NUCLEAR ANALYTICAL CHEMISTRY

Published papers submitted to the

University of Cape Town for the degree of

Doctor of Science

by

Max Peisach

M.Sc., Ph.D (Cape Town).

February 1974

It is often impossible to define a field of scientific endeavour with sufficient accuracy to cover the accepted sub-divisions of the field and yet to include the latest developments taking place on the borders of the domain. It may therefore be acceptable to refer to Nuclear Analytical Chemistry as a field in analytical chemistry in which the analysis is based principally on the measurement of products resulting from a nuclear interaction or a nuclear transition.

Historically the subject dates back to the early years of this century when naturally occurring radioactive elements were used as tracers. Probably the first application of this technique was by Paneth and Hevesy[1] who, in 1913, used radium-D (lead-210) as a natural tracer to determine the solubility of lead sulphide and lead chromate. Their technique remained limited in scope, however, until the discovery of artificial radioisotopes[2] in 1934. Thereafter the use of tracer techniques extended to every naturally occurring element.

The second major branch of the subject to develop was activation analysis. A few years after the discovery of neutrons, Hevesy and Levi[3] in 1936 bombarded impure yttrium with these particles and determined the dysprosium content by the amount of radiodysprosium generated in the sample. Similarly, shortly after the invention of the cyclotron, Seaborg and Livingood[4] in 1938 activated iron with deuterons to determine low concentrations of gallium. These two papers marked the start respectively of neutron and charged particle activation analysis.

After the discovery of nuclear fission, the construction of nuclear reactors served to accelerate developments in neutron activation analysis because large fluxes of neutrons became available to the analyst. As a result, research in neutron activation analysis mushroomed during the early

fifties but towards the end of that decade the research tempo started decreasing, even though the number of papers on the subject continued to grow as application of the technique spread to wider fields. When the limitations of neutron activation analysis became more evident and about the time when research on the analytical use of neutrons began to flag, the neglected complementary field of charged particle and photon activation analysis began to draw the attention of research analysts once more.

During the past decade the number of laboratories actively concerned with charged particle activation analysis has been increasing and a variety of accelerators has become available for analytical work. At about this time too, important advances were being made on nuclear detection systems. These influences made it possible for a third branch of nuclear analytical chemistry to come to the fore. Whereas previously only radioactive products of nuclear reactions were of interest to the analyst, the improved techniques showed that useful analytical information could be obtained from the spectrometry of the prompt reaction products. Probably the first occasion when prompt products were used for analysis was in 1951 when Gajdin and Pannell[5] determined beryllium by counting the prompt neutrons induced by photon irradiation. Since then more refined techniques of prompt particle spectrometry have been used to obtain analytical information not readily available by other means.

The growth of nuclear analytical chemistry can be judged from the growth rate of the literature on the subject. It is estimated[6] that there were about 250 papers on activation analysis, in 1955. This figure reached about 8000 in 1970 when the accretion was about 1000 papers per year. Under such conditions of growth new ideas are rapidly assimilated by many workers and papers dealing with applications of the methods outnumber those describing advances in methodology.

REFERENCES

1) F. Paneth and G. von Hevesy, Z.Anorg. Chem. 82, 323 (1913).

2) F. Joliot and I.Curie, Nature, 133, 201 (1934).

3) G. Hevesy and H.Levi, Kgl. Danske Videnskab. Selskab, Mat-fys. Medd. 14, 5 (1936).

4) G.T. Seaborg and J.J. Livingood, J.Amer.Chem.Soc. 60, 1784 (1938).

5) A.M. Gajdin and J.H. Pannell, Anal. Chem. 23, 1261 (1951).

6) G.J. Lutz, R.J. Boreni, R.S. Maddock and J. Wing (Eds.) - "Activation analysis: a bibliography through 1971" US.Bureau of Standards, Report TN 467, August, 1972.

CURRICULUM VITAE

Name : Max PEISACH

Personal Details : Born 3rd August 1926. Married 1950, children born in 1953 (twins), 1956, 1960

Education

1943 : Matriculation 1st Class Cape Province Senior Certificate Boys' High School, Worcester, South Africa.

1946 : B.Sc. University of Cape Town (Chemistry with Physics and Mathematics)

1948 : M.Sc. University of Cape Town (Inorganic Chemistry)
Thesis: "Germanium Ferrocyanide"

1954 : Ph.D. University of Cape Town
Thesis: "The reaction between stannic chloride and silver perchlorate in anhydrous media"

Professional Societies :

(1) Royal Institute of Chemistry
Associate 1951 to 1961, Fellow 1962 to date.

(2) South African Chemical Institute, Member 1962 to date.

(3) Chemical Society (London), Fellow 1952 to date

Professional Awards :

(a) Medal

(1) South African Chemical Institute, AE & CI Gold Medal 1965

(b) Fellowships

(1) University of Cape Town. Kings Scholarship, 1943

(2) The Ernest Oppenheimer Memorial Trust, Travelling Fellowship, 1965

(3) South African Council for Scientific and Industrial Research, Senior Bursary, 1970

Employment

1948-53 : University of Cape Town
1948 : Demonstrator
1949 : Junior Lecturer
1950 : Lecturer

1953-60 : S.A. Council for Scientific and Industrial Research
1953 : Research Officer; Inorganic and Analytical Chemistry
1955 : Research Officer; Radiochemistry
1957 : Senior Research Officer; Head, Radiochemistry

1960-63 : Israel Atomic Energy Commission
1960 : Head, Isotope Production Unit

1963 to date : Southern Universities Nuclear Institute
1963 : Head, Chemistry Division

Professional Appointments

(a) International bodies

(1) International committee on Modern Trends in Activation Analysis, 1969 to date.

(b) National bodies

(1) South African Atomic Energy Board
Isotopes and Radiation committee, 1967, 1968, 1972

(2) University of Stellenbosch.
Science Faculty, 1968, 1970, 1972

(3) Activation Analysis Co-ordination committee
Member, 1972 to date.

(c) Editorial boards.

(1) Journal of Radioanalytical Chemistry
Editorial Advisory Board, 1969 to date

(2) Journal of the South African Chemical Institute
Editorial Board, 1974

(d) Foreign laboratories

(1) England
(i) University of Durham, Radiochemistry visiting scientist, 1957
(ii) Atomic Energy Research Establishment, Harwell
Member, Isotope School, 1957
Vacation Associate, 1971

(2) France
(i) Nuclear Research Centre (C.E.N.), Saclay
Visiting scientist, 1957
(ii) National Centre of Scientifique Research (C.N.R.S.),
Laboratoire d'Analyse par Activation "Pierre Sue", Saclay
Research Associate, 1970-71

(3) U.S.A.
(i) Oak Ridge National Laboratory, Oak Ridge, Tennessee
Visiting scientist, 1965

(4) Austria
(i) International Atomic Energy Agency, Vienna
Research Agreement, Chief Investigator, 1973.

PUBLISHED PAPERS

PART I: NUCLEAR ANALYTICAL CHEMISTRY

1) The routine counting of carbon-14.
J.S. Afr. Chem. Inst. 12, 57 (1959).
M. Peisach

2) Determination of deuterium concentration in heavy water by the reaction $O^{16}(d,n)F^{17}$ induced by reactor neutrons.
(a) Israel At. Energy Comm. report IA-692 (1961).
(b) Anal. Chem. 34, 1305 (1962).
S. Amiel and M. Peisach.

3) Determination of oxygen by F^{18} counting in organic Li-O systems.
Bull. Res. Council Israel 10A No. 3 (1961).
M. Anbar, M. Peisach and R. Rafaeloff.

4) Oxygen-18 analysis by counting delayed neutrons of nitrogen-17.
(a) Israel At. Energy Comm. report IA-691 (1962).
(b) Anal. Chem. 35, 323 (1963).
S. Amiel and M. Peisach.

5) Analytical aspects of delayed neutron emission.
(a) Israel At. Energy Comm. report IA-784 (1962).
(b) Atomnaya Energiya 14, 535 (1963).
S. Amiel and M. Peisach.

6) Radioactivation analysis of sodium by counting photoneutrons.
(a) Israel At. Energy Comm. report IA-799 (1963).
(b) Anal. Chem. 35, 1072 (1963).
S. Amiel and M. Peisach.

7) A critical study of isotopic analysis of uranium by radioactivation using the method of delayed neutron counting.
Israel J. Chem. 1, 306 (1963).
S. Amiel and M. Peisach.

8) The determination of gold coating thicknesses by proton scattering.
J.S. Afr. Chem. Inst. 18, 61 (1965).
M. Peisach and D.O. Poole.

9) The use of semi-conductor detectors for surface analysis by elastic scattering of accelerated charged particles.
Proc. 1965 Intern. conf. "Modern Trends in Activation Analysis", College Station, Texas (1966) p. 206.
M. Peisach and D.O. Poole.

10) Isotopic determination of calcium-48 by proton activation.
Anal. Chem. 38, 956 (1966).
M. Peisach and R. Pretorius.

11) Analysis of surfaces by scattering of accelerated particles.
Anal. Chem. 38, 1345 (1966).
M. Peisach and D.O. Poole.

12) The determination of carbon, nitrogen and oxygen and their stable isotopic tracers in gases by neutron time-of-flight spectroscopy.
Chem. Communications 632 (1966).
M. Peisach.

13) Determination of alumina film thickness by alpha particle scattering.
Talanta 14, 187 (1967).
M. Peisach, D.O. Poole and H.F. Röhm.

14) Determination of deuterium in gases by neutron time-of-flight spectrometry.
(a) Anal. Chem. 39, 650 (1967).
(b) "Convention Handbook", S. Afr. Chem. Inst. 20th Convention, Durban (1967) p. 321.
M. Peisach and R. Pretorius.

15) Radioactivation analysis of calcium-48 tracers by proton irradiation.
Proc. Symposium "Medical Electronics and Nuclear Instrumentation in Medicine", Johannesburg, 1965, Leech 37, 11 (1967).
M. Peisach and R. Pretorius.

16) A study of the Ca(P,n)Sc reactions. (I). Energy levels in scandium isotopes.
Nucl. Phys. A99, 6 (1967).
W.R. McMurray, M. Peisach, R. Pretorius, P. van der Merwe and I.J. van Heerden.

17) A study of the Ca(p,n)Sc reactions. (II). Fluctuation analysis of the reaction $^{48}Ca(p,n)^{48}Sc$.
Nucl. Phys. A99, 17 (1967).
W.R. McMurray, M. Peisach, R. Pretorius, P. van der Merwe and I.J. van Heerden.

18) Reactions on light elements induced by charged particles elastically scattered by fast neutrons.
J. Nucl. Energy 21, 893 (1967).
W.J. Naudé and M. Peisach.

19) Cross sections for proton and deuteron-induced activation of calcium isotopes.
"Convention Handbook", S. Afr. Chem. Inst. 20th Convention, Durban (1967) p. 299.
M. Peisach, R. Pretorius and D.S. Rossettenstein.

20) Attempts at analysing volatile organic compounds by neutron time-of-flight spectrometry.
"Convention Handbook", A. Afr. Chem. Inst. 20th Convention, Durban (1967) p. 311.
M. Peisach, R. Pretorius and P.J. Strebel.

21) Isotopic determination of calcium-43 and calcium-48 by neutron time-of-flight spectrometry.
Anal. Chem. 40, 266 (1968).
W.R. McMurray, M. Peisach, R. Pretorius, P. van der Merwe and I.J. van Heerden.

22) The fast neutron facility at the Pretoria cyclotron.
Proc. 3rd Conf. "Accelerator Targets designed for the production of Neutrons" Euratom Report EUR 3895-d-f-e Brussels (1968) p. 261.
W.J. Naudé, M. Peisach, and W.L. Rautenbach.

23) Analytical use of prompt neutrons produced by pulses of charged particles. Proc. 2nd Conf. "Practical Aspects of Activation Analysis with Charged particles" Euratom Report EUR 3896 d-f-e Brussels (1968) p. 65.
M. Peisach.

24) Isotopic determination of oxygen-18 in gases by neutron time-of-flight spectrometry.
Anal. Chem. 40, 850 (1968).
M. Peisach, R. Pretorius and P.J. Strebel.

25) The determination of carbon, nitrogen and oxygen in gases by neutron time-of-flight spectrometry.
J. Radioanal. Chem. 1, 231 (1968).
W.J. Naudé, M. Peisach, R. Pretorius and P.J. Strebel.

26) The use of alpha particle scattering for the qualitative analysis of elements in solution.
J.S. Afr. Chem. Inst. 22, 50 (1969).
M. Peisach.

27) Isotopic determination of calcium-48 by deuteron activation.
Anal. Chem. 41, 416 (1969).
T.J. de Waal, M. Peisach and R. Pretorius.

28) The determination of stable calcium isotopes by charged particle irradiation.
"Modern Trends in Activation Analysis", J.R. de Voe (Editor), Nat. Bur. Stand. (U.S.) Spec. Publ. 312 (June 1969) Vol. II, p. 802.
M. Peisach and R. Pretorius.

29) Surface analysis of medium weight elements by prompt charged particle spectrometry.
"Modern Trends in Activation Analysis", J.R. de Voe (Editor) Nat. Bur. Stand. (U.S.) Spec. Publ. 312 (June 1969) Vol. II. p. 946.
C. Olivier and M. Peisach.

30) Isotopic determination of calcium-43 by proton activation.
J. Radioanal. Chem. 3, 345 (1969).
R.J.N. Brits and M. Peisach.

31) Microanalysis of surfaces by ion beam scattering.
"Electron and Ion Beam Science and Technology", R. Bakish, Ed., Amer. Inst. Mining, Mettalurg. Petroleum Engineers Inc. Gordon and Breach, New York (1969) Vol II, p. 1195.
M. Peisach and D.O. Poole.

32) The determination of nickel on metal surfaces by prompt proton spectrometry.
J.S. Afr. Chem. Inst. 23, 77 (1970).
C. Olivier and M. Peisach.

33) Determination of chromium on metal surfaces by prompt proton spectrometry.
J. Radioanal. Chem. 5, 391 (1970).
C. Olivier and M. Peisach.

34) Activation cross sections for deuteron-induced reactions on calcium isotopes, up to 5,5 MeV.
Radiochimica Acta 15, 123 (1971).
T.J. de Waal, M. Peisach and R. Pretorius.

35) Activation cross sections for proton-induced reactions on calcium isotopes, up to 5,6 MeV.
J. Inorg. Nucl. Chem. 33, 2783 (1971).
T.J. de Waal, M. Peisach and R. Pretorius.

36) Determination of oxygen by the spectrometry of prompt gamma-rays from triton-induced reactions.
Radiochem. Radioanal. Letters 8, 119 (1971).
M. Peisach.

37) Rapid neutron activation analysis of bromine using 6.1 min bromine-82m.
Radiochem. Radioanal. Letters 8 267 (1971).
M. Peisach, D. Comar and C. Kellershohn.

38) Activation cross sections for deuteron-induced reactions on some elements of the first transition series, up to 5,5 MeV.
Radiochimica Acta 17, 1 (1972).
P.P. Coetzee and M. Peisach.

39) Prompt proton spectrometry from high Q-value (d,p) reactions and its use for determining ^{10}B.
J. Radioanal. Chem. 11, 105 (1972).
C. Olivier and M. Peisach.

40) The use of charged nuclear particles for analysis.
Proc. Nat. conf. "Technological Applications of Nuclear Techniques", Atomic Energy Board, Pretoria (1972), paper 13.
M. Peisach and R. Pretorius.

41) Deuteron activation analysis of geological samples.
J. Radioanal. Chem. 12, 139 (1972).
R. Pretorius, F. Odendaal and M. Peisach.

42) Prompt gamma-rays from triton-induced reactions on oxygen and their use for analysis.
J. Radioanal. Chem. 12, 251 (1972).
M. Peisach.

43) The determination of boron-10 by prompt proton spectrometry.
J. Radioanal. Chem. 12, 313 (1972).
C. Olivier and M. Peisach.

44) Isotopic determination of calcium-48 by photon activation.
J. Radioanal. Chem. 13, 193 (1973).
M. Peisach.

45) Elemental analysis by differentiated backscatter spectrometry.
Thin Solid Films 19, 297 (1973).
M. Peisach.

PART II: TRACER AND RADIOCHEMISTRY.

46) Separations in radiochemistry with special reference to the isolation of carrier-free isotopes.
S.Afr. Indust. Chem. 11, 7 (1957).
M. Peisach.

47) The asscciation of vitamin A alchohol with rat serum proteins.
S.Afr. J. Med. Sci. 23, 24 (1958).
C.F. Garbers, J. Gillman and M. Peisach.

48) The carrier-free separation of UZ from 100 kg. uranyl nitrate.
Proc. U.N. Intern. conf. "Peaceful Uses At. Energy", 2nd Geneva, 1958, 20, 62.
J. v. R. Smit, M. Peisach and F.W.E. Strelow.

49) Skin decontamination of phosphorus-32.
S.Afr. Indust. Chem. 12, 245 (1958).
W.R. McMurray and M. Peisach.

50) A preliminary report on the metabolism of 2 - ^{14}C - pyruvate in diabetic baboons.
S. Afr. J. Med. Sci. 23, 278 (1958).
N. Savage, J. Gillman, C. Gilbert and M. Peisach.

51) The isolation of radiosilver by isotopic exchange.
J.S. Afr. Chem. Inst. 12, 116 (1959).
M. Peisach and S.J. van der Walt.

52) The chemical effects of radiation.
S.Afr. Indust. Chem. 13, 204 (1959).
M. Peisach.

53) The transport of vitamin A in rat serum with reference to the occurrence of unidentified metabolites of vitamin A in the rat.
Biochem. J. 75, 124 (1960).
C.F. Garbers, J. Gillman and M. Peisach.

54) Radiolytic oxidation of ferrous sulphate solutions with standardised internal sources of phosphorus-32.
Nature 187, 58 (1960).
M. Peisach and J. Steyn.

55) Radiolysis of ferrous sulphate solutions with standardised internal sources of phosphorus-32.
(a) J.S. Afr. Chem. Inst. 13, 34 (1960).
(b) S. Afr. Indust. Chem. 14, 232 (1960).
M. Peisach and J. Steyn.

56) Reactor-produced carrier-free iridium-194.
(a) Israel At. Energy Comm. report IA-855 (1963).
(b) Radiochimica Acta 2, 197 (1964).
M. Peisach.

57) Current interest in nuclear chemistry.
S. Afr. Indust. Chem. 18, 111 (1964).
M. Peisach.

58) The preparation of potassium hexacyanocobaltate (III) labelled with cobalt-58 and 60 for hydrological studies.
J.S. Afr. Chem. Inst. 18, 1 (1965).
M. Peisach.

PART III: MISCELLANEOUS

59) Germanium (Germanyl) ferrocyanide.
J. Chem. Soc. 1950, 949.
M. Peisach, W. Pugh and F. Sebba

60) The system sodium chloride - sodium sulphate - water, with reference to the recovery of sodium chloride and sodium sulphate from natural brines in South Africa.
S. Afr. Indust. Chem. 9, 210 (1955).
M. Peisach.

ADDENDUM

Papers published since completion of foregoing list

PART I: NUCLEAR ANALYTICAL CHEMISTRY

61) Some analytical investigations into the use of X-rays emitted during charged-particle irradiation.
J. Radioanal. Chem. 16, 445 (1973)
M. Peisach, D.A. Newton, P.F. Peck and T.B. Pierce

62) The elemental and isotopic determination of lithium by the coincident measurement of complementary particles.
J. Radioanal. Chem. 16, 551 (1973)
R. Pretorius, P.P. Coetzee and M. Peisach

63) Analysis of glass by simultaneous spectrometry of scattered alpha particles and prompt protons.
J. Radioanal. Chem. 16, 559 (1973)
M. Peisach and R. Pretorius

64) Rapid neutron activation of Bromine using 6.1-min Bromine-82m: Application to the determination of Bromine in blood plasma.
J. Radioanal. Chem. 19, 269 (1974)
M. Peisach, B. Mazière, C. Loc'h, D. Comar and C. Kellershohn

No. 1

THE ROUTINE COUNTING OF CARBON—14

by

M. PEISACH

OPSOMMING

'n Verbeterde metode vir die montering van bariumkarbonaat gemerk met koolstof-14 is ontwikkel. Die bariumkarbonaat word oor 'n groot oppervlakte in 'n dun lagie op 'n metaalplaat gesentrifugeer. Die metode maak dit moontlik om monsters maklik en vinnig vir analise voor te berei; die koëffisiënt van variasie van die resultate is kleiner as 2·5%.

SUMMARY

An improved method of mounting carbon-14 labelled barium carbonate is described. Barium carbonate is centrifuged on to a metal plate to produce a thin deposit over a large area. The method permits rapid and easy preparation of samples for analysis; the coefficient of variation of the results is better than 2·5%.

In most tracer work with carbon-14 the labelled sample is ultimately combusted to carbon dioxide which may be analysed as such or precipitated and counted as barium carbonate. This paper deals with a simple procedure for preparing barium carbonate samples by centrifugation.

Most existing methods for mounting carbon-14 labelled barium carbonate for counting purposes depend either on filtration on to paper or some other porous material such as sintered Perspex, or on evaporation of a slurry of the precipitate suspended in some volatile solvent. Although these methods are capable of yielding good results for thick sources, the reported error of 2% is exceeded when thin sources have to be measured. Calvin and others[1] state that "the evaporation (of slurries) is actually a somewhat more complicated process . . . when thin samples have to be made" and Gora and Hickey,[2] who investigated the self-absorption of carbon-14 samples, consider that for very thin samples "it is not possible to spread them out evenly". Winteringham[3] states explicitly that the results obtained from solid counting with internal gas flow counters have an error of ±5%. Wick, Barnet and Ackerman[4] stress the need for extreme care in preparing thin samples, and, whilst they do not give any data on their errors, their published curves show a wide scatter of results with thin deposits. It is thus evident that the method described below is of value where the other methods fail, especially for routine analyses when a large number of samples have to be analysed.

In connection with biological work, it frequently happens that samples of low specific activity have to be analysed and usually only a limited weight of material is available. Under such circumstances with existing methods it is necessary to form a thick deposit over a small surface and to correct for the self-absorption of the sample. This self-absorption can be reduced if the sample is deposited in a thinner layer over a larger area with the result that the counting rate will be higher and hence a shorter time will be necessary for counting. To achieve this, precipitated barium carbonate is suspended in alcohol and centrifuged on to a metal plate of large area. Homogeneous reproducible deposits are obtained easily and quickly, especially when thin deposits are prepared. Mention of such a method was made by Calvin *et al.*,[5]

pressure with "Tracerlab" proportional gas, a mixture of about 10% methane and 90% ragon.

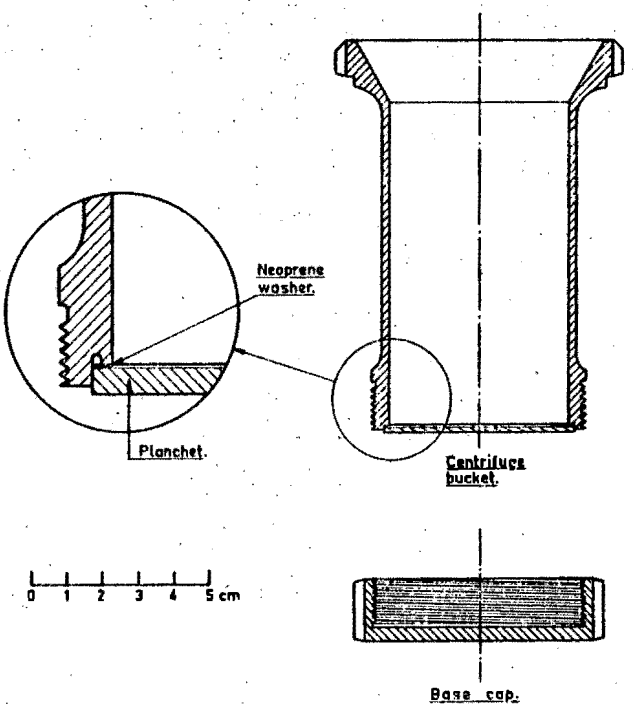

FIG. 1—Centrifuge bucket with base cap showing design of the bottom of the bucket where the washer is placed

RESULTS

A test series of 71 analyses was carried out. The results are shown in Figs. 2 and 3 and some are listed in Table I. In the former curve the activity is plotted against the thickness of the deposit, whilst the latter shows the same results plotted against the percentage transmission, R, where (100-R) represents the percentage loss of activity due to self-absorption and possibly other causes. The form of the curve in Fig. 3 corresponds to the well-known self-absorption expression

$$R = \frac{100\ (1 - e^{-\mu s})}{\mu s}$$

where s is the thickness of the deposit in mg/cm^2 and μ the mass absorption coefficient which, in this case, was found to have the value 0·55 cm^2/mg and is in good agreement with published values[7] for windowless counters.

A statistical analysis of the results showed that the coefficient of variation, v, of the corrected specific activity of a sample, $\bar{a}$, has the value 2·4(2)% over the range of thicknesses from 1 to about 6 mg/cm^2

$$\text{where } v = \frac{100\sigma}{\bar{a}}$$

σ is the standard deviation and $\bar{a}$, the mean specific activity.

TABLE I

Some values obtained for thin deposits of $BaCO_3$

No.	$BaCO_3$ mg	Thickness mg/cm²	Corrected Specific Activity c/m/mg	R Exptl.	R Calculated
55	14·9	0·77	14·78	80·3	81·6
54	18·1	0·93	15·07	78·5	78·2
46	19·6	1·01	14·95	76·3	76·7
41	23·0	1·19	14·90	72·7	73·5
19	34·3	1·77	15·12	64·3	64·0
13	35·5	1·83	14·90	62·5	63·0
4	35·7	1·84	15·23	63·7	62·9
20	38·0	1·96	15·01	61·2	61·2
3	39·2	2·02	15·14	60·9	60·4
8	46·1	2·38	15·09	55·1	55·8
10	46·6	2·40	14·87	55·0	55·5
23	47·1	2·43	15·00	55·1	55·2
24	52·1	2·69	14·97	52·1	52·2
33	62·6	3·23	15·03	46·8	46·8
61	82·2	4·24	15·14	38·9	38·7
70	99·8	5·14	15·19	33·6	33·3
70	111·5	5·75	14·70	30·2	31·6

For the series of 71 analyses, the mean corrected specific activity was 14·96 c/m/mg with a standard deviation of 0·36; *i.e.* coefficient of variation v=2·4%.

In addition to the series of analyses mentioned above, this method has been used in our Laboratories for several thousands of analyses over the past four years. During that time the method was tested repeatedly and analyses were carried out with deposits thinner than 1 mg/cm² and thicker than 6 mg/cm². The thinner samples were prepared with great ease and the results were within the stated limits of precision, but thick deposits tended to crack on drying and to break at the edges when removed from the centrifuge bucket. Accordingly, this method is not recommended for thick deposits.

The author wishes to thank Mr. I. Roth for assistance during the development stages and Mrs. A. Slaa and Mrs. M. M. Pols for assistance with the analyses.

This paper is published with the permission of the South African Council for Scientific and Industrial Research.

Radiochemistry Section,
National Chemical Research Laboratory,
S.A. Council for Scientific and Industrial Research,
Pretoria.

Received March 3, 1959.

REFERENCES

[1] Calvin, Heidelberger, Reid, Tolbert and Yankwich, *Isotopic Carbon*, John Wiley & Sons, London, 1949, p. 119.
[2] Gora and Hickey, *Anal. Chem.*, 1954, **26**, 1158.
[3] Winteringham, *Analyst*, 1951, **76**, 367.
[4] Wick, Barnet and Ackerman, *Anal. Chem.* 1949, **21**, 1511.
[5] Langham, private communication, mentioned in reference 1, p. 121.
[6] Evans and Huston, *Anal. Chem.*, 1952, **24**, 1483.
[7] Calvin, Heidelberger, Reid, Tolbert and Yankwich, *Isotopic Carbon*, John Wiley & Sons, London, 1949, p. 105.

No. 2

Reprinted from

ANALYTICAL CHEMISTRY

Determination of Deuterium Concentration in Heavy Water by the Reaction Oxygen-16 (*d, n*) Fluorine-17 Induced by Reactor Neutrons

SAADIA AMIEL and MAX PEISACH

Israel Atomic Energy Commission/Laboratories, P.O. Box 527, Rehovoth, Israel

Volume 34, Number 10

Page 1305–1307, September 1962

at the prevailing conditions of the energy spectrum of the neutron flux. The ratio of the effective cross sections for the (d, n) and (p, γ) reactions with O^{16}, R, should be given by the ratio of the fluorine-17 activities obtained from D_2O (100%) and H_2O (100%). It was found that

$$R = \frac{\bar{\sigma}(d, n)}{\bar{\sigma}(p, \gamma)} = 60 \pm 20 \qquad (1)$$

which showed that for equal numbers of atoms of the corresponding recoiling hydrogen isotope, the contribution of the (p, γ) reaction was about $1^1/_2\%$ of that of the (d, n) reaction. Because the container was made of polyethylene, a hydrogen-containing material, part of the (p, γ) contribution could have been due to protons recoiling from the walls.

Because the ratio, R, of yields of the (d, n) and (p, γ) reactions is large, it enables analysis of samples in the region where the fluorine-17 activity remains directly proportional to the deuterium content to be carried out relative to a single standard. This procedure is suitable for samples containing above 15 mg.-atoms deuterium per gram of water. However, this limitation depends on the value of the ratio, R, which in turn is dependent on the energy distribution of the fast neutron flux due to the difference in the threshold energies of the two competing reactions. Accordingly, the value of R with an undistorted fission spectrum neutron flux might be expected to exceed 60, and hence would extend the range of applicability of this procedure.

When the deuterium content is less than about 15 mg.-atoms per gram of water, analyses can no longer be referred to a single standard, but a linear calibration curve such as given in Figure 2 has to be used. The method is then applicable to the entire range of concentrations.

Neutron activation of water and container material components which could yield positron emitters either directly or by proton or deuteron recoils are given in Table I (*2*), which shows that N^{13} and F^{18} are the nuclides most likely to accompany F^{17}. These nuclides were both observed but because of their widely different half lives, their presence can easily be allowed for. However,

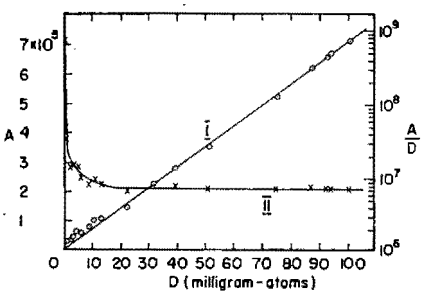

Figure 3. Variation of F^{17} with deuterium content

(I) Specific activity of F^{17} per mole water, A
(II) Specific activity of F^{17} per mole water per mole deuterium, A/D, plotted against deuterium content, D

their formation introduces a source of error which becomes appreciable in samples of very low deuterium content, below about 1% D_2O by weight, and may be considered as a limiting factor of the method.

The relative accuracy of this method, using fluorine-17 as a monitor for the deuterium content, depends on the stability of the neutron flux, reproducibility of sample position and on counting statistics. The first two cease to be important if a standard is irradiated simultaneously with the sample. The relative standard deviation of the result due to the statistical errors of counting samples of high deuterium content is about 0.1%, but in practice a value of 0.5% is generally obtained, considering the stability of the irradiation parameters and the counting equipment. The activity of the sample may be obtained either by extrapolation of the decay curve or by measuring the integrated count over a fixed period. As the activity is proportional to the sample weight, the sample may be reduced at the expense of accuracy. The minimum sample size is determined by the accuracy of sample preparation and the activity obtained rather than by the loss of recoiling deuterons from the sample, because the range of deuterons of several million electron volts energy is of the order of 0.1 mm. (*1*).

The observed constancy of the fluorine-17 yield over a wide range of deuterium concentration suggests that there is no observable difference in the corresponding energy losses of the recoiling deuterons at different isotopic concentrations of hydrogen—i.e.,

$$\frac{dE_D}{dx_{H_2O}} = \frac{dE_D}{dx_{D_2O}} \qquad (2)$$

The present method provides a simple and rapid nondestructive method for determining heavy water concentrations useful for heavy water reactors or heavy water process control. It could meet the required accuracies in both fields, 1% for D_2O production and down to 0.1% for heavy water reactors. With a conventional counting arrangement near a reactor, several dozens of samples per day could be analyzed.

The method is readily applicable to high-energy neutron distribution measurements in water systems, as in reactors. It is superior to foil techniques because the homogeneity of the medium is preserved.

ACKNOWLEDGMENT

We thank the operating crew of IRR-1 for the reactor irradiations and D. H. Samuel for supplying analyzed heavy water. Thanks are due to I. Dostrovsky for his continuous interest and criticism.

LITERATURE CITED

(1) Aron, W. A., Hoffman, B. G., Williams, F. C., U. S. At. Energy Comm. **AECU-663**, (1951).
(2) Ajzenberg-Selove, F., Lauritsen, T., *Nucl. Phys.* **11**, 150 (1959).
(3) Baranov, V. I., Kristianov, V. K., Karasev, B. V., *Dokl. Akad. Nauk S.S.S.R.* **129**, 1035 (1959).
(4) Dostrovsky, I., Samuel, D. H., Israel Atomic Energy Commission Laboratories, P.O. Box 527, Rehovoth, Israel, private communication, 1960.
(5) Duke,, D. W., Babcock and Wilcox Co. Rept. **BAW-1209**, (1960).
(6) Ernst, M. L., E. I. du Pont de Nemours and Co. Rept. **DP-202**, (1957).
(7) Glickstein, S. S., Winter, R. G., *Nucl. Instr. Methods* **9**, 226 (1960).
(8) Gokhale, V. A., Navalkar, M. P., Srinivasan, M., Subbaramu, K. R., India At. Energy Establishment, U. S. At. Energy Comm. **NP-9166**, (1960).
(9) Hughes, D. J., Schwartz, R. B., "**BNL-325** Neutron Cross Sections," U. S. Govt. Printing Office, 1958.
(10) Roy, J. C., Bresesti, M., Hawton, J. J., *Can. J. Phys.* **38**, 1428 (1960).
(11) Stehn, J. R., *Trans. Am. Nucl. Soc.* **3**, 467 Paper 25-10, Dec. 13, 1960.

RECEIVED for review December 18, 1961. Accepted March 30, 1962.

PRINTED IN U. S. A.

No. 3

Determination of oxygen by F^{18} counting in organic Li-O systems

M. ANBAR*, M. PEISACH AND R. RAFAELOFF**

The reactions $Li^6(n,L)t$, $O^{16}(t,n)F^{18}$ were used to determine the oxygen content of organic compounds[1].

Using solid mixtures, lithium fluoride and the oxygen - containing organic compounds in the form of fine powders were mixed mechanically. Ratios of lithium to oxygen ranged from unity to about ten. Activities of about 1μc for 150mg oxygen were obtained and measured by β-γ coincidence counting. Fluorine 18 yields were found to be proportional to oxygen content in the range 25–250mg oxygen. When however attempts were made to decrease the oxygen content below about 10mg difficulties were encountered due to the small oxygen impurity in lithium fluoride as well as to the competing production of fluorine-18 by the reaction $F^{19}(n,2n)F^{18}$. Of various organic solvents investigated at temperatures above their melting point, succinonitrile gave the best results. Lithium thiocyanate was dissolved in succinonitrile and the oxygen-containing organic compound was added at elevated temperatures. On cooling, the solid pellets were immersed in wax and irradiated. However,

* Isotope Dept., Weizmann Institute of Science, Rehovot: Consultant to the I.A.E.C.
** Israel Atomic Energy Commission.

at oxygen contents < 10 mg, the method could not be applied because of interference due to oxygen impurities in the lithium thiocyanate and the limited solubility of lithium thiocyanate in succinonitrile.

REFERENCE

1. OSMOND, R.G. AND SMALES, A.A., 1954, *Anal. Chim. Acta*, **10**, 117–128.

Bull. Research Council Israel. 10A No. 3 pp 23-4 (1961)

No. 4

Reprinted from

ANALYTICAL CHEMISTRY

Oxygen-18 Determination by Counting Delayed Neutrons of Nitrogen-17

SAADIA AMIEL and MAX PEISACH

Soreq Research Establishment, Israel Atomic Energy Commission, P.O.B. 527, Rehovoth, Israel

Volume 35, Number 3

Pages 323-327, March 1963

Oxygen-18 Determination by Counting Delayed Neutrons of Nitrogen-17

SAADIA AMIEL and MAX PEISACH

Soreq Research Establishment, Israel Atomic Energy Commission, P.O.B. 527, Rehovoth, Israel

▶ Neutron counting of 4.14-second nitrogen-17 is used for the analysis of oxygen-18 in solutions containing known of amounts lithium-6. Nitrogen-17 is produced by the successive nuclear reactions $Li^6(n, \alpha)t$; $O^{18}(t, \alpha)N^{17}$ on irradiation with thermal neutrons. The total delayed neutron emission of a sample irradiated to saturation at a thermal neutron flux of $10^{13}n/cm.^2$-second is about 4×10^5 neutrons per mg. of lithium-6 per atom per cent oxygen-18. The nitrogen-17 formation is proportional to the atom fraction of oxygen-18 and is independent of the sample size.

THE IMPORTANCE of oxygen-18 as a tracer for oxygen in various fields of research created the need for suitable analytical techniques. The common method of determining oxygen-18 content is by mass spectrometry (*10*), but radioactivation techniques have been tried as well (*11*). Although mass spectrometry is a very sensitive high precision method, its use is sometimes restricted by the relatively high cost of the equipment; additional drawbacks are the need to use vacuum apparatus, the relatively long procedure, and the destruction of the sample analyzed. It frequently happens that the more rapid methods of analysis by radio activation are sufficient and are preferred even though they are less accurate and sensitive than mass spectrometry.

In the main, analysis of oxygen-18 by radioactivation is carried out by measuring the activity of oxygen-19 or fluorine-18 (*6*). These methods are based on γ-ray spectrometry, coincidence counting, or, to a more limited extent, autoradiography where beta emission is measured by the blackening of photographic emulsions (*7*). The main limitation of all these methods is the interference from other components in the sample, which frequently may be major constituents. Recently attempts to determine oxygen-18 were reported in which the number of particles emitted during a nuclear reaction were measured—e.g., neutrons (*3*) from the reaction $O^{18}(\alpha,n)Ne^{21}$ and alpha particles (*5*) from the reaction $O^{18}(d,\alpha)N^{16}$.

In this work an attempt was made to assay oxygen-18 in water samples by measuring the delayed neutron emission from nitrogen-17. Neutrons can be counted selectively and efficiently without interference from β- or γ-ray background. Furthermore, neutron emission in radioactive decay is a sufficiently rare phenomenon to be specific for the detection and measurement of a particular neutron precursor. The formation of nitrogen-17 in neutron irradiated samples was recently used for the analysis of lithium-6 in aqueous systems (*4*).

Nitrogen-17 decays as follows:

$$N^{17} \xrightarrow[4.14\ \text{sec.}]{\beta^-} O^{17*} \xrightarrow{\text{prompt}} O^{16} + n,\ Q_m = 4.57\ \text{m.e.v.}$$

It can be formed directly from oxygen isotopes with fast neutrons in a reactor, by the reactions (*1*):

$$O^{17}(n, p)N^{17},\quad Q_m = -7.93\ \text{m.e.v.} \quad \text{(I)}$$

and

$$O^{18}(n, d)N^{17},\quad Q_m = -13.77\ \text{m.e.v.} \quad \text{(II)}$$

With thermal neutrons nitrogen-17 cannot be produced directly, but in the presence of lithium-6, secondary reactions with the 2.7-m.e.v. tritons from $Li^6(n,\alpha)t$ can lead to nitrogen-17 formation by the reactions

$$O^{18}(t, \alpha)N^{17},\quad Q_m = 3.82\ \text{m.e.v.} \quad \text{(III)}$$

and in the presence of nitrogen by

$$N^{15}(t, p)N^{17},\quad Q_m = 0.15\ \text{m.e.v.} \quad \text{(IV)}$$

The cross section of reaction I for unmoderated fission neutrons is not well established and has on separate occasions been reported to be 5 and 9 μb. (*9*, *13*). The cross section for reaction II is not known, but can be taken to be about two orders of magnitude smaller than for reaction I, because of the corresponding drop in the abundance of neutrons in fission with the appropriate energy. In natural water, the contribution of reaction II might account for a few per cent of the total nitrogen-17 produced by fast neutrons. Nevertheless, in oxygen-enriched water where the ratio of oxygen-18 to oxygen-17 may be higher than in natural water, the relative contribution of reaction II to the total yield of nitrogen-17 may become important or even comparable to that of reaction I (*2*).

The number of delayed neutrons obtained by reaction I from the nitrogen-17 produced from a 1-gram sample of natural water irradiated to saturation in a fission spectrum neutron flux of $10^2n/cm.^2$-second should be about 325, when the cross section is taken as 5 μb.

When lithium-6 is introduced into the water, the formation of nitrogen-17 proceeds predominantly by reaction III because of its high effective cross section with thermal neutrons (*4*). A 1-gram natural water sample containing 1 mg. of lithium-6 yields about 9000 delayed neutrons by this reaction when irradiated to saturation in a thermal neutron flux of $10^{12}n/cm.^2$-second. It follows that in water samples containing lithium-6 irradiated in a mixed flux, containing thermal and fast neutrons caused by partial moderation, the production of nitrogen-17 by reactions I and II is relatively small and reaction III could then be used for the measurement of the oxygen-18 content of the water.

The rate of formation of tritons by thermal neutron bombardment of lithium-6 is given by

$$A_t = [Li^6]\sigma_{n,\alpha}\Phi_n \quad (1)$$

where

A_t = the number of tritons produced per second,
$[Li^6]$ = the number of atoms of Li^6
Φ_n = the thermal neutron flux per cm.^{2} per second,
$\sigma_{n,\alpha}$ = the thermal reaction cross section of $Li^6(n, \alpha)\ t$.

Since the range of tritons is very small (*14*), the probability of a triton producing an atom of nitrogen-17 is proportional to the atom fraction of oxygen-18 provided that the solution is sufficiently dilute with respect to lithium to ignore collisions with the solute. It is assumed that the energy loss of the triton per collision with an oxygen atom is independent of the isotopic composition of oxygen and that the hydrogen composition is kept constant.

Thus

$$A_n \propto A_t f(O^{18}) \quad (2)$$

where

A_n = the number of nitrogen-17 atoms produced per second

$f(O^{18})$ = the atom fraction of oxygen-18

Reprinted from **ANALYTICAL CHEMISTRY**, Vol. 35, Page 323, March 1963

combining Equations 1 and 2 one gets

$$A_n \propto \sigma_{n,\alpha}\, \Phi_n\, [Li^6]\, f(O^{18})$$

which, for a known constant thermal neutron flux reduces to

$$A_n \propto [Li^6]\, f(O^{18}) \qquad (3)$$

Thus, the rate of production of nitrogen-17, in a sample of Li^6–H_2O^{18} irradiated with thermal neutrons, should be independent of the water content and should be proportional to the total lithium-6 content and the atom fraction of oxygen-18.

The above derivation implies that the analysis of the oxygen-18 concentration in water can be carried out with thermal neutrons with any sample size. The only proviso is that the lithium concentration should be low for two reasons; first, to avoid extra energy loss of the tritons by collision with the relatively light lithium, which will result in a lower effective cross section, and second, to obviate attenuation of the irradiation neutron flux within the sample by self-shielding.

In a well-thermalized flux, interference by reactions I and II is made negligibly small. When a mixed neutron flux is used for the analysis care should be taken to subtract the nitrogen-17 yield produced with fast neutrons by the direct reactions. Such a correction can be made by reirradiating the sample in a cadmium box which will absorb thermal neutrons and thus effectively eliminate the contribution from reaction III without changing those from reactions I and II. Another way of correcting for the above mentioned interference relies on the fact that the yield of nitrogen-17 from reactions I and II is proportional to the heavy oxygen content or sample size, while that from reaction III is independent of this parameter and depends on the lithium-6 content. Accordingly by reirradiating the sample with a changed lithium-6 concentration, the net effect of reaction III could be obtained.

EXPERIMENTAL

Preparation of Samples. Samples of water containing up to 97.04 atom per cent oxygen-18 were obtained from the Weizmann Institute of Science, Rehovoth, Israel, and were analyzed by mass spectrometry. From the supplied water, samples of lower oxygen-18 concentration were prepared by mixing known weights of enriched and natural water. Lithium-6 was obtained as metal containing 96.1 atom per cent Li^6 from Oak Ridge National Laboratory, Oak Ridge, Tenn., U.S.A., and from it all lithium salts were prepared. Synthesized lithium salts were checked for lithium content by chemical analysis, due account being taken of the decrease in atomic weight with increasing proportion of lithium-6.

The water samples used in this investigation contained lithium-6 as iodide, nitrate, or carbonate. Because of the hygroscopic nature of lithium iodide the preparation of its solutions was carried out in a glove box by weighing the water sample before and after the addition of the salt. With the other lithium salts, stock solutions of known lithium-6 content were prepared with water highly enriched with oxygen-18. Small weights of the stock solutions were used to prepare samples with decreasing atom per cent oxygen-18 water. Errors of the order of 0.2 mg., which were inherent in the direct addition of about 10 mg. of LiI to 1-gram water samples, were excluded in this second procedure. In all cases the lithium-6 concentration was kept well below the level where self-shielding might introduce unnecessary errors.

Sample Containers. The irradiation sample containers were polyethylene vials 51 mm. in length and of 8.5-mm. i.d. The vials were closed with caps which themselves could serve as miniature vials 7.3 mm. deep and with 8.3-mm. i.d. Samples were placed either in the main body of the vial or, when small samples had to be irradiated, into the caps, and were heat-sealed with polyethylene disks before irradiation. By placing small volumes of solution into the caps, the decreased free volume of the container restricted the movement of the sample thus ensuring better reproducibility of irradiation position.

Sealed samples were mounted in polyethylene carriers (rabbits) which were used in the pneumatic tube facility of IRR-1 (the Israel 5-Mw. swimming pool reactor at Soreq).

Irradiation. The rabbits were irradiated at the face of the reactor core where the thermal flux was 4.7×10^{12} $n/cm.^2$-second and the fast (fission spectrum) neutron flux was 1.1×10^{12} when the reactor operated at 1 Mw., the power level at which all the experiments were carried out.

Samples were irradiated for 30 seconds to reach saturation activity of nitrogen-17 and counted for 25 seconds after a delay of 5 seconds. Cadmium boxes of 0.03-inch wall thickness were used when discrimination against thermal neutrons was necessary.

Counting. The counting assembly consisted of a ring of six $B^{10}F_3$ neutron counters connected in parallel and embedded in a block of paraffin 40 × 40 × 40 cm. with a cavity in the center of the ring along the axis of the counters. During counting the sample was positioned half-way along the cavity in the center of the block.

Pulses from the counters were fed through an amplifier to a fast scaler which was started automatically by an electronic timer 5 seconds after the end of irradiation. The timer was triggered by the rabbit leaving the irradiation position. Discrimination against γ-rays was checked by placing a 6-mc. Co^{60} source in the counting position. Photoneutron emission due to (γ,n) reactions induced by high energy γ-rays from activation of sample and container impurities on the deuterium of the paraffin block, were negli-

Table I. Calibration of Neutron Count from Oxygen-18 Enriched Samples

I	II	III	IV	V	VI	VII	VIII
			Neutron counts				Counts per mg. of Li^6 per atom % O^{18}
O^{18} atom %	O^{17} μg. atoms	Li^6 mg.	Unscreened	Screened Cd	Difference (IV) − (V)	Ratio (IV)/(VI)	(VI)/(I)(III)
			Li^6 as nitrate or carbonate				
97.04	222.3	0.3915	228832	4074	224758	1.018	5916
66.53	166.5	0.5102	206485	4084	202401	1.020	5963
30.13	114.9	0.01368	2844	447	2397	1.186	5815
21.06	93.7	0.01357	2046	348	1698	1.205	5945
17.39	76.9	0.01722	2082	300	1782	1.168	5952
13.53	65.3	0.03431	2986	282	2704	1.104	5824
9.317	424.7	0.1119	7666	1469	6197	1.237	5944
7.085	44.9	0.1553	6523	273	6250	1.043	5680
4.257	39.4	0.1142	2956	80	2876	1.028	5916
1.965	27.6	0.3064	3563	141	3422	1.041	5683
0.204	29.8	0.3214	430	50	380	1.132	5796
					Mean:	5858	
					Standard deviation: ±105		
					Relative standard deviation ±1.8%		
			Li^6 as iodide				
88.29	207.1	0.6366	332961	5850	327111	1.018	5820
77.32	187.1	0.5187	237846	4576	233270	1.019	5816
65.16	27.8	0.01264	5027	203	4824	1.042	5857
56.42	147.3	0.4131	145407	3010	142397	1.021	6110
35.73	104.6	0.2994	62749	1623	61126	1.027	5714
9.33	43.2	0.2058	12289	367	11922	1.031	6209
2.52	127.8	0.0990	1685	322	1363	1.236	5463
0.204	20.8	0.2353	318	37	281	1.132	5854
					Mean:	5855	
					Standard deviation:	±229	
					Relative standard deviation ±3.9%		

gible. Stability was checked daily with a standard RaD–Be neutron source. A counting efficiency of about 7% was obtained for a known spontaneous fission neutron source. The counting duration of 25 seconds was sufficient to record most (>98%) of the neutron counts obtainable from nitrogen-17.

RESULTS

Calibration. Neutron activities obtained, with and without cadmium screening, from 1-gram water samples of varying isotopic composition of oxygen and containing known amounts of lithium-6 are given in Table I where the more consistent results with nitrate and carbonate are separated from those with iodide. The difference between the two measured counts as given in Column VI of Table I was taken as the net delayed neutron count induced by thermal neutrons in the irradiated samples.

The value, normalized to unit atom per cent O^{18} (Column VIII), gave a mean value of 5858 counts per mg. of Li^6 per atom per cent O^{18} for samples irradiated at a power level of 1 Mw. (rel. std. dev. ±1.8%). The fact that this value is constant irrespective of what lithium compound was used proves that the neutron count obtained per mg. of Li^6 is directly proportional to the atom fraction of oxygen-18 over the entire range as given in Equation 3. The relative standard deviation of the results for samples prepared by adding solid lithium iodide to the water was about 4%, largely due to the hygroscopic nature of the salt; but results from samples prepared by mixing weighed solutions of lithium and water had a relative standard deviation of about 2%, the over-all relative standard deviation of the method.

Some results of analyses on water samples of known concentration of oxygen-18 are given in Table II. The individually calculated error of the determinations, reaffirm that the method has a relative standard deviation of about 2%, but the errors in replicate analyses tend to fall together rather than to give a random spread, thus showing that errors in sample preparation make up a large part of the over-all error.

Effect of Sample Size. To determine the extent of escape of tritons with diminishing sample dimensions, which would show up as a decreased neutron count, weighed portions from 1 to 1000 μl. of a single solution were irradiated and counted. The solution contained 25.1 mg. of lithium-6 per ml. in water enriched to about 15 atom per cent oxygen-18. The variation of the neutron count per unit volume with the sample size is shown in Figure 1. It was found that the neutron count per unit volume is independent of sample size down to less than half a drop, 10 μl., below which the activity falls rapidly with decreasing sample size.

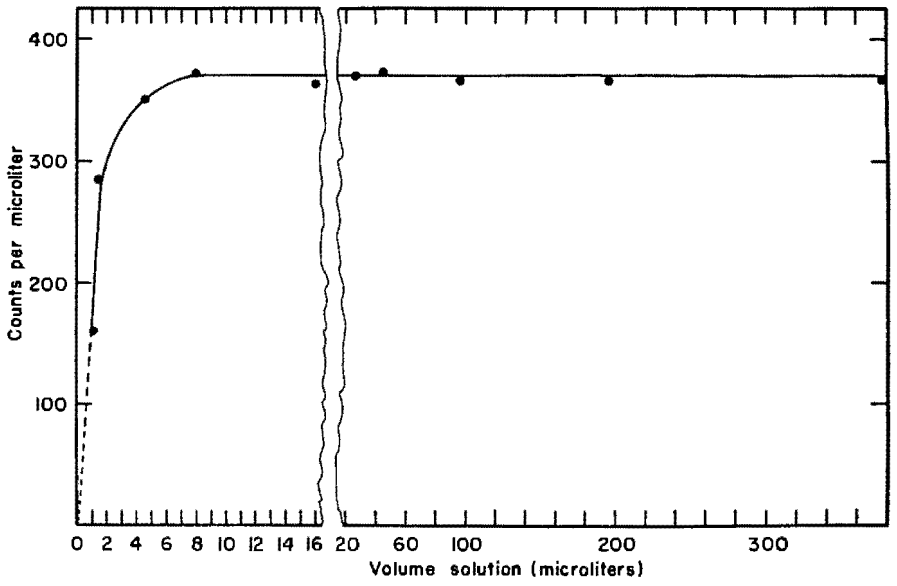

Figure 1. Variation of neutron counts with sample volume

The concentration of lithium-6 in the solution used for this test was much greater than for the main investigation. Such a high concentration was necessary to obtain sufficient counts from small solution volumes without resorting to repetitive irradiations and cumulative counting. The expected loss of neutron counts due to self-shielding of lithium-6 was observed for sample volumes exceeding 400 μl. (not shown in Figure 1) and increased to about 17% for a volume of 1000 μl.

The observed self-shielding in this series of experiments consists in practice of three effects; self-shielding by the solute during irradiation, attenuation of the tritons produced in the sample, and the absorption of the moderated neutrons of nitrogen-17 during counting. All three effects depend on the concentration of lithium-6 and the shape of the sample. When cadmium screens are used in the experiment, an apparent self-shielding effect of up to ~10% is observed as the result of absorption of thermalized neutrons in the counting assembly.

DISCUSSION

It has been verified that the delayed neutron count of nitrogen-17 in aqueous solutions of lithium-6 irradiated with thermal neutrons is proportional to the atom fraction of oxygen-18 in the water, provided the lithium-6 concentration is kept constant. This relationship, which has been derived in Equation 3, appears to be valid over the entire range of concentration of oxygen-18; furthermore, the count per milligram of lithium-6 does not seem to be affected by variations in the lithium-6 concentration (Column VIII, Table I).

Type of Neutron Flux. As the irradiations were carried out with a mixed neutron flux, the activities obtained in unscreened samples (Column IV, Table I) were higher than expected by reaction III alone. This difference is due to reactions I and II which proceed with fast neutrons, the contribution of which is eliminated by taking the difference between the neutron counts obtained from the bare and cadmium screened sample (Column VI, Table I). The values thus obtained give a measure of the nitrogen-17 formation by a pure thermal neutron flux whereas the values obtained from unscreened samples also include the contribution of the $O^{17}(n,p)$ and the $O^{18}(n,np)$ reactions as well as an additional contribution of reaction III induced by the epicadmium neu-

Table II. Comparative Analysis of Oxygen-18 in Water

Atom % O^{18}		
Known	Found	Error, %
61.11	62.94	+3.0
	62.27	+1.9
	61.97	+1.4
40.42	39.57	−2.1
	39.53	−2.2
	39.77	−1.6
15.17	15.26	+0.6
	14.87	−2.0
	14.82	−2.3
13.77	14.05	+2.0
	14.03	+1.9
	13.67	−0.7
4.843	4.836	−1.4
	4.854	+2.3
	4.855	+2.5
0.204	0.198	−2.9
(natural)	0.209	+2.5
	0.199	−2.5
	0.206	+1.0
	0.200	−2.0

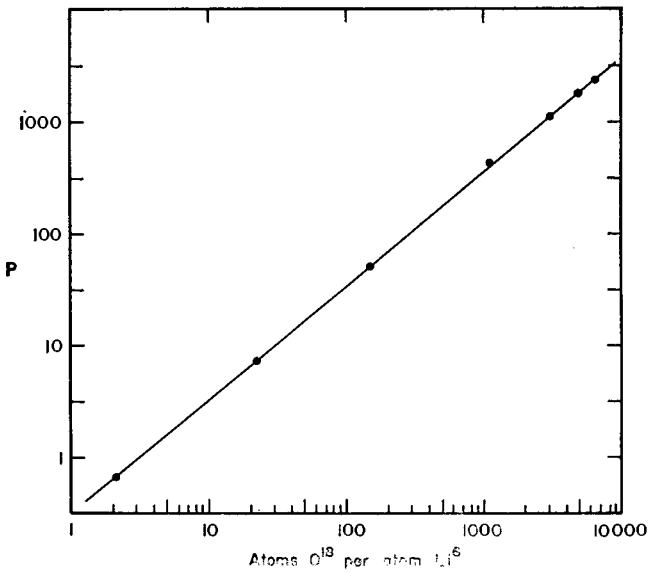

Figure 2. Variation of activity parameter, P (see text), with atom ratio of O^{18} to Li^6

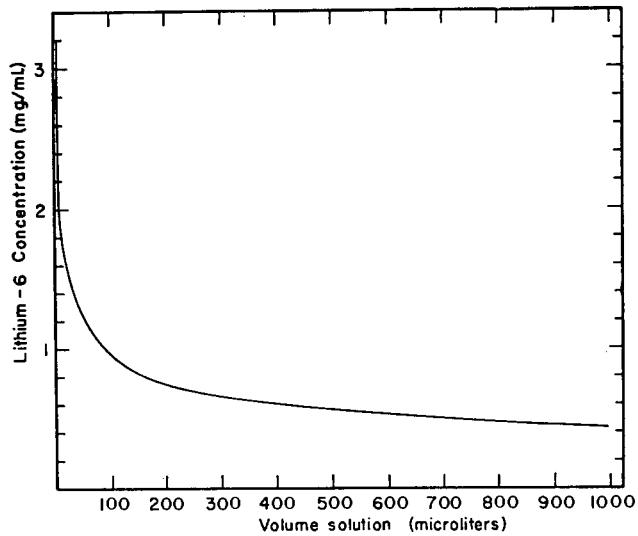

Figure 3. Variation of concentration of lithium-6 with volume, for spheres in which self-shielding effect amounts to 2%

rons. The ratio of these two values, (Column VII, Table I) gives the extent of interference by fast neutrons. For about 1 gram of oxygen-18 enriched samples containing about 0.2 to 0.5 mg. of lithium-6 the interference amounts to 2 to 4%, but with lower lithium-6 content the effect intensifies and may reach about 20%.

The formation of nitrogen-17 by reactions I and II depends on the content of heavy oxygen isotopes and hence on the sample size, while that by reaction III is independent of volume. For analysis, the use of smaller size water samples with the same lithium-6 content should reduce the extent of interference by fast neutrons corresponding to the decrease in the total amounts of oxygen-17 and -18 in the sample.

The relative contribution of fast neutrons to the formation of nitrogen-17 as indicated by the values in Column VII of Table I is representative of the ratio of slow to fast neutrons prevailing during the irradiation of the sample. A neutron flux with a different energy distribution should yield different results, but the contribution of the thermal neutrons as obtained by difference between counts of bare and screened samples (Column VI, Table I) is proportional to the atom fraction of oxygen-18 and is independent of the energy distribution of the reactor neutrons. Clearly, the use of a well thermalized neutron flux eliminates the need for cadmium screening and a double irradiation, since the count obtained from the unscreened sample is due only to reaction III.

Ratio of Oxygen-18 to Lithium-6. To obtain neutron counts that are neither too high and may be subject to coincidence losses nor too low and subject to relatively large statistical errors, the lithium-6 content of samples may be suitably adjusted. It then becomes necessary to establish that the results are not affected by differences in the oxygen-18 to lithium-6 ratio. This can be derived from Equation 3, which can be transformed into:

$$\frac{A_n}{[Li^6]^2} = \frac{K.f(O^{18})}{[Li^6]} = \frac{K}{[H_2O]} \cdot \frac{[O^{18}]}{[Li^6]} \quad (4)$$

where $f(O^{18}) = [O^{18}]/[H_2O]$ and where square brackets are used to denote the number of atoms O^{18} and molecules of water.

A plot of the ratio $[O^{18}]/[Li^6]$ against the parameter $P = A_n[H_2O]/[Li^6]^2$ should be linear. Such a test was carried out and the results, plotted in Figure 2, show that the relationship holds over a range of ratios from about 1 to 10^4 and hence that the nitrogen-17 yield per mg. of Li^6 per atom per cent O^{18} is independent of the relative composition of the nuclides that take part in the reaction. This extends the validity of Equation 3, beyond the range covered by Table I.

Effect of Sample Size and Self-shielding. The nitrogen-17 activity per unit volume solution induced by thermal neutrons is independent of sample size as is shown in Figure 1. This suggests that samples as small as a drop or even less can be used for analysis.

The increase in sample activity obtained by using higher concentration of lithium-6 will be partially counteracted by self shielding which will introduce an error in the analysis. This effect as calculated for spherical samples, and approximated to other geometrical shapes (*8*, *12*), is a function of three factors, which are the reaction cross section, the concentration, and a geometry factor of the form $4V/S$ where S is the surface area of the sample of Volume V. It follows that as the volume of a sample decreases the effect of self shielding diminishes and larger concentrations of lithium-6 become tolerable. Figure 3 shows the calculated variation of lithium-6 concentration with sample volume for spheres in which the self shielding effect is 2%—i.e., where the error introduced by ignoring the effect of self-shielding reaches the value of the standard deviation of the calibration samples. The attenuation of the tritons by lithium-6, which may be appreciable, is not taken into account.

Accuracy and Sensitivity. The accuracy and sensitivity of the determination of oxygen-18 can be derived from the statistical considerations of the delayed neutron count of the sample, provided the statistical error is the major error in the determination. The neutron emission of the sample, integrated from 5 seconds after the end of irradiation, irradiated to saturation at a thermal neutron flux of $10^{13}n/cm.^2$-second is 178,200 neutrons, per mg. of lithium-6 per atom per cent oxygen-18. This suggests that for example, a drop size sample of water (say, 33 μl.) of 1 atom per cent oxygen-18 containing 40 μg. of lithium-6 can be analyzed with a standard error of 4% in a single irradiation at $10^{13}n/cm.^2$-second when counted with an efficiency of 10%. For larger samples where the lithium-6 content can be increased the count increases correspondingly and the errors become smaller.

Repeating the measurement and accumulating the counts decreases the statistical fluctuations and thus in-

IA-784

0.17

No. 5a

ORIGINAL VERSION

ANALYTICAL ASPECTS OF DELAYED NEUTRON EMISSION

Preprint

by

S. AMIEL and M. PEISACH

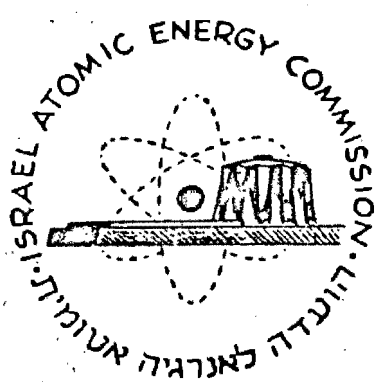

Israel Atomic Energy Commission

IA-784

ANALYTICAL ASPECTS OF DELAYED NEUTRON EMISSION

by

S. Amiel and M. Peisach

Israel Atomic Energy Commission
Soreq Research Establishment
October, 1962

ABSTRACT

A review of recent work in our laboratory on the use of delayed neutron emission for analysis. The use of this technique opens a new direction in activation analysis of great practical significance. The application of delayed neutron emission from fission is discussed in connection with the analysis of uranium, thorium and other fissionable nuclides and that from nitrogen-17 for the analysis of lithium, lithium-6 and oxygen-18. Other possibilities are mentioned as well.

CONTENTS

INTRODUCTION

The purpose of this article is to review recent work in our laboratory on the use of delayed neutron emission for analysis[1,2,3]. The use of this technique opens a new direction in activation analysis of great practical significance. The application of delayed neutron emission from fission will be discussed in connection with the analysis of uranium, thorium and other fissionable nuclides and that from nitrogen-17 for the analysis of lithium, lithium-6 and oxygen-18. Other possibilities will be mentioned as well.

Except for isotopes of the heavy elements, which emit neutrons when undergoing spontaneous fission, the number of radioactive nuclides known to emit neutrons in the course of their decay is very limited and their half-lives are short, ranging from a fraction of a second to some tens of seconds. These nuclides, known as delayed neutron precursors, originate from nuclear reactions leading to neutron-rich nuclides having a few neutrons more than a closed shell configuration. They decay by beta-ray emission to an excited state of the daughter from which de-excitation by neutron emission is energetically possible. Neutron emission from the excited daughter nucleus - the neutron emitter - is an instantaneous process, but its rate is determined by the decay of the precursor and has the same half-life. A schematic representation of the delayed neutron emission process is given in Figure 1

Most of the delayed neutron precursors are fission products; others have been observed in the products of high energy spallation of medium weight nuclei and in fast-neutron or triton-induced reactions on some light nuclei. Table I lists the properties of known delayed neutron precursors and their mode of formation.

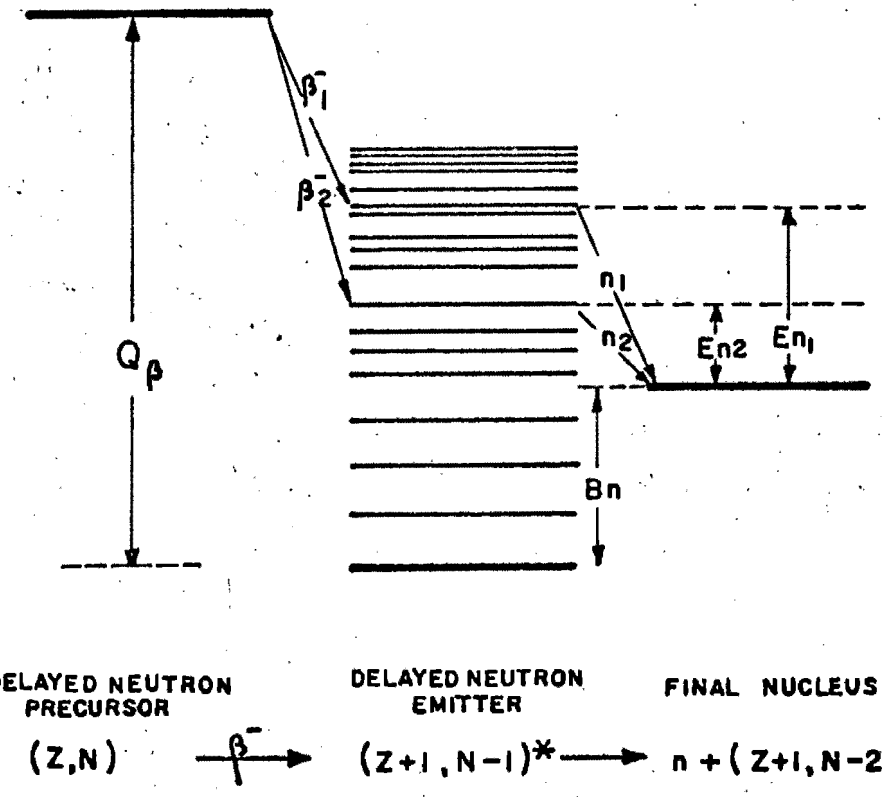

Fig. 1

Schematic Representation of Delayed Neutron Emission

Delayed neutron precursors can be detected against any β- or γ-ray background, because the neutrons can be counted without interference from other radiations. This is of great importance since a strong background is always present as a result of the radioactivation of other components of the sample. It make possible the application of delayed neutron counting as an analytical method in which either a target nuclide is assayed or the radiation leading to delayed neutron emission is measured. Delayed neutron precursors are quite rare, they have significantly different half-lives and their production can be made specific by appropriate choice of source material and irradiation conditions.

The usually available neutron sources which may serve for the production of delayed neutron precursors, are portable radioactive neutron sources, nuclear reactors and accelerators. Portable radioactive sources have a low neutron output which seldom exceeds 10^7 neutrons per second and thus are of little practical value. Nuclear reactors, which can provide fluxes of 10^{13} neutrons per cm^2 per second, or more, are very useful. Reactors can also be used as important triton sources for reactions with light nuclides by the use of intermediate reactions such as $Li^6(n,\alpha)t$. Accelerators provide many different kinds of radiations with a wide range of energies, but except for some low cost Van der Graaff and Cockcroft-Walton accelerators which are used as 14 MeV neutron generators with an output of 10^8 to 10^{10} neutrons per second, these machines are not generally available to the analyst. The major portion of this review deals with the observation of delayed neutron from reactor irradiation, although, in principle, any accelerator or source of neutron can be used.

DELAYED NEUTRON EMISSION FROM FISSION(1)

In Table I, the delayed neutrons emitted after fission have been divided into six groups whose half-lives range from a fraction of a second to just under one minute. There is a general similarity in the half-lives of the various groups from different fissioning nuclides. The groups themselves are probably mixtures of several unresolved activities as can be seen from the small discrepancies between the same groups from different fissioning sources but these differences are of no importance when the total neutron emission is measured for analytical purposes.

When delayed neutron emission is observed in a sample irradiated with either thermal or fast neutrons, the presence of a heavy nuclide, which undergoes fission, or of oxygen or nitrogen and Li^6 can be inferred, (see Table I). If Li^6 is present in the sample in conjunction with oxygen, or nitrogen (and most samples do contain oxygen, and some might contain nitrogen as well) delayed neutron emission is due to 4.1-second N^{17}. The same delayed neutron precursor results from fast neutron irradiation of oxygen in the absence of lithium. The presence of a fissionable nuclide is indicated unambiguously by delayed neutron emission with a longer half-life. If the sample is of natural origin and is irradiated with thermal neutrons, the delayed neutron emission arises from U^{235}. If the sample is not of natural origin, U^{233}, Pu^{239} or other transuranic nuclides which undergo fission with thermal neutrons might also be present. Natural heavy nuclides in which fission is induced by energetic neutrons from a reactor are Th^{232} and U^{238}. Many other nuclides should be taken into account when transuranic elements might be present as well.

The conventional methods for determining trace quantities of uranium in complex matrices are time-consuming and require elaborate chemical processing prior to measurement. The determinations are usually carried out by photometry, colorimetry, polarography, fluorimetry or radioactivity measure-

TABLE I

Delayed Neutron Emission: Nuclides, Properties, and Formation

(A) from Fission*

Group Index (i)	$T_{\frac{1}{2}}$ (sec)	Identified Precursors	Absolute Group Yield (%)									
			Thermal fission				Fast fission					
			U^{235}		Pu^{239}		U^{235}		U^{238}		Th^{232}	
			σ = 582 b		σ = 746 b							
1	52-56	Br^{87}(54s)	0.052	±0.005	0.021	±0.006	0.063	±0.005	0.054	±0.005	0.169	±0.012
2	21-23	Br^{88}(16s) I^{137}(24s)	0.346	±0.018	0.182	±0.023	0.351	±0.011	0.564	±0.025	0.744	±0.037
3	5-6	Br^{89}(4.4s) I^{138}(6.3s)	0.310	±0.036	0.129	±0.030	0.310	±0.028	0.667	±0.087	0.769	±0.108
4	~2	Br^{90}(1.6s) I^{139}(2s)	0.624	±0.026	0.199	±0.022	0.672	±0.023	1.599	±0.081	2.212	±0.110
5	~0.6		0.182	±0.015	0.052	±0.018	0.211	±0.015	0.927	±0.060	0.853	±0.073
6	~0.2		0.066	±0.008	0.027	±0.010	0.043	±0.005	0.309	±0.024	0.213	±0.031
No of delayed neutrons per fission			0.0158	±0.0005	0.0061	±0.0003	0.0165	±0.0005	0.0412	±0.0017	0.0496	±0.0020

(B) Not from Fission

Delayed Neutron Precursor	$T_{\frac{1}{2}}$ (Sec)	Target Nuclide	Reaction	Q (MeV)	Ref.	Remarks
Li^9	0.17	Li^7	t,p	-2.9		
		Be^9	n,p	-13.3		
C^{16}	0.74	C^{14}	t,p	-3.01	H	
N^{17}	4.14	N^{15}	t,p	-0.15		
		O^{17}	n,p	-7.93		
		O^{18}	n,d	-13.77		
		O^{18}	t,α	3.82		
Tl^{210}	~80					0.02% of decay by neutron emission
?	short	Cu	High energy protons	-	R	
?	8	Cu		-		
?	18	Cu		-		
?	6	Nd		-		Tentatively assigned to I^{138}(6.3s)
?	20	Nd		-		Tentatively assigned to I^{137}(24s)

Keepin, G.R., Wimett, T.F. and Ziegler, R.H. Phys. Rev. 107 1044 (1957)
H: Hinds, S., Middleton, R., Litherland, A.E. and Pullen, D.J. - Phys. Rev. Letters 6, 113 (1961)
R: Rudstam G., Svanheden, A., and Pappas, A.C. - Nature, 188, 1178 (1960).

ments. The experimental difficulties in these methods and the need to cope with large numbers of analyses for geological survey programs and the nuclear energy raw material industries emphasize the need for a faster, though reliable, and preferably non-destructive analytical procedure such as is provides by the method of delayed neutron counting.

When a sample containing N_f atoms of a fissionable nuclide of cross-section σ_f is irradiated in an effective flux of Φ neutrons per cm^2 per sec for t_b seconds, the number of fissions is given by $N_f \sigma_f t_b \Phi$. If a fraction a_i of these fissions lead to the production of the delayed neutron group i with decay constant λ_i, and an interval t_d elapses between the end of the irradiation and the start of counting, the number of delayed neutrons emitted over a period t_c is given by N_d, where :

$$N_d = N_f \sigma_f \Phi \frac{a_i}{\lambda_i} (1 - e^{-\lambda_i t_b}) e^{-\lambda_i t_d} (1 - e^{-\lambda_i t_c})$$

From this equation the optimum irradiation and measuring conditions for analysis can be deduced.

Since the half-life of delayed neutron activity is short, prolonged irradiation does not improve the accuracy of the analyses; it only increases the total radioactivity of the sample without contributing markedly to the delayed neutron emission. An irradiation of about 60 seconds produces saturation activity of the four short-lived groups, (Table I), about 85% of the saturation value for the 22-sec. group and half saturation of the longest lived group. When the yields of the groups are taken into account it is clear that irradiation for a longer period is unnecessary.

Some delay between the end of irradiation and the start of counting is inevitable because of the time required to transfer the sample from the irradiation position to the counting assembly. This delay period should be short, though too short a delay would require exacting specifications on the

timers controlling the delay period and fluctuations in the delay period could then introduce appreciable errors in the results. When the three short-lived groups are allowed to decay, the major component becomes the 22-second group which contributes about 80% of the counts. A delay of about 20 seconds is acceptable for the 22-second group and would effectively eliminate the contribution from all shorter lived groups. The 55-sec. group has a low abundance and small changes in the delay time will not introduce any errors from this source. The interference from N^{17}, which is produced by fast-neutron irradiation of oxygen (see Table I), is eliminated by the same delay period.

The duration of counting should be chosen as long as possible commensurate with the half-life of the group counted. The 22-sec. group, which is the major contributor to the measured counts, could be counted for about a minute which is long enough to record most of the neutrons emitted. Too long a counting period increases the contribution of background without adding appreciably to the net neutron count and thus actually reduces the accuracy of the measurement. An optimal counting period of 40 to 60 seconds appears to be most convenient.

These considerations lead a priori to the following conditions for the analyses: an irradiation lasting about 60 seconds, followed by a delay of about 20 seconds and counting for about 60 seconds.

The application of this method to the assay of uranium in natural samples, the determination of isotopic composition of uranium and the assay of thorium will be discussed. Other similar uses will be indicated.

The Analysis of Uranium[1]

Of the isotopes of natural uranium, U^{235} (which is the most important though the less abundant one) undergoes fission with thermal neutrons

with a high cross section (σ = 582b) whilst U^{238} requires fast neutrons with energies over 1 MeV and has a cross section smaller by about two orders of magnitude. For analysis of the total uranium content of natural isotopic composition, use of thermal neutrons is preferred since fast neutrons can cause fission in other nuclides as well. However, neutrons in reactors usually consist of thermal neutrons mixed with partially moderated fission-spectrum neutrons with sufficient energy to cause fission of U^{238}. Even under such conditions, fission of U^{235} is predominant and when uranium is the only fissionable element in the sample to be analyzed, the presence of fast neutrons in the reactor flux is not disadvantageous. If other fissionable elements as, for example, thorium, are present in relatively large amounts, fission by fast neutrons can introduce errors in analysis for uranium, and the use of thermal neutron screens and comparison with standards become necessary.

When irradiation and counting conditions are well defined, the delayed neutron emission in samples containing a known amount of natural uranium can be calculated from the values given in Table I. The experimental results are in good agreement with the calculated value. Under the conditions derived a priori for uranium analyses, 1µg natural uranium irradiated for 60 seconds at a flux of 10^{13} thermal neutrons per cm^2 per sec. gave, after a delay of 20 seconds, an emission of about 11700 neutrons during the 60-second counting period. A calibration curve obtained similarly for known uranium standards is given in Figure 2 and the delayed neutron count is directly proportional to the uranium content.

Some typical analysis are shown in Table II for samples selected to cover a large range of ore types. The values obtained by chemical analysis are given for comparison.

With a counting efficiency of 10% and a blank of 120 counts a sample containing about 10µg uranium can be analyzed with a precision of $\pm$1%.

TABLE II

Results of Uranium Assay of Several Different Samples

Sample	Concentration (in parts per million)	
	Present method*	Chemical processing and fluorimetry
1. 837 Granite	4.40 ± 0.05	4.2 ± 0.2
2. 643 Basalt	0.55 ± 0.05	0.9 ± 0.5
3. 694 Gneiss	1.98 ± 0.12	2.4 ± 0.2
4. 684 Schist	2.3 ± 0.2	2.6 ± 0.3
5. 665 Limestone	3.95 ± 0.10	4.0 ± 0.5
6. 777 Dolomite	2.92 ± 0.05	3.1 ± 0.2
7. 611 Marl	31.0 ± 0.3	33.7 ± 1.7
8. 664 Clay	3.8 ± 0.1	4.5 ± 0.5
9. 708 Sandstone	0.85 ± 0.02	0.9 ± 0.5
10. 613 Bituminous chalk	19.7 ± 0.7	23.3 ± 2.0
11. 644 Phosphate ore	153 ± 1.2	168 ± 8
12. 667 Manganese shale	37.3 ± 0.5	36.4 ± 1.6
13. Spring deposit	0.6 ± 0.2	1.3 ± 1.3

* The error recorded refers to the observed deviation from the mean.

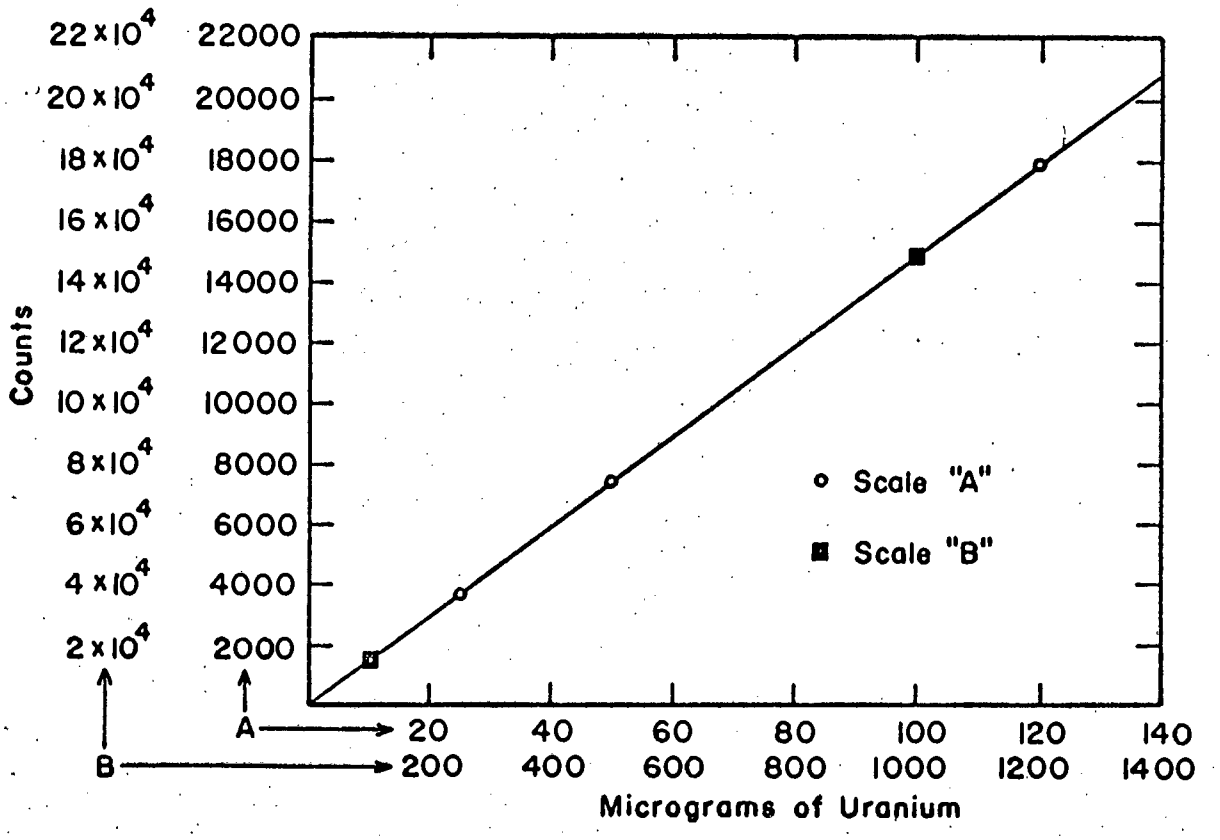

Fig. 2

Variation of delayed neutron count with uranium content.
Samples irradiated at 1.9×10^{12} neutrons/cm^2 - sec.

Because the total uranium content is assayed rather than its concentration, this precision can be attained for a concentration of 1 p.p.m. with a 10-g. sample and correspondingly larger weight of even lower concentrations. The maximum weight of sample to be analyzed is limited only by the load that can be carried by the pneumatic tube system of the reactor, in which the irradiations are carried out.

Improved precision for lower uranium contents is obtainable by repeating the irradiation and summing the neutron counts obtained. Thus a precision of ±1% would require 4 irradiations for a sample containing 4μg U, but as each analysis takes only a little over 2 minutes, the need to repeat an analysis is not a serious disadvantage. Another important advantage is that the analysis is non-destructive and if the samples are weighed out into suitable containers, analyzed samples may be stored for reference or returned unopened.

Attenuation of neutrons within the sample under irradiation or in the counting assembly might interfere with the analysis. This is serious only when relatively large weights of materials with high neutron absorption cross-sections are present. Such concentrations do not usually occur within the samples, but when cadmium screens are used in the irradiation, the presence of large amounts of cadmium can decrease the delayed neutron count by absorption of the delayed neutrons which have been moderated in the paraffin block. The extent of this effect was obtained by measuring the apparent cadmium ratio for pure thorium for which the ratio should be unity; values of 1.08 were obtained, indicating that the cadmium causes an 8% decrease in the delayed neutron count.

The Isotopic Analysis of Uranium[4]

For the isotopic analysis of uranium, the analysis must be carried out on a sample free from other nuclides which undergo fission with thermal

neutrons. In such a sample, fission induced by thermal neutrons can be due only to U^{235} and counting the delayed neutrons gives a measure of the content of this isotope, irrespective of the uranium-238 content or the presence of other elements. The isotopic ratio of U^{235} to U^{238} can then be derived if the total uranium content is known.

When a mixed neutron flux is used for the analysis, delayed neutrons are emitted from both U^{235} and U^{238}, but as the role of the lighter isotope is predominant, this value can serve as a measure of the uranium-235 content. The value obtained for the same sample re-irradiated in a flux from which the thermal neutrons have been removed by a cadmium screen, enables the uranium-238 content to be deduced, since much of the contribution from the fission of uranium-235 is eliminated. The use of standards of varying isotopic composition is, however, necessary as the contribution of uranium-235 to the delayed neutron counts, measured in a sample irradiated with epithermal neutrons, is still of the same order of magnitude as that of the same amount of uranium-238. The extent of the interference of uranium-235 by fast neutron fission in the analysis for uranium-238 in a pure uranium sample depends only on the energy spectrum of the irradiation neutron flux. Thus a double irradiation of the uranium sample with and without a cadmium screen enables the determination of both U^{235} and U^{238} to be made irrespective of the presence of foreign non-fissionable materials.

A typical calibration curve for uranium-235 content in U_3O_8 obtained with thermal neutrons is given in Figure 3. The delayed neutron emission is directly proportional to the U^{235} content. Deviations from proportionality will be observed at high concentrations due to self shielding; at high count rates coincidence counting losses will introduce negative errors. To overcome both these effects smaller samples or lower neutron fluxes should be used because the precise calculation of these errors is usually difficult and an approximate calculation could affect the precision of the result.

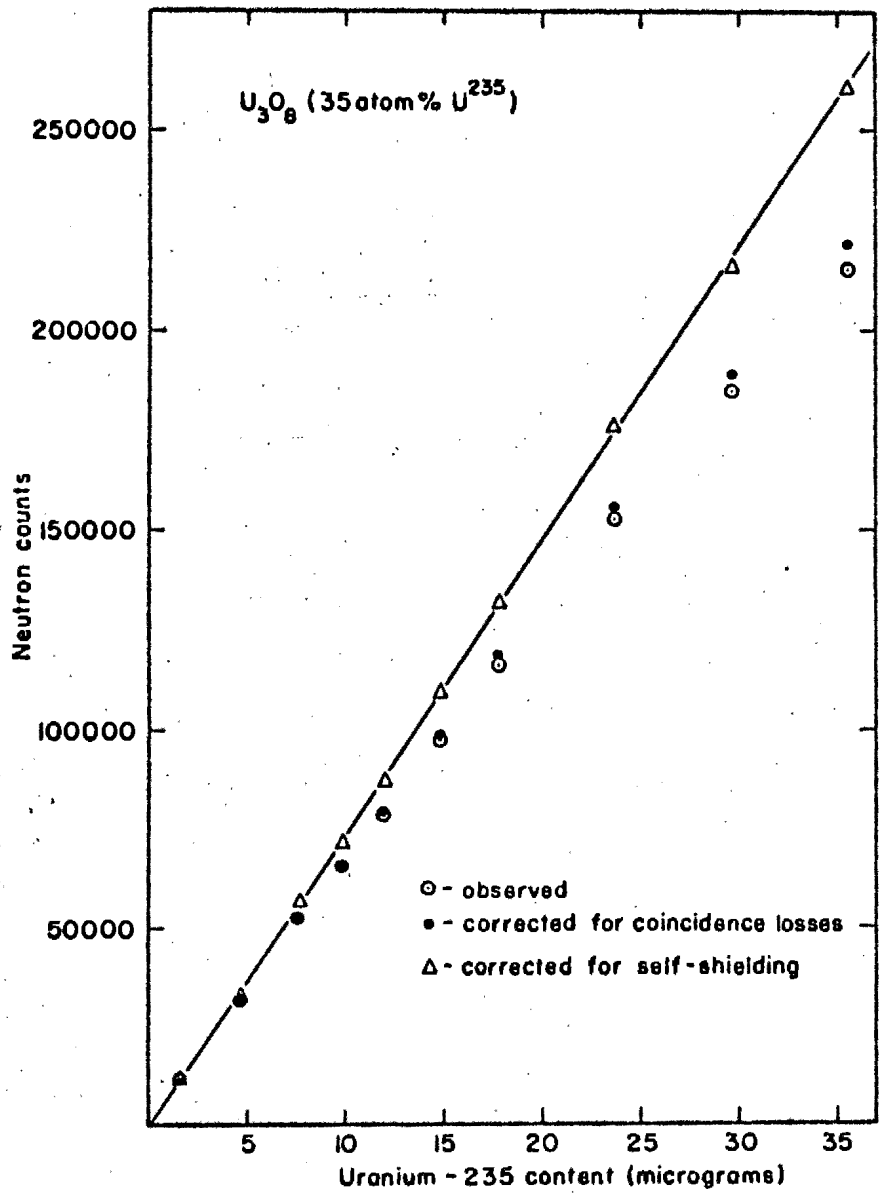

Fig. 3

Variation of delayed neutron count with uranium-235 content showing the corrections of coincidence loss and self-shielding for high U^{235} content. Samples were counted after a delay of 8 seconds and counts were normalized to a flux of 4.2×10^{11} neutrons/cm^2-sec. (0.1 M.W.)

Assay of U^{235} with a mixed neutron flux is presented in Figure 4. The U^{238} contribution to the delayed neutron count accounts for the rapid apparent increase in the count per unit weight U^{235} but this effect is eliminated when the result is corrected for the amount of U^{238} present in the sample. It is seen that corrections are not necessary for samples in which U^{235} exceeds 5 atom %. At lower enrichments, it is necessary to assay U^{238} content as well. The determination of both U^{235} and U^{238} in a mixed flux with and without cadmium screen is shown in Table III, where corrections due to the mutual interference of the uranium isotopes as well as self shielding are listed.

A precision of better than 0.5% is obtainable for the isotopic analysis of uranium. The principal sources of error are fluctuation of the reactor flux and errors due to self-shielding. The former may be eliminated by calibration of the reactor fluctuations by repeated measurements with a standard unopened sample, whilst the latter may be corrected for by calibration or by repeating the measurement on a smaller sample.

The Analysis of Thorium[1]

Thorium resembles U^{238} in undergoing fission with fast neutrons above a threshold of about 1 MeV but has a somewhat lower cross section. Since thorium has a lower fission rate and a lower delayed neutron emission than uranium-238 under identical irradiation conditions, the sensitivity for thorium analysis is lower than for uranium. As the sensitivity depends on the abundance of fast neutrons, thorium analysis requires the use of more intense neutron fluxes of fast neutrons and relatively larger samples than for uranium analysis. Some analytical results of analyses of pure thorium samples and of standards containing a known concentration of uranium are given in Table IV.

A major hindrance in the assay of thorium is that thorium ores

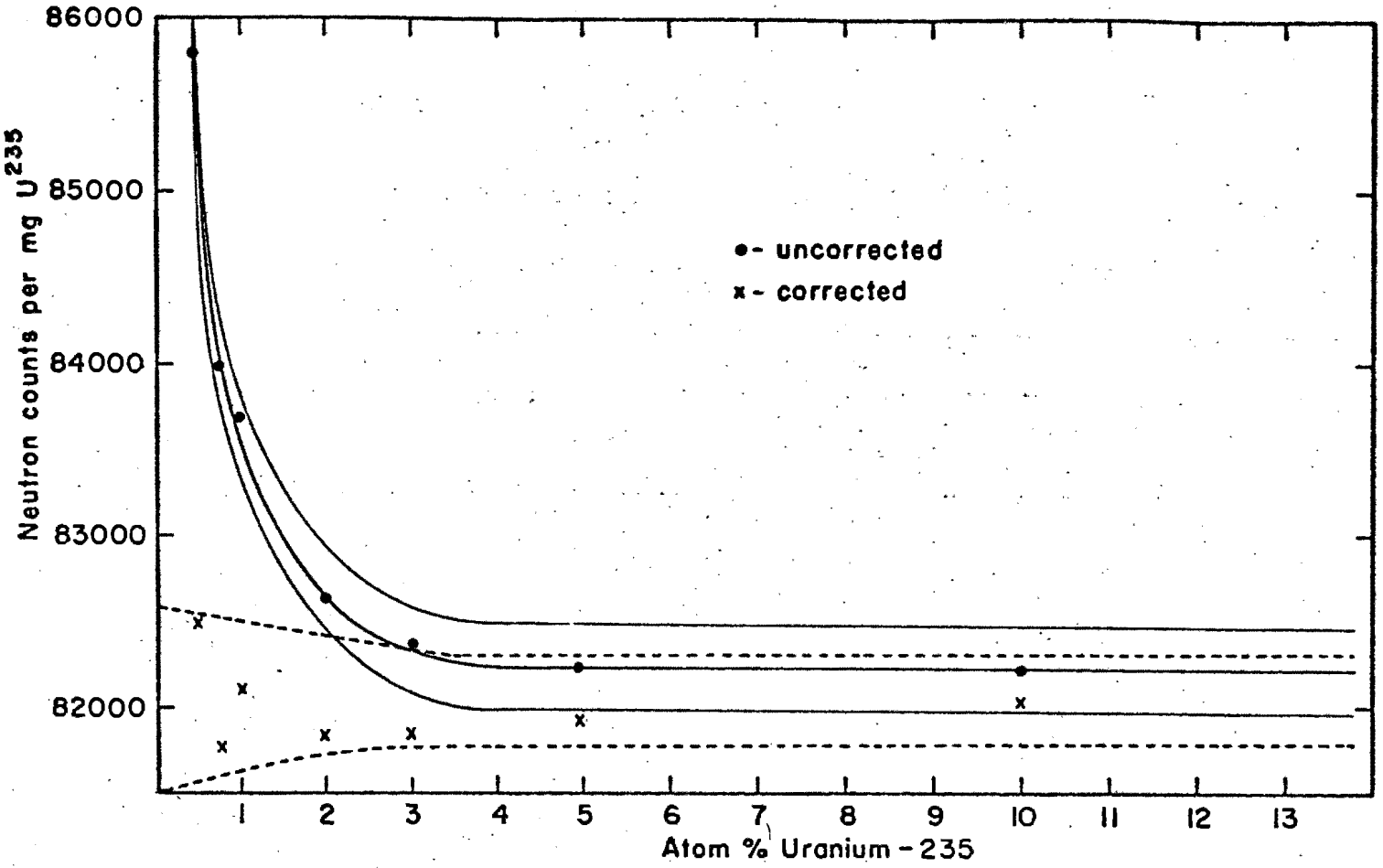

Fig. 4

Assay of U^{235} showing the contribution of U^{238}. Uncorrected values refer to gross counts observed, corrected values were obtained by deducting the contribution of U^{238}. The solid lines on either side of the curve show the range within one standard deviation ($\pm\sigma$) for the observed results. The dotted lines refer to the similar range for the corrected values. These two ranges approach each other and become identical at 100 atom % U^{235}. Irradiations were carried out at 7.5×10^9 neutrons/cm^2-sec.

TABLE III

Analysis of Isotopic Composition of Uranium

Irradiations were carried out at a power level of 2kw. (7.5×10^9 n/cm^2-sec.)

NBS Isotopic standards Sample No.	Atom % U^{235}	Sample weight (mg)	U^{235} content (mg)	Measured counts	Counts per mg U^{235}		U^{238} contribution	Net U^{235} counts per (mg)
					measured	corrected for self-shielding		
U - 005	0.483	207.45	0.85	72,740	85607	85798	3296	82502
U - 010	0.991	198.75	1.67	138,806	83107	83688	1599	82089
U - 020	2.01	156.50	2.67	218,408	81887	82625	780	81845
U - 030	3.01	79.95	2.04	166,909	81794	82364	516	81848
U - 050	4.95	45.00	1.89	154,402	81746	82235	314	81921
U - 100	10.07	23.40	2.00	163,123	81647	82217	143	82074
950	0.72 (natural)	224,00	1.37	114,440	83728	83977	2206	81771

Mean: 82007 ± 249

Std. deviation: 0.3%

TABLE IV

Determination of Thorium and Uranium in Mixtures of The Two

Samples 101, 102, 103, 104 are used as standards for the calculation of the Th-U mixtures. Irradiations were carried out at a flux of 3.75×10^{11} n/cm^2-sec.

Sample No.	Content (in mg)		Experimental count	Calculated count			Th+U Calculated/ Experimental
	Thorium	Uranium		Th	U	Th+U	
a) with cadmium cover							
101	-	2.10	2786	-	-	-	-
102	-	2.10	2755	-	-	-	-
103	2.01	-	604	-	-	-	-
104	2.02	-	584	-	-	-	-
105	5.96	2.07	4,150	1,565	2,720	4,285	1.03
106	10.25	2.00	5,587	2,990	2,630	5,620	1.01
107	20.60	2.02	9,150	6,070	2,660	8,730	0.96
108	40.25	2.04	14,424	11,880	2,690	14,570	1.01
109	67.50	2.06	20,590	17,750	2,710	20,460	0.99
110	108.0	2.12	32,985	30,750	2,790	33,540	1.02
111	201.5	2.08	64,167	59,400	2,740	62,140	0.97
b) without cadmium cover							
101	-	2.10	61,000	-	-	-	-
102	-	2.10	61,800	-	-	-	-
103	2.01	-	600	-	-	-	-
104	2.02	-	665	-	-	-	-
105	5.96	2.07	61,670	1,740	60,400	62,140	1.02
106	10.25	2.00	62,540	3,325	58,250	61,575	0.99
107	20.60	2.02	66,824	6,750	59,000	65,750	0.98
108	40.25	2.04	73,043	13,200	59,500	72,700	0.98
109	67.50	2.06	80,843	19,700	60,000	79,700	0.99
110	108.0	2.12	93,173	34,150	61,600	95,750	1.03
111	201.5	2.08	124,113	66,000	60,700	126,700	1.02

usually contain uranium, and hence the contribution from fast neutron fission of uranium has to be determined in order to correct for the thorium content. These analyses require the removal of thermal neutrons, by screens of cadmium or similar material, from the irradiation flux. The interference by uranium is corrected for by determining the content of uranium-235 as described above and, assuming the sample to be of natural isotopic composition, the corresponding contributions from the epithermal neutron fission of both uranium isotopes can be deduced. Table IV gives a comparison between calculated and experimental values for known mixtures of uranium and thorium. It can be deduced from the table that amounts of about 1mg. thorium can be determined with a precision of about 2%. The detection limit under the present conditions appears to be about 10µg. or about 1p.p.m. for a 10-g. sample, at which concentration the summed counts for three irradiations lead to a precision of about 15%.

Determination of U^{233} and Pu^{239} in Thorium and Uranium Breeding.

Determination of the Pu^{239} and U^{233} produced by breeding from their parent elements is usually done by remotely controlled radiochemical techniques. U^{233} and Pu^{239} have similar fission properties to U^{235} while thorium resembles U^{238}. The assay of Pu^{239} produced in U^{238} or natural uranium fuel elements, or U^{233} in thorium blankets, is again therefore analogous to the uranium-thorium determination. The adaptation of the delayed neutron emission technique for process control might have great advantages, since the need for chemical processing prior to assay is avoided or minimized considerably. A further in-line control could also be developed along the lines of the present method, using portable neutron sources.

Prospecting for Uranium and Thorium

By introducing a neutron source into a bore hole, fission will be

caused in the uranium and thorium present in the irradiated volume, resulting in delayed neutron emission.

The presence of delayed neutron activity of half-life longer than about 4 seconds would establish the presence of uranium and thorium and give us an indication of the concentration.

DELAYED NEUTRON EMISSION FROM NITROGEN-17

The characteristics of the delayed neutron precursor, nitrogen-17, are given in Table I. It can be produced by fast neutron irradiation of oxygen-17, by the reaction $O^{17}(n,p)N^{17}$ for which the threshold is about 9.5 MeV and oxygen-18 by the reaction $O^{18}(n,d)N^{17}$ for which the threshold is about 15.5 MeV[5]. Because of the low abundance of the heavy oxygen isotopes in nature and the relatively small reaction cross section for fission spectrum neutrons, 7.5 μb[6], the amount of nitrogen-17 which can be produced from natural oxygen is small and the application of delayed neutron counting for its analysis is possible only with high fluxes of fast neutrons; an integrated yield of only about 80 delayed neutrons is expected per mg. natural oxygen irradiated to saturation at a flux of 10^{13} n/cm^2-sec. However, if lithium-6 is present together with oxygen, the production of N^{17} from the reaction $O^{18}(t,\alpha)N^{17}$, induced by 2.7 MeV tritons emitted from the reaction $Li^6(n,\alpha)t$, becomes predominating. The very high cross section of the reaction $Li^6(n,\alpha)t$ with thermal neutrons [σ = 960b) leads to a high yield of N^{17} and makes it possible to use its delayed neutron emission for analysis. When nitrogen is present together with lithium-6, nitrogen-17 can also be produced by the reaction $N^{15}(t,p)N^{17}$, but the cross section for this reaction is somewhat lower than for $O^{18}(t,\alpha)N^{17}$.

The extent of production of nitrogen-17 depends on the degree of intimacy of mixing of lithium-6 with the oxygen-, or nitrogen-containing

medium, because of the short range of the tritons produced in the primary reaction. A solution is the most suitable form because conditions of maximum intimacy and homogeneity are met and when dilute, corrections due to self shielding and attenuation of tritons are avoided.

It has been shown[3] that the rate of production of N^{17} in dilute Li^6 solutions irradiated with thermal neutrons is proportional to the total lithium content of the sample and to the concentration of oxygen-18. It follows that the neutron emission from nitrogen-17 can be used to determine the lithium-6 content of a solution if the atom fraction of oxygen-18 of the sample is known, or if the lithium-6 content is known, the atom fraction of oxygen-18 can be determined. The same applies, by analogy, to nitrogen-15. The analysis of Li^6, O^{18} or N^{15} by this technique need not be limited to solutions since any other intimate mixtures of Li^6 - O^{18} or Li^6 - N^{15} will yield N^{17} when irradiated with neutrons. The production parameters for solid mixtures, colloidal systems or compounds should be determined specifically for each case since they depend on the physical properties of the sample.

Irradiation of 25 seconds builds up N^{17} virtually to its saturation level and counting its activity over an equal period is sufficient to record > 98% of its decay. The delay period between the end of irradiation and the start of counting should be as short as possible, provided a precisely reproducible delay is attainable.

The Analysis of Lithium[2]

Since the production of nitrogen-17, in a thermal neutron flux is a specific property of the Li^6 isotope, the determination of total lithium can be carried out only on samples known to be of natural isotopic composition or in which the isotopic composition is known.

When irradiation is carried out with a mixed reactor flux, reactions

leading to the direct production of nitrogen-17 from the oxygen in the sample will interfere with the analysis and the count obtained from this source must be deducted as part of the background effect. This can be done by repeating the analysis with cadmium screens which absorb the thermal neutrons and the difference between the results obtained from unscreened and screened irradiation thus represents the net effect of the $O^{18}(t,\alpha)$ reaction.

A calibration curve of delayed neutron counts from N^{17} obtained for lithium in solution in natural water is shown in Figure 5. At higher concentrations of lithium, deviation from linearity due to self shielding is observed. Approximate correction factors for self-shielding may be calculated. Experimentally, corrections may be made by repeating the measurement with a smaller sample.

Neutron absorption by other sample components depends on the amount of the absorber and its effective cross-section. This effect is shown in Figure 6. The extent of neutron absorption due to ions commonly present in samples containing lithium, as compared to a highly neutron-absorbing impurity such as boron, is shown in Figure 7.

Attention should always be paid to possible interference, from delayed neutron emission due to fission, in the analysis of lithium. Interference from this source can be detected by following the decay of the neutron emission. A half-life appreciably longer than 4.1 seconds is indicative of the presence of fissionable material. The amount of fissionable material can then be determined following the procedure for the analysis of uranium outlined above, and the extent of interference by this amount of uranium in the lithium analysis can be obtained by the comparison with a uranium standard irradiated and measured under the same conditions as the lithium sample.

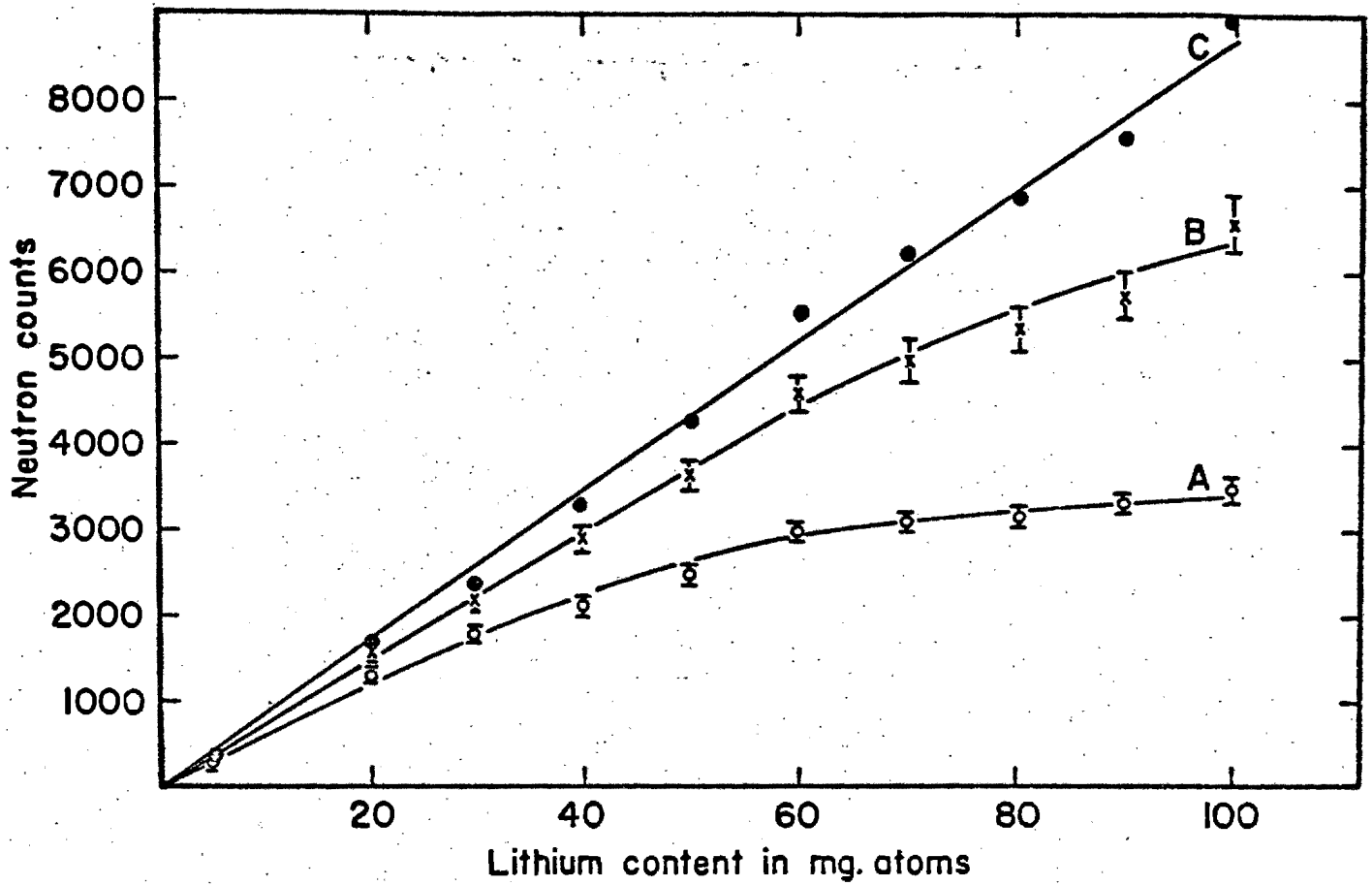

Fig. 5. Variations of neutron counts from N^{17} with lithium content, for LiCl solutions in natural water.

A. Observed values
B. Corrected for Chlorine attenuation
C. Further corrected for self-shielding.

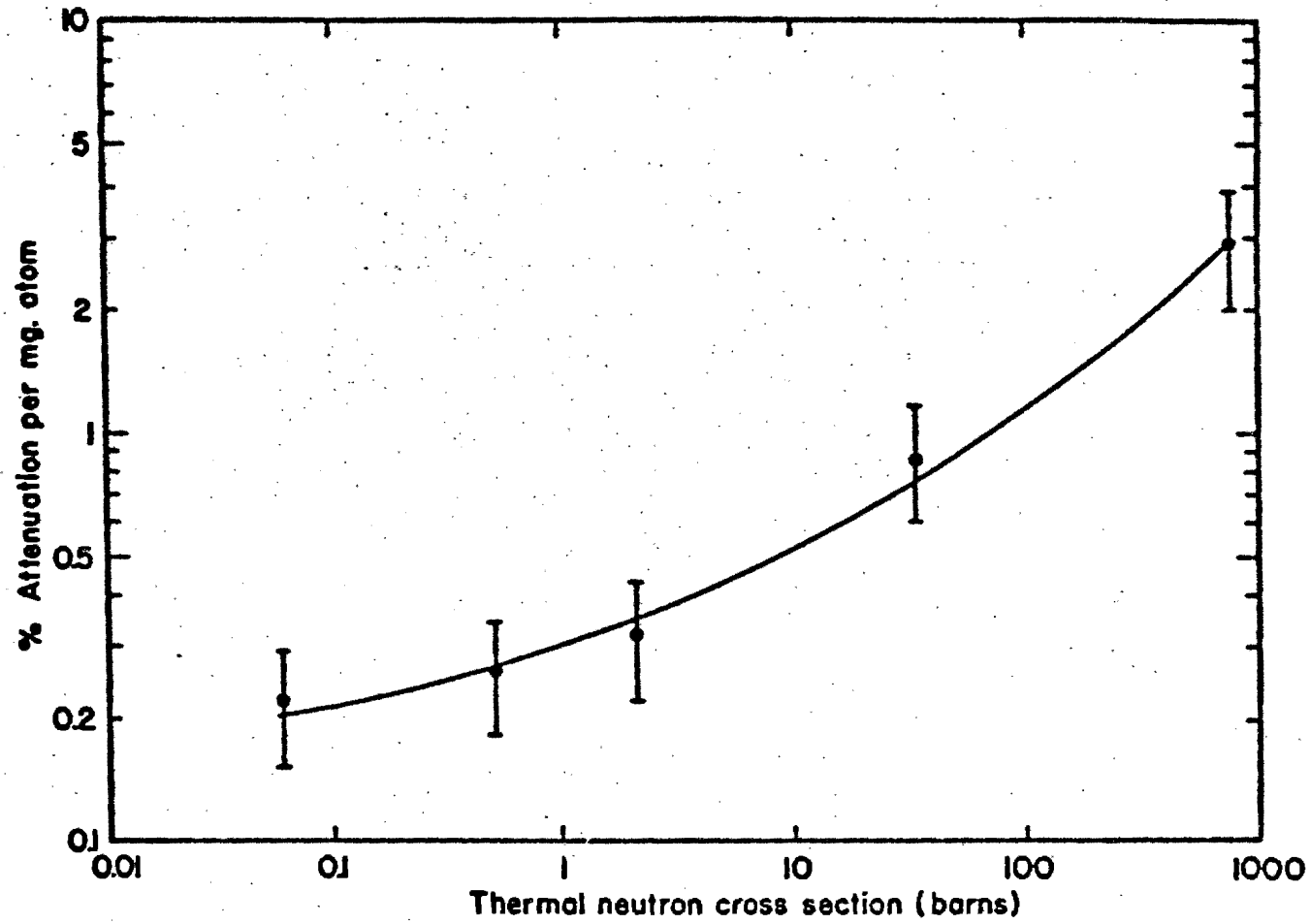

Fig. 6

The effect of cross-section of sample components on the attenuation of neutron activity.

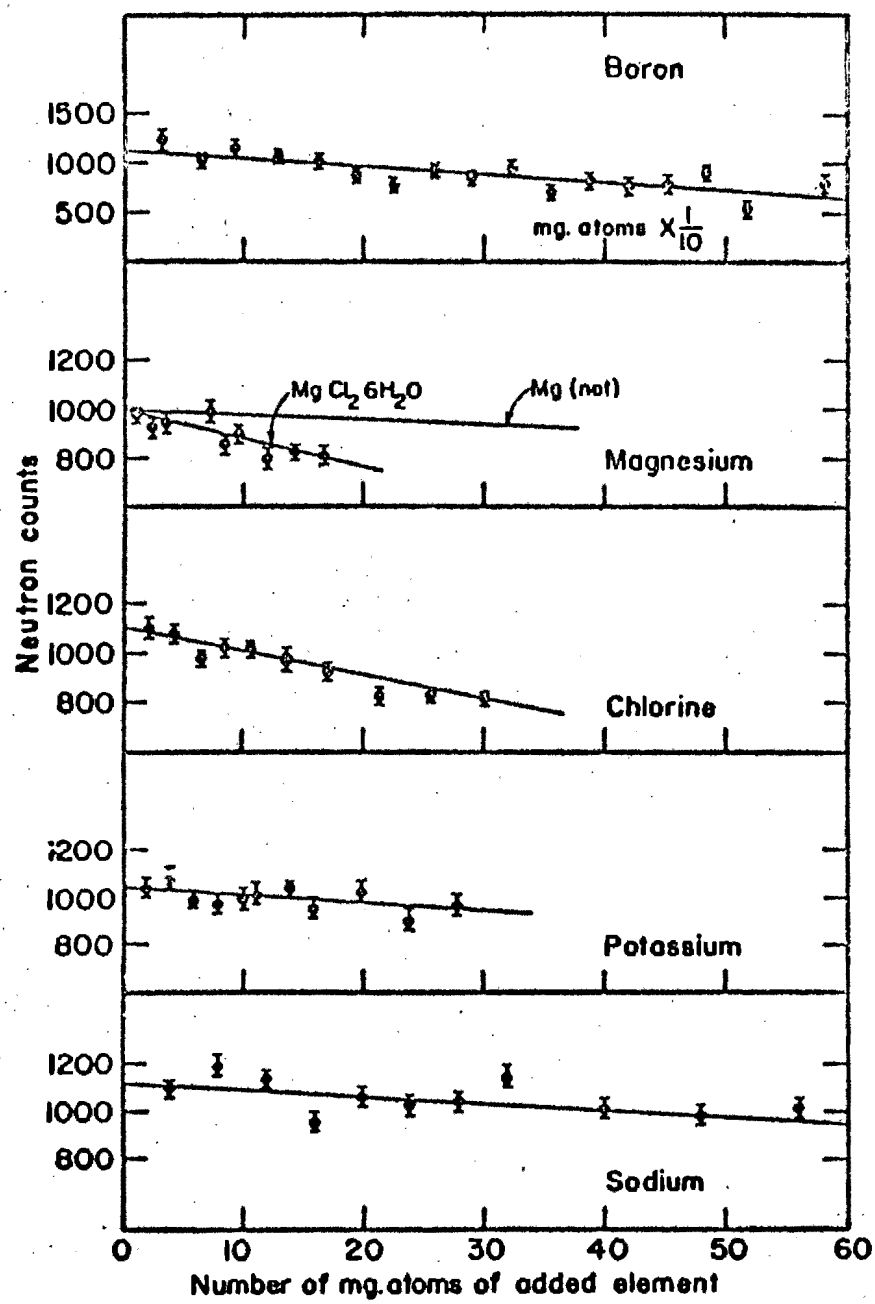

Fig. 7

The extent of neutron absorption by common ions present in lithium samples. Boron, for comparison, shows the effect of an element with a high absorption cross section.

The Isotopic Analysis of Lithium[2]

The usual method for the isotopic analysis of lithium is by mass spectrometry[7], which is laborious and time-consuming. Other methods, by activation analysis, require the measurement of tritium[8] from the primary reaction $Li^6(n,\alpha)H^3$, or of fluorine-18[9] produced by the secondary reaction $O^{16}(t,n)F^{18}$ induced by the tritons from lithium-6. The precision of both these procedures is affected by the efficiency of recovery of the product and is decreased by the inevitable presence of background radiations from impurities. Both these disadvantages are virtually eliminated by the method of delayed neutron counting.

The determination of lithium as described in the previous section is essentially a determination of Li^6. With samples in which the total lithium content is known, analysis by counting delayed neutrons from nitrogen-17 gives the isotopic composition. Figure 8 is a calibration curve obtained for a series of enriched samples, analyzed by mass-spectrometry, containing a fixed total weight of lithium dissolved in natural water. The neutron count is proportional to the atom fraction of lithium-6 over the entire range. For Li^6-depleted samples, the low count obtained with natural water can be overcome either by using water enriched with oxygen-18 as described in the next section, or by using larger samples of more concentrated solutions. Larger volumes of dilute solutions might lead to an increase in counts obtained from the heavy oxygen isotopes if fast neutrons are present in the irradiation flux. This effect may be measured as stated above by the use of cadmium screens in a subsequent irradiation.

Analysis of Oxygen-18[3]

The importance of oxygen-18 as a stable tracer for oxygen has created the need for suitable rapid analytical methods. The method of delayed neutron counting enables an analysis to be carried out within one

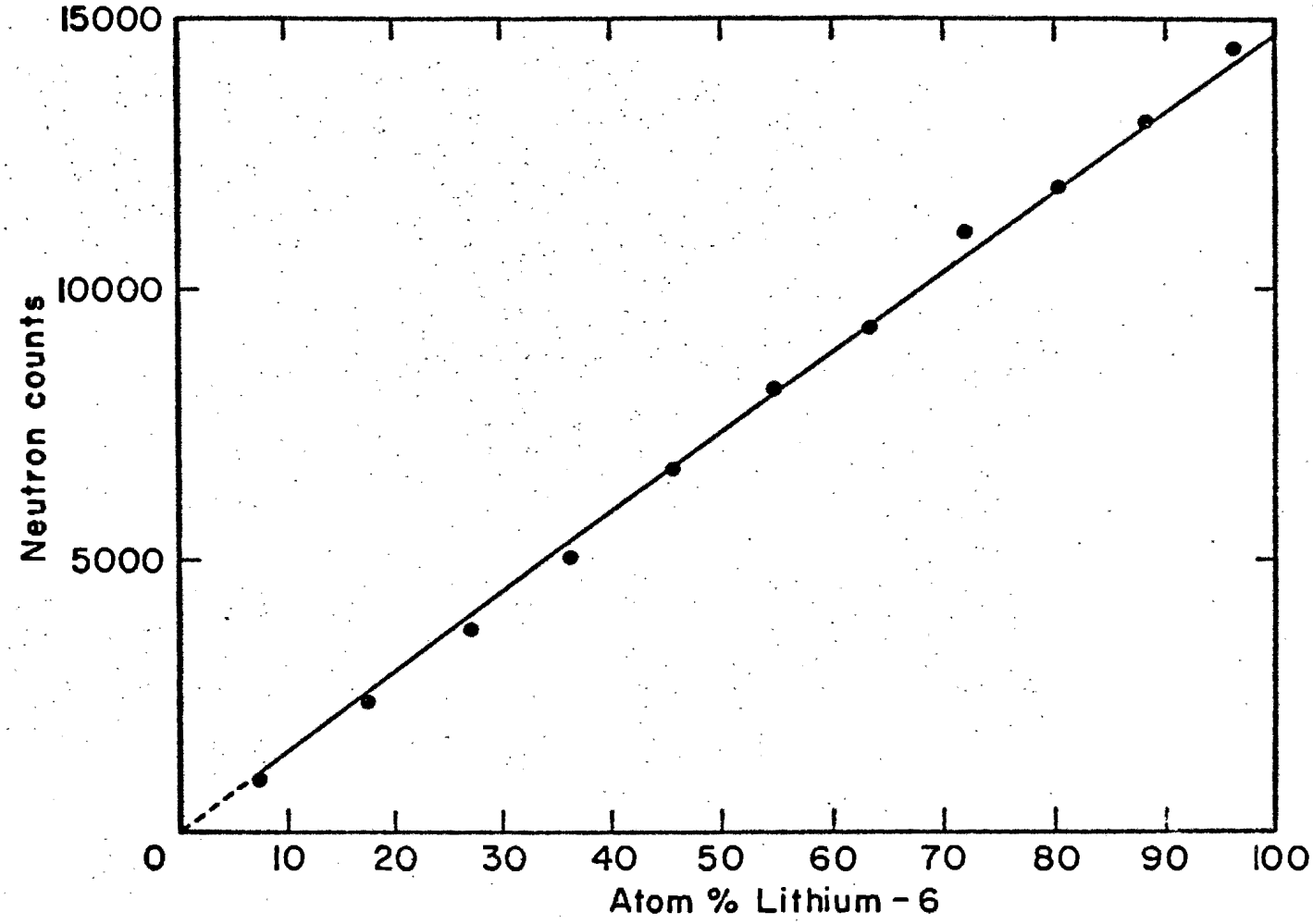

Fig. 8

The variation of neutron counts with isotopic composition of lithium for samples containing a fixed total amount of lithium.

minute without destroying the sample. It follows from the proceeding case, (of Li^6) that the delayed neutron count is directly proportional to the atom per cent of O^{18}, provided that the lithium content is fixed and that the irradiation conditions are kept constant. Figure 9 shows that the neutron count obtained is directly proportional to the atom percent of oxygen-18 over the entire range of O^{18} concentration. The proportionality is retained independent of sample size, as shown in Figure 10 where the neutron count per unit volume of solution is shown to be independent of the volume measured, down to less than 10µl. This indicates that analysis could be carried out even on a single drop of solution. It was shown[3] that the ratio of oxygen-18 to lithium-6 atoms does not affect the proportionality between the neutron counts per unit weight of Li^6 and the O^{18} concentration over a range of ratios from about 1 to 10^4. This enables a selection of suitable Li^6 content to be made to give a neutron count in a predetermined range and thus to reduce statistical errors in counting, provided lithium-6 content is kept below a level where errors from self-shielding become important.

The error of the analysis consists of errors of sample preparation and inaccuracies in the standards. Reactor fluctuations are also an important source of error which together with the counting statistics limit the precision of the method.

Although the usual method of determining oxygen-18 is by mass spectrometry the advantage of delayed neutron counting is that the analysis is rapid and non-destructive and that it does not require elaborate equipment and vacuum apparatus to be built at the irradiation site. The method is best suited for cases where rapid results are required without the high accuracy of mass spectroscopic analysis.

The reaction $O^{18}(t,\alpha)N^{17}$ may find important application for the determination of total oxygen. Intimate mixtures of the sample and lithium-6 can be made with fine particles in an inert gas atmosphere, or by fusing them

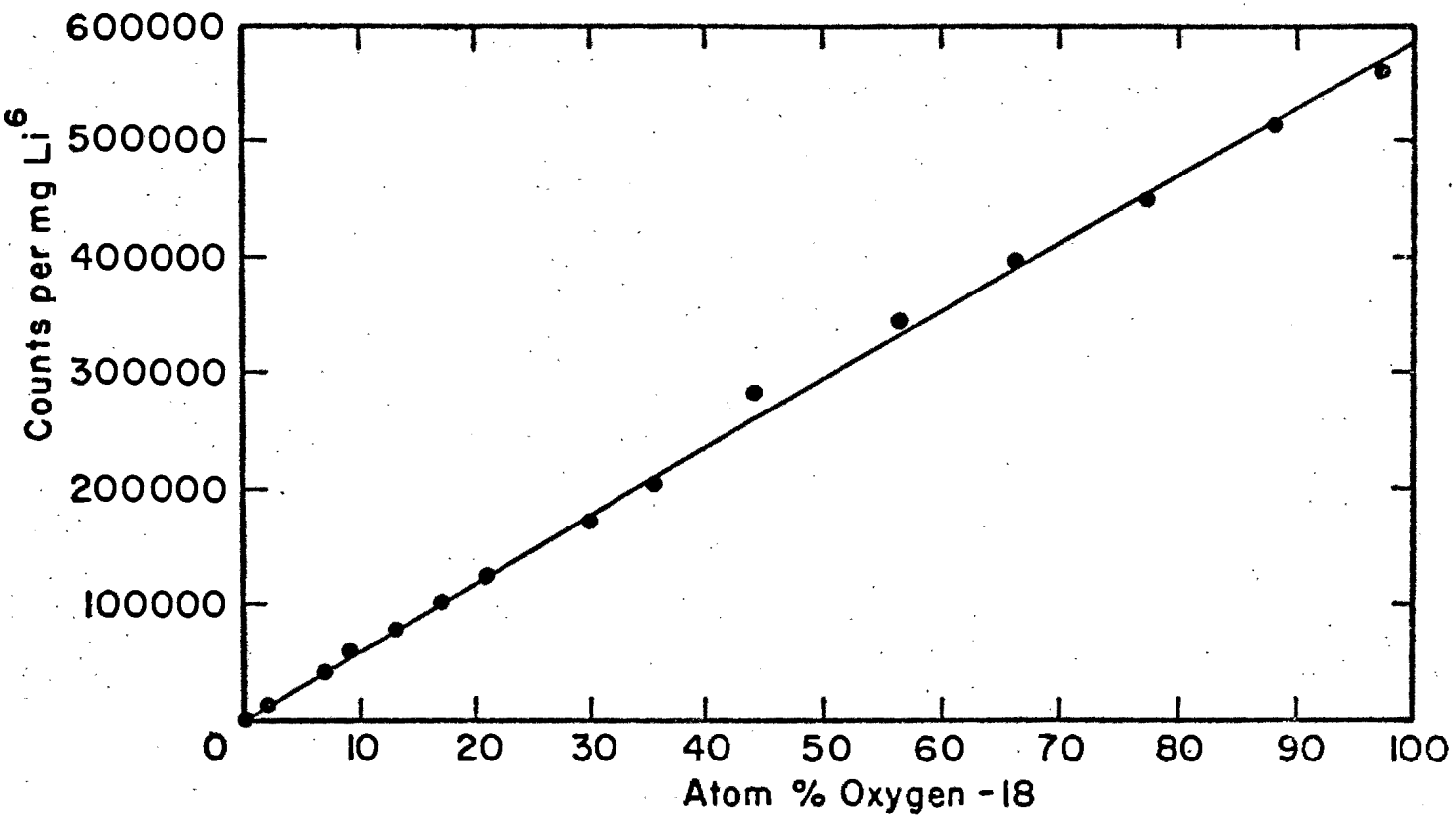

Fig. 9

The variation of neutron count per mg. lithium-6 with isotopic composition of oxygen.

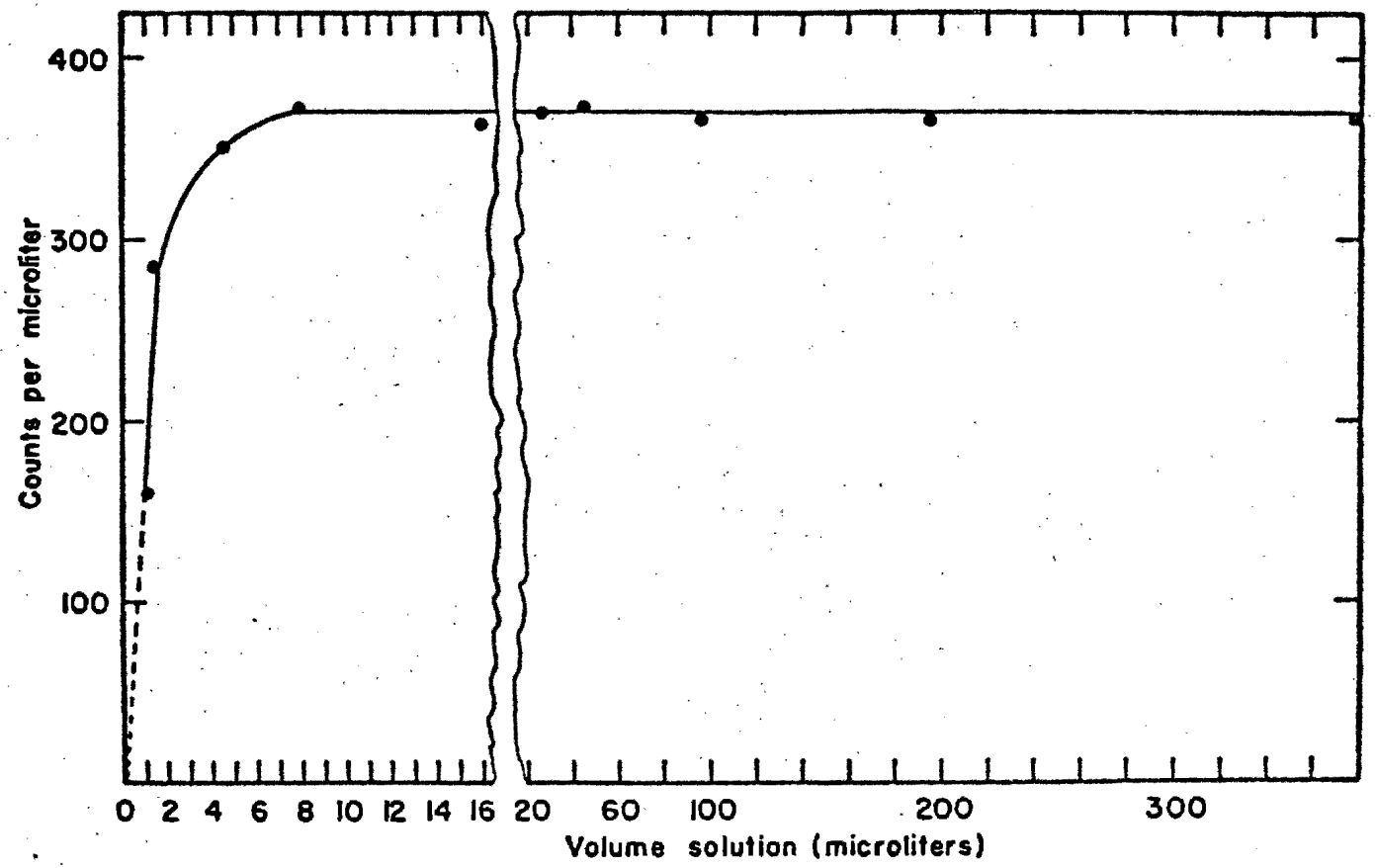

Fig. 10

The effect of sample volume on the N^{17} neutron counts obtained from Li^{6} - O^{18} solutions.

together or by dissolution in an inert medium. The measurement can be made in a way analogous to the analysis for oxygen-18 and it is clear that the total oxygen content can be derived if the isotopic composition of the oxygen is known.

Other Analytical Uses of Nitrogen-17

The formation of nitrogen-17 by fast neutron irradiation of oxygen in the absence of lithium-6 can form the basis of a non-destructive method for the analysis of total oxygen in a sample. This can be done either with a high flux of fast neutrons in a reactor or with neutrons from an accelerator. A fission spectrum neutron flux of 10^{14} neutrons/cm^2-sec. will give a saturation activity of 135 neutrons per second from 1 mg of oxygen or a total neutron emission of about 800 per mg oxygen.

The production of nitrogen-17 by the reaction $N^{15}(t,p)N^{17}$ could form the basis for the analysis of nitrogen-15, which is an important stable tracer for nitrogen. Such an analysis would require oxygen-18 to be absent from the sample, or to be present only in known and very low amounts, since its presence would show itself as a background which would have to be deducted from measured sample count, thus decreasing the precision of the measurement. The use of precisely prepared standards would be essential. Under such circumstances, nitrogen-15 could be determined in compounds such as lithium nitride or in oxygen-free solutions, solidified melts or mixtures where nitrogen-15 has been introduced.

APPARATUS AND PROCEDURE FOR COUNTING DELAYED NEUTRONS

In principle, the procedure of analysis by counting delayed neutrons involves the irradiation of the sample in a neutron flux from a reactor or

from another neutron source of sufficient strength, transfer to a neutron-counting assembly and counting after a certain delay.

An efficient apparatus, used in the course of analysis with the reactor IRR-1* is outlined diagrammatically in Figure 11.

Samples were irradiated in a pneumatic tube of the reactor for a predetermined time which was controlled by an electric timer. At the end of the irradiation period the sample in its carrier was transferred to the counting assembly.

The 4π-geometry counting assembly consisted of a ring of six $B^{10}F_3$ neutron counters connected in parallel and embedded in a large block of paraffin wax, with a cavity in the centre of the ring along the axis of the counters. During counting the sample was situated half way along the cavity in the centre of the block. Pulses from the counters were fed through an amplifier to a fast scaler, which was started automatically by an electronic timer a definite preset delay period after the end of irradiation. The timer was triggered by the solenoid which actuated the return of the sample from the irradiation position. The above-mentioned apparatus can be made completely automatic by the introduction of a programmer. An array of borated paraffin bricks around the counting assembly was used to shield the counters against background radiation.

Gamma ray background was efficiently discriminated against. The counting assembly was found to be stable and reproducible over long periods of time. Photo-neutron emission by (γ,n) reactions induced by high-energy gamma rays from other activities in the sample or sample container on the deuterium of the paraffin was found to be negligible.

The counting efficiency of delayed neutrons from fission in the equipment described was about 10% and somewhat lower for delayed neutrons from N^{17}.

---

* Israel Research Reactor No. 1 at Soreq.

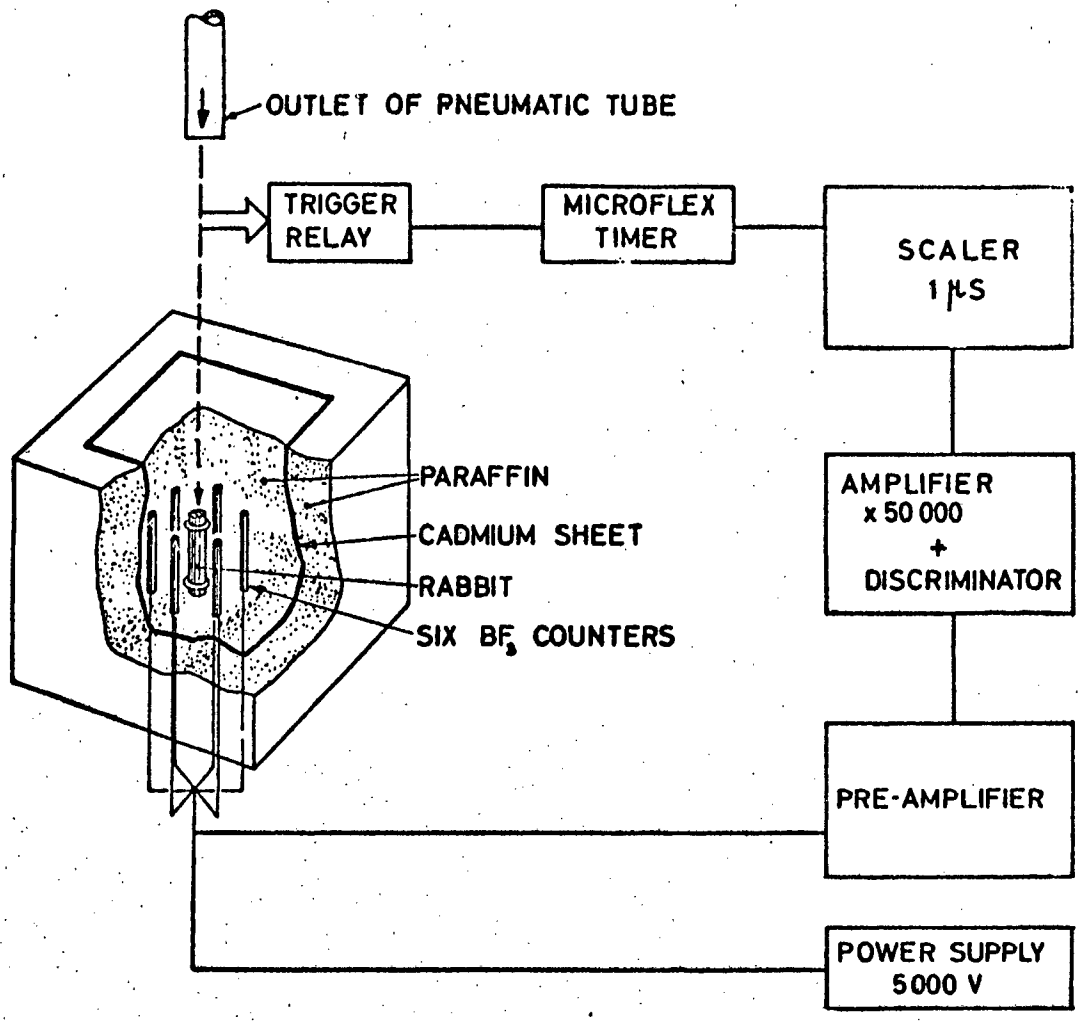

Fig. 11

Neutron counting assembly and block diagram of electronic circuit.

REFERENCES

1. AMIEL, S., I.A.E.C. Report No. IA-621, 1961
2. AMIEL, S. and WELWART, Y., I.A.E.C. Report No. IA-690, 1962
3. AMIEL, S. and PEISACH, M., I.A.E.C. Report No. IA-691, 1962
4. AMIEL, S. and PEISACH, M., Unpublished data, (1962)
5. AJZENBERG-SELOVE, F. and LAURITSEN, T., Nuclear Phys. 11, 221 (1959)
6. AMIEL, S. and GILAT, J., I.A.E.C. Report No. IA-755, 1962
7. COLEMAN, R. F., Analyst 85, 285 (1960)
8. KAPLAN, L. and WILZBACH, K. E., Anal. Chem. 26, 1797 (1954)
9. WINCHESTER, J. W., BATE, L. C. and LEDDICOTTE, G. W., U.S. Report No. CF-59-7-127, 1959

No. 5b

Отдельный оттиск

Атомная энергия

ИЮНЬ
ТОМ 14 1963 ВЫП. 6

543.53

Использование запаздывающих нейтронов в активационном анализе*

С. Амиел, М. Пейсах

*Израильская комиссия по атомной энергии,
Исследовательский центр Сорек, Реховот, Израиль*

Дается обзор последних работ Лаборатории, посвященных использованию запаздывающих нейтронов в активационном анализе [1—3]. Применение этого метода открывает новые и практически очень важные направления в анализе. Использование запаздывающих нейтронов, сопровождающих деление, обсуждается в связи с анализом урана, тория и других делящихся ядер; использование запаздывающих нейтронов, сопровождающих распад N^{17}, — в связи с анализом лития Li^6 и O^{18}. Кроме того, рассматриваются и другие возможности.

Число радиоактивных ядер, испускающих нейтроны в процессе распада, оказывается очень небольшим, если исключить спонтанно делящиеся изотопы тяжелых элементов. Периоды полураспада таких ядер — в пределах от долей секунды до нескольких десятков секунд. Эти ядра, известные как предшественники запаздывающих нейтронов, образуются в ядерных реакциях, приводящих к появлению обогащенных нейтронами изотопов. В результате их β-распада могут образоваться дочерние ядра в возбужденных состояниях, для которых энергетически возможно испускание нейтрона. Испускание нейтронов возбужденным дочерним ядром — излучателем нейтронов — мгновенный процесс, но период полураспада нейтронной активности равен периоду полураспада ядра-предшественника. Схематически процесс испускания запаздывающих нейтронов показан на рис. 1.

В табл. 1 и 2 приведены свойства известных предшественников запаздывающих нейтронов и способы их получения.

Предшественники запаздывающих нейтронов могут быть обнаружены, несмотря на присутствие любого фона β- и γ- излучений, поскольку детекторы нейтронов малочувствительны к указанным излучениям. Это обстоятельство имеет первостепенное значение и дает возможность использовать запаздывающие нейтроны для определения тех или иных ядер, входящих в состав образца, или для измерения радиации, под действием которой образуются излучатели запаздывающих нейтронов. Предшественники запаздывающих нейтронов крайне редки; их периоды полураспада существенно различаются.

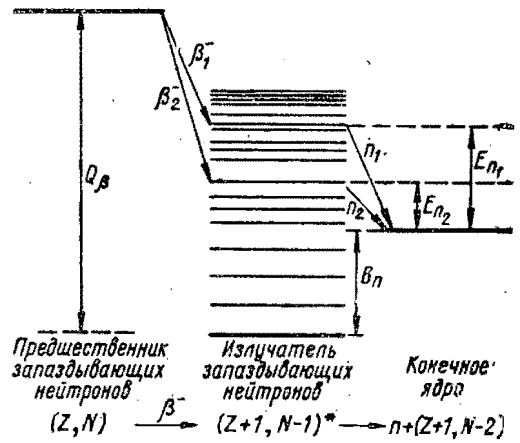

Рис. 1. Схема испускания запаздывающих нейтронов.

Путем соответствующего выбора материала образца и условий облучения можно получить вполне определенные предшественники запаздывающих нейтронов. Большая часть настоящего обзора касается работ, проведенных на реакторе, хотя в принципе может быть использован любой другой источник нейтронов.

* Перевод с английского.

Таблица 1

Характеристики предшественников запаздывающих нейтронов
(реакция деления [4])

Номер группы	Период полураспада, *сек*	Идентифицированные предшественники	Абсолютный выход групп, %				
			тепловые нейтроны		быстрые нейтроны		
			U^{235} (σ=582 *барн*)	Pu^{239} (σ=746 *барн*)	U^{235}	U^{238}	Th^{232}
1	52—56	Br^{87} (54 *сек*),	0,052±0,005	0,021±0,006	0,063±0,005	0,054±0,005	0,169±0,012
2	21—23	Br^{88} (16 *сек*), J^{137} (24 *сек*)	0,346±0,018	0,182±0,023	0,351±0,011	0,564±0,025	0,744±0,037
3	5—6	Br^{89} (4,4 *сек*), J^{138} (6,3 *сек*)	0,310±0,036	0,129±0,030	0,310±0,028	0,667±0,087	0,769±0,108
4	~ 2	Br^{90} (1,6 *сек*), J^{139} (2 *сек*)	0,624±0,026	0,199±0,022	0,672±0,023	1,599±0,081	2,212±0,110
5	~ 0,6	—	0,182±0,015	0,052±0,018	0,211±0,015	0,927±0,060	0,853±0,073
6	~ 0,2	—	0,066±0,008	0,027±0,010	0,143±0,005	0,309±0,024	0,213±0,031
Число запаздывающих нейтронов на деление			0,0158±0,0005	0,0061±0,0003	0,0165±0,0005	0,0412±0,0017	0,0496±0,0020

Запаздывающие нейтроны, сопровождающие деление [1]

В табл. 1 предшественники запаздывающих нейтронов, образующиеся при делении, разбиты на шесть групп в соответствии с их периодами полураспада, лежащими в пределах от долей секунды до 1 *мин*. Группы сами по себе представляют, вероятно, смеси нескольких неразделенных излучателей, что можно видеть из небольших различий между одними и теми же группами, относящимися к разным делящимся ядрам. Однако эти различия не играют роли, если с целью анализа измеряется полная нейтронная эмиссия.

Если при облучении образца тепловыми или быстрыми нейтронами наблюдаются запаздывающие нейтроны, то можно заключить, что в образце присутствуют или тяжелые делящиеся ядра, или кислород, или азот и Li^6 (см. табл. 1, 2). Если Li^6 присутствует в образце вместе с кислородом или азотом (большинство образцов действительно содержит кислород, а некоторые могут содержать и азот), то запаздывающие нейтроны обязаны N^{17} (4,1 *сек*), образующемуся в результате двух последовательных реакций $Li^6(n, \alpha)H^3$ и $O^{18}(t, \alpha)N^{17}$ или $N^{15}(t, p)N^{17}$. Этот же изотоп может образоваться при облучении кислорода быстрыми нейтронами, даже если в образце нет лития. На присутствие делящихся ядер однозначно указывает появление запаздывающих нейтронов с большими периодами полураспада. Если облучению тепловыми нейтронами подвергается образец естественного происхождения, то появление запаздывающих нейтронов обязано U^{235}. В случае облучения искусственного образца появление запаздывающих нейтронов может указывать на присутствие U^{233}, Pu^{239} и других трансурановых элементов, делящихся под

Таблица 2

Характеристики предшественников запаздывающих нейтронов (другие реакции)

Предшественник запаздывающих нейтронов	Период полураспада, *сек*	Ядро-мишень	Реакции	Энергия, *Мэв*
Li^9	0,17	Li^7	t, p	—2,9
		Be^9	n, p	—13,3
C^{16}	0,74	C^{14}	t, p	—3,01 [5]
N^{17}	4,14	N^{15}	t, p	—0,15
		O^{17}	n, p	—7,93
		O^{18}	n, d	—13,77
		O^{18}	t, α	3,82
Tl^{210}*	~80			
?	Короткий	Cu	Протоны	—
?	8	Cu	с большой	—
?	18	Cu	энергией	
? **	6	Nd		— [6]
? ***	20	Nd		—
				—

* 0,02% распадов с излучением нейтронов.
** По-видимому, J^{138} (6,3 *сек*).
*** По-видимому, J^{137} (24 *сек*).

действием тепловых нейтронов. Естественными тяжелыми ядрами, делящимися под действием быстрых нейтронов из реактора, являются Th^{232} и U^{238}. Если же в образце могут содержаться трансурановые элементы, то следует принимать во внимание еще ряд ядер.

Обычные методы определения следов урана в веществах сложного состава занимают много времени и требуют тщательной предварительной химической обработки. В геологии и ядерной энергетике необходим быстрый и доступный метод анализа, не требующий разрушения исследуемого образца. Таким методом может быть метод регистрации запаздывающих нейтронов.

Если образец, содержащий N_f делящихся ядер с сечением σ_f, облучается потоком Ф (*нейтр/см²·сек*) в течение t_b (*сек*), то число делений равно $N_f\sigma_f\Phi t_b$. Примем, что доля a_i этих делений приводит к образованию группы i излучателей запаздывающих нейтронов с постоянной распада λ_i и время между окончанием облучения и началом счета составляет t_d. Тогда число запаздывающих нейтронов, испущенных за время t_c, можно представить в виде

$$N_d = N_f\sigma_f\Phi\,\frac{a_i}{\lambda_i}\,(1-e^{-\lambda_i t_b})\,e^{-\lambda_i t_d}\,(1-e^{\lambda_i t_c}).$$

Из этого выражения можно найти оптимальные условия облучения и измерений.

Поскольку период полураспада нейтронной активности мал, то длительное облучение не улучшает точности анализа. Облучение в течение 60 *сек* приводит к насыщению активности, соответствующей первым четырем группам (см. табл. 1), дает 85% от величины насыщения для активности с периодом 22 *сек* и половину величины насыщения для самой долгоживущей группы.

Некоторая задержка между окончанием облучения и началом измерений неизбежна, поскольку требуется определенное время для переноса образца из нейтронного потока к счетчикам. Она должна быть невелика, хотя очень малая задержка требует повышенной точности ее измерения, так как разброс во времени задержки может внести заметные ошибки в результат. Задержка, составляющая около 20 *сек*, приемлема для 22-секундной группы, но почти полностью исключает вклад от всех короткоживущих групп. Группа с периодом полураспада 55 *сек* имеет малую интенсивность, и небольшие изменения во времени задержки не приводят к заметной ошибке. Вклад от N^{17}, который образуется при облучении кислорода быстрыми нейтронами, при такой задержке также исключается.

Продолжительность измерений устанавливается в соответствии с периодом регистрируемой группы. Для 22-секундной группы это время должно составлять ~1 *мин*. Более длительные измерения приводят к увеличению относительного вклада фона.

Эти соображения приводят *a priori* к следующим условиям анализа: времени облучения 60 *сек*, задержки 20 *сек* и измерений 60 *сек*.

Анализ урана [1]. Из естественных изотопов урана тепловыми нейтронами делится U^{235} (σ=582 *барн*); U^{238} делится нейтронами, энергия которых превышает 1 *Мэв*, и его сечения деления в ~100 раз меньше сечения деления U^{235}. Чтобы определить полное содержание урана естественного изотопного состава в образце, предпочтительнее использовать тепловые нейтроны, поскольку быстрые нейтроны могут вызывать деление и других ядер. Однако в спектре нейтронов реактора наряду с тепловыми присутствуют несколько замедленные нейтроны деления, энергия которых достаточна для того, чтобы вызвать деление U^{238}. Но даже в этих условиях преобладающим процессом будет деление U^{235}, и если уран является единственным анализируемым делящимся изотопом в образце, то быстрые нейтроны не создадут существенных помех. Если присутствуют относительно большие количества других делящихся элементов, таких, как, например, торий, деление быстрыми нейтронами может внести заметную ошибку в результаты анализа урана. В таких случаях необходимо использовать поглотители тепловых нейтронов и проводить калибровку по стандартным образцам.

Если условия облучения и измерения хорошо известны, то число испускаемых запаздывающих нейтронов можно найти на основе величин, приведенных в табл. 1 и 2. Экспериментальные результаты хорошо согласуются с найденными таким образом. Облученный в течение 60 *сек* в потоке тепловых нейтронов 10^{13} *нейтр/см²·сек* образец естественного урана весом 1 *мкг* после задержки в 20 *сек* испускает за 60 *сек* 11 700 нейтронов. На рис. 2 приведена калибровочная кривая, полученная с помощью стандартных образцов урана. Видно, что число зарегистрированных запаздывающих нейтронов прямо пропорционально содержанию урана в образце.

В табл. 3 приведены результаты анализа различных руд. Для сравнения там же даны результаты химического анализа.

Если эффективность регистрации нейтронов составляет 10%, то образец, содержащий около 10 *мкг* урана, может быть проанализирован с точностью ±1%. Поскольку определяется

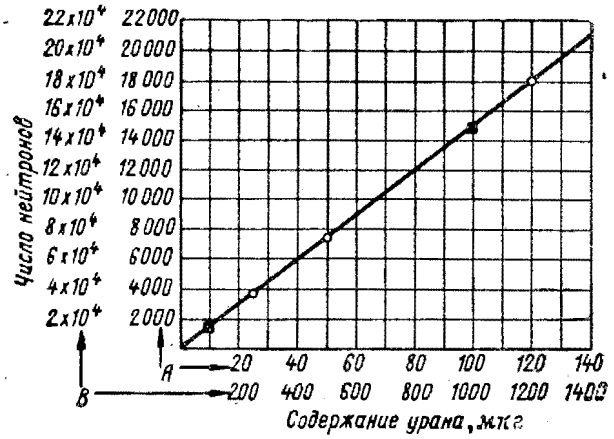

Рис. 2. Зависимость числа запаздывающих нейтронов от содержания урана в образце. Образцы облучались в потоке $1{,}9 \cdot 10^{12}$ *нейтр/см²·сек*:
○ — шкала *A*; ■ — шкала *B*.

скорее полное содержание урана в образце, чем его концентрация, то такую точность можно получить при концентрации порядка 10^{-6} для образцов весом 10 *г* и соответственно при меньшей концентрации урана для более тяжелых образцов. Максимальный вес анализируемого образца ограничивается лишь системой, переносящей образец из реактора к счетчикам.

Частичное поглощение нейтронного потока внутри образца при облучении или при измерении может повлиять на результаты анализа. Однако этот эффект играет существенную роль лишь для сравнительно больших образцов вещества с большим сечением поглощения нейтронов.

Анализ изотопного состава урана [7]. Анализ изотопного состава урана должен проводиться с образцами, не содержащими других ядер, делящихся под действием тепловых нейтронов. В таких образцах тепловыми нейтронами делится лишь U^{235} и число запаздывающих нейтронов является мерой его содержания независимо от присутствия U^{238} или других элементов. Относительное содержание U^{235} и U^{238} в образце можно получить, если известно полное содержание урана.

Если образец облучается смешанным потоком нейтронов, то запаздывающие нейтроны соответствуют делению как U^{235}, так и U^{238}, но поскольку главную роль играет U^{235}, число запаздывающих нейтронов может служить мерой содержания этого изотопа. Облучение того же образца в потоке, из которого кадмиевым экраном удалены тепловые нейтроны, позволяет определить содержание U^{238}. Однако в этом случае необходимо сравнение со стандартными образцами, имеющими различный изотопный состав, так как число запаздывающих нейтронов, соответствующих делению U^{235} надтепловыми нейтронами, того же порядка, что и число нейтронов, соответствующих делению U^{238}. Вклад, связанный с присутствием U^{235} при анализе содержания U^{238} в случае облучения образцов из чистого урана быстрыми нейтронами, полностью зависит от энергетического спектра этих нейтронов. Таким образом, двукратное облучение уранового образца с кадмиевым экраном и без него позволяет определить содержание U^{238} и U^{235} независимо от присутствия других неделящихся элементов.

Типичная калибровочная кривая для определения содержания U^{235} в U_3O_8, полученная при облучении тепловыми нейтронами, приведена на рис. 3. Число запаздывающих нейтронов прямо пропорционально содержанию U^{235}.

На рис. 4 приведены результаты анализа содержания U^{235} при облучении смешанным нейтронным потоком. Подъем кривой вызван присутствием U^{238} и исчезает с введением соответствующих поправок. Видно, что поправки

Таблица 3

Результаты анализа содержания урана в различных образцах

Образец	Концентрация (в миллионных долях)	
	метод запаздывающих нейтронов *	химический и флуорометрический методы
837 гранит	4,40±0,05	4,2±0,2
643 базальт	0,55±0,05	0,9±0,5
694 гнейс	1,98±0,12	2,4±0,2
684 сланец	2,3±0,2	2,6±0,3
665 известняк	3,95±0,10	4,0±0,5
777 доломит	2,92±0,05	3,1±0,2
611 мергель	31,0±0,3	33,7±1,7
664 глина	3,8±0,1	4,5±0,5
708 песчаник	0,85±0,02	0,9±0,5
613 битумный мел	19,7±0,7	23,3±2,0
644 фосфатная руда	153±1,2	168±8
667 марганцевый сланец	37,3±0,5	36,4±1,6
Отложение источника	0,6±0,2	1,3±1,3

* Ошибки представляют наблюдавшееся отклонение от средних значений.

не нужны, если содержание U^{235} превышает 5 ат.% . При меньших количествах U^{235} необходимо оценить содержание U^{238}. Результаты

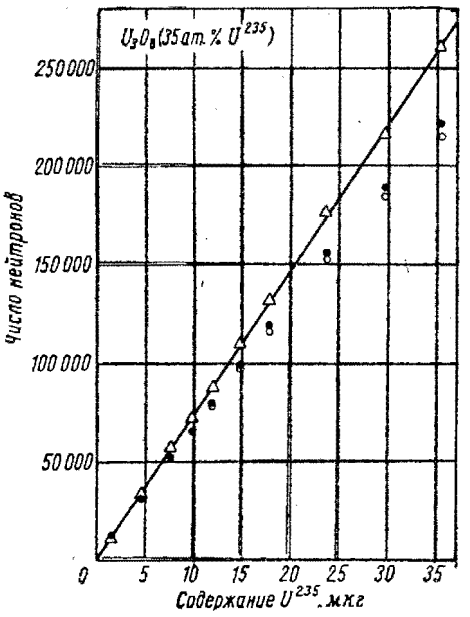

Рис. 3. Зависимость числа запаздывающих нейтронов от содержания U^{235} в образце. Измерения проводились после задержки 8 *сек*. Результаты нормированы на поток $4{,}2 \times 10^{11}$ *нейтр/см²·сек*:

○ — измеренные значения; ● — значения с учетом просчетов схемы совпадений; △ — значения с учетом самоэкранирования.

определения содержания U^{235} и U^{238} при облучении смешанным нейтронным потоком с кадмиевым фильтром и без него приведены в табл. 4.

Точность определения изотопного состава урана лучше 0,5%. Источниками ошибок являются флуктуации нейтронного потока реактора и самоэкранирование образцов. Влияние флуктуаций можно учесть с помощью повторных измерений со стандартным образцом.

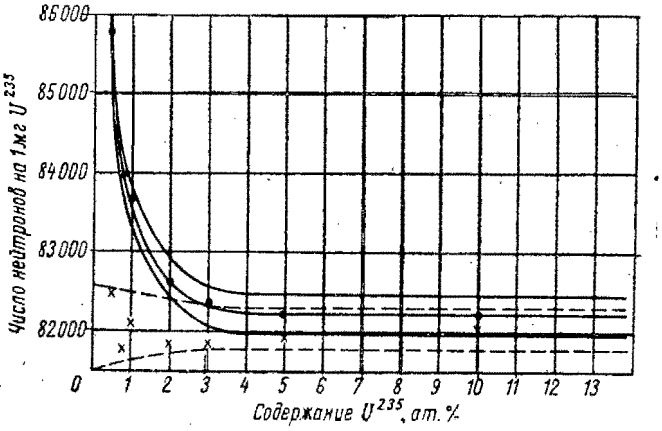

Рис. 4. Анализ содержания U^{235}.

Подъем неисправленной кривой (●) обязан присутствию U^{238}. Исправленные значения представлены крестиками. Пунктирными и внешними сплошными линиями обозначены пределы ошибок. Пределы ошибок исправленных и неисправленных значений сближаются и становятся одинаковыми при содержании U^{235}, равном 100 ат.%. Облучение проводилось в потоке $7{,}5 \cdot 10^9$ *нейтр/см²·сек*.

Поправка на самоэкранирование определяется в результате измерений, проведенных с меньшим образцом.

Анализ тория [1]. Деление Th^{232} напоминает деление U^{238}. Поскольку сечение деления Th^{232} несколько меньше, чем U^{238}, то для определения содержания тория требуются бо́ль-

Таблица 4

Анализ изотопного состава урана (облучение проводилось в потоке $7{,}5 \cdot 10^9$ *нейтр/см²·сек*)

Номер стандартного образца	Вес образца, *мг*	Содержание U^{235}, ат. %	Содержание U^{235}, *мг*	Измеренное число нейтронов	Число нейтронов на 1 *мг* U^{235}		Вклад U^{238}	Число нейтронов на 1 *мг* чистого U^{235}
					измеренное	исправленное на самоэкранирование		
U-005	207,45	0,483	0,85	72 740	85 607	85 798	3 296	82 502
U-010	198,75	0,991	1,67	138 806	83 107	83 688	1 599	82 089
U-020	156,50	2,01	2,67	218 408	81 887	82 625	780	81 845
U-030	79,95	3,01	2,04	166 909	81 794	82 364	516	81 848
U-050	45,00	4,95	1,89	154 402	81 746	82 235	314	81 921
U-100	23,40	10,07	2,00	163 123	81 647	82 217	143	82 074
950	224,00	0,72 (естеств.)	1,37	114 440	83 728	83 977	2 206	81 771
								Среднее 8200 7±249 Стандартное отклонение 0,3%

шие образцы и более интенсивные потоки нейтронов. Так, например, 1 *мкг* естественного тория, облученного до насыщения потоком нейтронов спектра деления 10^{13} *нейтр/см²·сек*, испускает 412 нейтронов. Некоторые результаты анализа приведены в табл. 5.

Таблица 5

Определение содержания тория и урана в смесях этих элементов

Номер образца *	Содержание, *мг*		Экспериментально измеренное число нейтронов	Вычисленное число нейтронов			Th+U (вычисление/эксперимент)
	Th	U		Th	U	Th+U	
С кадмиевым экраном							
101	—	2,10	2786	—	—	—	—
102	—	2,10	2755	—	—	—	—
103	2,01	—	604	—	—	—	—
104	2,02	—	584	—	—	—	—
105	5,96	2,07	4150	1565	2720	4285	1,03
106	10,25	2,00	5587	2990	2630	5620	1,01
107	20,60	2,02	9150	6070	2660	8730	0,96
108	40,25	2,04	14 424	11 880	2690	14 570	1,01
109	67,50	2,06	20 590	17 750	2710	20 460	0,99
110	108,0	2,12	32 985	30 750	2790	33 540	1,02
111	201,5	2,08	64 167	59 400	2740	62 140	0,97
Без кадмиевого экрана							
101	—	2,10	61 000	—	—	—	—
102	—	2,10	61 800	—	—	—	—
103	2,01	—	600	—	—	—	—
104	2,02	—	665	—	—	—	—
105	5,96	2,07	61 670	1740	60 400	62 140	1,02
106	10,25	2,00	62 540	3325	58 250	61 575	0,99
107	20,60	2,02	66 824	6750	59 000	65 750	0,98
108	40,25	2,04	73 043	13 200	59 500	72 700	0,98
109	67,50	2,06	80 843	19 700	60 000	79 700	0,99
110	108,0	2,12	93 173	34 150	61 600	95 750	1,03
111	201,5	2,08	124 113	66 000	60 700	126 700	1,02

* Образцы 101—104 использовались в качестве стандартов для вычисления состава смесей Th+U. Облучение проводилось в потоке $3{,}75 \cdot 1011$ *нейтр/см²·сек*.

Основное препятствие при анализе тория — обычное присутствие урана в ториевых рудах, поэтому сначала облучением в потоке тепловых нейтронов определяют содержание U^{235}, затем, предполагая естественный изотопный состав урана, находят содержание U^{238} и оценивают вклад этих изотопов в число делений при облучении образца надтепловыми нейтронами. В табл. 5 приведены вычисленные и экспериментальные значения для известных смесей урана и тория. Из таблицы видно, что присутствие 1 *мг* тория можно определить с точностью около 2%. Точность определения при содержании тория 10^{-6} в образце весом 10 *г* составляет 15%.

Определение содержания U^{233} и Pu^{239}. Анализ содержания Pu^{239}, образующегося в урановых тепловыделяющих элементах, или U^{233}, образующегося в брикетах из тория, аналогичен анализу ураново-ториевых смесей. Метод запаздывающих нейтронов обладает большими преимуществами по сравнению с химическими методами контроля за процессом бридинга.

Поиски урана и тория. Введение в буровую скважину нейтронного источника вызовет деление урана и тория, присутствующих в облучаемом объеме, и приведет к появлению запаздывающих нейтронов. Наблюдение нейтронной активности с периодом полураспада, бо́льшим 4 *сек*, указывает на присутствие урана или тория и позволяет оценить их концентрацию.

Запаздывающие нейтроны, сопровождающие распад N^{17}

Характеристики предшественника запаздывающих нейтронов N^{17} приведены в табл. 2. Изотоп N^{17} может быть получен при облучении O^{17} и O^{18} быстрыми нейтронами в реакциях $O^{17}(n, p)N^{17}$ и $O^{18}(n, d)N^{17}$. Пороги этих реакций равны соответственно 9,5 и 15,5 *Мэв* [8]. Вследствие малой распространенности тяжелых изотопов кислорода и сравнительно малого сечения реакции для нейтронов спектра деления 7,5 *мкбарн* [9] количество N^{17}, образующегося при облучении естественного кислорода нейтронами, весьма невелико и анализ содержания кислорода с помощью запаздывающих нейтронов можно проводить лишь в очень интенсивных нейтронных потоках. При облучении естественного кислорода до насыщения в потоке 10^{13} *нейтр/см²·сек* интегральный выход запаздывающих нейтронов составляет 80 *нейтр/мг*. Однако если в образце вместе с кислородом присутствует Li^6, то основным процессом, приводящим к образованию N^{17}, становится реакция $O^{18}(t, \alpha)N^{17}$, вызываемая тритонами с энергией 2,7 *Мэв*, получающимися в реакции $Li^6(n, \alpha)H^3$. Большое сечение последней реакции на тепловых нейтронах (960 *барн*) обеспечивает высокий выход N^{17} и позволяет использовать запаздывающие нейтроны для анализа. Так, например, при облучении до насыщения раствора 1 *мг* Li^6 в обыкновенной воде потоком тепловых нейтронов 10^{13} *нейтр/см²·сек* испускается около 40 000 нейтронов. Используя в качестве растворителя воду, обогащенную изотопом O^{18}, можно соответственно увеличить выход нейтронов и повысить чувствительность анализа. Если в образце вместе с Li^6 присутствует азот, то N^{17} образуется в реакции $N^{15}(t, p)N^{17}$, но сечение этой реакции несколько ниже сечения реакции $O^{18}(t, \alpha)N^{17}$.

Выход N^{17} зависит от степени близости атомов лития и атомов кислорода или азота в образце, поскольку пробег тритонов в веществе очень мал. Оптимальные условия в этом смысле встречаются в растворах.

Было показано [3], что интенсивность образования N^{17} в разведенном растворе лития, облучаемом тепловыми нейтронами, пропорциональна полному содержанию лития в образце и концентрации O^{18}. Отсюда следует, что запаздывающие нейтроны N^{17} могут быть использованы для анализа содержания Li^6 в растворе, если известна доля атомов O^{18} в образце. Наоборот, если известно содержание Li^6 в образце, то можно найти долю атомов O^{18}. Эти же рассуждения справедливы и для N^{15}. Анализ Li^6, O^{18} или N^{15} таким методом не обязательно ограничен растворами, поскольку в любых других смесях с близким расположением атомов Li^6 — O^{18} или Li^6 — N^{15} также будет образовываться N^{17} при облучении их нейтронами. Характеристики выхода N^{17} для твердых смесей, коллоидных систем или соединений должны определяться в каждом случае, поскольку они зависят от физических свойств образца.

Облучение в течение 25 *сек* приводит к насыщению N^{17}, и измерения в течение такого же времени позволяют зарегистрировать больше 98% всех нейтронов. Задержка между окончанием облучения и началом измерений должна быть минимальной при условии возможности точного ее повторения.

Анализ содержания лития [2]. Поскольку образование N^{17} в потоке тепловых нейтронов — специфическая особенность Li^6, то полное содержание лития можно определить лишь в том случае, если известен изотопный состав лития в образце.

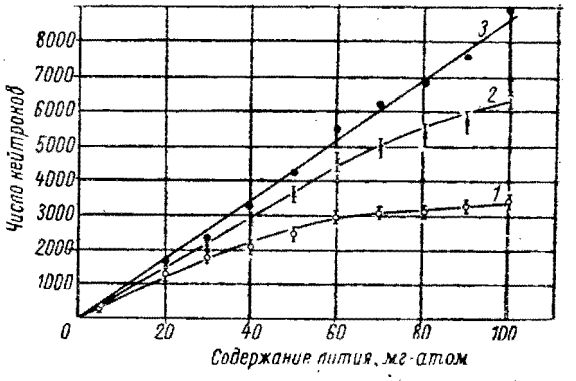

Рис. 5. Зависимость числа запаздывающих нейтронов от содержания лития в растворе LiCl в обыкновенной воде:

1 — измеренные значения; *2* — с поправкой на поглощение нейтронов хлором; *3* — с поправкой на полное самоэкранирование в образце.

Если образец облучается смешанным нейтронным потоком, то вносят свой вклад реакции прямого образования N^{17} из кислорода. Величина этого вклада должна определяться повторными измерениями с кадмиевым экраном.

Калибровочная кривая, полученная для раствора лития в обыкновенной воде, показана на рис. 5. Поглощение нейтронов другими веществами, содержащимися в образце, зави-

сит от количества этих веществ и сечений поглощения. Этот эффект иллюстрируется на рис. 6.

При анализе содержания лития всегда следует учитывать то, что в образце могут присутствовать делящиеся элементы. Прямое свидетельство этого — наблюдающаяся нейтронная активность с периодом, заметно бо́льшим 4,1 *сек.*

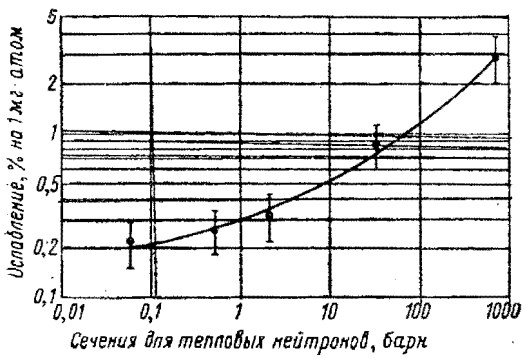

Рис. 6. Влияние величины сечения поглощения присутствующих в образце элементов на нейтронную активность.

Анализ изотопного состава лития [2]. Обычно для изотопного анализа лития используется масс-спектрометрия — трудоемкий и медленный метод [10]. При использовании других методов анализа требуется измерение трития [11], образующегося в первичной реакции $Li^6(n, \alpha)H^3$, или F^{18} [12], образующегося во вторичной реакции $O^{16}(t, n)F^{18}$. Точность такого анализа зависит от эффективности выделения измеряемой активности и неизбежного присутствия фоновых активностей. Эти недостатки исключаются, если используется метод запаздывающих нейтропов.

Описанный выше анализ содержания лития является по существу анализом содержания Li^6. Для образцов с известным полным содержанием лития такой анализ указывает и изотопный состав. На рис. 7 приведена калибровочная кривая, полученная для растворенных в обычной воде образцов, проанализированных масс-спектрометрическим методом и содержащих известное полное количество лития. Число запаздывающих нейтронов пропорционально доле атомов Li^6 в образце. Для увеличения выхода запаздывающих нейтронов из обедненных образцов следует использовать либо обогащенную изотопом O^{18} воду, либо образцы больших размеров с повышенной концентрацией раствора. Однако следует помнить, что в таких образцах с большей вероятностью может идти реакция на тяжелых изотопах кислорода, если в потоке имеются быстрые нейтроны.

Анализ O^{18} [3]. Метод запаздывающих нейтронов позволяет проанализировать содержание кислорода в образце (по O^{18}) в течение 1 *мин*

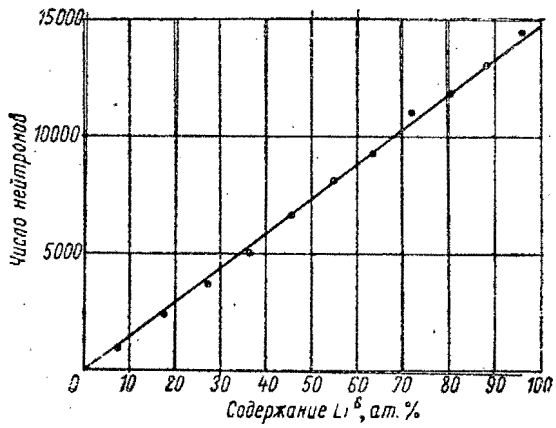

Рис. 7. Зависимость числа запаздывающих нейтронов от изотопного состава лития для образцов, содержащих одинаковое полное количество лития.

и без разрушения образца. Как следует из предыдущего раздела, посвященного Li^6, число запаздывающих нейтронов прямо пропорционально доле атомов O^{18}, если содержание лития и условия облучения постоянны. На рис. 8 видно, что число нейтронов пропорционально доле

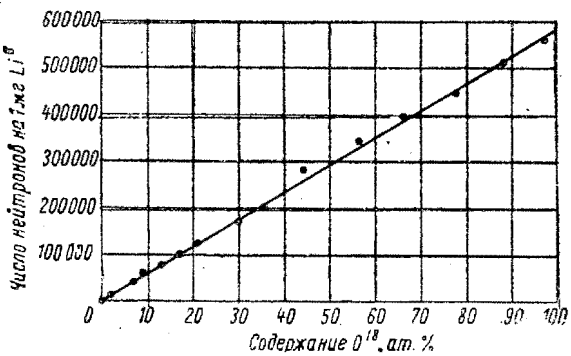

Рис. 8. Зависимость числа запаздывающих нейтронов, соответствующих 1 *мг* Li^6, от изотопного состава кислорода.

атомов O^{18} во всем интервале концентраций O^{18}. Пропорциональность не изменяется при изменении размеров образцов, и анализ может проводиться даже с одной каплей раствора. Было показано [3], что пропорциональность между числом запаздывающих нейтронов на единицу веса Li^6 и концентрацией O^{18} не нару-

шается в интервале отношений числа атомов O^{18} к числу атомов Li^6 от 1 до 10^4. Это позволяет вводить в образец столько Li^6, сколько нужно для получения оптимальной скорости счета запаздывающих нейтронов. Однако содержание Li^6 должно быть ниже того уровня, когда начинает существенно сказываться самоэкранирование образца.

Точность анализа определяется точностью изготовления образцов и точностью использованных стандартов. Кроме того, существенным источником ошибок являются флуктуации потока нейтронов реактора.

Другие применения N^{17} для анализа. Образование N^{17} при облучении кислорода быстрыми нейтронами в отсутствие Li^6 позволяет определять полное содержание кислорода в образце без его разрушения. Это можно сделать либо в интенсивных потоках быстрых нейтронов из реактора, либо в потоке нейтронов ускорителя. Поток нейтронов спектра деления интенсивностью 10^{14} *нейтр/см²·сек* дает при насыщении нейтронную активность 135 *нейтр/сек* на 1 *мг* кислорода или полное число запаздывающих нейтронов 800 *нейтр/мг*.

Образование N^{17} в реакции $N^{15}(t, p)N^{17}$ дает возможность определять содержание N^{15}. Для такого анализа требуются образцы, не содержащие кислорода.

Метод регистрации запаздывающих нейтронов

В принципе анализ заключается в облучении образца потоком нейтронов реактора или другого источника нейтронов, переносе образца к нейтронным счетчикам и после некоторой задержки регистрации числа запаздывающих нейтронов. Установка, используемая для анализа на реакторе IRR-I (Израильский исследовательский реактор I, Сорек), схематически показана на рис. 9. Образцы облучаются в пневматической системе реактора в течение контролируемого электрическим таймером времени. После окончания облучения образцы в своих контейнерах переносятся к счетчикам.

Шесть соединенных параллельно нейтронных счетчиков, наполненных $B^{10}F_3$, расположены кольцом и образуют установку с 4π-геометрией. Счетчики помещены в большой блок парафина с полостью в центре кольца, образованного счетчиками. Во время измерений образец находится в этой полости в центре

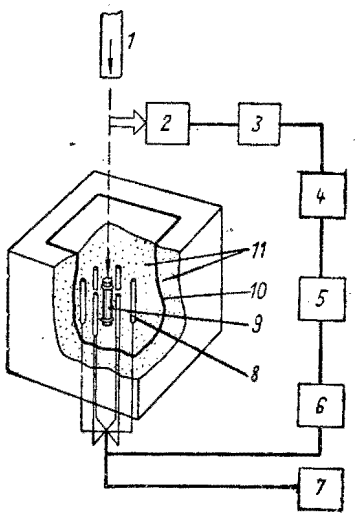

Рис. 9. Схема установки для регистрации запаздывающих нейтронов:
1 — пневматическая линия; *2* — пусковое реле; *3* — таймер; *4* — нумератор с «мертвым» временем 1 *мксек*; *5* — усилитель с коэффициентом усиления 50 000 и дискриминатор; *6* — предусилитель; *7* — источник питания 5000 *в*; *8* — шесть счетчиков с BF_3; *9* — контейнер; *10* — слой кадмия; *11* — парафин.

блока. Импульсы счетчиков после усиления подаются на быстрый нумератор, запускаемый автоматически электронным таймером, определяющим время задержки между окончанием облучения и началом измерений. Таймер управляется сигналом с соленоида, с помощью которого образец переносится из реактора к счетчикам. Всю систему можно полностью автоматизировать, и она может управляться программирующим устройством. Парафиновый блок со счетчиками окружен защитой из смеси парафина с бором, снижающей нейтронный фон. Эффективность регистрации запаздывающих нейтронов, сопровождающих деление, составляла 10%; эффективность регистрации нейтронов N^{17} несколько ниже.

Поступила в Редакцию 7/I 1963 г.

ЛИТЕРАТУРА

1. S. Amiel. Israel Atomic Energy Commission, Report IA-621, 1961.
2. S. Amiel, Y. Welwart. Israel Atomic Energy Commission, Report IA-690, 1962.
3. S. Amiel, M. Peisach. Israel Atomic Energy Commission, Report IA-691, 1962.
4. G. Keepin et al. Phys. Rev., 107, 1044 (1957).
5. S. Hinds et al. Phys. Rev. Lett., 6, 113 (1961).
6. G. Rudstam et al. Nature, 188, 1178 (1960).
7. S. Amiel, M. Peisach. Неопубликованные данные, 1962.
8. F. Ajzenberg-Selove, T. Lauritsen. Nucl. Phys., II, 221 (1959).
9. S. Amiel, J. Gilat. Israel Atomic Energy Commission, Report IA-755, 1962.
10. R. Coleman. Analyst, 85, 285 (1960).
11. L. Kaplan, K. Wilzbach. Analyt. Chem., 26, 1797 (1954).
12. J. Winchester, L. Bate, G. Leddicotte. U. S. Report, No. CF-59-7-127, 1959.

539.1

Выход нейтронов из некоторых материалов под действием α-частиц радона и продуктов его распада

Г. В. Горшков, В. А. Зябкин, О. С. Цветков

В работе измерены выходы нейтронов по реакции (α, n) для некоторых легких элементов, химических соединений, минералов и горных пород под действием α-частиц Rn + RaA + + RaC′, а также определены отношения выходов от Rn + RaA к выходам от Rn + RaA + + RaC′. Полученные экспериментальные значения выходов для некоторых горных пород и минералов сравниваются с расчетными. Показано, что выход нейтронов из горных пород и минералов в основном обусловлен выходами на алюминии, кремнии, кислороде, натрии, магнии и фторе.

Цель настоящей работы — определить нейтронный выход из некоторых материалов под действием α-частиц Rn*+ RaA + RaC′, а также отношение выхода от Rn + RaA к выходу от Rn + RaA + RaC′, которое позволяет найти выход на RaC′.

Нейтронные источники изготовлялись в виде стеклянных ампул цилиндрической формы диаметром 20 и высотой 40 *мм* (выбор ампул такого размера обоснован в работе [1]). Ампулы заполнялись порошкообразными материалами мишени, размеры зерен которых не превышали 40—50 *мк*. Наполнение ампул радоном производилось на обычной эманационной установке. Количество радона в каждой ампуле определялось на электрометре по внешнему γ-излучению путем сравнения с эталоном радия. Для устранения влияния самопоглощения γ-лучей в нейтронных источниках все электрометрические измерения производились через свинцовый фильтр толщиной 1 *см*. При сравнении результатов измерений с фильтром и без фильтра было установлено, что самопоглощение в материале источника в зависимости от плотности наполнителя составляло 1—5% от полного γ-излучения.

В качестве исследуемых материалов использовались «химически чистые» или «чистые для анализа» элементы и химические соединения природного изотопного состава. Кроме того были исследованы выходы нейтронов для некоторых пород и минералов. Химический состав был известен для следующих пород и минералов: флюорит, порода с гатчетолитом, гранит Рапакиви, глауконит, сланец, Дубовский гранит, мрамор, карбуран и монацит.

В табл. 1 представлены некоторые характеристики (α, n)-реакций легких элементов. Энергии и пороги реакций для изотопов углерода, азота, кислорода, кремния, фосфора, серы и хлора вычислены по дефектам соответствующих масс [2, 3].

Описание установки

Измерения полного числа нейтронов, испускаемых источниками, производили на стандартной установке типа СЧ-3. Нейтронный счетчик СНМ-5А был окружен парафиновым экраном-отражателем в виде трубы с внутренним диаметром 22, высотой 50 и толщиной стенок 3 *см* (рис. 1). Наличие этого экрана повышало скорость счета от Ac + Be-источника примерно в два раза. Для снижения присчета γ-квантов борным счетчиком между ним и ампулами помещался свинцовый фильтр толщиной 5 *см*, что обеспечивало практически полное отсутствие счета от γ-излучения эталона, содержащего 100 *мг* радия.

Для определения зависимости эффективности $Э_н$* установки от средней энергии нейтронов

* Под Rn подразумевается равновесное состояние Rn + RaA + RaC′.

* Под эффективностью установки $Э_н$ понимается отношение числа зарегистрированных импульсов к полному числу нейтронов, испускаемых источником.

No. 6

Reprinted from

ANALYTICAL CHEMISTRY

Radioactivation Analysis of Sodium by Counting Photoneutrons

SAADIA AMIEL and MAX PEISACH

Israel Atomic Energy Commission, Soreq Research Establishment, P.O.B. 527, Rehovoth, Israel

Volume 35, Number 8

Pages 1072-1076, July 1963

Radioactivation Analysis of Sodium by Counting Photoneutrons

SAADIA AMIEL and MAX PEISACH

Israel Atomic Energy Commission, Soreq Research Establishment, P.O.B. 527, Rehovoth, Israel

▶ A method is described for a nondestructive radioactivation analysis of sodium in complex matrices, in which Na^{24} is assayed by counting photoneutrons emitted from deuterium by the 2.75-m.e.v. gamma ray, in an assembly consisting of D_2O and neutron detectors. This principle offers efficient discrimination against large amounts of radioactivities with energies below 2.23 m.e.v., the threshold for the photodisintegration of deuterium. The photoneutron activity was proportional to the Na^{24} content in the sample, and microgram quantities of sodium were analyzed with a precision of 2%. Sensitivities better than 0.1 μg. are indicated. Interference from other radionuclides is discussed. Possible extension for the analysis of elements other than sodium is discussed as well.

Because of the widespread occurrence of sodium and its importance in many fields, accurate methods for its analysis have been developed. Flame photometry is mainly used when high sensitivity is required, but this sensitivity can be affected by the presence of other components which frequently occur together with sodium (*2*). Nuclear methods of analysis utilizing characteristic nuclear properties indicate a more specific method of analysis with a greater sensitivity (*6*).

Radioactivation analysis of sodium is generally based on the formation of sodium-24 by neutron capture. This isotope decays with a half life of 15.0 hours and can be measured either by its 2.75-m.e.v. gamma ray or by the coincidence measurement of the cascade of this gamma ray and the one of 1.37 m.e.v. In most cases it is sufficient to discriminate against gamma rays of less than 2 to $2^1/_2$ m.e.v. (*11*) and to measure the gross activity of radiation above this level. Further differentiation between sodium-24 and other activities in the same energy range is made by following the half life.

When sodium occurs in a complex matrix, sodium-24 activity frequently forms only a small part of the gross activity of a highly active sample, and analysis by radioactivation without chemical processing is then hindered by overloading the detector, paralyzing it for most of the counting time. Electronic discrimination at a preset energy level then becomes difficult, if not altogether impossible. In such cases there is a decrease in accuracy and sensitivity, and hence the need arises either for chemical separations or, if nondestructive analysis is essential, for a detector insensitive to gamma radiation below about 2 m.e.v. The photodisintegration of deuterium and the emission of photoneutrons require gamma ray energies greater than 2.23 m.e.v. This suggests that a detecting system based on counting the emission of photoneutrons from deuterium would be naturally biased and would be entirely insensitive to energy quanta below the photoneutron threshold of 2.23 m.e.v. Such a detector would have an additional advantage because the emitted neutrons can be counted without interference from other radiations and may be detected against any beta- or gamma-ray background.

The number of radionuclides which emit gamma rays of energy greater than 2.23 m.e.v. is relatively small and their number is still further reduced when only those with half lives within a factor of about 10 of that of sodium-24, say 1 to 100 hours, are considered as possible sources of photoneutron emission from deuterium. Thus the counting of photoneutrons emitted from the interaction between the high energy gamma rays of sodium-24 and deuterium can form the basis for the assay of sodium-24 and the determination of sodium by neutron radioactivation. The emission of photoneutrons from deuterium was used for the analysis of deuterium in water samples (*4*, *9*) when their neutron activities were compared with those of standards placed as targets around an intense source of sodium-24. The present method for sodium analysis is the same in principle, but has the roles of source and target interchanged. That is, whereas for deuterium analysis the source is constant and the target is the unknown, here the source is unknown and the target constant.

The Sample. It is clear that the form of the sample is immaterial. For optimal conditions it is undesirable that the sample should contain large quantities of neutron absorbers, or should contain material which could lead directly to neutron emission. It would also be inconvenient if the sample contained relatively large amounts of material which on neutron radioactivation would emit high-energy gamma rays.

Sample components which could lead to a higher neutron count are nuclides undergoing spontaneous fission and alpha-particle emitters inducing (α,n) reactions on light elements in the sample and container. Direct interference by delayed neutrons is not serious since all delayed neutron emitters have half lives less than about 1 minute and they may be allowed to decay. Samples which contain beryllium would certainly lead to high results due to the production of photoneutrons by gamma rays above 1.67 m.e.v., the threshold for photoneutron emission from beryllium. The extent of interference from the above sources can be checked experimentally and will be discussed later.

High-energy gamma-ray emitters with short half lives of, say, less than 1 hour, can be left to decay without losing too much activity of sodium-24, while those with half lives longer than 100 hours would add a nearly constant count rate during the period of measurement and this can be treated as part of the background. Radionuclides falling between these groups, such as 2.6-hour manganese-56 and 40-hour lanthanum-140, can have their presence corrected for by following the decay of photoneutron emission. The only serious source of interference appears to be from gallium-72 which emits high-energy gamma rays and decays with a half life very close to that of sodium-24. It would appear that the accuracy of the method for sodium analysis would be affected if gallium is present in the sample. Interference from the presence of fission products in the sample during measurement is expected but can be checked experimentally.

Irradiation Conditions. Besides being produced by neutron capture in sodium, for which the thermal neutron, cross section is 536 mb. (*5*), sodium-24 can be produced with fast neutrons by an (n,α) reaction on aluminium or an (n,p) reaction on

Reprinted from **ANALYTICAL CHEMISTRY**, Vol. 35, Page 1072, July 1963

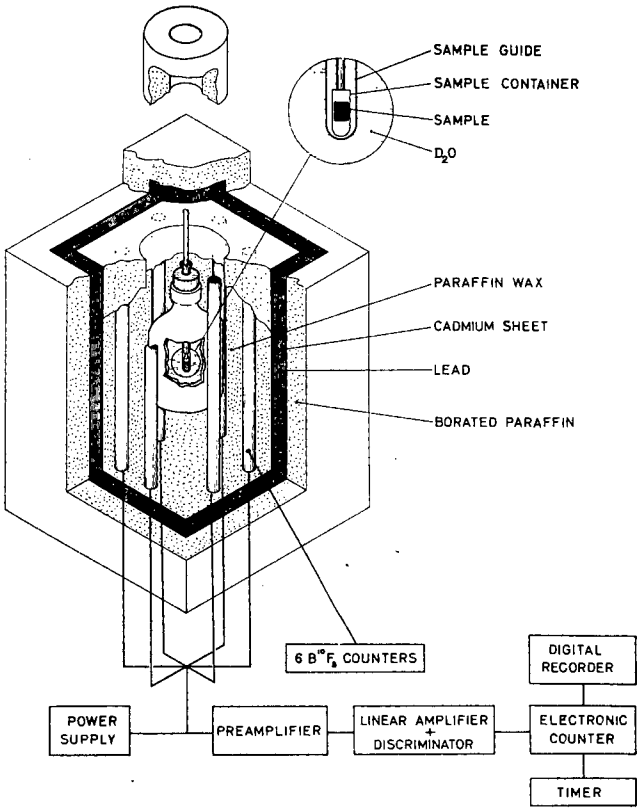

Figure 1. Photoneutron measurement assembly and block diagram of electronic circuit

magnesium. The effective cross sections for these reactions with fission spectrum neutrons are 0.6 and 1.2 mb., respectively (*10*). Because the production rate of sodium-24 from these elements in a mixed neutron flux normally available in a reactor (partially thermalized fission spectrum neutron flux) is lower by two or more orders of magnitude than that of the (n,γ) reaction on sodium, mixed fluxes can be used for the analysis of sodium, except where the method is used at its ultimate sensitivity in samples where the aluminium or magnesium content far exceeds the sodium content.

The duration of the irradiation is best adjusted to the approximate sodium content of the sample. However, irradiations lasting longer than about a day do not add significantly to the sensitivity or accuracy of the method

Neutron Detection. To obtain the maximum output of photoneutrons from a source of sodium-24 it is necessary to surround the source with a sufficiently thick layer of deuterium. Since light hydrogen has an appreciable cross section for neutron capture, 0.3 barn, it is desirable to keep its concentration as low as possible. An efficient way to detect neutrons is to count them after they have been thermalized by a moderator such as heavy water, paraffin, graphite, or ordinary water. Ideally, the counters could be immersed in a bath of heavy water, but for economy paraffin wax or graphite could be used as moderator surrounding a volume of heavy water in which the neutrons are produced. A 4-π arrangement of enriched $B^{10}F_3$ proportional neutron counters placed in the moderator around the photoneutron source provides an efficient detection system of very low sensitivity to gamma radiation.

Counting Conditions. The duration of counting depends on the activity of the sample and the precision required. The delay between irradiation and counting is determined by the absence or presence of other activities in the sample and the nature of the radiations they emit, and those interfering activities also determine for how long the sodium-24 decay should be followed. To be able to correct for longlived interferences it is required that the counting equipment be stable over a long period of time. It is desirable that the counting equipment be constructed from materials with low neutron absorption.

EXPERIMENTAL

Samples for analysis were weighed out into polyethylene vials and were irradiated in the Israel Research Reactor No. 1 where thermal fluxes of up to 5×10^{13} neutrons/cm.^{2}-second were available. Because of radiation damage to the vials, the irradiation did not exceed 1 hour. The irradiated sample was dropped into the counting assembly (Figure 1) so as to lie at the center of a flask of 1 liter of heavy water containing more than 99% deuterium. Neutrons generated from this container were counted with a ring of six $B^{10}F_3$ proportional neutron counters connected in parallel to a scaler and supplied from a common high voltage source. The entire assembly was embedded in a block of paraffin wax 40 × 40 × 50 cm. which served as a moderator to thermalize the fast neutrons. Screening from external neutron sources was provided by a structure of bricks of borated paraffin and sheets of cadmium metal, and radiation from extraneous gamma sources was shielded off by a wall of lead bricks on the outside. Pulses from the counters were fed to a recording scaler, the counting period of which was controlled by an electric timer.

The stability of the apparatus was regularly checked with a radioactive neutron source placed in the counting position and the lack of response to gamma rays was checked with a 10-mc. cobalt-60 source which gave no rise in the background count rate [very high cobalt-60 activities gave the expected rise over background due to the 2.5-m.e.v. gamma ray of 4×10^{-5}% abundance (*8*)]. It was incidentally observed that the efficiency of the counters was 6.7% with standard Pu-Be neutron source placed in the sample position.

Although the counters were biased to discriminate against gamma radiation, it was still possible that under intense gamma radiation some spurious counts could be obtained. To remove this source of error the heavy water container was replaced by an identical one filled with natural water, and a measurement was again taken. The difference between the count rate obtained with heavy water and that with natural water gave the photoneutrons' count rate of the source. Since natural water itself contains 0.015% deuterium it was expected that for perfect discrimination against gamma rays, the ratio of the counts obtained with the two waters could be the ratio of their deuterium contents, in this case about 1.5×10^{-4}. The values obtained were in good agreement with this value showing that the counters were sufficiently well biased against gamma rays.

The possible interference from sample materials which themselves could lead to neutron emission was checked and determined in the same way. Thus, samples in which (α,n) reactions or fission could occur, leading to neutron counts not arising from deuterium, were detected and counted with natural water around the sample. The same was true for photoneutron emission from beryllium when that element was present in the sample. In all these cases the photoneutron emission from sodium was given by the differences between the count rates with the heavy water and natural water placed around the sample.

RESULTS

Irradiated samples of pure sodium compounds were counted over long periods of time to check the stability of the apparatus by following the decay of sodium-24. In all cases no deviation

from the 15.0-hour half life was observed. Counting was continued for periods over a week during which time the activity decayed by more than a factor of 2000.

Absolute calibration of the apparatus was carried out by observing the count rate of photoneutron emission from standardized sodium-24 sources. In the experimental apparatus described above, sodium-24 gave one photoneutron count for every 2.45×10^4 disintegrations (Table I).

Samples of known sodium content were irradiated in various fluxes for varying amounts of time, and their photoneutron emission rates were determined in order to calibrate the apparatus and to determine the precision of the method. To obtain sufficiently high counting rates, relatively large amounts of sodium were used for these tests. Table II shows results obtained from such standards, some of which were irradiated simultaneously and others in quick succession in order to obviate errors due to long-term drifts in the reactor flux. The normalized count rates refer to the number of counts per minute obtained per μg. of Na irradiated at a flux of 10^{13} neutrons/cm.^{2}-second for 1 hour. The counts from which the results in Table II were calculated, had a relative standard deviation of about 0.6% whereas the relative standard deviation of the results in the Table is about 1.8% which shows that the counting errors played little part in the result and that the observed precision is the precision of the method, under the prevailing experimental conditions.

The accuracy of the method was checked on a large number of samples of known sodium content ranging from 2 mg. down to 0.3 μg. Some results of these tests are given in Table III.

Table I. Absolute Efficiency of Photoneutron Counting

Sample number	Neutron count rate (min.$^{-1}$)	Activity, d.p.m.	Ratio disintegrations per neutron count
8A	1661	4.042×10^7	2.433×10^4
8B	1674		2.414
9A	1909	4.742	2.484
9B	1955		2.425
10A	2400	5.957	2.482
10B	2452		2.429
11A	2891	6.968	2.410
11B	2834		2.459
12A	3195	7.862	2.461
12B	3233		2.431
13A	3504	8.626	2.462
13B	3548		2.431
14A	3896	9.627	2.471
14B	3912		2.461
			Mean 2.447×10^4
			Std. dev. ±247 (1%)

Table II. Calibration of Photoneutron Count Rate for Sodium Analysis

Weight sodium (mg.)	Irradiation: Duration (min.)	Irradiation: Flux, neutrons/cm.^{2}-sec.	Observed count rate per min. per mg.	Normalized[a] count rate per min. per μg.
3.11	2	7.1×10^{12}	3.792×10^3	15.63
3.29	60	3.2×10^{13}	5.066×10^4	15.83
3.95	2	6.7×10^{12}	3.461×10^3	15.14
4.78	60	3.2×10^{13}	4.912×10^4	15.35
5.21	60	3.2×10^{13}	4.966×10^4	15.52
7.08	2	6.7×10^{12}	3.503×10^3	15.32
12.25	2	6.7×10^{12}	3.635×10^3	15.90
28.48	1	2.4×10^{12}	6.449×10^1	15.75
32.03	2	7.1×10^{12}	3.867×10^3	15.96
			Mean	15.60
			Std. dev.	±0.29 (1.86%)

[a] Normalized to an irradiation of 1 hour at a flux of 10^{13} neutrons/cm.^{2}-sec.

Table III. Some Results of Sodium Determinations

Range	Sodium content (μg.): Present	Sodium content (μg.): Found	Error: μg.	Error: %
10 to 2200	2175.7	2204.0	+28.3	+1.30
	1271.0	1270.1	−0.9	−0.07
	841.8	836.2	−5.6	−0.67
	74.40	74.97	+0.57	+0.77
	20.61	21.00	+0.39	+1.89
	18.16	18.09	−0.07	−0.39
1 to 10	7.34	7.21	−0.13	−1.77
	2.960	2.849	−0.111	−3.75
	2.282	2.281	−0.001	−0.04
	2.010	2.031	+0.021	+1.04
	1.883	1.916	+0.033	+1.75
	1.024	1.088	+0.064	+6.25
<1	0.923	0.896	−0.027	−2.93
	0.712	0.727	+0.015	+2.11
	0.326	0.307	−0.019	−5.83

DISCUSSION

Precision and Sensitivity. The sources of error that affect the precision of the method arise at three stages—the preparation of the sample, its irradiation, and its counting. Because sample preparation requires simple operations the errors inherent in them are considered to be small and of the same order as similar procedures in other analytical methods. For this reason this source of error is not discussed here.

Errors that may arise at the irradiation stage are errors arising from reactor flux variations and difference between irradiation fluxes through the sample and the standard with which it is compared. Relative errors occurring at this stage do not depend on the weight of sodium in the sample as the amount of sodium-24 activity built up in the sample varies linearly with the weight of sodium it contains and with the neutron irradiation flux to which it is exposed. As a result, the values given in Table II can be used as an indication of the precision of the method as a whole since errors due to counting those results do not play an important role, and sampling errors there are assumed to be constant and small.

When the over-all precision for the analysis of small amounts of sodium has to be determined, the additional errors of counting should also be taken into account. These errors arise from the statistical errors normally involved in counting random events, errors due to background activity, and errors due to the presence of other components in the sample that could yield neutron counts.

For a gross sample count of S and a background, B, the standard deviation of the net sample count, $\Delta = S - B$, is given by σ_Δ where

$$\sigma_\Delta = \pm\sqrt{S + B} = \pm\sqrt{2B + \Delta}$$

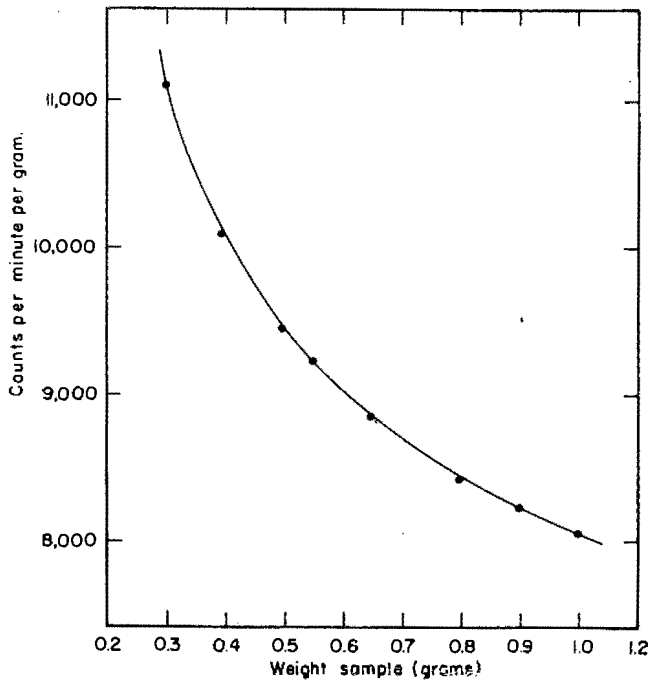

Figure 2. Variation of count rate with sample size, of sample containing high concentration of strongly neutron-absorbing material

Sample contained 0.188% Na and 39.4% w./w. Cd. Curve calcd. for self-absorption of cadmium and points are experimental

With a background of about 12 counts per minute, as measured in this investigation, a precision of ±10% (relative standard deviation) can be obtained for a sample containing 0.34 μg. of sodium which is irradiated for 1 hour at a flux of 10^{13} neutrons per cm.^{2}-second and is counted for about 2 hours. The sensitivity of the method can be much improved by longer irradiations at higher fluxes. A flux of 5×10^{13} n/cm.^{2}-second can be obtained readily. For practical considerations irradiations should not extend much more than a day, say 30 hours or two half lives, when the activity would be about 16 times greater than for the same sample irradiated for 1 hour at the same flux. Hence the sensitivity of the method for the same ±10% precision can be improved to about 0.004 μg. Conversely, it can be shown that the minimum weight which can be determined with a precision of say, 2% (the relative standard deviation of the results under the experimental conditions of irradiation), is about 2 μg., but with the longer irradiation and the higher flux it reduces to about 0.025 μg.

When samples are to be analyzed for sodium in the presence of elements which can cause (α,n) reactions or undergo fission, or in the presence of beryllium which would yield photoneutrons as well, the additional activity can be measured with natural water in place of D_2O in the counting assembly (as was described above). This extra activity is then treated as an added background.

Accuracy. The results in Table III give a clear indication of the accuracy of the method. However, because of the sensitivity of the method, careless handling of the samples can lead to systematically-high results especially when small weights of sodium are analyzed. This was shown by a series of aluminum samples that were irradiated to determine the extent of sodium-24 formation by the reaction $Al^{27}(n,\alpha)Na^{24}$. Irradiation of vials handled only with pincers and tongs gave consistent results (see value in Table IV), but samples handled with gloves showed contamination of about 40% (due to about 0.5 μg. of sodium from the talc used with the gloves). Samples touched with bare hands showed nearly three times as much activity as in the clean vials (equivalent to about 4 μg. of Na).

Systematically-low results were obtained from samples containing appreciable amounts of strongly neutron-absorbing material. Figure 2 shows the decrease of count rate per unit weight sample for a material containing 0.188% sodium and 39.4% cadmium. In the figure the experimental points are shown against the curve calculated for self-absorption of cadmium (*3*) and normalized for the known sodium content of the sample. The addition of a known amount of sodium as internal standard (spike) enables the correct sodium content to be computed.

Interference from Other Elements. The most common elements that occur together with sodium do not interfere with the analysis by photoneutron emission. Potassium-42 emits a γ-ray of 2.44 m.e.v. but only with an abundance of 0.04% of its disintegrations; the amount of potassium would have to be 500 times higher than the sodium content of the sample to introduce an error of 2% to equal the experimental error (precision) of this method. Calcium does not yield any interfering isotope on neutron irradiation while magnesium interferes only in so far as it produces sodium-24 by the reaction $Mg^{24}(n,p)Na^{24}$ with fast neutrons, which is discussed below. Most elements which occur in the anions usually associated with sodium do not interfere because of the absence of gamma rays over 2.23 m.e.v. emitted in their decay, so that sodium can be analyzed in any chemical form.

The main elements which can interfere because of the high-energy gamma rays they emit after neutron irradiation are listed in Table IV. In the same table are listed the calculated and observed photoneutron emission from 1 μg. of element irradiated for 1 hour at a

Table IV. Calculated and Observed Photoneutron Count Rates for Common Elements Likely to Interfere in Sodium Analysis, Compared with Count Rate for Sodium

Element	Isotope	Half life (hours)	Activity[a] Calcd.	Activity[a] Observed	Sodium[b] equivalent, μg.
Sodium	Na^{24}	15.0	14.84	14.90	1
Manganese	Mn^{56}	2.58	12.65	11.99	1.24
Gallium	Ga^{72}	14.1	3.28	3.04	4.90
Lanthanum	La^{140}	40.2	0.515	0.50	2.98×10^1
Magnesium	Na^{24}	15.0	0.00247[c]	0.003[c]	4.97×10^3
Aluminum	Na^{24}	15.0	0.00142[c]	0.0017[c]	8.76×10^3
Potassium	K^{42}	12.4	0.00059	0.00058[d]	2.53×10^4

[a] Normalized counts per minute for 1 μg. of metal irradiated for 1 hour at a thermal neutron flux of 10^{13} n/cm.^{2}-sec. and counted 1 hour after irradiation.

[b] Wt. element in micrograms yielding a neutron count rate equivalent to 1 μg. of Na 1 hour after the end of irradiation.

[c] For a fission-spectrum neutron flux of 10^{12} n/cm.^{2}-sec. Assuming a thermal to fission flux ratio of 10:1.

[d] Measured for "Analar" grade $KHCO_3$ containing approximately 0.03% Na and corrected for the sodium-24 contribution.

thermal neutron flux of 10^{13} neutrons/-cm.^{2}-second, and counted 1 hour after the end of irradiation. The calculated values were obtained from the measured efficiency for sodium-24 gamma rays of 2.75 m.e.v. corrected for the cross section of the deuterium (γ,n) reaction (*7*) for the energy of the gamma ray concerned. The observed results are in very good agreement with the calculated values. Column 6 of Table IV gives the weight of element in micrograms necessary to produce a photoneutron count rate equivalent to that of 1 μg. of sodium, both being irradiated for 1 hour at a thermal flux of 10^{13} neutrons/cm.^{2}-second and counted 1 hour after irradiation. From these values it is clear that the determination of sodium offers some difficulties in samples where the manganese or lanthanum concentration is high and is almost impossible in samples containing gallium as long as the gallium-72 is not removed before counting. Naturally, the shorter-lived interference from manganese-56 can be reduced by waiting for a longer time before counting.

Depending on the nature of the interfering element, it is frequently possible to alter irradiation conditions to improve the ratio of sample to interference count rates. Thus, the photoneutron count rate of a sample containing equal weights of sodium and manganese irradiated for 1 hour will, according to the values in Table IV, consist of almost equal contributions from the two components, at the start of counting. If, however, the same sample is irradiated for a longer time, say 10 hours, even at a lower flux, the relative contribution of sodium at the start of counting is doubled. On the other hand, if the sample is rich in lanthanum, short high-flux irradiations are preferable because long irradiations will favor the relatively higher yield of the longer-lived nuclide.

Aluminum and magnesium which produce sodium-24 by fast neutron reactions obviously interfere in the analysis for sodium. From Table IV it can be seen that an aluminum content about 175 times that of sodium and a magnesium content of about 100 times that of sodium, would only add about 2% to the photoneutron count rate. However, the values given in Table IV do not reflect how little the true extent of interference is, since both aluminum and magnesium results have been normalized to a fission spectrum neutron flux of 10^{12} neutrons/cm.^{2}-second, and compared with that for a thermal neutron flux of 10^{13} for sodium. In an actual irradiation with a mixed flux (partially moderated fission spectrum neutron flux), the interference from these two elements is still further decreased when the ratio of thermal to fast neutrons is more than 10. Sodium analysis in large concentrations of aluminum and magnesium can still be carried out if the samples are irradiated first unshielded and then shielded with cadmium. The cadmium ratio for sodium was measured and found to be 45.8 ± 0.8. (This result was obtained for an irradiation flux consisting of fast and thermal neutrons in the unusually high ratio of about 1:3.) As the sodium-24 production from Al or Mg is unaffected by the cadmium screen, the difference between the two results enables the sodium content to be calculated.

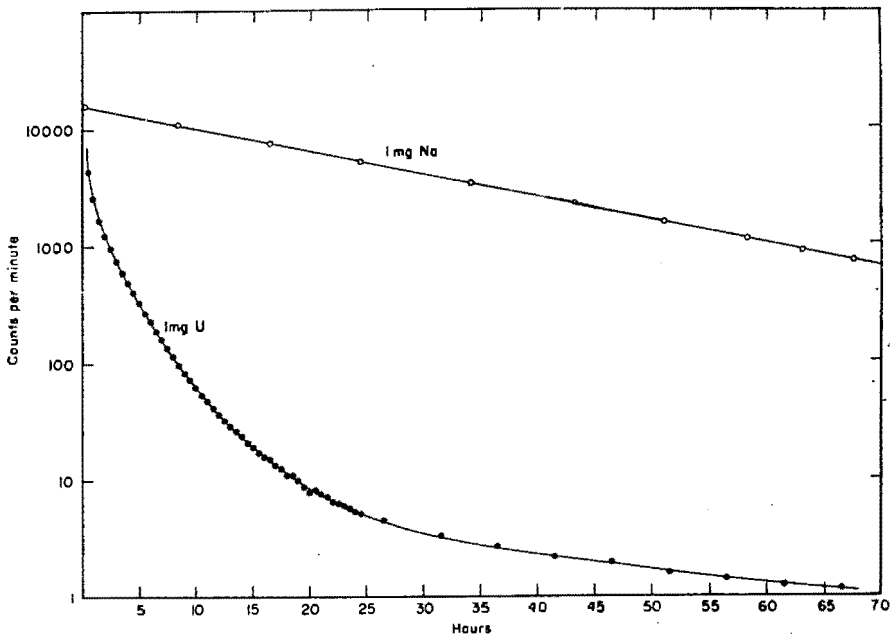

Figure 3. Comparison of photoneutron count rate from 1 mg. of sodium and 1 mg. of natural uranium after irradiation for 1 hour at flux of $10^{13}n/cm.^2$-sec.

When samples contain uranium, the formation of fission products on neutron irradiation could lead to higher photoneutron emission. The count rates obtained from 1 mg. of natural uranium and from 1 mg. of sodium both irradiated for 1 hour at a neutron flux of 10^{13} neutrons/cm.^{2}-second are compared in Figure 3. Although shortly after irradiation the count rates are comparable, the fission product decay is so much faster than that of sodium, that 15 to 20 hours later, the count rate of sodium is about 400 to 800 times greater. So even if uranium and sodium are present in equal proportions in the sample to be analyzed, it is sufficient to wait for about one half life (15 hours) to eliminate the interference altogether. The small amounts of uranium normally present in samples assayed for sodium obviously do not interfere. The determination of sodium in the presence of high concentrations of uranium is still possible for uranium concentrations up to 10 times that of sodium, at which concentration the mixed fission products would contribute a little more than 1% to the sodium count rate, 20 hours after irradiation. If the ratio of uranium to sodium (by weight) exceeds 10, the error due to the presence of fission products becomes large, and nondestructive analysis by this method is then possible only if an accurate analysis of uranium is made and its presence corrected for. Such analysis can be carried out nondestructively as well (*1*) using essentially the same experimental apparatus and counting delayed neutrons.

ACKNOWLEDGMENT

Thanks are due to the operating crew of IRR-1 who attended to the irradiations, to Yoram Gurfinkel and Amos Nutes who helped with the construction of the apparatus, and to Vili Carbunaru for his assistance with the experiments.

LITERATURE CITED

(1) Amiel, S., ANAL. CHEM. **34**, 1683 (1962).
(2) Dean, J. A., "Flame Photometry," p. 163, McGraw-Hill, New York, 1960.
(3) Gilat, J., Gurfinkel, Y., Israel Atomic Energy Comm. *Rept.* IA-756 (1962).
(4) Haigh, C. P., "Second Radioisotope Conference Oxford 1954," Vol. II Butterworth, London, 1954.
(5) Hughes, D. J., Schwartz, R. B., "Neutron Cross Sections," 2nd ed., Brookhaven National Laboratory, Upton, N. Y., 1958.
(6) Koch, R. C., "Activation Analysis Handbook," p. 44, Academic Press, New York, 1960.
(7) Marion, J. B., Fowler, J. L., "Fast Neutron Physics Part I," p. 28, Interscience, New York, 1960.
(8) Morinaga, H., Takahashi, K., *J. Phys. Soc. Japan* **14**, 1460 (1959).
(9) Odeblad, E., *Clin. Chim. Acta* **1**, 67 (1956).
(10) Roy, J. C., Hawton, J. J., Atomic Energy of Canada *Rept.* AECL-1181 (1960).
(11) Schroeder, G. L., Winchester, J. W., ANAL. CHEM. **34**, 96 (1962).

RECEIVED for review February 11, 196[illegible] Accepted April 29, 1963.

PRINTED IN U. S. A.

No. 7

A critical study of isotopic analysis of uranium by radioactivation using the method of delayed neutron counting

S. AMIEL and M. PEISACH, Department of Nuclear Chemistry, Israel Atomic Energy Commission

Activation analysis methods are suitable for the isotopic analysis of uranium because of the differences in the type of neutrons required to cause fission of the two main isotopes and the large fission cross section of the less abundant, though important isotope-U^{235} with slow neutrons. A critical study of the factors affecting the precision of determining the ratio U^{235}/U^{238} has been undertaken. The method investigated was the delayed neutron emission method [1]. It was concluded that when the total uranium content was known, the isotopic ratio can be determined with a precision of ±1%. If the total uranium content is not known, the same precision is obtainable in samples of up to 5 atom -% U^{235}, with lower precision up to about 10 atom -%, but the method fails for higher enrichment of U^{235}. Corrections are made for reactor neutron energy and flux variations, self shielding, coincidence losses, sample size and shape etc. The advantage of the delayed neutron counting technique is discussed.

REFERENCES

1. Amiel, S., 1962, Anal. Chem., 34, 1683.

No. 8

THE DETERMINATION OF GOLD COATING THICKNESSES BY PROTON SCATTERING

by

M. PEISACH and D. O. POOLE*

OPSOMMING

'n Metode word beskryf vir die nie-vernietigende bepaling van oppervlaktelae goud met 'n dikte tussen 0 en 10μg/cm^2 op aluminium, mika, staal en tinplaat deur elastiese verstrooiing van protone, met behulp van halfgeleier detektore. Die presisie van die metode is $\pm 0{\cdot}2\mu$g/cm^2 en die gevoeligheid is beter as 5×10^{-10}g goud by die bestralingspunt.

SUMMARY

A method is described using semi-conductor surface barrier detectors for non-destructively measuring the thickness of surface films of gold in the range 0 to 10μg/cm^2 on aluminium, mica, steel and tin plate, by elastic proton scattering. The precision of the method is $\pm 0{\cdot}2\mu$g/cm^2 and its sensitivity is better than 5×10^{-10}g gold at the point of incidence of the proton beam.

INTRODUCTION

The limited penetration of charged particles with energies of a few MeV makes them suitable for the investigation of surface layers. By measuring the energy spectrum of the particles scattered from a monoenergetic incident beam, the chemical composition of surfaces has been determined.[1, 2, 3, 4, 5] Such measurements required the use of a magnetic spectrometer set to receive scattered particles of a predetermined energy; by varying the magnetic field in the spectrometer the entire energy range could be scanned.[2]

Modern developments in the manufacture of solid state devices has simplified the instrumentation for measuring energies of charged particles with the result that a multi-channel analyser can record the entire energy spectrum of the scattered particles in a single irradiation. The negligible cost of solid state detectors, makes them more readily available for analysis. Despite the fact that their resolution cannot match that of the more expensive magnetic spectrometers, the advantages of small size, low cost and speed of analysis, outweigh this disadvantage.

THEORY

For non-relativistic proton energies, the Rutherford equation states that P, the differential scattering cross-section per unit solid angle at a mean scattering angle θ, for a target material with nuclear charge Z_2e is,

$$P = \frac{(Z_2 e^2)^2}{16\, E^2 \sin^4\left(\frac{\theta}{2}\right)} \text{ cm}^2 \quad \ldots \quad (1)$$

* S.A. Atomic Energy Board, Isotope Unit.

where E is the incident proton energy. After being scattered, the energy of the proton, E', is given by

$$E' = E\left[1 - 2\,(1 - \text{Cos}\,\theta)\frac{M_1 M_2}{(M_1 + M_2)^2}\right] \quad .. \quad .. \quad .. \quad .. \quad .. \quad (2)$$

where M_1 is the mass of the bombarding particle (proton) and M_2 of the scattering nucleus. Thus, for a monoenergetic proton beam scattered off a monolayer of an isotopic target through a predetermined angle, the energy spread in the measured spectrum is determined by the resolution of the detecting system, σ, the standard deviation of a normal distribution.

For finite target thicknesses, the incident proton loses energy by ionization at a rate $\frac{dE}{dx}$ and similarly, after being scattered, at a rate $\frac{dE'}{dx}$, where the average energy loss $\frac{dE}{dx}$ per cm path length is given,[6] by

$$-\frac{dE}{dx} = \left[\frac{4\pi e^4 Z_1^2}{m_0 v^2}\right] \text{N.B.} \quad .. \quad .. \quad .. \quad .. \quad .. \quad .. \quad .. \quad (3)$$

where $B = Z_2 . \text{Ln}\,\frac{2m_0 v^2}{I}$ for non-relativistic velocities and $Z_1 e$ is the charge of the bombarding proton, N the number of atoms per cm^3 material, e and m_0 respectively the charge and rest mass of the electron, v the velocity of the incident particle and I the average excitation potential of the stopping material, usually determined empirically.

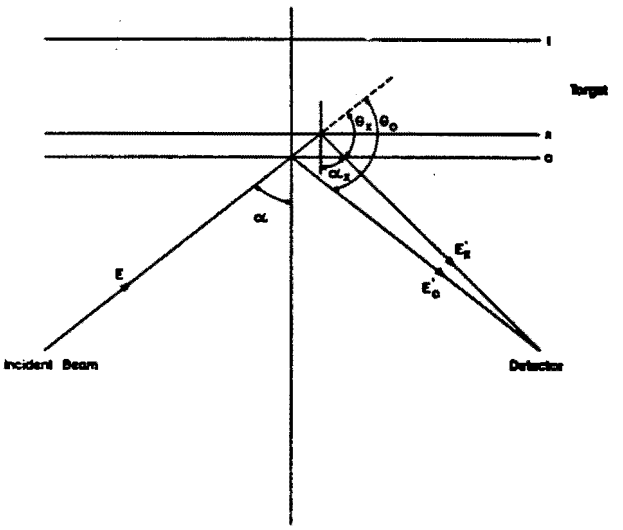

FIG. 1—Diagrammatic representation of scatter from a layer x within the target thickness t.

The energy, E'_x of a proton scattered from a depth x below the surface (see Fig. 1) is

$$E'_x = E - \frac{dE}{dx}\frac{x}{\cos a}\left[1-2(1-\cos\theta_x)\frac{M_1M_2}{(M_1+M_2)^2}\right] - \frac{dE_x}{dx}\frac{x}{\cos a_x} \quad .. \quad (4)$$

The energy spectrum measured by the detector will show the same normal distribution for each energy E'_x and the whole energy spectrum will be the sum of all such distributions for x ranging between 0 and t, the thickness of the target. Fig. 2 represents the

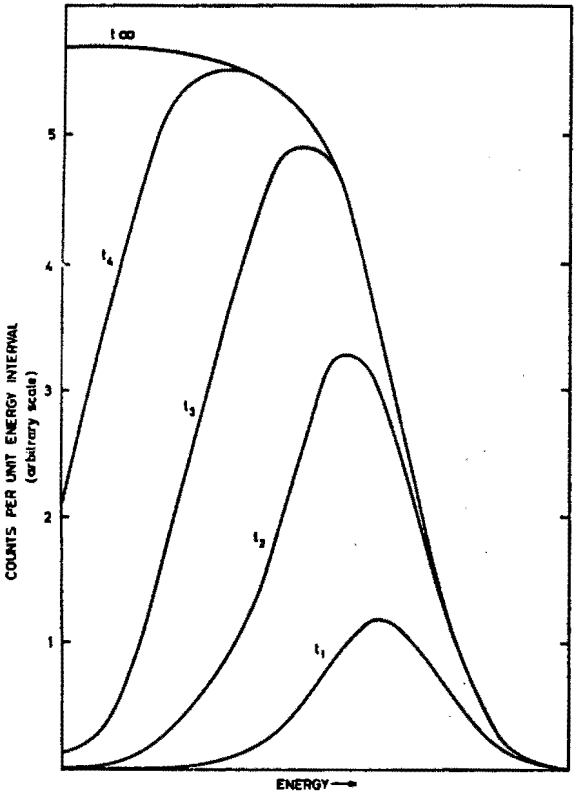

FIG. 2—The shape of the energy spectrum of scattered protons for increasing target thickness.

change in shape of the energy spectrum for increasing target thicknesses, t_1, t_2, t_3 and t_4. Targets thicker than t_4 for which $E'_x=0$, are called "infinitely" thick and would produce a spectrum consisting of a plateau terminating in a single step, (as t_∞ is in Fig. 2) the position of which is given by equation (2) and which has a slope $(\pi\sigma)^{-1}$ at its inflexion point.

When one element is coated on another, the energy of the proton beam incident

on the underneath layer is degraded an extent given by equation (3), resulting in a shift of the maximum scattered energy from this layer. Should a thin layer of a heavy element cover a thick backing of a light element, the spectrum of the scattered protons will show a peak separated from the step by an energy difference depending on the mass difference between the heavy element and the backing; on the other hand a film of a light element will show up as a peak on the plateau of the curve. In both cases the area under the peak gives a measure of the surface thickness. In Fig. 3 the ratio of

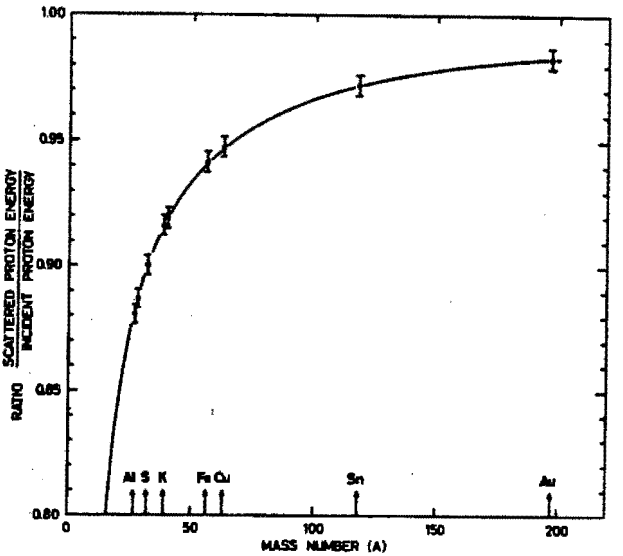

FIG. 3—The variation of scattered proton energy with the mass number of the scatterer. Experimental points are plotted on a calculated line. The indicated range represents resolution limits.

the maximum scattered energy to the incident proton energy is plotted as a function of the mass of the scattering nucleus for a scattering angle of 135°. This curve shows that the energy difference between protons scattered from nuclei with unit mass difference, decreases rapidly as the mass numbers of the target nuclei increase. Because the measuring system has a finite resolution, it is clear that heavy elements would be more difficult to distinguish from each other, than light elements. Similarly, if the energy of the scattered protons is used as a criterion for establishing the identity of an element on the surface, the error in the experimental determination of the mass number would be larger the heavier the element.

In this work a heavy element, gold, was measured on backings of light, medium and moderately heavy elements.

EXPERIMENTAL

Construction of solid state detectors.—N-type silicon of resistivity 1500 ohm-cm and cut along the (1,1,1) plane into discs 20 mm diameter and 1 mm thick were

obtained, lapped on both sides, from Messrs. Wacker Chemie GMBH. of Munich, Germany. The silicon was used to prepare surface barrier type[7] charged particle detectors with an active area of about 0·2 cm^2. These were mounted on brass supports which also held a collimating disc of brass with an aperture of about 0·07 cm^2 fixed 5 mm in front of the detector. The complete assembly was mounted inside a scattering chamber such that the active surface of the detector was 15 cm away from the point of scatter.

The resolution of each detector was measured using the 5·48 MeV alpha particles from a standard americium-241 source as supplied by The Oak Ridge Technical Enterprises Corporation. Typical values of the full width at half height ranged from 25 to 30 keV, which corresponds to a resolution of about 0·5%.

Preparation of surfaces.—Gold films of varying thicknesses were evaporated on clean metal surfaces of aluminium, stainless steel and tin plate, and on mica. The area of the deposit was well-defined by the use of accurately cut mica masks.

Calibration of surface thicknesses.—1. By radiotracers. Gold was irradiated at Saclay, France, for a short time to produce low specific activity radiogold. Portions of this gold were used to prepare samples as above. The gold thickness of the film on each sample was deduced from the measured activity. After the radiogold had decayed, the samples were preserved for use as standards.

2. By radioactivation. Samples of gold deposits, after being measured by proton scattering, were sent to Saclay, France, for radioactivation, where they were irradiated in a thermal neutron flux of $2·2 \times 10^{12}$ neutrons/cm^2sec for 3 hours. It was found that for deposits on aluminium and mica, the gold activity could be measured non-destructively without interference. The gold deposits on tin, however, could only be determined by spectrum stripping because of the contribution to the total count rate from the radiotin. Serious interference on the other hand was found from activities in stainless steel; consequently, the gold on such samples had to be separated chemically before counting.

Measurement of scattered protons.—The scattering chamber in which this investigation was carried out, is based on a design used at Harwell. The insulated target support, could be rotated, but in this investigation it was kept at 75° to the incident beam. Two targets could be mounted on the support and each could be placed in the beam in turn. The detector was mounted on an arm which could be rotated around the target, thus enabling angular variations to be measured. A current integrator measured the total current falling on the target. The beam could also be passed through the scattering chamber into a Faraday cup via a hole between the two mounted targets to check the total beam current directly.

The solid state detector was mounted on the detector arm and amplified pulses from it were recorded by a multichannel analyzer, or by a scaler coupled to a single channel analyzer set to pass pulses corresponding to a predetermined energy range.

Proton beams of energies 1·0, 1·5, 2·0, 2·5 and 3·0 MeV were obtained from the SUNI Van de Graaff accelerator. To prevent damage to the targets, the beam current was as low as could be maintained in the accelerator, and was reduced still further by two collimating plates which allowed a parallel beam of 0·5 mm^2 cross-sectional area to pass through to the target.

Preliminary tests showed that with proton energies above 3 MeV, inelastic scattering effects became marked. Although the relative energies of incident and scattered proton beams remain constant, the absolute energy difference increases with increasing energy (see equation [2]). For this reason the incident proton energy of 2·5 MeV was chosen. The scattering angle was selected by taking measurements at 45°, 90°, 105°, 120° and 135°. Although the cross-section decreases with increased scattering angle, (see equation [1]) the energy difference between the incident and scattered proton also increases, (see equation [2]) making it easier to detect and count scattered protons at backward angles. The geometrical arrangement inside the scattering chamber made it impossible to measure at angles much greater than 135°.

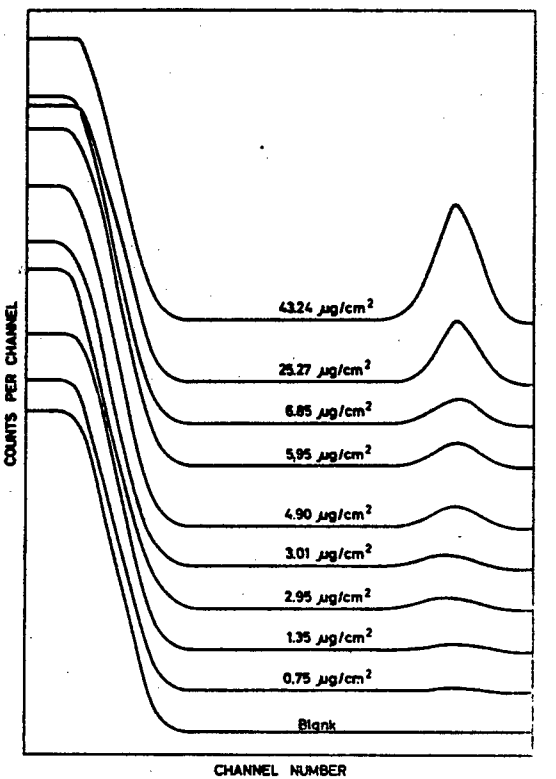

FIG. 4—Energy spectra of protons scattered from increasingly thick gold films on aluminium. To facilitate comparison, the zero of each curve has been shifted vertically by an arbitrary amount.

RESULTS

Typical spectra obtained for increasing thicknesses of gold film on aluminium plates are shown in Fig. 4. Similar families of curves were obtained for gold films on backings of mica, steel and tin plate, typical examples of which are shown in Fig. 5.

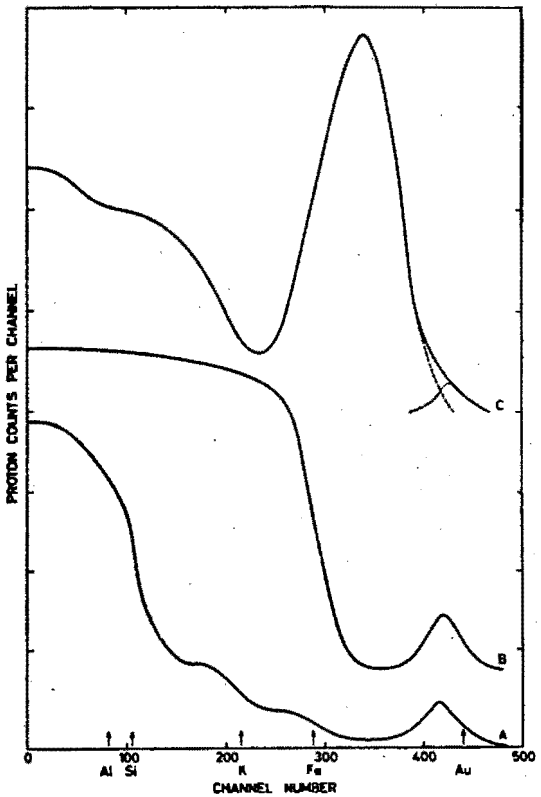

FIG. 5—Energy spectrum of protons scattered from a gold film on mica (A), showing steps corresponding to Al, Si, K and Fe, stainless steel (B) and tin plate (C). In C the gold spectrum (dotted curve) is not resolvable from that of the thick tin coating (dashed line).

Whilst the energy of the leading edge of the gold peak remained fixed, that of the backing increased with increasing atomic number. The energy corresponding to the inflexion point of the front edge of the plateau representing the backing material, is shown in Fig. 3, plotted together with the calculated energy variation with mass number. These results confirm that gold can readily be resolved from light or moderately light elements, but when the mass number of the backing is about 100 or more, resolution of gold becomes difficult (see Fig. 5C).

The number of proton counts, as given by the area under the gold peak was shown to be proportional to the gold film thickness, as measured with radiotracers and by

radioactivation analysis as described earlier. The calibration curve for films on aluminium up to 10μg/cm^2 thick is shown in Fig. 6 where the dotted lines show the range for one standard deviation.

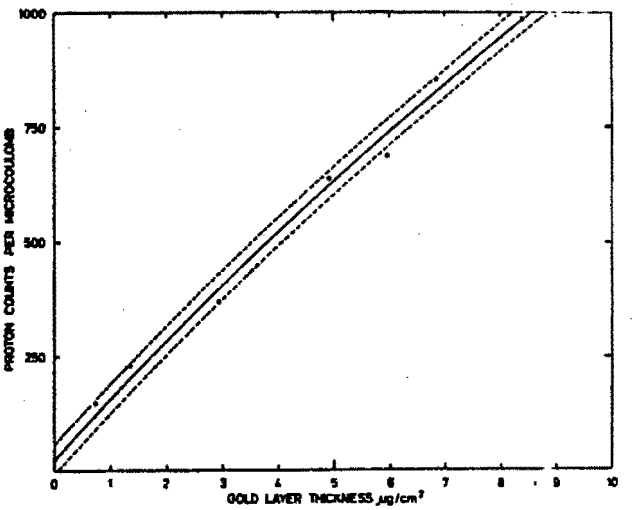

FIG. 6—The variation of scattered proton counts with gold film thickness.

The analyses of various samples are given in Table I.

DISCUSSION

Comparison with earlier scattering methods.—The use of semi-conductor detectors in place of magnetic spectrometers for the measurement of the energy of scattered protons simplifies the experimental procedure and shortens the time required for surface analysis. With the aid of these devices it has been shown that the entire energy spectrum can be measured in one operation. When a single element is to be measured, as in the present work, the instrumentation can be further simplified by the use of a single channel analyzer set to receive pulses corresponding to the entire energy range under the peak, in place of a multichannel analyzer. Because of the small size of the detecting system, the potential use of the method is much increased, especially for extra-terrestrial investigations.

The method, in common with earlier scattering procedures, still suffers from the disadvantage that the scattered particle can only be measured *in vacuo*, but its most serious disadvantage is the lower resolution of solid state detectors when compared with that of magnetic spectrometers. It is likely that resolution could be improved with charged particles heavier than protons, and with further development of more suitable solid state devices.

TABLE I

Some comparative results of thickness determinations

Gold thickness $\mu g/cm^2$	
By activation analysis	By proton scattering
0·71	0·91
1·25	1·15
1·35	1·55
1·76	1·60
2·10	2·03
2·93	2·68
4·91	5·04
5·55	5·52
6·84	7·09
8.30	8.47
8.40	8.42
9·31	9·18

Accuracy and precision.—From the results in Table I, the accuracy of the method for analyzing surfaces by proton scattering was shown to be good for gold film thicknesses of between 0 and $10\mu g/cm^2$, the average difference between the two methods being sufficiently close to zero to indicate no bias.

Intercomparison of results and replicate analyses have shown that the precision of thickness measurement is $\pm 0{\cdot}2\mu g/cm^2$ for gold films in the range studied. It is thus possible to use this method to measure gold thicknesses in the microgram/cm^2 range, even when those films are difficult to see. It follows that by using an incident beam with cross-sectional area of 0·5 mm^2, the sensitivity is better than 5×10^{-10}g gold at the position of incidence.

Sources of Error.—Because of the small energy change suffered by the proton on being scattered, the energy spread in the incident beam can be a source of error. For this reason, high stability accelerators such as Van de Graaff machines are suitable; the beam obtained with the SUNI instrument had an energy spread of less than 1 keV at 2·5 MeV. Although, the resolution of the detector was as little as 0·5%, it was still the major factor determining the resolution of the measuring system.

The incident beam has low penetration into the target, so that most of the energy is deposited in a small volume, causing a disproportionately large temperature change at the point of incidence. If the rise in temperature is high enough to cause loss of gold from the surface, the measured surface concentration would be too low. To overcome

this danger, very low beam intensities were used. Currents as low as 1 to 10×10^{-9} amps were obtained by defocussing the incident beam onto the first of two collimator plates and using the second collimator to define the diameter of the beam falling onto the target. This had the disadvantage that it extended the time required for measurement. When the targets had good thermal conductivity, currents as high as 5×10^{-7} amps could be used without "burn through". It is possible that with liquid cooling, the current could be increased appreciably.

As all measurements were determined by integrating the current falling on the sample, errors in the current integration directly affect the measurement. For this reason the incident beam was periodically checked in a Faraday cup placed directly behind the targets.

The relatively large statistical errors due to low count rates which are incurred in the measuring of very thin film thicknesses, can be reduced by increasing the counting time.

Use for qualitative analysis.—The high sensitivity of the proton scattering method for detecting gold on surfaces makes it useful for qualitative analysis. However, the method is not limited to minor components. The results obtained for different backing materials (see Fig. 4) show that the position of the step in the energy spectrum can identify an element provided its atomic weight is sufficiently different from other elements to be resolved by the detecting system.

The curve for gold on mica (Fig. 5A) serves as an example. It shows a series of steps, the inflexion points of which correspond to the elements Al, Si, K and Fe, each a major component of mica.

The authors acknowledge with thanks the assistance of Messrs. Rene Pretorius and Albert Bottega. Dr. R. Cherry is thanked for the loan of the americium-241 calibration source. The staff of the Southern Universities Nuclear Institute is thanked for much valued discussion, advice and criticism, and the patient co-operation of the accelerator operators is gratefully acknowledged.

One of us (D.O.P.) thanks the South African Atomic Energy Board for permission to include his work in this publication.

Southern Universities Nuclear Institute,
Faure.

Received February 22nd, 1965.

REFERENCES

[1] S. Rubin, T. O. Passell, and L. E. Bailey, *Anal. Chem.*, 1957, **29**, 736.
[2] S. Rubin, *Nucl. Instr. Methods*, 1959, **5**, 177.
[3] R. F. Sippel, and E. D. Glover, *Ibid.*, 1960, **9**, 37.
[4] W. M. Buechner, and J. E. Robertshaw, *Trans. Am. Nucl. Soc.*, 1962, **5**, 197.
[5] F. L. Green, M. D. Cooper, and J. E. Robertshaw, *ibid.*, 1962, **5**, 197.
[6] M. S. Livingston, and H. A. Bethe, *Rev. Mod. Phys.*, 1937, **9**, 271.
[7] G. Dearnaley and A. B. Whitehead, *At. Energy Res. Estab.* G. Brit., 1960, Rep. R 3437.

No. 9

THE USE OF SEMICONDUCTOR DETECTORS FOR SURFACE ANALYSIS BY ELASTIC SCATTERING OF ACCELERATED CHARGED PARTICLES

by

MAX PEISACH, DARRELL O. POOLE*
Southern Universities Nuclear Institute
Faure, C.P., South Africa

ABSTRACT

Charged particles with energies of a few Mev and having a limited range in solid material undergo their reactions within a short distance from the surface rather than in the depth of the target and by so doing enable the surface layers of the target to be studied. Such a method of surface analysis has been investigated with protons.

Elastically-scattered protons have proved suitable for the determination of the chemical elements in the surface of solids. Targets were bombarded with a collimated beam of particles at constant energy from the 5.5-Mev Van de Graaff accelerator at Southern Universities Nuclear Institute (SUNI). Scattered particles were analyzed 10 cm from the source at 90° to the incident beam. Other angles are currently under investigation. Elements such as carbon, aluminum, iron and gold were identified and measured on the surfaces of other metals with a sensitivity of the order of 10^{-6} gm/cm^2. The sensitivity of the method increases with increasing scattering angle and with the energy of the incident particle.

By using surface-barrier semiconductor detectors with a window less than 0.05 μ thick the energy of the measured particle is not altered within the resolution limits of the detector. The main advantages of these detectors are their compactness, stability and cheapness that enable surface analyses to be carried out at a fraction of the cost with more usual methods using mass-spectrometry. Their disadvantage lies in the decreased resolution when compared with the more conventional method.

Gold was measured on surfaces of aluminum, quartz, steel, brass and similar metals, and aluminum layers on heavy metals could readily be analyzed. However, the quantitative determination of aluminum on light metals presented difficulties owing to the resolution limits of the detectors. This problem is being investigated with heavier charged particles at comparable energies.

INTRODUCTION

The uncertainty attached to the chemical composition of the surface of silicon for solid-state detectors prompted the investigation of a method suitable for the analysis of surfaces nondestructively. A method has been described (1, 2) using the elastic scattering of protons off surface layers and analyzing their energy spectrum with a magnetic spectrometer. This method has been used to analyze aerosols on aluminum (1), calcium concentrations on glass surfaces (1) and sulphur deposits on niobium (3); a modification using scattered deuterons was also used to analyze organic materials on surfaces (4).

The high cost of the analyzing magnetic spectrometer has restricted the availability of the instrument and hence deterred general exploitation of this method of surface analysis. Modern developments in the manufacture of solid-state devices has removed this restriction as well as simplified the instrumentation for measuring charged-particle energies. The good energy resolution of semiconductor detectors that has made them very useful in other fields is an added consideration; but in this case, because the energy range of scattered particles is small, the high resolution of the magnetic spectrometer is still superior to semiconductor detectors. Nevertheless, the advantages of small size, low cost and speed of analysis outweigh this disadvantage.

This paper describes the use of semiconductor detectors for analyzing surfaces by measuring the energy distribution of scattered protons and alpha particles.

THE PRINCIPLE OF THE METHOD

From the Rutherford scattering equation P the number of charged particles with nuclear charge Z_1e scattered into unit-solid angle at a mean-scattering angle Θ by a target of nuclear charge Z_2e is

$$P = \frac{(Z_1\ Z_2e^2)^2}{16\ E^2\ \mathrm{Sin}^4\left(\frac{\Theta}{2}\right)} \text{ per atom per incident particle} \qquad (1)$$

where E is the energy of the incident particle. The energy E′ of the scattered particle is given by

$$E' = E\left[1 - 2(1-\mathrm{Cos}\ \Theta)\frac{M_1M_2}{(M_1+M_2)^2}\right] \qquad (2)$$

where M_1 and M_2 are respectively the masses of the incident particle and the target material. If scatter takes place from other than surface atoms, the values of E and E′ are degraded to account for loss of energy by ionization within the target.

From Eq. 1 we may deduce that the scatter cross section decreases as the square of the incident-particle energy, and with the scattering angle Θ as $\mathrm{Sin}^4\left(\frac{\Theta}{2}\right)$ but increases as the square of the atomic number of the target. Similarly, Eq. 2 shows that the energy difference between the incident and scattered particle increases with the energy and mass of the bombarding particle. A plot of the ratio $\frac{E'}{E}$ against the mass number of the target nucleus is shown in Fig. 1 for protons and alphas.

*South African Atomic Energy Board Isotope Unit at the Southern Universities Nuclear Institute, Faure, C.P., South Africa.

Reprinted from
Proceedings, 1965 International Conference: Modern Trends in Activation Analysis

To differentiate between targets of different mass numbers M_2 and M'_2, it is desirable to have a wide as possible energy difference between their corresponding values of E′ in order to overcome the inherent resolution limitation of the measuring system. It follows that the use of high-energy heavy-particle beams would be advantageous especially if the scattered particle is measured at a large backward scattering angle. However, since the method is based entirely on elastic scattering, an upper limit is imposed on the bombarding-particle energy to the level where inelastic scattering ceases to be insignificant. An important consideration in the selection of the mass of the bombarding particle involves penetration into the target; if information is sought from layers at a depth from the surface (5), it may be necessary to use light particles even at the expense of resolution.

APPARATUS

The 5.5-Mev Van de Graaff accelerator at SUNI provided proton- and alpha-particle beams which at 2.5 Mev had a maximum energy spread of 1 kev. The current falling on the target was controlled to between 1 and 10 nanoamps and collimated to produce a beam with cross-sectional area of $\sim$ 0.5 mm^2. Larger currents were found to cause a disproportionately large temperature rise at the point of incidence resulting in local vaporization from the surface and correspondingly low results for thin-film analysis. When the target films had good thermal conductivity, currents as high as 500 nanoamps could be used without "burn through."

Initial experiments were conducted in a scattering chamber which allowed measurements to be made at a scattering angle of 90° only. However, a more versatile chamber, constructed subsequently, made provision for a continuously variable detector position that because of the physical size of the detector assembly limited the maximum scattering angle to 135°. The target mount made provision for two targets, each of which could be placed in the beam in turn, and had a port between them to allow direct measurement of the beam current in a Faraday cup at the rear of the chamber.

From Messrs. Wacker-Chemie G.M.B.H., Munich, 1500 ohm-cm n-type silicon was obtained and used to construct surface-barrier type semiconductor detectors (6) with an active area of $\sim$ 0.2 cm^2. The resolution as measured by the 5.48-Mev alpha particle of Am^{241} was 0.5%. The window thickness was less than $\sim$ 0.05 μ which gave rise to a maximum energy loss of $\sim$ 50 kev from a 2.5-Mev particle. This almost constant energy loss over the energy range of interest occurred in both measurement and calibration and was automatically compensated for. However, spectrum distortion due to straggling was estimated to be less than 10 kev over the same range and could not be detected within the resolution limits of the detecting system. The detector was mounted on a brass support 5 mm behind a collimator with an aperture of $\sim$ 0.07 cm^2. The whole assembly was fixed inside the scattering chamber 15 cm from the point of scatter on the target. Pulses from the detector were passed through a charge-sensitive preamplifier to a 512-channel analyzer or a single-channel analyzer preset as required.

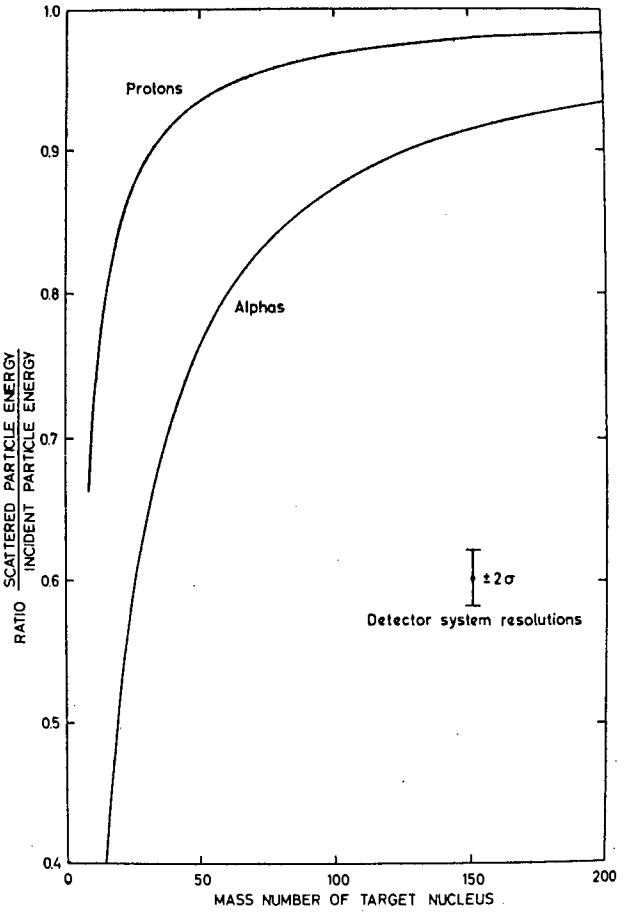

Fig. 1—Calculated energies of alpha and proton particles scattered through 135° as a function of scattering nucleus mass. The range shown represents the resolution limits of the detecting system

A current integrator connected to the target mount made it possible to compare different targets on the same backing material directly. This method of current measurement gives relative results because it also responds to secondary electron emission from the target; the absolute current can be obtained from Faraday-cup measurements.

MEASUREMENT OF GOLD FILMS

In order to place the scattering results on a quantitative basis calibrated gold films were deposited on various backings. The calibration was carried out by evaporating radiogold onto a known area of the sample plates and measuring the radioactivity of the deposit. A second method of standardization after the scattering measurements had been taken was by neutron-activation analysis of a known area of surface. In the latter method the gold was counted nondestructively on backings of aluminum, mica and tin plate, but chemical separation was needed to analyze the gold deposits on steel.

Proton scattering. Proton beams suitable for surface analysis ranged from 1 to 3 Mev above which energy inelastic-scattering effects became marked. Because higher-energy beams were advantageous most of the experiments were carried out with 2.5 Mev protons.

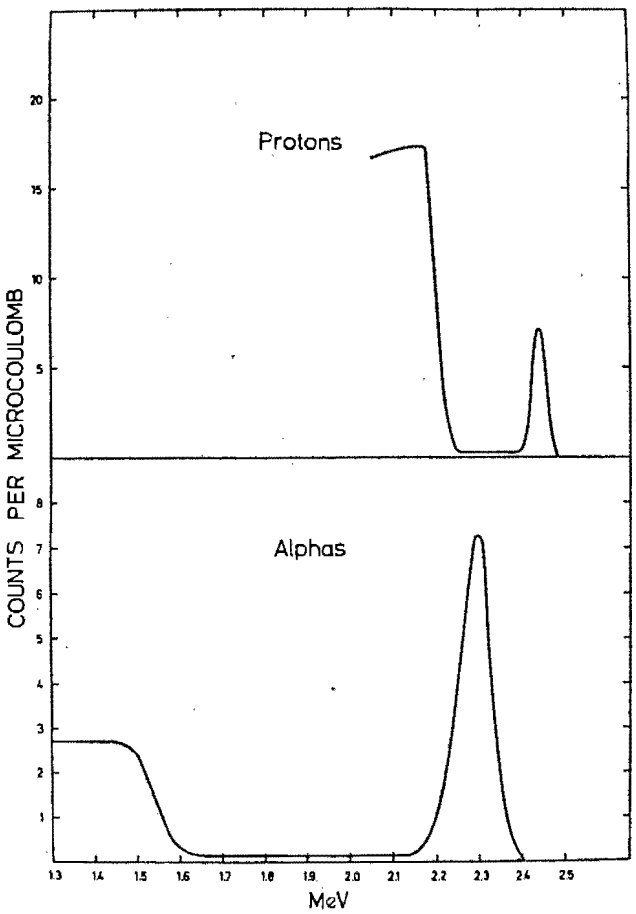

Fig. 2—Energy spectra obtained for the irradiation of gold on aluminum targets with 2.5-Mev alpha and proton particles

Proton-scattering measurements carried out on targets of different thicknesses of gold film on aluminum (7) showed that the gold peak in the energy spectrum of the protons could be readily resolved from the plateau due to the backing. The area under the gold peak (see Fig. 2) was directly related to the gold-film thickness as is shown in the calibration curve in Fig. 3. Errors within one standard deviation are shown dotted in the figure from which it can be deduced that the thickness of gold in the range 1 to 10 $\mu g/cm^2$ can be measured with a precision of $\pm$ 0.2 $\mu g/cm^2$. However, it should be noted that the measured error reflects the overall error of both the method of proton scattering and of neutron-activation analysis. From a knowledge of the errors involved in neutron-activation analysis it may be concluded that the errors involved in the scattering method alone are considerably smaller.

The values plotted in Fig. 3 for gold on aluminum were not directly applicable to gold on other backings because the apparent current as measured by the current integrator included secondary electron emission from the target that varied from backing to backing. For routine analyses it was more convenient to preset the current integrator to sum a suitable total current, usually 40 microcoulombs, at the completion of which it automatically switched off the counting system measuring proton

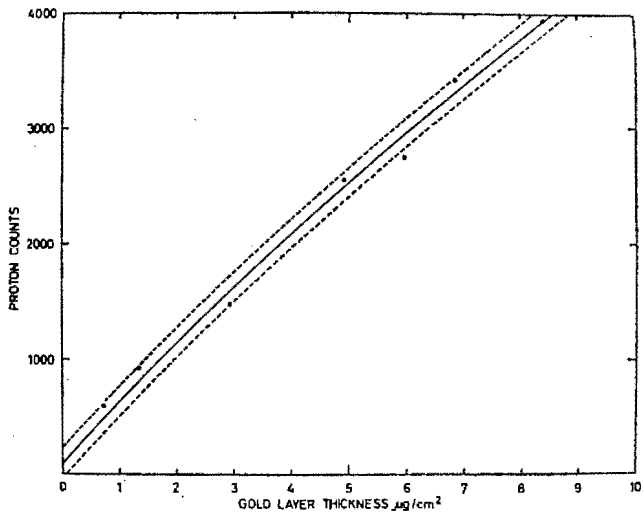

Fig. 3—Calibration curve for gold thickness on aluminum by proton scattering

counts. For the same reason the ordinates in Fig. 3 represent proton counts.

Similar calibration curves were obtained for other backings, but the energy spectra for scattered protons differed from that in Fig. 2; the front edge of the plateau moved to higher energies with increasing mass number until the gold peak could no longer be resolved from plateaux corresponding to mass numbers greater than about 100.

Alpha scattering. To utilize the advantage offered by heavier bombarding particles the same targets were irradiated with alpha particles of similar energy for comparison. Figure 2 shows the difference between the spectra obtained. The most obvious difference is the much larger energy range of scattered alphas as compared with scattered protons that allows for some relaxation of the severe stability criteria demanded of the electronics of the measuring system. Also noticeable is the much lower count obtained from the aluminum backing in the case of alpha scattering as compared with proton scattering. This emphasizes the higher penetration of protons. An example of the response of the measuring system is shown in Fig. 4 for increasing gold film thicknesses on aluminum, measured by alpha scattering; this calibration curve is shown in Fig. 5.

Similar families of curves were obtained for different backings, and examples with approximately equal gold thicknesses are shown in Fig. 6. These examples for aluminum, steel, brass and tin plate show similar effects to those obtained with protons. In both cases the maximum scattered-particle energy from the backing material varied in accordance with the plots in Fig. 1.

Of practical importance is the observation that whereas gold could not be resolved from tin plate with protons, the use of alpha particles makes analysis of gold films on tin plate possible. The theoretical plot in Fig. 1 demonstrates that to resolve two peaks in the energy spectrum of scattered particles, corresponding to two elements with mass numbers M_2 and M'_2, should be easier with alpha particles than with protons because all bar the

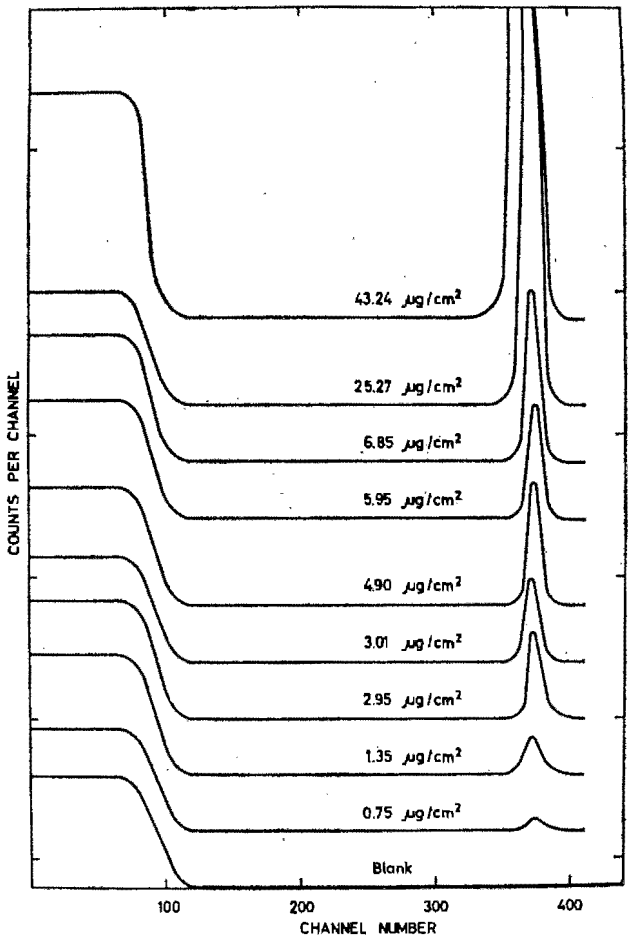

Fig. 4—Recorded spectra for increasing thicknesses of gold on aluminum using 2.5-Mev alpha particles

very lightest elements with A<7. Experimental verification of this fact was obtained by attempting to analyze a special target of a thin layer of tin over a thin layer of gold on a backing of aluminum. Comparative results for 2.5-Mev protons and alphas are shown in Fig. 7.

MEASUREMENT OF OTHER THIN SURFACES

The above investigation of gold films served to establish the use of semiconductor detectors for surface

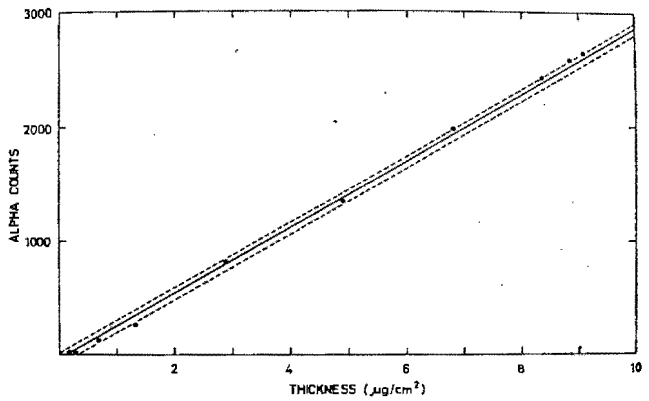

Fig. 5—Calibration curve for gold thicknesses on aluminum by alpha scattering

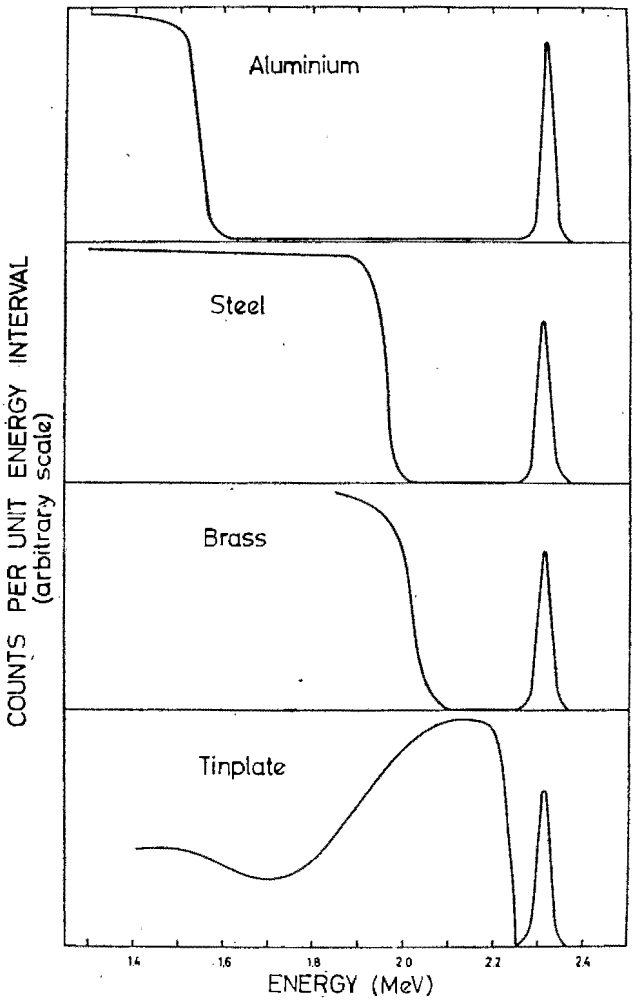

Fig. 6—Alpha scattering from gold showing the effect of increasing mass number of backing material

analysis of heavy element films on backings of lighter elements. The problem that prompted this investigation being borne in mind, attention was diverted towards lighter elements. Two representative cases may be mentioned: tin plate and aluminum layers on iron.

In Fig. 6 the energy spectrum of alpha particles scattered from tin plate (tin on iron) shows a broad maximum corresponding to the relatively-thick tin coating. Also the energy corresponding to the inflection point for iron is observed to be considerably lower than for the case of steel in the same figure. This energy shift corresponds to an overall loss of energy for an alpha particle traversing the tin layer and hence affords a method for determining the coating thickness. The method is only applicable to coatings thick enough to cause an appreciable shift in the energy spectrum of scattered particles from the backing material. In the example cited the energy shift was about 300 kev corresponding to approximately 600 $\mu g/cm^2$. By comparison previous work with gold films in the range 1 to 10 $\mu g/cm^2$ should result in a maximum shift of a few kev which is much lower than the resolution limit of the detecting system and would therefore be undetectable.

When the mass number of the backing exceeds that of the surface element, the energy spectrum of scattered

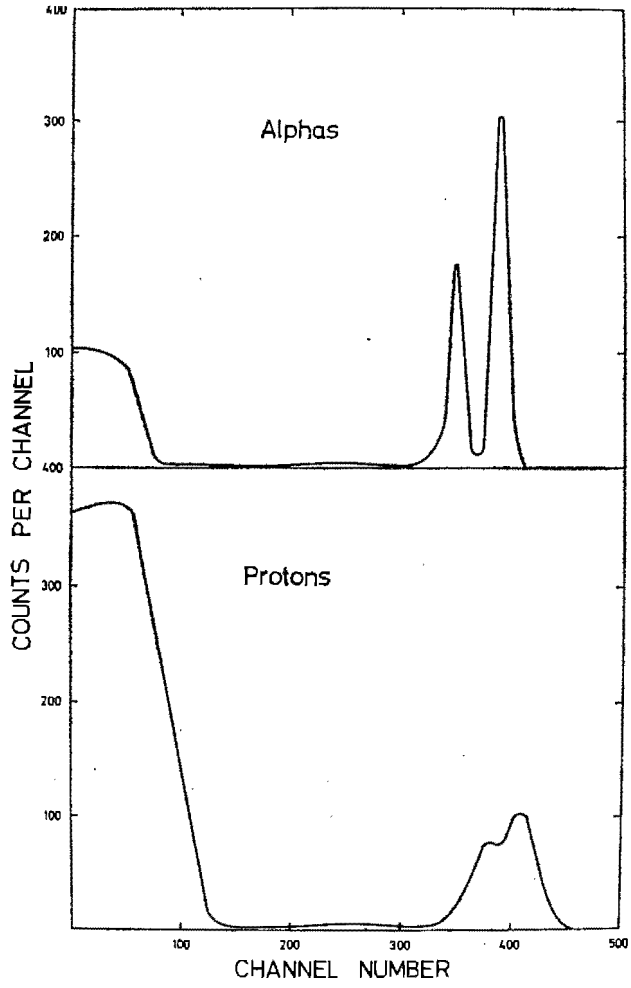

Fig. 7—Comparison of the resolution of gold from tin by proton and alpha scattering

particles would appear as a gently sloping plateau on which a peak is superimposed. The energy corresponding to the edge of the plateau represents the element of the backing while as before the energy at the inflection point of the peak is characteristic of the surface element. An example is shown in Fig. 8 where a peak due to a thin layer of aluminum and a broadened distribution due to a diffused layer of oxygen are shown on the plateau corresponding to iron. In this case quantitative measurement of film thicknesses by integrating the number of counts under the peak is less accurate due to statistical errors inherent in the subtraction of large counts.

Quantitative analysis of surface concentration of the light elements by measuring the distribution of scattered particle momenta with solid-state detectors is currently under investigation.

GEOLOGICAL SAMPLES

In previous work (7) it was noticed that while measuring gold film thicknesses on mica, the plateau from the mica backing showed a series of steps, the inflection points of which corresponded to the elements aluminum, silicon, potassium and iron, each a major component of mica. Pursuing the possibility of applying

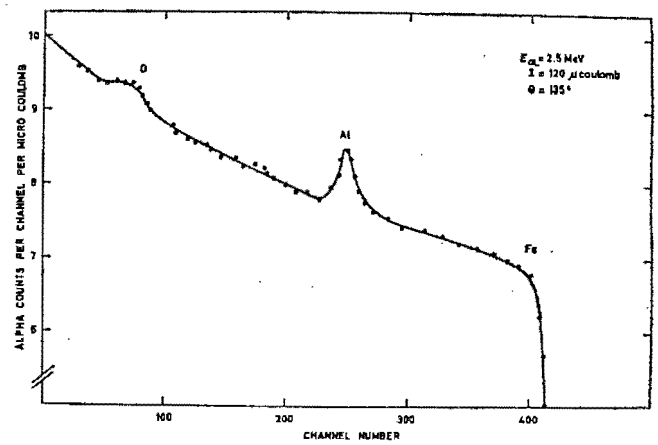

Fig. 8—An example of the spectra obtained from coatings of light elements on heavy backings: oxygen and aluminum on iron

the method to qualitative and semiquantitative analysis of unknown samples, a series of geological specimens was investigated with alpha-particle beams of 2.5 and 3.0 Mev. Some typical spectra of widely differing ores obtained with beam energies of 2.5 Mev are shown in Fig. 9.

Qualitatively the curves are self-explanatory, but semiquantitatively the curves can be used to deduce the weight ratio of constituent elements by measuring the respective step heights. Owing to difficulties in measuring the step height accurately, results have as yet only been semiquantitative. For example, quartz can be seen to consist of approximately equal weights of silicon and oxygen, and fluorite of about equal proportions of calcium and fluorine. The calculated ratios for ideal SiO_2 and CaF_2 are respectively 0.878 and 1.055. It is interesting to note that the sample of galena as submitted for analysis was considered to be reasonably pure lead sulphide, but the analysis showed it to contain relatively high concentrations of copper/zinc that frequently are found in this mineral.

The analysis of most geological samples required a slight modification of the experimental procedure because, being nonconducting, the current integrator could not function. In these cases irradiations were carried out for predetermined times and the flux measured independently in the Faraday cup. For some surface studies the variations in beam current would increase the experimental error of the determination. This series of investigations for the analysis of major components in thick targets constitutes a new line of study which is also currently proceeding.

* * *

The authors acknowledge with thanks the willing cooperation of Messrs. Rene Pretorius and Albert Bottega and of the staff of the Southern Universities Nuclear Institute. Geological samples were kindly loaned by the Geology Department, University of Stellenbosch. One of us (D.O.P.) thanks the South African AEB for permission to include his work in this project.

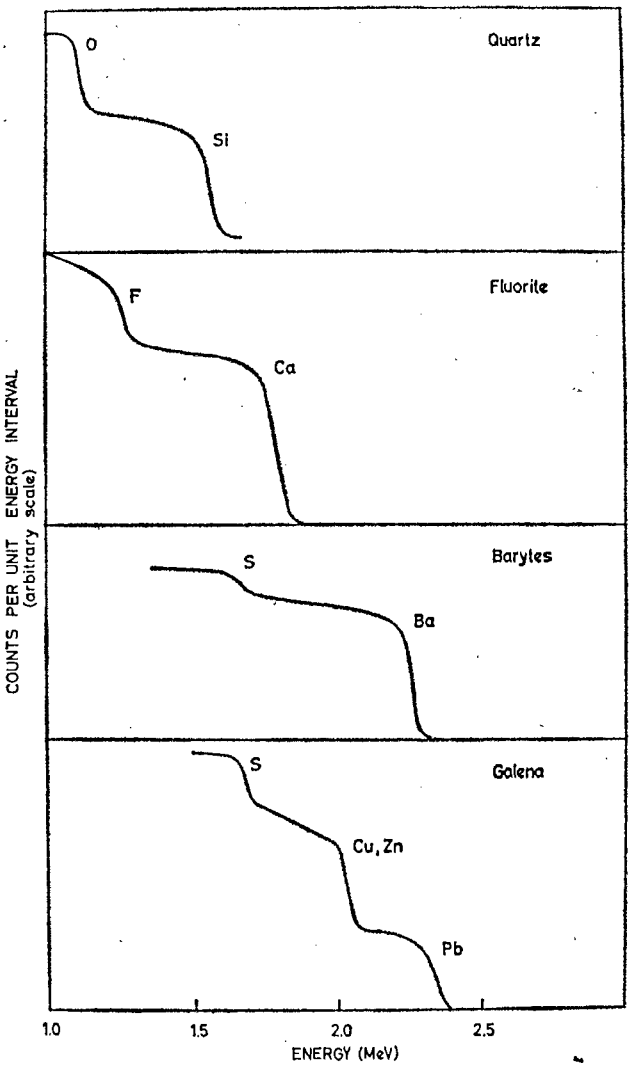

Fig. 9—Alpha scattering spectra from various geological samples

REFERENCES

1. S. Rubin, T. O. Passell, L. E. Bailey. Chemical analysis of surfaces by nuclear methods, Anal. Chem. 29, 736 (1957)
2. S. Rubin. Surface analysis by charged particle spectroscopy, Nuclear Inst. and Methods 5, 177 (1959)
3. W. W. Buechner, J. E. Robertshaw. Surface analysis by means of nuclear particle scattering, Trans. Amer. Nuc. Soc. 5, 197 (1962)
4. F. L. Green, M. D. Cooper, J. E. Robertshaw. Surface composition studies based on nuclear bombardment data, Trans. Amer. Nuc. Soc. 5, 197 (1962)
5. R. F. Sippel. Diffusion measurements in the system Cu-Au by elastic scattering, Phys. Rev. 115, 1441 (1959)
6. G. Dearnaley, A. B. Whitehead, AERE-R 3437 (1960)
7. M. Peisach, D. O. Poole. The determination of gold coating thicknesses by proton scattering (to be published, 1965)

QUESTIONS-ANSWERS

O. U. Anders: At Dow we have carried out charged-particle analyses and found that secondary electron losses, etc. from different targets make the current-integrator readings nonreproducible within more than 10^6/O. We now use a Faraday hood electrically connected to the target with our entrance hole for the primary beam and a second hole for the scattered particles to leave in the direction of the detector. Do you also find this necessary for your quantitative work?

Pleisach: We observe that the current measurements for gold samples deposited on reproducible backings are sufficiently reproducible. Nonconductive targets require that thin samples are used, and the transmitted beam is captured in a Faraday cup.

No. 10

Isotopic Determination of Calcium-48 by Proton Activation

MAX PEISACH and RENÉ PRETORIUS

Southern Universities Nuclear Institute, Faure, C.P., South Africa

▶ Activation with 4.75-m.e.v. protons of calcium samples containing enriched calcium-48 as tracer, leads to the formation of 44-hour scandium-48 and 4-hour scandium-43 and 44. The ratio of these activities gives a measure of the isotopic concentration of calcium-48. Other calcium isotopes do not interfere. The relative standard deviation over the concentration range from 0.18 (natural) to 4 atom % Ca^{48} is 2.7%.

Radiotracers are being used for calcium tracing in vivo, but the reluctance of the medical profession to use radioactive material on healthy subjects prompted the use of stable calcium isotopes for tracing purposes. However, the utilization of stable isotopes depended, among other considerations, on the availability of a suitable method of analysis. The most sensitive method of isotopic analysis is by mass spectrometry. Nuclear methods of analysis, though not as sensitive, can serve a useful purpose in this field.

Natural calcium consists of six stable isotopes, of which calcium-40 makes up almost 97% of the natural element. Accordingly any one of the five heavier isotopes could serve as a tracer in biological studies. In this paper the determination of the isotopic concentration of calcium-48 used as a tracer is described.

Nuclear methods have been developed for determining calcium-48 by neutron activation either through measuring the high energy gamma-rays emitted by calcium-49 (*2*), or by allowing the calcium-49 to decay and measuring the daughter scandium-49 after chemical separation (*5*). These methods, though useful for calcium-48 analysis, have the disadvantage that the total calcium content has to be determined separately. It would therefore be advantageous to devise a direct method which would lead to the isotopic ratio of tracer to total calcium directly.

In order to obtain reasonable yields from the proton activation of calcium, it would be advisable to irradiate at energies somewhat above the coulomb barrier, 4.1 m.e.v. At such energies (p,n) reactions are most likely to occur. Table I lists the Q-values of (p,n) reactions on calcium isotopes and some nuclear characteristics of the products obtained.

From Table I it follows that a (p,n) reaction is impossible with calcium-40 or calcium-42 for incident proton energies between 4 and 5 m.e.v. If it is assumed that the (p,n) reaction cross sections for the remaining four isotopes are comparable, the main activities that can be expected in a proton irradiated calcium target are the scandium isotopes 43, 44, and 48. The yield of scandium-46 is expected to be very small because of the low natural abundance of calcium-46 (0.0033%) and the relatively short half-life of scandium-46m and relatively long one of scandium-46.

The activity, A, produced in w gram of a target element irradiated for a time t in a constant flux of ϕ particles per cm.^{2}-second by a reaction with cross section σ is given by

$$\frac{A}{w} = \frac{N\sigma\phi a}{M}(1 - e^{-\lambda t}) \qquad (1)$$

where N is the Avogadro number, 6.025×10^{23}, M the atomic weight of the target element, a the fractional abundance of the target nuclide producing the required activity, and λ the decay constant of the radioactive product. Proton activation of calcium samples containing enriched calcium-48 would produce readily distinguishable scandium-48 activity and some other identifiable scandium isotope whose activity could be used as a measure of natural calcium within the target. The ratio of these activities, R, would be given by

$$R = \frac{A_l}{A_n} = \frac{\sigma_l a_l (1 - e^{-\lambda_l t})}{\sum_n \sigma_n a_n (1 - e^{-\lambda_n t})} \qquad (2)$$

where the subscripts l and n refer, respectively, to the scandium isotopes obtained from the label, calcium-48, and the natural calcium isotopes. In Equation 2 it is assumed that the enrichment of calcium-48 is not large enough to change the value of M appreciably.

Because a_n is constant and the cross sections are determined by the energy of the irradiation beam, then, for a fixed irradiation duration, it is clear that the isotopic concentration of calcium-48 would be proportional to the activity ratio, R

$$R = ka_l \qquad (3)$$

Charged particle irradiation is limited to thin deposits because of the very short range of charged particles in matter. At the same time, the entire energy of the beam is deposited within a very short distance in the target, thus resulting in large temperature rises. Indeed, the thermal properties of a material frequently determine whether

Table I. Nuclear Properties of Target Nuclides

Target nuclide	Natural abundance (%)	Q-value (*1*) (p,n) (m.e.v.)	Product: Nuclide	Product: Half-life	Product: Main[a] decay gamma-rays (m.e.v.)
Ca^{40}	96.97	−14.680	Sc^{40}	0.18 sec.	(β^+) 3.75
Ca^{42}	0.64	−6.700	Sc^{42m}	62 sec.	(β^+) 1.52, 1.23 0.44
Ca^{42}	0.145	−3.003	Sc^{43}	3.9 hr.	(β^+) 0.37
Ca^{44}	2.06	−4.431	Sc^{44m}	2.4 d	0.271
			Sc^{44}	4.0 hr.	(β^+) 1.16
Ca^{46}	0.0033	−2.165	Sc^{46m}	20 sec.	
			Sc^{46}	84 d	1.12, 0.89
Ca^{48}	0.18	−0.515	Sc^{48}	44 hr.	1.31, 1.04, 0.99
O^{16}	99.759	...	F^{16}	10^{-12} sec.	
O^{17}	0.037	−3.544	F^{17}	66 sec.	(β^+)
O^{18}	0.204	−2.450	F^{18}	110 m.	(β^+)
F^{19}	100	−4.031	Ne^{19}	18 sec.	(β^+)
Ta^{180}	0.0123	−0.083 (*3*)	W^{180m}	5 msec.	0.10
			W^{181}	stable	
Ta^{181}	99.988	+0.242 (*3*)	W^{181m}	14 μsec.	0.15, 0.14
			W^{181}	130d	

[a] (β^+) refers to positron decay and hence the appearance of 0.51 m.e.v. gamma-rays.

Reprinted from ANALYTICAL CHEMISTRY, Vol. 38, Page 956, July 1966

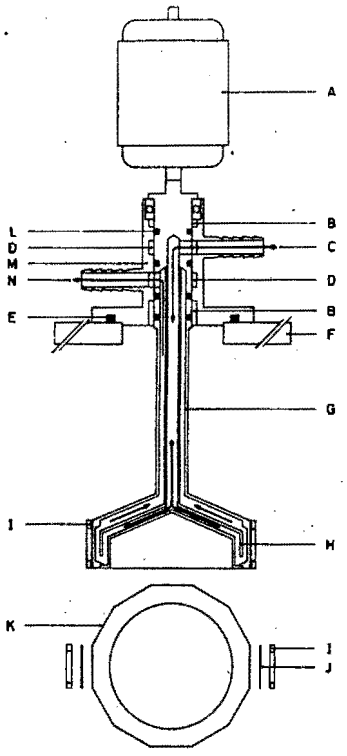

Figure 1. Rotating sample holder cooled by circulating water

A. Motor and gear box
B. Nylon bearings
C. Water inlet
D. Water chambers
E. Vacuum seal
F. Base plate
G. Rotating cooled target holder
H. Cooling water stream guide
I. Target clamps
J. Target
K. 12 flats for mounting target
L. Water and vacuum seals
M. Target holder support
N. Water outlet

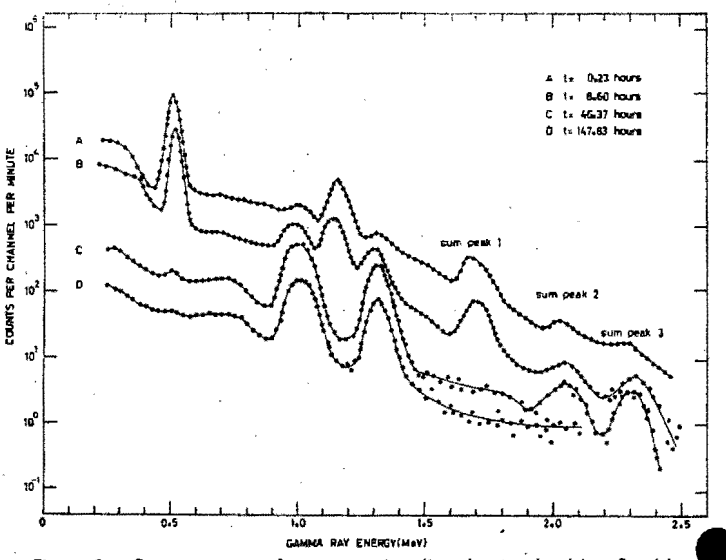

Figure 2. Gamma spectra from proton irradiated natural calcium fluoride

irradiation with charged particles is practical or not.

For the analysis of calcium by proton irradiation, few forms of the target material are suitable. The more common calcium compounds usually precipitated in analyses, such as the carbonate and oxalate, decompose on heating. Possible interference from the nuclear reactions of other elements also make it desirable that only simple compounds such as the oxide and fluoride which melt at 2580° and 1360° C., respectively, be considered.

Proton activation of oxygen will result in the formation of 66-second fluorine-17 and 110-minute fluorine-18 by (p,n) reactions on the stable isotopes of oxygen, while fluorine will only form 18-second neon-19. Comparing the properties of these radio-nuclides with the (p,n) products of calcium in Table I it is clear that fluoride would be preferable to oxide.

The backing material for the target should be inert to activation and capable of withstanding relatively high temperatures. Tantalum meets these requirements, because the only activity that could be measured with the sample is tungsten-181 (see Table I). However, even this nuclide is not expected to be present in any appreciable concentration, because the coulomb barrier for protons is about 10.5 m.e.v.

EXPERIMENTAL

Preparation of Samples and Standards. Calcium, separated from biological material as oxalate or carbonate, was redissolved and converted to calcium fluoride by evaporation with HF in a platinum crucible. The calcium fluoride was transferred to a tungsten boat and distilled in vacuum onto tantalum discs over an area compatible with the cross sectional area of the irradiation beam.

Standards were similarly prepared from calcium carbonate enriched to 97.98% in calcium-48, obtained from the Oak Ridge National Laboratory, U.S.A., which was diluted with natural calcium to the required isotopic concentration.

Irradiation and Measurement. Sample discs were mounted on a rotating holder cooled by circulating coolant (see Figure 1) inside a vacuum chamber which fitted onto the beam tube of the 5.5 m.e.v. Van de Graaff accelerator at the Southern Universities Nuclear Institute. The irradiation beam was defocussed until its cross section exceeded that of the calcium fluoride deposit. Targets were irradiated up to 2 hours with 4.75 m.e.v. protons in a beam current of about 2 μa.

After irradiation, samples were analysed either by gamma-ray spectrometry or by gross gamma-ray counting with a 3- × 3-inch NaI(Tl) scintillation detector. Counting usually started about 15 minutes after irradiation, thereby allowing sufficient time for very short-lived activities to decay, and continued periodically until sufficient data had been accumulated to allow the major components to be separately determined.

RESULTS AND DISCUSSION

Gamma-Ray Spectrometry. Gamma-ray spectra recorded during the decay of an irradiated sample of natural calcium fluoride are shown in Figure 2. Immediately after irradiation, the presence of scandium-44 was proved by the pronounced peak from positron annihilation radiation of 0.51 m.e.v. and the photopeak from the 1.16 m.e.v. gamma-ray, the apparent photopeak at 1.67 m.e.v. is a sum peak (Sum peak 1 in Figure 2).

After 8.6 hours the presence of the longer-lived scandium-48 could already be distinguished by the appearance of photopeaks from gamma-rays of 0.99 and 1.04 m.e.v. (unresolved) and 1.31 m.e.v. Sum peak 1 was still evident, and similar but smaller sum peaks (2 and 3) could be distinguished at about 2 and 2.3 m.e.v.

After about 46 hours the characteristics of scandium-44 had almost disappeared. The shape of the spectrum thereafter remained virtually unaltered, but for the disappearance of sum peaks as a result of the decreased count rate. The identity of each radionuclide

was confirmed by the rate of decay of the respective gamma-rays.

At lower proton energies scandium-43 was shown to be the only positron emitter formed (4), but under the conditions of the irradiation described above, scandium-43 was not observed for the following reasons: the calcium isotope from which it would be produced has an abundance of 0.145% which is low compared to that of calcium-44, 2.06%. Apparently the cross section of the reaction $Ca^{43}(p,n)Sc^{43}$ is too small to compensate for the lower concentration; it emits only a 0.37-m.e.v. gamma-ray for about 21% of its disintegrations, so that the intensity of this gamma-ray would be too small to be distinguished from the high Compton continuum caused by higher energy gamma-rays emitted by other nuclides; it has a half-life so close to that of scandium-44 that its positron annihilation radiation cannot be resolved from that of scandium-44 by decay measurements alone.

Because of the above last-mentioned reason, it was convenient to consider the mixture of scandium-43 and scandium-44 as a single radioactive species. The half-life was found to be 4 hours whether measured by the decay of the positron annihilation radiation or the decay of the 1.16 m.e.v. gamma-ray.

The Effect of Irradiation Duration. The intensity of the 4-hour activity was taken as a measure of the total natural calcium content of the sample. The time-dependent factor $(1 - e^{-\lambda_l t})/(1 - e^{-\lambda_s t})$ in Equation 2 could then be considered as relating to two radionuclides. The variation of this time-dependent factor with the irradiation duration is shown in Figure 3 from which it can be seen that the yield of scandium-48 relative to that of the 4-hour activity (scandium-43 and scandium-44) would change slowly with time. An irradiation of 20 hours would approximately double the activity ratio obtained after 2 hours, but despite the increase in sensitivity this would offer, the increased radiation cost would not be warranted.

Accuracy and Precision. The activity ratio of scandium-48 to the 4-hour activity at the end of the irradiation changes linearly with calcium-48 content, so that one standard sample and a sample of natural composition are sufficient to fix the calibration line, provided targets of approximately the same thickness are irradiated for a fixed duration. If the variation in thickness is such as to cause an appreciable variation of the proton energy within the target from sample to sample, the change in cross section of the (p,n) reaction at the lower proton energies would affect the activity ratios differently, thereby giving erroneous results. A variation in the length of irradiation would result in a change in the activity ratio from sample to sample as well, but this could be corrected for by using the appropriate values from Figure 3.

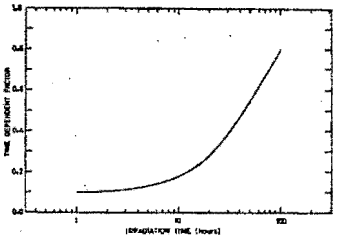

Figure 3. The variation of the time-dependent factor $\frac{(1 - e^{-\lambda_l t})}{(1 - e^{-\lambda_s t})}$ with irradiation time

λ_s and λ_l refer respectively to the 4 and 44-hour activities

Table II shows a typical set of results from an irradiation of 2 hours at a proton energy of 4.75 m.e.v. The relative standard deviation was 2.7% while the mean value of the activity ratio in this case was 0.252 per atom % calcium-48. The relative standard deviation is a measure of the precision of the method, but the absolute value of the activity ratio changes with the length of irradiation and may further vary if the irradiation flux undergoes appreciable change during irradiation.

The precision was thus sufficient to measure a 10% increase over the natural calcium-48 isotopic concentration. The mean error, −0.004 atom %, was sufficiently close to zero to indicate no bias. The main source of error affecting the accuracy of a determination would be contamination from other calcium salts, which would not be immediately obvious during activity measurements, and it would thus require stringent precautions to be taken to prevent such contamination.

Contamination from other sources would have very little effect. If any contamination occurs before the evaporation of the calcium fluoride, the contaminant is unlikely to follow calcium through the chemical stages. Should the contamination occur after the target is prepared, it would still be possible to discriminate against it by half-life and energy measurements. It should be noted that the elements likely to be activated by proton irradiation at 4.75 m.e.v. would be those lighter than calcium, and the activities they would produce would not interfere in the analyses. The coulomb barrier for elements heavier than calcium would tend to decrease the activation cross sections thus still further discriminating against the contaminant.

Advantages and Limitations. The method offers a simple procedure for determining isotopic concentrations of calcium-48, and, in the sense that the analyzed sample is still available after analysis, is nondestructive. The procedure, being based on the determination of activity ratios, does not require yields, weights of targets, or irradiation fluxes to be known. If samples are irradiated successively or singly, it is necessary that the irradiation flux remains constant for all the samples. However, when the samples and standards are irradiated together, as is possible by the use of the rotating target holder shown in Figure 1, flux variations would only result in a calibration line with a different slope. It is essential, that the standard and sample should be counted under identical conditions and that the irradiation duration be known.

The method is applicable to samples of natural isotopic concentration of calcium-48 (0.18%) and samples enriched with calcium-48. When the isotopic concentration of calcium-48 is about 4%, the count-rates of the scandium-48 and the 4-hour activities are about equal. At higher enrichments the yield of scandium-48 becomes so great that the error involved in measuring the shorter-lived activity lowers the precision of the method. Accordingly the method is best suited for low isotopic concentrations of calcium-48. It would thus be advisable to dilute very highly concentrated samples with a known amount of natural calcium.

The method is not suitable for microamounts of calcium. Approximately a milligram of calcium fluoride is the least

Table II. A Typical Set of Results

(I) Known Ca^{48} concn. (atom %)	Activity ratio (×100)	Activity ratio per unit atom %	(II) Measured Ca^{48} concn. (atom %)	Observed difference (II) − (I)
0.185	4.75	0.257	0.188	+0.003
0.192	4.83	0.252	0.191	−0.001
0.375	9.32	0.249	0.369	−0.006
0.825	21.57	0.262	0.854	+0.029
1.040	26.38	0.254	1.045	+0.005
1.370	33.15	0.242	1.313	−0.057

Mean activity ratio 0.252 ± 0.007 per unit atom %
Relative standard deviation ±2.7%
Mean error −0.004 atom %

needed to prepare the target. However, this amount is readily obtainable from most biological systems where the method would find ready application.

ACKNOWLEDGMENT

The assistance of Robbie Verbruggen especially with the design and construction of the rotating sample holder is gratefully acknowledged.

LITERATURE CITED

(1) Everling, F., Koenig, L. A., Mattauch, J. H. E., Wapstra, A. H. "Nuclear Data Tables, Part I," National Academy of Sciences, Washington, 1961.
(2) Junod, E., Laverlochere, J., "Proceed. 3rd Intern. Colloquium on Biology," Saclay, 1963.
(3) Koenig, L. A., Mattauch, J. H. E., Wapstra, A. H., "Nuclear Data Tables Part II," National Academy of Sciences, Washington, 1961.
(4) Peisach, M., Pretorius, R., unpublished data, Southern Universities Nuclear Institute, Faure, C. P. (1965).
(5) Strelow, F. W. E., Staerk, H., ANAL. CHEM. **35**, 1154 (1963).

RECEIVED for review March 9, 1966. Accepted April 18, 1966. R. P. thanks Dr. H. P. Malan, his Promotor at the University of Stellenbosch, for permission to publish his results which will form part of his doctorate thesis to be submitted to the University of Stellenbosch.

Reprinted from ANALYTICAL CHEMISTRY, Vol. 38, Page 1345, September 1966

Analysis of Surfaces by Scattering of Accelerated Alpha Particles

MAX PEISACH and DARRELL O. POOLE[1]

Southern University Nuclear Institute, Faure, C. P., South Africa

▶ Elastic scattering of monoenergetic alpha particles has been used for qualitative and quantitative analysis of surface layers nondestructively. Energy spectra were obtained with surface barrier semiconductor detectors. Surface concentrations of films were measured between 0 and 40 μg./cm.^{2} with a precision of $\pm$0.2 μg./cm.^{2} over an area of 0.5 mm.^{2} The method was also applied to thick coatings and to geological samples. A nomogram is presented for selecting experimental conditions and for the rapid interpretation of experimental data.

ELASTIC scattering of accelerated particles has been used for the analysis of surface layers. Rubin (*8*) described a suitable method for the analysis of aerosol on aluminum and the determination of calcium concentrations on glass surfaces using proton scattering. Robertshaw and coworkers determined sulphur deposits on niobium, also with accelerated protons (*2*), and organic materials on surfaces with accelerated deuterons (*4*). Sippel (*9*) utilized the penetration of accelerated light particles to determine the concentration of a diffused metal at a depth from the surface.

In all the above-mentioned work a magnetic spectrometer was used to determine the energy spectrum of the scattered particles. Although this apparatus has good resolving power, its main disadvantages are its high cost and bulk. With the development of semiconductors, small cheap detectors have been made for measuring the energy of charged particles (*3*). Peisach and Poole (*6*) used these solid state detectors and showed that despite the lower resolution obtainable, surface layers of gold could be measured by proton scattering.

The Rutherford differential scattering cross section, P, per unit solid angle at a mean scattering angle ϕ, for nonrelativistic bombarding particles is given by

$$P = \frac{(Z_1 Z_2 e^2)^2}{16E^2 \sin^4 \frac{\phi}{2}} \text{ per atom} \qquad (1)$$

where Z_1 = the atomic number of the bombarding particle
Z_2 = the atomic number of the target nucleus
e = the electronic charge
E = the energy of the bombarding particle

Equation 1 shows that the number of alpha particles scattered from a monoatomic surface layer through a particular angle would be four times that of protons scattered through an equal angle, provided the bombarding beams had equal energy and intensity. It follows that methods for analyzing very thin targets or surface layers by particle scattering could be more sensitive with alpha particles than with protons or deuterons. The rate of energy loss of alpha particles, and hence the stopping cross section for alpha particles in matter, is greater than for protons or deuterons, so that if information is sought at some depth below the surface, the lighter particles would be advantageous.

The energy E' of a particle scattered through an angle θ in center-of-mass coordinates, is given by

$$\frac{E'}{E} = 1 - 2(1 - \cos\theta)\frac{M_1 M_2}{(M_1 + M_2)^2} \qquad (2)$$

where M_1 and M_2 are, respectively, the masses of the bombarding particle and target nucleus. The value of θ may be obtained from θ_L, the angle in laboratory coordinates, by

$$\theta = \theta_L + \arcsin\left(\frac{M_1}{M_2}\sin\theta_L\right) \qquad (3)$$

[1] South African Atomic Energy Board, Isotope Unit.

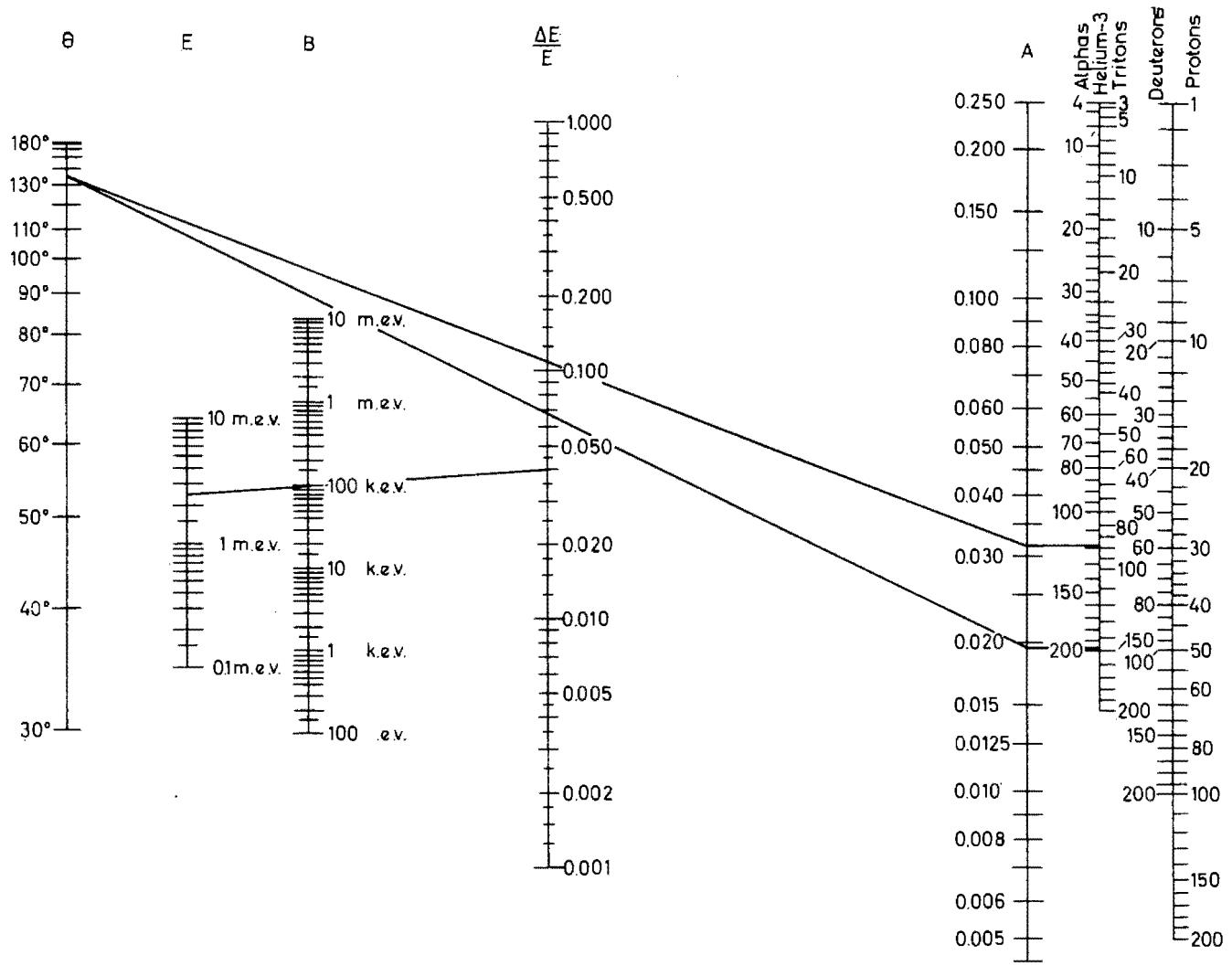

Figure 1. Nomogram for the calculation of data from charged particle scattering and for selection of experimental conditions

The lines drawn refer to Exomple 1 in the text

but for most practical purposes, and especially when $M_1 \ll M_2$, the error incurred in assuming the center-of-mass and laboratory angles to be equal, is small.

From Equation 2 it follows that the relative energy loss, $(E - E')/E = \Delta E/E$, for an alpha particle would be $4\left(\frac{M_2+1}{M_2+4}\right)^2$ times that of a proton under similar measuring conditions. For analytical purposes, therefore, the use of alpha particles in preference to protons is again indicated, this time because better resolution between different target masses results.

When a monoenergetic beam of alpha particles is scattered by a target consisting of a monolayer of isotopic nuclei, the energy spectrum of the scattering particles at a fixed scattering angle is expected to consist of a single line. However, due to the nonideal behaviour of the measuring apparatus, the line should appear as a narrow, normal distribution, the width of which is determined by the resolution of the system. Also, as most elements are a mixture of isotopes, the presence of target nuclei with different masses would further distort the ideal spectrum, each mass appearing as a normal distribution about an energy given by Equation 2 and the spectrum being the sum of all the normal distributions. As the target thickness increases, each isobar at each subsequent layer will generate a similar normal distribution, but at a lower energy, the energies of the incident and scattered particle being degraded by traversing the target material. The number of particles scattered from each isobar at a particular layer will be determined by the flux pertaining to that layer and the relative concentration of the isobar in question, but the height of the component distribution will depend on the number of these scattered particles that reach the detector. As before, the shape of the spectrum will be the sum of all the component distributions. The number of particles scattered from a particular isobar and counted over an energy interval determined by the resolution of the detecting system is given by Equation 3 in Reference (*8*).

When trying to differentiate between targets of different mass numbers M_2 and $M_{2'}$, it is desirable to have a wide as possible energy difference between their corresponding values of E' to overcome the inherent resolution limitation of the measuring system. It follows from Equation 2 that the use of high energy heavy particle beams would be advantageous, especially if the scattered particle is measured at a large backward scattering angle. However, because the method is based entirely on elastic scattering, an upper limit is imposed. The energy of the bombarding particle should not reach the level where inelastic scattering becomes significant.

SELECTION OF EXPERIMENTAL CONDITIONS

When two target elements having masses M_2 and $M_{2'}$ are considered in a sample to be analyzed, the parameters that determine the experimental conditions are θ and E, which in turn have to be chosen to obtain a suitable value for ΔE in relation to the resolution of the detecting system. The selection of experimental conditions would require

repeatedly solving Equation 2, for which the nomogram given in Figure 1 has been constructed.

The lines in the nomogram are labelled θ, E, B, $\Delta E/E$, and A where B, the difference in energy between the scattered particles from two target nuclei M_2 and $M_{2'}$ as derived from Equation 2, is

$$B = |(\Delta E)_{M_2} - (\Delta E)_{M_{2'}}| \qquad (4)$$

and A is the mass factor given by

$$A = \frac{M_1 M_2}{(M_1 + M_2)^2} \qquad (5)$$

Extra scales have been included for converting the mass of a target, M_2, to the mass factor A for M_1 values of 1, 2, 3, and 4 corresponding to irradiation with protons, deuterons, tritons or helium-3 ions, and alpha particles. The following two examples, which refer to samples analyzed experimentally, show how the nomogram may be used.

Example 1. Thin sandwiches of tin on gold on aluminum plates are to be measured by alpha particle scattering. The resolution of the detecting system being about 50 k.e.v., it is desirable to have $B > 100$ k.e.v. In this case $M_1 = 4$, $M_2 = 197$ for gold, and $M_{2'} = 119$, the integer nearest the atomic weight of tin. To obtain a suitable irradiation energy E, the procedure is as follows. Arbitrarily choosing a value $\theta = 135°$ as convenient for measurement, values of $\Delta E/E$ are read off the nomogram for each of the two elements. The difference between them is now plotted on the same $\Delta E/E$ scale and the energy of the irradiation beam is obtained by joining this point to the value 100 k.e.v. on the B scale and reading off the intercept on the E scale. As indicated in Figure 1, the value of E is 2.5 m.e.v.

Example 2. A geological sample irradiated with 2.5-m.e.v. alpha particles and measured at $\theta_L = 135°$ gave steps in the energy spectrum corresponding to ΔE values of 154, 497, and 920 k.e.v., respectively. To identify the elements associated with these steps, each value is considered as representing a $M_{2'}$ and, in turn, compared with an hypothetically infinite M_2 for which $\Delta E = 0$—i.e., B and ΔE are considered equal. By aligning the B value with $E = 2.5$ m.e.v. to obtain $\Delta E/E$, a second line may be drawn joining this value of $\Delta E/E$ with $\theta = 135°$ to give a value of A. It is assumed that $\theta_L = \theta$. The value of the mass factor, read in association with the alpha scale, identifies the mass numbers of the target element as 204, 64.5, and 32 being, respectively, Pb, Cu or Zn, and S.

EXPERIMENTAL

Apparatus. The scattering chamber consisted of an evacuated hemispherical bowl, 35 cm. in diameter, with an attached beam port which fitted onto a beam tube of the 5.5-m.e.v. Van de Graaff accelerator at the Southern Universities Nuclear Institute. The beam port held the first of two collimators used to define the beam diameter and direction. A second collimator was positioned at the end of the beam port near the bowl of the chamber, about 25 cm. from the first. Diametrically opposite the beam port, protruding from the bowl, was a Faraday cup used to measure the beam current.

The target was mounted on an insulated center arm to which a current integrator (*1*) was attached for directly measuring the net current falling on the target. By allowing the irradiation beam to by-pass the targets, comparison of the currents falling on the target and that passing to the Faraday cup could be made. Discrepancies between these readings were attributed to charge loss from the target by secondary particle emission.

The construction and mounting of the detector has been described (*7*). The underside of the lid plate of the scattering chamber carried the target arm and detector assembly. All relative positions of the target, detector, and beam could be adjusted independently without breaking the chamber vacuum. The geometrical arrangement within the scattering chamber made it possible to measure scattered particles at all angles up to 140°.

Pulses from the solid state detectors were recorded by a multichannel analyzer or by a scaler coupled to a single channel analyzer set to pass pulses in a predetermined energy range.

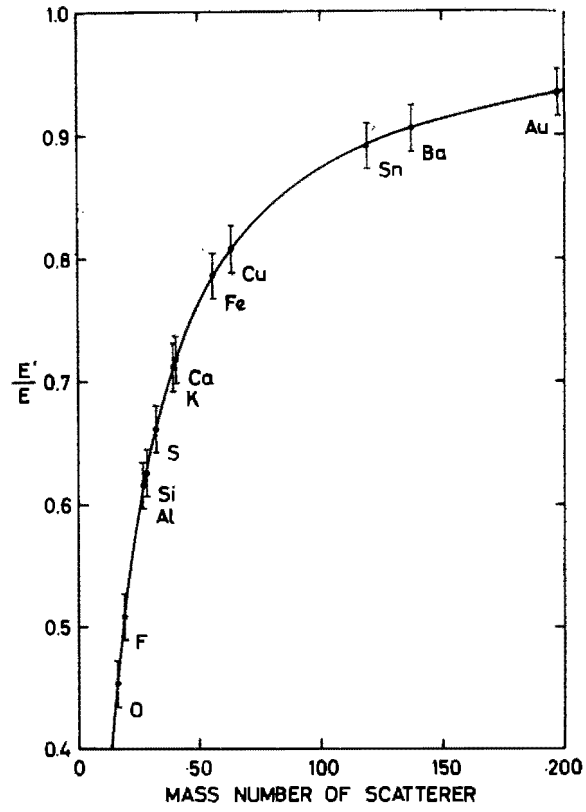

Figure 2. Effect of the mass number of the scatterer on the energy of the scattered particle

$\theta = 135°$. Error flags indicate resolution limits for an incident beam of 2.5 m.e.v.

Irradiation and Measurement. The area of the beam determined the area of the surface analyzed. It was thus necessary to collimate the beam spot to as small an area as could be obtained without losing too much on the count rate. By using a beam spot of 0.5 mm.^{2} a reasonable count rate could be obtained; even thin deposits required not more than 40 minutes of irradiation.

A beam current between 1 and 10 na. was used to measure very thin deposits over the range 0 to 10 μg./cm.^{2} Larger currents cause a sharp temperature rise at the point of irradiation, resulting in local vaporization from the surface with correspondingly low results. When the target had good thermal conductivity or refractory surfaces, currents as high as 0.5 μa. could be used without burn-through.

At 2.5 m.e.v. the alpha beam as obtained from the accelerator had an energy spread of about 1 k.e.v., while the value of B for alpha particles scattered from heavy elements such as gold or lead and light elements such as aluminium was between 500 and 800 k.e.v. at scattering angles between 90° and 135°. If higher energies were used, the scattering cross sections would fall according to Equation 1 and at lower energies the value of B decreases according to Equation 2.

The resolution of detectors as checked with an americium-241 source gave the full width of the peak at half maximum from 30 to 50 k.e.v. for the 5.48-m.e.v. alpha particles.

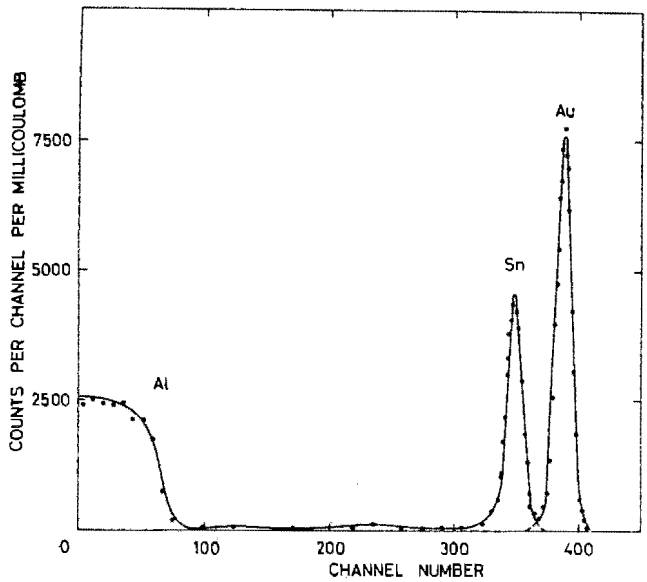

Figure 3. Resolution test

Energy spectrum of alpha particles scattered from aluminum coated with a layer of tin over a layer of gold. E_α = 2.5 m.e.v.

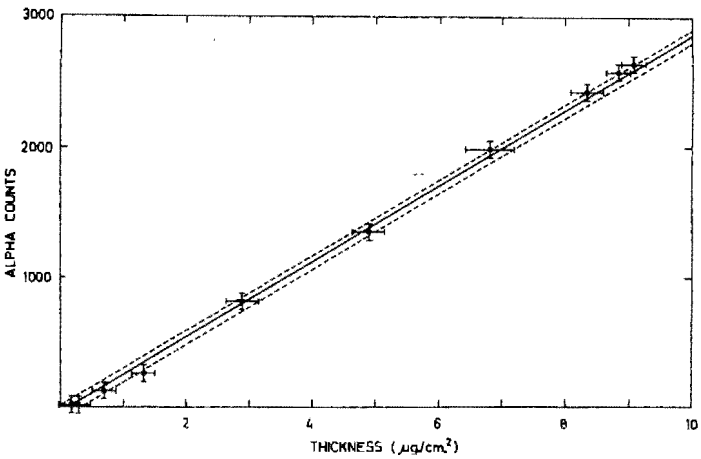

Figure 4. Measurement of the thickness of gold films on aluminum by alpha particle scattering

RESULTS AND DISCUSSION

Verification of Formulae. The validity of Equations 1 and 2 for the elastic scattering of alpha particles was checked by varying the incident beam energy from 1.5 to 4.0 m.e.v. and by changing the scattering element and measuring angle at a constant energy of 2.5 m.e.v. Using a target of a thin film of gold on aluminum, the product of the area under the gold peak in the observed energy spectra and the square of the energy of the incident beam remained constant, per unit current, within experimental limits, as expected from Equation 1. With the same target, the energy difference between the alpha particles scattered from aluminum and gold—i.e., B (Al-Au)—varied as $(1 - \cos \theta)$ in accordance with Equation 2.

Resolution. The effect of using different elements as targets is shown in Figure 2 where experimentally determined values of E'/E are shown plotted against the corresponding atomic weights of the target and compared with the theoretical curve, also drawn. The range shown for each experimental point indicates the resolution limit of the detector system at 2.5 m.e.v. It was observed from Figure 2 that an element with mass number of 120 should readily be resolvable from gold. Accordingly a target was prepared by evaporating a thin deposit of about 1 μg./cm.² gold onto aluminum and covering it with an approximately equally thin layer of tin. The energy spectrum of the scattered alpha particles, Figure 3, showed that the overlap between the two peaks corresponding to tin and gold, respectively, was negligibly small, thus verifying the conclusion drawn from Figure 2.

Measurement of Gold Film Thicknesses. Gold films of varying thicknesses were evaporated onto aluminum, stainless-steel, and tin plates and onto mica, and were analyzed by monoenergetic alpha particle scattering to determine their thicknesses. The results were compared with results obtained from neutron activation analyses of the same samples, Figure 4, and showed that in the range 1 to 10 μg./cm.² the two methods differed by less than ±0.2 μg./cm.² The thickness errors shown in Figure 4 refer to estimated errors associated with the neutron activation analysis, while those in the alpha counts to current measurements and statistical errors in counting.

The emission of secondary electrons from the bombarded target makes direct current integration open to error, unless the entire scattering chamber is used as a Faraday cage. For the same reason, data obtained from measurements of the surfaces of aluminum cannot be used directly for those of stainless steel. Correction for this type of error can be determined, but for routine use it is simpler to calibrate different metals separately. Curves similar to that shown in Figure 4 were obtained in each case, with about the same relative error.

The measurement of gold films was further checked by using radioactive gold to prepare samples standardized by counting. This intercalibration yielded results in complete agreement with the above, and was extended to film thicknesses up to 40 μg./cm.²

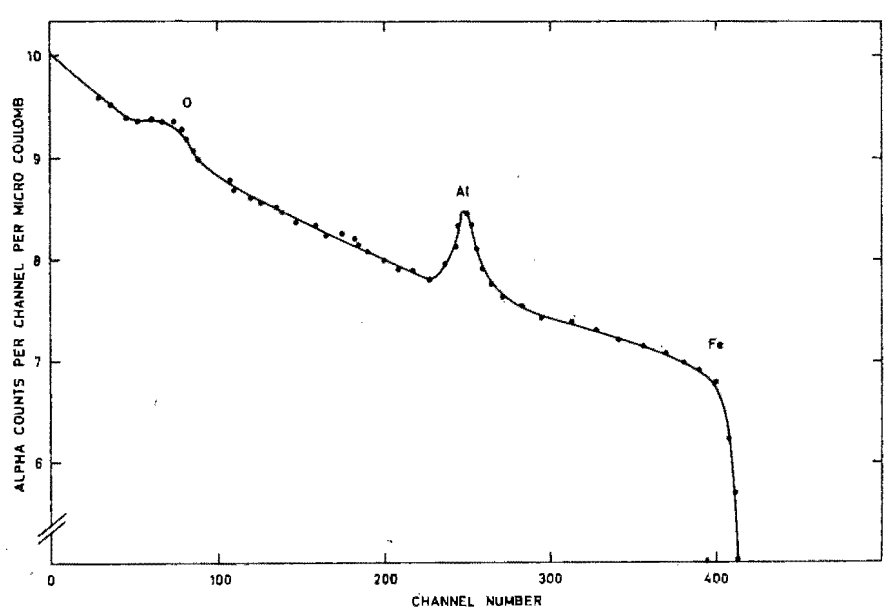

Figure 5. Alpha particle energy spectrum obtained from a target of light elements, aluminum and oxygen, on a heavier element, iron

E_α = 2.5 m.e.v.; θ_L = 135°

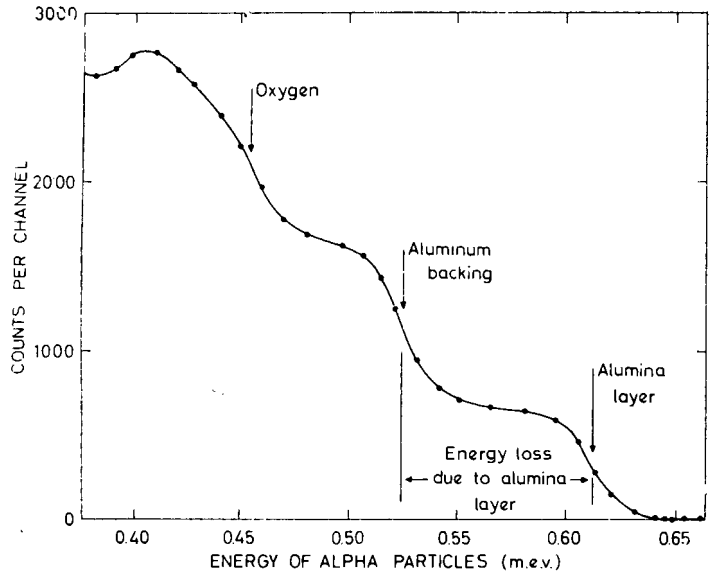

Figure 6. Measurement of oxide thickness by the energy loss of charged particles passing through the surface film

Anodized aluminum, 58.6 μg./cm.² Al_2O_3

Measurement of Light Element Coatings. When the mass number of the surface element is less than that of the backing material, the low energy alpha particles scattered from within the sample contribute to the counts obtained from the surface elements. The energy spectrum then shows the peak positioned over the plateau as shown in Figure 5, where the peak due to a thin layer of aluminum and a broadened distribution due to a diffused layer of oxygen are shown on the plateau corresponding to iron. The quantitative measurement of the aluminum film thickness, made by integrating the number of counts under the peak, was less precise due to the large statistical errors inherent in the subtraction of nearly equal counts.

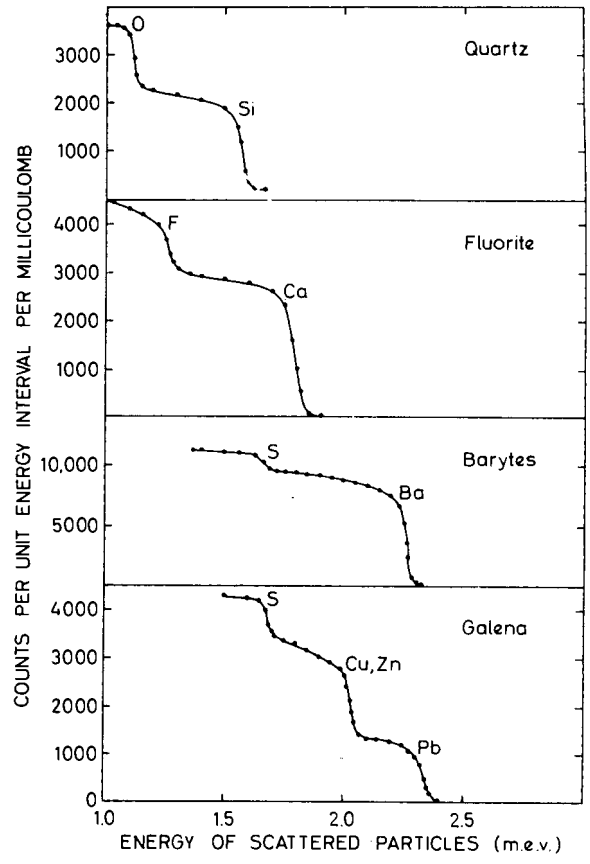

Figure 8. Analysis of some geological samples

E_α = 2.5 m.e.v.

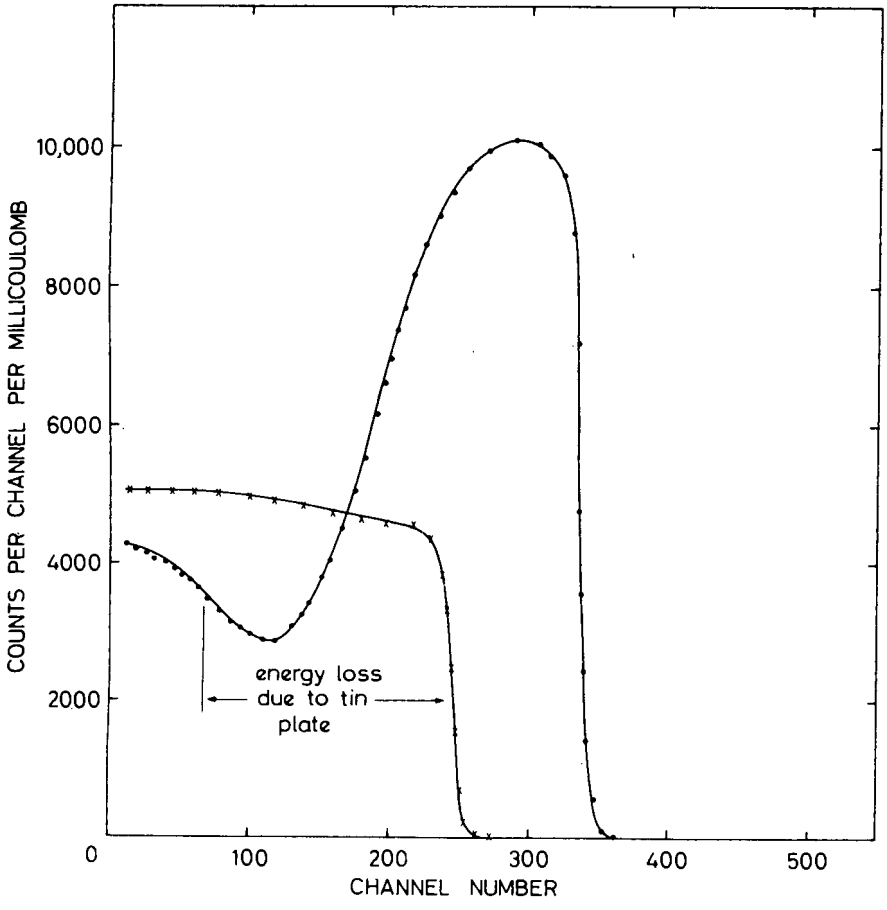

Figure 7. Measurement of thick coatings

0.55 mg./cm.² tin plate on iron measured with E_α = 3.0 m.e.v. Iron -*-*-; tin-plated iron -●-●-

The precision for measuring light elements can be improved by decreasing the incident energy of the bombarding alpha particles, thus decreasing the penetration, but the gain is counteracted by the accompanying loss in resolution. Alternatively, an indirect method can be used for relatively thick films (coatings). The decrease in the maximum energy of the alpha particle scattered by the backing material—i.e., the shift in the position of the plateau step—is determined by the energy loss of the alpha particle passing through the surface layer before and after scatter, and thus gives a measure of the coating thickness. An example of the analysis of an anodized aluminum sample by this method is shown in Figure 6.

Measurement of Thick Surface Coatings. The indirect method described above for light elements can similarly be used for heavy metal

coatings. Samples of tin-plated iron were analyzed to determine the thickness of the tin cover. In Figure 7 the spectrum from a typical sample is compared with that of polished iron. The shift in the position of the iron edge is clearly indicated, but in the example shown the tin coating was so thick, about 0.55 mg./cm.^{2}, that the alpha particles scattered from the iron showed an appreciable energy spread due to straggling. The inflexion point corresponding to the iron in the energy spectrum was then used as the reference point.

Because the sharpness of the plateau step in the energy spectrum deteriorates with increasing coating thicknesses, the error inherent in defining the position of the inflexion point increases, but the relative error in ascertaining the coating thickness remains about ±2%.

Measurement of Geological Samples. Homogeneous samples infinitely thick with respect to the alpha particle range can be analyzed for their major components by alpha particle scattering. Each component is identified by a step in the energy spectrum, as shown in the examples in Figure 8. The position of the step determines the element and its concentration is obtained from the height.

A variety of geological samples were analyzed and some spectra are shown in Figure 8. The results are comparable with those obtained when large sources of alpha-emitting radioisotopes were used (*5*). The sample of galena was submitted as a pure lead ore, but the analysis showed it to contain copper and/or zinc (these elements are irresolvable by the method used) in relatively high concentrations, a common occurrence in this mineral.

ACKNOWLEDGMENT

The authors acknowledge the willing assistance of René Pretorius and Albert Bottega. Hermann Röhm is thanked for his analysis of the anodized aluminium targets. Geological samples were kindly loaned by the Geology Department, University of Stellenbosch.

LITERATURE CITED

(1) Blignaut, E., Kritzinger, J. J., *Nucl. Inst. Methods* **36**, 176 (1965).
(2) Buechner, W. W., Robertshaw, J. E., *Trans. Am. Nucl. Soc.* **5**, 197 (1962).
(3) Dearnaley, G., Whitehead, A. B., At. Energ. Res. Estab. (Gt. Brit.) *Rept.* **R 3437** (1960).
(4) Green, F. L., Cooper, M. D., Robertshaw, J. E., *Trans. Am. Nucl. Soc.* **5**, 197 (1962).
(5) Patterson, J. H., Turkevich, A. L., Franzgrote, E., *J. Geophys. Res.* **70**, 1311 (1965).
(6) Peisach, M., Poole, D. O., *J.S. African Chem. Inst.* **18**, 61 (1965).
(7) Peisach, M., Poole, D. O., Proc. 1965 Intern. Conf. Modern Trends in Activation Analysis, College Station, Texas, **ICAA-II/37**, in press.
(8) Rubin, S., Passell, T. O., Bailey, L. E., ANAL. CHEM. **29**, 736 (1957).
(9) Sippel, R. F., *Phys. Rev.* **115**, 1441 (1959).

RECEIVED March 21, 1966. Accepted May 20, 1966. One of us, (D.O.P.) thanks the South African Atomic Energy Board for permission to include his work in this publication.

PRINTED IN U. S. A.

No. 12

The Determination of Carbon, Nitrogen, and Oxygen and their Stable Isotopic Tracers in Gases by Neutron Time-of-flight Spectroscopy

By Max Peisach

(*Southern Universities Nuclear Institute, Faure, C.P., South Africa*)

Reprinted from Chemical Communications, 1966,

THE CHEMICAL SOCIETY
BURLINGTON HOUSE, LONDON, W.1

PERGAMON PRESS
OXFORD NEW YORK LONDON PARIS

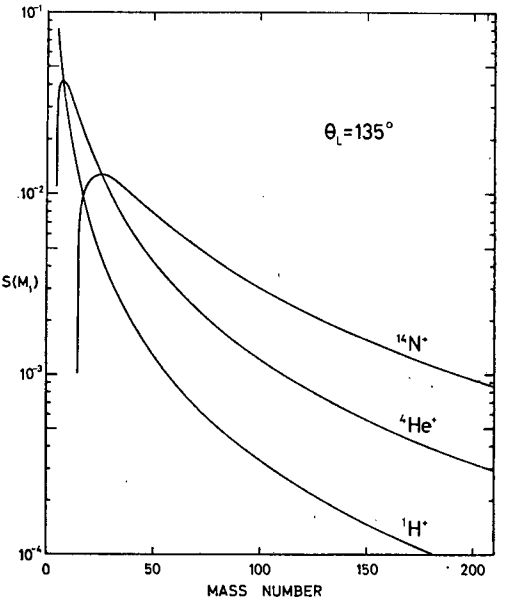

FIG. 1.—Mass sensitivity for protons, alpha particles and nitrogen ions scattered through a laboratory angle of 135°.

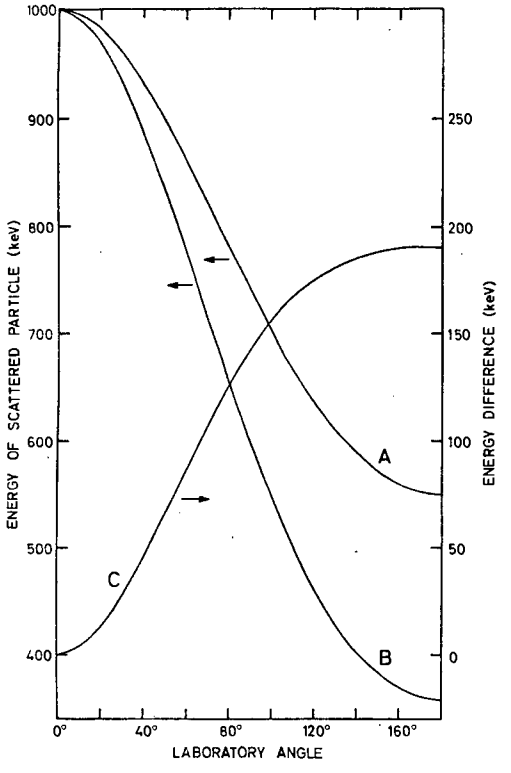

FIG. 2.—Effect of variation of scattering angle on the energy of the alpha particles scattered from aluminium (A), oxygen (B) and the difference between them (C). Incident energy = 1·00 MeV

and for oxygen. In the same figure, the energy difference between particles scattered from aluminium and oxygen at the same depth is shown as a function of the scattering angle for an incident beam of 1 MeV. Although the energy difference increases, there is relatively little change for angles greater than 135°. Accordingly this angle was selected.

The bombarding energy was chosen on the criterion that the rate of energy loss of the alpha particles should be as large as possible, within the alumina, so that penetration into the aluminium metal should be minimized. The lower the energy E, the lower the penetration, but the Van de Graaff accelerator could not give a stable beam much below 0·6 MeV. However, at this energy, the separation between E_1' and E_2' was not sufficiently large. The energy was thus stepped up to 1 MeV as a compromise between better resolution and poorer penetration properties.

EXPERIMENTAL

Apparatus

The 5·5 MeV Van de Graaff accelerator at the Southern Universities Nuclear Institute provided the beam of singly charged helium-4 ions of 1 MeV with energy spread of ± 1 keV. In all cases the incident beam was collimated to a cross-sectional area of 5×10^{-3} cm². With currents of up to 1 μA no vaporization could be detected from the targets, because of the refractory nature of alumina. When gold was used for calibration, lower currents were used to prevent gold volatilization.

The scattering chamber with the collimation for the incident beam was the same as described previously.[3] The detector assembly consisted of a surface barrier silicon solid state detector[4] with an active area of 0·2 cm², mounted 12·7 cm from the point of scatter. When required, collimators could be inserted in the scattered beam to reduce background from multiply scattered alpha particles.

The target assembly allowed for two 17 mm metal plates to be mounted for analysis. An aperture between them enabled the beam to be passed directly to a Faraday cup for current measurement. The entire target assembly was insulated and connected to a current integrator.[5]

Measurement and resolution

Pulses from the solid state detector were amplified and transmitted to a multichannel analyser on which the entire observed spectrum was recorded. The resolution of the detector, as measured by the full width at half the height of the spectrum peak obtained from the 5·48 MeV alpha particles from americium-241 was never more than 55 keV.

Calibration of the measuring system

The scattering of alpha particles at $\theta_L = 135°$ was measured for gold, aluminium and carbon. On adjustment of the scattering angle to centre-of-mass co-ordinates, the three energies obtained from equation (3) gave a straight line calibration. With thick targets the inflection point of the plateau edge in the spectrum was taken as E'.

Preparation of alumina targets

Alumina films of different thicknesses were prepared by anodizing one side of an aluminium foil in 3% w/v triammonium citrate at voltages ranging from 20 to 280 V. The foils were washed in water and stored in vacuum desiccators till required.

Standardization of film thicknesses

Previous work[8–10] has shown that the thickness of alumina formed during anodization is a linear function of the voltage. The mean value of the proportionality constant was accepted as 0·478 μg of alumina/V. As a check on the alumina film thickness, the oxygen content of anodized films was determined by helium-3 activation and measurement of the induced fluorine-18 activity.[11]

RESULTS AND DISCUSSION

Energy spectra of alpha particles scattered from untreated aluminium and from anodized aluminium with thin and thick layers of oxide are shown in Fig. 3. As was expected, the energy spectrum for a thin oxide layer showed a single plateau, caused

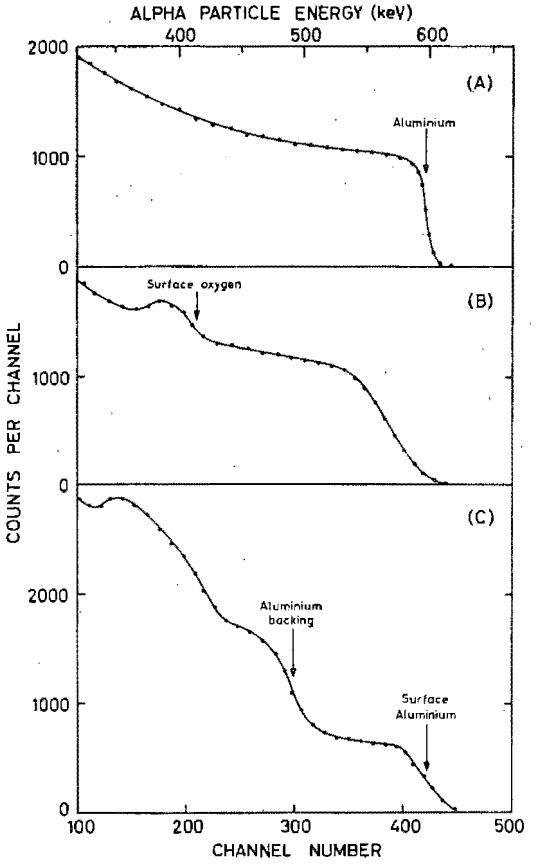

FIG. 3.—Energy spectra of alpha particles scattered from untreated aluminium (A), and from anodised aluminium with thin (B) and thick (C) layers of oxide. $\theta_L = 135°$, $E = 1{\cdot}00$ MeV, counted for 30 min.

by alpha particles scattered from a thick layer of aluminium, with a broadened peak corresponding to a much thinner layer of oxygen, superimposed on the plateau. It was found that the calculated value of E' for oxygen (0·417 MeV) agreed with the maximum energy of particles scattered from oxygen (as measured by the inflection point of the protruding peak in the spectrum). However, the inflection point of the plateau was found to be at a somewhat lower energy than that calculated for E' for aluminium (0·598 MeV). Examination of the same spectrum showed that the leading edge of the spectrum did not fall to zero as rapidly as was the case with unanodized aluminium foil. With increasing target thickness the difference between the measured and the calculated energies corresponding to aluminium increased. At the same time the number of counts recorded in the leading edge of the spectrum increased with thickness until the leading edge resolved into another plateau, the energy of the inflection point of which corresponded exactly to the energy of alpha particles scattered from surface layers of aluminium. An example of a spectrum with three plateaux is shown in Fig. 3C.

The inflection point of the edge of the intermediate step in the energy spectrum

corresponding to an energy intermediate between that of oxygen and aluminium, was found to vary with the thickness of alumina and was displaced to lower energies with increasing thickness of the alumina. If the energy measured from scatter occurring from aluminium in the last layer of alumina is E_{di} [see equation (4)], then the maximum energy measured from scatter at the surface of the aluminium metal, $E_{d(i+1)}$, is related to $(S_1 + S_2)$, the total path length of the alpha particle in alumina. The difference between the energy of a particle scattered from a surface atom of aluminium in alumina and $E_{d(i+1)}$, represents the total energy loss of the particle in alumina. Thus the energy $E_{d(i+1)}$, corresponding to the inflection point of the intermediate plateau can serve as a measure of alumina thickness.

The crystal structure of aluminium metal is cubic close packed with a unit cell of 4·04 Å and an average distance between aluminium atoms[13] of 2·86 Å. In the case of γ-alumina, the unit cell[12] is 7·90 Å with oxygen atoms in cubic close packing. The 24 aluminium atoms are randomly situated in 8 of the 64 sites which have oxygen tetrahedrally arranged around them and 16 of the 32 sites where oxygen is octahedrally arranged. The shortest distance between two octahedrally surrounded aluminium atoms is about 2·8 Å, while between tetrahedrally and octahedrally surrounded ones it is 3·1 Å and between tetrahedrally surrounded atoms, about 3·4 Å. The overall effect is that the average distance between aluminium atoms in alumina is appreciably greater than in aluminium metal. The difference in intensity of the alpha particles scattered from within the alumina and those from the aluminium metal, and hence the appearance of the intermediate plateau in the energy spectrum, is attributed to the increased concentration of aluminium atoms per unit area of the beam.

Recent work[14–17] has indicated that energetic ions could penetrate ordered crystalline structures along favoured crystallographic directions without appreciable loss of energy. Thus, for an alumina layer which is deposited as an ordered crystal and on which the alpha particle irradiation beam is incident in precisely the favoured direction, scattering data could lead to a low result. However, as anodization is unlikely to lead to ordered crystals and because the thickness of the film is obtained from the difference in energy between particles scattered from *surface* aluminium atoms of alumina and *surface* aluminium atoms from the underlying metal, this effect can be neglected. Alternatively, penetration of the underlying metal by channelling would result in a small change of the number of particles scattered from *within* the aluminium, which would again have little bearing on the analysis.

A calibration curve of the maximum energy of an alpha particle scattered from the aluminium metal as a function of alumina thickness is given in Fig. 4. The energy error flags shown in Fig. 4 refer to the errors involved in determining the inflection point in the spectrum, while the thickness error flags refer to the standardization errors from the determination of oxygen by helium-3 activation.

The results of a typical series of analyses are shown in Table I. The values of the known thickness in the table were obtained from activation analysis. The precision of the method as given by the relative standard deviation was found to be 3·5%, while the statistical scatter of results and the mean error indicated no bias. It should be noted that the relative standard deviation included errors from activation analysis, the results of which were assumed to be absolute for purposes of calculation. Because the precision of the standardization by activation analysis[11] or by the variation of film thickness with the anodizing voltage[6–10] is about the same as the value of 3·5% found

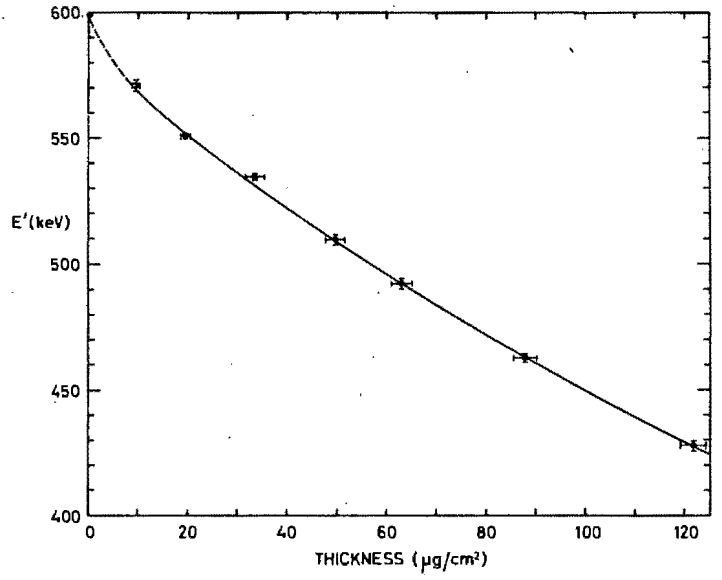

FIG. 4.—The variation of the maximum energy of alpha particles scattered from aluminium metal with thickness of alumina film.

TABLE I.—SOME ANALYSES OF ALUMINA LAYERS ON ALUMINIUM

Sample number	*E, keV*	Thickness, $\mu g/cm^2$			Relative error, %
		Found	Known	Difference	
1	559	15·54	14·34	+1·20	+8·37
2	557	16·83	16·73	+0·10	+5·98
3	549	21·84	22·94	−1·10	−4·80
4	543	25·62	26·29	−0·67	−2·55
5	539	28·49	29·64	−1·15	−3·88
6	520	41·78	41·11	+0·67	+1·63
7	502	55·45	54·01	+1·44	+2·67
8	497	59·37	57·84	+1·53	+2·65
9	490	65·25	67·40	−2·15	−3·19
10	480	73·04	72·18	+0·86	+1·19
11	476	76·48	77·44	−0·96	−1·24
12	438	110·75	110·42	+0·33	+0·30

Mean error +0·00833 $\mu g/cm^2$
Mean relative error +0·59%
Relative standard deviation ±3·5%

here, it may be deduced that the method of alpha particle scattering is, at worst, as precise as these two methods.

Applications

The method of alpha particle scattering affords a convenient method for measuring oxide films on aluminium from 10 to about 150 $\mu g/cm^2$ by the technique of determining the energy lost by the incident and scattered particles passing through the film. The method may be extended to thin films of light elements on metals and heavy elements. For thicker films the incident energy of the alpha particle may be increased,

thus increasing the range of applicability of the method without appreciable loss of sensitivity.

In corrosion studies the oxide film on iron may be measured *in situ*, without having to float the oxide film off the underlying metal.[18] Alternatively films of iron oxide floated off corroded surfaces may be analysed for homogeneity.

Acknowledgements—One of us (D. O. P.) thanks the South African Atomic Energy Board for permission to include his work in this report. Another of us (H. F. R.) thanks the South African Council for Scientific and Industrial Research for a bursary enabling him to take part in this work, which forms part of his Master's thesis accepted by the Chemistry Department, University of Stellenbosch. The assistance of O. B. E. Teuteberg with the construction of some apparatus and of P. A. d'A. Hill with the activation analysis, is gratefully acknowledged.

Résumé—On a utilisé la diffusion des particules alpha accélérées pour déterminer l'épaisseur du film superficiel d'oxyde sur l'aluminium oxydé anodiquement. Les mesures sont basées sur la détermination de la différence entre l'énergie d'une particule alpha diffusée par la couche d'oxyde superficiel et celle d'une particule diffusée par le métal sous-jacent. On a analysé de façon non destructive des films d'épaisseur comprise entre 10 et 130 μg/cm^2 avec un écart type relatif de 3,5%. Le temps moyen nécessité par une analyse est de 30 min, avec une intensité de faisceau incident allant jusqu'à 1 μA environ.

Zusammenfassung—Die Streuung beschleunigter Alphateilchen wurde benutzt, um die Dicke des Oxydfilms auf der Oberfläche anodisch oxydierten Aluminiums zu bestimmen. Die Messungen beruhten auf der Bestimmung der Differenz der Energie eines Alphateilchens, das einerseits an der oberflächlichen Oxydschicht, andererseits am darunterliegenden Metall gestreut wurde. Filme der Dicke 10–130 μg/cm^2 wurden zerstörungsfrei mit einer relativen Standardabweichung von 3,5% analysiert. Die durchschnittliche Zeit für eine Analyse betrug 30 min mit einer Stromstärke des auftreffenden Strahls bis etwa 1 μA.

REFERENCES

1. M. Peisach and D. O. Poole, *Proc. 1965 Int. Conf. Modern Trends in Activation Analysis*, College Station, Texas, p. 206.
2. M. Peisach and D. O. Poole, *Anal. Chem.*, 1966, **38**, 1345.
3. E. Rutherford, J. Chadwick and C. D. Ellis, *Radiations from Radioactive Substances*, p. 194. Cambridge University Press, London, 1930.
4. G. Dearnaley and A. B. Whitehead, *The Solid-state Surface Barrier Charged Particle Detector*, A.E.R.E., R-3437, 1960.
5. E. Blignaut and J. J. Kritzinger, *Nucl. Inst. Methods*, 1965, **36**, 176.
6. W. Walkenhorst, *Naturwissenschaften*, 1947, **34**, 373.
7. J. R. Young, *Phys. Rev.*, 1954, **94**, 960; 1956, **103**, 292.
8. L. Harris, *J. Opt. Soc. Am.*, 1955, **45**, 27.
9. S. Anderson, *J. Appl. Phys.*, 1944, **15**, 477.
10. G. Haas, *J. Opt. Soc. Am.*, 1948, **39**, 532.
11. S. S. Markowitz and J. D. Mahoney, *Anal. Chem.*, 1962, **34**, 329.
12. R. W. G. Wyckoff, *The Structure of Crystals*, pp. 9, 36. Reinhold, New York, 1935.
13. D. F. Eggers, Jr., N. W. Gregory, G. D. Halsey, Jr. and B. S. Rabinovitch, *Physical Chemistry*, Wiley, London, 1964.
14. C. Lehmann and G. Liebfried, *J. Appl. Phys.*, 1963, **34**, 2821.
15. J. R. Beeler, Jr. and D. G. Besco, *ibid.*, 1963, **34**, 2873.
16. B. Domeij, F. Brown, J. A. Davies and M. McCargo, *Can. J. Phys.*, 1964, **42**, 1624.
17. D. S. Gemmell and R. E. Holland, *Phys. Rev. Letters*, 1965, **14**, 945.
18. T. J. Nurse and F. Wormwell, *J. Appl. Chem.*, 1952, **2**, 550.

No. 14

Reprinted from

ANALYTICAL CHEMISTRY

Determination of Deuterium in Gases by Neutron Time-of-Flight Spectrometry

MAX PEISACH AND RENÉ PRETORIUS

Southern Universities Nuclear Institute, P.O. Box 17, Faure, C.P., South Africa

Volume 39, Number 6
Pages 650-657, May 1967

Determination of Deuterium in Gases by Neutron Time-of-Flight Spectrometry

Max Peisach and René Pretorius

Southern Universities Nuclear Institute, P.O. Box 17, Faure, C.P., South Africa

A new method for the determination of deuterium in gases uses time-of-flight spectrometry of neutrons emitted in (d,n) reactions. A pulsed deuteron beam of 2.0, 2.4, or 3.0 mev was used. Deuterium was determined in hydrogen, nitrogen, oxygen, and carbon dioxide at partial pressures ranging from 1 to over 100 mm. The average time taken for an analysis was about 10 minutes. The relative standard deviation was ±3.4% and the sensitivity, 2.5 × 10^{-8} grams per sq cm beam area, was sufficient to detect deuterium in natural hydrogen.

WITH THE INCREASING USE of deuterium as a tracer in chemical systems, the need has arisen for a method of determining deuterium rapidly and, where possible, without disturbing the system by sampling. Nuclear methods have already proved successful for determining the deuterium content in water (*1*) and hydrogenous organic liquids (*2*) using reactions induced by recoil deuterons in neutron-irradiated samples. However, the use of "knock-on" deuterons depends on the presence of suitable nuclides in the sample which undergo deuteron reactions yielding measurable radioactivities. Furthermore, the method is not readily applicable to gases where difficulties arise either from the low activity produced in the irradiated sample or from the techniques for irradiating large amounts of gases under pressure in reactors.

A novel method for the determination of deuterium in the surface layers of Zircaloy was described by Butler (*3*), who used accelerated deuterons with energies up to 3 mev to induce the nuclear reaction $^{2}H(d,n)^{3}He$ and counted the neutrons produced. This method (*3*) breaks down when the sample contains other nuclides capable of yielding neutrons by (*d,n*) reactions at the energy of the bombarding deuteron beam. In fact, at deuteron energies above 1.85 mev, Butler observed interference from oxygen when the threshold for the reaction $^{16}O(d,n)^{17}F$ was exceeded. The sensitivity of his method was further reduced by neutrons produced from (*d,n*) reactions on nitrogen-14 in the residual air in the vacuum system and from deuterons striking the aluminum beam tube.

The energy of a neutron, E_n, emitted from a nuclear reaction is determined by the Q-value of the reaction, the energy of the deuteron incident on the target nucleus, E_d, and the angle θ_L at which it is emitted. From the kinematics of a nuclear reaction, the energy of the neutron is given (*4*) by

$$\sqrt{E_n} = v \pm \sqrt{v^2 + w} \tag{1}$$

where

$$v \equiv \frac{\sqrt{m_d m_n E_d}}{(m_n + M)} \operatorname{Cos} \theta_L \tag{2}$$

$$w \equiv \frac{MQ + E_d(M - m_d)}{(m_n + M)} \tag{3}$$

and m_d, m_n, and M refer to the masses of the deuteron, neutron, and product nucleus, respectively. For a specific nuclear reaction, the neutrons will have energies related to the different Q-values pertaining to the corresponding excited states in which the product nucleus is left. It may then be possible to utilize some selected neutron energy for determining the concentration of a specific nuclide in the target sample nondestructively, and any experimental method by which neutron energies may be determined could be suitable for analysis.

A convenient and accurate method for determining neutron energies is by the time-of-flight technique where the time, t, taken by a neutron to cover a fixed distance, d, is measured. The relationship between t and E_n is given, nonrelativistically, by

$$t = \frac{72.3 \times d}{\sqrt{E_n}} \tag{4}$$

where the constant includes the mass of the neutron and conversion units, while E_n is given in mev, t in nanoseconds, and d in meters. The energy resolution attainable will thus depend on the precision in measuring t. Recent developments of fast electronics have made it possible to measure nanosecond time intervals. The two signals marking the start and end of the neutron flight are obtained from some electronic device coupled with the incident pulsed beam and a neutron detector. Clearly the duration of the pulse represents an error in the time measurement and constitutes a limiting factor in the technique. The application of neutron time-of-flight spectroscopy to analysis was first discussed by Peisach and Pretorius (*5, 6*).

When solids or liquids are irradiated with charged particle beams, the entire energy of the beam is deposited within a relatively short distance in the sample, thus generating high temperatures which are frequently sufficient to destroy the sample. For this reason charged particle irradiations usually require refractory targets or targets with very good cooling. This problem does not arise in the case of gases, because the density of a gas is so low that only a small fraction of the beam energy is transferred to the gas per unit path length. For this reason charged particle irradiation can readily be carried out on gases, provided the container has a sufficiently thin window through which the beam may enter. Analyses based on such irradiations would then be nondestructive and the gas under investigation could readily be part of a closed system which need not be disturbed by sampling.

(1) S. Amiel and M. Peisach, ANAL. CHEM., **34**, 1305 (1962).
(2) E. Fabbri, E. Lazzarini, and V. Sanguist, *Intern. J. Appl. Radiation Isotopes*, **15**, 437 (1964).
(3) J. P. Butler, "Radiochemical Methods of Analysis," Vol. I, p. 393, Proceedings of Symposium, Salzburg, October 1964, Intern. At. Energy Agency, Vienna, 1965.
(4) R. D. Evans, "The Atomic Nucleus," p. 412, McGraw-Hill, New York, 1955.
(5) M. Peisach, *Chem. Communications*, **632** (1966).
(6) M. Peisach and R. Pretorius, *S. African Ind. Chem.*, **20**, 5 (1966)

Reprinted from **ANALYTICAL CHEMISTRY**, Vol. 39, Page 650, May 1967

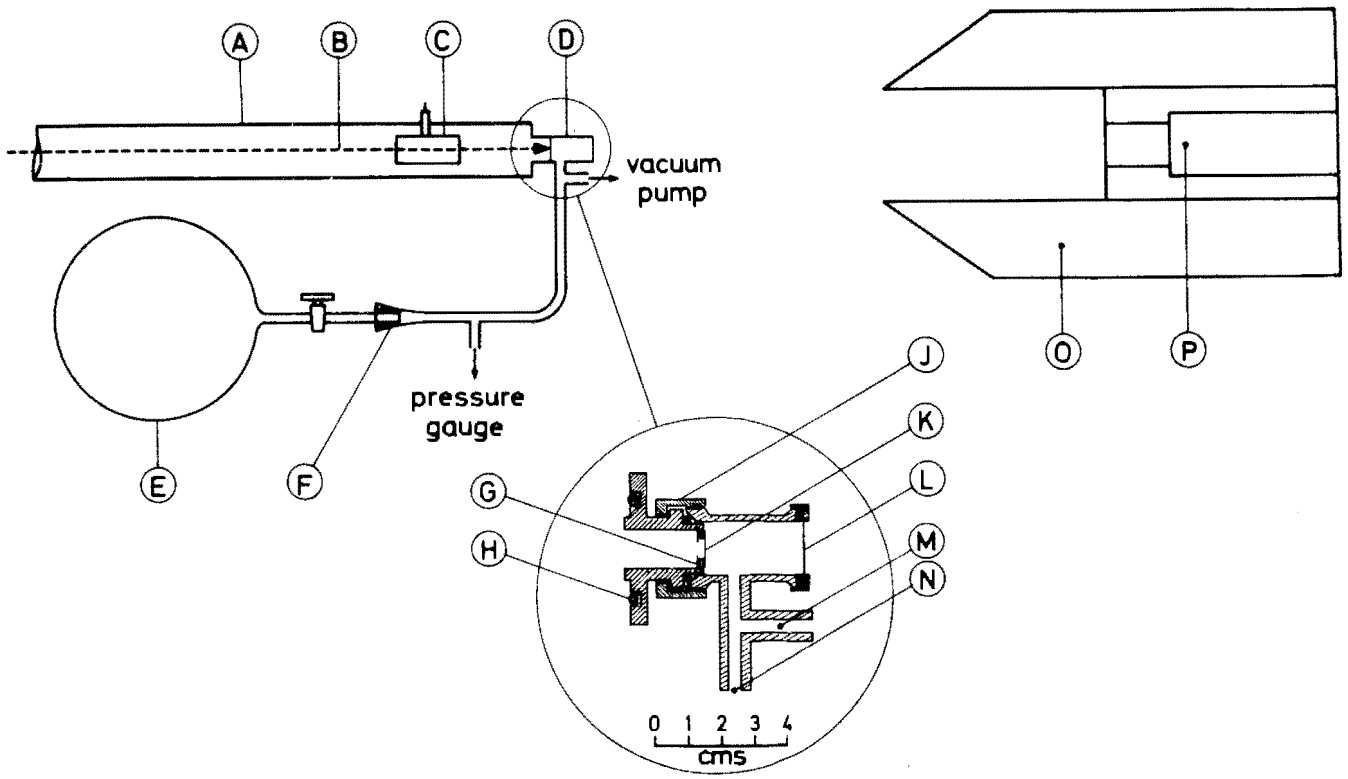

Figure 1. Gas-handling apparatus and irradiation cell

A. Beam tube
B. Irradiation beam
C. Pickup probe
D. Irradiation cell
E. Gas-sampling bottle
F. Sample connection point
G. Tantalum collimator and window support
H. Vacuum O-ring
J. Screw-on clamp
K. Nickel window
L. Platinum back of cell
M. Connection to vacuum pump
N. Connection to gas-handling apparatus
O. Detector shield
P. Scintillation detector

EXPERIMENTAL

Apparatus. A diagrammatic sketch of the apparatus is shown in Figure 1. Gas samples could either be inserted from a gas-sampling bottle (shown) or fed directly into the irradiation cell at the point where the gas sample bottle was inserted. The dead space was made as small as possible to reduce losses when handling gases not condensable with liquid nitrogen.

The nickel window through which the irradiation beam passed was mounted with Araldite on the window support in such a way that the gas pressure helped to keep the window in position. Window supports of different lengths could be inserted, thus changing the path length of the beam through the gas. A beam path length of 3 cm was suitable for most purposes, but when the gases had a relatively high density, or when relatively high pressures were used, better energy resolution could be attained with shorter path lengths. The entire gas cell assembly was insulated, so that the total current could be measured with a current integrator (*7*).

Electronic Equipment. A block diagram of the electronic equipment (*8*) is shown in Figure 2. Neutrons generated by the pulsed beam at the target were detected in a NE 213 liquid scintillation detector placed at a distance d and an angle θ_L from the target. The time of arrival of the pulsed irradiating beam on the target was given by a signal from a pickup probe placed near the target in the beam tube. The difference in time between the signal from the detector and that caused by the beam pulse was converted by the time converter to a pulse, with amplitude proportional to time, and recorded by the multichannel analyzer.

Because the neutron detector was sensitive to γ-rays as well as neutrons, signals caused by γ-rays from whatsoever source were rejected by pulse shape discrimination (*8*) and low-level electronic noise, by the energy discriminator. The current integrator (not shown in Figure 2) was set to accumulate a predetermined total current and automatically switched off the measuring system when this value was reached.

Irradiation and Measurement. Samples of gas at measured pressures were irradiated with a pulsed deuteron beam of energy between 2 and 3 mev obtained from the 5.5-mev van de Graaff accelerator at the Southern Universities Nuclear Institute. Pulses were 5 nsec long and 400 nsec apart. Low average beam currents of between 0.2 and 0.5 μa were used to prevent damage to the thin (0.0001-inch) nickel window which could not be cooled. The platinum back of the cell where most of the energy of the beam was dissipated was cooled externally with a jet of compressed air. Measurements were usually made at $\theta_L = 30°$ to reduce the background of neutrons caused by the beam striking the beam tube, collimator holders, and other material in its path.

From Equation 4 it is clear that better energy resolution is attained with longer flight paths. However, the count rate decreases with d^2, so that a compromise has to be reached between resolution and the duration of the analysis. At

(7) E. Blignaut and J. J. Kritzinger, *Nucl. Instr. Methods*, **36**, 176 (1965).

(8) W. R. McMurray, P. van der Merwe, and I. J. van Heerden, *Nucl. Phys.*, **A92**, 401 (1967).

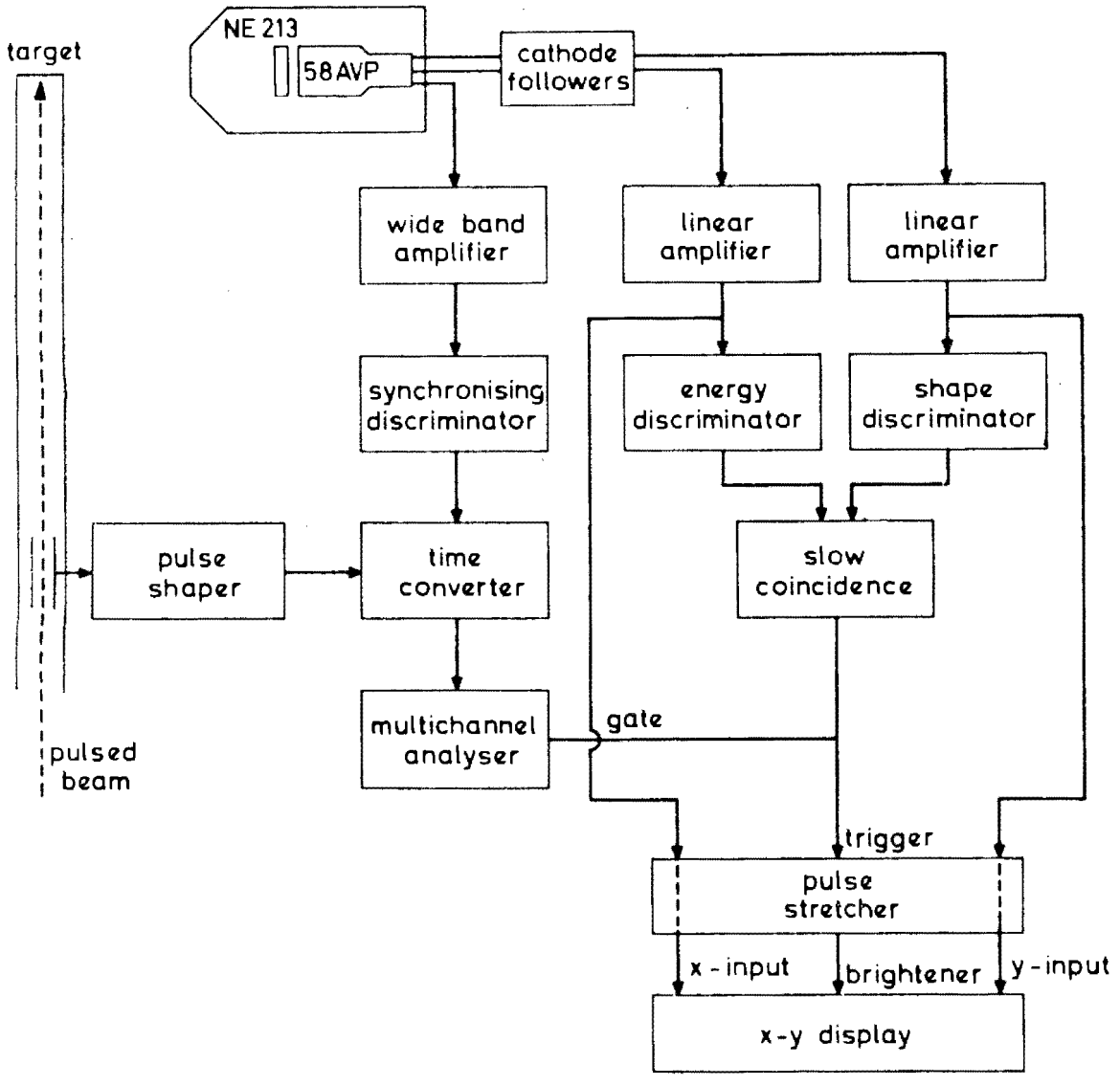

Figure 2. Block diagram of electronic equipment (8)

about 3 meters the resolution was adequate and sufficient counts could be accumulated in 8 to 10 minutes to complete the analysis. To improve the precision, especially for gas samples in which the deuterium partial pressure was low, longer irradiations were carried out to increase the number of neutron counts and thereby decrease the relative statistical errors.

RESULTS AND DISCUSSION

Background. Measurements carried out on the empty gas cell showed that the background spectrum consisted of a peak corresponding to 2.6-mev neutrons from ^{12}C due to a carbon deposit which was gradually built up during irradiation, from the decomposition of oil vapors from the pumping system on the hot nickel window at the point of incidence of the irradiation beam. In addition there was a low continuum covering the entire energy range, due to γ-rays not completely eliminated by pulse shape discrimination, and neutrons scattered into the detector. The contribution from scattered neutrons increased with the number of neutrons generated in the gas cell and accordingly was a function of the pressure and composition of the gas.

When deuterium was determined in a sample, the neutrons from the carbon deposit did not interfere, because their energy was much lower than neutrons from deuterium. However, the background continuum did add to the deuterium peak in the neutron energy spectrum and had to be subtracted. This was carried out for all analyses and in all spectra shown in this paper. The error incurred in using data from an empty cell to correct for this background was negligible when the deuterium content was relatively high. For samples containing relatively small amounts of deuterium, this error could become appreciable; it was then advisable to determine the background by irradiation of a sample with approximately the same composition and pressure in which deuterium was absent.

Neutron Spectra. Table I lists the neutron energies expected from the irradiation of ^{12}C, ^{14}N, ^{16}O, and ^{2}H with deuterons, as calculated from Equation 1 for $E_d = 3.0$ mev and $\theta_L = 30°$; n_i refers to the ith excited state in which the product nucleus is left after neutron emission.

Typical neutron time-of-flight spectra obtained from samples of deuterium (at partial pressures, p_d) in hydrogen, oxygen, carbon dioxide, and nitrogen (at total pressures, P) are shown in Figure 3. From this figure it is obvious that neutrons emitted from deuterium can readily be distinguished from those emitted from the other major components in the mixtures. Accordingly, the number of counts under the

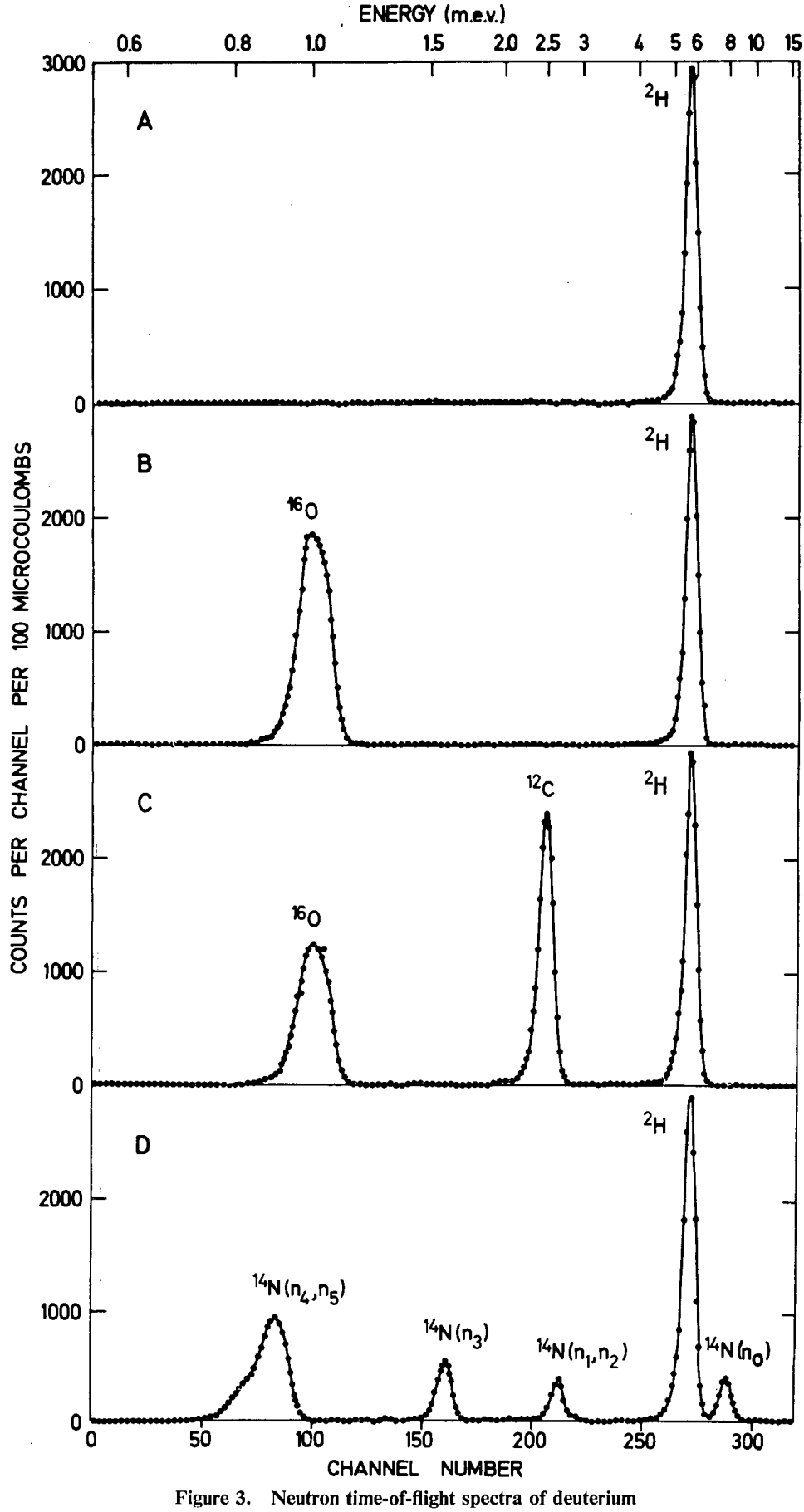

Figure 3. Neutron time-of-flight spectra of deuterium

A. Hydrogen (P = 81.9 mm, P_d = 46.7 mm)
B. Oxygen (P = 128.1 mm, P_d = 46.5 mm)
C. Carbon dioxide (P = 87.2 mm, P_d = 46.7 mm)
D. Nitrogen (P = 84.9 mm, P_d = 47.1 mm)
for E_d = 3.0 mev and θ_L = 30°

Table I. Some Neutron Energies from (*d*, *n*) Reactions

E_d = 3.0 mev, θ_L = 30°

Target	^{12}C	^{14}N	^{16}O	^{2}H
Natural abundance, %	98.89	99.63	99.759	0.015
Q(*d*, n_0), mev (*9*)	− 0.281	5.066	− 1.627	3.268
Neutron energy				
n_0	2.582	7.932	1.223	5.738
n_1		2.771	0.685	
n_2		2.710		
n_3		1.763		
n_4		1.098		
n_5		1.033		
n_6		0.693		
n_7		0.235		

deuterium peak can be integrated and used as a measure of the deuterium content.

When low concentrations of deuterium are determined in nitrogen, the tail of the $^{14}N(n_0)$ neutron peak may overlap a portion of the deuterium peak. This interference may be overcome by changing θ_L. The effect of such a change calculated for E_d = 3.0 mev is shown in Figure 4, where the energy calibration of the channel number is the same as that in Figure 3 for easy comparison. The position of the deuterium peak in the neutron spectrum can thus be shifted to a position between the (n_0) and (n_1) peaks of ^{14}N by measuring at an angle of 70°. However, the differential cross section for neutron emission from the reaction $^{2}H(d,n)^{3}He$ is angle-dependent and drops by a factor of about 2 (*10*) between 30° and 70°.

The energy of each neutron group in Figure 3 is about 200 kev lower than the values in Table I. This is due to the energy lost by the deuteron beam passing through the nickel window.

Neutrons with energies below about 700 kev could not be distinguished from γ-rays by pulse shape discrimination. Accordingly, neutron groups below 700 kev, that might have been expected from Table I, were not observed.

When the deuteron beam passes through the gas in the irradiation cell its energy is degraded by an amount depending on the pressure and composition of the gas mixture. For example, a cell 3 cm long, containing CO_2 at 100-mm pressure, will cause a loss of 128 kev from an incident beam of 3-mev deuterons. This loss will appear to broaden low energy neutron peaks in the energy spectrum much more than peaks occurring at higher energies, because the energy interval per channel increases with increasing energy. Accordingly, the shape of the high energy peak due to deuterium is little affected by the variation of total pressure in the irradiation cell.

(9) F. Everling, L. A. Koenig, J. H. E. Mattauch, and A. H. Wapstra, "Nuclear Data Tables," Part I, National Academy of Sciences, Washington, 1961.

(10) J. E. Brolley and J. L. Fowler, in "Fast Neutron Physics," Part I, J. B. Marion and J. L. Fowler, eds., p. 80, Interscience, New York, 1960.

Table II. Determinations of Deuterium

Gas containing deuterium	E_d	Deuterium partial pressure, mm Hg, 20° C: Known *A*	Found *B*	Error (*B* − *A*)	Relative error, % 100(*B* − *A*)/*A*	Neutron counts per 100 microcoulombs *N*	Neutron counts per unit pressure, *N*/*A*
H_2	2.0	107.3	107.1	−0.2	− 0.2	47825	445.7
		41.6	42.7	+1.1	+ 2.6	19088	458.8
		5.3	5.1	−0.2	−3.7	2279	430.0
H_2	2.4	97.3	97.6	+0.3	+ 0.3	41242	423.9
		38.1	37.7	−0.4	− 1.1	15916	417.7
		24.2	23.5	−0.7	− 2.9	9945	411.0
		10.9	10.9	0.0	0.0	4584	420.6
		1.60	1.66	+0.06	+ 3.8	701	438.1
H_2	3.0	78.9	78.46	−0.44	− 0.6	33072	419.2
		55.8	55.76	−0.04	− 0.1	23501	421.2
		46.7	46.64	−0.06	− 0.1	19659	421.0
		42.9	43.53	+0.63	+ 1.5	18348	427.7
		13.85	14.30	+0.45	+ 3.2	6028	435.2
		5.15	5.18	+0.03	+ 0.6	2181	423.5
		1.15	1.03	−0.12	−10.4	436	379.1
O_2	3.0	87.4	88.23	+0.83	+ 0.9	37191	425.5
		46.5	46.21	−0.29	− 0.6	19479	418.9
		21.4	21.02	−0.38	− 1.8	8859	414.0
		9.63	9.75	+0.12	+ 1.2	4109	426.7
CO_2	3.0	46.7	46.22	−0.48	− 1.0	19481	417.2
		4.33	4.43	+0.10	+ 2.3	1867	431.2
		2.01	2.08	+0.07	+ 3.5	878	436.8
N_2	3.0	47.1	47.47	+0.37	+ 0.8	20009	424.8
		18.07	17.20	−0.87	− 4.8	7249	401.2
		5.36	5.15	−0.21	− 3.9	2169	404.7

Mean error = −0.02 mm Hg (mean value of *B* − *A*).
Mean neutron count per mm pressure D_2 = 419.2 at 3.0 mev.
Relative standard deviation = ±3.4%.

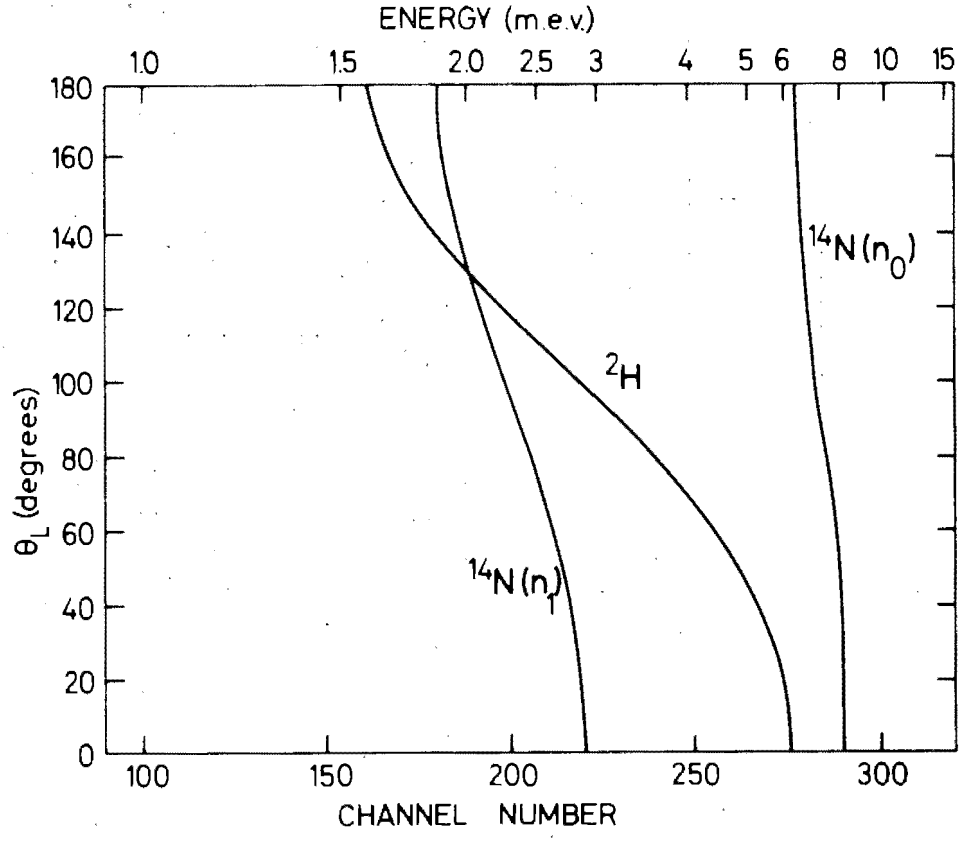

Figure 4. Effect of measuring angle, θ_L, on relative neutron energies from nitrogen and deuterium

E_d = 3.0 mev

ACCURACY AND PRECISION

The variation of neutron counts with partial pressure of deuterium was calibrated with deuterium gas enriched to 99.5% D at different deuteron bombarding energies over the pressure range up to 400 mm. The calibration curves remained linear over the entire pressure range. For E_d = 2.0, 2.4, and 3.0 mev, the number of neutron counts obtained per millimeter pressure of deuterium per 100 microcoulombs of beam current was respectively 446.7, 422.6, and 421.5. These values follow the trend expected from the variation of the reaction cross section with deuteron energy (see Figure 5). Because there is little variation in reaction cross section between 2.4 and 3.0 mev, the calibration curve obtained at the latter energy was applicable to all gas samples in which the energy loss of the bombarding beam was less than about 600 kev.

Local heating of the gas in the path of the deuteron beam could decrease the density of the gas and thus decrease the rate of neutron production. With the low average current used in this investigation, this effect was not observed, in agreement with similar observations by Butler (*3*).

The results of some determinations of deuterium in different gases are shown in Table II. For samples analyzed with 3.0-mev deuterons the mean error (given by the mean value of $B-A$) was −0.02-mm pressure, which was a measure of the accuracy of the method and showed that there was no bias. The mean value of the number of neutrons produced per 100 microcoulombs per mm pressure was 419.2, which is in agreement with the calibration value within the precision of the method. The relative standard deviation was ± 3.4%.

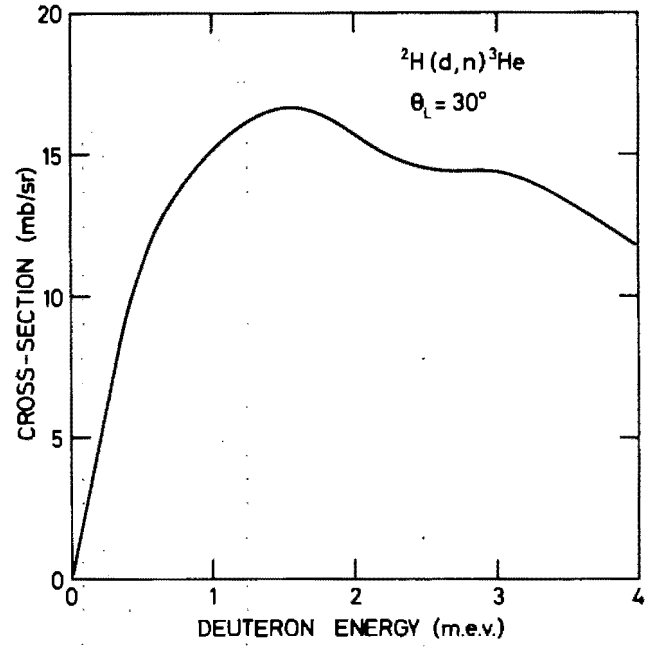

Figure 5. Variation of differential cross section (in laboratory coordinates) for reaction $^2H(d,n)^3He$ with deuteron energy at θ_L = 30°

Because the background count rate is a function of the content of the gas cell, the precision with which deuterium can be determined will vary with the gas composition. The minimum partial pressure of deuterium that could be mea-

sured with a precision of about ±3.4% in a sample containing either nitrogen or carbon dioxide at about 300-mm pressure was about 0.8 mm for an irradiation lasting an hour with 2000-μcoulomb beam current. When a lower precision of about ±10% was acceptable, 0.25-mm partial pressure deuterium could be measured with the same current.

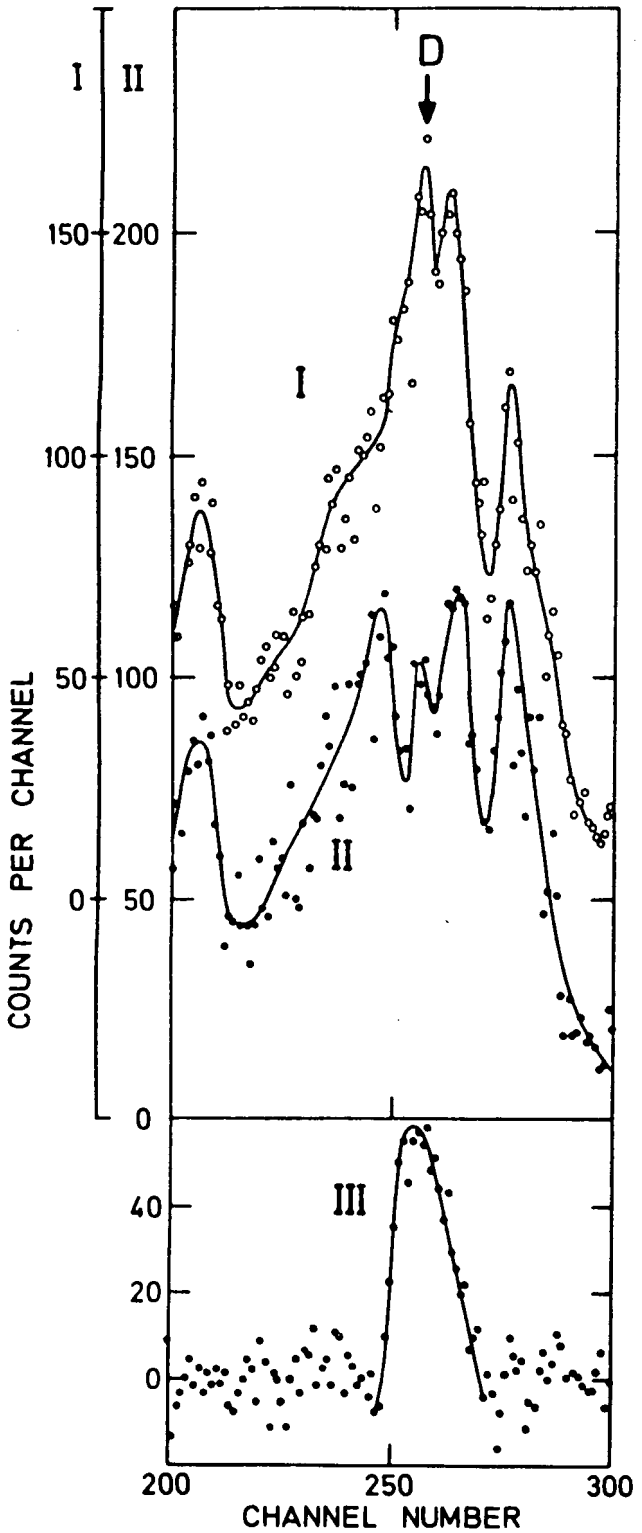

Figure 6. Neutron time-of-flight spectrum for deuterium in natural hydrogen

Observed spectrum (I), background (II), and difference between them (III)
P = 508 mm, E_d = 2.0 mev, θ_L = 0°
Total current 400 microcoulombs
Arrow shows calculated energy for neutrons from deuterium

SENSITIVITY

With a fresh nickel window the background count over the energy region where the deuterium peak appears in the energy spectrum was about 250 counts per 100 microcoulombs for E_d = 2.0 mev and θ_L = 0°. Under these conditions the determination of 1-mm pressure deuterium required an irradiation with a 500-microcoulomb beam (lasting between 15 and 30 minutes) for the relative standard deviation of the count to lie below that of the precision of the method. However, much shorter irradiations would have been sufficient for qualitatively detecting the presence of deuterium.

From the experience gained in the analyses it was considered that the method was sufficiently sensitive to detect the presence of a partial pressure of 0.1-mm deuterium in the irradiation cell. As this amount would be present in "natural hydrogen" at pressures somewhat less than atmospheric, commercial hydrogen (the deuterium content varies appreciably from the 0.015 atom % of natural hydrogen, but the value 0.010 atom % represents a fair average) was used to check the sensitivity of the method. A sample of commercial hydrogen at 508-mm pressure and 20°C was analyzed with a 2-mev deuteron beam and an integrated current of 400 microcoulombs. The resulting spectrum, which is compared in Figure 6 with the background spectrum obtained immediately afterwards with an empty cell under the same irradiation conditions, clearly shows the presence of deuterium above the background. The signal to noise ratio was 0.46. Considering the difficulty in evaluating the background counting rate, it is estimated that a signal of about half that observed here would be significant. Since the amount of deuterium in the 7-cc cell was 117 ng, and the deuterium traversed by the 4-mm diameter beam in the 3-cm long cell was 50.4 ng per sq cm, the sensitivity would thus be about 25 ng per sq cm. In terms of molecular concentration this limit is equivalent to about 50 ppm of deuterium.

INTERFERENCES AND LIMITATIONS

Interference in deuterium determinations may be expected when other components in the gas under investigation contain nuclides which could yield neutrons with energies sufficiently near to those from deuterium. One such case, ^{14}N, where the interference could be overcome by a change in the measuring angle, has already been discussed. An example of interference where little could be gained from a change in measuring direction is the case where the gas contains a component enriched in carbon-13. This nuclide yields a relatively large number of neutron groups on irradiation with deuterons. Interference would be experienced from n_1, n_2, n_3, n_4, or n_5 neutron groups, depending on the angle of measurement. The relative error introduced by such interference would decrease with an increase in the partial pressure of deuterium being determined but would increase with increasing enrichment of carbon-13. Similar interferences could be expected from gases containing enriched nitrogen-15 and oxygen-17 and/or 18.

A possible limitation in this method would be the presence in the gas sample under analysis, of a component which would decompose in contact with the heated spot on the nickel window or the rear platinum wall of the gas cell, to yield nonvolatile products. The decomposition products would be deposited in the path of the beam and could become points where relatively intense neutron generation could occur.

If this were the case, the background would become overwhelming. Furthermore, irradiation of such a sample would make the gas cell unusable for any subsequent sample. Even if the decomposition products did not cause excessive neutron generation, the deposition of material on the nickel window would increase the energy loss in the irradiation beam and would widen the energy spread of the bombarding particles, resulting in a distortion of the expected neutron energy spectrum.

ACKNOWLEDGMENT

The advice of Roy McMurray, Philip van der Merwe, and Izak van Heerden on the use of the time-of-flight spectrometer and their assistance during the course of the investigation sare gratefully acknowledged. Johan Kritzinger helped to design the irradiation cell which was made by Tobias Swart.

RECEIVED for review October 11, 1966. Accepted February 13, 1967.

PRINTED IN U. S. A.

No. 15

RADIOACTIVATION ANALYSIS OF CALCIUM-48 TRACERS BY PROTON IRRADIATION*

MAX PEISACH AND RENÉ PRETORIUS

Southern Universities Nuclear Institute

Faure, South Africa

Radiocalcium tracers have in the past been used to trace the movement of calcium *in vivo*. The first radioisotope so used was calcium-45 but with the increased availability of calcium-47 this shorter-lived isotope gained favour. However, because of the reluctance to use radioactive material for experimental purposes on healthy subjects, especially children, possible use of non-radioactive tracers has been receiving attention all over the world.

Natural calcium consists of six stable isotopes (see Table I), the most abundant of which, calcium-40, makes up almost 97% of the element. Because the other isotopes occur in low isotopic concentrations, they can each serve as a tracer, the usefulness of which would depend on the extent to which they can be enriched.

TABLE I
STABLE ISOTOPES OF CALCIUM

Isotope	Natural Abundance %	Price* $ per mg.	Isotopic Concentration of Separated isotope	Enrichment Factor
^{40}Ca	96·97	5·25	99·9	1·03
^{42}Ca	0·64	10·00	85	133
^{43}Ca	0·145	37·00	65	448
^{44}Ca	2·06	2·70	98	48
^{46}Ca	0·0033	635·00	40	12,000
^{48}Ca	0·18	26·00	95	528

Current price at Oak Ridge National Laboratory, Oak Ridge, Tenn., U.S.A. for isotopic concentration listed. Lower concentrations can be obtained at a reduced price.

In selecting the stable isotope to be used, two factors have to be considered:—

(1) the extent to which the tracer can be diluted
(2) the ease with which it can be determined at the dilution pertaining to the experiment.

In addition, practical considerations include the cost of the tracer. From Table I it is clear that calcium-40 offers virtually no scope for use as a tracer, whilst the enrichment factor for calcium-46 is far higher than that of any other isotope. Though much lower than calcium-46, the enrichment factors of calcium-43 and 48, and hence the range of dilutions over which they can prove useful, are comparable, but because of their lower cost the use of these isotopes as tracers of calcium is being studied.

The most sensitive method of isotopic analysis is by mass spectrometry. Unfortunately the extent of stable tracer research does not often reach the stage where such expensive equipment is warranted. Nuclear methods of analysis, though not as sensitive as mass spectrometry, can serve a useful purpose in this developing field. This paper describes such a method that enables isotopic concentrations of calcium-48 tracers to be determined.

Neutron activation analysis has long been used to determine small amounts of calcium-48, either by measuring the activity of 8.8-min calcium-49 produced in the activation, or by allowing this short-lived activity to decay to 57.5-min scandium-49 which can then be separated chemically and counted. In addition to calcium-49 the radioisotopes of calcium that are formed are produced in relatively low amounts — 165-day calcium-45 because of its long half-life and 4.7-day calcium-47 which is formed from a very low abundance target isotope. Thus, when the ratio of the tracer calcium-48 to total natural calcium has to be measured, rather than the content of tracer alone, neutron activation is not always a convenient method. Furthermore, if calcium-43 is used for tracing purposes neutron activation is of no use at all, because the product is not radioactive (see Table II).

TABLE II
NUCLEAR REACTION PRODUCTS OF CALCIUM ISOTOPES

Isotope	ACTIVATION PRODUCT			
	NEUTRON IRRADIATION (n,γ) reaction	*Q MeV	PROTON IRRADIATION (p,n) reaction	*Q MeV
^{40}Ca	^{41}Ca 7.7×10^4y	+ 8·361	^{40}Sc 0.18 s	−14·680
^{42}Ca	^{43}Ca stable	+ 7·929	^{42}Sc 62 s; 0.66 s	− 6·700
^{43}Ca	^{44}Ca stable	+11·136	^{43}Sc 3.9 h	− 3·003
^{44}Ca	^{45}Ca 165 d	+ 7·420	^{44}Sc 2.4d; 4.0h	− 4·431
^{46}Ca	^{47}Ca 4.7 d	+ 7·305	^{46}Sc 20 s; 84 d	− 2·165
^{48}Ca	^{49}Ca 8.8 m	+ 5·144	^{48}Sc 44 h	− 0·515

* Everling, F., Koenig, L. A., Mattauch, J. H. E., Wapstra, A. H. "Consistent set of energies liberated in nuclear reactions" Part I. National Academy of Sciences, National Research Council, Washington (1961).

When the isotopic concentration of a tracer has to be determined relative to the total content of the element, it is advisable to compare the tracer content with a naturally occurring isotope of about the same concentration level to increase the sensitivity of the analysis and to improve the precision. For this reason it would not be sufficiently sensitive to compare calcium-48 concentrations with those of calcium-40, but rather to use calcium-43, say, as an internal standard.

Charged particle irradiation is limited to thin deposits because of the very short range of charged particles in

* *This Paper was read at a Symposium on Medical Electronics and nuclear instrumentation in Medicine during September 1965, in Johannesburg.*

matter. At the same time, the entire energy of the beam is deposited within a very small distance in the target, thus resulting in large temperature rises. Indeed, the thermal properties of a material frequently determine whether irradiation with charged particles is practical or not.

For the analysis of calcium by proton irradiation, few forms of the target material are suitable. The more common calcium compounds usually precipitated in analysis, such as the carbonate and oxalate decompose on heating. Possible interference from the nuclear reactions of other elements also make it desirable that only simple compounds such as the oxide and fluoride which melt at 2580° and 1360°C respectively be considered.

The proton activation of oxygen will result in the formation of fluorine-17 (66 s) and fluorine-18 (110 m) by (p, n) reactions on the stable isotopes of oxygen, whilst fluorine will form only 18-sec neon-19. Comparing the properties of these radionuclides with the (p, n) products of calcium listed in Table II it is clear that fluoride would be preferable to the oxide.

The Coulomb barrier for proton activation of calcium is about 4.1 MeV. It is thus desirable to irradiate at energies somewhat above this level, in order to obtain increased yields. Furthermore at energies of between 4 and 5 MeV no reaction with calcium-40 or calcium-42 can occur because they are too endoergic (see Table II column 5). Thus apart from the short-lived neon activity, proton irradiation in this energy range can only produce (p, n) products with the heavier calcium isotopes, calcium-43, 44, 46 and 48. The activities that would thus be produced in the irradiated material would consist of a 4-hour activity from scandium-43 and 44 which cannot be resolved by halflife measurements, and a 44-hour activity of scandium-48 with possibly some scandium-44 m. It is not expected that calcium-46 would produce appreciable amounts of scandium-46 because of its low abundance. The determination of the isotopic concentration of calcium-48 would thus require a measurement of the ratio of the activities of scandium-48 and the mixture of scandium-43 and 44, the latter representing the total natural calcium.

EXPERIMENTAL.

PREPARATION OF SAMPLES

Samples of a separated calcium compound, in which the isotopic concentration of calcium-48 was to be determined, were converted to calcium fluoride by evaporation with HF in a platinum crucible. After all volatile materials had been expelled, the calcium fluoride was transfered to a tungsten boat and heated electrically *in vacuo*. Under these conditions thin deposits of calcium fluoride were distilled onto tantalum metal discs over an area compatible with the cross-sectional area of the irradiation beam.

PREPARATION OF STANDARDS

Calcium carbonate, enriched to 97.98% in calcium-48, was obtained from Oak Ridge National Laboratory, U.S.A. A standard solution of this material was made in dilute hydrochloric acid and diluted to required levels of isotopic concentrations of calcium-48 by the addition of predetermined volumes of a standard solution of natural calcium. From these solutions, calcium fluoride was obtained and suitable targets for irradiation were prepared with calcium-48 concentrations between that of natural calcium (0.18%) and about 3% for use as standards and to evaluate the method.

Because ratios of activities were to be measured, neither the weight of calcium fluoride, nor the area of the deposit had to be determined.

IRRADIATION AND MEASUREMENT

Sample discs were mounted on a rotating holder cooled by circulating coolant inside a vacuum chamber which fitted onto the beam tube of the 5.5 MeV Van de Graaff accelerator at the Southern Universities Nuclear Institute. The irradiation beam was defocussed until its cross-section exceeded that of the calcium fluoride deposit. With a continuous current of about 2μA, targets were irradiated at a proton energy of 4.75 MeV. From Figure 1 it can be seen that the ratio of the activities at the end of the irradiation of scandium-48 to that of scandium-43 and 44 increases only slightly when the duration of the irradiation changes by a few hours. Accordingly the irradiation usually lasted between 1 and 2 hours; much longer irradiation would have led to an increased ratio, but the cost of a long irradiation was not justified by the rise in sensitivity.

After irradiation, samples were analysed either by gamma-ray spectroscopy, or by gross gamma-ray counting with 3″ × 3″ NaI(Tl) scintillation detectors. Counting usually started about 15 minutes after irradiation, thereby allowing sufficient time for all very short-lived activities to decay, and continued until sufficient data had been accumulated to allow the 4-hour and 44-hour activities to be separately determined.

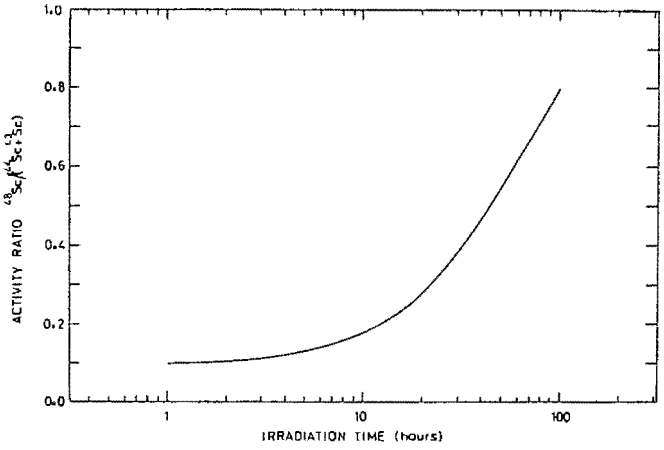

FIGURE 1.

The change of the activity ratio with the irradiation time.

RESULTS.

Gamma-ray spectra recorded during the decay of an irradiated sample of natural calcium fluoride are shown in Figure 2. Immediately after the irradiation, the presence of scandium-44 is identified by the pronounced peak due to positron annihilation radiation of 0.51 MeV and the photopeak from the 1.16 MeV gamma-ray. As expected, the formation of scandium-43 was not clearly obvious, because the abundance of calcium-43 is so much less than that of calcium-44 and the intensity of the 0.37 MeV gamma-ray is low. An apparent photopeak corresponding to a gamma-ray of 1.67 MeV is caused by coincidence summing of β+ and 1.16 MeV radiation (sum peak I in Figure 2).

After 8.60 hours the presence of the longer-lived

scandium-48 could already be shown by the appearance of photopeaks from gamma-rays of 0.99 and 1.04 MeV (unresolved) and 1.31 MeV. At the same time the sum peak I was still obvious and similar sum peaks at about 2 MeV, (sum peak 2) from chance coincidence between 0.99 and 1.04 gamma-rays, and at about 2.3 MeV, (sum peak 3) from one of these gamma-rays coinciding with the 1.31MeV gamma-ray, also became distinguishable. After about 46 hours, the characteristics of scandium-44 had almost disappeared, but the positron annihilation peak was still discernable. But for the disappearance of the latter peak, the shape of this curve remained unaltered even after about 150 hours, although by then the count rate had fallen so much that random coincidence peaks were no longer visible.

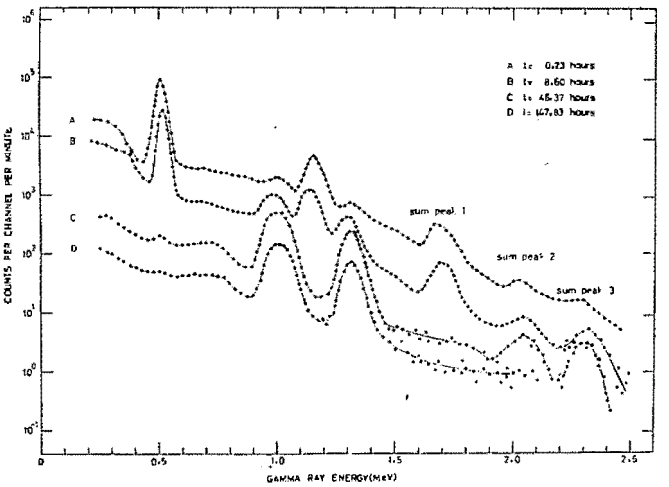

FIGURE 2.

Gamma-ray spectra obtained from natural calcium fluoride irradiated with 4.75 MeV protons.

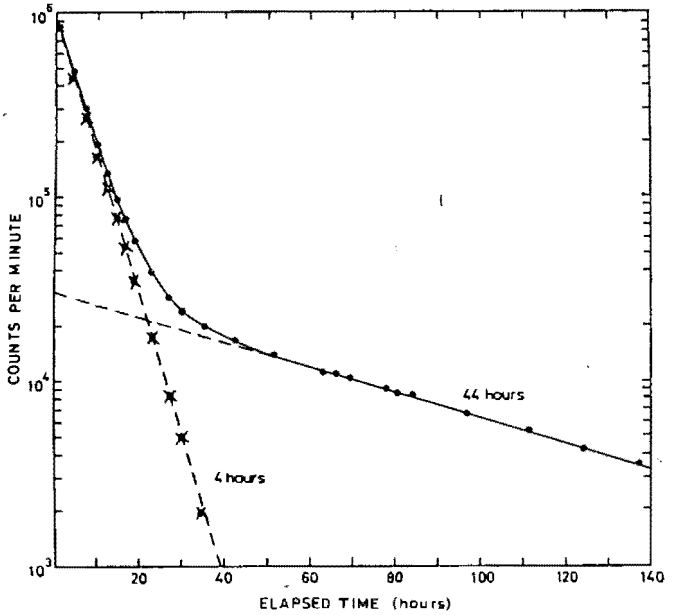

FIGURE 3.

Decay curve of proton-irradiated natural calcium fluoride.

Decay measurements were carried out on each of the above-mentioned gamma-rays and these served to confirm the original identification.

A specially prepared thick target of 6.3 mg/cm² natural calcium fluoride was activated to confirm that no interfering activities were produced. The decay of this material is shown in Figure 3. From an activation of about 2 hours the activities of the 44-hour and 4-hour halflife radionuclides were 31,000 and 900,000 c.p.m. respectively, for the counting conditions prevailing at the time of measurement. These values change according to the total weight of calcium fluoride on the target, the thickness of the deposit, the irradiation current and the counting geometry, but as ratios have to be determined, the absolute values of the measurements may vary over a wide range, without necessarily affecting the precision of the determination.

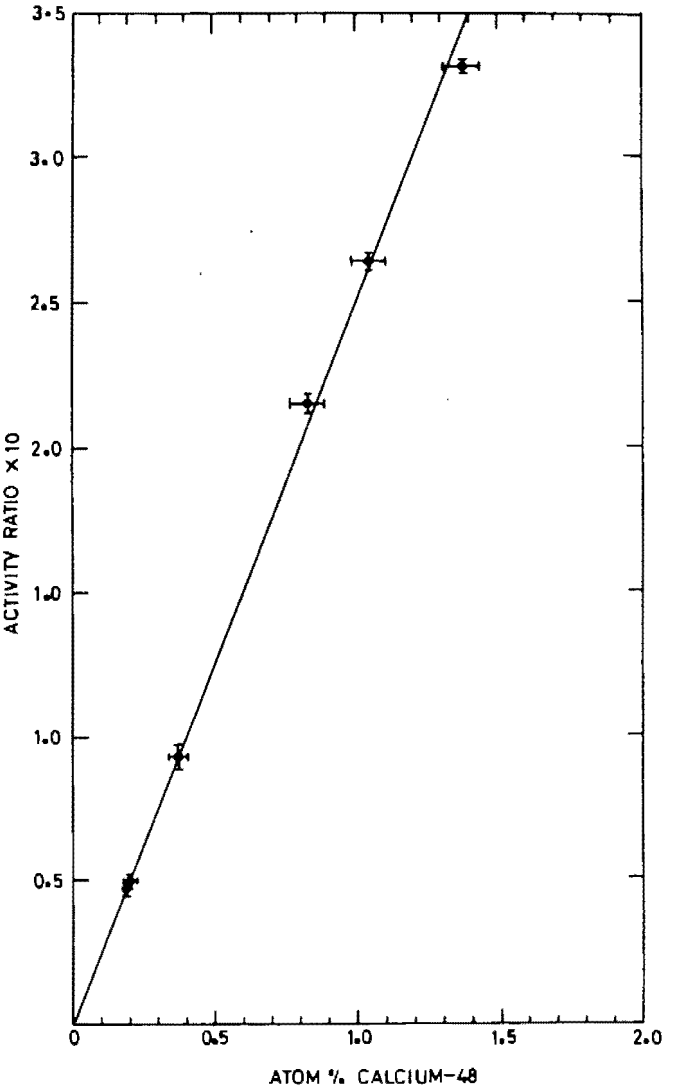

FIGURE 4.

Calibration curve showing the change of the activity ratio with isotopic concentration of calcium-48. The error flags refer to estimated errors in preparing the standards.

The variation of the activity ratio at the end of the irradiation, of scandium-48 to scandium-43 and 44 with isotopic composition constitutes the calibration curve of the method, provided targets of approximately the same thickness are irradiated for a fixed duration. One such calibration curve obtained at Ep = 4.75 MeV for an irradiation of 2½ hours is shown in Figure 4 over the range from natural composition to 1.4 atom % calcium-48. The activity ratio changes linearly with calcium-48 content, so that one sample prepared as standard and a natural composition sample are sufficient to fix the calibration line. Table III shows that for the above conditions the mean value of the activity ratio was 0.252, with a relative standard error of 2.7%, per atom % calcium-48. To obtain the values in column 4 and 5, each sample was considered as an unknown, and the result of the measurement expressed in terms of the calibration line obtained from the other points.

TABLE III
RESULTS OF ANALYSES

Known Atomic % ^{48}Ca (A)	Activity Ratio × 100	Activity Ratio per unit atom %	Measured Atomic % ^{48}Ca (B)	Observed Difference (B − A)
0·185	4·75	0·257	0·188	+ 0·003
0·192	4·83	0·252	0·191	− 0·001
0·375	9·32	0·249	0·369	− 0·006
0·825	21·57	0·262	0·854	+ 0·029
1·040	26·38	0·254	1·045	+ 0·005
1·370	33·15	0·242	1·313	− 0·057

Mean value 0·252 ± 0·007 Mean Error = − 0·004 atom %
Relative standard error ± 2·7 %

DISCUSSION

ADVANTAGES OF THE METHOD

The main advantage of the method lies in its simplicity and the cancellation of errors normally occurring during activation analysis. The activity **A**, produced in **w** g. of a target element irradiated in a flux of ϕ particles per cm²-sec by a reaction with cross-section σ is given by

$$\frac{A}{w} = \frac{N \delta \phi a (1 - e^{-\lambda t})}{M}$$

where **N** is the Avogadro number, 6.023×10^{23}, and **M** the atomic weight of the target element. The fractional abundance of the target isotope producing the required activity is **a**.

In an analysis such as described here the ratio of activities is given by

$$R = \frac{A_p}{A_q} = \frac{\delta_p a_p (1 - e^{-\lambda_p t})}{\delta_q a_q (1 - e^{-\lambda_p t})}$$

where p and q refer to the two measured activities, 44-hour scandium-48 and the sum of 4-hour scandium-43 and 44 respectively. It is clear that for a fixed irradation time **t**

$R = K \frac{a_p}{a_q}$ $R = Ka_p$

provided the isotopic concentration of calcium-43 and 44 remained constant at the level found in nature. The proportionality constant, K, includes the ratio of the reaction cross-sections and the time dependence factor plotted in Figure 1.

Experimentally it is not necessary to determine the weight of the target element, the irradiation flux or any variation in it, the cross-section of the beam of irradiating particles nor even the absolute activities of the products, if the standards are measured under the same conditions.

As a result of the wide difference in the halflives of the measured products, the activities of each radionuclide can readily be separated. The close resemblance between scandium-43 and scandium-44 makes it difficult to distinguish between them, but this is an advantage rather than a disadvantage, as it enables the two activities to be considered as one which is a measure of the total natural calcium content of the sample.

Because the only measurements made are non-destructive gamma-ray counting and spectroscopy, the sample remains intact after analysis. Consequently standard samples may be used repeatedly, and analysed samples may be retained for future requirements.

DISADVANTAGES OF THE METHOD

As the method depends on determining a ratio of activities, the main source of error lies in determining the separate activities. At low enrichments, the 4-hour activity can readily be observed even after a relatively short irradiation, but as the enrichment increases, the activity of scandium-48 increases rapidly relative to the total activity of the sample; it is expected that when the isotopic concentration of calcium-48 exceeds 4% scandium-48 would become the main activity in the irradiated sample. Accordingly the method is best suited for samples of low isotopic concentrations of calcium-48. Very highly concentrated samples could, however, be diluted with natural calcium before analysis.

The main purpose of the method was to determine the isotopic concentration of calcium-48, accordingly no attempt was made to refine the techniques to utilize micro amounts of calcium. The prior separation of at least 5 mg of a calcium sample is required in order to overcome the large losses incurred during the evaporative preparation of the target disc. However, present investigations are directed towards developing techniques suitable for quantities of calcium less than 1 mg, as this would enable the calcium in about 1 cc of blood serum to be analysed.

ACCURACY AND PRECISION

The results in Table III gave a mean error of —0.004 atom %, a value sufficiently close to zero to indicate no bias in the analysis. Similarly the relative standard error of ± 2.7% shows that the precision of the method is better than the large errors frequently occurring in biological work. For medical purposes a method of analysis capable of distinguishing samples in which tracer concentration vary by 10%, would be acceptable.

This condition is readily met in the present investigation.

The main source of error in the analysis is contamination but as proton activation reactions of many nuclides occur above relatively high threshold energies, such nuclides would not yield any radioactive products at the relatively low proton energies used. However, contamination from other calcium salts would not be immediately obvious and would require stringent precautions to be taken.

ACKNOWLEDGEMENTS.

The staff of the Institute is thanked for their interest, assistance and constructive criticism. One of us (R.P.) thanks Dr. H. P. Malan, his Promotor at the University of Stellenbosch, for permission to publish his results which will form part of his doctorate thesis to be submitted to the University of Stellenbosch.

No. 16

Reprinted from:

NUCLEAR PHYSICS, VOLUME A99 (1967) No. 1

W. R. McMURRAY, M. PEISACH, R. PRETORIUS,
P. VAN DER MERWE and I. J. VAN HEERDEN
Southern Universities Nuclear Institute, Faure, C.P., South Africa

A STUDY OF THE Ca(p, n)Sc REACTIONS
(I). Energy levels in scandium isotopes

NORTH-HOLLAND PUBLISHING COMPANY - AMSTERDAM

1.E.1 *Nuclear Physics* A99 (1967) 6—16;

A STUDY OF THE Ca(p, n)Sc REACTIONS
(I). Energy levels in scandium isotopes

W. R. McMURRAY, M. PEISACH, R. PRETORIUS,
P. VAN DER MERWE and I. J. VAN HEERDEN
Southern Universities Nuclear Institute, Faure, C.P., South Africa

Received 17 March 1967

Abstract: Time-of-flight measurements have been made on the neutrons emitted from enriched targets of ^{43,44,48}Ca bombarded by 4.0 to 5.5 MeV protons. Two additional levels have been found in ^{43}Sc at 1347±10 and 1424±10 keV in agreement with recent work on the ^{40}Ca(α, p) reaction; in ^{48}Sc, knowledge of the level structure has been extended up to 4169 keV with the observation of 34 additional levels; and the measurements for the low-lying states in ^{44}Sc agree with previous work. The measured (p, n_0) Q-values for ^{43}Ca, ^{44}Ca and ^{48}Ca are −2998±10, −4447±10 and −534±15 keV, respectively.

E NUCLEAR REACTIONS ^{43}Ca, ^{44}Ca, ^{48}Ca (p, n), E = 4.0−5.5 MeV; measured $\sigma(E_n)$; deduced Q. ^{43}Sc, ^{44}Sc, ^{48}Sc, deduced levels, nuclear temperature. Enriched targets.

1. Introduction

Since this work was initiated, (p, nγ) and (p, γ) studies have been reported by Broman and Du Bois [1]) and Chasman *et al.* [2]) concerning the level structures of ^{43}Sc and ^{48}Sc, respectively. The high resolution of Ge-Li drifted detectors has been used by these workers to determine the energies of the low-lying levels of these nuclei. The intrinsic energy resolution of neutron time-of-flight equipment as used in the present work cannot compare with that obtained with Ge-Li drifted detectors but a systematic approach to level structure measurements gives an unambiguous level scheme with uncertainties only a few times larger than when using the semi-conductor detectors.

Levels in ^{43}Sc have also been obtained from several, charged-particle, reaction studies; most recently by Čujec [3]) using a magnetic spectrograph.

2. Experimental details

2.1. TIME-OF-FLIGHT SYSTEM

The measurements were made with the pulsed beam from the SUNI 5.5 MV Van de Graaff accelerator. The beam pulse length was usually about 4 ns for the proton beam with pulse separation times of either 400 or 600 ns. The detector and associated electronics has been described elsewhere [4]). The use of NE 213 liquid

scintillator makes it possible to discriminate against γ-backgrounds using pulse shape discrimination. The spectra then obtained had negligible residual background relative to the Ca(p, n) groups even at flight paths exceeding 6 m. The relative detector efficiency is determined as a function of energy by comparison with the known response of a standard long counter and the detector bias conditions can be duplicated as described in ref. [4]).

The time scale of the time-to-amplitude converter was calibrated with cables of known delay. The dispersions used were between 0.75 and 1.05 ns per channel. Random spectra were obtained to check the linearity of the time-to-amplitude converter.

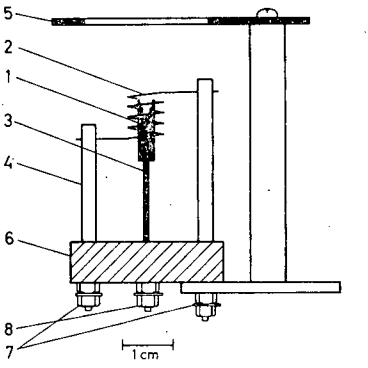

MICRO-EVAPORATOR

1) Crucible (Ta), 2) Tungsten filament: diam. 0.25mm
3) Crucible-holder (W): diam. 2mm
4) Filament support, 5) Target-holder
6) Insulator and system base
7) Filament connections
8) High-voltage connection

Fig. 1. Sketch of the micro-evaporator used to evaporate enriched CaO material.

The target in the form of CaO was evaporated onto 0.025 cm tantalum discs 2.5 cm in diam. These were supported on an O-ring seal at the end of a thin walled (0.025 cm) brass can which also acts as a Faraday cup. A beam current integrator and long counters were used as reference monitors. A jet of compressed air gave direct cooling to the target backing. No deterioration of targets was observed after prolonged bombardment with 5 μA of protons.

The energy of the accelerated protons was monitored by an NMR probe in the magnetic field of the accelerator analysing magnet. This was calibrated up to an NMR frequency of 18.964 MHz by measuring (p, n) reaction thresholds on ^{7}Li, ^{13}C, ^{45}Sc and ^{63}Cu and ^{65}Cu, and confirmed up to 33.250 MHz by observation of a strong ^{30}Si(α, γ)^{34}S resonance [5]).

2.2. TARGET PREPARATION

CaO targets were prepared using enriched $CaCO_3$ material obtained from Oak Ridge National Laboratory. Enriched $CaCO_3$ (1 to 3 mg) was placed in a platinum

crucible and reduced to CaO in a muffle furnace before it was transferred to the tantalum crucible of a micro-evaporator designed for the evaporation of enriched materials at high temperatures, CaO evaporates at about 2500° C.

Fig. 1 shows the form of the micro-evaporator which was based on a more elaborate design which has been reported [6]). A high temperature is achieved by bombarding the crucible (0.32 cm diam by 1.27 cm length) with up to 0.5 A of electrons emitted from a heated tungsten or thoriated tungsten coil around the crucible. A variable bombarding potential of up to 500 V enables the temperature to be adjusted up to about 3000° C (sufficient even to soften the tungsten rod support below the crucible). A suitable power source was constructed using Hg vapour rectifier valves in a conventional full wave rectifier circuit which is undamaged by accidental current surges, which occur in the event of sparks or mechanical shorts. A high current cut-out is added to protect the supply.

In order to obtain a uniform deposit on the target, the top half of the crucible was flared. The targets used in this work had a thickness immediately after evaporation of about 100 $\mu g/cm^2$ corresponding to 5 keV energy loss for 5 MeV protons. The precision of the weighings on which thickness was based varied between 10 and 20 %. If the CaO changed completely to $CaCO_3$ (a slow process) these targets would become 8.5 keV thick to 5 MeV protons.

3. Energy levels of ^{43}Sc

The targets used to study the ^{43}Sc level structure were made with enriched material obtained from Oak Ridge National Laboratory and contained ^{40,42,43,44,48}Ca with percentage abundances of 46.28, 7.61, 24.15, 21.88 and 0.08, respectively. Only the last three isotopes can contribute to the neutron emission at the proton energies used in this work. Neutron spectra were observed at proton energies ranging from 4.0 MeV to 5.5 MeV. Fig. 2(a) is a neutron spectrum obtained at 0° with a bombarding energy of 5.25 MeV, and fig. 2(b) was obtained with a different target viewed at 90° with a proton energy of 5.535 MeV. Because of their Q-values, groups a–c are ascribed to the ^{44}Ca(p, n)^{44}Sc reaction. The level schemes of ^{43}Sc and ^{44}Sc deduced from the observed neutron spectra are given in fig. 3 where the present work is compared with the previously published data. The levels assigned to ^{43}Sc are also tabulated in table 1. The ground state Q-values are given in table 2.

Neutron group n_8 in fig. 2(b) is assigned to ^{43}Sc because (i) its energy agrees more closely with a level in ^{43}Sc than with the level scheme of ^{44}Sc [8]), and (ii) if the third excited state in ^{44}Sc has the high spin value tentatively assigned to it (6 or 7^+), it is unlikely to be excited with significant intensity in the present work.

Neutron groups 6 and 7 are assigned to levels in ^{43}Sc. Such levels were not observed in the work of Broman and Du Bois [1]). These authors also tentatively assigned a level at 1150 ± 10 keV close to a definite assignment at 1175 ± 4 keV. The present work has shown no evidence of a doublet in this position (see group 5 in fig. 2). If two

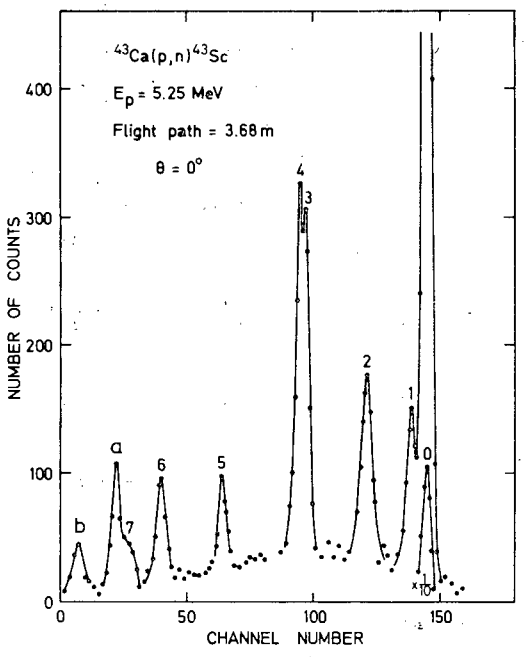

Fig. 2(a). Neutron time-of-flight spectrum obtained at 0° by bombarding an enriched target containing ^{43}Ca and ^{44}Ca with 5.25 MeV protons.

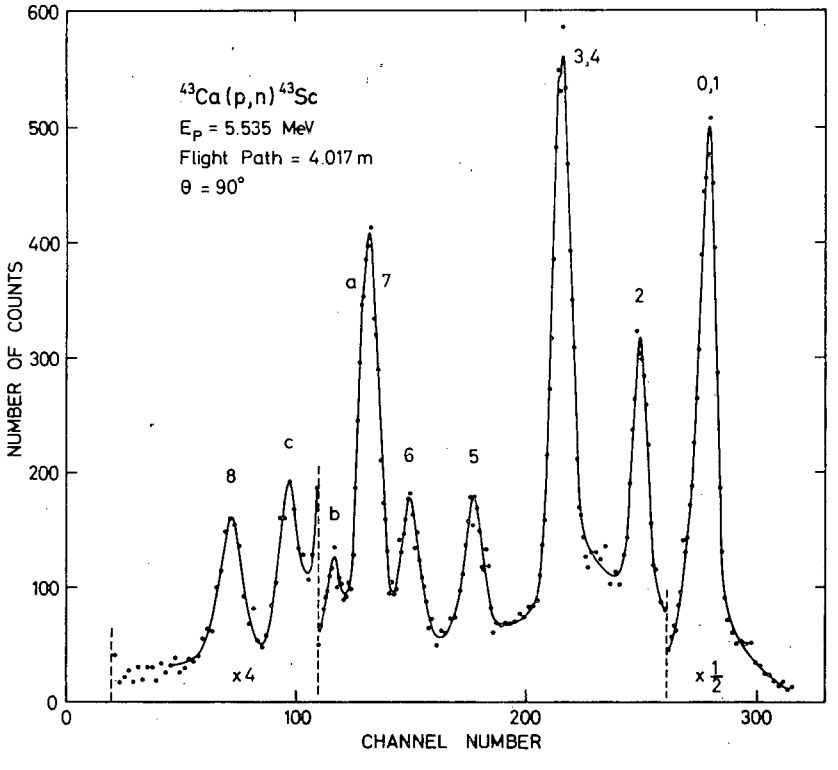

(b). Neutron time-of-flight spectrum obtained at 90° with 5.535 MeV protons.

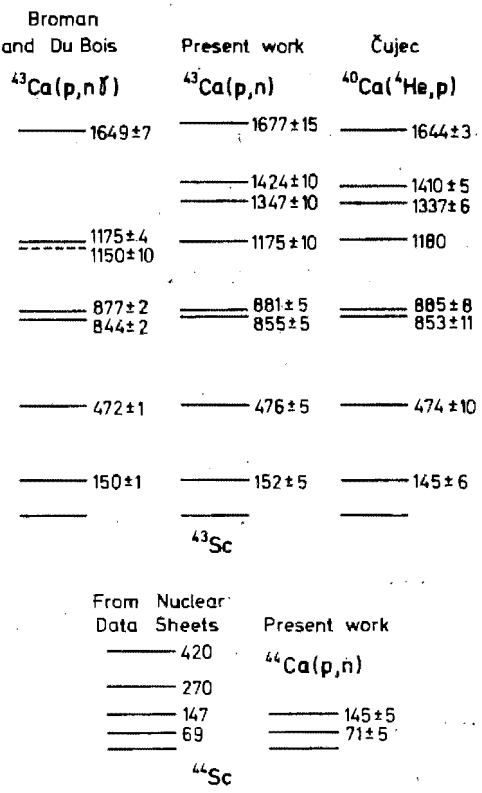

Fig. 3. Energy level schemes for ^{43}Sc and ^{44}Sc.

TABLE 1
Energies of ^{43}Sc levels

Level	Energy (keV)	Level	Energy (keV)	Level	Energy (keV)
1	152±5	4	881± 5	7	1424±10
2	476±5	5	1175±10	8	1677±15
3	855±5	6	1347±10		
			Energies of ^{45}Sc levels		
1	151±20	16	2776± 6	31	3515± 5
2	237±20	17	2800± 6	32	3557±10
3	628± 6	18	2885± 6	33	3617±10
4	1139± 7	19	2920± 4	34	3640±10
5	1397± 7	20	2969± 4	35	3667± 5
6	1883± 6	21	3021± 6	36	3705±10
7	2080± 7	22	3050± 6	37	3805± 5
8	2175± 5	23	3146± 4	38	3682±10
9	2267± 6	24	3208± 4	39	3919±10
10	2380± 5	25	3258± 6	40	3975±10
11	2508± 4	26	3292± 6	41	4017±10
12	2548± 4	27	3322± 6	42	4060±10
13	2630±10	28	3353±10	43	4086±10
14	2661±10	29	3370±10	44	4139±10
15	2725±10	30	3479± 5	45	4169±10

neutron groups of roughly equal intensity are present in these spectra they would have to be less than 20 keV apart. The presence of a second neutron group cannot be excluded, but no evidence has been found for its existence in this work. This is in agreement with the measurements of Čujec [3]) who observed only one level at 1180 keV with an experimental resolution of 25 keV. Phillips *et al.* [9]), however, have confirmed the work of Broman and Du Bois. Also using a Ge-Li drifted detector to observe the decay gammas, they excited the levels of ^{43}Sc with the ^{40}Ca(α, p)^{43}Sc reaction.

TABLE 2

Reaction	Ground state Q-values (keV)	
	present work	other work [7,8])
^{43}Ca(p, n_0)^{43}Sc	-2998 ± 10	-3005 ± 11
^{44}Ca(p, n_0)^{44}Sc	-4447 ± 10	-4431

A striking feature of the ^{43}Ca(p, n)^{43}Sc reaction is the relatively high cross section to the ground state of ^{43}Sc. Limited measurements were made of the excitation and angular distribution cross sections. Uncorrelated fluctuations were observed implying a predominantly compound nucleus mechanism. It would follow that the relative cross sections for the excitation of different final states in ^{43}Sc are determined by statistical considerations as modified by barrier penetration probabilities. As the spin of both the ^{43}Ca target and ^{43}Sc ground state is $\frac{7}{2}$, the reaction to this state can proceed with incoming proton and outgoing neutron having zero angular momentum thus minimizing Coulomb and centrifugal barrier effects. The first excited state in ^{43}Sc has been assigned [1]) a spin $\frac{3}{2}$ so that the formation of this state involves significant barrier inhibition to either or both the incoming proton and outgoing neutron and hence occurs with reduced probability. The same considerations imply that all the other levels excited in this study have spins different to $\frac{7}{2}$. This qualitative argument places some doubt on the $\frac{7}{2}$ spin assignments by Phillips *et al.* [9]) for the ^{43}Sc levels at 1347 and 1424 MeV corresponding to neutron groups 6 and 7 in the present work.

No low-lying levels are expected on the basis of a simple shell model assuming a ^{40}Ca core and additional nucleons in the $1f_{\frac{7}{2}}$ shell [10]). Bansal and French [11]) have, however, calculated that a $d_{\frac{3}{2}}$ hole state in the $f_{\frac{7}{2}}$ shell region (described as the coupling of a hole directly with the ground state) should have a very low excitation in ^{43}Sc. This could correspond to the $\frac{3}{2}^+$ state [1]) at 150 keV. Other low-lying levels could be explained using a deformed Nilsson well. Čujec [3]) finds that this model predicts the existence of several bands of low-lying levels with small spins (up to $\frac{7}{2}$).

It is clear from fig. 2 that the cross sections for the ^{43}Ca(p, n) and ^{44}Ca(p, n) reactions are of roughly equal magnitude. From the measured absolute efficiency of the detector and the integrated beam current, values could be obtained for the magni-

tude of the differential cross sections, which varied from about 1 mb/sr to 12 mb/sr for the different levels (the latter figure is the cross section for the formation of the ^{43}Sc ground state). This information is relevant to the discussion of possible contaminant groups in the ^{48}Ca(p, n)^{48}Sc spectra (see sect. 4 below).

4. Energy levels of ^{48}Sc

A series of time spectra were obtained to resolve the neutron groups emitted from a CaO target containing 76.1 % ^{48}Ca. The target also contained ^{40,42,43,46}Ca with

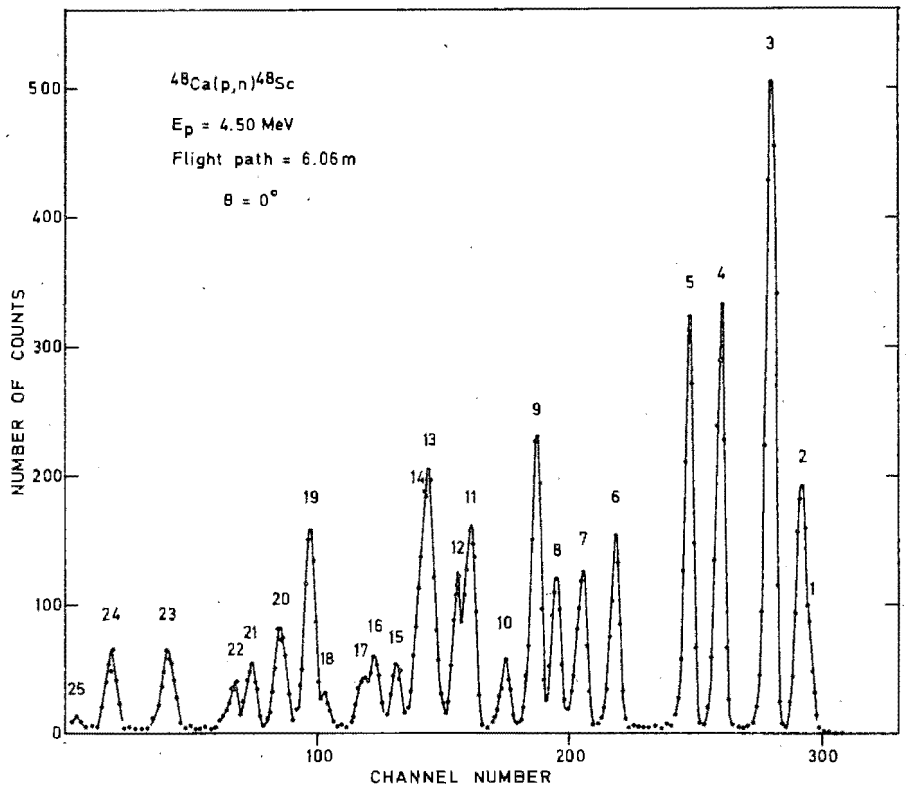

Fig. 4. Neutron time-of-flight spectrum obtained at 0° by bombarding an enriched target containing ^{48}Ca with 4.5 MeV protons.

percentage abundances of 22.6, 0.16, 0.04, 0.59 and 0.47, respectively. The proton energy was again varied from 4.00 to 5.50 MeV, and a large number of neutron groups was observed.

Energy resolution in a time-of-flight system is best at low energies. It is therefore necessary to observe closely spaced levels near the threshold of detection in order to obtain sufficient separation from neighbouring levels. From successive spectra at increasing proton energies, it is not difficult to build up a consistent energy level

scheme. In this work (on the ^{48}Sc levels), neutron groups could usually be clearly separated in two or more spectra. Typical neutron spectra are reproduced in figs. 4 and 5.

The absolute cross sections for the production of individual neutron groups is found to be between 0.5 and 5.0 mb/sr. The cross sections therefore have the same order of magnitude as those reported for the other energetically possible calcium (p, n) reactions (see sect. 3). From their low percentage abundance in this target, it follows

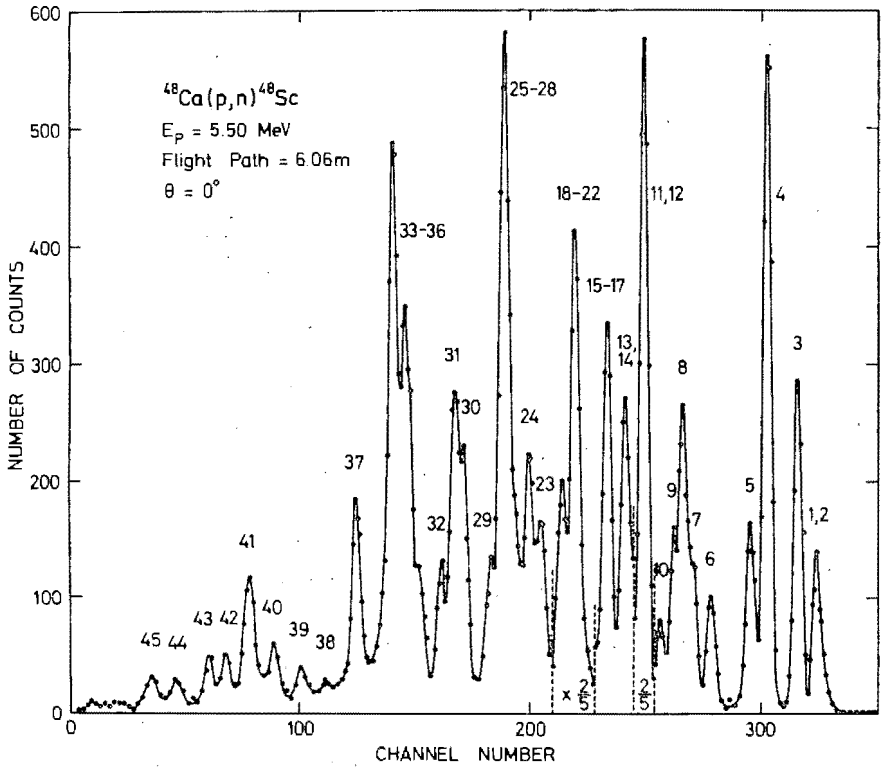

Fig. 5. Neutron time-of-flight spectrum obtained at 0° by bombarding an enriched target containing ^{48}Ca with 5.5 MeV protons.

that they cannot give neutron groups with sufficient intensity to confuse the assignment of levels to ^{48}Sc.

The levels in ^{48}Sc thus obtained are tabulated in table 1. The lower portion of the level scheme is also compared in fig. 6 with that derived from earlier time-of-flight work by Elwyn *et al.* [12]) and Ferguson and Paul [13]), and the (p, nγ) measurements of Chasman *et al.* [2]). The latter authors presented convincing evidence to show that the (p, n_0) transition to the ground state of ^{48}Sc was not observable presumably because of its very high spin value (6^+). This has been taken into account in the present work. The Q-value for the ground state transition is found to be 534 ± 15 keV compared

to 529±10 keV which Chasman *et al.* based on a Q-value of 660±10 keV for the first excited state as determined by Johnson [quoted in ref. [7])].

The close agreement of the energies of the levels of ^{48}Sc determined in the present

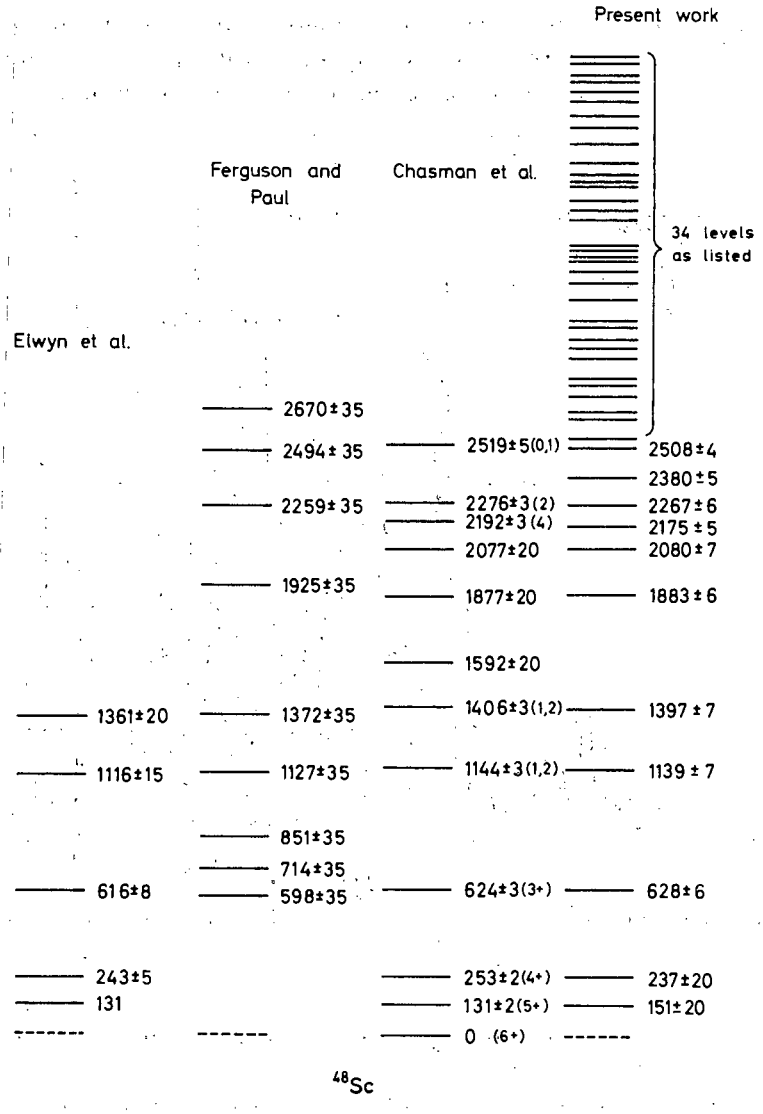

Fig. 6. The lower portion of the ^{48}Sc level scheme derived from the present work compared with results of other workers.

work with those obtained by Chasman suggests that the overall uncertainties on the present work are not very much larger than theirs. The uncertainties quoted in table 1 for the present work are based on the experimental reproducibility from one spectrum

to another. As the level energies are here determined from each spectrum, the values (based on Q-value differences) are more precise than the Q-value determination for any one level. The energies of the first two levels are not accurately determined in the present work because, at these energies, they could not be adequately resolved.

Using a ^{3}He proportional counter, Chasman *et al.* also observed levels not extracted from the γ-decay measurements. The existence of a level at 1592 keV is, however, not confirmed by the present study notwithstanding the use of much higher proton energies. An additional level is found at 2380 keV as well as 34 other levels between 2508 keV and 4169 keV.

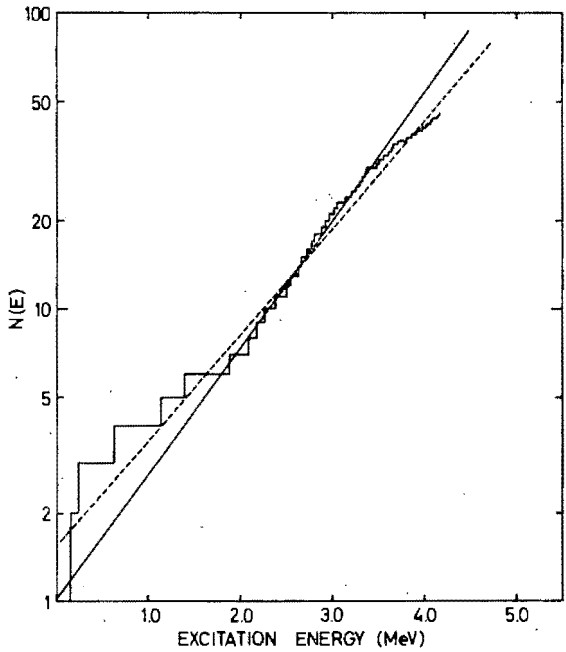

Fig. 7. An Ericson plot of $N(E)$, the number of levels in ^{48}Sc below the excitation energy E as observed in the present work. The full straight line has a slope corresponding to a nuclear temperature of 1.0 MeV, and the dashed straight line corresponds to a temperature of 1.2 MeV.

Unlike the low-lying levels of ^{43}Sc, those of ^{48}Sc are in reasonable agreement both as regards energy and spin with calculations based on the simple shell model [10]).

The level structure at high excitations in ^{48}Sc as determined by this study might be an over-simplification. It is possible that some peaks have not been resolved. Deviation from a straight line in an Ericson plot [14]) is assumed to be indicative of unrecognized structure. Fig. 7 is such a plot of the present data where the superposed unbroken line corresponds to a nuclear temperature of 1.0 MeV and the dashed line to 1.2 MeV. The unbroken line deviates considerably from the level scheme above an excitation of about 3.7 MeV but the corresponding nuclear temperature (1 MeV)

is lower than other values in the literature [15,16]). If the nuclear temperature of 1.2 MeV is more correct, there is less likelihood of lost level structure in the present work.

Financial assistance from the South African Atomic Energy Board is gratefully acknowledged. One of us (R.P.) thanks his Promotor for permission to publish results which will form part of a doctorate thesis to be submitted to the University of Stellenbosch.

References

1) L. Broman and J. Du Bois, Nuclear Physics **72** (1965) 529
2) C. Chasman, K. W. Jones and R. A. Ristman, Phys. Rev. **140B** (1965) 212
3) B. Čujec, Nuclear Physics **81** (1966) 523
4) W. R. McMurray, P. van der Merwe and I. J. van Heerden, Nuclear Physics **A92** (1967) 401
5) W. R. McMurray, I. J. van Heerden and G. Wiechers, Nuclear Physics **73** (1965) 113
6) W. Menti, M. Martin, E. B. Bas and O. Vogt, Nuclear Instr. **31** (1964) 25
7) G. J. McCallum, A. T. G. Ferguson and G. S. Mani, Nucl. Physics **70** (1960) 116
8) Nuclear Data Sheets, compiled by K. Way *et al.* (Printing and Publishing Office, National Academy of Sciences – National Research Council, Washington 25, D.C.)
9) W. R. Phillips, R. de La Pena and T. A. Critchley, Nuclear Physics **A90** (1967) 379
10) J. D. McCullen, B. F. Bayman and L. Zamick, Phys. Rev. **134** (1964) B515
11) R. K. Bansal and J. B. French, Phys. Lett. **11** (1964) 145
12) A. J. Elwyn, H. H. Landon, S. Oleksa and G. N. Glasoe, Phys. Rev. **112** (1958) 1200
13) A. T. G. Ferguson and E. B. Paul, Nuclear Physics **12** (1959) 426
14) T. Ericson, Nuclear Physics **8** (1958) 265, **11** (1959) 481
15) N. Macdonald and A. C. Douglas, Nuclear Physics **24** (1961) 614
16) J. Jänecke, Nuclear Physics **48** (1963) 129

No. 17

Reprinted from:

NUCLEAR PHYSICS, VOLUME A99 (1967) No. 1

W. R. McMURRAY, M. PEISACH, R. PRETORIUS
P. VAN DER MERWE and I. J. VAN HEERDEN
Southern Universities Nuclear Institute, Faure, C.P., South Africa

A STUDY OF THE Ca(p, n)Sc REACTIONS
(II). Fluctuation analysis of the reaction ^{48}Ca(p, n)^{48}Sc

NORTH-HOLLAND PUBLISHING COMPANY - AMSTERDAM

2.D

Nuclear Physics **A99** (1967) 17—27; © *North-Holland Publishing Co., Amsterdam*

A STUDY OF THE Ca(p, n)Sc REACTIONS
(II). Fluctuation analysis of the reaction ^{48}Ca(p, n)^{48}Sc

W. R. McMURRAY, M. PEISACH, R. PRETORIUS
P. VAN DER MERWE and I. J. VAN HEERDEN
Southern Universities Nuclear Institute, Faure, C.P., South Africa

Received 17 March 1967

Abstract: The ^{48}Ca(p, n)^{48}Sc reactions to the first 11 excited states in ^{48}Sc have been studied as a function of angle and proton energy from 4.03 to 5.63 MeV. Absolute cross sections (±25 %) have been obtained using a calibrated, time-of-flight detection system. The cross sections are observed to have random fluctuations in accordance with the Ericson fluctuation theory. There is no indication of any direct reaction contributions to the cross sections. The average angular distributions are symmetric about 90°. The coherence energy Γ is observed to be $\leqq 9$ keV at 15 MeV excitation in ^{49}Sc. Autocorrelation analysis of the cross sections for exciting the third to 11th excited states of ^{48}Sc leads to probable spins of (3,4), (1,2), (1,2), 2, (1,2), 1, (2,3), 2 and 0, respectively.

E | NUCLEAR REACTIONS ^{48}Ca(p, n)^{48}Sc, $E = 4.03 - 5.63$ MeV; measured $\sigma(E; E_n, \theta)$. ^{49}Sc levels deduced Γ; ^{48}Sc levels deduced J. Enriched target.

1. Introduction

Compound nucleus effects have been observed in the ^{48}Ca(p, n) reaction at energies below 4 MeV by El Nadi *et al.* [1]) and Ricci *et al.* [2]). They associate peaks in their excitation curves with levels in ^{49}Sc. Jones *et al.* [3]) in a study of the ^{48}Ca(p, p) reaction observed resonances on a background of sharp fluctuations. They ascribed the fluctuations to overlapping $T = \frac{7}{2}$ states in the ^{49}Sc compound nucleus and the resonances to $T = \frac{9}{2}$ states which are isobaric analogues of low-lying levels in ^{49}Ca. These they observed at $E_p = 1.935$, 1.945, 3.86, 5.952 and 5.994 MeV centre-of-mass energies. The present work on the (p, n) reaction was undertaken in the proton energy range 4.0 to 5.6 MeV and, therefore, is not affected by the isobaric analogue resonances.

The cross sections of many reactions show rapid fluctuation with energy in satisfactory agreement with statistical theory developed by Ericson [4]) and Brink and Stephen [5]) for reactions proceeding via highly-excited, overlapping, compound states. Besides delineating the reaction mechanism, application of fluctuation theory can enable an estimate of the relative direct interaction amplitude and the mean lifetime of the compound states. In favourable cases, the analysis can give information on the spins of the particles in the exit channel [6]). Several careful studies are available of the detailed analysis of experimental data in terms of fluctuation theory. For example, Allardyce *et al.* [7]) investigated the ^{26}Mg(p, α) reaction, Dearnaley *et al.* [8])

the ^{27}Al(α, p) reaction and von Witsch *et al.* [9]) the ^{37}Cl(p, α) reaction. On the other hand, Van der Woude [10]) and Dallimore and Hall [11]) generated synthetic excitation functions to study the effects of finite energy range of data and finite resolution on experimentally determined quantities.

The criterion for the application of fluctuation theory is that the mean level width Γ should considerably exceed the mean level spacing D at the relevant excitation of the compound nucleus. With $E_p = 5.5$ MeV, the excitation in ^{49}Sc attained by proton capture in ^{48}Ca is about 15 MeV. This is not a high energy in view of the wide spacing of levels near the ground state of ^{49}Sc. Calculations of level spacings are not very reliable. An estimate of $D \approx 50$ eV at 15 MeV excitation is obtained by using the accepted dependence of level density on excitation energy and the mean level spacing at the neutron binding energy for nuclei of mass about 50. The theoretical work of Eder *et al.* [12]) gives $D \approx 0.05$ eV for ^{48}Ca at this excitation. A value of $D \leqq 100$ eV is obtained for ^{49}Sc by extrapolating from its known low-lying level structure using an Ericson plot of the form shown in fig. 7 of part (I) of this report. With $\Gamma \approx 10$ keV, the ratio Γ/D for ^{49}Sc is certainly much larger than 2, a value shown by Dallimore and Hall [11]) to be adequate for fluctuation analysis. The effects of a small Γ/D have been discussed by Moldauer [13]).

2. Cross-section measurements

The absolute efficiency of the neutron detector was determined for 4 MeV neutrons from the known ^{12}C(^{3}He, n) cross section [14]) with a target 180 μg/cm^2 thick. The efficiency at lower energies up to 2 MeV was obtained from measurements on various Li targets using the ^{7}Li(p, n) reaction cross section [15]). The absolute cross sections for the ^{48}Ca(p, n)^{48}Sc reaction are based on the deduced detector efficiency, the target thickness measured by weighing, the integrated proton beam current and the counts in the neutron spectrum for the reaction to a particular level. The major sources of uncertainty are the detector efficiency (± 20 %), the target thickness (± 15 %) and the counting statistics (usually better than ± 5 %). Relative uncertainties should be purely statistical.

The reaction ^{48}Ca(p, n)^{48}Sc has been studied as a function of energy and angle for incident protons between 4.03 MeV and 5.63 MeV. Measurements were made at 0° between 4.03 and 5.03 MeV in steps of 20 keV and at 90° in steps of 10 keV between 4.83 and 5.63 MeV. The results combined into one excitation curve for the reactions going to the first 11 excited states of ^{48}Sc are presented in fig. 1.

Angular distributions were measured at eleven energies between 4.43 and 5.53 MeV and eight angles from 0° to 150°. Two representative sets of results are given in figs. 2 and 3 for the reaction to levels 3 and 5 of ^{48}Sc, respectively. The angular distributions averaged over energy are shown in fig. 4.

The structure in the angular distributions is asymmetrical and rapidly fluctuating. The average cross sections, however, even when averaged over only 250 keV,

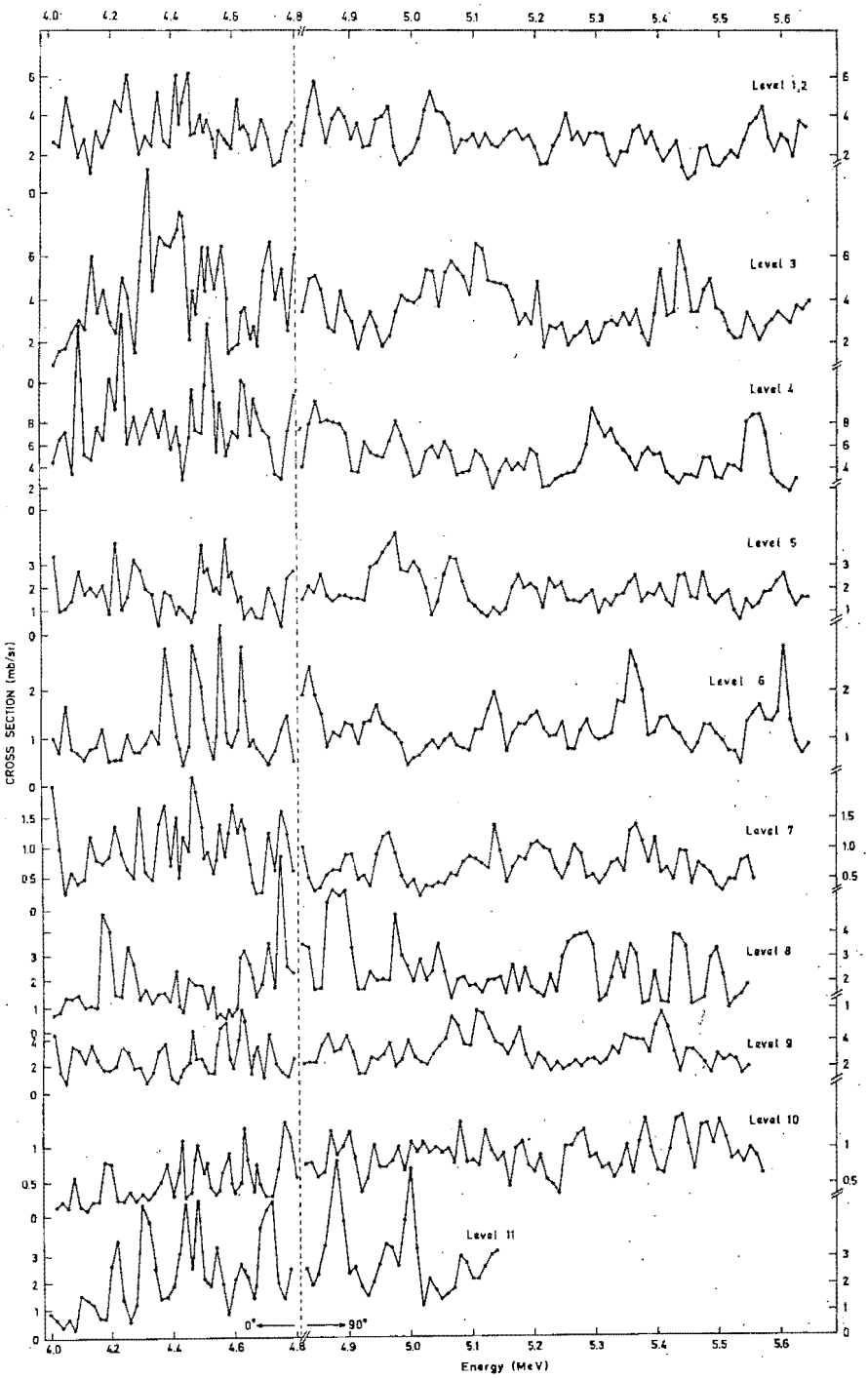

Fig. 1. The excitation cross sections for ^{48}Ca(p, n)^{48}Sc reactions to levels 1 to 11 in ^{48}Sc measured at 0° in the proton energy range 4.03 to 4.83 MeV and at 90° in the range 4.83 to 5.63 MeV. The ground state reaction was not observed.

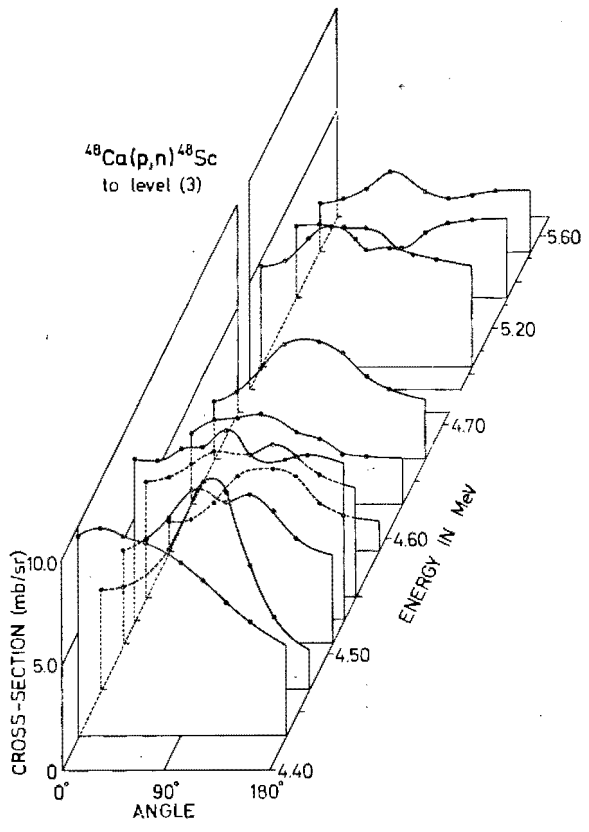

Fig. 2. The ^{48}Ca(p, n)^{48}Sc differential cross sections as a function of angle for the reaction to the third excited state of ^{48}Sc. The shape of the angular distributions shows rapid fluctuations with changing proton energy.

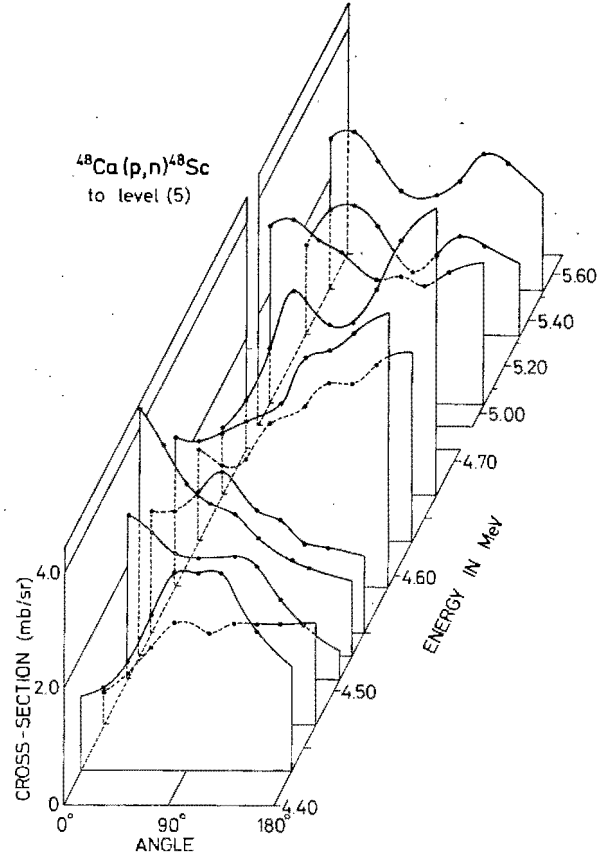

Fig. 3. The ^{48}Ca(p, n)^{48}Sc differential cross sections as a function of angle for the reaction to the fifth excited state of ^{48}Sc.

all have approximate symmetry about 90°. These features of the angular distributions as well as the sharp fluctuations observed in the excitation cross section curves are characteristic of a reaction proceeding via a highly-excited compound nucleus satisfying the requirements of Ericson fluctuation theory.

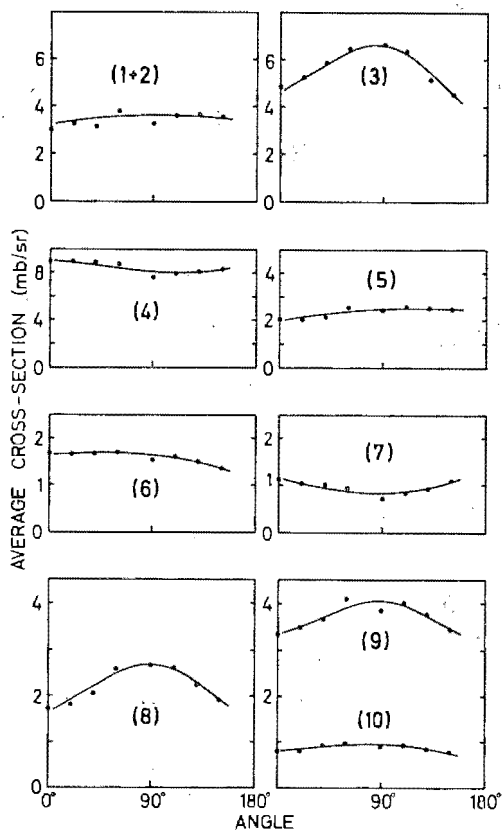

Fig. 4. The angular distributions for the ^{48}Ca(p, n)^{48}Sc reactions averaged over the proton energy interval 4.43 to 4.67 MeV. Each distribution is labelled with a number indicating the excited state of ^{48}Sc to which the reaction proceeded.

3. Correlation functions and coherence energy

If the width of compound states at the relevant excitation is Γ, then only states within an energy region of order Γ can be simultaneously excited and must be treated coherently. If this coherence energy embraces a large number of levels, then the total reaction cross section is a sum of a large number of terms with random phase and hence itself becomes a random number. If transitions to different final states are compared, the transition probabilities are independently random. It is therefore a basic conclusion of Ericson theory that cross correlations between cross sections to different exit channels a and b should be zero while auto-correlations for any one

channel should only be other than zero within the coherence energy Γ. As used in this work, correlation coefficients for the cross sections as a function of the energy E are defined as

$$R_{(ab)}(\varepsilon) = \left\langle \left(\frac{\sigma_a(E)}{\langle \sigma_a(E) \rangle} - 1 \right) \left(\frac{\sigma_b(E+\varepsilon)}{\langle \sigma_b(E) \rangle} - 1 \right) \right\rangle,$$

where ε is an increment of energy.

The auto-correlation coefficient is obtained for a = b in which case the indices will be omitted.

Ericson [4]) has shown that

$$R(\varepsilon) = \frac{R(0)}{1+\varepsilon^2/\Gamma^2},$$

while Stephen [5]) has obtained

$$R(0) = (1-y^2)/N,$$

which describes the damping of the statistical fluctuations by the presence of a competing fraction y of direct reaction cross section and by N-independent effective channels for the reaction via the compound state. For the purely statistical case $N = 1$, and hence $R(0) = 1$ for a one-channel reaction with no competing direct interaction.

In the work presented here, there is no evidence of a direct contribution. In particular there is no tendency toward forward peaking of the angular distributions. The average angular distribution is, in several cases, peaked at 90°. The parameter y will therefore be assumed equal to zero. This assumption should at least be reliable for the 90° excitation measurements.

Dearnaley [7]) has described a method for analysing cross-section excitation measurements for a non-stationary process (such that the average cross section is not a constant). An alternative procedure has been used here viz. the replacement of $\langle \sigma(E) \rangle$ by a running average $\langle \sigma_R(E) \rangle$ averaged over an energy interval δE as in the work of Elliott and Spear [16]). In order to analyse the present work using the running average method, the auto-correlation function $R(0)$ was first computed as a function of δE. The results are presented in fig. 5. It is clear that besides structure with width less than 100 keV there is additional non-stationary behaviour (at least for the reactions going to levels 3, 6 and 9 of ^{48}Sc).

Auto-correlation curves $R(\varepsilon)$ were therefore computed for δE = 160, 200 and 240 keV where the full range of data collection was in most cases 800 keV. Fig. 6 contains the auto-correlation curves for δE = 160 keV. The fact that $R(\varepsilon)$ for $\varepsilon > \Gamma$ is found to remain nearer zero for δE = 160 keV and appears to depart progressively from zero for larger δE suggests $\delta E \approx$ 160 keV gives the most reasonable values of $R(0)$ and Γ.

The mean value of Γ deduced from these curves is 9 keV, which, as the energy resolution of these measurements is between 5 and 8 keV, must be regarded as an

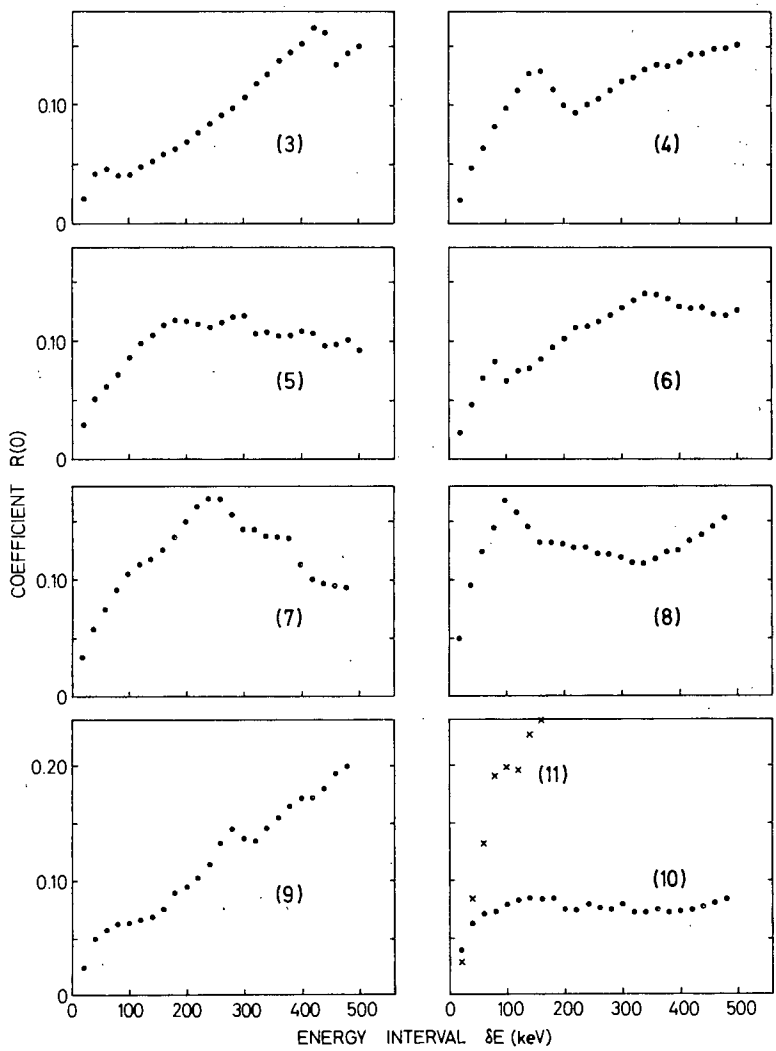

Fig. 5. The computed auto-correlation coefficients $R(0)$ plotted as a function of the running average interval δE for the reactions going to the indicated levels of ^{48}Sc at $\theta = 90°$.

upper limit. The peak counting method using the average number of maxima per unit energy

$$K = 0.55/\Gamma \quad [\text{ref. } ^{11})],$$

gives $\Gamma = 25$ keV. This confirms the conclusion that the energy resolution is inadequate for a precise determination of Γ. From interpolation in the graphical sum-

mary of available data as prepared by Papineau [17]), the expected value for the coherence energy at 15 MeV in ^{49}Sc is around 6 keV corresponding to a mean lifetime of the compound states of about 10^{-19} sec.

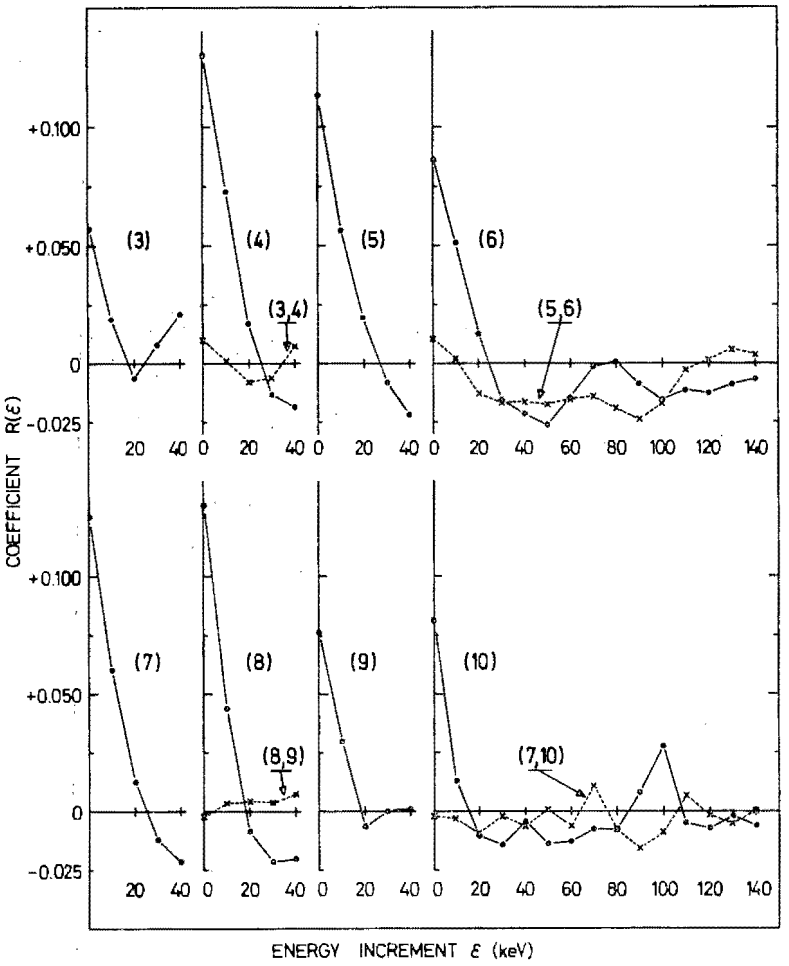

Fig. 6. The computed auto-correlation coefficients $R(\varepsilon)$ plotted as a function of the energy increments ε(keV). The averaging interval used was $\delta E = 160$ keV. Four cross correlation coefficients $R_{ab}(\varepsilon)$ are also plotted in this figure. The full data are only shown for levels 6 and 10 to illustrate the behaviour of $R(\varepsilon)$ for $\varepsilon > 40$ keV.

Fig. 6 also contains computed cross correlations for $\delta E = 160$ keV, $\theta = 90°$ for four pairs of excitation curves. The lack of cross correlation, suggested by a visual examination of the excitation curves, is confirmed by these results.

4. The spins of ^{48}Sc final states

The value of the auto-correlation coefficient $R(0)$ for a pure compound nucleus reaction is given by $1/N$, where N is the number of effective channels. Several authors

(refs. [4, 5, 9])) have shown that a good approximation for N is given by

$$N = \tfrac{1}{2}(2I+1)(2i+1)(2I'+1)((2i'+1)$$

for observations around 90°. The quantities I and i are the spins of target and projectile and I' and i' the spins of residual nucleus and emitted particle, respectively. For the reaction ^{48}Ca(p, n)^{48}Sc at 90°, N has the values 2, 6, 10, 18, 22 etc. for reactions proceeding to ^{48}Sc levels with spin 0, 1, 2, 3, 4 etc., respectively. The auto-correlation coefficient $R(0)$ is thus strongly spin dependent.

TABLE 1

Measured and calculated $R(0)$ values

Sc^{48} level	Possible spin value	$R(0)$ at 90°		Probable spins		$R(0)$ at 0° measured value [a])
		calculated (I/N)	measured value [a])	present work	Chasman *et al.* [18])	
3	3	0.071	0.059±0.017	3, 4	3+	0.26±0.15
	4	0.056	0.058±0.013			
4	1	0.167	0.13 ±0.04	1, 2	1, 2	0.24±0.15
	2	0.10	0.125±0.023			
5	1	0.167	0.12 ±0.04	1, 2	1, 2	0.23±0.15
	2	0.10	0.115±0.023			
6	2	0.10	0.090±0.023	2		0.25±0.15
	3	0.071	0.089±0.017			
7	1	0.167	0.13 ±0.04	1, 2		0.20±0.15
	2	0.10	0.127±0.026			
8	1	0.167	0.147±0.04	1		0.30±0.15
	2	0.10	0.142±0.026			
9	2	0.10	0.082±0.026	2, 3	4	0.25±0.15
	3	0.071	0.080±0.018			
10	2	0.10	0.092±0.026	2	2	0.26±0.15
	3	0.071	0.090±0.018			
11	0	0.50	0.405±0.18	0	0, 1	
	1	0.167	0.30 ±0.06			

[a]) The $R(0)$ correction and uncertainty due to the finite-energy range of data (FRD) are calculated using formulae derived by Dallimore and Hall [11]).

For measurements where the neutrons are detected at 0° or 180°, the number of effective channels is severely restricted by the required conservation of magnetic substates along the direction of the incident beam. A full discussion of this point is given by von Witsch *et al.* [9]). For the reaction being studied here, N is reduced to 1 (hence $R(0) = 1$) for a reaction leading to a zero-spin state of ^{48}Sc, and $N = 2$ (so that $R(0) = 0.5$) for reactions to states with spin $\geqq 1$.

The results from an analysis of the present work are given in table 1. It should be noted that the measured $R(0)$ values for the 0° measurements (column 7 of table 1) are all smaller than the expected value 0.5. It is nonetheless significant that all these $R(0)$ values for the 0° data are about equal and relatively large in comparison with the 90° measurements. The reduction of $R(0)$ values is presumably another result of the inadequate energy resolution of the measurements. The resultant suppression of peaks and filling in of sharp troughs in the excitation curve would depress the value of $R(0)$. The measured $R(0)$ values at 0° are therefore in qualitative agreement with the expected $R(0)$ values for reactions to final states of spin $\geqq 1$.

Table 1 also lists the measured $R(0)$ values for the 90° data. These are corrected for the fact that the analysis is made over a finite-energy range of data (FRD). Dallimore and Hall [11]) have derived a correction term for the "bias" introduced by the FRD. The FRD statistical uncertainty on $R(0)$ (again using an expression derived by Dallimore and Hall [11])) is also given in table 1. The finite-energy resolution also introduces a negative bias as discussed above. Bearing this in mind, the most probable spin assignments based on the present work are given in column 5. Comparison with the spins suggested by Chasman *et al.* [18]) on the basis of γ-ray transition probabilities (see column 6, table 1) shows general agreement with the conclusions based on the present work.

5. Discussion

Ericson [19]) and Macdonald [20]) have shown that under certain conditions the cross section for populating a definite final state of spin I when averaged over bombarding energy may be proportional to $(2I+1)$. The $(2I+1)$ rule should be valid for the same conditions which make application of the Ericson fluctuation theory valid, viz. the purely statistical nature of the compound nucleus reaction in the region of overlapping states. The $(2I+1)$ rule has been verified experimentally for certain reactions but its applicability is limited by additional requirements.

(i) The energy of the incoming particle must be such that a sufficient number of angular momenta can participate or the spins of the reacting particles be large enough to enable compound states of different I to be populated with equal probability.

(ii) The energy of the outgoing particle should be large enough to ensure that the barrier penetration does not suppress any l-values compatible with I and I'.

Such conditions unfortunately are not satisfied for the present study of the ^{48}Ca(p, n)^{48}Sc reaction. Even for reactions going to different states of equal spin, the cross sections are not necessarily equal as the penetrabilities will also be determined by the parity of the final state. This has been illustrated by Jänecke [21]) in a study of the ^{40}Ca(d, α)^{38}K reaction. It is therefore not surprising that the average cross sections in the present work show little obvious correspondence with the spin assignments.

On the other hand, the overall agreement (except for level 9) with the spins suggested by Chasman *et al.* on the basis of gamma-ray transition probabilities gives weight to the additional spin values deduced from the fluctuation analysis of the present work. The probable spins of the lower levels are also compatible with the spin values expected on the basis of a simple shell model [22]).

Financial assistance from the South African Atomic Energy Board is gratefully acknowledged. One of us (R.P.) thanks his Promotor for permission to publish results which will form part of a doctorate thesis to be submitted to the University of Stellenbosch.

References

1) L. M. El Nadi *et al.*, Nuclear Physics **64** (1965) 449
2) R. A. Ricci *et al.*, Proc. Int. Conf. on the study of nuclear structure with neutrons, Antwerp (July 1965) p. 500.
3) K. W. Jones *et al.*, Phys. Rev. **145** (1966) 894
4) T. Ericson, Phys. Rev. Lett. **5** (1960) 430; Ann of Phys. **23** (1963) 390; Phys. Lett. **4** (1963) 258
5) D. M. Brink and R. O. Stephen, Phys. Lett. **5** (1963) 77;
R. O. Stephen, thesis, University of Oxford (1963);
D. M. Brink, R. O. Stephen and N. W. Tanner, Nuclear Physics **54** (1964) 577
6) G. M. Temmer, Phys. Rev. Lett. **12** (1964) 330
7) B. W. Allardyce, W. R. Graham and I. Hall, Nuclear Physics **52** (1964) 239
8) G. Dearnaley, W. R. Gibbs, R. B. Leachman and P. C. Rogers, Phys. Rev. **139** (1965) 1170
9) W. von Witsch, P. von Brentano, T. Meyer-Kuckuk and A. Richter, Nuclear Physics **80** (1966) 394
10) A. van der Woude, Nuclear Physics **80** (1966) 14
11) P. J. Dallimore and I. Hall, Nuclear Physics **88** (1966) 193
12) G. Eder, A. Kitz and W. Schwetje, Nuclear Physics **79** (1966) 417
13) P. A. Moldauer, Phys. Lett. **8** (1964) 70
14) J. H. Towle and B. E. F. Macefield, Proc. Phys. Soc. **77** (1961) 399
15) F. Gabbard, R. H. Davis and T. W. Bonner, Phys. Rev. **114** (1959) 201
16) R. V. Elliott and R. H. Spear, Nuclear Physics **81** (1966) 209
17) L. Papineau, French Commissariat A L'Energie Atomique report CEA-R2876 (1966)
18) C. Chasman, K. W. Jones and R. A. Ristman, Phys. Rev. **140** (1965) 212
19) T. Ericson, Nuclear Physics **17** (1960) 250
20) N. MacDonald, Nuclear Physics **33** (1962) 110
21) J. Jänecke, Nuclear Physics **48** (1963) 129
22) J. D. McCullen, B. F. Bayman and L. Zamick, Phys. Rev. **134** (1964) 515

PERGAMON PRESS
OXFORD NEW YORK LONDON PARIS

Journal of Nuclear Energy, 1967, Vol.21, pp. 893 to 898. Pergamon Press Ltd. Printed in Northern Ireland

REACTIONS ON LIGHT ELEMENTS INDUCED BY CHARGED PARTICLES ELASTICALLY SCATTERED BY FAST NEUTRONS*

W. J. NAUDÉ
Merensky Institute for Physics, The University of Stellenbosch, Stellenbosch, S.A.

and

M. PEISACH
Southern Universities Nuclear Institute, Faure, Cape, S.A.

(*First received* 15 *May* 1967 *and in final form* 26 *June* 1967)

Abstract—Average cross sections for reactions induced by recoil-charged particles, obtained in an irradiating flux of 14·5 MeV neutrons, have been measured in boric acid, wax, cyclohexane, NH_4F, NH_4SCN, water and D_2O. In addition the cross section for the reaction $^{11}B(n, p)^{11}Be$ induced by 14·5 MeV neutrons was found to be 7·1 ± 2 mb.

1. INTRODUCTION

SINCE the first reports on the reactions induced by recoil protons elastically scattered by reactor neutrons (GLICKSTEIN and WINTER, 1960; STEHN, 1960; ROY *et al.*, 1960), the study and application of such reactions have drawn considerable attention. While studying irradiations with fast neutrons GILMORE and HULL (1962) found that the reactions induced by 'knock-on' protons caused an increase in the activity of nitrogen-13 from the reaction $^{13}C(p, n)^{13}N$ and thus interfered with the attempted determination of nitrogen in organic compounds. The use of nuclear reactions induced by recoil-charged particles for analytical purposes was first shown by AMIEL and PEISACH (1962) who measured the activity of fluorine-17 obtained from the reaction $^{16}O(d, n)^{17}F$ induced by reactor neutrons, to determine the deuterium content of heavy water. The same approach was used to determine the content of deuterium-labelled organic materials by FABBRI *et al.* (1964) who measured the activity of nitrogen-13 from the reaction $^{12}C(d, n)^{13}N$ and also to determine the isotopic concentration of oxygen-18 in hydrogen-containing materials through the reaction $^{18}O(p, n)^{18}F$ induced by reactor neutrons (AUMANN and BORN, 1965; HUNT and MILLER, 1965).

In this work average cross sections have been measured for reactions on boron, carbon, nitrogen and oxygen induced by recoil-protons and recoil-deuterons from 14·5 MeV neutrons.

2. THEORETICAL CONSIDERATIONS

It can be shown that the saturation activity per unit volume of a product nuclide, obtained by the irradiation with charged particles elastically scattered by mono-energetic neutrons, is given by

$$a_\infty = N_i N_p \sigma_{\text{scat}} \phi_n \int_{E_{\text{th}}}^{E_{\max}} \sigma(E) P(E) (\mathrm{d}E/\mathrm{d}x)^{-1} \, \mathrm{d}E, \qquad (1)$$

* This work forms part of a dissertation to be submitted by W. J. N. to the University of Stellenbosch in partial fulfillment of the requirements for a doctorate.

where N_t and N_p are the number of target and charged particle atoms per unit volume respectively, σ_{scat} the total cross section for elastic scattering of the recoiling nucleus, ϕ_n the neutron flux per unit area, E_{max} the maximum energy of the charged particle, $\sigma(E)$ and E_{th} the cross section and threshold of the reaction leading to the product nuclide and dE/dx the differential rate of energy loss of the recoiling particle. The probability that the scattered particle will have an energy greater than E is $P(E)$.

From equation (1) an average cross section $\bar{\sigma}$ may be defined as

$$\bar{\sigma} = a_\infty (N_t N_p \sigma_{scat} \phi_n \int_{E_{th}}^{E_{max}} P(E)(dE/dx)^{-1} dE)^{-1}. \quad (2)$$

The probability $P(E)$ was calculated for protons, assuming isotropic scattering at 14·5 MeV, and for deuterons using the differential cross sections given by SEAGRAVE (1955) and ALLRED *et al.* (1953), for 14·1 MeV neutrons, by the relationship

$$P(E) = \frac{\int_E^{E_{max}} \sigma(\phi)\, dE}{\int_0^{E_{max}} \sigma(\phi)\, dE}, \quad (3)$$

where $\sigma(\phi)$ was the differential elastic scattering cross section in the centre-of-mass system and ϕ the angle through which the neutron was scattered. The variation of $P(E)$ as a function of E/E_{max} is shown in Fig. 1.

The differential rate of energy loss was approximated by means of the equation

$$-\frac{dE}{dx} = \frac{K}{E}, \quad (4)$$

where K is a constant.

3. EXPERIMENTAL

3.1 *Neutron source*

Samples were irradiated with 14·5 ± 0·4 MeV neutrons generated by the reaction $^3H(d, n)^4He$. A tritium gas target, 3 cm long was used and operated at a gas pressure of about 500 mm. The gas cell was constructed according to the design of NOBLES (1957) in which a double window was used to allow better cooling so that deuteron currents up to 5 μA could be used. The total neutron yield was not measured but the averaged neutron flux through the samples was determined (see below).

3.2 *Irradiation and measurement*

To ensure a good yield with the available neutron flux, large samples of about 250 cm^3 were used in all cases except for D_2O. The cylindrical sample containers were made of Perspex and were constructed with a cavity which enabled the sample to be mounted in a position completely surrounding the tritium gas cell in the forward direction. In the case of D_2O, a 3 cm^3 capsule of polyethylene was used in close contact with the gas cell. Irradiations lasted between 1–20 min. As monitors of the gross neutron flux, the deuteron current falling on the tritium cell was used, as well as the counts recorded by a BF_3-counter placed at a fixed distance from the cell at a backward angle.

where N_i and N_p are the number of target and charged particle atoms per unit volume respectively, σ_{scat} the total cross section for elastic scattering of the recoiling nucleus, ϕ_n the neutron flux per unit area, E_{max} the maximum energy of the charged particle, $\sigma(E)$ and E_{th} the cross section and threshold of the reaction leading to the product nuclide and dE/dx the differential rate of energy loss of the recoiling particle. The probability that the scattered particle will have an energy greater than E is $P(E)$.

From equation (1) an average cross section $\bar{\sigma}$ may be defined as

$$\bar{\sigma} = a_\infty (N_i N_p \sigma_{scat} \phi_n \int_{E_{th}}^{E_{max}} P(E)(dE/dx)^{-1} dE)^{-1}. \tag{2}$$

The probability $P(E)$ was calculated for protons, assuming isotropic scattering at 14·5 MeV, and for deuterons using the differential cross sections given by SEAGRAVE (1955) and ALLRED *et al.* (1953), for 14·1 MeV neutrons, by the relationship

$$P(E) = \frac{\int_E^{E_{max}} \sigma(\phi)\, dE}{\int_0^{E_{max}} \sigma(\phi)\, dE}, \tag{3}$$

where $\sigma(\phi)$ was the differential elastic scattering cross section in the centre-of-mass system and ϕ the angle through which the neutron was scattered. The variation of $P(E)$ as a function of E/E_{max} is shown in Fig. 1.

The differential rate of energy loss was approximated by means of the equation

$$-\frac{dE}{dx} = \frac{K}{E}, \tag{4}$$

where K is a constant.

3. EXPERIMENTAL

3.1 *Neutron source*

Samples were irradiated with 14·5 ± 0·4 MeV neutrons generated by the reaction $^3H(d, n)^4He$. A tritium gas target, 3 cm long was used and operated at a gas pressure of about 500 mm. The gas cell was constructed according to the design of NOBLES (1957) in which a double window was used to allow better cooling so that deuteron currents up to 5 μA could be used. The total neutron yield was not measured but the averaged neutron flux through the samples was determined (see below).

3.2 *Irradiation and measurement*

To ensure a good yield with the available neutron flux, large samples of about 250 cm^3 were used in all cases except for D_2O. The cylindrical sample containers were made of Perspex and were constructed with a cavity which enabled the sample to be mounted in a position completely surrounding the tritium gas cell in the forward direction. In the case of D_2O, a 3 cm^3 capsule of polyethylene was used in close contact with the gas cell. Irradiations lasted between 1–20 min. As monitors of the gross neutron flux, the deuteron current falling on the tritium cell was used, as well as the counts recorded by a BF_3-counter placed at a fixed distance from the cell at a backward angle.

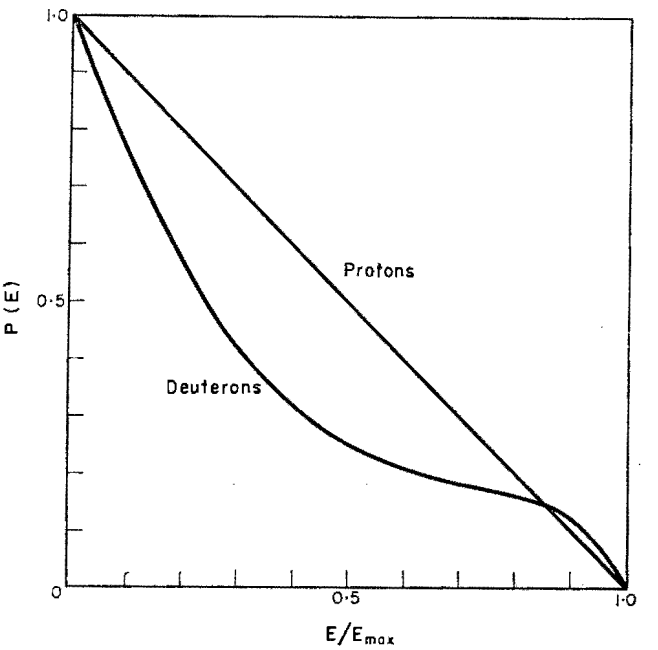

FIG. 1. The probability that a recoiling proton or deuteron will have an energy greater than E when elastically scattered by a 14·5 MeV neutron.

Samples were counted by means of a 5 × 4 in. NaI(Tl) scintillation crystal coupled to a multichannel analyser in the multiscaler mode. Counting was continued for several half-lives and the absolute disintegration rates at the end of the irradiation were determined. Where necessary, the decay rate of specific γ-rays was followed to minimize interference from other radioactive species in the sample.

3.3 *Neutron flux measurement*

The value of the neutron flux, averaged over the volume of the sample, was determined in samples where suitable fast neutron induced reactions occurred. This method of averaging the neutron flux is based on internal standardization and is preferable to the use of external standards or monitors because the variation of the neutron flux caused by sample components and geometrical effects are more readily compensated for.

The results are given in Table 1, together with the cited values (JESSEN *et al.*, 1966) of the corresponding reaction cross sections from which the neutron flux was calculated. The average value of the neutron flux was found to be $(7{\cdot}3 \pm 1{\cdot}0) \times 10^6$ neutrons/cm^2.sec. The error given is the probable error, calculated from the experimental results, taking into account discrepancies in the neutron reaction cross sections as obtained by different workers. In the case of D_2O which was irradiated much closer to the tritium gas cell, the corresponding flux was about 10 times higher.

4. RESULTS AND DISCUSSION

4.1 *Cross section for the reaction* $^{11}B(n, p)^{11}Be$

The cross section of the reaction $^{11}B(n, p)^{11}Be$ with 14·5 MeV neutrons was measured by determining the yield of 13·6 sec beryllium-11. The value obtained was

This observation is in complete agreement with the work of WILKNISS (1966) who found that the yield of radioactive products from reactions induced by the recoil protons obtained from irradiation with 14·7 MeV neutrons were, in most cases, higher than the corresponding calculated values.

Acknowledgment—Financial assistance from the South African Atomic Energy Board is gratefully acknowledged.

REFERENCES

ALLRED J. C., ARMSTRONG A. H. and ROSEN L. (1953) *Phys. Rev.* **91,** 90.
AMIEL S. and PEISACH M. (1962) *Analyt. Chem.* **34,** 1305.
AUMANN D. C. and BORN H. J. (1965) *Int. J. appl. Radiat. Isotopes* **16,** 727.
BLASER J. P., BOEHM F., MARMIER P. and SCHERRER P. (1951) *Helv. phys. Acta* **24,** 465.
BLASER J., MARMIER P. and SEMPERT M. (1952) *Helv. phys. Acta* **25,** 442.
BORMANN M. (1965) *Nucl. Phys.* **65,** 257.
DAGLEY P., HAEBERLI W. and SALADIN J. X. (1961) *Nucl. Phys.* **24,** 353.
FABBRI E., LAZZARINI E. and SANGIUST V. (1964) *Int. J. appl. Radiat. Isotopes* **15,** 437.
FOWLER J. L. and BROLLEY J. E. (1956) *Rev. mod. Phys.* **28,** 103.
GIBBONS J. and MACKLIN R. (1959) *Phys. Rev.* **114,** 571.
GILMORE J. T. and HULL D. E. (1962) *Analyt. Chem.* **34,** 187.
GLICKSTEIN S. S. and WINTER R. G. (1960) *Nucl. Instrum. Meth.* **9,** 226.
HILL H. A., HAASE E. L. and KNUDSEN D. B. (1961) *Phys. Rev.* **123,** 1301.
HUNT L. H. and MILLER W. W. (1965) *Analyt. Chem.* **37,** 1269.
JARMIE N. and SEAGRAVE J. (1956) *Charged Particle Cross Sections*, Report La-2014.
JESSEN P., BORMANN M., DREYER F. and NEUERT H. (1966) *Nucl. Data* (A) **1,** 103.
KANTELE J. and GARDNER D. G. (1962) *Nucl. Phys.* **35,** 353.
KUAN HSIN-MIN and RISSER J. R. (1964) *Nucl. Phys.* **51,** 518.
NEWSON H. W. (1937) *Phys. Rev.* **51,** 620.
NOBLES R. (1957) *Rev. scient. Instrum.* **28,** 962.
ROY J. C., BRESESTI M. and HAWTON J. J. (1960) *Can. J. Phys.* **38,** 1428.
SEAGRAVE J. D. (1955) *Phys. Rev.* **97,** 757.
STEHN J. R. (1960) *Trans. Am. nucl. Soc.* **3,** 467.
WAPSTRA A. H., NIJGH G. T. and VAN LIESHOUT R. (1959) *Nuclear Spectroscopy Tables*, p. 26, North Holland, Amsterdam.
WHALING W. (1958) *Encyclopedia of Physics*, Vol. 34, p. 193, Springer, Berlin.
WHITEHEAD A. B. and FOSTER J. S. (1958) *Can. J. Phys.* **36,** 1276.
WILKNISS P. E. (1966) *Radiochim. Acta* **6,** 135.

No. 19

CROSS SECTIONS FOR PROTON AND DEUTERON-INDUCED ACTIVATION OF CALCIUM ISOTOPES

by

Max Peisach, René Pretorius and David S. Rosettenstein

Southern Universities Nuclear Institute, P.O. Box 17, FAURE, C.P., South Africa.

Reprinted from "Convention Handbook", South African Chemical Institute
20th Convention, Durban (1967) p.299

CROSS SECTIONS FOR PROTON AND DEUTERON-INDUCED ACTIVATION OF CALCIUM ISOTOPES

Max Peisach, René Pretorius and David S. Rosettenstein

Southern Universities Nuclear Institute, P.O. Box 17, Faure, C.P., South Africa

S U M M A R Y

With the increase in the use of stable isotopes for tracing calcium in vivo the need for determining their isotopic concentration in calcium, routinely, has increased. Recently a method using proton activation has been developed, but to utilize this technique to its best advantage, a knowledge of the variation of the activation cross section with particle energy is essential.

Because charged particles lose their energy within a relatively short distance in the irradiated material, the calcium was prepared as a thin layer of oxide or fluoride on a backing of tantalum. Protons or deuterons at energies ranging up to 5 MeV and currents between 0.2 and 0.5 μA were used in the irradiation.

Natural calcium targets and targets enriched in ^{40}Ca, ^{42}Ca, ^{43}Ca, ^{44}Ca and ^{48}Ca were irradiated and the activities generated were measured by gamma-ray scintillation spectrometry with a NaI(Tl) crystal. Relative cross sections for the various proton and deuteron-induced reactions were obtained.

INTRODUCTION

Nuclear methods have been used to determine calcium-48 absolutely by neutron activation (1,2) and recently a method using charged particle activation has been developed (3) to determine the relative enrichment of calcium-48. To utilize this latest technique to its best advantage, a knowledge of activation cross sections would be essential. In addition, the variation of cross section with particle energy has to be known, because unlike neutrons, charged particles undergo a rapid change of energy within the sample. Information on the cross sections of reactions induced by charged particles on the calcium isotopes is not available. For this reason this investigation was undertaken with protons and deuterons.

For target materials irradiated with a constant current of particles at a fixed energy, the specific activity produced would be directly proportional to the reaction cross section. At the end of the irradiation, the activity in the sample would be the sum of all the activities produced by various reactions on the components of the targets. By gamma-ray spectrometry and decay measurements the various radioactivities may be resolved and hence individual cross sections may be determined relative to one another. Absolute values may be obtained if the activities are determined absolutely or by comparison with a reaction of known cross section.

Radioactive nuclides expected from the irradiation of calcium isotopes with protons and deuterons are listed in Tables I and II respectively. The criteria for inclusion of radioactive products in these Tables are

(i) the Q-value of the reaction leading to that radioactive product should exceed -5 MeV. This condition was determined by the maximum energy attainable by the bombarding particles in the S.U.N.I. Van de Graaff accelerator.

(ii) the radioactive product should decay with the emission of gamma-rays, or beta-rays of sufficient energy to be detected in the measuring system.

(iii) the half-life of the product should lie between 4 min. and 1 year. The lower limit is imposed by the time taken to transfer the target to the measuring position and the upper limit by the fractional change in activity that would be detected in a relatively short counting period of a few weeks.

PREPARATION OF SAMPLES

Enriched calcium isotopes were obtained from the Oak Ridge National Laboratory, U.S.A. as calcium carbonate. The carbonate was dissolved in hydrochloric acid and precipitated as fluoride with hydrofluoric acid in a platinum crucible. The fluoride was selected as target material because it could stand up to relatively high temperatures and did not form interfering activities.

Because charged particles lose their energy within a relatively short distance in the irradiated material, it is preferable that the target material be as thin as possible. However, the activity yield is a function of the weight of material irradiated, thus, when targets are prepared, a compromise has to be struck between energy loss in the target and activity yield. Thin targets of calcium fluoride were prepared by evaporation in vacuo, onto tantalum backings which, at the bombarding energies used, did not produce interfering activities. When small amounts of material were available, as, for example, was the case for some highly enriched calcium isotopes, a tungsten microcrucible (5) [1] heated by electron bombardment was used; in this way it was possible to prepare targets of about 130 $\mu g./cm.^2$ thickness

from 1 mg. of fluoride.

IRRADIATION

Irradiations were carried out with the 5.5 MV Van de Graaff accelerator at the Southern Universities Nuclear Institute. The beam energy was defined with a precision of ± 0.1%. Irradiation currents ranged between 0.2 and 7.0 μA. but when the current exceeded about 0.5 μA external cooling of the targets became necessary. Irradiations lasted for two hours. The current falling on the target was obtained by insulating the target assembly and measuring the current with a suitably designed current integrator (6).

Single samples were irradiated inside a Faraday cup which enabled the total current falling on the sample to be measured with a precision of ± 1%. These samples were used for intercalibration of flux and for normalisation of the results from different irradiations.

To enable several samples to be irradiated simultaneously with a beam at a constant energy, a rotating sample holder accommodating up to 12 samples (Figure 1) could be mounted on the beam tube. This sample holder could also be used to irradiate several samples at different energies simultaneously, by using stacked foils of aluminium to degrade the energy of the irradiating beam.

ACTIVITY MEASUREMENT

After irradiation samples were counted and analysed by gamma-ray spectrometry using a 3 x 3 inch NaI(Tl) scintillation detector. The spectra were recorded on a multichannel analyser and gross counts were simultaneously measured with a single channel analyser preset to cover selected energy regions. Counting started about ten minutes after the end

of the irradiation and continued periodically until sufficient data had been accumulated to enable the components to be separately determined.

Decay data was analysed with the IBM 1620 computer of the University of Stellenbosch, to determine the component activities at the end of the irradiation, using a programme based on the principle of maximum likelihood (7). Calibrated sub-standards were used to obtain absolute activities.

PROTON CROSS SECTIONS

Gamma-ray spectra obtained during the decay of a sample of natural calcium fluoride irradiated with protons of 4.75 MeV is shown in Figure 2. Immediately after irradiation the presence of scandium-44 was proved by the pronounced peak from positron annihilation of 0.51 MeV and the photopeak from the 1.16 MeV gamma-ray. After a few hours the presence of the longer-lived scandium-48 could already be distinguished by the appearance of the (unresolved) photopeaks from gamma-rays of 0.99 and 1.04 MeV and of 1.31 MeV. Thereafter the decay followed without any sign of longer-lived activities being present.

Because the yields of scandium-44 and 48 from natural calcium were sufficiently high for ready measurement, natural calcium could be used for the cross section measurements of the reactions $^{44}Ca(p,n)^{44}Sc$ and $^{48}Ca(p,n)^{48}Sc$. However, for proton energies above about 3 MeV, but below about 4.5 MeV when the reaction $^{44}Ca(p,n)^{44}Sc$ was energetically not possible, any 4-hour activity had to be ascribed to scandium-43. The activity yield of ^{43}Sc was then still sufficiently high to use natural calcium for the determination. When protons of energy less than the threshold for the reaction $^{43}Ca(p,n)^{43}Sc$ was used, the scandium-43 activity could only have been formed by the reaction $^{42}Ca(p,\gamma)^{43}Sc$.

Accordingly natural calcium was suitable for determining the cross section of the reaction $^{42}Ca(p,\gamma)^{43}Sc$ up to an energy of about 3 MeV, the sum of the scandium-43 yield from this reaction and $^{43}Ca(p,n)^{43}Sc$ over the proton energy range 3.1 to 4.5 MeV and, with suitable gamma-ray energy discrimination, the cross section for the reaction $^{44}Ca(p,n)^{44}Sc$ above 4.5 MeV. In the energy ranges where different reactions led to the same product or to products with similar half-lives, enriched targets were used.

Cross sections near to the reaction thresholds were open to large errors because of the difficulties in measuring low activities. Accordingly the thresholds for (p,n) reactions were determined by measuring the variation of neutron emission from the target with proton energy. The neutrons were counted with a BF_3-detector at 0^o placed as close to the target as possible in order to subtend a large solid angle. Reaction thresholds measured in this way are given in Table III. Because the Q-value for the reaction $^{48}Ca(p,n)^{48}Sc$ is only -0.515 MeV the threshold for this reaction can be considered as a semi-quantitative measure of the Coulomb barrier for calcium isotopes.

The measured variation of the relative cross section with proton energy is given in Figure 3 for the (p,γ) reaction on ^{42}Ca, and the (p,n) reactions on ^{43}Ca and ^{48}Ca.

DEUTERON CROSS SECTIONS

Gamma-ray spectra obtained from the decay of a sample of natural calcium fluoride irradiated with 4.75 MeV deuterons is shown in Figure 4. A few minutes after irradiation the most prominent peaks in the spectrum are those due to ^{49}Ca (3.10 and 4.05 MeV), ^{38}K (2.20 MeV) and β^+ annihilation radiation (0.51 MeV).

In attempting to measure the yield of scandium-49, the 1.76 MeV gamma-ray produced in its decay was found to be of too low intensity for convenient measurement. Accordingly the yield of this product was obtained from gross measurement of the radioactive decay without absorbers interposed to stop the beta-particles. The decay curve then showed the presence of a 57.5-min. component which was identified as scandium-49. The gamma-ray spectra measured under the same conditions showed considerable contribution from beta-particles of up to 2.01 MeV, as may be deduced from the shape of spectrum A in Figure 4.

After some time, when the two short-lived components, ^{38}K and ^{49}Ca, had decayed, the main photopeak in the spectrum was due to the 1.16 MeV gamma-ray from scandium-44, but after some 50 hours, the spectrum (B of Figure 4) contained many photopeaks including those corresponding to 0.27 MeV from ^{44m}Sc, 0.99, 1.04 and 1.31 MeV from ^{48}Sc and higher energy gamma-rays of low intensity.

It is thus clear that the radioactive mixture obtained from the deuteron irradiation of natural calcium is complex, with several components having half-lives relatively close to each other, so that yields for specific reactions could not readily be measured. Accordingly, calcium targets enriched in the selected isotopes had to be used. The following are the main reactions which are currently being investigated:

(1) $^{40}Ca(d,\alpha)^{38}K$

(2) $^{42}Ca(d,n)^{43}Sc$

(3) $^{43}Ca(d,n)^{44}Sc$

(4) $^{48}Ca(d,n)^{49}Sc$

(5) $^{48}Ca(d,2n)^{48}Sc$

(6) $^{48}Ca(d,p)^{49}Ca$

The results obtained for reactions 3 and 5 are shown in Figure 5, where the relative cross sections are shown as a function of deuteron energy.

It is noteworthy that the activity yield for the (d,2n) reaction on ^{48}Ca is so high at comparatively low deuteron energies. In a three-body reaction such as this, activation is, to date, the only method for measuring the cross section.

REFERENCES

(1) JUNOD, E., LAVERLOCHERE, J., Proc. 3rd Intern. Colloquium on Biology, Saclay, 1963.

(2) STRELOW, F.W.E., STAERK, H., Anal. Chem. 35, 1154 (1963).

(3) PEISACH, M., PRETORIUS, R., Anal. Chem. 38, 956 (1966).

(4) EVERLING, F., KOENIG, L.A., MATTAUCH, J.H.E., WAPSTRA, A.H., "Nuclear Data Tables, Part I", National Academy of Sciences, Washington, 1961.

(5) MENTI, W., MARTIN, M., BAS, E.B., VOGT, O., Nucl. Inst. Methods 31, 25 (1964).

(6) BLIGNAUT, E., KRITZINGER, J.J., Nucl. Inst. Methods 36, 176, (1965).

(7) MONK, R.G., MERCER, A., DOWNHAM, T., Anal. Chem. 35, 178 (1963).

(8) McMURRAY, W.R., PEISACH, M., PRETORIUS, R., van der MERWE, P., van HEERDEN, I.J., Nucl. Phys. (in press).

TABLE I

RADIONUCLIDES EXPECTED FROM CALCIUM ISOTOPES IRRADIATED WITH PHOTONS

Product Nuclide	Half Life	Gamma-ray Energies MeV	Target Nuclide	Reaction Type	Q-value (4)
^{43}Sc	3.9h.	(β+), 0.37	^{42}Ca	(p,γ)	4.927
			^{43}Ca	(p,n)	-3.003
^{44m}Sc	2.4d.	0.27	^{43}Ca	(p,γ)	6.705
^{44}Sc	4.0h.	(β+), 1.16	^{44}Ca	(p,n)	-4.431
^{46}Sc	84d.	1.12, 0.89	^{46}Ca	(p,n)	-2.165
^{47}Sc	3.4d.	0.16	^{46}Ca	(p,γ)	8.487
^{48}Sc	44h.	0.99, 1.04, 1.31	^{48}Ca	(p,n)	-0.515
^{49}Sc	57.5m.	1.76	^{48}Ca	(p,γ)	9.550
^{43}K	22h.	0.37, 0.61	^{46}Ca	(p,α)	-1.696

TABLE II

RADIONUCLIDES EXPECTED FROM CALCIUM ISOTOPES

IRRADIATED WITH DEUTERONS

Product Nuclide	Half Life	Gamma-ray Energies MeV	Target Nuclide	Reaction Type	Q-value (4)
^{43}Sc	3.9h.	(β+), 0.37	^{42}Ca	(d,n)	2.702
^{44m}Sc	2.4d.	0.27	^{42}Ca	(d,γ)	12.410
^{44}Sc	4.0h.	(β+), 1.16	^{43}Ca	(d,n)	4.481
^{46}Sc	84d.	1.12, 0.89	^{44}Ca	(d,γ)	13.431
			^{46}Ca	(d,2n)	-4.390
^{47}Sc	3.4d.	0.16	^{46}Ca	(d,n)	6.262
^{48}Sc	44h.	0.99, 1.04, 1.31	^{46}Ca	(d,γ)	14.493
			^{48}Ca	(d,2n)	-2.740
^{49}Sc	57.5m.	1.76	^{48}Ca	(d,n)	7.330
^{47}Ca	4.7d.	1.31, 0.81, 0.49	^{46}Ca	(d,p)	5.080
			^{48}Ca	(d,t)	-3.670
^{49}Ca	8.8m.	3.10, 4.05, 4.70	^{48}Ca	(d,p)	2.919
^{38}K	7.7m.	(β+), 2.20	^{40}Ca	(d,α)	4.655
^{42}K	12.4h.	1.52	^{42}Ca	(d,2p)	-4.972
			^{44}Ca	(d,α)	4.257
^{43}K	22h.	0.37, 0.61	^{43}Ca	(d,2p)	-3.259
^{44}K	22m.	1.16, 2.1	^{46}Ca	(d,α)	2.930

TABLE III

THRESHOLD ENERGIES OF (p,n) REACTIONS ON CALCIUM ISOTOPES

Reaction	Measured Values (MeV)	
	Q-value (8)	Threshold
$^{43}Ca(p,n)^{43}Sc$	-2.998	3.075 ± 0.003
$^{44}Ca(p,n)^{44}Sc$	-4.447	4.545 ± 0.003
$^{48}Ca(p,n)^{48}Sc$	-0.534	1.16 ± 0.01

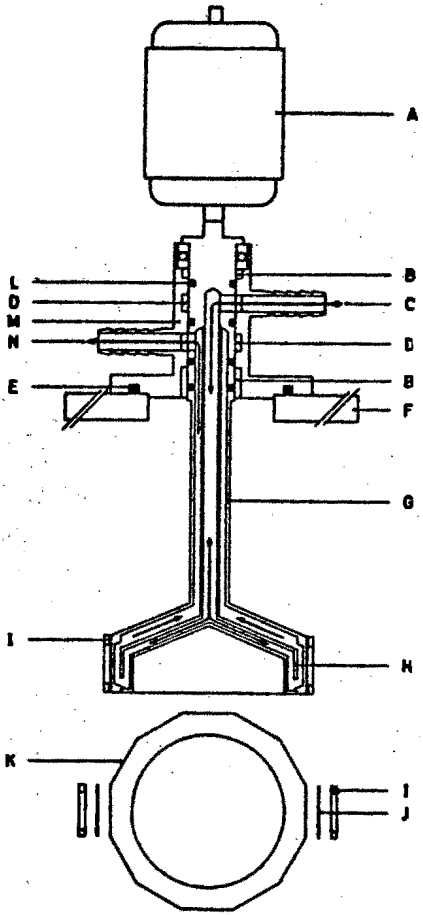

FIGURE 1

Rotating sample holder cooled by circulating water

A : Motor and gear box

B : Nylon bearings

C : Water inlet

D : Water chambers

E : Vacuum seal

F : Base plate

G : Rotating cooled target holder

H : Cooling water stream guide

I : Target clamps

J : Target

K : 12 flats for mounting targets

L : Water and vacuum seals

M : Target holder support

N : Water outlet

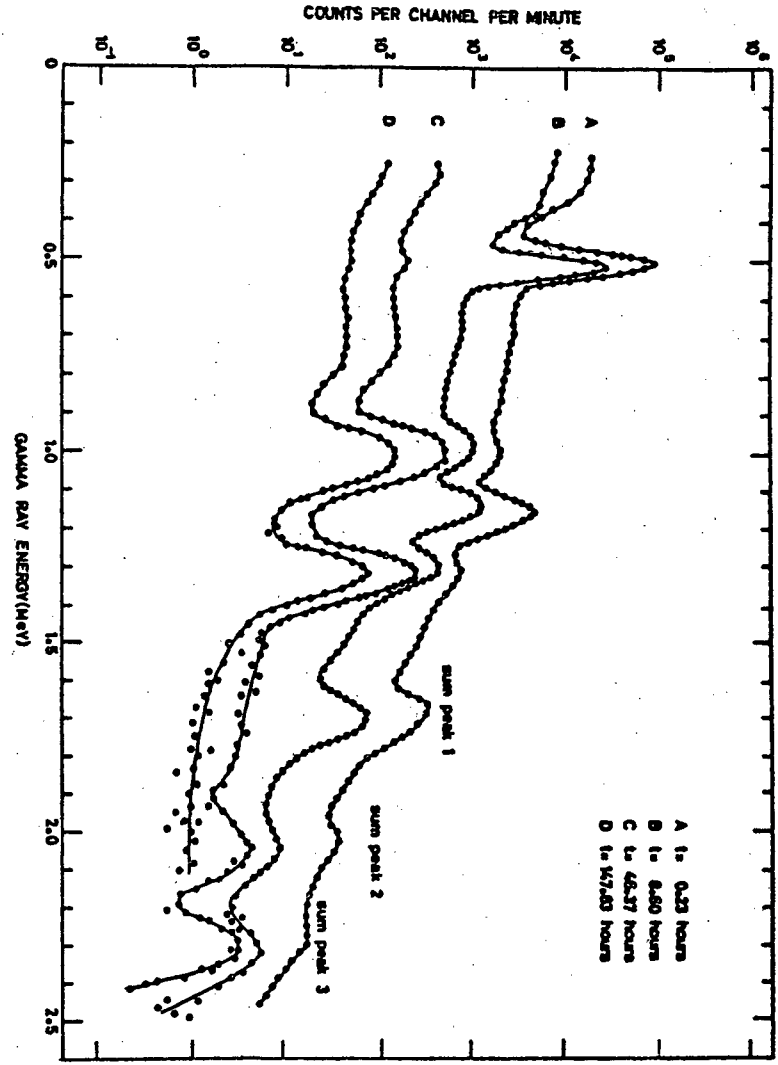

FIGURE 2

Gamma spectra from proton irradiated natural calcium fluoride E_p = 4.75 MeV

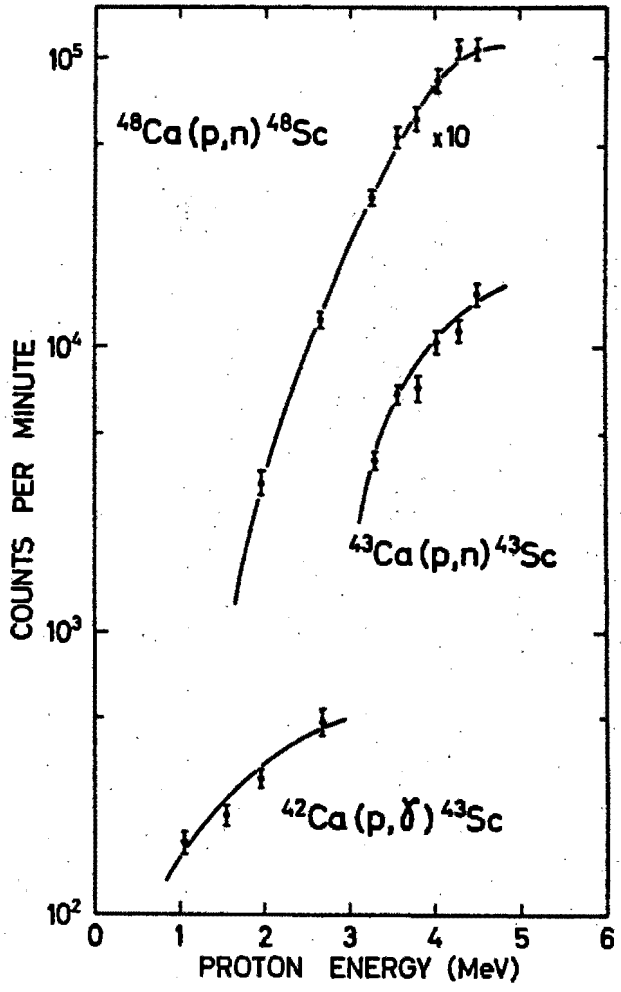

Figure 3

Relative excitation curves from proton activation

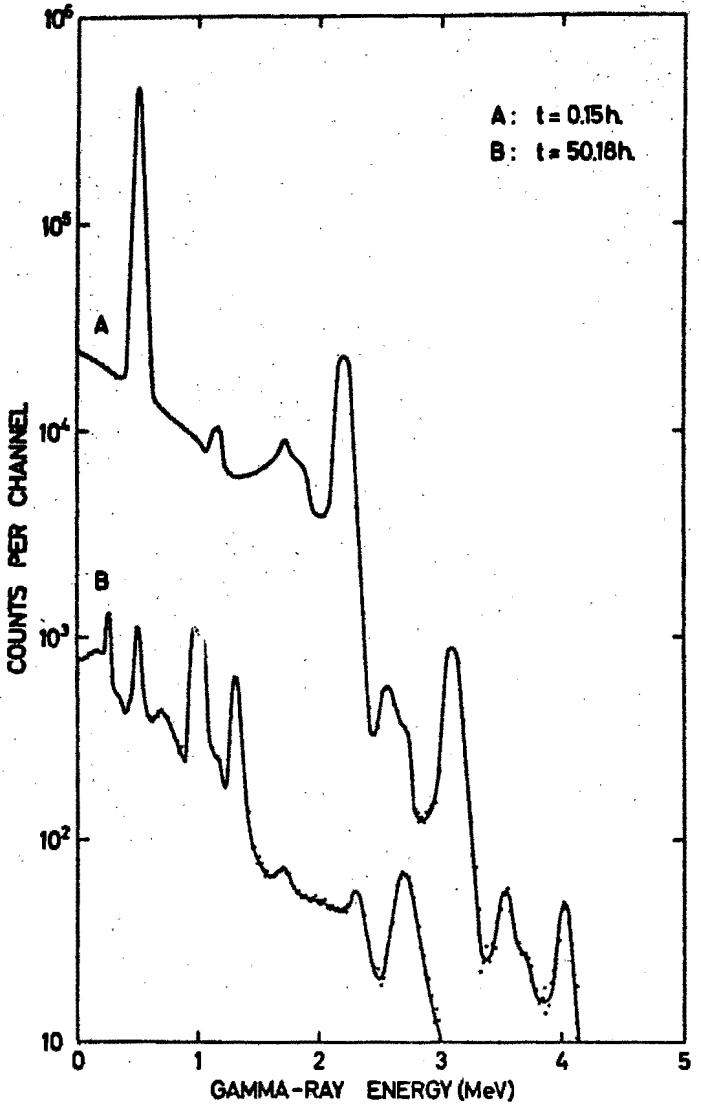

Figure 4

Gamma spectra from deuteron irradiated natural calcium fluoride E_d = 4.75 MeV

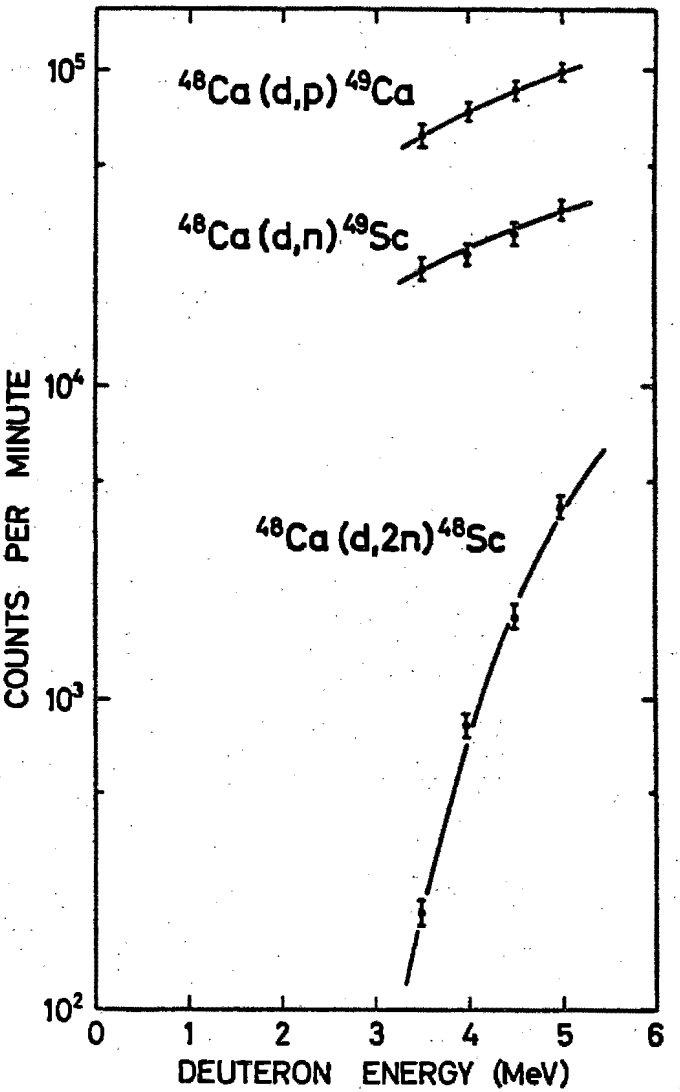

Figure 5

Relative excitation curves from deuteron activation

No. 20

ATTEMPTS AT ANALYSING VOLATILE ORGANIC COMPOUNDS BY NEUTRON TIME-OF-FLIGHT SPECTROMETRY

by

Max Peisach, René Pretorius and Paul J. Strebel

Southern Universities Nuclear Institute, P.O. Box 17, FAURE, C.P., South Africa.

Reprinted from "Convention Handbook", South African Chemical Institute 20th convention, Durban (1967), p.311

ATTEMPTS AT ANALYSING VOLATILE ORGANIC COMPOUNDS BY NEUTRON TIME-OF-FLIGHT SPECTROMETRY

Max Peisach, René Pretorius and Paul J. Strobel

Southern Universities Nuclear Institute, P.O. Box 17, Faure, C.P., South Africa

SUMMARY

Neutron time-of-flight spectroscopy provides a sensitive means of elemental analysis. Carbon, nitrogen and oxygen were determined in the gaseous phase by using neutrons emitted from (d,n) reactions induced by a beam of pulsed deuterons of 3.0 or 3.4 MeV. Pulses were of 5 nsec duration and 400 nsec apart. The number of neutrons in each energy group varied linearly with the partial pressure of the gas under investigation, provided the energy loss of the irradiating beam in the gas sample was negligible. Carbon dioxide, methane, oxygen, nitrogen and mixtures of D_2O/H_2O, CO_2/CO and CO_2/H_2 were analyzed. Minimum sample size was about 10 µg and the relative standard deviation was about $\pm$ 3%.

The vapours of most organic compounds could not be analyzed in the gas irradiation cell because the high temperatures generated by the beam at the cell window caused decomposition of the sample. Non-volatile carbonaceous material, deposited on the cell window in the path of the beam, led to comparatively high neutron yields from carbon-12 and made the cell unusable for subsequent samples. Possible ways of overcoming this difficulty are discussed and the experimental approach described.

INTRODUCTION

Neutron activation analysis has established itself as a sensitive method for determining most elements, but the method is inapplicable to the analysis of light elements such as carbon, nitrogen and oxygen, since neutron capture by their most abundant isotopes leads to stable nuclides. The method is also, with few exceptions, limited to solid and liquid samples, because the irradiation of gaseous samples with reactor neutrons presents serious technical difficulties. The advantages of nuclear methods of analysis may be extended to these fields through use of reactions induced by charged particles, especially those producing neutrons, which lend themselves to spectrometry by time-of-flight techniques.

The use of neutron time-of-flight spectrometry for analysis was first suggested at the 19th Convention of the South African Chemical Institute in February, 1966 (1), and has already been used for solid samples (2) and for gases which do not decompose at high temperatures (3,4). The analysis may be carried out on a few tens of micrograms of material and because C, N and O are each separately determinable (6), the method could be potentially useful for the analysis of volatile organic material. Unfortunately, most organic materials are not stable at the high temperatures which may be generated by the charged particles irradiation beams. This paper discusses some limitations of the technique and suggests an extention of the method to enable carbon, nitrogen and oxygen to be determined in volatile organic substances.

IRRADIATION AND MEASUREMENT

Pulsed deuteron beams obtained from the 5.5 MeV Van de Graaff accelerator at the Southern Universities Nuclear

Institute were used to generate neutrons by (d,n) reactions in gaseous samples at measured pressures. Pulses were 5 nsec long and 400 nsec apart. The beam energy used was between 3.0 and 3.5 MeV and the average current ranged between 0.3 and 0.8 μa. The neutrons were usually measured at 30° and their flight paths were about 3 metres.

The electronic equipment has been described (5) and the construction of the irradiation cell used for samples which do not decompose under the irradiation conditions, is shown in Figure 1. Neutron time-of-flight spectra were recorded on a multichannel analyser. The finite duration of the irradiation pulse introduces a limitation on the time-of-flight resolution of the neutron energy, so that neutrons of a single energy are recorded as a neutron group having a distribution with a minimum full width at half peak height equal to the pulse duration.

For a particular nuclear reaction and at a selected deuteron energy the number of neutrons emitted will depend on the number of target nuclei in the path of the beam. In a single set of measurements the neutron count per unit beam current at a fixed angle will be directly proportional to the partial pressure of the thermally stable gas, provided the beam cross section and cell length remain constant. It was thus possible to calibrate the equipment by a series of measurements on a single gas over a range of pressures. The calibration curves remained linear provided the energy loss of the irradiating beam in the gas sample was negligible. The extent of the energy loss depended on the composition and pressure of the gas sample.

The efficiency of the measuring system decreased rapidly for neutrons below 1.0 MeV, falling to zero for neutron energies of about 700 keV. For this reason neutrons of energies between 700 and 1000 keV were not suitable for

quantitative measurements.

NEUTRON SPECTRA

Samples

The energies of some neutrons from (d,n) reactions induced by 3.0 MeV-deuterons on C, N and O, and measured at 30° are listed in Table 1 where i refers to the ith excited state in which the product nucleus is left after neutron emission. The values given suggest that neutrons of some selected energies may be counted to determine the corresponding nuclides in the target sample, quantitatively.

Typical spectra obtained from methane, oxygen and nitrogen are given in Figure 2. The spectra have the following features

(i) the spectra are based on time measurements with channel number proportional to the neutron flight time, accordingly the energy scale is not linear.

(ii) the peaks correspond to neutron groups with energies about 200 keV lower than those given in Table 1 because this is the energy lost by the beam in passing through the nickel window (see Figure 1).

(iii) the spectra depict no neutron groups with energy lower than 700 keV since such groups are eliminated by the pulse shape discrimination in the electronic circuit (5).

The calibrations were performed on those neutron groups least likely to be affected by neutron groups from other nuclides. Thus ^{14}N-calibrations used n_0 and n_3 neutrons because the n_1 and n_2 groups have energies comparable to the

energy of neutrons from ^{12}C, and the n_4, n_5 and n_6 groups overlap those from ^{16}O.

Background

The predominant feature in the background spectra was the peak corresponding to 2.5 MeV neutrons from ^{12}C due to the residual vacuum oil vapour in the beam tube which deposited on the hot spot generated at the point of incidence of the beam on the nickel window of the cell. The remainder of the background consisted of a continuum of counts over the entire energy range due to gamma rays not entirely eliminated by the pulsed shape discrimination and neutrons scattered into the detector.

LIMITATIONS OF THE METHOD

From sample components

When the sample contains other nuclides which yield neutrons with energies near to those of the neutron groups being used for analytical purposes, these nuclides would interfere with the precision of the analyses. Thus interference could be expected from gases containing enriched carbon-13, nitrogen-15 and oxygen-17 and 18. Interference from the same nuclides could also be encountered when one element in the sample is present in very high concentrations relative to the other elements; for example, a sample containing many carbon and only one nitrogen atom per molecule may contain carbon-13 in amounts comparable to the nitrogen content even though the carbon-13 is not enriched.

From heating the sample

Local heating of the gas in the path of the beam could decrease the density of the gas and cause a decreased rate of

neutron production. This effect was, however, not observed at the low average current densities used in this investigation.

From heating the container

On passing through the nickel window into the cell, a fraction of the energy of the irradiating beam is dissipated as local heating on the window. At the tantalum backing the beam is entirely stopped causing a very high temperature over a small area of the metal. The high temperature at these two hot spots would severely restrict the usefulness of the method if the gas sample under analysis contained a component which decomposed to non-volatile products at the temperatures concerned. The non-volatile products would tend to deposit in the path of the beam and become a source of neutrons. The background would then become overwhelming and would make accurate analyses difficult. The cell would, moreover, be rendered unusable for subsequent analyses.

As an example of thermal decomposition, the irradiation of acetonitrile vapours may be cited. A sample of liquid CH_3CN was connected directly to the irradiation cell to build up the saturation vapour pressure. During irradiation it was observed that the neutron count from the sample increased rapidly, the increase being due to neutrons from carbon-12. However, the peak caused by carbon in the spectrum was noticeably displaced to an apparently lower energy, compared with the corresponding peak in the methane spectrum. The apparent energy displacement of the peak was due to the fact that the ^{12}C-neutrons from acetonitrile were mostly generated at the backing whereas those from methane were generated about the middle of the cell. The magnitude of displacement was determined by the time taken by the deuterons to traverse the extra distance. Examination of the cell after irradiation

showed a carbon deposit on the inside of the nickel window and a thick tarry residue on the backing. Clearly the amount of decomposition products on the backing would have been considerably lower, had the cell been isolated from the liquid during the irradiation.

APPLICATION TO ORGANIC VAPOURS

If the method is to be of use in the analysis of thermally unstable organic vapours, either decomposition must be prevented or the deleterious effects of decomposition must be minimised.

Prevention of decomposition

A possible approach would be the use of materials with better heat conducting properties in the construction of the cell, and the use of some cooling device. Such an approach is, however, unlikely to solve the problem since the heating effect generates a temperature of nearly 1000°C and is very localised. Also, any cooling system would have to make contact with the nickel window and yet not result in energy degradation of the deuteron beam.

A second approach would be to decrease the heating effect of the beam by decreasing the average beam current, but the neutron count rate would then drop and hence the time required for an analysis would have to be increased. Attempts to increase the neutron count rate could then be made by increasing the length of the irradiation cell, or by increasing the cross sectional area of the beam. However, an increase in the cell length would increase the uncertainty of the flight path of the neutron, resulting in a broadening of the spectral peaks. Changes in the cross section of the beam are limited the maximum cross sectional area obtainable from the accelerator.

Utilisation of decomposition

An entirely different approach involves decomposition of the sample under controlled conditions. Non-volatile decomposition products may then be deposited over a selected area and subsequently removed from the path of the beam to make analyses of the volatile materials possible. This procedure transforms the analysis into a four-stage process and necessitates the construction of a different irradiation cell shown in Figure 3.

Firstly, the cell and its measured contents are irradiated for a short period with a d.c. beam of deuterons at a high current (8-12 μa) in the position shown in Figure 4. During this operation the high temperature generated at the tantalum backing causes decomposition of most organic vapours and the deposition of the non-volatile materials at the hot spot. The tantalum backing is 0.01 inches thick, sufficient to stop the beam entirely, and its thermal conductivity is suitable to ensure localisation of the carbonaceous deposit. The flanged adapter (see Figure 3) is used to move the point of incidence of the beam on the backing to a markedly off-centre position. The dimensions of the dummy cell were chosen such that the deposit could be placed in the path of the beam during a subsequent irradiation.

Secondly, the cell without its dummy is mounted in position B as shown in Figure 4 with the nickel window and attached to the adapter and the carbonaceous deposit on the tantalum backing in the path of the beam. A second irradiation is carried out with a pulsed deuteron beam of a cross sectional area large enough to cover the entire deposit. The time-of-flight spectrum recorded at this stage represents neutrons emitted both from the deposit and from any volatile materials in the cell and the background.

Thirdly, the cell is rotated through 180° about its length (Position C, Figure 4). Because the carbon deposit is not in the centre of the tantalum backing, the rotation of the cell effectively removes the deposit from the path of the beam. The time-of-flight spectrum recorded at this stage represents neutrons emitted from the volatile material and the background.

Fourthly, the cell is evacuated and the time-of-flight spectrum recorded at this stage represents the background.

From the data obtained at the second, third and fourth irradiation, the required analytical results may be computed.

Advantages

The main advantage of this procedure is that analysis of volatile organic material becomes possible. In addition the cell is available for subsequent analyses after replacing the tantalum backing. No deposit forms on the inside of the nickel window, because at no stage does the irradiation beam strike it while decomposable material is the cell.

REFERENCES

(1) PEISACH, M., PRETORIUS, R., S. African Industrial Chemist 20, 5 (1966).

(2) McMURRAY, W.R., PEISACH, M., PRETORIUS, R., van der MERWE, P., van HEERDEN, I.J. (in preparation for publication).

(3) PEISACH, M., Chem. Communications, 632 (1966).

(4) PEISACH, M., PRETORIUS, R., Anal. Chem. (in press)(1967).

(5) McMURRAY, W.R., PEISACH, M., PRETORIUS, R., van der MERWE, P., van HEERDEN, I.J., Nucl. Phys. (in press)(1967).

(6) NAUDE, W.J., PEISACH, M., PRETORIUS, R. (in preparation for publication).

TABLE I

SOME NEUTRON ENERGIES FROM (d,n) REACTIONS

E_d = 3.0 MeV $\theta_L = 30^\circ$

Target		^{12}C	^{14}N	^{16}O
Natural Abundance (%)		98.89	99.63	99.759
Q (d,n_0) MeV		-0.281	5.066	-1.627
Neutron Energy (MeV)	n_0	2.582	7.932	1.223
	n_1		2.771	0.685
	n_2		2.710	
	n_3		1.763	
	n_4		1.098	
	n_5		1.033	
	n_6		0.693	
	n_7		0.235	

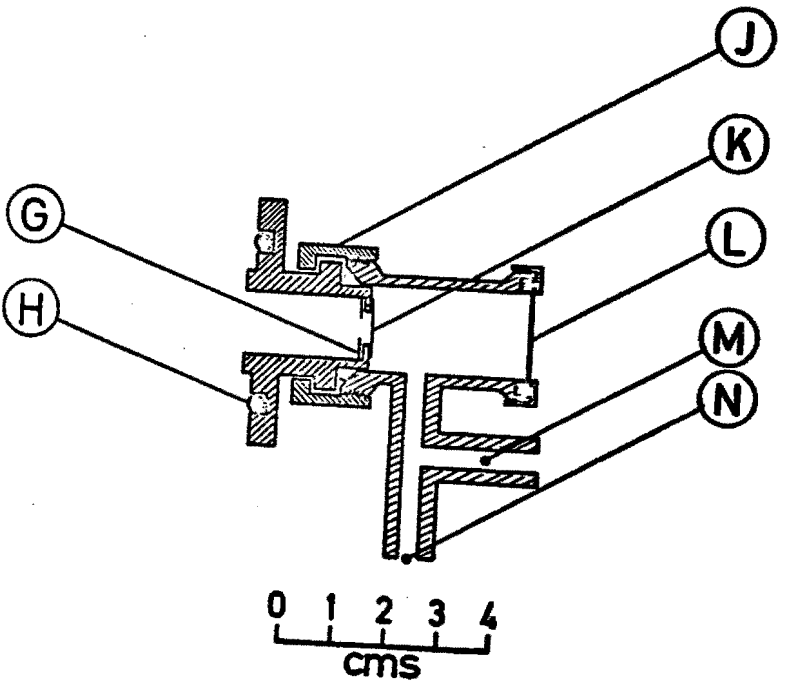

Figure 1

Irradiation cell for thermally stable samples

G : Tantalum collimator

H : Vacuum O-ring

J : Screw-on clamp

K : Nickel window

L : Tantalum back of cell

M : Connection for vacuum pump

N : Connection for gas handling apparatus

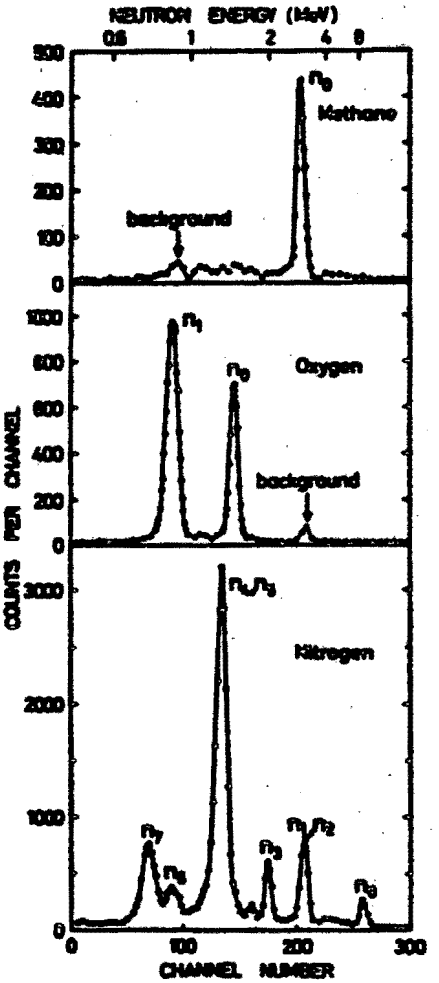

Figure 2

Typical neutron time-of-flight spectra

E_g = 3.9 MeV

Flight path = 3.0 meters

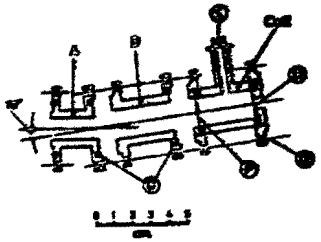

Figure 3

Irradiation cell assembly for decomposing and analysing organic vapours

A : Flanged adapter

D : Dummy cell

O : Vacuum O-rings

P : Tantalum back of cell

Q : Centre line for assembly screws

R : Nickel window

S : Connection for vacuum apparatus

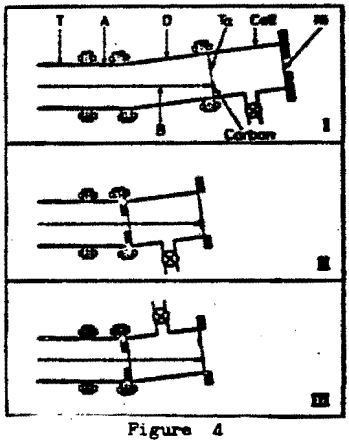

Figure 4

The mounted cell assembly as used for a sequence of irradiations

I : Preliminary decomposition

A : Flanged adapter

B : Path of irradiating beam

D : Dummy cell

II : Analysis of carbon deposit

III : Analysis of residual gas phase and measurement

No. 21

Reprinted from

ANALYTICAL CHEMISTRY

Isotopic Determination of Calcium-43 and Calcium-48 by Neutron Time-of-Flight Spectrometry

W. ROY McMURRAY, MAX PEISACH, RENÉ PRETORIUS, PHILIP VAN DER MERWE, AND IZAK J. VAN HEERDEN

Southern Universities Nuclear Institute, P. O. Box 17, Faure, C. P., South Africa

Volume 40, Number 2

Pages 266–270 February 1968

Isotopic Determination of Calcium-43 and Calcium-48 by Neutron Time-of-Flight Spectrometry

W. Roy McMurray, Max Peisach, René Pretorius, Philip van der Merwe, and Izak J. van Heerden
Southern Universities Nuclear Institute, P. O. Box 17, Faure, C. P., South Africa

Neutron time-of-flight spectrometry was used to determine the isotopic concentration of ^{43}Ca and ^{48}Ca in calcium fluoride targets irradiated with a pulsed proton beam of 4.5 meV. For the determination of ^{43}Ca, neutron counts from ^{48}Ca were used as an internal standard to represent total calcium, and vice versa for the determination of ^{48}Ca. ^{43}Ca was determined over the range 0.145 (natural) to about 2 atom % and ^{48}Ca over the range 0.18 (natural) to about 1.2 atom % with relative standard deviations of ±4.3 and ±5.8%, respectively. The duration of an analysis was between 30 and 60 minutes. The method can be extended to determine higher enrichments of either isotope. The effects of proton energy, measuring angle, and target thickness were investigated.

THE HEAVIER ISOTOPES OF CALCIUM occur in such low concentrations in nature that preparations enriched in them are suitable for stable isotopic tracing. However, the widespread use of this technique has been hampered by difficulties in determining the isotopic concentration of the tracer. Neutron activation methods have been used for determining calcium-48 (*1–4*) by measuring the generated calcium-49, but these methods require a separate determination of total calcium content. Recently a method using proton activation has been reported (*5*) in which the activity produced from calcium-43 and -44 served as a measure of the total calcium content and was used as an internal standard to obtain the ratio of calcium-48 to total calcium directly. The disadvantage of this method (*5*) lies in the fact that the irradiated sample has to be counted over a long period to enable the shorter-lived activities to decay, so that the activity formed from calcium-48 may be measured with sufficient precision. For this reason it was desirable to develop a method which would retain the advantage of directly determining the ratio of tracer to total calcium, but reduce the over-all duration of the analysis.

The duration of the analysis would be reduced if shorter-lived activities could be measured, but, in this case, no such activities can readily be generated by neutron or proton activation. However, the half lives of the product cease to be the determining factor if prompt nuclear reaction products are measured during irradiation. When calcium isotopes are irradiated with protons, the prompt neutrons emitted from (p, n) reactions can conveniently be measured against high backgrounds of other prompt or delayed reaction products. The energy of neutrons emitted will be related to the Q-values of the reactions leading to the excited states in which the product nuclei are left, and their relative yields will depend on the reaction cross sections and the isotopic concentrations of the calcium isotopes. The ground state Q-values for (p, n) reactions of the stable calcium isotopes are given in Table I, from which it is clear that no neutrons can be emitted from calcium-40 or -42 with proton energies below 6.7 meV. At such energies the only calcium isotopes from which a measurable neutron yield may be expected are those of mass number 43, 44, and 48; the low natural abundance of calcium-46 makes it unlikely that the relative neutron yield from this isotope would be appreciable.

The measurement of prompt neutrons by neutron time-of-flight spectrometry has already been used for analytical purposes and the principles of the method have been discussed (*6*, *7*). This paper describes the application of neutron time-of-flight spectrometry to the determination of calcium-43 and -48 using proton irradiation.

EXPERIMENTAL

Preparation of Samples and Standards. Calcium carbonate enriched in calcium-43 or -48 was obtained from the Oak Ridge National Laboratory, United States of America. Calcium fluoride targets of samples and standards were prepared by the method described previously (*5*). The thickness of targets prepared in this way could be controlled and reproduced with a relative standard deviation of ±3.8% for target thicknesses ranging from 300 to 1000 μg per sq cm Targets analyzed in this investigation were about 600 μg per sq cm thick. The microevaporator shown in Figure 1 was used to prepare targets from samples weighing between 0.5 and 2.0 mg. A high temperature was achieved by bombarding the crucible containing the calcium fluoride with up to 0.5 A of electrons emitted from a heated thoriated tungsten coil around the crucible. A variable bombarding potential of up to 500 V enabled the temperature to be adjusted to a maximum of 3000° C.

Irradiation and Measurement. Pulsed proton beams were obtained from the 5.5-mV Van de Graaff accelerator at the Southern Universities Nuclear Institute. Pulses were about 4 nsec in duration and 400 nsec apart. Average beam currents were between 0.6 and 3.0 μA. The tantalum backings on which the targets were deposited were cooled externally by compressed air. For convenience a current integrator, set to a predetermined value, automatically switched off the measuring system. On the average the measurements required from 30 to 60 minutes per sample.

The electronic equipment was the same as used previously (*7*) and is described in detail by McMurray, van der Merwe, and van Heerden (*8*). The time of arrival of the pulsed irradiating beam on the target was given by a signal from a pickup probe placed near the target in the beam tube. Neutrons generated by the pulsed beam at the target were detected in an NE 213 liquid scintillation detector placed a distance d meters and at an angle θ from the target. Pulses from gamma rays were rejected by pulse shape discrimination. The difference in time, t nsec, between the signals from

(1) E. Junod and J. Laverlochere, "Proceedings of 3rd International Colloquium on Biology," Saclay, 1963.
(2) F. W. E. Strelow and H. Staerk, ANAL. CHEM., **35**, 1154 (1963).
(3) S. Amiel and J. O. Juliano, Israel Atomic Energy Commission, Rept. IA-933 (1964).
(4) J. T. Corless, ANAL. CHEM., **38**, 810 (1966).
(5) M. Peisach and R. Pretorius, ANAL. CHEM., **38**, 956 (1966).
(6) M. Peisach, *Chem. Commun.*, **1966**, p 632.
(7) M. Peisach and R. Pretorius, ANAL. CHEM., **39**, 650 (1965).
(8) W. R. McMurray, P. van der Merwe, and I. J. van Heerden, *Nucl. Phys.*, **A92**, 401 (1967).

Reprinted from **ANALYTICAL CHEMISTRY**, Vol. 40, Page 266, February 1968

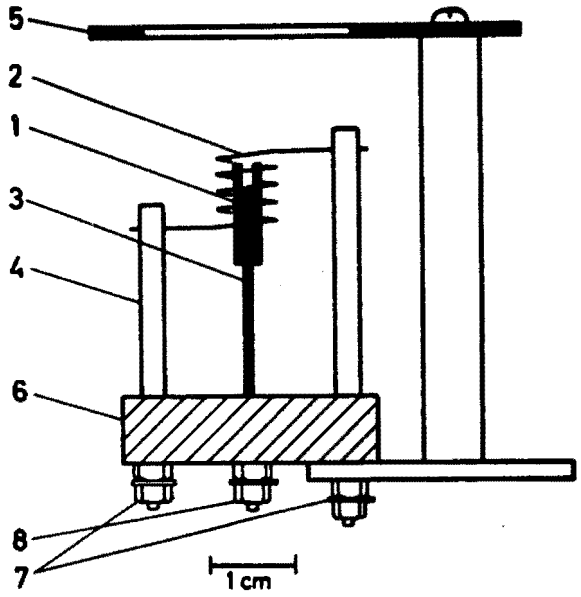

Figure 1. Microevaporator used to prepare calcium fluoride targets from small amounts of material

1. Tantalum crucible
2. Tungsten filament, 0.25-mm diameter
3. Tungsten crucible support, 2.0-mm diameter
4. Brass filament support
5. Target holder
6. Insulator and system base
7. Filament connections
8. High voltage connection

the detector and the pickup probe was converted by a time-amplitude converter and recorded by a multichannel analyzer. The neutron energy, E_n meV, may be obtained from the time-of-flight, t, by the nonrelativistic relationship:

$$t = \frac{72.3 \times d}{\sqrt{E_n}} \qquad (1)$$

NEUTRON TIME-OF-FLIGHT SPECTRA

Time-of-flight spectra of the neutrons emitted from ^{43}Ca, ^{48}Ca, and natural calcium targets irradiated with a proton beam of 4.5 meV are shown in Figure 2. Neutrons of specific energy groups appear as peaks broadened by uncertainties in the measurement of the neutron flight time from the target to the detector and by the spread of kinetic energy of neutrons caused by the energy loss of the irradiating protons within the target thickness. The energy of the neutron group is related to the excited state in which scandium-43 or scandium-48 is left. The nuclear level structure of these two product nuclei was deduced from such data and is reported elsewhere (*9*).

The detection threshold for the measuring system was about 700 keV, so that at proton bombarding energies below about 4.7 meV, no neutron groups could be observed for the reactions ^{19}F(p, n)^{19}Ne and ^{44}Ca(p, n)^{44}Sc. These proton energies are also below the threshold for neutron emission from the tantalum backing. It thus follows that all the measured neutron groups originate from ^{43}Ca and ^{48}Ca. These are observed on a low background continuum in the time-of-flight spectrum, which can easily be subtracted.

With a proton energy of 4.5 meV the highest neutron energy obtainable from the reaction ^{43}Ca(p, n)^{43}Sc at 0° is 1.477 meV

(9) W. R. McMurray, M. Peisach, R. Pretorius, P. van der Merwe, and I. J. van Heerden, *Nucl. Phys.*, A 99, 6 (1967).

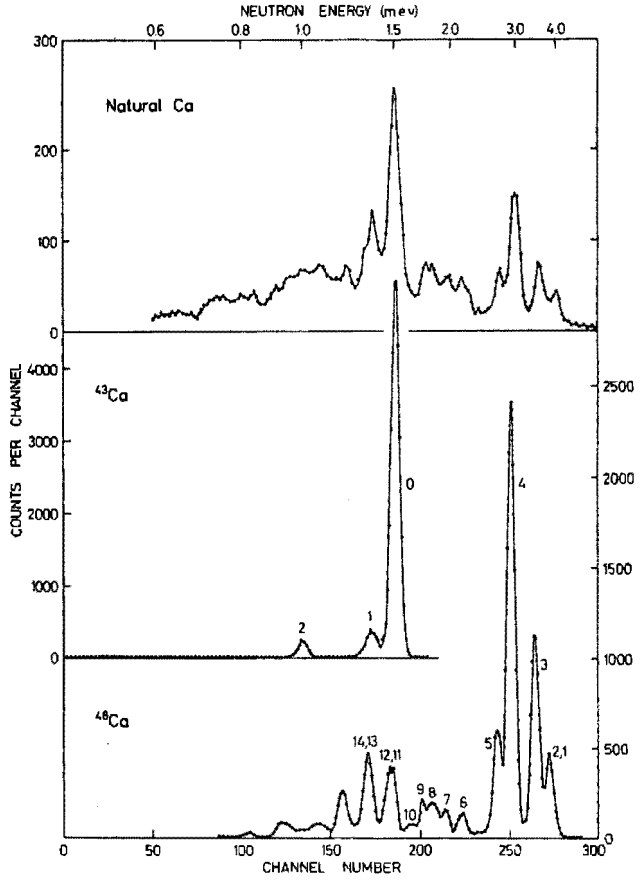

Figure 2. Time-of-flight spectra of neutrons from (p, n) reactions on targets of natural calcium and enriched ^{43}Ca and ^{48}Ca

E_p = 4.5 meV. θ = 0°. d = 2.991 meters

Table I. Ground-State Q-Values for (p, n) Reactions

Target nuclide	Natural abundance, %	Q-value (*10*), meV
^{40}Ca	96.97	−14.680
^{42}Ca	0.64	−6.700
^{43}Ca	0.145	−3.003
^{44}Ca	2.06	−4.431
^{46}Ca	0.0033	−2.165
^{48}Ca	0.18	−0.515
^{19}F	100	−4.031
^{180}Ta	0.0123	−0.083
^{181}Ta	99.988	+0.242

Table II. Neutrons with Energies above 700 keV Emitted at 0° in (p, n) Reactions on Calcium-43 and -48 by 4.5-meV Protons

Group	Energy, ^{43}Ca	Energy, ^{48}Ca	Group	Energy, ^{48}Ca
n_0	1.477	...	n_{13}	1.327
n_1	1.325	3.806	n_{14}	1.296
n_2	1.001	3.720	n_{15}	1.232
n_3	...	3.329	n_{16}	1.181
n_4	...	2.818	n_{17}	1.157
n_5	...	2.560	n_{18}	1.072
n_6	...	2.074	n_{19}	1.037
n_7	...	1.877	n_{20}	0.988
n_8	...	1.782	n_{21}	0.936
n_9	...	1.690	n_{22}	0.907
n_{10}	...	1.577	n_{23}	0.811
n_{11}	...	1.449	n_{24}	0.749
n_{12}	...	1.409		

(10) F. Everling, L. A. Koenig, J. H. E. Mattauch, and A. H. Wapstra, "Nuclear Data Tables," Part I, National Academy of Sciences, Washington, 1961.

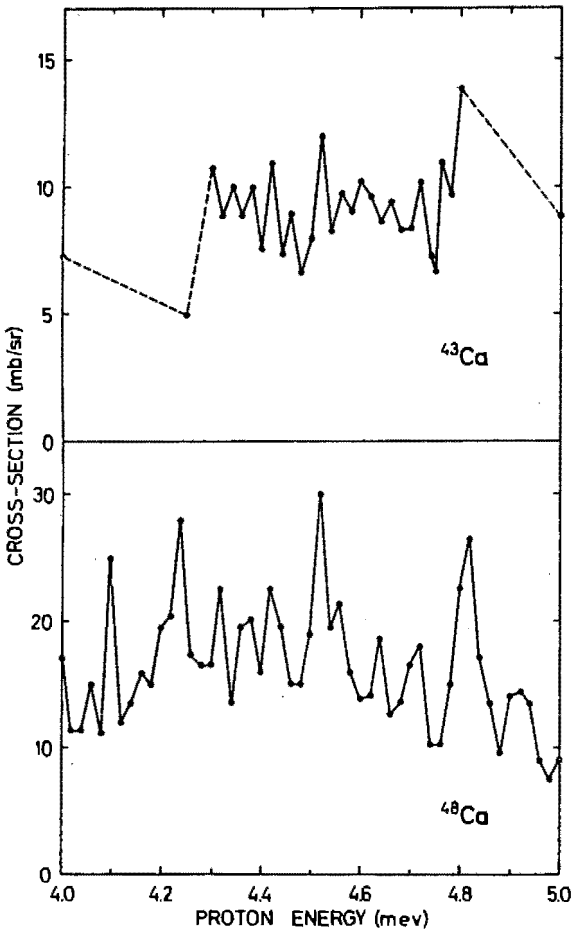

Figure 3. Excitation curves for reaction $^{43}Ca(p,n)^{43}Sc$, summed for n_0 and n_1 neutron groups, and reaction $^{48}Ca(p,n)^{48}Sc$, summed for n_1 to n_5 neutron groups, measured at 0°

(see Table II), while from the reaction $^{48}Ca(p, n)^{48}Sc$ neutron energies up to 3.966 meV may be expected. [The (p, n_0) transition to the ground state of ^{48}Sc is not observable (*11*), presumably because of its very high spin value of 6+, so that under these conditions the highest neutron energy from the latter reaction is in fact 3.806 meV.]

In this investigation the net integrated count for neutrons between 1.267 and 1.642 meV, corresponding to the n_0 and n_1 neutron groups from calcium-43 (see Figure 2) and including the n_{10} to n_{14} neutron groups from calcium-48 (see Table II), is used as a measure of the calcium-43 concentration and is referred to as "the calcium-43 count" and is written as [43]. In the same way the net integrated count obtained from neutrons between 2.416 and 4.151 meV, corresponding to the n_1 to n_5 neutron groups from calcium-48 (see Table II), is used as a measure of the concentration of this isotope and is referred to as "the calcium-48 count" and written as [48].

SELECTION OF EXPERIMENTAL PARAMETERS

The excitation curves for calcium-43 and -48 summed for the neutron groups (n_0, n_1) and (n_1 to n_5), respectively, as obtained from enriched targets, are shown in Figure 3. The sharp fluctuations (*12*) are characteristic of a reaction proceeding through a highly excited compound nucleus satisfying the requirements of the Ericson fluctuation theory (*13*). From Figure 3 it is clear that the over-all trend in neutron yield varies little over the energy range studied, so that any selected proton energy in the range 4 to 5 meV could be suitable for analytical purposes.

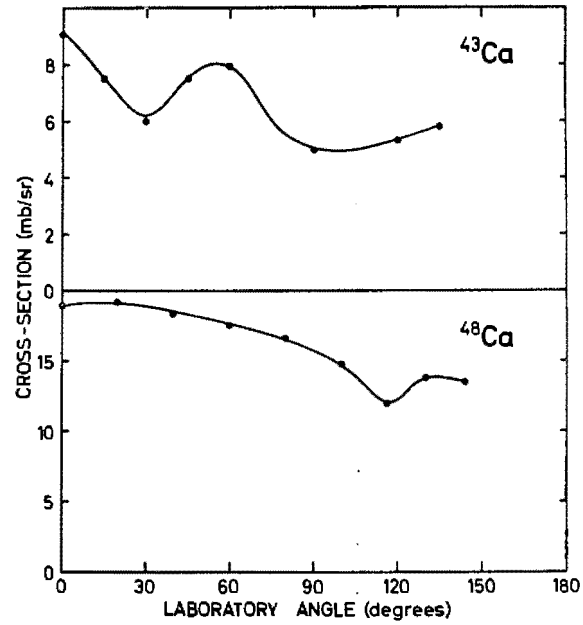

Figure 4. Angular variation of neutron yield for (p,n) reactions on ^{43}Ca, summed for n_0 and n_1 neutron groups, and ^{48}Ca, summed for n_1 to n_5 neutron groups, measured at 4.5 meV

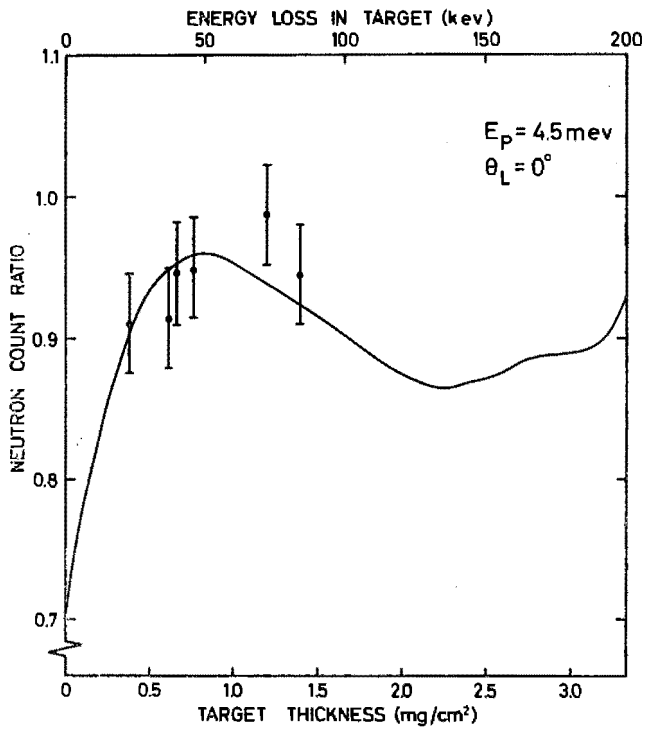

Figure 5. Effect of target thickness on ratio of neutron count from calcium-43 to that from calcium-48 in natural calcium

Curve calculated from excitation curves and points experimentally determined

(11) C. Chasman, K. W. Jones, and R. A. Ristman, *Phys. Rev.*, **140B**, 212 (1965).
(12) W. R. McMurray, M. Peisach, R. Pretorius, P. van der Merwe, and I. J. van Heerden, *Nucl. Phys.*, A **99**, 17 (1967).
(13) T. Ericson and T. Mayer-Kuckuk, *Ann. Rev. Nucl. Sci.*, **16**, 183 (1966).

Table III. Determinations of Calcium-43

I	II	III	IV	V	VI	VII
Sample No.	Known ^{43}Ca concn., atom %	Neutron count ratio	Net[a] neutron count, ratio per atom %	Found ^{43}Ca concn., atom %	Error, V-II, atom %	Relative error $\frac{100\ VI}{II}$, %
Nat. C	0.145	0.911	2.166	0.132	−0.013	−8.97
Nat. D	0.145	0.945	2.400	0.146	+0.001	+0.69
Nat. E	0.145	0.914	2.186	0.133	−0.012	−8.28
Nat. F	0.145	0.940	2.366	0.144	−0.001	−0.69
28–43	0.175	1.009	2.354	0.173	−0.002	−1.14
30–43	0.266	1.292	2.613	0.292	+0.026	+9.77
		1.213	2.316	0.259	−0.007	−2.63
31–43	0.320	1.330	2.291	0.308	−0.012	−3.75
		1.354	2.366	0.318	−0.002	−0.63
27–43	0.354	1.523	2.616	0.389	+0.035	+9.89
		1.439	2.379	0.354	Zero	Zero
33–43	0.490	1.760	2.373	0.489	−0.001	−0.02
		1.772	2.398	0.494	+0.004	+0.82
32–43	0.505	1.800	2.382	0.506	+0.001	+0.02
34–43	1.058	3.057	2.325	1.034	−0.024	−2.27
		3.123	2.388	1.062	+0.004	+0.38
35–43	1.216	3.642	2.504	1.280	+0.064	+5.26
		3.399	2.304	1.178	−0.038	−3.13
36–43	1.430	3.884	2.299	1.382	−0.048	−3.36
		3.998	2.378	1.430	Zero	Zero
37–43	1.794	4.850	2.371	1.788	−0.006	−0.33
		4.831	2.360	1.780	−0.014	−0.78
38–43	1.990	5.483	2.455	2.055	+0.065	+3.27
		5.259	2.343	1.960	−0.030	−1.51

Mean value of net neutron count ratio per atom % = 2.372
Relative standard deviation = ±4.34%
Mean error = −0.0004 atom %

[a] Net value obtained from observed value (III) minus intercept value of calibration line (0.597).

For this investigation a proton energy of 4.5 meV was chosen. At this energy, neutrons from the reaction $^{19}F(p, n)^{19}Ne$ would not be recorded and the energies of the measured neutrons from the calcium isotopes would be above the value at which the detection efficiency (*8*) begins to decrease rapidly with decreasing neutron energy.

Angular distribution curves for the appropriate neutrons at E_p = 4.5 meV are shown in Figure 4, from which it is clear that little can be gained by changing the measuring angle. In this investigation measurements were made at 0°.

Effect of Target Thickness. From the excitation curves in Figure 3, it is obvious that the neutron yield changes appreciably with a small change in proton energy. If the target is sufficiently thick, such energy changes will take place within the target. For this reason it was necessary to investigate the effect of target thickness.

From the excitation curves, the ratio [43]/[48] was calculated, for natural calcium, as a function of target thickness for an incident beam of 4.5 meV. The calculations were verified experimentally and the results are shown plotted over the calculated curve in Figure 5. The error bars shown in Figure 5 refer mainly to statistical errors in the measured neutron count from which the ratios were obtained. The calculated value of the neutron count ratio does not change rapidly with target thickness above 300 μg per sq cm, and for target thicknesses above 300 μg per sq cm a relative variation of ±4% will not introduce errors greater than ±1% in the determination.

DETERMINATION OF CALCIUM-43

Results of some determinations of calcium-43 with isotopic concentrations from 0.145 (natural) to about 2 atom % are listed in Table III. The value in column III is [43]/[48]. A calibration curve relating the neutron count ratio to the isotopic concentration of calcium-43 was linear with a slope of 2.378 ± 0.047 per atom % and an intercept value of 0.597 at zero calcium-43 concentration. From this calibration curve, the values given in Table III (column V) were obtained. For each determination given in Table III the neutron count ratio per atom per cent was calculated and is shown in column IV. These values show that the relative standard error was ±4.34%. The mean error was negligibly different from zero. The mean value of the neutron count ratio, 2.372 per atom per cent of ^{43}Ca, was in agreement with the slope of the calibration curve within the errors of the method.

In the analyses mentioned above, each irradiation lasted about an hour, during which time approximately 3000 net counts were accumulated with natural calcium for each of the numerator and denominator in the neutron count ratio. The relative standard error in the neutron count ratio due to statistical fluctuations of the counts obtained from the sample and in the measurement of backgrounds was calculated to be about ±4%. This value is not appreciably different from the relative standard deviation of the method (see Table III), so that precision could be improved if larger numbers of neutron counts are accumulated during an irradiation. Even with the present precision, however, the method is sufficiently sensitive to determine a relative variation of 10% in the isotopic concentration of calcium-43 at the level of natural calcium.

With increasing calcium-43 concentration, the number of neutron counts obtained from this isotope increases, so that the relative standard deviation of the neutron count ratio decreases until limited by the precision with which the neutron counts from calcium-48 may be measured. The method is thus applicable to isotopic concentrations of calcium-43 far beyond the range of values analyzed in Table III.

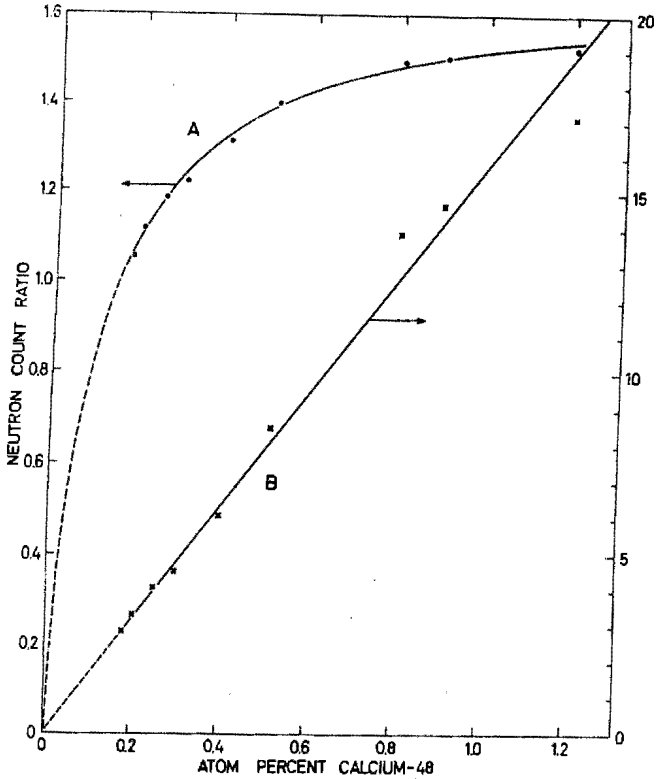

Figure 6. Variation of ratio of neutron count from calcium-48 to that from calcium-43 with isotopic concentration of ^{48}Ca

A. **Ratio of observed counts**
B. **Ratio corrected for contribution of calcium-48 neutron counts to calcium-43 count**

For semiquantitative purposes it would be sufficient to use the number of neutron counts from calcium-43 as a measure of the concentration of this isotope. To use this approach for a precise determination, it would, in addition, require a knowledge of the irradiation current, the accurate calcium content of the irradiated material, and the area and thickness of the sample irradiated. Such an analysis would be sensitive to inhomogeneity in the target. Despite the increased statistical errors incurred by measuring ratios, the advantages through the use of calcium-48 as an internal standard have to be considered against the difficulties involved in measuring the other parameters.

DETERMINATION OF CALCIUM-48

Unlike the case of calcium-43, where the denominator for calculating the neutron count ratio was independent of the calcium-43 concentration, the determination of the similar ratio or its reciprocal in the case of calcium-48 includes terms which are functions of the calcium-48 concentration in both the numerator and denominator. Accordingly, the curve showing the relationship between the neutron count ratio and the isotopic concentration of calcium-48 is not expected to be linear. One such curve obtained from samples of known isotopic concentrations, analyzed under the experimental conditions used for the determination of calcium-43, is shown in Figure 6*A* where the neutron count ratio is [48]/[43]. At low isotopic concentrations of calcium-48 the rate of change of neutron count ratio with isotopic composition is high and hence the method promises to be useful for the determination of this isotope in the concentration region up to about 0.4 atom % calcium-48. At higher isotopic concentrations the curve levels off and tends to the value 1.675, which is the ratio of the counts obtained from calcium-48 in the two energy regions concerned, the calcium-43 contribution becoming comparatively smaller with increased enrichment of calcium-48.

The relative standard deviation of the results shown in Figure 6*A* was about ±5.8% ,so that the determination of calcium-48 by this method is somewhat less precise than the determination of calcium-43. However, the comparatively large relative errors of the more highly enriched calcium-48 samples tended to raise the value of the relative standard deviation of the results.

The contribution of neutrons from calcium-48 to [43] is proportional to [48] and the proportionality constant was 0.597 under the conditions of the measurement. When [43] is corrected for counts contributed by calcium-48, the ratio R_c = [48]/([43] −0.597 [48]) should be a linear function of the isotopic concentration of calcium-48. This correction is applied to the observed values in Figure 6*B*. At low isotopic concentrations of calcium-48 the measured isotopic concentration is in good agreement with the known value, but the agreement becomes poor at higher concentrations of calcium-48. The deterioration is due to the fact that the relative size of the correction term increases, thus increasing the relative statistical error of [43] − 0.597 [48].

The method of measuring ratios is clearly not suited for the determination of calcium-48 above an isotopic concentration of about 0.4 atom %. For higher concentrations the method of neutron time-of-flight spectrometry can be used reliably if the calcium-48 count is used as a direct measure of the concentration of this isotope. Although this value would not be affected by other components in the sample, the total calcium content would then have to be determined separately, as is the case for neutron activation methods.

ACKNOWLEDGMENT

One of us (R. P.) thanks his promotor for permission to publish results which will form part of a doctorate thesis to be submitted to the University of Stellenbosch.

RECEIVED for review June 20, 1967. Accepted October 10, 1967. Financial assistance from the South African Atomic Energy Board is gratefully acknowledged.

Reprinted from Proc. 3rd Conf. on 'Accelerator, Targets Designed for the Production of Neutrons' held in Liege, September 1967. Euratom, Brussels (1968) pp 261-282

No.22

THE FAST NEUTRON FACILITY AT THE PRETORIA CYCLOTRON

W.J. Naudé*, Max Peisach** and W.L. Rautenbach
Nuclear Physics and Radioactivity Division, National Research Laboratory
Pretoria.South Africa
* The Merensky Institute for Physics, University of Stellenbosch
** Southern Universities Nuclear Institute, Faure C.P.

ABSTRACT

The construction of a beryllium target for use with the internal beam from the Pretoria 110-cm. cyclotron, as a neutron source, is described. The beryllium is mounted on a copper support through which a rapid current of cooling water flows. The transfer of heat is improved by grooving the underside of the target and by spreading the charged particle beam over the entire surface.

Samples for neutron irradiation are mounted in a cylindrical pipe in six positions from 6.5 to 23.6 cm. from the beryllium and at angles from 14° to 70° to the direction of incidence of the charged particle beam. The pipe protrudes through the vacuum lock so that samples can be irradiated outside the vacuum system of the cyclotron.

Activation reactions with thresholds between 1.8 and 20.3 MeV. were used to calibrate the neutron flux. Ten reactions were so chosen that it was possible to use only 5 target materials, viz., KOH, Al, MgO, NH_4F and C. Thus only 6 irradiations were sufficient to measure the flux at each irradiation site. The activities were measured with a NaI(Tl) scintillation detector, the efficiency of which had been calibrated as a function of gamma-ray energy.

Flux calibrations were performed on the neutrons emitted in the reaction $^{9}Be(d,n)^{10}B$ with 15.7 MeV. deuterons and the reaction $^{9}Be(\alpha,n)^{12}C$ with 31.8 MeV. alpha particles.

Total fluxes, depending on the irradiation site, ranged from 1.8×10^{8} to 2.1×10^{10} neutrons/cm.^{2}-sec. The energy distribution was measured and found to be in excellent agreement with published data obtained from 15, 24 and 26 MeV. deuterons. Agreement was also good when the angular distribution of the emitted neutrons was compared with previously reported values. Total fast neutron emission from deuteron bombardment at 15.7 MeV. was 2.28×10^{12} neutrons/sec. per 100 μA., which may be compared with the reported value of 1.90×10^{12} neutrons/sec. at 15 MeV.

The Pretoria 110-cm. cyclotron (1) can produce internal and external proton, deuteron and alpha-particle beams with maximum energies of about 8, 16 or 32 MeV. respectively, and is capable of producing internal beam currents of up to 800 μA of hydrogen ions or 200 μA helium ions. External beams with well-defined energy (within ± 0.3%) can be obtained at currents of a few microamperes. The large difference between internal and external beam currents makes it attractive to use the internal beam for neutron production.

Measurements by other authors (2) have shown that the total neutron yield obtainable from the irradiation of thick targets with accelerated deuterons or alpha-particles increases rapidly with decreasing atomic number of the target. Moreover, the angular distribution of the neutron flux from light elements has a pronounced peak in the forward direction. It follows that the optimum ratio of useful neutron flux to charged particle beam current is obtainable in a position as close as possible to a light element target, in the direction of the incoming charged particle beam.

Because the neutron flux obtainable from a target is directly proportional to the incident charged particle beam current, the practical limitation to the intensity of the neutron flux is imposed by the thermal properties of the target which determine the rate of removal of heat from the region irradiated. The light element, beryllium, has thermal properties which meet

the requirements for neutron production; it has very good thermal conductivity, a comparatively high melting point and low vapour pressure over a wide temperature range, thus making it useful for a target material inside the vacuum of the cyclotron.

The paper describes the beryllium target used at the Pretoria cyclotron and the calibration of the flux and energy distribution of neutrons obtained from it by irradiation with 15.7 MeV. deuterons and 31.8 MeV. alpha-particles.

DESCRIPTION OF THE TARGET AND IRRADIATION ASSEMBLY

The target consisted of a block of beryllium soldered onto a copper plate (see Figure 1), by placing a foil of silver, 0.1 mm. thick, between the copper and beryllium, and heating the system, under an inert atmosphere, to 900°C. The copper plate was, in turn, silver-soldered onto a copper block through which the cooling water circulated rapidly. To improve heat transfer from the copper plate to the water, the area of contact was increased by grooving the underside of the copper plate. The entire target head could be fitted onto a standard target support, thereby making it a simple operation to change target dimensions and materials.

By selecting the correct angle between the beryllium surface and the target support, a well-centred cyclotron beam could be spread over the entire surface of the beryllium target

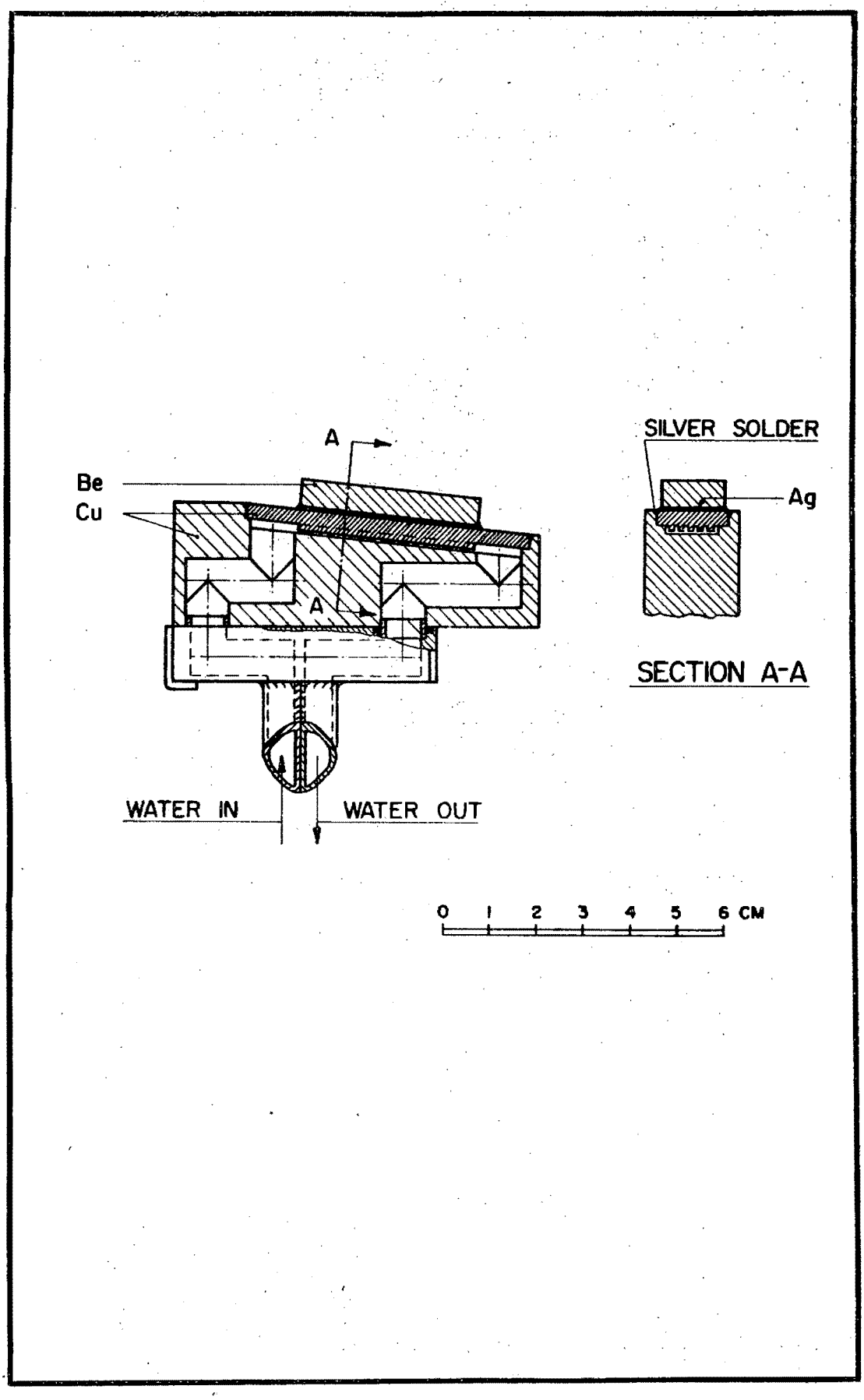

Figure 1. The construction of the beryllium target head.

whereby the heat generated could be dissipated over a larger area. The centering of the beam was achieved by adjusting the current through the first harmonic coils of the cyclotron so as to obtain equal beam currents onto the beryllium target and onto an auxiliary target placed at the same radius from the centre of the cyclotron, 180^{o} away (see Figure 2). When the auxiliary target was retracted a short distance, the entire internal beam fell on the beryllium. Erroneous measurements of the beam current due to secondary electron emission was prevented by copper shielding plates above and below the targets.

Samples for neutron irradiation were positioned in a cylindrical brass pipe, closed at one end and situated immediately behind the beryllium target (see Figure 3). The open end of the pipe protruded through the vacuum lock through which the entire assembly could be introduced into, and removed from, the cyclotron. The sample holder, into which the samples were mounted, fitted into the pipe and could be inserted into any depth required, and withdrawn rapidly. The advantage of such an assembly lies in the fact that the sample is irradiated at atmospheric pressure, thus simplifying sample preparation and irradiation procedure. A fast pneumatic transfer system can readily be incorporated. Since the brass pipe is situated within the radio frequency field of the cyclotron, and because the danger exists that a small fraction of the circulating cyclotron beam may strike the tube, a jet of compressed air was

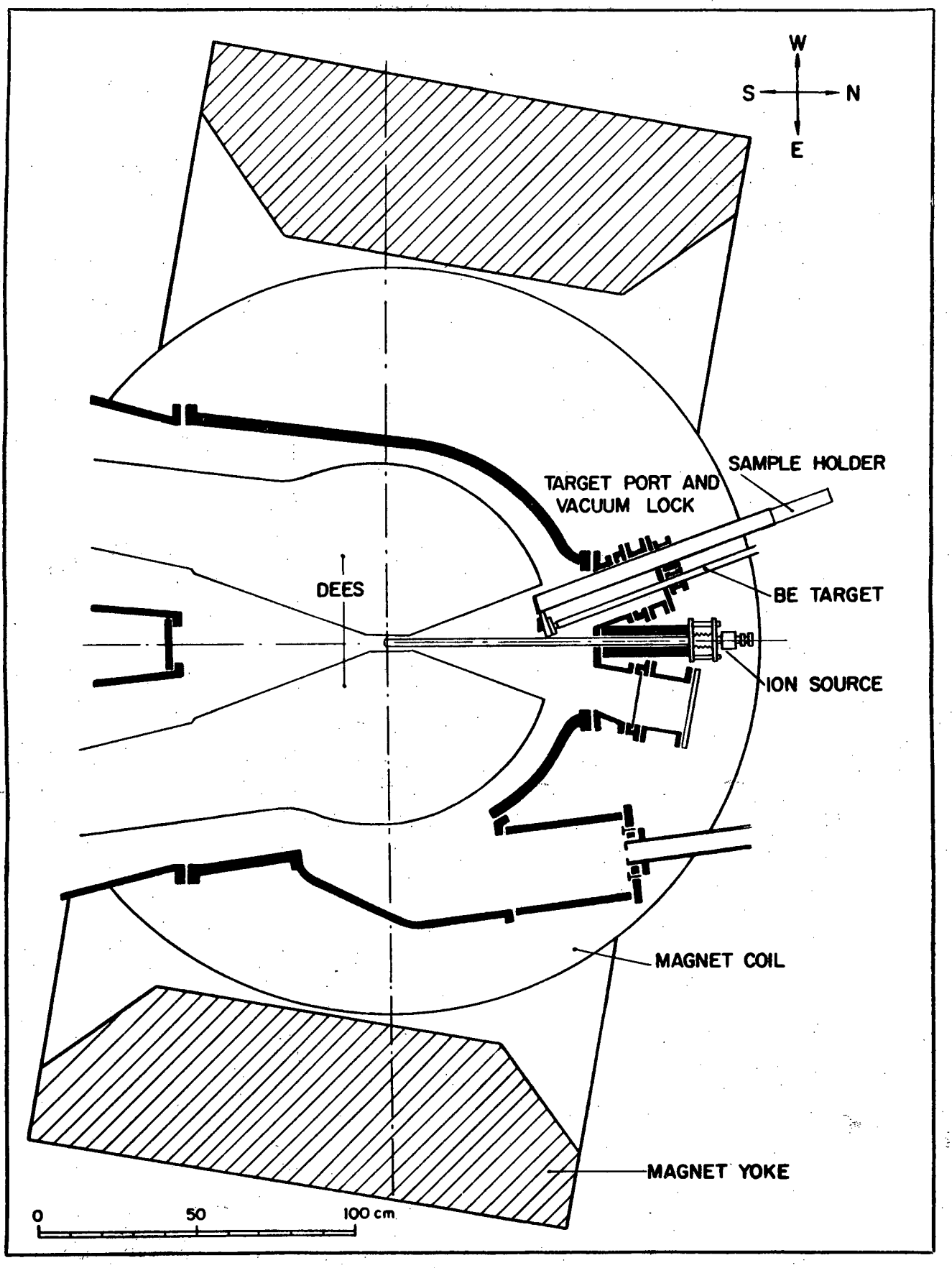

Figure 2. The position of the neutron facility in the cyclotron.

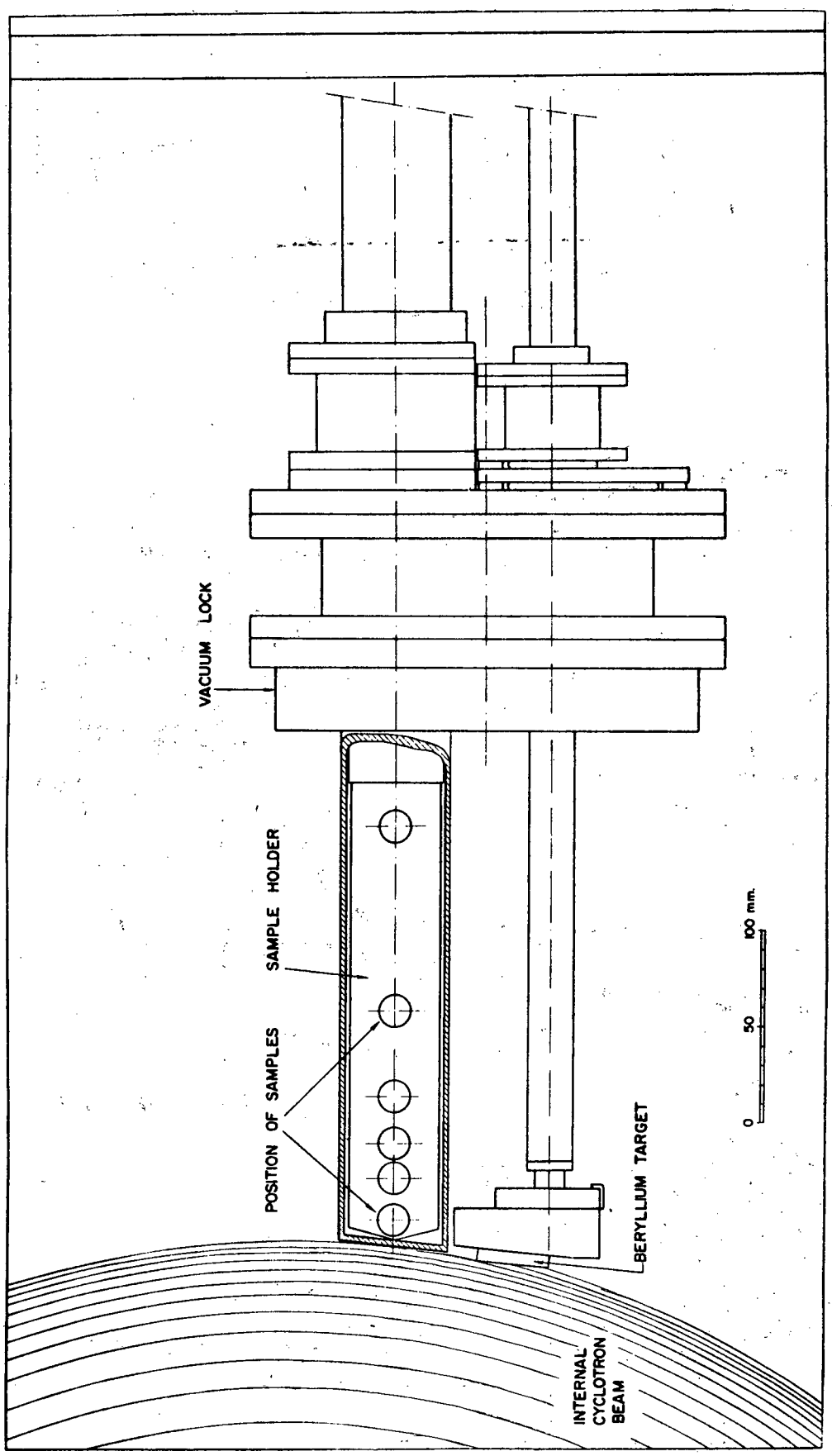

Figure 3. The neutron irradiation assembly.

usually directed onto the closed end in order to cool the pipe and to provide air cooling for the irradiated samples, if necessary.

CALIBRATION OF NEUTRON FLUX

The use of activation threshold detectors still represents a useful technique for measuring neutron fluxes and their energy distribution. This method was used to determine the flux and energy distribution of neutrons produced by 15.7 MeV. deuterons and 31.8 MeV. alpha particles incident on a thick beryllium target.

Selection of reactions with suitable thresholds

Neutrons with energies up to about 20 MeV. were expected from bombarding the target with deuterons and up to about 35 MeV. from the alpha particle irradiation. It was thus necessary that the reactions selected for calibrating the neutron flux should have thresholds ranging over as wide an energy as possible within the expected neutron energy range. Furthermore, reactions had to be selected for which the excitation curves were available, at least in part, and from which the activities that were produced were readily observable. The half-life of the products could not have been too short, as this would have led to difficulties in transporting the activated sample to the counting assembly, nor too long, requiring a

comparitively long irradiation time. In addition it was desirable that some target nuclides should be chemically combined in stable and readily available pure compounds so that results of more than one reaction could be observed from a single irradiated sample.

The reactions that were selected are given in Table I together with the half-life of the product concerned in each case and the energies of important gamma-rays that were used to measure the activities. The 10 listed reactions were selected because they met the requirements outlined above. All the reaction products could be observed by the irradiation of only 5 target materials, KOH, Al, MgO, NH_4F and C, which were counted with a single counting assembly, at appropriate times after the end of the activation, even when all five target materials were simultaneously activated. Reference to Figure 3 shows that the six irradiation positions could thus be simultaneously calibrated, in a series of only six irradiations during which every target material was irradiated in every position and a blank container could be accommodated in every position in turn to allow for subtraction of unwanted activities generated in it.

The only drawback with the abovementioned set of reactions lies in the fact that no reaction is included with its threshold between 5 and 11 MeV. However, the advantages of the selected reactions in other ways were so great as to outweigh this disadvantage.

TABLE I

NEUTRON THRESHOLD REACTIONS

Reaction	Approximate threshold (MeV)	Half-life of product	Energies of important gamma-rays* (MeV)
$^{41}K(n,p)^{41}Ar$	1.8	1.83 h.	1.29
$^{27}Al(n,p)^{27}Mg$	1.9	9.5 m.	0.84, 1.01
$^{41}K(n,\alpha)^{38}Cl$	3.3	37.3 m.	1.62, 2.16
$^{27}Al(n,\alpha)^{24}Na$	4.0	15 h.	1.37, 2.75
$^{24}Mg(n,p)^{24}Na$	4.9	15 h.	1.37, 2.75
$^{19}F(n,2n)^{18}F$	11.0	110 m.	(β^+)
$^{14}N(n,2n)^{13}N$	11.4	10 m.	(β^+)
$^{39}K(n,2n)^{38}K$	13.4	7.7 m.	(β^+), 2.16
$^{16}O(n,2n)^{15}O$	16.6	124 s.	(β^+)
$^{12}C(n,2n)^{11}C$	20.3	20.5 m.	(β^+)

* (β^+) refers to positron emission and hence the appearance of 0.51 MeV. gamma-rays.

Irradiation and measurement

Weighed quantities of the selected target materials were irradiated in polyethylene vials of 3 $cm.^3$ capacity. The polyethylene containers were mounted in each of the six positions shown in Figure 3. These positions correspond respectively to directions of 14, 31, 40.5, 50, 60 and 70° relative to the incident charged particle beam, calculated with respect to the centre of the beryllium target and the midpoint of the irradiated samples, and were at distances of 6.5, 7.5, 8.7, 10.6, 14.5 and 23.6 cm. respectively.

The beryllium target was irradiated with internal beam currents of about 100 μA. for 10 minutes and the total current falling on it was measured with a current integrator. Additional monitoring was carried out using cylinders of copper, placed about a meter from the beryllium target, in which the relative yields of both copper-62 and copper-64 from the reactions $^{63}Cu(n,2n)^{62}Cu$ and $^{65}Cu(n,2n)^{64}Cu$ respectively, were compared with the current integrator values. For intercomparison between different irradiations, all values were normalised to a total charge of 60 millicoulombs, but the normalisation factors were always within ± 10% of unity. The neutron-induced activities in the samples and the copper monitors were measured with a 3 x 3" NaI(Tl) scintillator crystal the efficiency of which was calibrated using substandards of ^{137}Cs, ^{84}Mn, ^{60}Co and ^{22}Na. Counting of the samples was in most cases continued for several half-lives of the product nuclide, from which, the

activities at the end of the irradiation were deduced.

Flux calibrations

The excitation curves for the reactions used for calibrating the neutron flux are shown in Figures 4 and 5, where the solid curves are based on published data (3,4) and the dotted lines are the assumed shapes in the region where experimental data were not available. The integral neutron flux, as obtained from the activation reactions on samples placed in positions 3 and 6 are given as examples, in Figure 6, and in position 1 in Figure 7, where deuterons and alpha particles were respectively used to generate the neutron flux. These figures both show the variation of the neutron flux, for neutrons of energy greater than E, with neutron energy, E.

The energy distribution of the neutrons from the reaction $^{9}Be(d,n)^{10}B$ is shown in Figure 8 for all the irradiation positions, and for the reaction $^{9}Be(\alpha,n)^{12}C$ in Figure 9 for irradiation position 1.

The results shown in Figures 6-9 were calculated by an iteration process for which initially it was assumed that the energy distribution of the neutrons was independent of neutron energy. Three iterations were sufficient to reproduce the reported values.

The shape of the energy distribution curves in Figure 8 is in excellent agreement with previous work (5,6,7) reported for incident deuteron beams of 15, 24 and 26 MeV., especially

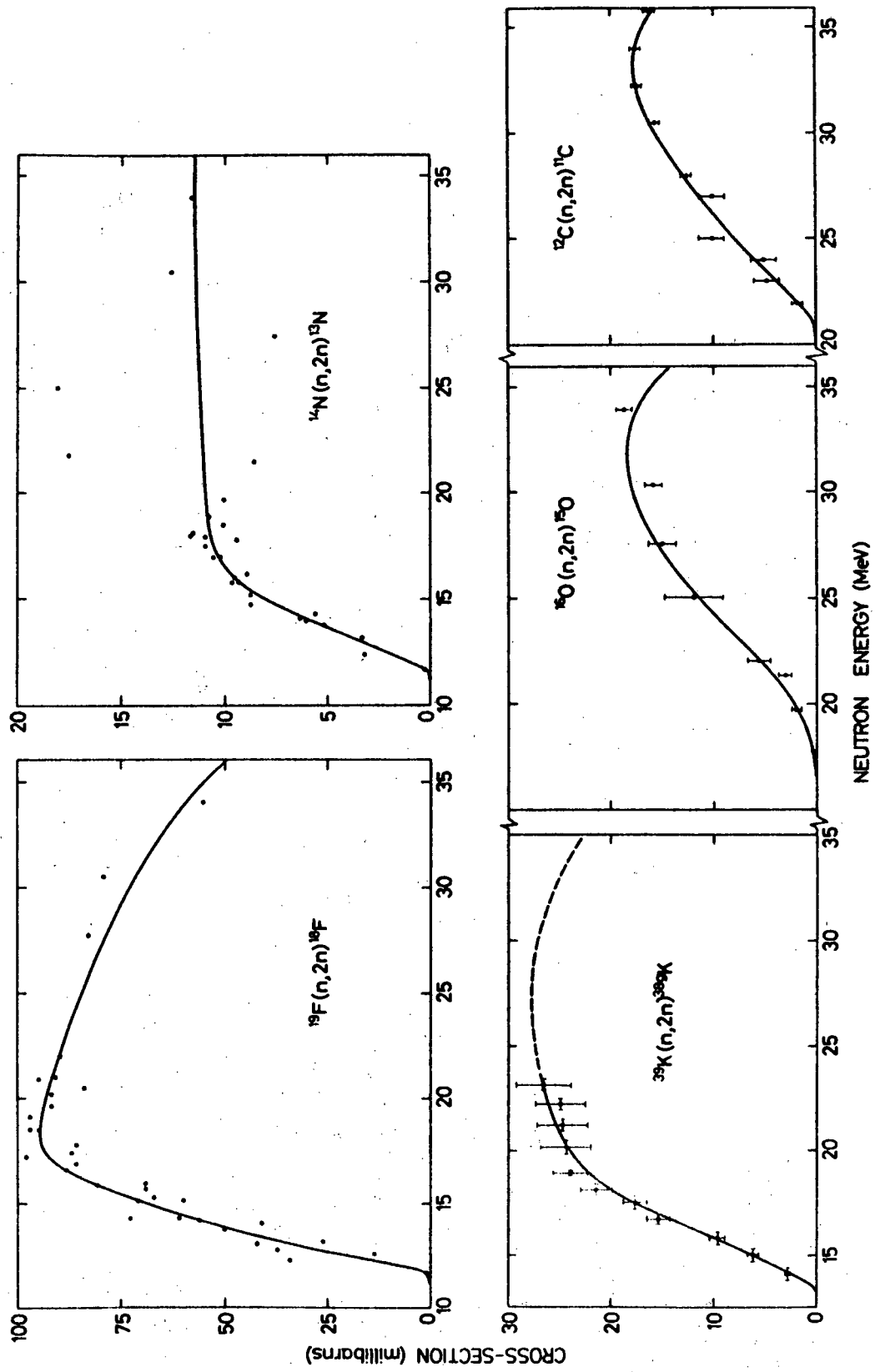

Figure 4. Excitation curves for some (n,2n) reactions used to determine the neutron flux. The broken line shows the assumed shape of the curve in a region of insufficient data.

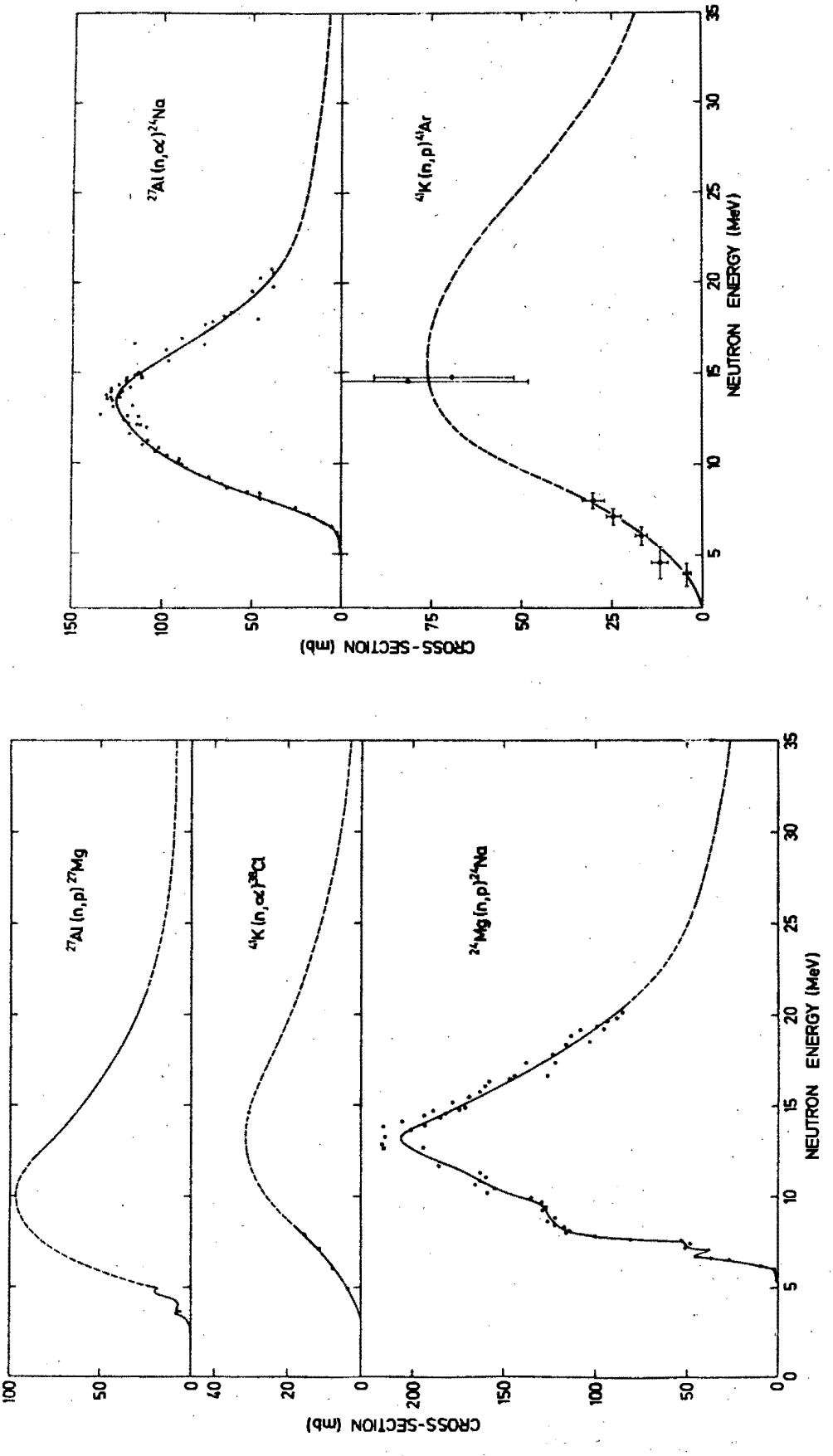

Figure 5. Excitation curves for some (n,p) and (n,α) reactions used to determine the neutron flux. The broken lines show assumed shapes of the curves in regions of insufficient data.

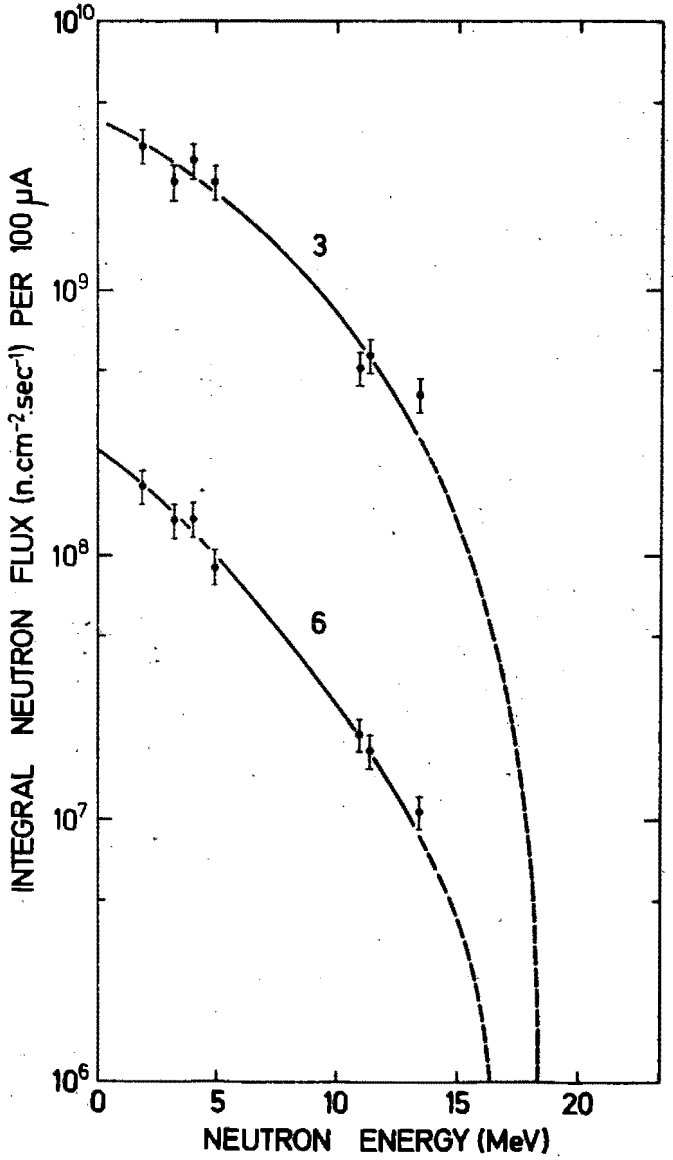

Figure 6. The variation with the neutron energy E, of the total neutron flux, for neutrons with energy greater than E, as obtained at irradiation positions 3 and 6 from the reaction $^{9}Be(d,n)^{10}B$.

E_d = 15.7 MeV.

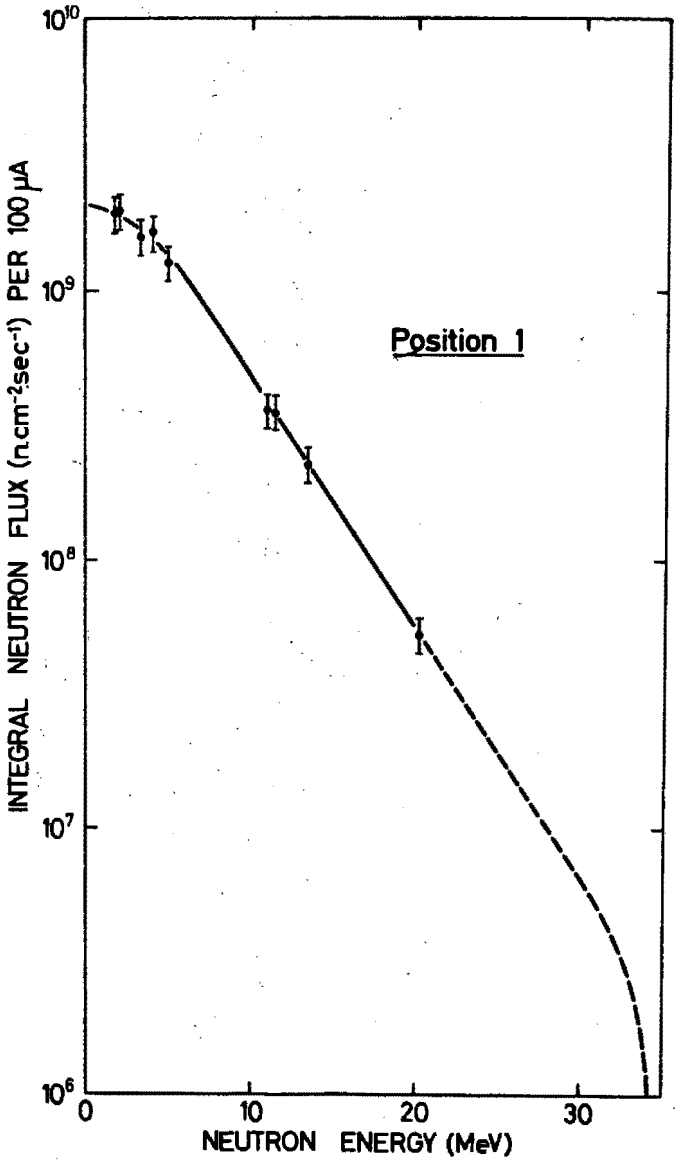

Figure 7. The variation with the neutron energy E, of the total neutron flux, for neutrons with energy greater than E, as obtained at irradiation position 1 from the reaction $^{9}Be(\alpha,n)^{12}C$

E_α = 31.8 MeV.

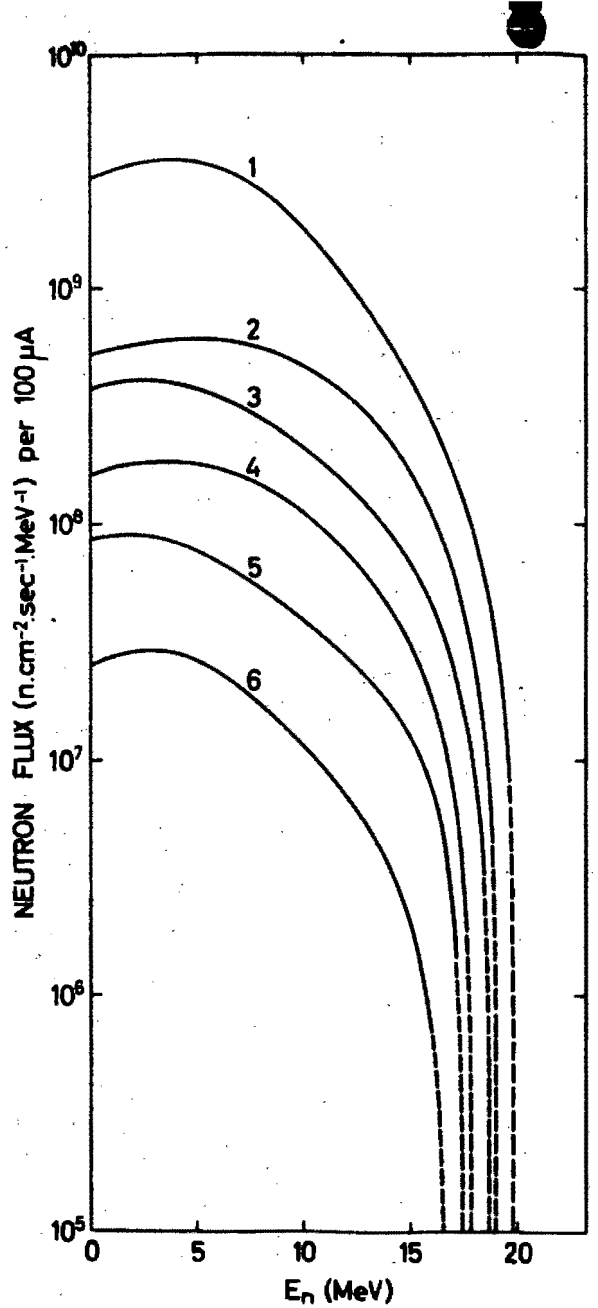

Figure 8. Energy distribution of neutrons from the reaction $^{9}Be(d,n)^{10}B$ at all six irradiation positions.

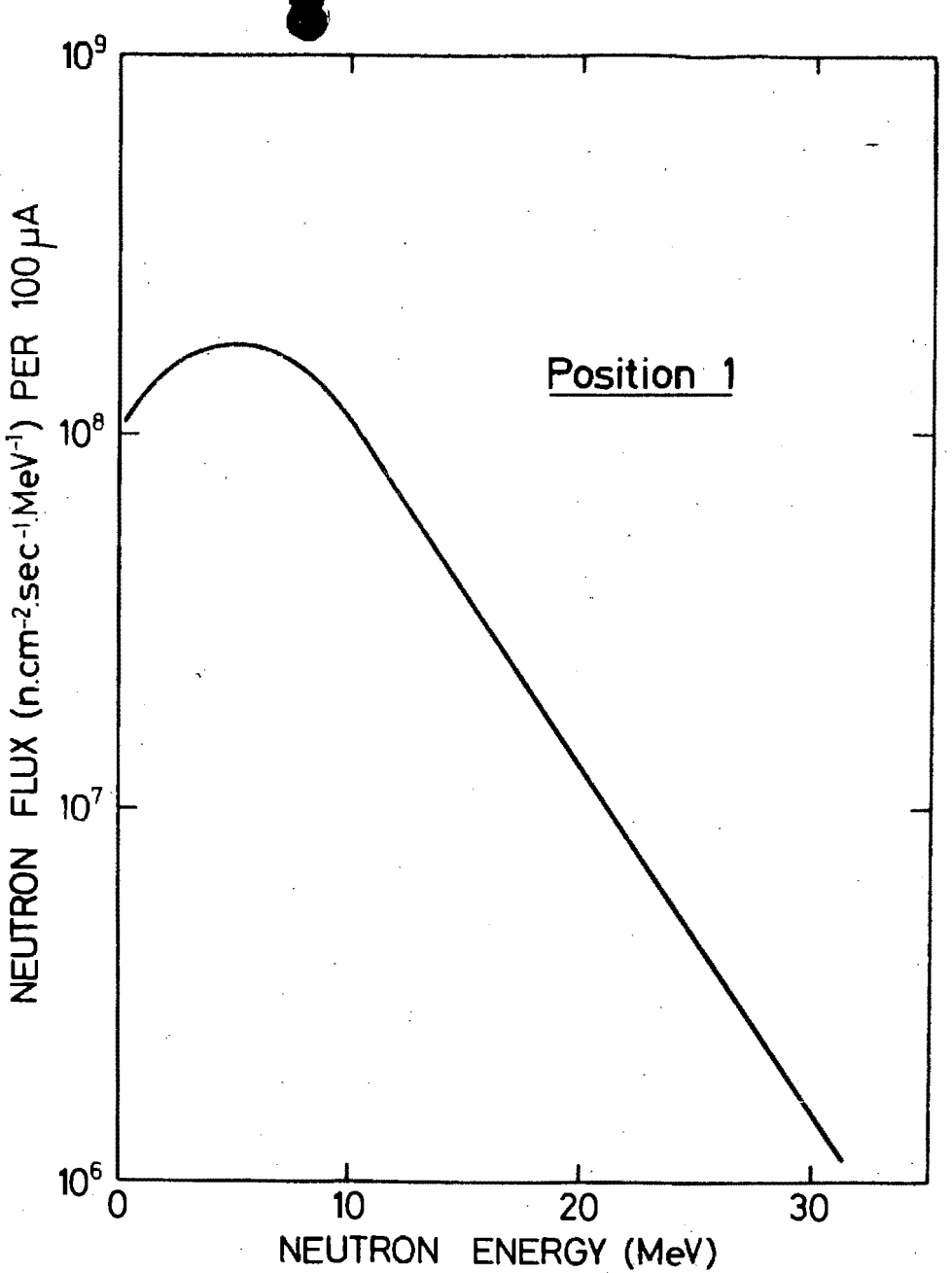

Figure 9. Energy distribution of neutrons from the reaction $^{9}Be(\alpha,n)^{12}C$ at irradiation position 1.

when allowance is made for the difference in bombarding conditions. In the case of the reported data for 15 MeV. deuterons (5), the rate of flux decrease with neutron energy was somewhat greater than that observed in this work, but as the conditions of the deuteron bombardment were not defined, quantitative comparison between the reported (5)and observed results was not possible.

The angular distribution of the neutron flux can be deduced if correction is made for the different distances between the irradiation positions and the centre of the beryllium target. However, in this connection the errors in determining the mean angle between the target and the internal cyclotron beam incident on the beryllium, arising from the fact that neither the beryllium target, nor the irradiated samples, can be considered as points, become large, especially with decreasing angle. Furthermore, the uncertainty in the actual distance between the sample and some mean point of neutron generation in the beryllium introduces very large errors in the relative neutron flux intensity at small angles. The sizes of the probable errors from these sources are marked in Figure 10 where the experimental results are shown as points and are compared with the reported (2) angular distribution of neutrons

from the reaction $^{9}Be(d,n)^{10}B$, shown as a smooth curve.

When the observed angular distribution from 0^{o} to 90^{o} (see Figure 10) and the reported data (2) from 90^{o} to 180^{o} were used to calculate the total neutron emission with energy above 1 MeV. from a thick target of beryllium by a deuteron beam of 15.7 MeV., the value obtained was 2.28×10^{12} neutrons/sec. per 100 μA. This value should be compared with the corresponding result (2) for 15 MeV. deuterons of 1.90×10^{12} neutrons/sec. per 100 μA.

ACKNOWLEDGEMENTS

We would like to thank the Director of the National Physical Research Laboratory for the use of the cyclotron and the Director of the National Chemical Research Laboratory for supplying funds to cover travelling expenses of one of us (M.P.). The use of some equipment from the Southern Universities Nuclear Institute is gratefully acknowledged. Carl Verwey, Kobus van der Merwe and the operators of the Pretoria cyclotron are thanked for their valued assistance during the experiments. Hugh Schmitt and E. Thain prepared the drawings in this manuscript.

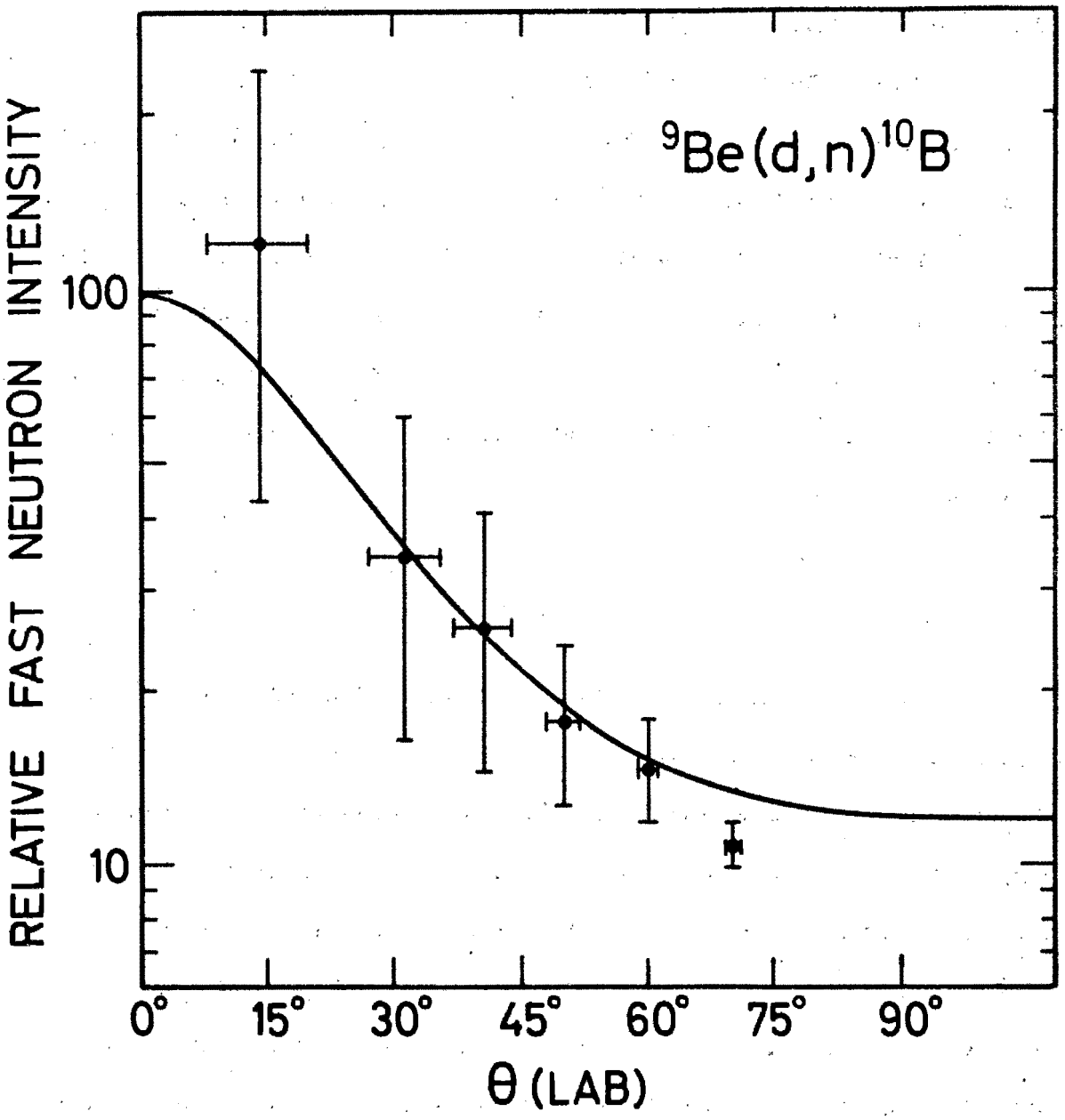

Figure 10. Angular distribution of the fast neutron flux. The points are experimentally determined and the curve represents reported results (2).

REFERENCES

(1) Rautenbach, W.L., de Velde Harsenhorst, Z., Bruins, L.D., Spoelstra, B. "Improvements on the 110-cm. fixed frequency cyclotron of the National Physical Research Laboratory", Tydskrif vir Natuurwetenskappe, (1967) (in press).

(2) Allen, A.J., Nechaj, J.F., Sun, K.-H., Jennings, B., Phys. Rev. 81, 536 (1961).

(3) Jessen, P., Bormann, M., Dreyer, F., Neuert, H., Nuclear Data 1A, 103 (1966).

(4) Stehn, J.R., Goldberg, M.D., Magurno, B.A., Wiener-Chasman, R., Brookhaven National Laboratory report BNL-325, 2nd Edition, Supplement 2, (May, 1964).

(5) Cohen, B.L., Phys. Rev. 81, 184 (1951).

(6) Tochilin, E., Kohler, G.D., Health Physics 1, 332 (1958).

(7) Heertje, I., Aten, A.H.W., Jr., Physica 30, 978 (1964).

DISCUSSION

Mr. MARKOWITZ

It may not be quite fair to ask about the choice of experimental method after your fine work with threshold detectors, but I do wonder about the rejection of proton-recoil scintillation spectrometry in your work or that of the previous speaker, Dr. BRUNINX. Is gamma-ray interference the reason ?

Mr. PEISACH

The space in the irradiation pipe holding the samples was so limited that proton-recoil detectors were difficult to mount. We also have little experience with that kind of measurement.

Mr. KUIN

Why do you use the internal and not the external beam ?

Mr. PEISACH

The external beam has already been adapted to high resolution physics experiments so that the total current obtainable externally was much smaller than the internal one. We thus had very little choice.

Reprinted from Proc. 2nd Conf. on 'Practical Aspects of Activation Analysis with Charged Particles', held in Liege, September 1967. Euratom, Brussels (1968) pp 65-102

No. 23

ANALYTICAL USE OF PROMPT NEUTRONS PRODUCED BY PULSES OF CHARGED PARTICLES

Max Peisach
Southern Universities Nuclear Institute, Faure, South Africa

ABSTRACT

With accelerated protons or deuterons, nuclear reactions on light nuclides leading to the emission of prompt neutrons occur at relatively low energies. By measuring the neutron flight time from its point of generation to the point of detection, the various neutron energies may be resolved and used to identify the target nucleus while their yield is proportional to the content of the nuclide in the irradiated sample.

Using 3 MeV deuterons, methods are described for the determination of deuterium, carbon, nitrogen and oxygen in microgram quantities in gases. The relative standard deviation of the analytical results are between 3 and 4%. Sensitivities are below a microgram of the corresponding element.

With protons, the Q-values of the (p,n) reactions on the abundant isotopes of carbon, nitrogen and oxygen are so low that a 5 MeV proton beam does not generate any neutrons from them. On the other hand the heavier isotopes undergo (p,n) reactions thus enabling their isotopic concentration to be determined.

Similarly the time-of-flight spectrometry of neutrons from the reactions Ca(p,n)Sc on the various calcium isotopes has been used as a means of isotopic determination of calcium-43 and 48.

Possible extension of the technique to other analyses is discussed.

Ever since 1936 when Hevesy and Levi (1) used thermal neutrons to determine dysprosium in impure yttrium, the use of nuclear reactions to solve analytical problems has increased rapidly, especially those nuclear reactions which lead to a radioactive product. Activation analysis has become a field that is being studied widely and intensely, so that its shortcomings and limitations are becoming better known. Some of the shortcomings become evident

(i) when the half-life of the product is very long, because the irradiation time required to produce sufficient radioactivity will be long, unless the reaction has a high cross section;

(ii) when the half-life of the product is very short, because special methods of fast transfer to the counting assembly become necessary;

(iii) when the detection efficiency of the radiation emitted by the product is poor.

The limitations of activation analysis make its application impossible

(i) when the sample under investigation, contains other elements which yield the same radioactive product;

(ii) when interfering radioactive nuclides cannot be separated and their radiation cannot be distinguished from that of the desired product;

(iii) when the product is stable.

The measurement of the rate of decay of a radioactive product is only one form of using a nuclear reaction for analysis. Another method to arrive at the same result may be to measure the rate of formation of a product, as obtained from measurement of the prompt radiation or particles emitted in the nuclear reaction. This technique increases the scope of using nuclear reactions for elemental and isotopic analysis because it makes such methods independent of the radioactive decay properties of the product and has the advantage that the rate of accumulation of data remains virtually constant with time. The energy of a particle emitted in a nuclear reaction depends, among other parameters, on the energy of the incident particle so that charged particle beams, the energy of which can more readily be controlled and selected, offer an a priori advantage over neutrons and gamma-rays, for use in analysis. They suffer from the obvious disadvantage of lack of penetration and the extent to which they generate heat at the target.

Reactions induced by charged particles lead to the emission of a variety of prompt products, any of which can in principle be used for analysis. Frequently, however, it happens that the emitted product cannot conveniently be measured near its point of generation. It then becomes important to choose those that have sufficient penetration through matter to leave the irradiated region, viz., gamma-ray photons and neutrons. In this paper the use of prompt neutrons for

analysis is described.

The energy E_n of a neutron emitted from a nuclear reaction is determined by the Q-value of the reaction, the energy of the incident particle, E, and the angle, θ, at which the neutron is emitted. From the kinematics of a nuclear reaction, the neutron energy is given by

$$\sqrt{E_n} = v \pm \sqrt{v^2 + w} , \qquad (1)$$

where

$$v = \frac{\sqrt{m.m_n.E}\ \mathrm{Cos}\theta}{m_n + M} \qquad (2)$$

and

$$w = \frac{MQ + E(M-m)}{m_n + M} , \qquad (3)$$

and the masses m, m_n and M refer respectively to the incident particle, the neutron and the product nucleus. In any specific case, the emitted neutrons will have energies related to the Q-values pertaining to the corresponding excited states in which the product nucleus is left. It may then be possible to select some neutron energy for determining the concentration of a specific nuclide in an irradiated target, and any experimental method by which neutron energies may be determined could be suitable for analysis.

A convenient and accurate method for determining neutron energies is by the time-of-flight technique where the

time, t (nanoseconds), taken by a neutron to cover a distance, s (metres), is measured. Non-relativistically the relationship between the time-of-flight and the neutron energy is given by

$$t = \frac{72.3 \times s}{\sqrt{E_n}} , \qquad (4)$$

where the constant includes the mass of the neutron and conversion units and E_n is given in Mev. Rewriting equation 4, the energy resolution may be shown to be

$$\frac{\Delta E_n}{E_n} = \left[\left(\frac{E_n^{1/2} \cdot \Delta t}{36.1 \times s} \right)^2 + \left(\frac{2 \Delta s}{s} \right)^2 \right]^{1/2} , \qquad (5)$$

where ΔE_n, Δt and Δs represent the uncertainties in the neutron energy, the flight time and the flight path respectively. From equation 5 it may be deduced that the energy resolution of the system will depend on the uncertainty in the flight path, which is usually small for paths of several metres, but largely on the precision in measuring the flight time. For a constant flight path, the energy resolution is best at lower energies.

With recent development in fast electronics, it has now become possible to measure short time intervals with a fair degree of precision. The flight time can be given by the interval between two pulses, marking respectively the start and the end of the flight. The signal marking the end of the flight

can be obtained from a pulse produced in a scintillation detector by the neutron. The signal marking the start of the flight may be obtained either from another prompt product of the reaction, with the consequent loss of efficiency introduced by the additional measurement, or by using a beam for irradiation that is pulsed at a known frequency, when the passage of the beam itself may be used to generate the required pulse. The application of neutron time-of-flight spectroscopy to analysis was first discussed by Peisach and Pretorius (2,3) when the latter course was followed, despite the fact that the duration of the pulse introduced an uncertainty in the flight time and constituted a limitation of the method. As a result, neutrons of the same energy, that should have taken the same flight time, arrived at the detector over a small time spread and were thus registered as an apparent group of neutrons.

THE ELECTRONIC EQUIPMENT

A block diagram of the electronic equipment (4) is shown in Figure 1. Neutrons generated by the pulsed beam at the target were detected in an NE 213 liquid scintillation detector placed at a distance, s, and an angle, θ, from the target. The time of arrival of the pulsed irradiating beam on the target was given by a signal from a pickup probe placed near the target in the beam tube. The difference in time between the signal from the detector and that caused by the beam

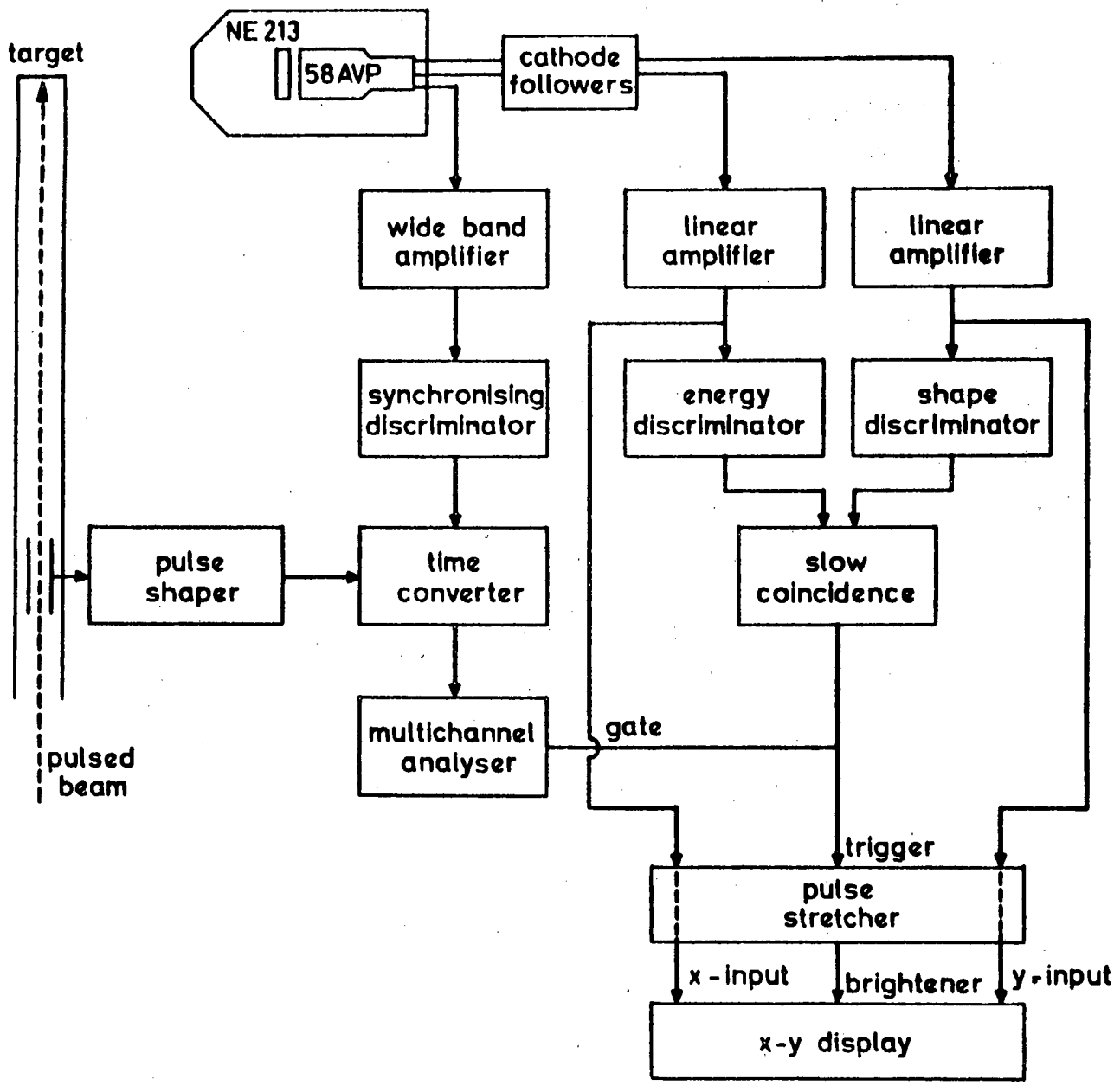

Figure 1 : Block diagram of the electronic equipment.

pulse was converted by the time converter to a pulse with amplitude proportional to time, and recorded by the multichannel analyzer. A current integrator (not shown in Figure 1) was set to accumulate a predetermined total current, and automatically switched off the measuring system when this value was reached.

Because the neutron detector was sensitive to gamma-rays as well as neutrons, signals caused by gamma-rays from whatsoever source were rejected by pulse shape discrimination (5) and low level electronic noise by the energy discriminator. The efficiency of the neutron detector was measured relative to that of a $^{10}BF_3$-filled neutron counter and is shown in Figure 2, from which it may be learnt that the relative efficiency falls rapidly for neutrons below 1 MeV and that the detection threshold for neutrons lies below about 700 keV.

ANALYSES USING PULSED DEUTERON BEAMS

When solids or liquids are irradiated with charged particle beams, the entire energy of the beam is deposited within a relatively short distance in the sample, thus generating high temperatures which are frequently sufficient to destroy the sample. Charged particle irradiations therefore usually require refractory targets or targets with very good cooling. This problem does not arise in the case of gases, and irradiation with charged particles can readily be carried out, provided the container has a sufficiently thin window through

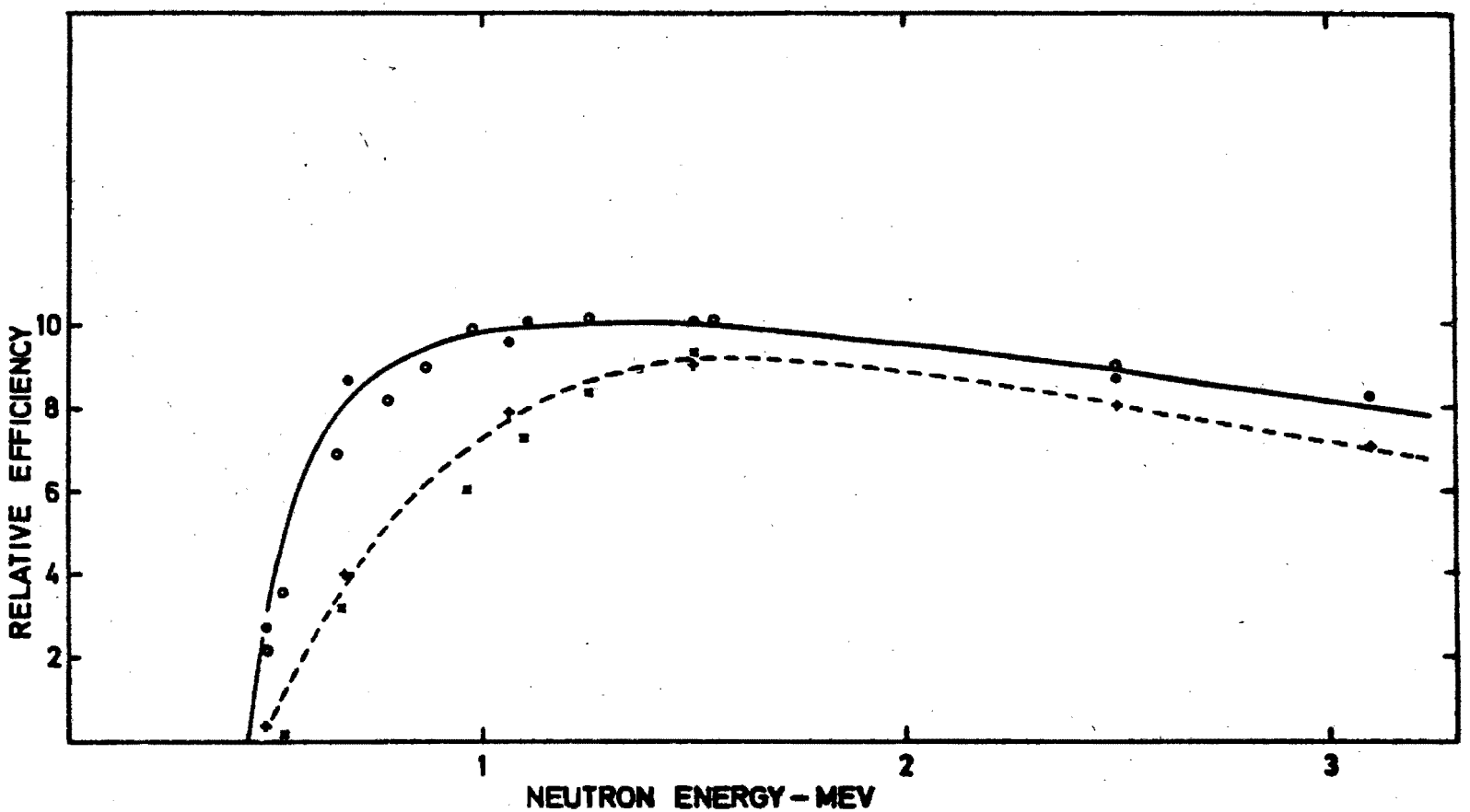

Figure 2 : Relative efficiency of the neutron counting assembly with pulse shape discrimination.

which the beam may enter. A diagrammatic sketch of the gas handling apparatus and the irradiation cell is given in Figure 3.

Because most (d,n) reactions are exoergic, neutrons may be expected to be produced from all components of a deuteron-irradiated sample. The extent to which neutrons from other sources would tend to decrease the usefulness of any analytical method, would depend on their relative energy and intensity. At comparatively low incident energies of deuterons, the Coulomb barrier of only the lightest elements are exceeded, so that interference from (d,n) reactions on other elements would be much reduced. The very important light elements carbon, nitrogen and oxygen are also those for which activation analysis methods are not very suitable. The determination of these elements in gases, by time-of-flight spectrometry of neutrons produced by a pulsed deuteron beam, was thus attempted.

Neutron energies that may be expected from the irradiation of ^{2}H, ^{12}C, ^{14}N and ^{16}O with 3.0 MeV deuterons, are given in Table I. It is clear that the energies of neutrons from (d,n) reactions on deuterium, carbon-12 and oxygen-16 differ sufficiently to enable the neutron groups to be resolved, but difficulties may be expected from neutrons of nitrogen-14. Typical time-of-flight spectra obtained from mixtures of deuterium gas with hydrogen, oxygen, carbon dioxide and nitrogen with 3.0 MeV deuterons are shown in Figure 4 and from

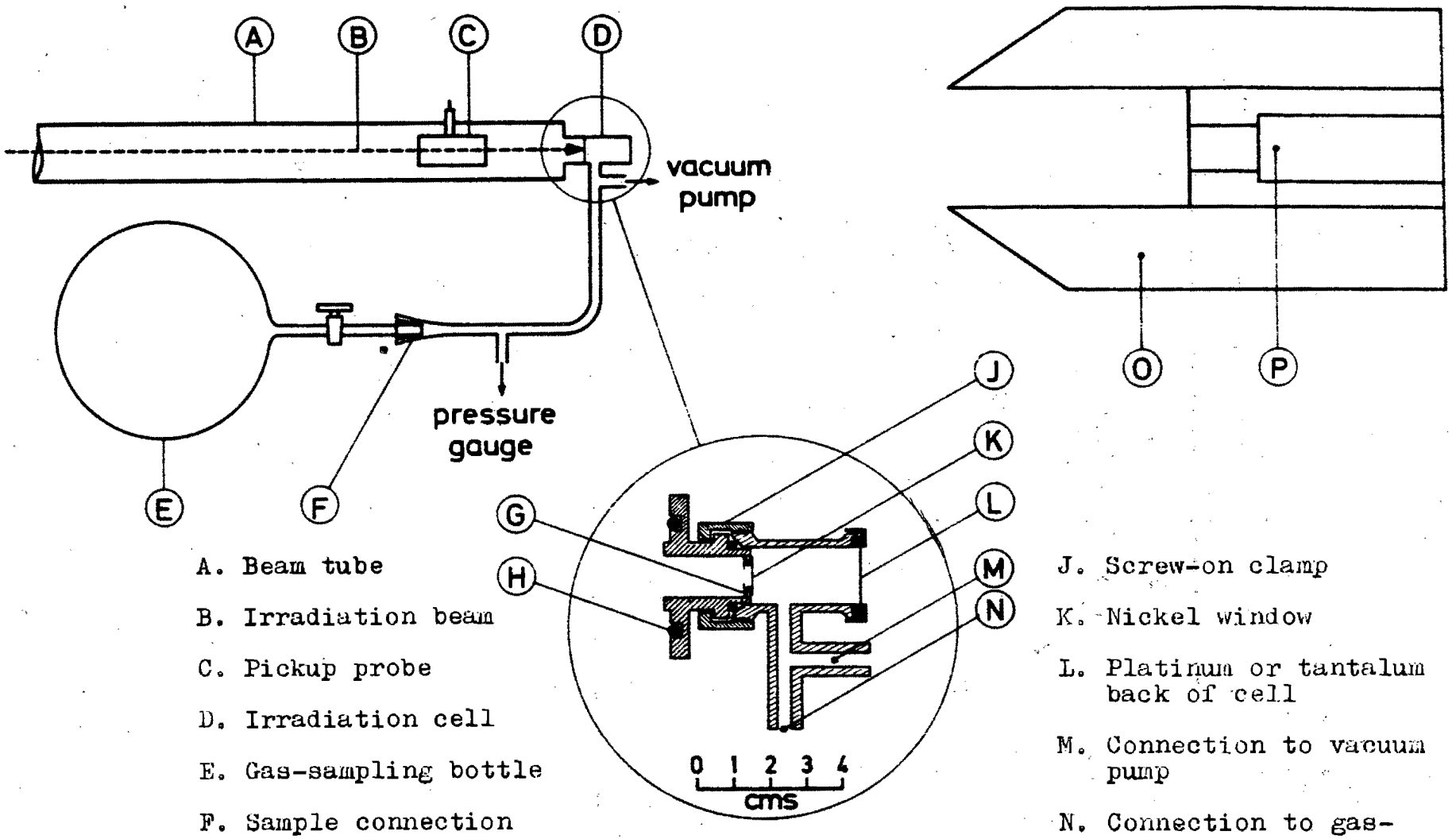

A. Beam tube

B. Irradiation beam

C. Pickup probe

D. Irradiation cell

E. Gas-sampling bottle

F. Sample connection point

G. Tantalum collimator and window support

H. Vacuum O-ring

J. Screw-on clamp

K. Nickel window

L. Platinum or tantalum back of cell

M. Connection to vacuum pump

N. Connection to gas-handling apparatus

O. Detector shield

P. Scintillation detector

Figure 3 : Gas handling apparatus and irradiation cell.

TABLE I

SOME NEUTRON ENERGIES FROM (d,n) REACTIONS

E_d = 3 MeV $\theta = 30^o$

Target	^2H	^{12}C	^{14}N	^{16}O
Natural Abundance %	0.015	98.89	99.63	99.759
Q (d,n_0) MeV. (6)	3.268	- 0.281	5.066	- 1.627
Neutron Energy MeV.				
n_0	5.738	2.582	7.932	1.223
n_1			2.771	0.685
n_2			2.710	
n_3			1.763	
n_4			1.098	
n_5			1.033	
n_6			0.693	
n_7			0.235	

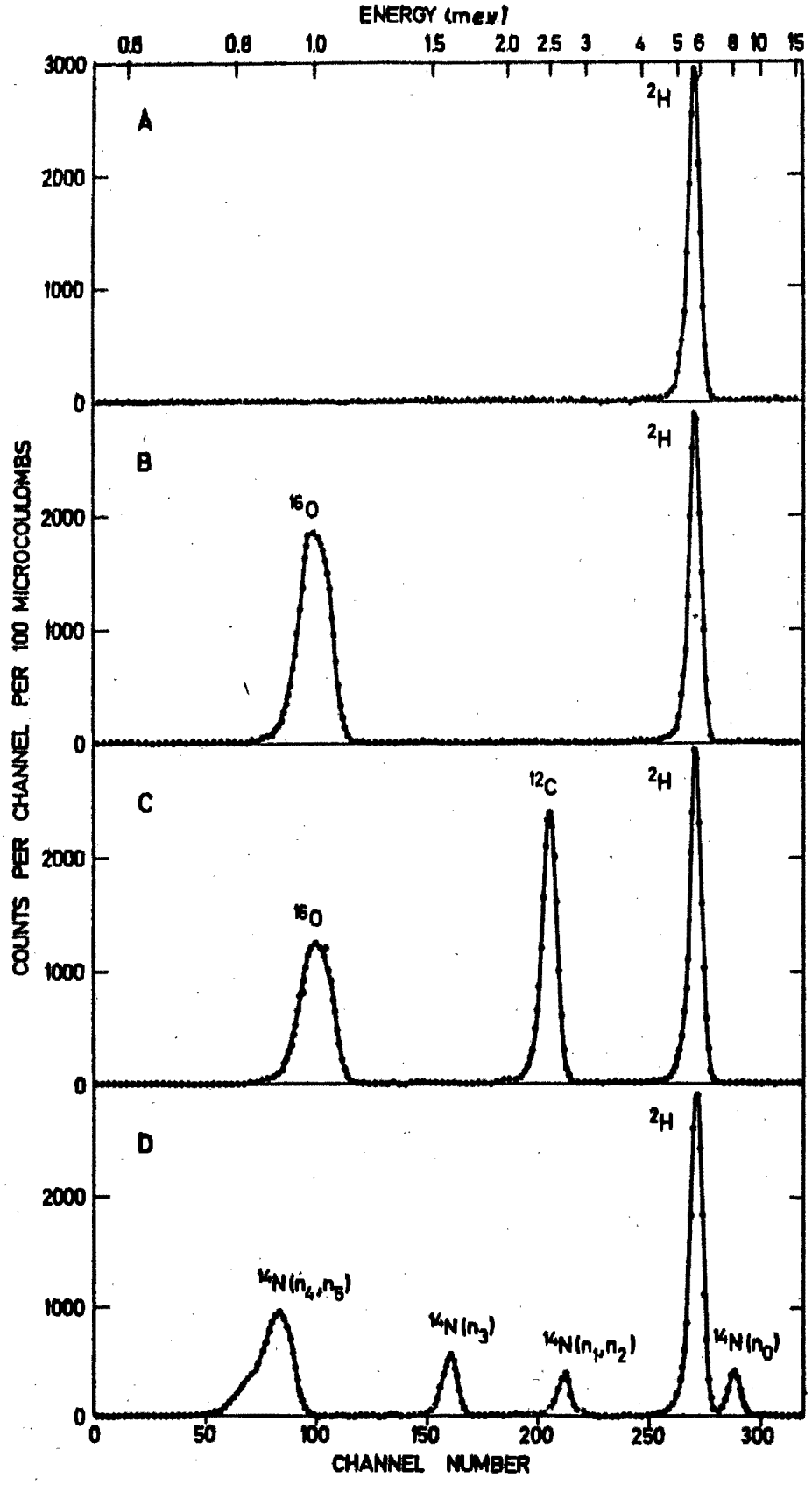

Figure 4 : Typical time-of-flight spectra of deuterium gas in hydrogen (A), oxygen (B), carbon dioxide (C) and nitrogen (D).

E_d = 3.0 MeV. s = 3 metres $\theta = 30^{\circ}$

methane, oxygen and nitrogen with 3.5 MeV deuterons are shown in Figure 5. Because the spectra are based on time measurements, the channel number is proportional to the flight time, and hence the energy scale cannot be linear; as a consequence, peaks appear to be wider at lower energies.

From Figures 4 and 5 the neutron groups with energies listed in Table I may be identified, but correction has to be made for the 160 keV energy lost by the beam in passing through the nickel window of the gas cell (see Figure 3). A convenient reference to "zero" flight time in the spectrum may be obtained from the position of a peak produced by pulses, from gamma-rays generated at the sample, not entirely eliminated by pulse shape discrimination. Figure 6 shows such a peak in a spectrum obtained from a sample of pure nitrogen gas at about 100 mm. pressure. A spectrum obtained under the same conditions, but for which pulse shape discrimination was not used, is shown in the same figure, for comparison, and clearly illustrates that it would be futile to use such data for analysing gas samples containing smaller amounts of elemental nitrogen.

The curves in Figures 4 and 5 show that the counts registered under each peak in the spectrum can readily be integrated to be used as a measure of the content of the corresponding element in the bombarded sample. It should be noted that if nitrogen is present, the determination of carbon and oxygen will require correction for the inclusion of counts

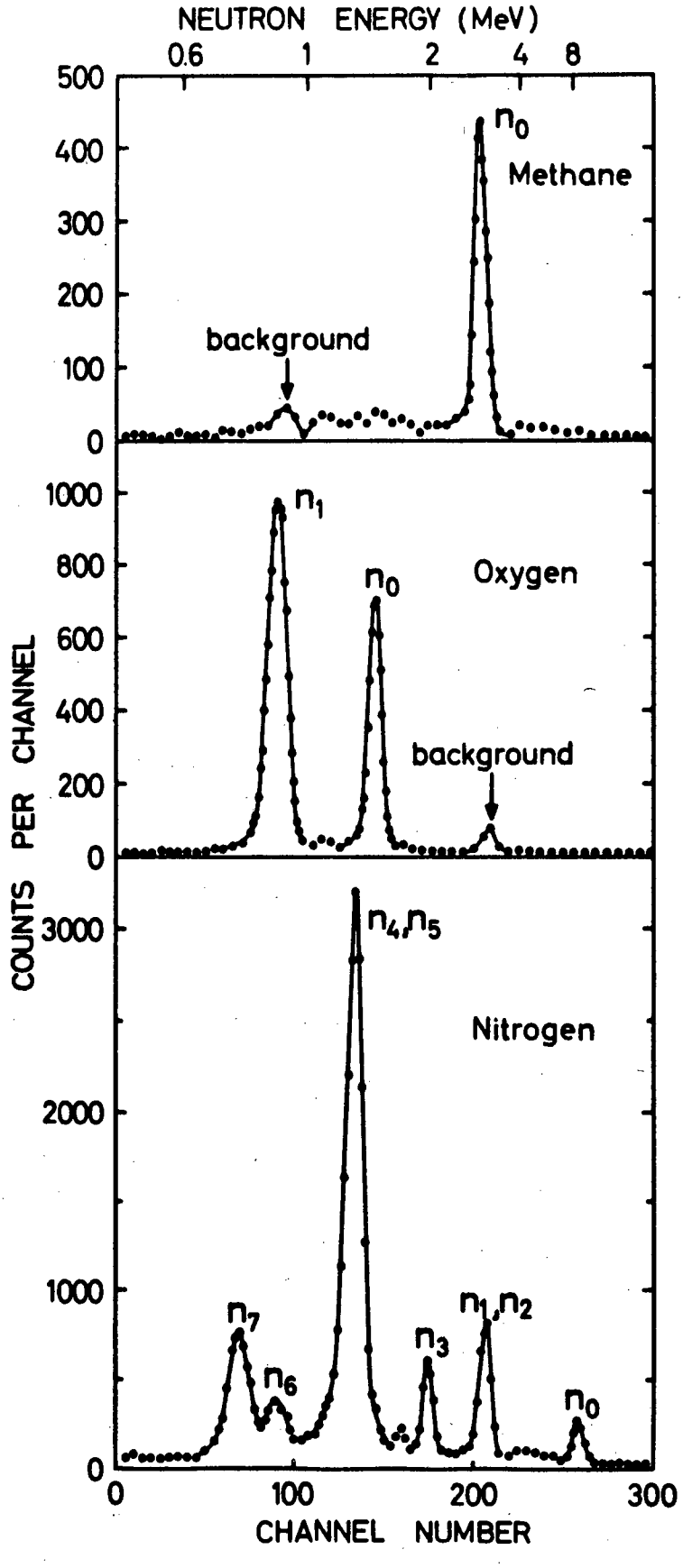

Figure 5 : Neutron time-of-flight spectra from methane, oxygen and nitrogen.

E_d = 3.5 MeV. s = 3 metres $\theta = 30^{\circ}$

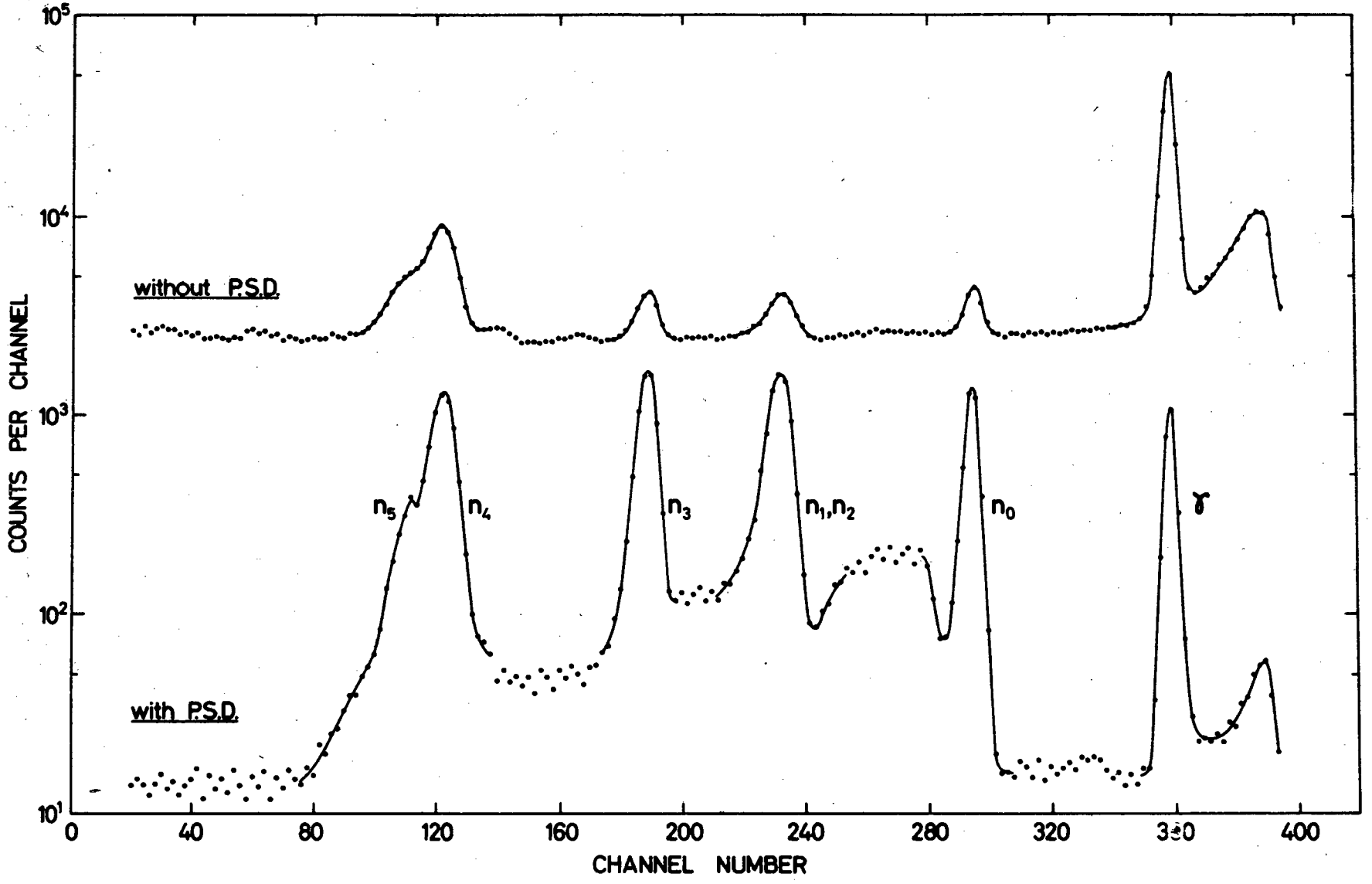

Figure 6 : Neutron time-of-flight spectra from nitrogen showing the effect of pulse shape discrimination. The peak due to gamma-rays not entirely discriminated against, is on the right in the lower spectrum.

from the $^{14}N(n_1,n_2)$ and $^{14}N(n_4,n_5)$ neutron groups respectively. Such correction can readily be determined, being proportional to the number of counts observed from the $^{14}N(n_0)$ or $^{14}N(n_3)$ neutron groups. This type of correction is needed for the analysis of mixtures of carbon-dioxide and nitrogen, when spectra such as shown in Figure 7 are obtained with 3.0 MeV deuterons and that shown in Figure 8 when the deuteron energy is 2.0 MeV.

The yield of any neutron group is a function of the number of target nuclei in the path of the beam. Accordingly a calibration curve can be obtained from a single gas chosen as reference and measured over a range of pressures. Such calibration curves were linear for elemental analysis of deuterium, carbon and nitrogen. In the case of oxygen, deviation from linearity became noticeable at pressures above 25 mm. due to the energy lost by the deuteron beam in the gas sample, when the reaction cross section was lower and the lower energy neutrons were measured with a lower efficiency. Figure 9 shows how correction for these effects yields a linear calibration line.

The results of determinations of deuterium, carbon, nitrogen and oxygen in gas samples have been reported (7,8). A typical set of results is given in Table II and a summary of different series of test analyses is given in Table III. The summary includes the value of the slope of the calibration line for each test and the observed mean neutron count per mm.

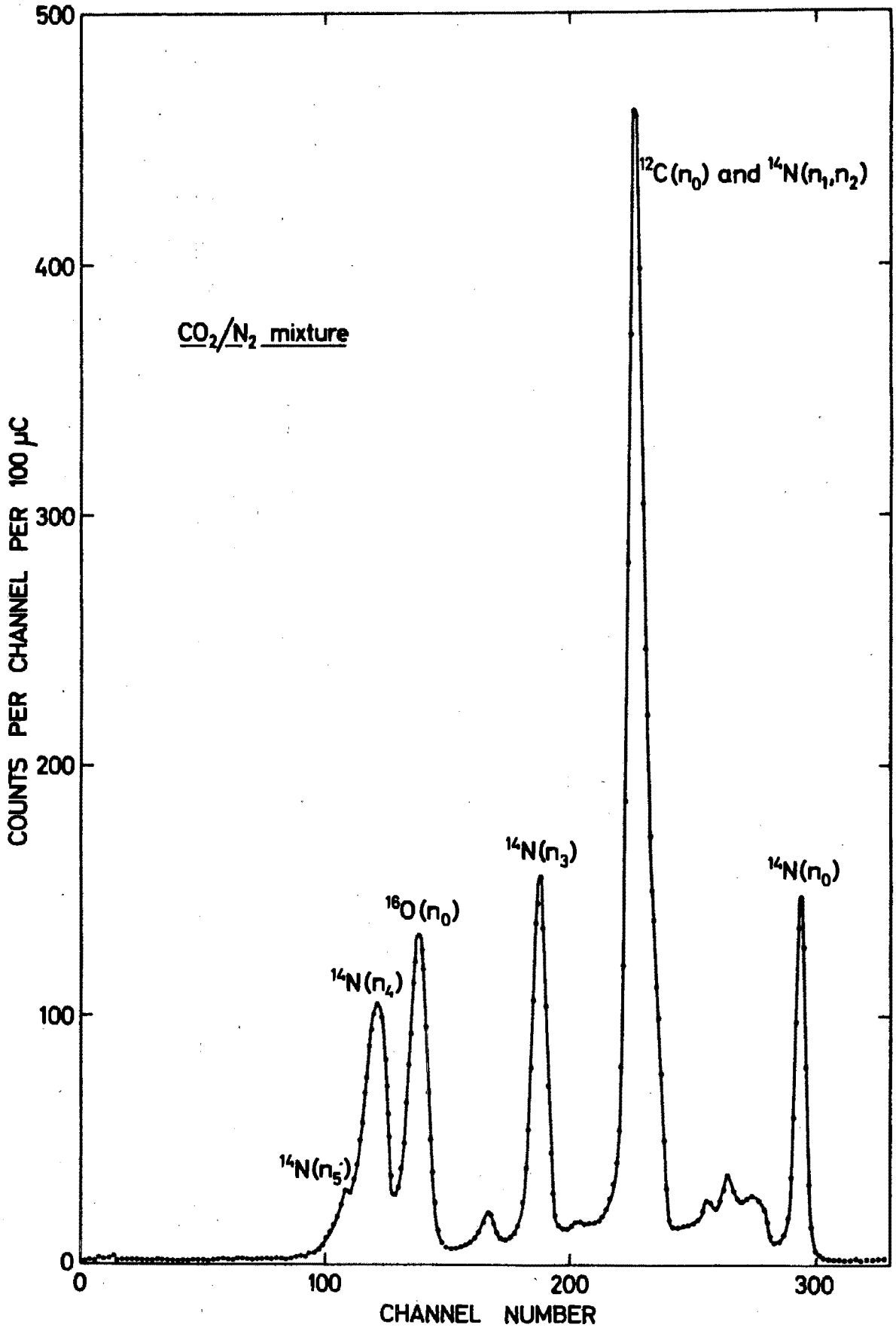

Figure 7 : Spectrum from a mixture of carbon dioxide and nitrogen showing that carbon and oxygen peaks are not resolved from (n_1, n_2) and (n_4) neutron peaks of nitrogen respectively. E_d = 3.0 MeV.

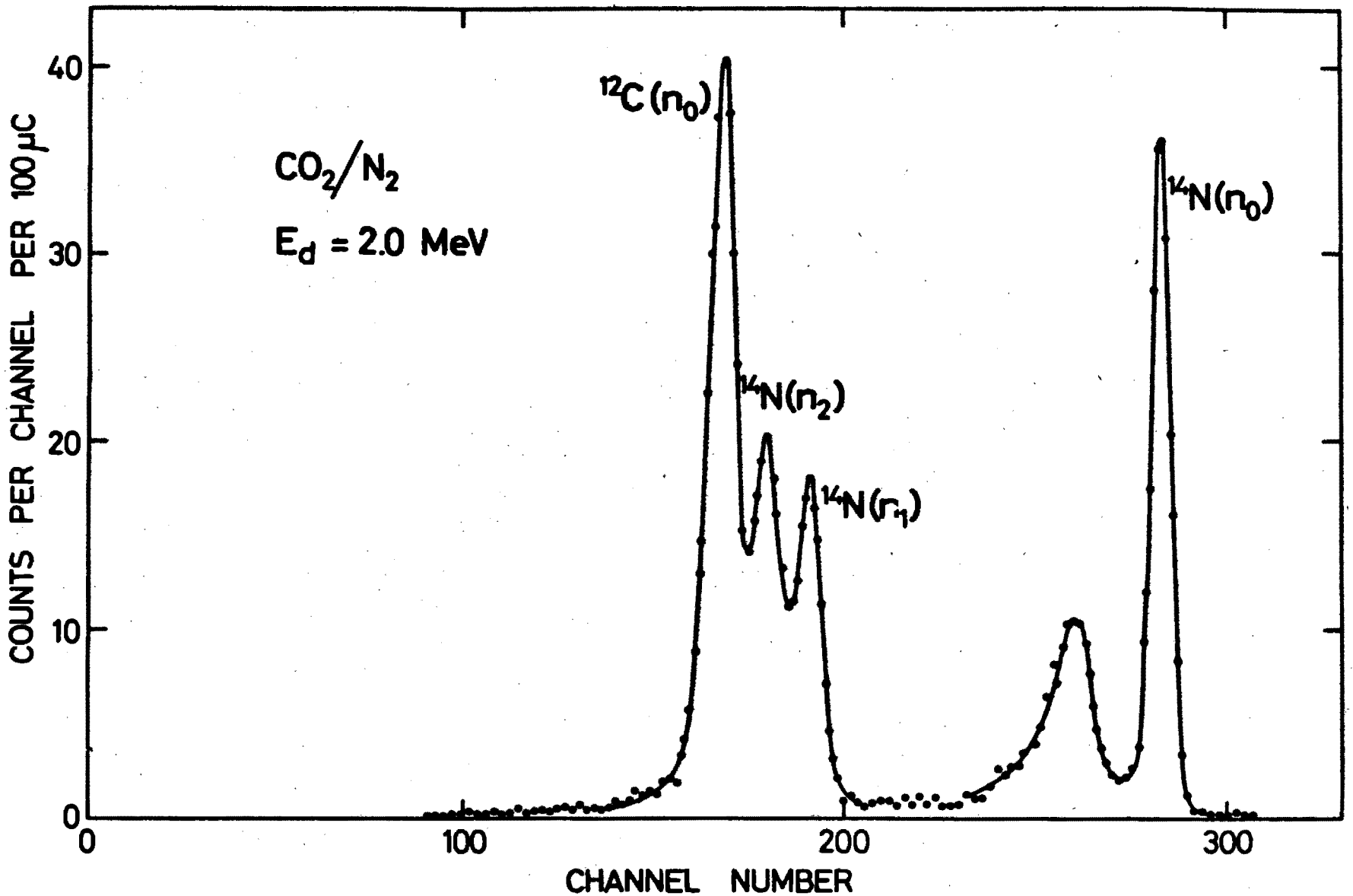

Figure 8 : Spectrum from CO_2/N_2 mixture obtained with 2.0 MeV deuterons.

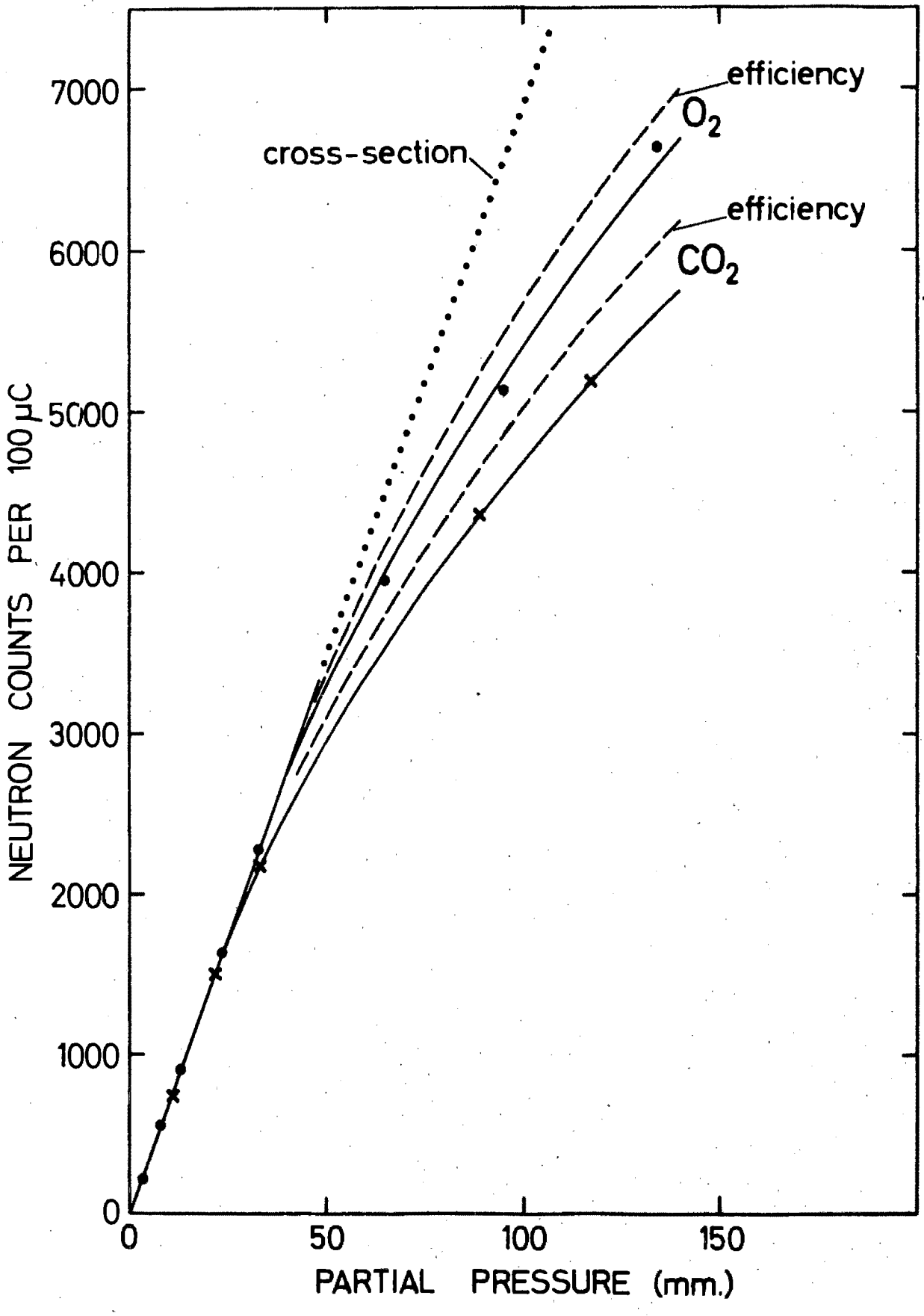

Figure 9 : The effect of energy loss on the neutron yield from oxygen. Observed values (solid line) are firstly corrected for decreased detection efficiency (broken line) and then for decreased reaction cross section (dotted).

TABLE II

SOME DETERMINATIONS OF CARBON IN CO_2/CO

E_d = 3.0 MeV $\theta = 30^o$

Sample number	Total pressure in cell (20°C)		Error	Relative error	Neutron counts per 100 μC	Neutron counts per 100 μC per mm. pressure
	Known A mm.	Found* B mm.	(B-A)	100 X (B-A)/A	N	N/A
78	89.70	92.40	+ 2.70	+ 3.01	16315	181.88
79	37.75	37.53	- 0.22	- 0.58	6453	170.95
85	40.75	41.63	+ 0.88	+ 2.16	7190	176.45
86	82.60	85.36	+ 2.76	+ 3.34	15046	182.15
87	40.17	39.33	- 0.84	- 2.09	6776	168.67
88	91.92	92.45	+ 0.53	+ 0.53	16324	177.58
89	41.55	41.19	- 0.36	- 0.87	7111	171.15
90	89.00	88.80	- 0.19	- 0.21	15669	176.06
91	37.67	37.19	- 0.48	- 1.27	6391	169.65
92	89.85	88.35	- 1.50	- 1.67	15588	173.49
93	35.12	36.14	+ 1.02	+ 2.90	6202	176.57
94	91.20	87.48	- 3.72	- 4.08	15432	169.21
95	38.70	38.17	- 0.53	- 1.37	6567	169.69

* Determined from $^{12}C(n_0)$ count

Mean error = + 0.0038 mm. Hg.

Mean neutron count per 100 μC per mm. total pressure = 174.12

Relative standard deviation = ± 2.27%

TABLE III

SUMMARY OF TEST ANALYSES ON GASES

WITH 3 MeV DEUTERONS

Gas Mixture	Nuclide Determined	Number of Samples	Calibration*	Mean* Neutron Count	Mean pressure error mm.	Relative Standard Deviation
H_2/D_2	^{2}H	15	421.5	419.2	- 0.020	± 3.4%
CO_2/D_2	^{2}H	12	421.5	422.0	+ 0.003	± 3.5%
CO_2/CO	^{12}C	13	179.8	174.1	+ 0.004	± 2.3%
	^{16}O	13	75.4	74.4	- 0.001	± 3.0%
CO_2/N_2	^{12}C	9	174.3	168.9	- 0.003	± 2.6%
	^{14}N	13	23.3	24.2	+ 0.004	± 4.6%
	^{16}O	11	68.9	69.8	- 0.002	± 3.4%
	^{14}N	10**	23.7	23.0	- 0.046	± 3.3%

* Counts per mm. pressure per 100 microcoulombs

** E_d = 2.0 MeV.

pressure per 100 microcoulombs. In all cases the agreement between the two values is within the precision of the method. It is satisfying to note that the precision of the method is comparable with that of most methods using activation analysis.

The background spectrum (see Figure 10) consists of a prominent peak due to neutrons generated from carbon-12, from residual oil vapours deposited on the nickel window at the point of incidence of the beam. A small contribution from neutrons from oxygen-16 is also identifiable. The remaining continuum is produced by neutrons from a variety of sources and by those scattered into the detector. Heavy isotopes of carbon and oxygen probably also contribute to the neutron background. Spectra obtained from carbon dioxide enriched in oxygen-18 and in carbon-13 are shown in Figure 11.

The precision of a determination will clearly deteriorate as the sample size decreases. From a knowledge of the background count (see Figure 10) and the values in Table III it is possible to calculate the size of the smallest sample for which the standard deviation of the integrated count will be comparable with or a given multiple of the relative standard deviation of the method. Such values for carbon, nitrogen and oxygen are given in Table IV, from which it is clear that the method is capable of analysing microgram quantities of these elements. The limit for qualitative identification is considerably less; for example using 20 millicoulombs, 60 ng ^{12}C,

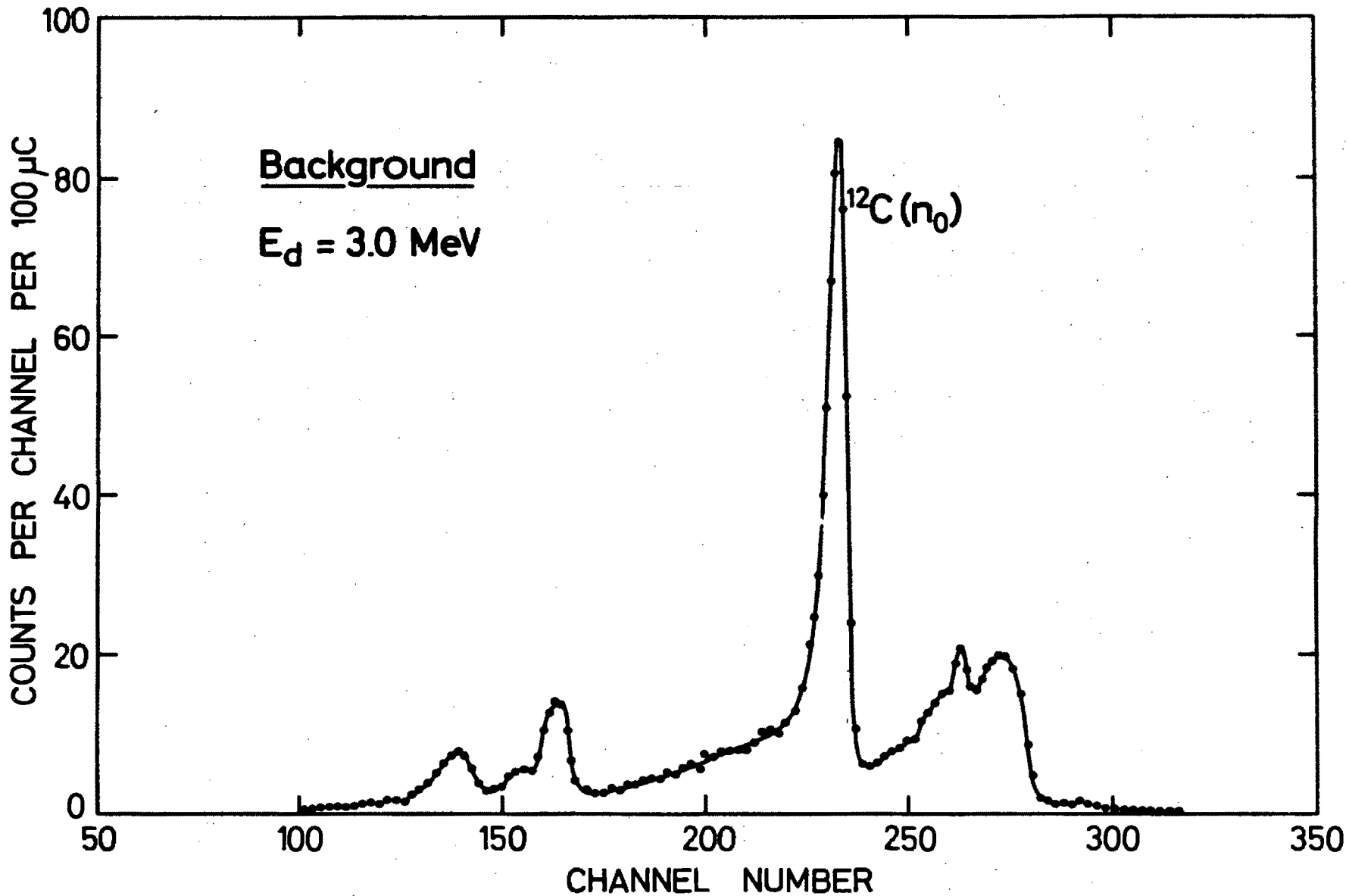

Figure 10 : Background spectrum obtained with 3.0 MeV deuterons.

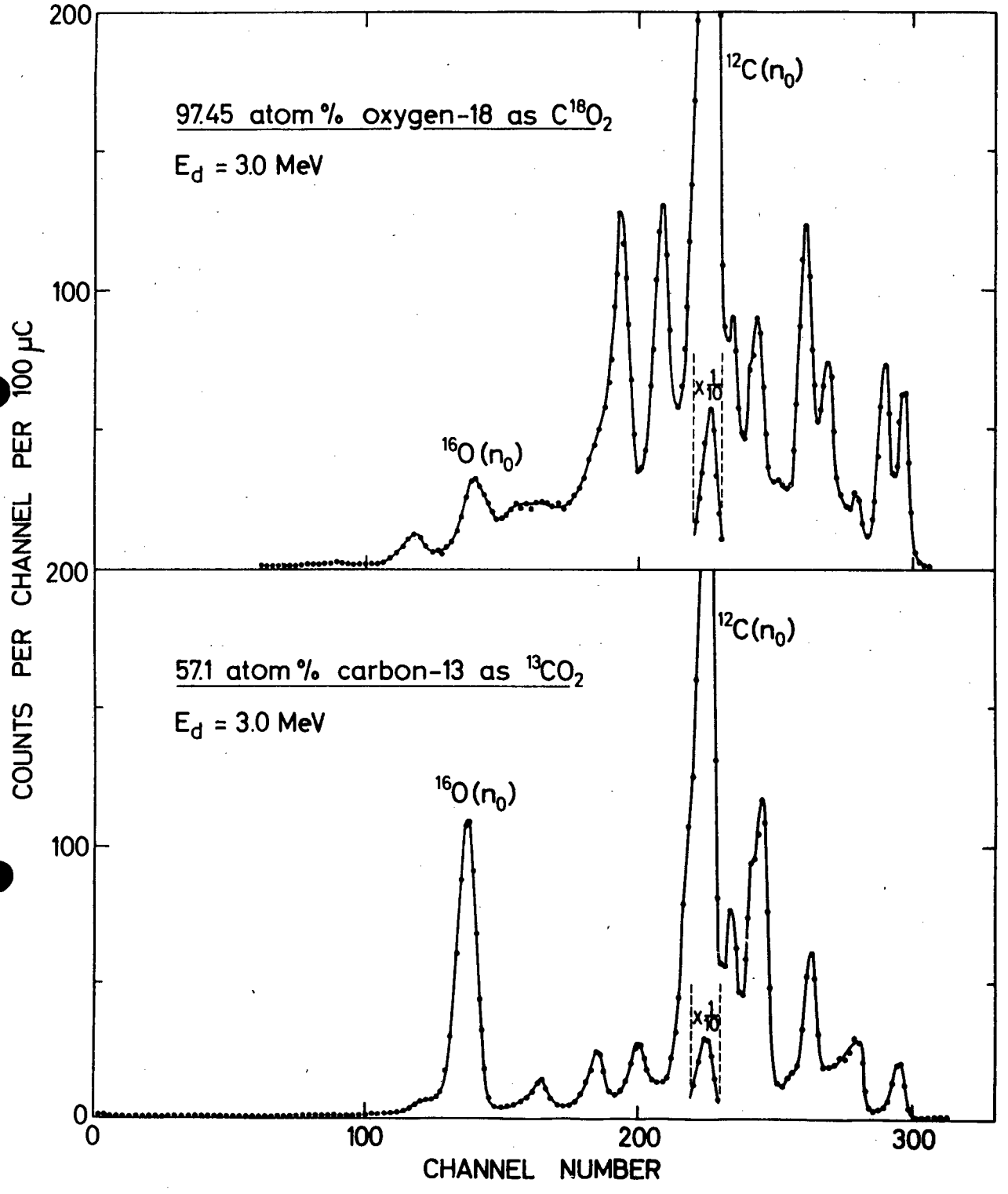

Figure 11 : Spectra obtained from carbon dioxide enriched in oxygen-18 (upper spectrum) and carbon-13 (lower spectrum).

TABLE IV

PRECISION LIMITS FOR ELEMENTAL ANALYSES

Relative Precision %	Total Current milli-coulombs	Micrograms per $cm.^2$ cross sectional area of beam		
		^{12}C	^{14}N	^{16}O
± 3.0%	1	5.18	28.40	16.79
	2	3.46	16.67	10.75
	10	1.50	5.60	4.25
	20	1.06	3.67	2.92
± 10.0%	1	1.42	5.29	3.99
	2	0.98	3.49	2.71
	10	0.44	1.43	1.18
	20	0.31	0.99	0.82

200 ng ^{14}N and 170 ng ^{16}O per cm.^{2} cross sectional beam area can be detected.

ANALYSIS USING PULSED PROTON BEAMS

Like deuterons, protons can be used for the analysis of gases, but unlike (d,n) reactions, most (p,n) reactions are endoergic. It thus becomes possible to use the energy of the irradiation beam as an additional parameter, not only to vary the energy of the emitted neutron, but also to control the total neutron emission from the sample by preventing the occurrence of nuclear reactions of lower Q-value. In this way the number of neutrons scattered into the detector is decreased and the general background against which the measurements have to be made, is smaller. A typical background neutron time-of-flight spectrum obtained with 5.0 MeV protons is shown in Figure 12. The general appearance of the spectrum is the same as that obtained with deuterons, but its intensity is much less.

The energies of neutrons that may be expected from (p,n) reactions on the isotopes of carbon, nitrogen and oxygen are given in Table V. From the table it is clear that no neutrons can be generated from the abundant lighter isotopes ^{12}C, ^{14}N and ^{16}O by proton beams of energy less than 5.931 MeV. It is also clear that in samples enriched in any of the heavier stable isotopes of these three elements, suitable neutron energies are expected, which would make their determination

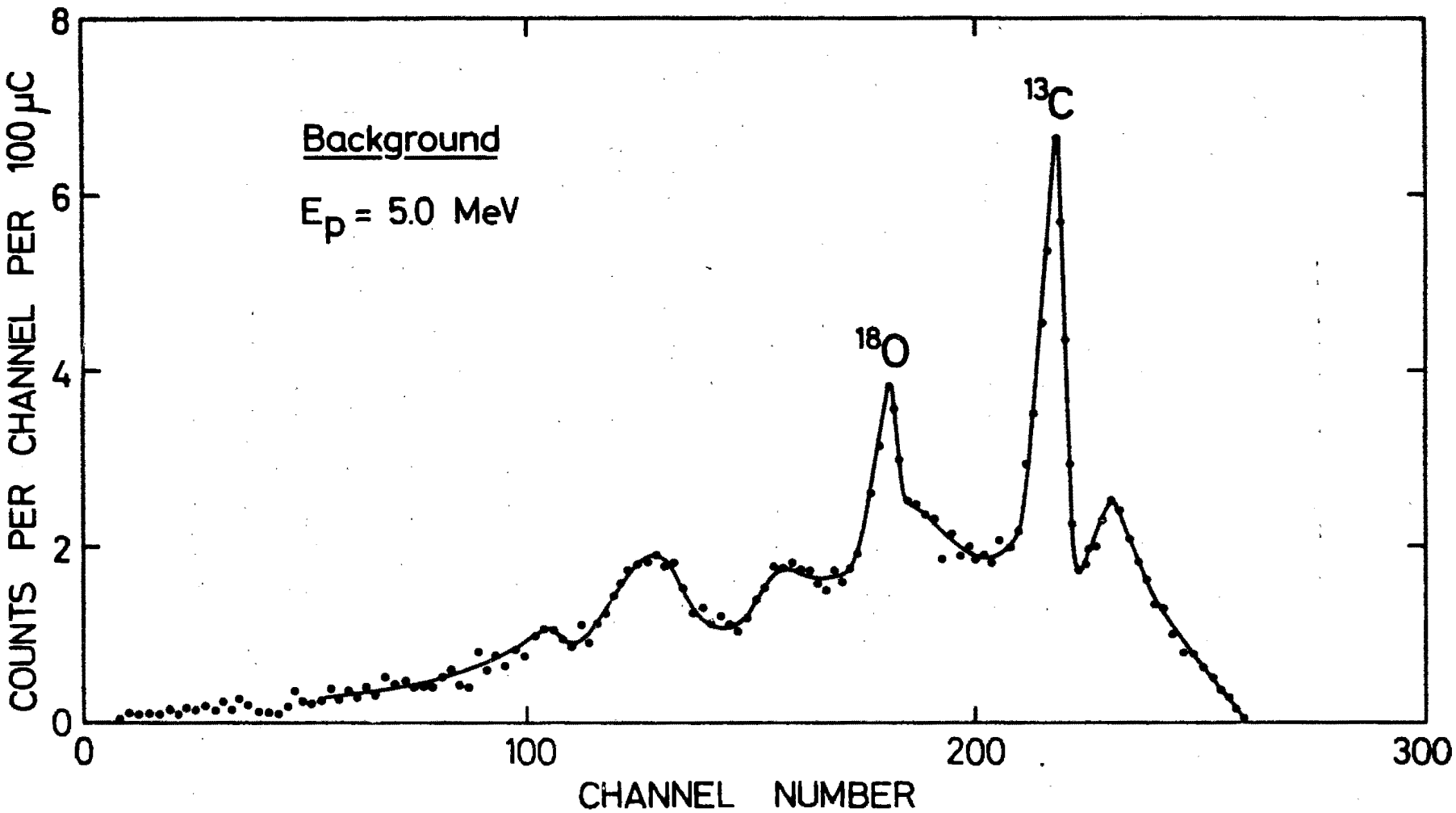

Figure 12 : Background spectrum obtained with 5.0 MeV protons.

TABLE V

NEUTRON ENERGIES FROM SOME (p,n) REACTIONS

E_p = 5.0 MeV $\theta = 0^o$

Target	Natural Abundance %	Q-value (p,n_o) MeV (6)	Neutron energy MeV
^{12}C	98.89	-18.390	-
^{13}C	1.11	- 3.004	1.941 (n_o)
^{14}N	99.63	- 5.931	-
^{15}N	0.37	- 3.543	1.381 (n_o)
^{16}O	99.759	-16.431	-
^{17}O	0.037	- 3.544	1.390 (n_o)
			0.854 (n_1)
^{18}O	0.204	- 2.450	2.495 (n_o)
			1.555 (n_1)
			1.445 (n_2)
			1.406 (n_3)
			1.361 (n_4)
			0.744 (n_5)
			0.288 (n_6)

possible. Time-of-flight spectra of the neutrons obtained from the proton irradiation of carbon dioxide enriched in oxygen-18 and in carbon-13 and of ammonia gas enriched in nitrogen-15 are shown in Figure 13. As before, the energy of each neutron group is about 160 keV lower than that given in the table. From the relative heights of the peaks in the spectra and from the neutron energies, little mutual interference is expected between oxygen-18 and carbon-13, nor is nitrogen-15 expected to cause interference in the determination of either of the other two nuclides (unless it is present in relatively enriched quantities in the sample under investigation). However, because the yield of $^{15}N(n_0)$ neutrons is so low relative to those of oxygen-18, comparatively small amounts of oxygen-18 could seriously hinder the determination of nitrogen-15.

The determination of the isotopic concentration of oxygen-18 in gases has been fully reported elsewhere (9). The relative standard deviation was found to be $\pm$ 3.4%. With a maximum total current of 20 millicoulombs, about 280 ng./cm.^{2} beam area could be measured. If a lower precision of $\pm$ 10% is acceptable, the lower limit may be decreased to 80 ng./cm.^{2}, but only some 900 ng./cm.^{2} of carbon-13 could be similarly determined. The sensitivity limit for detecting oxygen-18 qualitatively is about 16 ng./cm.^{2}

To apply this technique to other elements, it may be useful to refer to the diagrammatic representation of the

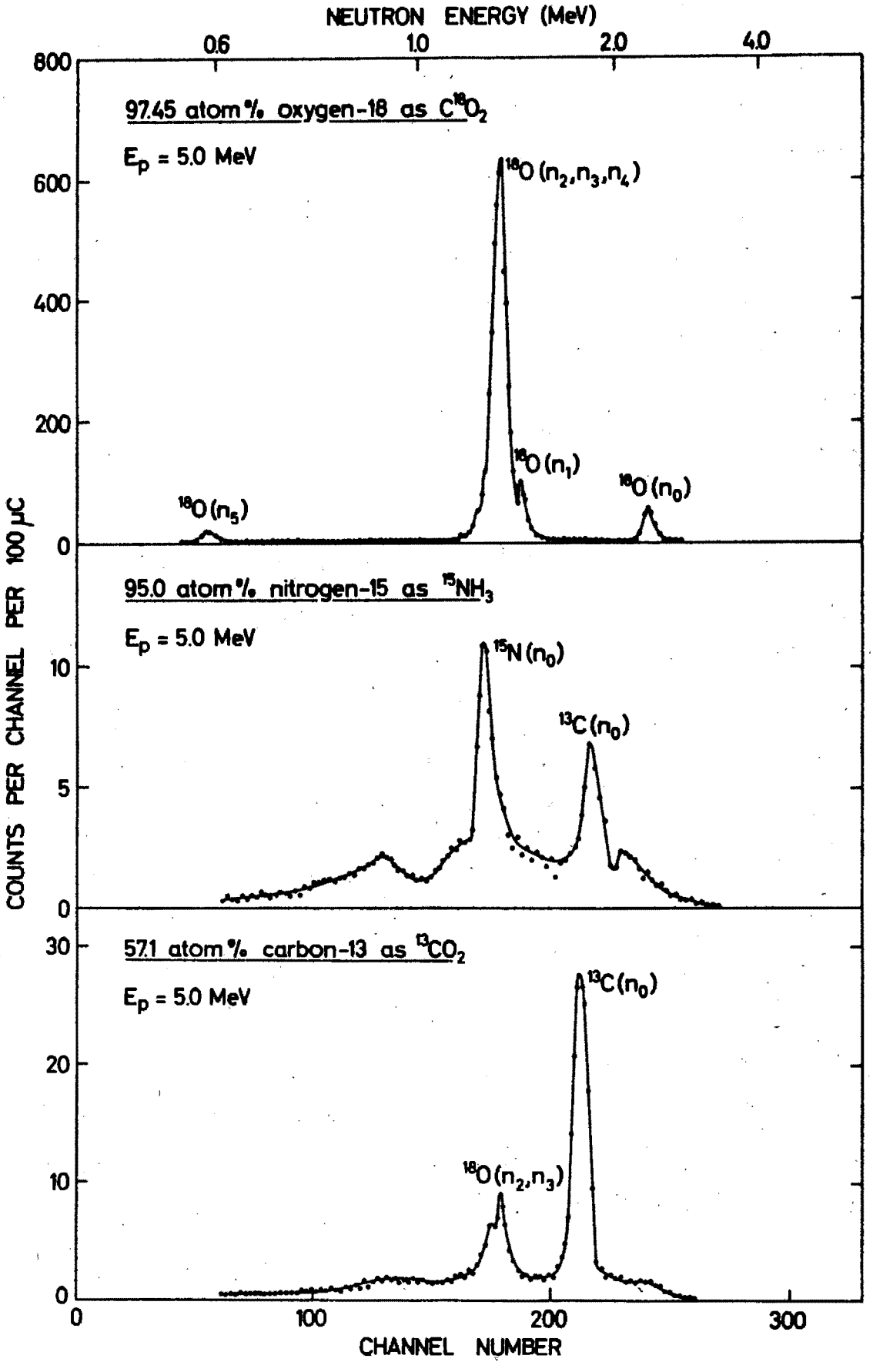

Figure 13 : Neutron time-of-flight spectra from carbon-13, nitrogen-15 and oxygen-18 irradiated with 5 MeV

Q-values (>-5 MeV) for the (p,n_i) reactions on elements with $Z < 20$, shown in Figure 14. The calculated Coulomb barrier for each nuclide is shown as a wavy line. Stable nuclides that are not listed are those for which the Q-value of the (p,n_0) reaction is less than -5 MeV. From this diagram many potential uses of this technique can be found, and possible sources of interference can be identified and avoided. Furthermore, provided suitable targets can be produced, the method may readily be adapted to the analysis of solids and to elements of higher atomic number. One such case is the isotopic analysis of calcium isotopes.

With proton energies below 6.7 MeV the only heavy isotopes of calcium from which a measurable neutron yield may be expected are those of mass numbers 43, 44 and 48; the low natural abundance of calcium-46 (0.0033%) makes it unlikely that the relative neutron yield from this isotope would be appreciable. At proton energies below 4.7 MeV calcium fluoride targets could be used for the isotopic determination (10) either of calcium-43 or 48, because the neutron detection threshold of about 700 keV is then too high for detecting neutrons from the reactions $^{19}F(p,n)^{19}Ne$ and $^{44}Ca(p,n)^{44}Sc$. Time-of-flight spectra of neutrons emitted from natural calcium fluoride and from enriched targets of calcium-43 and calcium-48 by 4.5 MeV protons are shown in Figure 15. By integrating the counts from $^{43}Ca(n_0,n_1)$ and $^{48}Ca(n_1-n_5)$ neutrons the concentra-

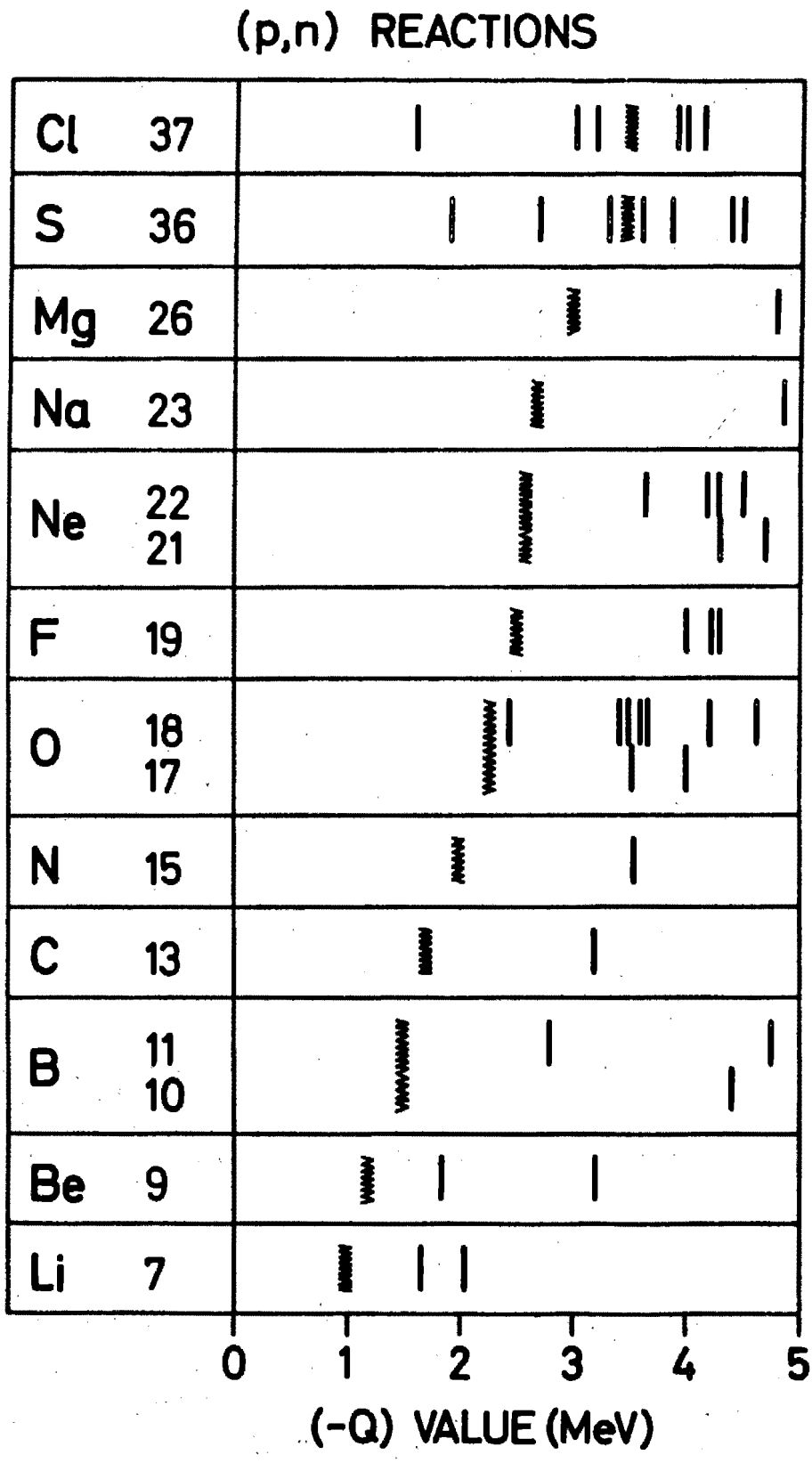

Figure 14 : Q-values for (p,n) reactions to different excited levels in the product nucleus, for stable nuclides with $Z<20$, and for Q-values >-5 MeV. The wavy line represents the calculated Coulomb barrier for each nuclide.

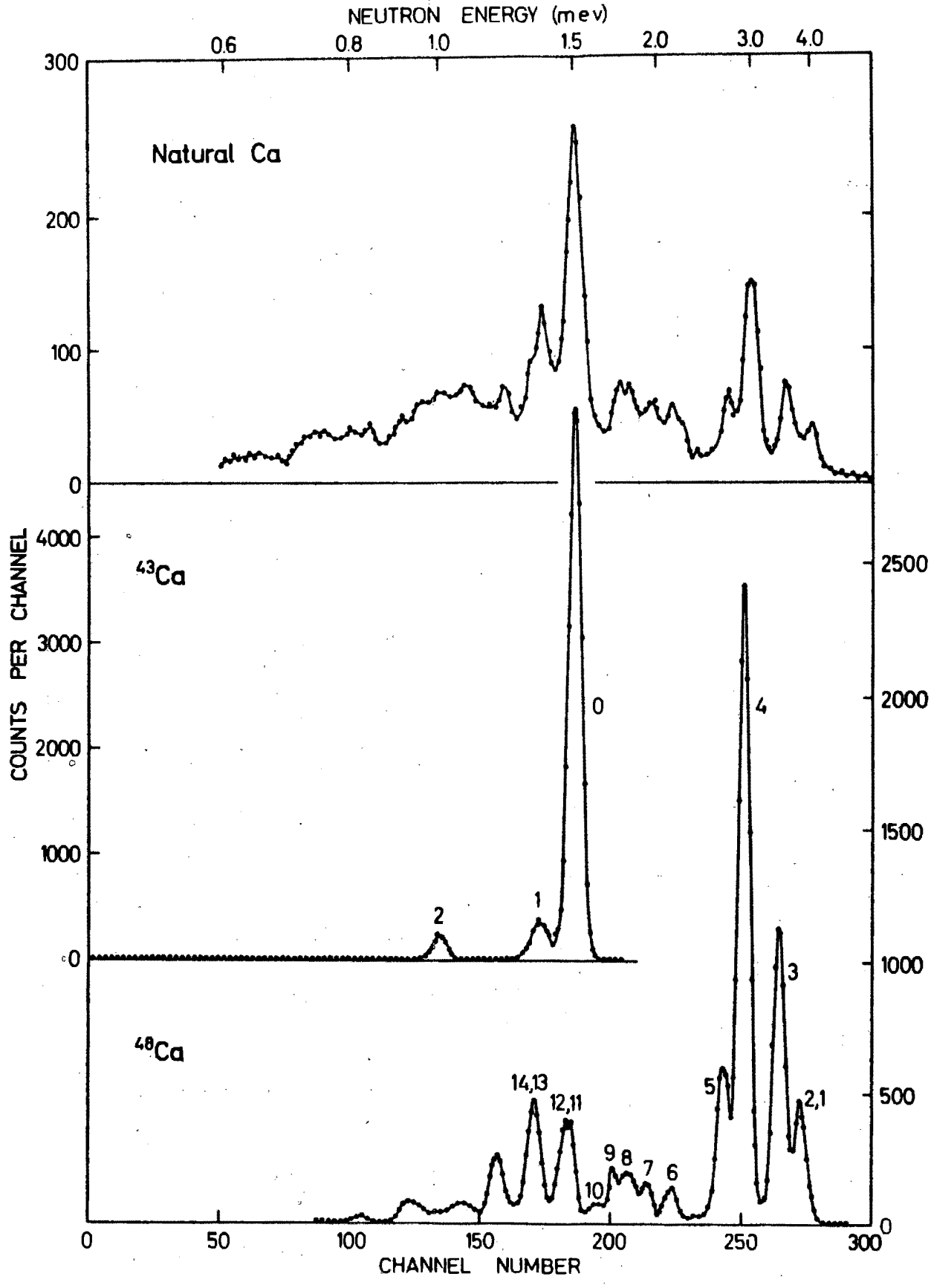

Figure 15 : Time-of-flight spectra of neutrons from (p,n) reactions on targets of natural calcium and enriched ^{43}Ca and ^{48}Ca. $E_p = 4.5$ MeV. $\theta = 0^\circ$. s = 3 metres.

tion of one isotope may be obtained relative to the other. The method can be used to determine either isotope when the other is present in known or natural concentrations. The method is, however, limited to comparatively low enrichments of ^{48}Ca, because the contribution of $^{48}Ca(n_{10}-n_{14})$ neutrons to the count representing the calcium-43 content could become overwhelming and make the determination open to large errors.

An interesting application of (d,n) reactions to analysis of solids has recently been reported (11) in which light elements were determined in metals by neutron time-of-flight spectrometry. By using thick targets and measuring the neutron yield as a function of depth below the target surface, a depth resolution of 4500 Å was attained.

This work was financially supported by the South African Atomic Energy Board.

REFERENCES

(1) Hevesy, G., Levi, H., Kgl. Danske Videnskab. Selskab, Math.-fys. Medd. 14, No. 5 (1936).

(2) Peisach, M., Chem. Communications, 632 (1966).

(3) Peisach, M., Pretorius, R., S. African Ind. Chem., 20, 5 (1966).

(4) McMurray, W.R., van der Merwe, P., van Heerden, I.J., Nucl. Phys. A92, 401 (1967).

(5) Owen, R.R., U.K. At. Energy Res. Establishment report EL/R 2712, (1958)."

(6) Everling, F., Koenig, L.A., Mattauch, J.H.E., Wapstra, A.H., "Nuclear Data Tables", Part I, National Academy of Sciences, Washington, 1961.

(7) Peisach, M., Pretorius, R., Anal. Chem., 39, 650 (1967).

(8) Naude, W.J., Peisach, M., Pretorius, R., Strebel, P.J. (in press).

(9) Peisach, M., Pretorius, R., Strebel, P.J. (in press).

(10) McMurray, W.R., Peisach, M., Pretorius, R., van der Merwe, P., van Heerden, I.J., (in press).

(11) Möller, E., Nilsson, L., Starfelt, N., Nucl. Instr. Methods 50, 270 (1967).

DISCUSSION

Mr. FLEISCHER

Have you ever looked at an impure or unknown sample ?
Do you have any examples ?

Mr. PEISACH

It is difficult to understand what you mean by an impure sample.
If the target contains nuclides that would produce neutrons above the detection threshold energy they would be observed and would be identified.
If not, their presence could not be detected.

Mr. ALBERT

Pouvez-vous nous rappeler les sensibilités que vous avez obtenues car je n'ai pas bien pu les relever ?

Mr. PEISACH

With protons using 20 mCb current 16 ng $^{18}O/cm^2$
with deuterons under the same conditions :

^{12}C 60 ng/cm^2 , ^{14}N 200 ng/cm^2, ^{16}O 170 ng/cm^2

Mr. TOUSSET

J'ai cru comprendre que la principale limitation de votre sensibilité est due à l'existence du "fond" parasite. Est-ce que l'assez longue durée de vos expériences ne risque pas d'être également une cause de limitation de sensibilité par suite de dérives de l'électronique de l'accélérateur ?

Mr. PEISACH

We did not observe any independent time factor in the background.
The total current through the cell is the only important determining factor. The sensitivity would thus, at a constant total current, depend only on the background. The values cited were strained without special attempts to reduce background. That such reduction is possible is certainly true, but how far the sensitivity would be increased if this were done, I do not dare to guess at.

Mr. HOLM

What is the effect of sample thickness ? In particular what happens with an infinitely thick sample ?

Mr. PEISACH

In some cases, especially for calibration purposes we had gases up to 150 mm pressure in a 3cm long cell. There was thus an appreciable amount of material in the beam path. Naturally with thin targets the peaks are expected to be sharp and they would appear wider with increased thickness.

In the extreme case of an infinitely thick target, I would expect the spectrum to consist of a series of steps corresponding in energy to the peaks obtained for thin targets.

Mr. QUAGLIA

N'avez vous jamais été ennuyé par la formation de deutérium sur les fenêtres et la reaction parasité d(d,n)T ?

Mr. PEISACH

Yes. The neutrons from ^{12}C are almost all due to the formation of a layer of carbon from the decomposition of oil vapours on the nickel window. Any oxydation of the nickel also showed up as a small peak due to neutrons from oxygen.

Mr. CUYPERS

La sensibilité donnée par votre méthode, tient-elle compte de la quantité d'oxygène et carbone présente sur la fenêtre d'entrée de la cellule ?

Mr. PEISACH

The sensitivities are calculated as the weight of material necessary to give the number of counts equal to 3 times the standard deviation of the integrated background count in the region where the spectrum peak is expected.

No. 24

Reprinted from

ANALYTICAL CHEMISTRY

Isotopic Determination of Oxygen-18 in Gases by Neutron Time-of-Flight Spectrometry

MAX PEISACH, RENÉ PRETORIUS, and PAUL J. STREBEL

Southern Universities Nuclear Institute, P.O. Box 17, Faure, C.P., South Africa

Volume 40, Number 6

Pages 850–853 May 1968

Isotopic Determination of Oxygen-18 in Gases by Neutron Time-of-Flight Spectrometry

Max Peisach, René Pretorius, and Paul J. Strebel[1,2]

Southern Universities Nuclear Institute, P.O. Box 17, Faure, C.P., South Africa

Oxygen-18 was determined in gases by time-of-flight spectrometry of the prompt neutrons from the reaction $^{18}O(p,n)^{18}F$ produced by a pulsed beam of protons of 5.0 MeV. The analysis is nondestructive and, with a beam current of 0.5 to 1.5 μA requires from 5 to 30 minutes per sample. The method is applicable to isotopic concentrations from 0.204 atom % (natural level) to 100%. The relative standard deviation was ±3.8% and the sensitivity, 7.2×10^{-8} g/cm².

MANY NUCLEAR METHODS for determining oxygen-18 have been developed, not only because of the use of this isotope as a tracer for oxygen, but also as a means of determining oxygen, the most abundant isotope of which has less favorable nuclear activation properties. Activation analysis has been carried out using the activities of fluorine-18, generated either by proton irradiation (*1*) or by neutron-induced "knock-on" protons (*2*, *3*), of oxygen-19, produced by thermal neutron capture (*4*), of carbon-15, generated by fast neutrons (*5*), or of nitrogen-17, produced by secondary tritons in the presence of lithium-6 by the successive nuclear reactions $^{6}Li(n,\alpha)^{3}H$ and $^{18}O(t,\alpha)^{17}N$ induced by thermal neutrons (*6*). Analytical methods, in which the emission of prompt nuclear reaction products was measured, were developed using alpha particle emitted in the (d,α) reaction (*7*) or neutrons emitted in the (α,n) reaction (*8*). These latter methods have the advantage that the conditions of measurement are not determined by the decay properties of radioactive products.

The technical difficulties connected with the irradiation of gaseous samples, with few exceptions, limit the use of methods such as described above, to liquids and solids. An attempt to determine oxygen-18 in carbon dioxide was reported (*4*) but the procedure involved the conversion of the gas to solid ammonium carbamate, which was then irradiated. There is thus need for an analytical method which could extend the advantages of nuclear methods to the determination of oxygen-18 in the gaseous phase. In this work an attempt was made to determine oxygen-18 nondestructively in gases by time-of-flight spectrometry of prompt neutrons emitted from the reaction $^{18}O(p,n)^{18}F$ induced by a pulsed beam of protons. This method has already been applied to the determination of deuterium (*9*) and other elements (*10*) using a pulsed deuteron beam and isotopes of calcium (*11*) using a pulsed proton beam.

Table I. Neutron Energies from (p,n) Reactions

E_p = 5.0 MeV

Target	Natural abundance, %	Q-value (p, n_0) MeV (*12*)	Neutron energy, MeV
^{12}C	98.89	−18.390	...
^{13}C	1.11	−3.004	1.941 (n_0)
^{14}N	99.63	−5.931	...
^{15}N	0.37	−3.543	1.381 (n_0)
^{16}O	99.759	−16.431	...
^{17}O	0.037	−3.544	1.390 (n_0)
			0.854 (n_1)
^{18}O	0.204	−2.450	2.495 (n_0)
			1.555 (n_1)
			1.445 (n_2)
			1.406 (n_3)
			1.361 (n_4)
			0.744 (n_5)
			0.288 (n_6)

Gaseous samples in which the isotopic concentration of oxygen-18 is to be determined frequently contain the elements carbon and nitrogen, in addition to oxygen. The nuclear properties of the stable isotopes of these elements under the conditions of proton irradiation are of considerable interest and are listed in Table I. The Q-values of the (p,n_0) reactions of the stable isotopes and the natural abundances are given in the table. Using proton beams with energies less than 5.5 MeV, the highest energy attainable in this investigation, neutron emission from the very abundant nuclides ^{12}C, ^{14}N, and ^{16}O is energetically impossible. In the same table, values are given for the energies of neutrons expected to be formed by a proton beam of 5 MeV from the heavier isotopes of these elements, the neutron group n_i corresponding to the i^{th} excited state in which the product nucleus is left. The neutron energies given in the last column of Table I were calculated from the kinematics of the nuclear reactions concerned, as were reported previously (*9*). Many neutron groups are obtainable from oxygen-18 and there is no *a priori* reason to prefer any one for use for analytical purposes, except that the n_0 neutrons from carbon-13 and nitrogen-15 have energies relatively close to those of the n_3 and n_4 neutrons from oxygen-18 and hence could be a possible source of interference.

EXPERIMENTAL

Isotopically enriched oxygen-18, as chemically pure carbon dioxide containing 97.45 atom % ^{18}O and 0.27 atom % ^{17}O was supplied by Yeda Research and Development Co.,

[1] Department of Chemistry, University of Cape Town, Rondebosch, C.P., South Africa.

[2] Present address, Graduate College, Princeton University' Princeton, N. J. 08540.

(1) B. A. Thompson, ANAL. CHEM., **33,** 583 (1961).
(2) L. H. Hunt and W. W. Miller, *Ibid.*, **37,** 1269 (1965).
(3) D. C. Aumann and H. J. Born, *Naturwissenschaften*, **51,** 159 (1964).
(4) G. J. Fritz, I. Han, and W. H. Ellis, *Intern. J. Appl. Radiation Isotopes*, **16,** 431 (1965).
(5) V. P. Guinn, *Trans. Amer. Nucl. Soc.*, **9,** 83 (1966).
(6) S. Amiel and M. Peisach, ANAL. CHEM., **35,** 323 (1963).
(7) G. Amsel and O. Smulkowski, *Compt. Rend.*, **251,** 950 (1960).
(8) S. Amiel and A. Nir, "Radiochemical Methods of Analysis Vol I," I.A.E.A., Vienna, 1965, p 287.
(9) M. Peisach and R. Pretorius, ANAL. CHEM., **39,** 650 (1967).
(10) M. Peisach, *Chem. Communications*, **1966,** 632.
(11) W. R. McMurray, M. Peisach, R. Pretorius, P. van der Merwe, and I. J. van Heerden, ANAL. CHEM. **40,** 266 (1968).
(12) F. Everling, L. A. Koenig, J. H. E. Mattauch, and A. H. Wapstra, "Nuclear Data Tables, Part I," National Academy of Sciences, Washington, 1961.

Reprinted from **ANALYTICAL CHEMISTRY**, Vol. 40, Page 850, May 1968

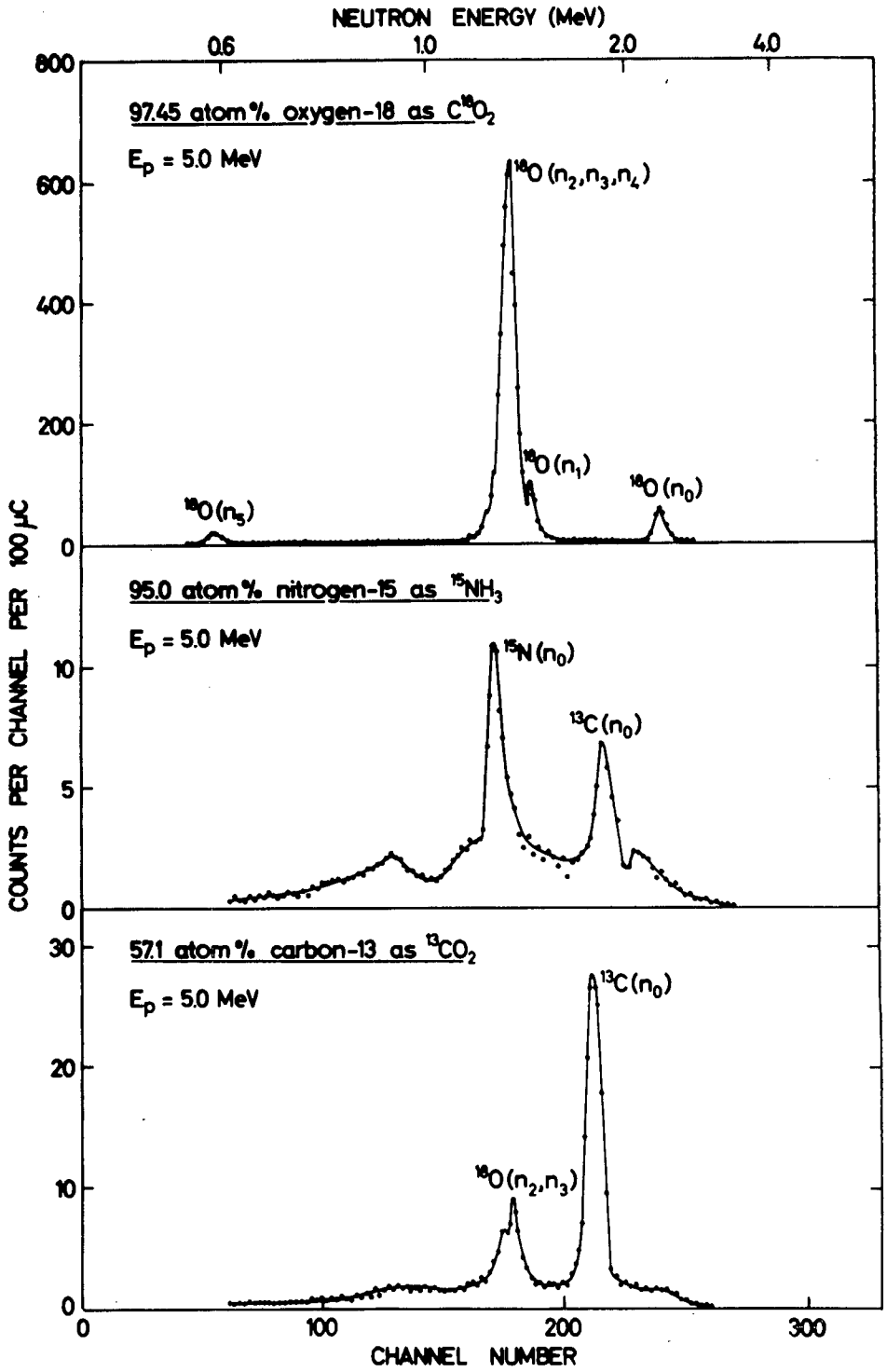

Figure 1. Neutron time-of-flight spectra of enriched oxygen-18, nitrogen-15, and carbon-13

Proton energy (E_p) = 5.0 MeV
Flight path = 3.13 m

Rehovoth, Israel. From this stock, samples were prepared containing known concentrations of oxygen-18 in natural oxygen, carbon dioxide, and nitrogen.

The irradiation cell, 3 cm long with a volume of about 7 cc, and the gas handling apparatus, have already been described (*9*). A circular tantalum collimator, 3.5 mm in diameter, defined the cross-sectional area of the beam. However, the beam area is irrelevant because the number of counts recorded during an irradiation with a predetermined integrated quantity of charge, is independent of the beam area. The beam entered the irradiation cell through a thin nickel window and was stopped in the thick tantalum rear wall of the cell. Neither the nickel nor the tantalum could yield neutrons at the proton energies used in this investigation.

Pulsed proton beams were obtained from the 5.5 MV Van de Graaff accelerator at the Southern Universities Nuclear Institute. Pulses were of 4-nsecond duration and 400 nseconds apart. Low average beam currents of between 0.5 and 1.5 A were used to prevent damage to the thin nickel window. Most measurements lasted between 5 and 30 minutes per sample.

The electronic equipment was the same as was used previously (*9*). Low level electronic noise was rejected by energy discrimination and pulses from gamma-rays by pulse shape discrimination. The neutron detection threshold was somewhat below 700 keV so that neutrons below this energy could not be observed.

NEUTRON SPECTRA

Enriched Samples. Typical neutron time-of-flight spectra obtained from enriched carbon-13 as $^{13}CO_2$, nitrogen-15 as $^{15}NH_3$ and oxygen-18 as $^{18}CO_2$ with 5.0-MeV protons are shown in Figure 1. The energy of each neutron group is

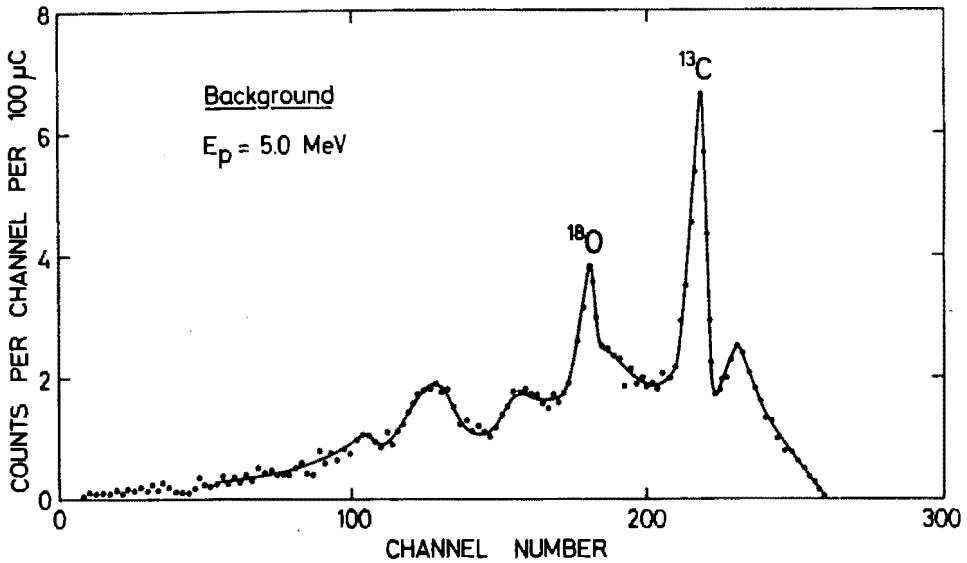

Figure 2. Typical background spectrum

E_p = 5.0 MeV
Flight path = 3.13 m

about 150 keV lower than the corresponding values given in Table I because of the energy lost by the proton beam in passing through the nickel window.

The spectrum obtained from oxygen-18 consisted of an isolated small single peak corresponding to the n_0 neutron group and a large composite peak which included counts from the neutron groups n_1, n_2, n_3, and n_4 that could not be resolved under the conditions of the experiment. For analytical purposes it is not necessary to resolve these neutron groups, because the relative number of counts obtained from each is constant at constant incident proton energy and constant measuring angle. The small peak due to n_5 neutrons is just detectable, but the detection efficiency for such low energy neutrons is much smaller than for neutrons of about 1 MeV or higher, so that the height of the peak is not a true reflection of the relative reaction cross section.

Background. A typical background spectrum as obtained from the irradiation of an empty gas cell with a beam of 5-MeV protons is given in Figure 2. This spectrum consisted of two relatively prominent peaks corresponding to 1.752- and 1.328-MeV neutrons from carbon-13 and oxygen-18, respectively, probably because of deposits formed from residual vacuum oil vapors in the beam tube which decomposed at heated points of incidence of the irradiation beam on the cell window. In addition there was a low continuum of counts due to gamma-rays not entirely eliminated by pulse shape discrimination and neutrons scattered into the detector.

Unlike the case for deuteron irradiation where all nuclidic components of carbon-, nitrogen-, or oxygen-containing gases generate neutrons at relatively low incident beam energies (*13*), proton irradiation at comparable energies does not generate neutrons in such large numbers because of the highly endoergic nature of the corresponding proton-induced reactions on the more abundant lighter isotopes. Accordingly, the total number of neutrons produced in the gas cell from sources other than the nuclide under investigation, does not vary appreciably with the composition of the gas unless the gas contains other enriched isotopes of carbon, nitrogen, or oxygen. Hence, the magnitude and spectral distribution of the background can be considered to be independent of the pressure and composition of the gas under analysis.

(13) W. J. Naudé, M. Peisach, R. Pretorius, and P. J. Strebel, *J. Radioanal. Chem.* (in press).

CALIBRATION

The n_0 neutrons from oxygen-18 are readily resolvable from all other neutron groups that can be generated in gases containing only carbon, nitrogen, and oxygen and would therefore appear to be most suitable for analytical purposes. However, the neutron yield from the (p,n_0) reaction induced by 5 MeV protons is so much lower than the yield from the combined (p,n) reactions leading to the first, second, third, and fourth excited states, that the integrated neutron count over the energy region covered by this combined group provides a better index of the oxygen-18 content of the gas. With 5 MeV protons, the appropriate energy region for integration lies between about 1.0 and 1.58 MeV. The integrated count in this region was used as a measure of the oxygen-18 content despite the fact that neutrons from nitrogen-15 and oxygen-17 might add to the total count.

As the neutron count is proportional to the number of target nuclei in the path of the beam, it was possible to utilize the integrated neutron count obtained from a single gas sample, but measured over a range of pressures, as a calibration curve. The linear calibration curve obtained with a 5-MeV proton beam and approximately 10 atom % oxygen-18 as $^{18}CO_2$ over pressures ranging from 0.7 to 63.3 mm had a slope of 1080 counts per millicoulomb for 1 μg per cm² cross-sectional area of the beam.

RESULTS OF ANALYSES

Table II lists the results of some determinations of oxygen-18 in oxygen gas and in the presence of natural carbon dioxide and natural nitrogen with a proton beam of 5.0 MeV. The mean neutron count was 1091 counts per millicoulomb for 1 μg per cm², which agrees with the calibration value, quoted above, within the precision of the method. The mean error, −0.045 μg per cm², provides a measure of the accuracy of the method and the statistical analysis of the results shows that there is no bias. The relative standard deviation was ±3.82%.

Table II. Some Determinations of Oxygen-18

E_p = 5.0 MeV

Gas mixed with $C^{18}O_2$	Oxygen-18 content μg/cm²			Relative error, %	Neutron counts per millicoulomb	
	Known A	Found B	Error (B-A)		Observed N	Per unit mass N/A
O_2	4.44	4.08	−0.36	−8.11	4639	1045
	9.95	9.71	−0.24	−2.41	10720	1077
	15.09	15.14	+0.05	+0.33	16584	1099
	20.69	21.40	+0.71	+3.44	23340	1128
N_2	3.32	3.08	−0.24	−7.23	3555	1071
	6.85	6.89	+0.04	+0.58	7667	1119
	12.08	12.19	+0.11	+0.91	13399	1109
	19.66	19.44	−0.22	−1.12	21228	1080
	27.36	26.72	−0.64	−2.34	29088	1063
	31.46	32.51	+1.05	+3.34	35342	1123
CO_2	3.88	3.66	−0.22	−5.67	4187	1079
	5.70	5.63	−0.07	−1.23	6314	1107
	17.71	18.23	+0.52	+2.94	19921	1125
	24.54	24.35	−0.19	−0.77	26526	1081
	36.83	35.85	−0.98	−2.66	38944	1057

Mean error = −0.045 μg/cm²
Mean neutron count per μg/cm² = 1091 for 1 mC
Relative standard deviation = ±3.82%

PRECISION

From a knowledge of the background and the slope of the calibration line, the minimum amount of oxygen-18 for which the neutron count could be determined with a precision of ±3% by irradiating with a total charge of 1 mC was found to be 1.76 μg per cm² cross-sectional area of the beam. By increasing the total charge to 20 mC thereby increasing the number of counts and hence reducing its statistical uncertainty, about 280 ng/cm² of oxygen-18 could be measured with the same precision. When a lower precision of ±10% was acceptable, this limit was reduced to 80 ng/cm².

SENSITIVITY

The background over the energy range of the n_1, n_2, n_3, and n_4 neutrons from oxygen-18 amounted to about 700 counts per millicoulomb. Under these conditions the sensitivity limit for the detection of oxygen-18 with 1 mC total charge was 72 ng per cm². The criterion selected for the calculation of the sensitivity was that weight of sample for which the net sample count was three times the standard deviation of the background count over the relevant energy interval.

INTERFERENCES

When the determination has to be carried out in the presence of oxygen in which the oxygen-17 concentration is not enriched, interference from this nuclide is unlikely. However, it frequently happens that preparations enriched in oxygen-18 are also enriched in oxygen-17, albeit to a smaller extent. In such cases interference from oxygen-17 *is* likely.

In the presence of carbon, oxygen-18 can readily be determined because none of the stable isotopes of this element can produce interfering neutrons. In the presence of nitrogen, interference from neutrons generated by nitrogen-15 may be expected when the concentration by weight of nitrogen-15 is about seven times that of oxygen-18. At the isotopic concentrations of oxygen-18 and nitrogen-15 found in nature, neutrons from nitrogen-15 would introduce errors in the determination of oxygen-18 when the nitrogen-to-oxygen atom ratio is greater than about 4:1.

Other elements from which interference is energetically possible, when 5 MeV protons are used, are neon (from ^{22}Ne) and sulfur (from ^{36}S). The presence of neon in samples containing enriched oxygen-18 is improbable. Sulfur-36 occurs in nature in an isotopic concentration of 0.014 atom %; interference from this nuclide is thus expected to be small in unenriched samples.

ACKNOWLEDGMENT

Acknowledgment is due to Bob Naudé who helped with the preliminary investigation.

RECEIVED for review September 11, 1967. Accepted January 15, 1968. This work was financially supported by the South African Atomic Energy Board. One of us (P.J.S.) was also supported by a bursary from the South African Council for Scientific and Industrial Research.

Journal of Radioanalytical Chemistry Vol. 1 (1968) 231—241

THE DETERMINATION OF CARBON, NITROGEN AND OXYGEN IN GASES BY NEUTRON TIME-OF-FLIGHT SPECTROMETRY

W. J. NAUDÉ*, M. PEISACH, R. PRETORIUS, P. J. STREBEL**

Southern Universities Nuclear Institute P. O. Box 17, Faure, C. P. (South Africa)

(Received September 15, 1967)

Carbon, nitrogen and oxygen were determined in gases by time-of-flight spectrometry of prompt neutrons from the respective reactions $^{12}C(d, n)^{13}N$, $^{14}N(d, n)^{15}O$ and $^{16}O(d, n)^{17}F$, produced by a pulsed beam of deuterons of 2 MeV (for nitrogen) or 3 MeV. The analysis is non-destructive and requires about 15 min. per sample. The relative standard deviation for all three elements was about $\pm$ 3%. Detection limits, using a total irradiation current of 20 millicoulombs, for carbon, nitrogen and oxygen, respectively, were $6 \cdot 10^{-8}$ g, $2 \cdot 10^{-7}$ g and $1.7 \cdot 10^{-7}$ g per cm^2 cross-sectional area of irradiating beam.

Introduction

Among the more common elements for which neutron activation analyses are not sufficiently sensitive, are carbon, nitrogen and oxygen. These elements are so important that attempts to extend the advantages of nuclear methods of analysis to their determination are justified. One such attempt, in which the radioactive products of photoactivation with high energy gamma-rays was used to determine microgram quantities, has recently been reported[1]. In this work, another attempt is described, in which the prompt neutrons from (d, n) reactions are measured by neutron time-of-flight spectrometry.

When deuterons of energy, E_d, induce (d, n) reactions, the energy of the emitted neutron, E_n, is determined by the Q-value of the reaction and the angle Θ at which it is emitted. From the kinematics of a nuclear reaction, the neutron energy is given by

$$\sqrt{E_n} = v \pm \sqrt{v^2 + w}\,, \tag{1}$$

where

$$v = \frac{\sqrt{m\, m_n\, E_d}\cos\Theta}{(m_n + M)} \tag{2}$$

* The Merensky Institute for Physics, University of Stellenbosch, Stellenbosch, C. P. (South Africa).

** The Department of Chemistry, University of Cape Town, Rondebosch, C. P., (South Africa).

and

$$w = \frac{MQ + E_d(M - m)}{(m_n + M)} . \tag{3}$$

m, m_n and M, respectively, refer to the mass of the deuteron, the neutron and the product nucleus.

The most accurate method available at present for neutron spectroscopy is the time-of-flight technique in which the time t (nanoseconds) taken by a neutron to cover a distance s (metres) is measured and related, non-relativistically, to the energy of the neutron, in MeV, by

$$t = \frac{72.3 \times s}{\sqrt{E_n}} , \tag{4}$$

where the constant includes the mass of the neutron and the relevant conversion constants. The energy resolution of a time-of-flight spectrometer, obtained from Equation 4, is given by

$$\frac{\Delta E_n}{E_n} = \left[\left(\frac{\Delta t \sqrt{E_n}}{36.1 \times s}\right)^2 + \left(\frac{2\Delta s}{s}\right)^2\right]^{1/2} , \tag{5}$$

where ΔE, Δt and Δs are the uncertainties in energy, time and distance, respectively. The uncertainty in a flight path of several metres is relatively small, so that the energy resolution of the system will depend largely on the precision in measuring the flight time, the time interval between two pulses, marking the start and end of the neutron flight.

When the irradiating deuteron beam consists of pulses of short duration, the arrival of a pulse at the target may mark the instant of neutron generation, and the arrival of the neutron at the detector may mark the end of the time-of-flight. Clearly, the duration of the irradiating pulse will introduce an uncertainty in the flight time, and constitutes a limitation of the method.

This technique[2] has already been applied to the determination of deuterium in gases[3] and to the isotopic analysis of calcium in thin deposits[4]. The determination of light elements in comparatively thick plates of metals has also been described using the same technique[5]. This paper describes the use of neutron time-of-flight spectrometry for the elemental determination of carbon, nitrogen and oxygen in gases.

The Q-values of (d, n_0) reactions on carbon-12, nitrogen-14 and oxygen-16 are given in Table 1, together with the calculated energies of neutrons emitted in the (d, n_i) reactions where the product nucleus is left in its i-th excited state. The detected neutrons will, however, be measured as a group with an energy spread about the calculated value, the extent of which is determined by the energy resolution of the spectrometer.

Table 1

Neutron energies from (d, n) reactions
$E_d = 3.0$ MeV $\Theta = 0°$

Target	Natural abundance, %	Q-value (d, n_0) MeV[6]	Neutron energy, MeV
^{12}C	98.89	− 0.281	2.582(n_0)
^{14}N	99.63	5.066	7.932(n_0)
			2.771(n_1)
			2.710(n_2)
			1.763(n_3)
			1.098(n_4)
			1.033(n_5)
			0.693(n_6)
			0.235(n_7)
^{16}O	99.759	− 1.627	1.223(n_0)
			0.685(n_1)

Experimental

The electronic equipment[7] was the same as used previously[3]. Because the neutron detector was sensitive to gamma-rays as well as to neutrons, signals caused by gamma-rays were rejected by pulse shape discrimination[8] and low level electronic noise by the energy discriminator. The efficiency of the neutron detector fell rapidly for neutrons below 1 MeV, while the detection threshold for neutrons was somewhat below 700 KeV.

The gas handling apparatus and the irradiation cell have been described[3]. Irradiations were carried out with the 5.5 MV Van de Graaff accelerator at the Southern Universities Nuclear Institute. Deuteron pulses lasted for 5 nsec. and were 400 nsec. apart. Low average beam currents, ranging between 0.7 and 1.2 μA, were used to prevent damage to the nickel window of the gas cell, which could not be cooled. For improved resolution, larger flight paths are necessary (see Equation 5), but as the count rate decreases with s^2, a compromise between resolution and the duration of the analysis has to be struck. At about 3 metres resolution was adequate, and the count rate sufficiently high to complete an analysis within 15 minutes.

Neutron spectra

Typical neutron time-of-flight spectra, obtained from methane, oxygen and nitrogen with 3.5 MeV deuterons, are given in Fig. 1. The energy scale is not linear, because the spectra are based on time measurements with channel number

proportional to the neutron flight time. For this reason, the peaks are spread over more channels towards the low energy ends of the spectra.

The peaks in the spectra correspond to the energies listed in Table 1, provided correction is made for the difference in deuteron energy and for the 160 KeV energy lost by the deuteron beam in the nickel window. Neutrons with energies

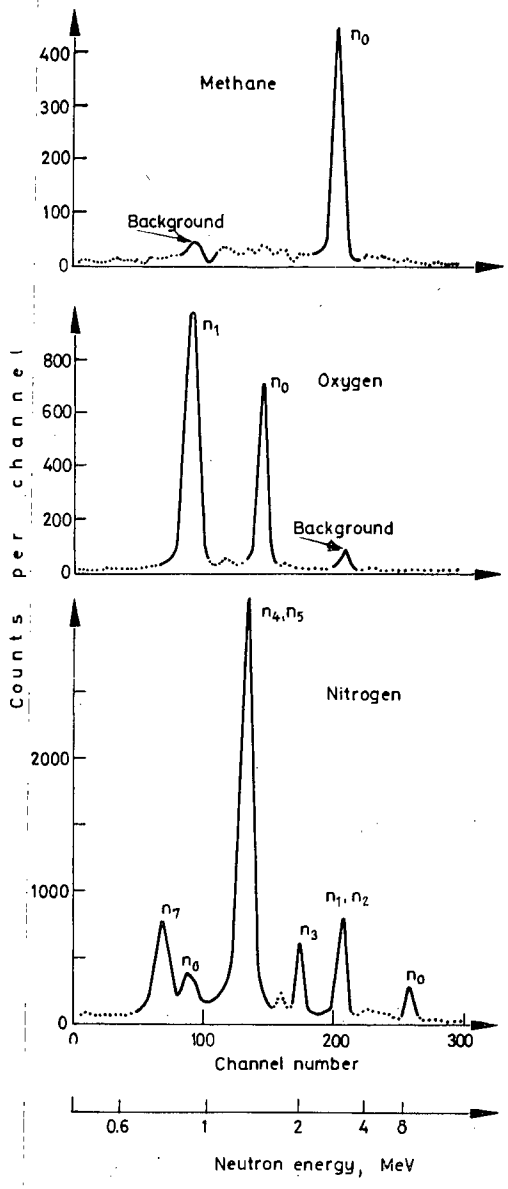

Fig. 1. Typical neutron time-of-flight spectra. $E_d = 3.5$ MeV, $\Theta = 30°$, $s = 2.99$ m

below 700 KeV could not be distinguished from gamma-rays by pulse shape discrimination. Accordingly, at lower deuteron energies, neutron groups which may have been expected from Table 1, with energies below this value, were not observed.

Carbon-12 produced only one characteristic neutron group which was used to provide a measure of the carbon content of the sample. By contrast, oxygen-16 gave rise to two neutron groups of which the n_1 groups had an energy below 1 MeV. Because in this energy range the neutron detection efficiency decreased rapidly with decreasing neutron energy, the number of neutrons counted would vary appreciably with the fluctuations in neutron energy caused, for example, by the varying energy loss of the irradiation beam in samples of different pressure and composition. In addition, because of low detection efficiency, small changes in the neutron yield might not be reflected in the observed neutron count. For these reasons, the n_1 neutron group from oxygen-16 was not suitable for measurement, and hence the n_0 group was used.

Nitrogen-14 generated seven neutron groups. The spectrum shows that the neutron group pairs (n_1, n_2) and (n_4, n_5) were not resolvable under the conditions of measurement, but this did not detract from their potential use as a measure of nitrogen content. However, the n_1 and n_2 groups had energies comparable with the energy of neutrons from carbon-12, the n_4 and n_5 groups had energies similar to those of the n_0 neutrons from oxygen-16, and the groups n_6 and n_7 had energies near to the range of rapidly decreasing detector efficiency. Consequently the n_0 and n_3 groups were used for determining the nitrogen content of a sample.

Calibration

The integrated count from a characteristic neutron group is proportional to the pressure of the gas, and its variation with pressure served as a calibration curve for the determination of the nuclide concerned. The calibration curves for nitrogen (using N_2) and carbon (using CH_4) remained linear up to pressures of 100 mm, despite the fact that the energy loss of the beam in a 3-cm sample was already significant above 50 mm. This is probably due to the fact that the reaction cross section varies little with deuteron energy in that range.

The oxygen-16 calibration curves obtained from measurements on carbon dioxide and oxygen are given in Fig. 2. The two curves (drawn as solid lines in Fig. 2) coincide and remain linear up to pressures of about 25 mm, but deviation from linearity occurs at higher pressures. The $^{16}O(n_0)$ neutrons had an observed energy of 1.039 MeV. At this energy there is an appreciable change in detector efficiency with decreasing neutron energy, but when correction is made for the efficiency loss, the calibration curve still deviates from linearity as shown dashed in Fig. 2. It can thus be deduced that the effective cross section for the reaction $^{16}O(d, n_0)^{17}F$ decreases with decreasing deuteron beam energy near 3 MeV. This conclusion is compatible with the fact that the values for carbon dioxide lie below

those obtained from oxygen because the energy loss of the beam in the former is greater.

It thus follows that when carbon and nitrogen are to be determined in thermally stable gas mixtures, analysis may be performed at any pressure over the range studied. If oxygen is also to be determined, the gas sample should be analyzed at a pressure below 20 mm. After such an analysis it may be found that an elemental component present in low concentration cannot be determined with sufficient precision. If the component is carbon or nitrogen, the analysis may be

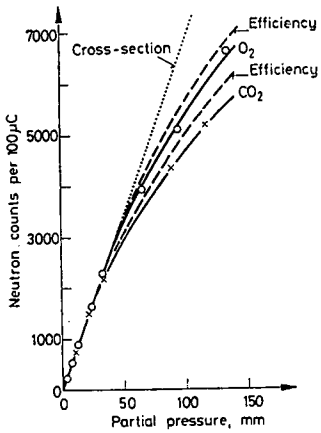

Fig. 2. Calibration curve for oxygen as measured with oxygen gas and carbon dioxide. Experimental curves (solid) are corrected for detector efficiency variation (dashed) and cross section variation (dotted)

repeated at a higher gas pressure, but if the low concentration component is oxygen, uncorrected neutron counts measured at higher pressures will lead to inaccurate results. However, the energy lost by the irradiation beam can be calculated from a knowledge of the concentrations of the major elemental components, and hence correction for variations in detector efficiency and reaction cross section can be made.

Background

The predominant feature in the background spectra (see Fig. 3) is the peak corresponding to 2.5 MeV neutrons from carbon-12 due to the residual vacuum oil vapour in the beam tube, which deposited on the hot spot generated at the point of incidence of the beam on the nickel window of the cell.

The background spectrum includes widened peaks of unknown origin. Such peaks may arise from neutrons produced by the interaction of the pulsed beam and material it strikes along the beam tube. Neutrons scattered into the detector would yield random pulses, the intensity of which would be a function of the total number of neutrons generated. In extreme cases it may be necessary to

correct for this background effect, which may be determined by irradiating a sample with approximately the same composition and pressure as the one under analysis, but in which the component to be measured is absent.

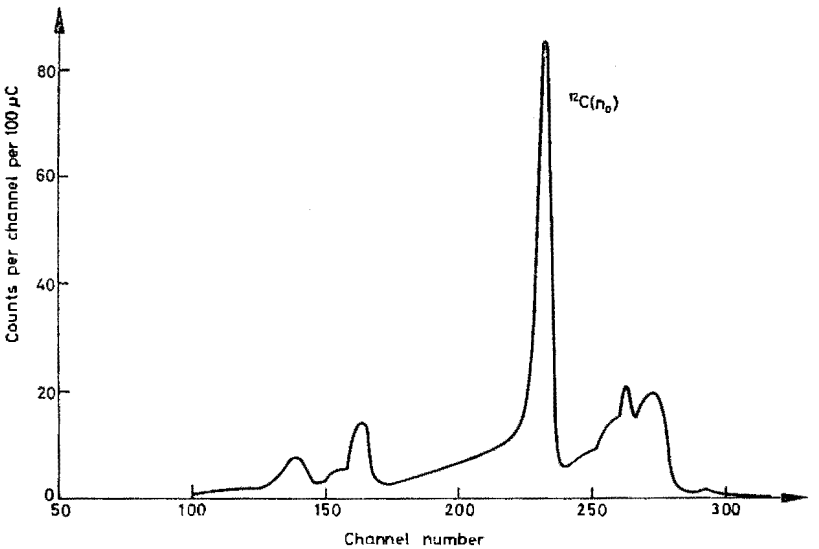

Fig. 3. Typical background spectrum. $E_d = 3.0$ MeV; $\Theta = 30°$; $s = 2.93$ m

Analyses of gas mixtures

A typical spectrum obtained from the irradiation of a CO_2/N_2 sample is given in Fig. 4. The $^{14}N(n_1, n_2)$ neutron groups have energies comparable with the energy of the $^{12}C(n_0)$ group, and the $^{14}N(n_4, n_5)$ neutron groups have energies comparable with those of $^{16}O(n_0)$ neutrons. Under constant experimental conditions, the number of counts obtained from the $^{14}N(n_1, n_2)$ and (n_4, n_5) group pairs relative to the number of $^{14}N(n_0)$ neutrons is constant and could be determined from a spectrum of nitrogen gas. From a knowledge of these ratios and the number of n_0 neutrons from nitrogen-14, the net neutron counts from $^{12}C(n_0)$ and $^{16}O(n_0)$ could be obtained.

Some typical results of elemental analyses of gas mixtures containing carbon, nitrogen and oxygen are given in Table 2, and a summary of different series of test analyses is given in Table 3. The summary includes the value of the slope of the calibration line for each test and the observed mean neutron count per mm pressure per 100 microcoulombs. In all cases the agreement between the two values was within the precision of the method. The apparent variation in the slope of the calibration curves of carbon-12 and oxygen-16 from one set of gas mixtures to the other reflects variations in the counting conditions used for the different analyses.

Table 2

Some determinations of carbon, nitrogen and oxygen in gas mixtures

Element determined	E_d (MeV)	Gas mixture	Relative composition (by pressure)	Elemental concentration, (μg per cm² of beam area)			Relative error %
				Known (A)	Found (B)	Error (B−A)	100 (B−A) / (A)
C	3.0	CO_2/CO	0.366 : 1.00	79.7	78.6	−1.1	−1.4
			1.10 : 1.00	84.9	83.2	−1.7	−2.0
			2.18 : 1.00	86.2	88.0	+1.8	+2.1
			0.365 : 1.00	188.2	187.8	−0.4	−0.2
			0.117 : 1.00	190.0	186.8	−3.2	−1.7
			0.508 : 1.00	194.4	195.5	+1.1	+0.6
N	2.0	N_2/CO_2	0.411 : 1.00	58.5	59.6	+1.1	+1.9
			19.5 : 1.00	108.0	107.5	−0.5	−0.5
			1.03 : 1.00	115.6	116.2	+0.6	+0.5
			9.16 : 1.00	166.4	163.7	−2.7	−1.6
			25.1 : 1.00	220.6	222.6	+2.0	+0.9
			40.7 : 1.00	256.3	247.8	−8.5	−3.3
O	3.0	CO_2/CO	0.117 : 1.00	109.4	108.1	−1.3	−1.2
			0.021 : 1.00	109.8	113.9	+4.1	+3.7
			0.508 : 1.00	156.7	156.5	−0.2	−0.1
			39.8 : 1.00	210.3	213.0	+2.7	+1.3
			0.366 : 1.00	318.1	319.1	+1.0	+0.3
			1.10 : 1.00	355.1	363.0	+7.9	+2.2

Table 3

Summary of test analyses on gases

$E_d = 3.0$ MeV

Gas mixture	Nuclide determined	Number of samples	Calibration*	Mean* neutron count	Mean pressure error, mm	Relative standard deviation %
CO_2/CO	^{12}C	13	179.8	174.1	+0.004	±2.3
	^{16}O	13	75.4	74.4	−0.001	±3.0
CO_2/N_2	^{12}C	9	174.3	168.9	−0.003	±2.6
	^{14}N	13	23.3	24.2	+0.004	±4.6
	^{16}O	11	68.9	69.8	−0.002	±3.4
	^{14}N	10**	23.7	23.0	−0.046	±3.3

* Counts per mm per 100 microcoulombs.
** $E_d = 2.0$ MeV

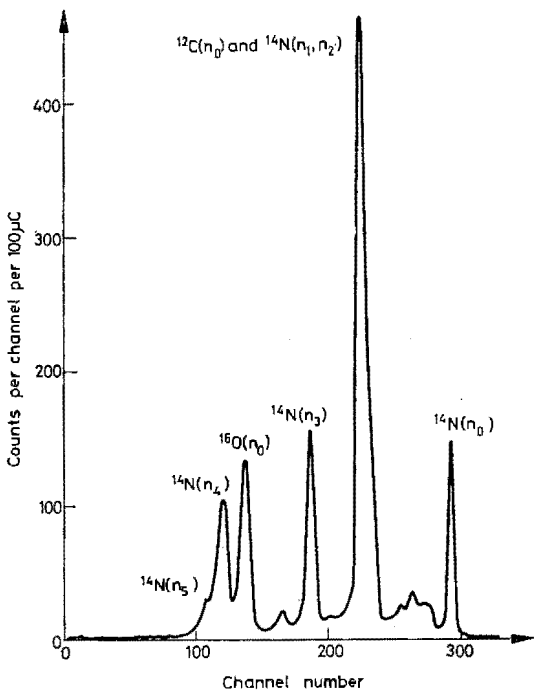

Fig. 4. Neutron time-of-flight spectrum of a mixture of carbon dioxide and nitrogen. $E_d = 3.0$ MeV; $\Theta = 30°$; $s = 2.93$ m; $P_{CO_2} = 18.46$ mm; $P_{N_2} = 31.04$ mm

Precision and sensitivity

The relative standard deviation of the method was about $\pm$ 3% for all three elements. It is satisfying to note that this precision is comparable with that of most nuclear methods used for analysis.

When nitrogen was present, the additional corrections required to obtain the net counts made a contribution to the total variance of the determinations resulting in a slightly higher relative standard deviation. The determination of nitrogen with a 2 MeV, rather than a 3 MeV, deuteron beam precluded the detection of neutrons from oxygen-16 (see Fig. 5), and resulted in a comparatively lower value of the $^{12}C(n_0)$ count, but the background continuum in the energy range corresponding to n_0 neutrons from nitrogen-14 was also lower. At the lower incident deuteron energy the $^{14}N(n_1)$ and (n_2) neutron groups were partially resolved.

Since the method requires a measurement to be made of events that are statistically random, the precision of an analysis will deteriorate as the relative statistical errors involved in determining the count rate increase. From a knowledge of the background and the slopes of the calibration lines, the minimum elemental concentration in the gas for which the neutron count can be determined with

a precision of ± 3% and ± 10% has been calculated and is given in Table 4 up to a maximum total current of 20 millicoulombs (requiring about 3 hours). When longer irradiations are practicable, the minimum quantity of these elements which can be determined without sacrificing precision, may be reduced.

The sensitivities with which the three elements that can quantitatively be detected using a charge up to 20 millicoulombs, are given in Table 5.

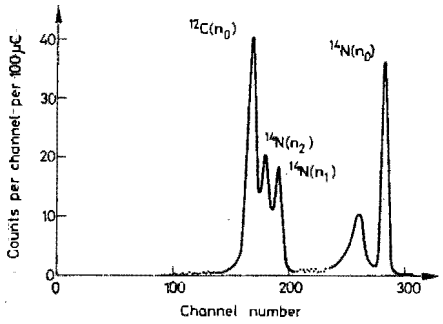

Fig. 5. Neutron time-of-flight spectrum of a mixture of carbon dioxide and nitrogen. $E_d = 2.0$ MeV; $\Theta = 30°$; $s = 2.93$ m; $P_{CO_2} = 11.66$ mm; $P_{N_2} = 19.61$ mm

Table 4

Precision limits for elemental analysis

Relative precision of neutron count	Total current, millicoulombs	Micrograms per cm² cross-sectional area of beam		
		^{12}C	^{14}N	^{16}O
±3%	1	5.18	28.40	16.79
	2	3.46	16.67	10.75
	10	1.50	5.60	4.25
	20	1.06	3.67	2.92
±10%	1	1.42	5.29	3.99
	2	0.98	3.49	2.71
	10	0.44	1.43	1.18
	20	0.31	0.99	0.82

Despite the comparatively high background in the energy region corresponding to neutrons from carbon, this element could be determined with greatest sensitivity because the reaction $^{12}C(d, n_0)^{13}N$ has a relatively high cross section. As the energies of their characteristic neutron groups were well resolved, the presence of both carbon and oxygen in the sample hardly reduced the sensitivity with which each could be determined. However, the presence of nitrogen in a sample affected the sensitivity with which the other two elements could be determined. Nevertheless, carbon and oxygen could be determined in microgram quantities with a 2 millicoulomb total current, even when the nitrogen to carbon ratio was about 2500 : 1 by weight and the nitrogen to oxygen ratio was about 75 : 1.

Table 5

Sensitivity of elemental analyses

Total current, millicoulombs	Nanograms per cm² cross-sectional area of beam		
	^{12}C	^{14}N	^{16}O
1	290	900	770
2	210	630	540
10	90	280	240
20	60	200	170

Interferences

When the sample contains other nuclides which yield neutrons with energies near to those of the neutron groups being used for analytical purposes, these nuclides would interfere with the precision of the analyses. Thus, nitrogen-14 interferes with the measurement of carbon and oxygen. Similar interference could be expected from gases containing enriched carbon-13, nitrogen-15 and oxygen-17 and 18. Even in samples in which the heavy isotopes are not enriched, neutrons generated from them may still interfere with the determination of a minor component. For example, a sample containing many carbon and only one nitrogen atom per molecule may contain carbon-13 in amounts comparable to the nitrogen content even though carbon-13 is not enriched.

If the gas under investigation contains components which decompose to form non-volatile products at high temperatures, these products could deposit at the heated point of incidence of the deuteron beam on the nickel window and at the back of the cell where high temperatures develop over small areas. The non-volatile material deposited in the path of the beam would become a source of neutrons and make accurate analysis difficult.

This work was financially supported by the South African Atomic Energy Board. One of us (P. J. S.) was supported by a bursary from the S. A. Council for Scientific and Industrial Research.

References

1. CH. ENGELMANN, *Intern. J. Appl. Rad. Isotopes*, 18 (1967) 569.
2. M. PEISACH, *Chem. Communications*, (1966) 632.
3. M. PEISACH and R. PRETORIUS, *Anal. Chem.*, 39 (1967) 650.
4. W. R. MCMURRAY, M. PEISACH, R. PRETORIUS, P. VAN DER MERWE and I. J. VAN HEERDEN, Anal. Chem., 40 (1968) 266.
5. E. MÖLLER, L. NILSSON and N. STARFELT, *Nucl. Instr. Methods*, 50 (1967) 270.
6. F. EVERLING, L. A. KOENIG, J. H. E. MATTAUCH and A. H. WAPSTRA, Nuclear Data Tables, Part I, National Academy of Sciences, Washington, 1961.
7. W. R. MCMURRAY, P. VAN DER MERWE and I. J. VAN HEERDEN, *Nucl. Phys.*, A 92 (1967) 401.
8. R. R. OWEN, U. K. AERE, EL/R-2712, 1958.

No. 26

THE USE OF ALPHA PARTICLE SCATTERING FOR THE QUALITATIVE ANALYSIS OF ELEMENTS IN SOLUTION*

By **M. PEISACH**

*Preliminary presentation in "Convention Handbook", 20th Convention S. African Chem. Inst., Durban (1967), pp. 199-207.

OPSOMMING

Ontleding deur elastiese verstrooiing van alfa-deeltjies, wat voorheen net van toepassing was tot oppervlaktelae en dun films, is gebruik vir die kwalitatiewe elementele bepaling van oplossings. 'n Mikroverstuiwer is beskrywe om die oplossing op dun selfondersteunende koolstoffolies neer te slaan. Die energiespektrum van die alfa-deeltjies wat deur 160° verstrooi is vanaf 'n bestralingsbundel van 5 MeV, is gebruik om die elemente te identifiseer.

SUMMARY

Analysis by elastic scattering of alpha particles, previously suitable only for surface films and thin layers, has been used for the qualitative elemental analysis of solutions. A micro-atomiser is described for depositing the solution onto a self-supporting thin carbon foil. The energy spectrum of alpha particles scattered through 160° from a beam of 5 MeV is used to identify the elements.

Although the elastic scattering of charged particles has been used for physical measurements for many years, it is only recently that the use of solid state detectors has so simplified the instrumentation for measuring the energy of charged particles, that the technique became readily available to chemists as a convenient tool for analysis. The potential value of the technique using surface barrier detectors[1] was demonstrated by the fact that a variety of charged particles at different energies could be used without any change in instrumentation.

With films of heavy metals, proton scattering provided an easy method for determining film thickness,[2] and by increasing the proton energy, the penetration of the particle could be increased so as to give information of the target composition at some depth below the surface.[3] For most analytical investigations of surfaces, however, alpha particles appear to be more suitable because the energy loss that alpha particles undergo is relatively greater than that of protons at corresponding incident energies, and the penetration is less, thus restricting the analysis to a smaller depth of material.[4] The rate of change of energy loss with the mass of the target nucleus was shown to be a function of the mass of the bombarding particle[5] so that the optimum resolution attainable with incident particles of equal energy measured through the same scattering angle depended not only on the mass of the target nucleus but also on the appropriate choice of bombarding particle. For the determination of alumina film thickness, for instance, it was shown that singly charged helium ions were preferable to hydrogen or nitrogen ions.[6]

The emphasis on the use of thin targets to attain good resolution has mitigated against the use of this technique for qualitative analysis because of the difficulty in producing suitable surfaces. Recently an attempt was made to obtain thin films of

organic polymers on which drops of solution could be evaporated.[7] Practical problems in preparing such samples have again emphasized the need for a technique more readily applicable to routine measurements and one which can readily be used by inexperienced personnel. This paper describes an attempt to provide a technique for the qualitative elemental analysis of solutions that would meet these requirements.

Principle of the Method. According to the classic theory of elastic scattering[8] when an incident particle of mass m and energy E is elastically scattered from a target nucleus of mass M, the energy of the scattered particle, E', is obtained from

$$\frac{E'}{E} = 1 - 2(1-\text{Cos } \theta)\ \frac{Mm}{(M+m)^2}, \quad .. \quad .. \quad .. \quad .. \quad (1)$$

where θ is the scattering angle measured in centre-of-mass coordinates, which may be obtained from the angle ϕ, in laboratory coordinates, by the relationship

$$\theta = \phi + \text{arc sin}\left(\frac{m}{M}\sin\phi\right). \quad .. \quad .. \quad .. \quad .. \quad (2)$$

From these equations it can readily be calculated that a light element such as carbon would be very suitable for a sample support because the maximum energy of an alpha particle scattered from the sample support would, for most elements, be less than that scattered from an element in the sample and would thus not interfere with the detection of the element. Obviously carbon would not be detectable in the sample, nor would the three lighter elements boron, beryllium and lithium be readily detected.

PREPARATION OF THE SAMPLE

Carbon foils. Self-supporting foils of carbon, in which alpha particles of 5 MeV lose less than 15 keV are available commercially, but can be made readily by sputtering carbon onto glass while striking an arc between carbon electrodes. The foils used in this investigation were made as follows: Microscope slides were thoroughly cleaned and mounted about 20 cm. above a tantalum boat containing barium chloride. The barium chloride was heated, in vacuum, by passing a current through the boat, and evaporated to form a thin deposit on the glass slides. Thereafter an arc was struck between two carbon electrodes placed in a similar position under the slides. By sputtering, a thin layer of carbon was built up. When sufficient carbon had been deposited, the glass slide was removed and the carbon foil floated off onto the surface of a warm 30% v/v alcohol in water mixture containing a few drops of "teepol". The high solubility of barium chloride facilitated the removal of the carbon foil and the alcohol decreased the surface tension, thus enabling the foil to be floated onto a suitable mount with a smaller danger of rupture. Foils prepared in this way usually contained traces of barium salts. Where the presence of barium interfered with the analysis, foils free from this contaminant, but showing signs of sulphur contamination, were prepared using "teepol" to coat the glass before sputtering carbon on it. The foil was mounted on a brass plate to cover a hole of 1 cm. diameter.

Deposition of the solution. Self-supporting carbon foils cannot be subjected to a direct spray from an atomiser, because the pressure from the jet is sufficient to destroy the foil. For this reason an atomiser of the design shown in Fig. 1 was used, in which

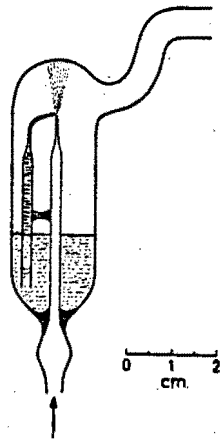

Fig. 1. Micro-atomiser for producing a mist of the solution to be analysed.

small volumes of the liquid under investigation could be atomised into a jet impinging on the inner wall of the glass. The pressure of compressed air applied at the atomiser caused a slow-moving current of air to waft tiny droplets of the liquid through the wide chimney outlet. In this way, atomised droplets could be brought into contact with and deposited on the carbon foil clamped near the outlet of the chimney.

With an applied pressure of 10 p.s.i.g., which was more than enough to operate the atomiser, the air escaping through the chimney did not damage the carbon foil. Under such conditions a few tens of micrograms material were deposited during 10 min. of spraying.

IRRADIATION AND MEASUREMENT

Foils were mounted at the centre of a hemispherical scattering chamber and irradiated in vacuum with a low intensity beam of 5 MeV alpha particles. The cross sectional area of the beam was 0·031 cm^2. The energy of scattered alpha particles was measured with a surface barrier-type silicon semiconductor detector placed at 160° to the incident beam 20 cm. from the target foil. Pulses from the detector were amplified and transmitted directly to a multichannel analyser.

A typical spectrum obtained from a solution containing a mixture of sodium, aluminium and magnesium sulphates is shown in Fig. 2A. Each element is clearly resolved and the expected peak due to barium in the carbon foil is shown at the extreme right. The peak on the extreme left is that due to the carbon foil itself. The spectrum obtained from a solution of manganese and potassium sulphates on a foil prepared without the use of barium chloride is shown in Fig. 2B.

As all measurements were made in vacuum, all volatile solvents and any volatile component would be removed. In Fig. 2A, barium was shown to be present in the foil, but no trace of chlorine could be found, because the chloride evaporated as HCl.

When the components are readily resolvable, an irradiation of a few minutes is sufficient to identify the components.

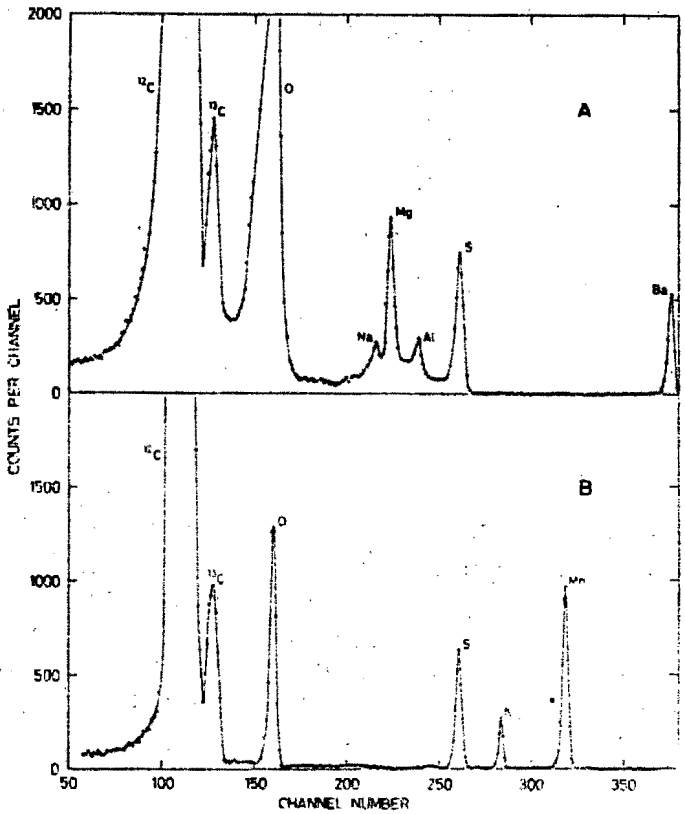

Fig. 2. Energy spectrum of 5-MeV alpha particles scattered through 160° from carbon foils on which solutions had been sprayed.

(A) Sodium, magnesium and aluminium sulphates on foils prepared with Ba Cl_2.
(B) Manganese and potassium sulphates on foils prepared with teepol.

RESOLUTION

The identification of an element depends on the precision with which the energy of the alpha particles can be determined. In the absence of interfering elements, the energy corresponding to the spectral peak could be measured with a precision of $\pm$ 16 keV. The resolution of the entire measuring system, as given by the full width at half maximum height of the spectrum peak obtained from the 5·48 MeV alpha particles from americium-241 was about 50 keV. It thus follows that the energy of a scattered alpha particle can be measured with a precision of $\pm$ 16 keV provided the sample does not contain a component, from which an alpha particle scattered

TABLE I

Energies of Alpha particles scattered from a beam of 5 MeV through an angle of 160°

Z	Element	Energy keV	Z	Element	Energy keV	Z	Element	Energy keV
6	C	1301	34	Se	4118	64	Gd	4532
7	N	1597	35	Br	4108	65	Tb	4535
8	O	1855	37	Rb	4165	66	Dy	4549
9	F	2181	38	Sr	4191	67	Ho	4551
11	Na	2529	39	Y	4199	68	Er	4554
12	Mg	2603	40	Zr	4208	69	Tm	4561
13	Al	2802	41	Nb	4231	70	Yb	4573
14	Si	2861	42	Mo	4267	71	Lu	4576
15	P	3022	44	Ru	4294	72	Hf	4587
16	S	3071	45	Rh	4300	73	Ta	4589
17	Cl	3203	46	Pd	4319	74	W	4596
19	K	3354	47	Ag	4325	75	Re	4602
20	Ca	3388	48	Cd	4363	76	Os	4612
21	Sc	3538	49	In	4369	77	Ir	4614
22	Ti	3616	50	Sn	4393	78	Pt	4617
23	V	3686	51	Sb	4398	79	Au	4621
24	Cr	3708	52	Te	4437	80	Hg	4631
25	Mn	3769	53	I	4425	81	Tl	4636
26	Fe	3788	55	Cs	4449	82	Pb	4641
27	Co	3842	56	Ba	4468	83	Bi	4643
28	Ni	3825	57	La	4472	84	Po	4644
29	Cu	3907	58	Ce	4475	88	Ra	4669
30	Zn	3922	59	Pr	4479	90	Th	4677
31	Ga	3992	60	Nd	4482	92	U	4685
32	Ge	4053	62	Sm	4515			
33	As	4065	63	Eu	4518			

under the same experimental conditions, would have an energy within $\pm$ 50 keV.

Table I lists the energies of alpha particles scattered through 160° from the most abundant isotope of each natural element from carbon to uranium, but excluding the rare gases. The uncertainty in identifying a sample component and the list of elements interfering with the identification of each are given in Table II. An element in column 1 of that Table will be reported as being the element(s) in column 2 provided no other element listed in column 3 is present in comparable concentrations. From Table II it may be seen that provided the elements in the solution to be analysed are present in comparable concentrations, a unique identification without interference

TABLE II

Uncertainties and interferences in qualitative identification

Element Present	Element(s) Reported	Atomic number(s) of interfering element(s)	Element Present	Element(s) Reported	Atomic number(s) of interfering element(s)
N	N	—	In	Cd, In	46-51
O	O	—	Sn	Sn, Sb	48-53
F	F	—	Sb	Sn, Sb	48-55
Na	Na	—	Te	Te, I, Cs	50-60
Mg	Mg	—	I	Te, I	50-58
Al	Al	—	Cs	Te, Cs	51-60
Si	Si	—	Ba	Ba, La, Ce, Pr, Nd	52-62
P	P	—	La	Ba, La, Ce, Pr, Nd	52-62
S	S	—	Ce	Ba, La, Ce, Pr, Nd	52-62
Cl	Cl	—	Pr	Ba, La, Ce, Pr, Nd	52-63
K	K	20	Nd	Ba, La, Ce, Pr, Nd	52-64
Ca	Ca	19	Sm	Sm, Eu	55-69
Sc	Sc	—	Eu	Sm, Eu, Gd	55-69
Ti	Ti	—	Gd	Eu, Gd, Tb	59-71
V	V	24	Tb	Gd, Tb, Dy	60-71
Cr	Cr	23	Dy	Tb, Dy, Hr, Er, Tm	61-74
Mn	Mn	26	Ho	Dy, Ho, Er, Tm	61-74
Fe	Fe	25, 28	Er	Dy, Ho, Er, Tm	61-75
Co	Co, Ni	28	Tm	Dy, Ho, Er, Tm, Yb, Lu	61-75
Ni	Co, Ni	26, 27	Yb	Tm, Yb, Lu, Hf	64-78
Cu	Cu, Zn	30	Lu	Tm, Yb, Lu, Hf, Ta	64-78
Zn	Cu, Zn	29	Hf	Yb, Lu, Hf, Ta, W, Re	65-82
Ga	Ga	—	Ta	Lu, Hf, Ta, W, Re	66-83
Ge	Ge, As	33	W	Hf, Ta, W, Re, Os	66-84
As	Ge, As	32, 35	Re	Hf, Ta, W, Re, Os, Ir	66-84
Se	Se, Br	33, 35, 37	Os	Re, Os, Ir, Pt, Au	70-84
Br	Se, Br	33, 34	Ir	Re, Os, Ir, Pt, Au, Hg	70-84
Rb	Rb	34, 38-40	Pt	Os, Ir, Pt, Au, Hg, Tl	70-88
Sr	Sr, Y	37, 41	Au	Os, Ir, Pt, Au, Hg, Tl	70-88
Y	Sr, Y, Zr	37-41	Hg	Pt, Au, Hg, Tl, Pb, Bi, Po	72-90
Zr	Y, Zr	37-41	Tl	Au, Hg, Tl, Pb, Bi, Po	72-92
Nb	Nb	38-42	Pb	Hg, Tl, Pb, Bi, Po	72-92
Mo	Mo	41, 44, 45	Bi	Hg, Tl, Pb, Bi, Po	72-92
Ru	Ru, Rh	42, 45-47	Po	Hg, Tl, Pb, Bi, Po	74-92
Rh	Ru, Rh	42, 44-47	Ra	Ra, Th, U	78-92
Pd	Pd, Ag	44-49	Th	Ra, Th, U	80-92
Ag	Pd, Ag	44-49	U	Ra, Th, U	80-92
Cd	Cd, In	46-51			

is possible for the elements nitrogen, oxygen, fluorine, sodium, magnesium, aluminium, silicon, phosphorus, sulphur, chlorine, scandium, titanium and gallium. Furthermore, unique identification is also possible for the following elements, provided the elements mentioned in parentheses are known to be absent:— potassium (Ca), calcium (K), vanadium (Cr), chromium (V), manganese (Fe), iron (Ni, Mn), rubidium (Se, Sr, Y, Zr), niobium (Sr, Y, Zr, Mo) and molybdenum (Nb, Ru, Rh). In all other cases there is an uncertainty in establishing the atomic number of the element ranging from ± 1 for medium weight elements, such as the pairs (Co, Ni), (Cu, Zn) and (Pd, Ag) to ± 3 for heavy elements such as Pt or Au, which could not be distinguished from Os, Ir, Hg or Tl.

CONCLUSION

The technique of analysis by elastic scattering of charged particles, which previously was useful only for the analysis of surface layers, has been extended to include the analysis of solutions. The method provides a rapid and sensitive identification of light and medium weight elements irrespective of the chemical form in which the elements occur. It suffers from the disadvantage that volatile components are lost, often before their presence can be noted.

The same technique makes it possible to prepare thin targets of any element for nuclear studies, particularly of those elements for which targets could not readily be prepared by distillation in vacuum.

Financial support from the South African Council for Scientific and Industrial Research is acknowledged.

Southern Universities Nuclear Institute,
P.O. Box 17,
Faure, Cape.

Received, September 13th, 1968.

REFERENCES

[1] M. Peisach and D. O. Poole, *Proc.* 1965 *Intern. Conf.* 'Modern Trends in Activation Analysis', College Station, Texas (1965) p. 206.
[2] M. Peisach and D. O. Poole, *J. S. African Chem. Inst.*, 1965, **18**, 61.
[3] R. F. Sippel, *Phys. Rev.*, 1959, **115**, 1441.
[4] M. Peisach and D. O. Poole, *Anal. Chem.*, 1966, **38**, 1345.
[5] M. Peisach and D. O. Poole, *Proc. 2nd Intern. Conf.* 'Electron and Ion beam Science and Technology', New York (in the press).
[6] M. Peisach, D. O. Poole and H. F. Röhm, *Talanta*, 1967, **14**, 187.
[7] F. Luthereau and J. Tousset, Report LYCEN/6647, University of Lyon, France 1966; *Compt. rend. Acad. Sc. Paris*, 1967, **264**, 77.
[8] E. Rutherford, *Phil. Mag.*, 1911, **21**, 669.

No. 27

Reprinted from

ANALYTICAL CHEMISTRY

Isotopic Determination of Calcium-48 by Deuteron Activation

TIELMAN J. de WAAL, MAX PEISACH, and RENÉ PRETORIUS
Southern Universities Nuclear Institute, P. O. Box 17, Faure, C.P., South Africa

Volume 41, Number 3
Pages 416-420, March 1969

Reprinted from **ANALYTICAL CHEMISTRY**, Vol. 41, Page 416, March 1969

Isotopic Determination of Calcium-48 by Deuteron Activation

Tielman J. de Waal,[1] Max Peisach, and René Pretorius[2]

Southern Universities Nuclear Institute, P.O. Box 17, Faure, C.P., South Africa

The biological use of the stable isotope calcium-48 for tracing required the determination of isotopic concentrations in calcium samples. The separated calcium was converted to fluoride and distilled in vacuum onto tantalum disks. After activation with 5-MeV deuterons the activities of 8.8-min ^{49}Ca gave a measure of the calcium-48 content and the 4-hour activities of scandium-43 and -44 a measure of the natural calcium content. By using the ^{42}Ca and ^{43}Ca of natural calcium as internal standard, the isotopic concentration of ^{48}Ca was determined without the need for measuring fluxes, yields, or sample weights. Milligram quantities of calcium fluoride were analyzed with a relative standard deviation of ±2.0%.

THE BIOLOGICAL half-life of calcium (*1*) is so long, 1.6×10^4 days, that the use of the radiocalcium tracers, ^{45}Ca or ^{47}Ca, is frowned upon by the medical profession for studying calcium metabolism in humans. This is especially true when healthy patients such as young children or pregnant women are involved, because the effect of long-term exposure to even relatively small amounts of radiation is not yet fully understood. The availability of stable isotopes of calcium has made it possible to carry out such investigations without exposing the patient to any radiation hazard. A calcium preparation enriched in a selected isotope is administered and thereafter the isotopic concentration in samples drawn from the patient has to be determined.

The following conditions (*2, 3*) will determine whether a stable isotopic tracer can usefully be applied: The isotope should have a relatively low abundance in nature; it should be available in adequate enrichment; it should be reasonably priced; and a method should be available whereby its isotopic concentration could be determined at the dilution pertaining to the experiment.

The heavier isotopes of calcium occur in nature in such low isotopic concentrations that each can serve as a stable isotopic tracer. The extent to which each meets the first three of the above requirements may be judged from Table I. It is clear that calcium-46 has a far higher enrichment factor than the other isotopes and thus has a wider potential use. However, although calcium-43 and -48 have lower enrichment factors than that of calcium-46, they can nevertheless be diluted over a considerable range and their much lower cost makes their use as tracer more practicable.

Calcium-43 cannot be activated with thermal neutrons because neutron capture leads to a stable product. Neutron activation has, however, been used for the determination of calcium-48 (*4, 5*) even though the method was not applicable to the isotopic determination of calcium-48 unless the total calcium content was known or separately determined. This disadvantage has been overcome by using proton activation (*6*) or by measuring the prompt neutrons emitted during proton irradiation (*7*) when the isotopic concentration of calcium-48 was determined directly, by expressing the count obtained from this isotope relative to that obtained from some other stable calcium isotope representing the total natural calcium in the same sample. By using an internal standard in this way, there are further advantages because there is then no need to know the irradiation flux, the reaction yield, or the sample weight.

[1] Formerly from the Department of Chemistry, University of Stellenbosch, C.P., South Africa. Present address, South African Titan Products (Pty) Ltd., Umbogintwini, Natal

[2] On leave at Activation Analysis Research Laboratory, Texas A & M University, College Station, Texas 77843

(1) *Health Phys.*, **3**, 161 (1960).
(2) M. Peisach and R. Pretorius, *Proc. Symp. Med. Electron. Nucl. Instr., Johannesburg, 1965*, Leech **37**, 11 (1967).
(3) W. F. Bethard, R. A. Schmitt, D. A. Olehy, S. A. Kaplan, S. M. Ling, R. H. Smith, and E. Dalle Molle, "Nuclear Activation Techniques in the Life Sciences," I.A.E.A., Vienna, 1967, p 533.
(4) E. Junod and J. Laverlochere, "Proc. 3rd Intern. Colloquium on Biology," Saclay, 1963.
(5) F. W. E. Strelow and H. Staerk, ANAL. CHEM., **35**, 1154 (1963).
(6) M. Peisach and R. Pretorius, *ibid.*, **38**, 965 (1966).
(7) W. R. McMurray, M. Peisach, R. Pretorius, P. van der Merwe, and I. J. van Heerden, *ibid.*, **40**, 266 (1968).

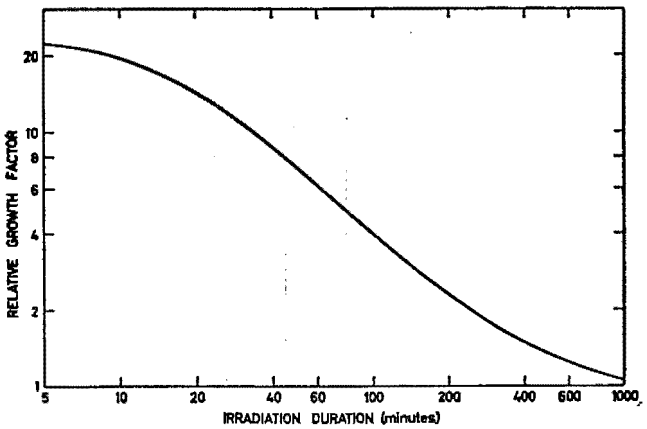

Figure 1. Variation, with duration of irradiation, of growth factor of calcium-49 relative to that of scandium-43 and -44

Proton activation (*6*) required the measurement of 4-hour scandium-43 and -44 to represent natural calcium and 44-hour scandium-48 to give the calcium-48 content. The disadvantage of this method lies in the fact that the irradiated sample has to be counted over a long period to enable the shorter-lived activities to decay, so that the scandium-48 can be measured with sufficient precision. The time required for an analysis is thus relatively long, even though many samples may be analyzed over the same period. By contrast, the method using prompt neutrons (*7*) is rapid, but the activation method may often be preferred because the instrumentation is less sophisticated.

When irradiations are carried out with deuterons of a few MeV, the cross sections of stripping reactions are usually higher than those of other reactions, so that the products most likely to be formed are from (d,p) and (d,n) reactions. If it is assumed that the cross sections for corresponding reactions with the various calcium isotopes do not differ appreciably from each other, activities formed from calcium-46 may be expected to be negligibly low because of the low natural abundance of this isotope (see Table I). If the duration of the deuteron bombardment is relatively short, say a few hours, it is not expected that significant amounts of long-lived activities would be generated and activities with very short half-lives would not be observed in samples that have to be transported some distance to the counting assembly. Accordingly, the main activities expected from the irradiation of natural calcium with deuterons are scandium-43 and -44 produced by the respective reactions

$$^{42}Ca(d,n)^{43}Sc \text{ and } ^{43}Ca(d,n)^{44}Sc$$

and calcium-49 and scandium-49 produced by the respective reactions

$$^{48}Ca(d,p)^{49}Ca \text{ and } ^{48}Ca(d,n)^{49}Sc.$$

As was the case with proton activation (*6*), the summed activities of scandium-43 and -44 could serve as a measure of the content of natural calcium in the irradiated sample. The activity of the short-lived 8.8-min calcium-49 could be used as a measure of the content of calcium-48, in contrast to the much longer-lived 44-hour scandium-48 used for the same purpose after proton activation. Deuteron activation could thus serve for determining the isotopic concentration of calcium-48 by a method which uses an internal standard and retains the simplicity of activation analysis, but requires less time than by proton activation because shorter-lived activities are involved.

Table I. Stable Isotopes of Calcium

Isotope	Natural abundance, %	Price (*8*), $ per mg[a]	% Isotopic concentration of separated isotope[a]	Enrichment factor
^{40}Ca	96.97	5.25	99.9	1
^{42}Ca	0.64	11.00	85	133
^{43}Ca	0.145	40.00	65[b]	450[b]
^{44}Ca	2.06	3.00	98	50
^{46}Ca	0.0033	640.00	31	12,000
^{48}Ca	0.18	24.00	95	500

[a] Current prices for isotopic concentrations listed. Lower isotopic concentrations are considerably cheaper.

[b] Isotopic concentrations of over 80 atom % have already been obtained from ORNL. For such samples, the enrichment factor is ~550.

If [m] denotes the activity produced from the calcium isotope of mass number m, the activity ratio, R, is given by

$$R = \frac{[48]}{[42 + 43]} = \frac{\sigma_{48}a_{48}}{\sigma_{42}a_{42} + \sigma_{43}a_{43}} \cdot F(t) \qquad (1)$$

where σ_m and a_m refer, respectively, to the reaction cross section and to the fractional abundance of the corresponding calcium isotopes in the irradiated target and

$$F(t) = \frac{1 - e^{-\lambda_1 t}}{1 - e^{-\lambda_2 t}} \qquad (2)$$

gives the growth factor of the 8.8-min activity (subscript 1) relative to that of the 4-hour activity (subscript 2), when the decay factors are λ and the duration of the irradiation is t. The variation of the growth factor with time is shown in Figure 1.

From Equation 1, it follows that for an irradiation lasting for a constant time, the activity ratio is proportional to the fractional isotopic abundance of calcium-48 if the abundance of calcium-42 and -43 are kept constant, or if it can be assumed that they are negligibly different from those in nature. This assumption is valid when the added tracer has been diluted with relatively large amounts of natural calcium and the starting material is not appreciably enriched in calcium-42 a -43. When the isotopic concentration of calcium-48 has be determined in samples where very little dilution has taken place and it is known that the fractional abundances of calcium-42 and -43 are different from those in natural calcium, Equation 1 cannot be usefully applied without a knowledge of the values a_{42} and a_{43} in the sample itself. However, just as in the use of radioactive tracers, what is usually required with stable tracers is to know the percentage, p, of the tracer that is found per gram of the analyzed sample. The value may be calculated from the equation

$$p = \frac{100\,[k_{48}^0 - L(k_{42}^0 + k_{43}^0)]}{[k_{48}^0 - L(k_{42}^0 + k_{43}^0)] - [k_{48}' - L(k_{42}' + k_{43}')]} \qquad (3)$$

where

$$L = \frac{R}{F(t)}$$

and

(8) "Catalog Radio and Stable Isotopes," Oak Ridge National Laboratory, 4th Ed., Oak Ridge, Tenn., 1963, p 62.

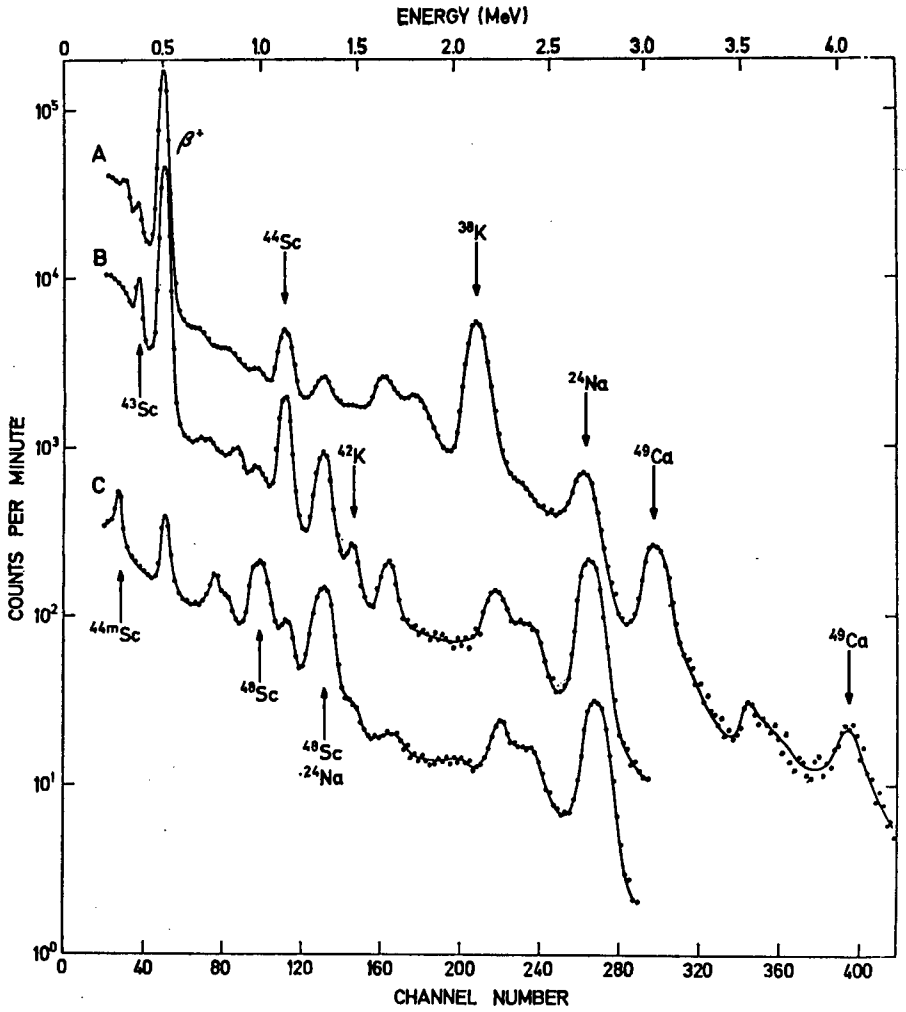

Figure 2. Typical gamma-ray spectra from deuteron irradiated natural calcium fluoride

A. t = **0.53 hours**
B. t = **3.95 hours**
C. t = **44.05 hours**

$$k_m^0 \equiv \frac{\sigma_m a_m^0}{M^0}, \qquad k_m' \equiv \frac{\sigma_m a_m'}{M'} \tag{4}$$

in which the zero superscript refers to values in natural calcium and primed superscripts to values in the original undiluted tracer. M^0 and M' are the average atomic weights of calcium in nature and in the tracer preparation, respectively.

EXPERIMENTAL

Preparation of Samples and Standards. From the chemical compounds of calcium which are refractory enough to withstand the heating effect of the deuteron beam, calcium fluoride was selected as target material because of its relatively high melting point (1360 °C) and because the only activation product from the fluorine, 11-second fluorine-20, did not interfere because it did not survive the transportation time from the irradiation site to the counting equipment. Tantalum was chosen as the backing material because it could withstand high temperatures and, at the available deuteron energies, was inert to activation.

Calcium samples were converted to fluoride by evaporation with HF in a platinum crucible, and distilled in vacuo from an electrically heated tungsten boat onto tantalum disks. Standards ranging from 0.18 to about 2 atom % calcium-48 were prepared by adding natural calcium to the enriched calcium-48 obtained from the Oak Ridge National Laboratory, U.S.A., converting them to fluoride and also distilling onto tantalum. By maintaining a constant distance between the heated boat and the tantalum disk, and by using a constant rate of heating, the weight deposited over an area of about 3 cm² could be reproduced with a relative precision of about ±4%, from equal weights of starting material. The recovery was about 10% and targets produced in this way had an average thickness between 300 and 1000 μg/cm². The variation of the thickness of the deposit did not affect the precision of the analyses. When small samples of a few milligrams were available, the microevaporator described previously (*7*) was used and yielded targets with an average thickness of about 150 μg/cm² and a recovery of about 25%.

Irradiation and Measurement. Up to 12 targets could simultaneously be irradiated on a rotating sample holder (*6*), cooled by circulating coolant, which fitted into a vacuum chamber on a beam tube of the 5.5 MV Van de Graaff accelerator at the Southern Universities Nuclear Institute. Irradiations with 5.0-MeV deuterons and beam currents between 2 and 8 μA usually lasted 2 hours.

The samples were analyzed either by gross gamma-ray counting or by gamma-ray spectrometry. Because the activated samples were pure calcium fluoride, routine analysis could be carried out by gross gamma-ray counting, when a count, [48], was obtained with a discriminator in the counting assembly set to record only pulses from gamma-rays above 2.90 MeV. The count, [42 + 43], was obtained with a single channel analyzer set to record pulses from positron annihila-

tion radiation. The activities at the end of the irradiation were computed from the decay data by a program using the criterion of maximum likelihood (*9*).

GAMMA-RAY SPECTROMETRY

Typical gamma-ray spectra obtained from the decay of a deuteron irradiated sample of natural calcium fluoride are shown in Figure 2. Some minutes after irradiation, the most prominent peaks in the spectrum (Curve *A*) indicated the presence of 7.7-min potassium-38, 8.8-min calcium-49, and 4-hour scandium-44. The large photopeak from positron annihilation was due to ^{38}K, ^{43}Sc, and ^{44}Sc. Gamma-rays from sodium-24 were due to sodium impurity in the tantalum. Although 57.5-min scandium-49 was produced, its presence was not shown by gamma-ray counting because the intensity of its 1.76 MeV gamma-ray, 0.03 gamma-rays per 100 disintegrations (*10*), is too low to be observed in the comparatively high Compton continuum, and because its beta-particles could not penetrate the "Perspex" absorber of 1.5 g/cm^2 around the scintillation detector.

After 3.95 hours, (Figure 2, Curve *B*), when the two short-lived components had decayed, the photopeak from scandium-44 was still very prominent, and the presence of 3.9-hour scandium-43 was indicated by a smaller photopeak at 0.37 MeV. Potassium-42, from the nuclear reaction ^{44}Ca(d,α)^{42}K, was identified by gamma-rays of 1.52 MeV.

The spectrum recorded 44.05 hours after irradiation (see Figure 2, Curve *C*), showed the presence of 44-hour scandium-48, formed by the reaction ^{48}Ca(d,2n)^{48}Sc. Gamma-rays of 0.27 MeV were due to 2.4-day scandium-44m, the presence of which explains the persistence of the characteristic photopeaks of 4-hour scandium-44.

The identity of each radionuclide was confirmed by half-life measurements and by irradiating targets highly enriched in the corresponding calcium isotope. The activities found by irradiating natural calcium fluoride with deuterons of 5.0 MeV are summarized in Table II.

ACCURACY AND PRECISION

The value of [48] was expected to include only the counts obtained from the decay of calcium-49. However, because of the presence of both ^{38}K and ^{24}Na in the irradiated sample, random coincidences added to the measured count. Pulses from sodium-24, which decayed with a half-life long compared to that of calcium-49, merely served to raise the effective background level somewhat, and could thus be eliminated by subtraction. The count rate of potassium-38 decayed at a rate comparable to that of calcium-49 and could not be similarly eliminated. Accordingly, the value of [48] always included counts from potassium-38.

Calcium-40, the target isotope from which potassium-38 is formed, makes up almost 97% of natural calcium and this value does not change appreciably, provided the extent of enrichment of calcium-48 is not too high—i.e., a_{40} can be considered to be constant and, hence, from Equation 1 under constant irradiation conditions,

$$\frac{[40]}{[42 + 43]} = \frac{\sigma_{40}a_{40}}{\sigma_{42}a_{42} + \sigma_{43}a_{43}} \cdot F_1(t) = \text{constant} \qquad (5)$$

(9) R. G. Monk, A. Mercer, and T. Downham, ANAL. CHEM., **35**, 178 (1963).
(10) I. Rezanka, J. Frana, M. Vobecky, and A. Mastalka, *J. Inorg. Nucl. Chem.*, **18**, 13 (1961).

Table II. Activities Observed in Natural Calcium Irradiated with Deuterons of 5 MeV

Product nuclide	Half life	Main gamma-ray energies (MeV)	Reaction
^{38}K	7.7 min	(β^+), 2.20	^{40}Ca(d,α)
^{49}Ca	8.8 min	3.10, 4.05, 4.70	^{48}Ca(d,p)
^{43}Sc	3.9 hour	(β^+), 0.37	^{42}Ca(d,n)
^{44}Sc	4.0 hour	(β^+), 1.16	^{43}Ca(d,n)
^{42}K	12.4 hour	1.52	^{44}Ca(d,α)
^{48}Sc	44 hour	0.99, 1.04, 1.31	^{48}Ca(d,2n)
^{44m}Sc	2.4 days	0.27	^{43}Ca(d,n)

where $F_1(t)$ is the relative growth factor of the 7.7-min potassium-38. The measured ratio of activities may then be written as

$$R = \frac{[48] + [40]}{[42 + 43]} = C_1 \cdot a_{48} + C_0$$

where C_0 and C_1 are constants.

This relationship was confirmed experimentally when a calibration plot of "activity ratio" against "atom per cent calcium-48" was linear, but had an extrapolated value of 1.2 at zero calcium-48 content. The absolute value of the intercept, C_0, was a function of the irradiation and measuring conditions, and accordingly had to be determined with each set of analyses where experimental conditions may have been altered. These corrections, due to other activities in the sample, decreased the precision of determining [48].

The measurement of [42 + 43] as a single radioactive species did not increase the relative errors of the results. Also, because of the relatively low total activities of the samples, photoproduction of positrons by high energy gamma-rays in shielding and other materials, was negligible. Added counts were, however, obtained from Compton-scattered gamma-rays of higher energy from longer-lived radionuclides in the target, but such counts were treated as an added background and were eliminated by subtraction.

Some typical results are shown in Table III, which includes results obtained from five replicate analyses of a calcium carbonate sample (0.946 atom %). The slope of the calibration line was 4.286 per atom per cent, which is in agreement with the mean value in Table III, 4.270, within the precision of the method. The relative standard deviation was ±2.03%. This precision is sufficient to measure an increase of somewhat more than 10% in the isotopic concentration of calcium-48 in natural calcium. The accuracy of the method may be judged from the low value of the mean error, −0.0006 atom %, and from the statistical evaluation of results which showed no bias.

ADVANTAGES AND DISADVANTAGES

The method is comparatively fast, accurate, and nondestructive. Like all methods using internal standards, the weight of the irradiated sample, the irradiation flux, or the reaction cross sections need not be known. It is, however, essential that samples and standards be irradiated at the same energy and measured under the same conditions. The method requires at least two standards of known calcium-48 concentration, but one of them could be natural calcium. The thickness of the sample does not have an effect on the precision of the result, if it is between 300 and 1000 μg per cm^2.

The method is applicable to all concentrations of calcium-48. The activity of calcium-49 in highly enriched samples

Table III. Some Results of Calcium-48 Determinations

Known ^{48}Ca concn, atom %, *A*	Activity ratio	Net activity ratio per atom %	Found ^{48}Ca concn, atom %, *B*	Error, *B* − *A*	Relative error, %
0.180	1.981	4.261	0.179	−0.001	−0.6
0.180	1.972	4.211	0.177	−0.003	−1.7
0.200	2.040	4.130	0.193	−0.007	−3.5
0.403	2.895	4.171	0.392	−0.011	−2.7
0.608	3.814	4.276	0.607	−0.001	−0.2
0.802	4.553	4.163	0.779	−0.023	−2.9
0.946	5.415	4.441	0.980	+0.034	+3.6
0.946	5.277	4.295	0.948	+0.002	+0.2
0.946	5.317	4.337	0.957	+0.011	+1.2
0.946	5.198	4.211	0.929	−0.017	−1.8
0.946	5.304	4.323	0.954	+0.008	+0.9
1.024	5.583	4.267	1.019	−0.005	−0.5
1.151	6.295	4.414	1.185	+0.034	+3.0
1.604	8.161	4.331	1.621	+0.017	+1.1
1.786	8.811	4.254	1.772	−0.014	−0.8
1.939	9.418	4.231	1.914	−0.025	−1.3

ean error = −0.0006 atom %.
ean activity ratio per atom % = 4.27 ± 0.09.
elative standard error = ±2.03%.

ay become very great compared to that of the 4-hour activity, thereby decreasing the precision with which the latter n be determined. In such cases the irradiation time may increased to obtain higher activities of ^{43}Sc and ^{44}Sc without appreciably altering the yield of ^{49}Ca.

It is a disadvantage that microgram quantities cannot be analyzed. At least 1 mg of calcium fluoride is required to make a target.

POSSIBLE INTERFERENCES

Apart from potassium-38, the generation of which is unavoidable, no other radionuclide with approximately the same half-life and gamma-ray energy can interfere with the measurement of calcium-49.

Many positron-emitting radionuclides with half-lives between ? and 6 hours can be generated with 5-MeV deuterons interfere with the measurement of the activities of m-43 and -44. The number may be considerably reif the nature and relative scarcity of target nuclides are into account. If inert gases and relatively rare ele- and isotopes are excluded and if it is considered that the elements with high atomic numbers have such large Coulomb barriers that the reaction cross sections at relatively low deuteron energies become negligibly small, the serious non-isotopic contaminants remaining are nickel (^{60}Ni) and tin (^{116}Sn), and, to a lesser extent, zinc (^{70}Zn), strontium (^{84}Sr), and cadmium (^{106}Cd). If any of these elements is present in such amounts that the radioactive products can be detected by gamma-ray spectroscopy, correction for their contribution to the count, [42 + 43], can be effected.

Contamination from other calcium salts constitutes the most serious danger. Such contamination will reduce the *accuracy* of the analysis without the analyst being aware of it.

RECEIVED for review August 19, 1968. Accepted November 12, 1968. Parts of this work were included in a Master's thesis (by T. J. de W.) and a doctorate thesis (by R. P.) presented to the Chemistry Department, University of Stellenbosch, and are published with their permission. The financial assistance of the South African Atomic Energy Board is acknowledged.

No. 28

THE DETERMINATION OF STABLE CALCIUM ISOTOPES BY CHARGED PARTICLE IRRADIATION

Max Peisach and Rene Pretorius[1]

Southern Universities Nuclear Institute
P. O. Box 17, Faure, C.P.
South Africa

MODERN TRENDS IN ACTIVATION ANALYSIS

Proceedings of the 1968 International Conference
held at the National Bureau of Standards
Gaithersburg, Maryland, October 7–11, 1968

James R. DeVoe, Editor
Philip D. LaFleur, Assistant Editor

Institute for Materials Research
Analytical Chemistry Division
National Bureau of Standards
Washington, D.C. 20234

Volume II of 2 Volumes

National Bureau of Standards Special Publication 312, Volume II

Nat. Bur. Stand. (U.S.) Spec. Publ. 312, Vol II, 676 pages (June 1969)

CODEN: XNBSA

Issued June 1969

THE DETERMINATION OF STABLE CALCIUM ISOTOPES BY CHARGED PARTICLE IRRADIATION

Max Peisach and Rene Pretorius[1]

Southern Universities Nuclear Institute
P. O. Box 17, Faure, C.P.
South Africa

I. Introduction

Calcium is not only the fifth most abundant element in the earth's crust [1], it is also the most abundant metal in the human body, where it makes up about 1.5% of the body weight [2]. In many systems the role of calcium can best be studied by tracer techniques using either radioactive or stable isotopes but, in biomedical research, stable isotopes are preferred due to the reluctance of the medical profession to administer radioactive material to humans.

Because the heavier isotopes of calcium occur in such low concentrations in nature, preparations enriched in calcium-43, 46 or 48 are suitable for tracing purposes. Neutron activation methods have been used for determining calcium-48 [3-6] and calcium-46 [7], but these methods require a separate determination of total calcium content. No activation method for the isotopic determination of calcium-43 has previously been reported.

II. Experimental

A. Preparation of Samples and Standards

Calcium separated from biological material as oxalate or carbonate was dissolved in dilute hydrochloric acid and converted to calcium fluoride by evaporation with hydrofluoric acid in a platinum crucible. The calcium fluoride was evaporated in vacuum onto tantalum discs for proton or deuteron irradiation and on aluminium foils for alpha activation. Target thicknesses were approximately 1 mg/cm^2.

Standards were similarly prepared from enriched calcium isotopes as obtained from the Oak Ridge National Laboratory, U.S.A., and diluted with natural calcium to the required isotopic concentration.

---

[1] Presently at Activation Analysis Research Laboratory, Texas A&M University, College Station, Texas 77843.

B. Activation

Proton and deuteron activation was carried out with the 6 MeV Van de Graaff accelerator at the Southern Universities Nuclear Institute, and alpha activation at the cyclotron of the Council for Scientific and Industrial Research at Pretoria where energies up to about 32 MeV could be attained. Irradiations lasted up to 2 hours and beam currents between 2 and 5 μA were used.

Samples were mounted on a rotating target holder (Fig. 1), cooled by circulating water or air. Up to 12 samples were irradiated simultaneously. After irradiations, samples were analyzed either by gamma-ray spectrometry or gross gamma-ray counting, with a 3 in. × 3 in. NaI(Tl) scintillation detector. The enhanced resolution afforded by Ge(Li) detectors was not needed in this investigation.

C. Prompt Neutrons

The energy of the prompt neutrons emitted during irradiation was measured by the time-of-flight technique [8]. The neutron energy, E_n(MeV), may be obtained from the time (nanoseconds) taken by the neutron to traverse a fixed known distance d (meters), by the non-relativistic relationship;

$$E_n = \left(\frac{72.3 \times d}{t}\right)^2$$

Proton beams in pulses of 4 nsec duration, 400 nsec apart were obtained from the Van de Graaff accelerator. Targets were irradiated singly with average beam currents between 0.6 and 3.0 μA.

III. Results and Discussion

The determination of isotopic concentrations as described here is based on measuring a ratio of either activities or prompt neutron counts. It is thus unnecessary to determine the total calcium content separately. Furthermore, no yields, weights of targets, or irradiation fluxes need to be known.

Flux variation during irradiation would affect the activity ratios in samples irradiated singly. However, when the samples and standards are irradiated together, flux variations would only result in a calibration line with a different slope. In the case of prompt neutron measurement (see below), the flux variation during irradiation produces no effect because the decay of the product nuclides is not involved.

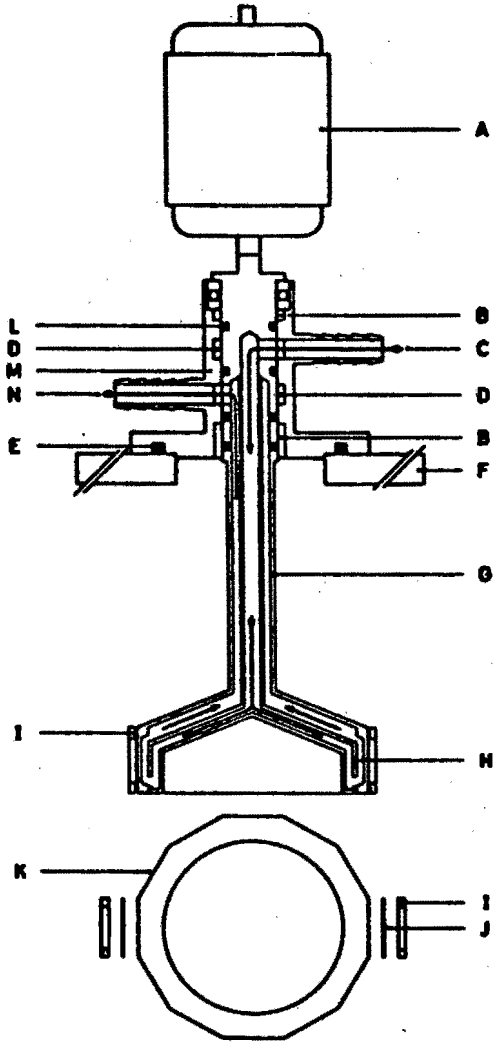

Figure 1. Rotating target holder.

A. Motor and gear box
B. Nylon bearings
C. Water inlet
D. Water chamber
E. Vacuum seal
F. Base plate
G. Rotating cooled target holder
H. Cooling water stream guide
I. Target clamps
J. Target
K. Flats (12) for mounting targets
L. Water and vacuum seals
M. Target holder support
N. Water outlet

A. Proton Activation

Activation of calcium samples, with 4.75 MeV protons leads to the formation of 44 hour scandium-48 and 4 hour scandium-44 and 43, from

(p,n) reactions on calcium-48, 44 and 43, respectively. The ratio of the 44 to 4 hour activity gives a measure of the isotopic concentration of calcium-48. Activities from other calcium isotopes, fluorine, or from the tantalum backing do not interfere.

Scandium-44 activity does not form at proton energies below about 4.56 MeV and analysis of calcium-43 as tracer is possible at such energies [9]. Although at higher proton energies scandium-44 activity interferes with the determination of calcium-43, its formation is advantageous for the determination of calcium-48, as the precision with which the 4 hour activity representing total calcium is measured, is improved.

Table 1 shows some results for the determination of calcium-48 and 43 by proton activation at energies of 4.75 and 4.50 MeV, respectively. The relative standard deviation over the concentration range from natural

Table 1. The determination of calcium–43 and 48.

I Known concentration (atom %)	Activity ratio	Activity ratio per unit (atom %)	II Measured concentration (atom %)	Observed difference (II – I)
Calcium–48; Ep = 4.75 MeV [8] (× 100)				
0.185	4.75	0.257	0.188	+ 0.003
0.192	4.83	0.252	0.191	– 0.001
0.375	9.32	0.249	0.369	– 0.006
0.825	21.57	0.262	0.854	+ 0.029
1.040	26.38	0.254	1.045	+ 0.005
1.370	33.15	0.242	1.313	– 0.057
Calcium–43; Ep = 4.50 MeV [9] (× 1)				
0.145	1.97	9.13	0.149	+ 0.004
0.379	3.98	8.79	0.376	– 0.003
1.004	9.56	8.87	1.006	+ 0.002
1.769	16.41	8.91	1.780	+ 0.011
2.010	18.46	8.86	2.012	+ 0.002

Calcium–48: Relative standard deviation = ± 2.7%
Mean error = – 0.004 atom %

Calcium–43: Relative standard deviation = ± 3.2%
Mean error = + 0.003 atom %

abundance to about 2 atom % was ± 2.7% for calcium-48 and ± 3.2% for calcium-43.

B. Deuteron Activation

When deuterons are used for activation, many radionuclides are produced from the stable isotopes of calcium. Of these, calcium-48 can be separately determined by measuring the high energy gamma rays of 8.8 minute calcium-49 formed by the reaction $^{48}Ca(d,p)^{49}Ca$. The 4 hour activity produced from calcium-42 and 43 served as a measure of total natural calcium and was determined by counting annihilation gamma rays [10].

A typical set of results for determining calcium-48 by deuteron activation is given in Table 2 where the activity ratio in column 2 represents the ratio of the 8.8 minute activity to the 4 hour activity. The relative standard deviation for the determination of calcium-48 concentrations ranging from natural (0.18%) to about 2 atom % was about ± 2%. The advantage of deuteron activation analysis over proton activation is its shorter duration because shorter-lived radionuclides are involved.

Table 2. Some determinations of calcium–48 by deuteron activation

I ^{48}Ca conc. known (atom %)	Activity ratio	Activity ratio per unit (atom %)	II ^{48}Ca conc. found (atom %)	Difference (II – I)	Relative error (%)
0.180	1.981	4.261	0.179	– 0.001	– 0.6
0.180	1.972	4.211	0.177	– 0.003	– 1.7
0.200	2.040	4.130	0.193	– 0.007	– 3.5
0.403	2.895	4.171	0.392	– 0.011	– 2.7
0.946	5.415	4.441	0.980	+ 0.034	+ 3.6
0.946	5.277	4.295	0.948	+ 0.002	+ 0.2
1.604	8.161	4.331	1.621	+ 0.017	+ 1.1
1.786	8.811	4.254	1.772	– 0.014	– 0.8

Number of samples in test series	= 16
Number of analyses in test series	= 25
Mean activity ratio per atom %	= 4.27 ± 0.09
Mean error	= – 0.0006 atom %
Relative standard error	= ± 2.03%
Slope of calibration line	= 4.286 per atom %
Intercept of calibration line; Activity ratio	= 1.214

C. Alpha Activation

Alpha activation was found to be unsuitable for the determination of calcium tracers, because of the formation of intense activities of scandium-43 from the most abundant calcium isotope, calcium-40, by the reaction $^{40}Ca(\alpha,p)^{43}Sc$.

However, this reaction could well serve for the determination of calcium-40. The variation of the yield of scandium-43 activity, formed by the reaction $^{40}Ca(\alpha,p)^{43}Sc$, with alpha particle energy is shown in Figure 2 from which it can be seen that the most favorable energy at which total calcium could be determined would be at about 14 MeV.

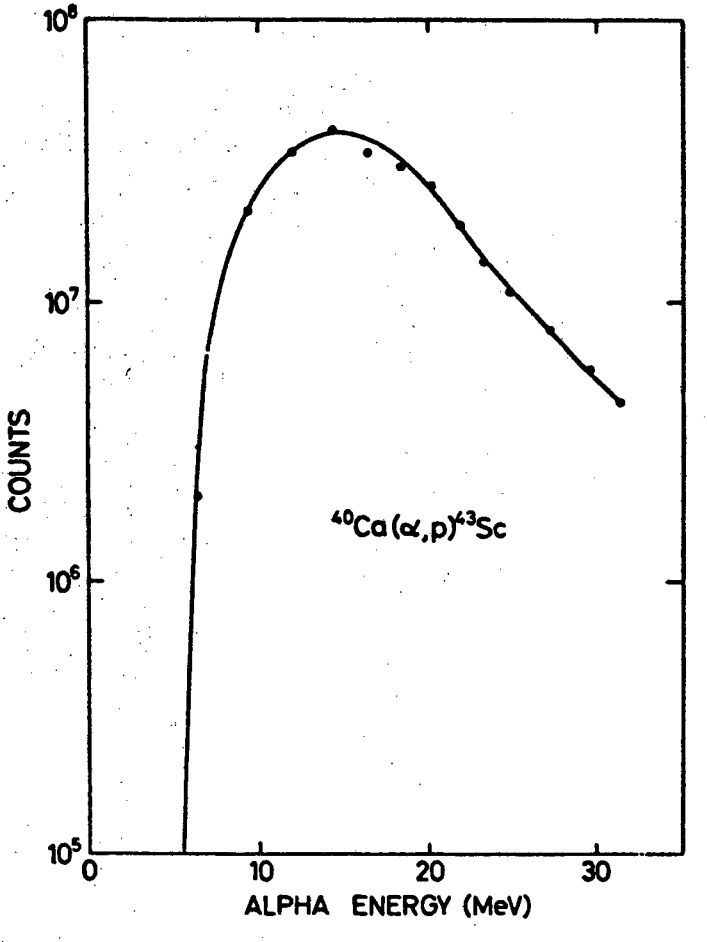

Figure 2. The variation of scandium-43 activity, formed by the reaction $^{40}Ca(\alpha,p)^{43}Sc$, *vs.* alpha irradiation energy.

D. Prompt Neutron Measurement

Time-of-flight spectra of neutrons emitted from calcium-43, calcium-48 and natural calcium targets irradiated with protons of 4.5 MeV are shown in Figure 3. At this bombarding energy neutrons from sources other than calcium-43 and calcium-48 could not be observed [11].

The net integrated counts of neutrons between 1.267 and 1.642 MeV (corresponding to the n_0 and n_1 neutron groups from calcium-43 and

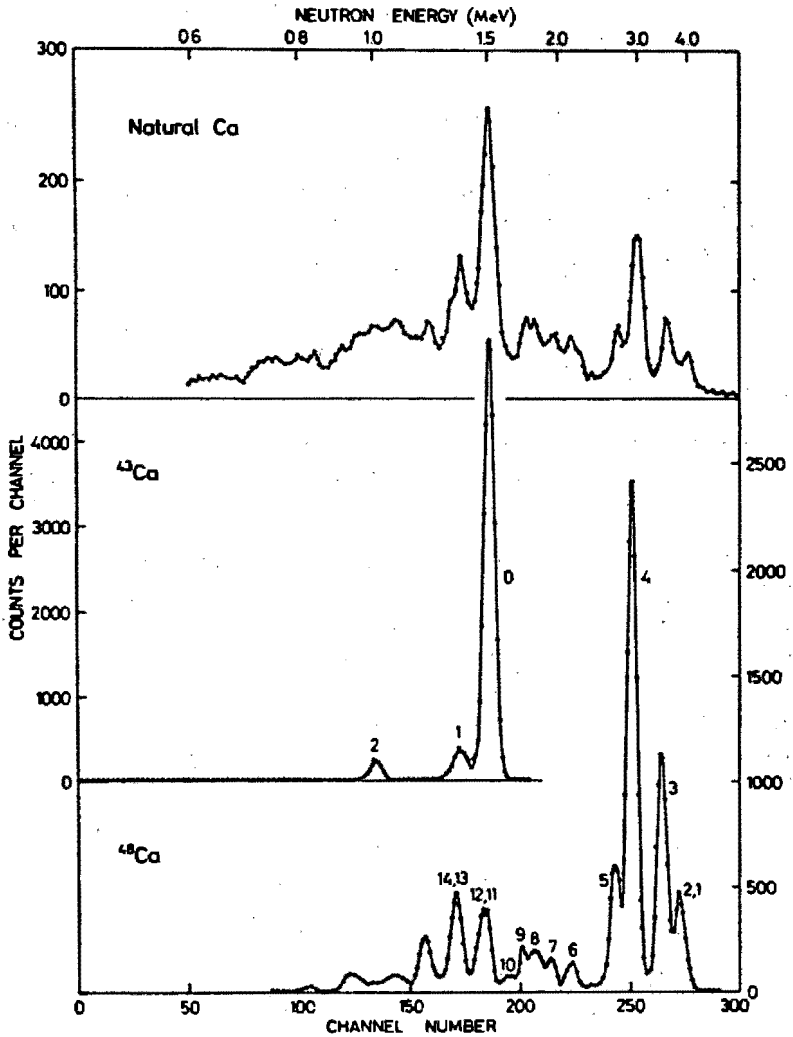

Figure 3. Time-of-flight spectra of neutrons from (p,n) reactions on targets of natural-calcium and enriched ^{43}Ca and ^{48}Ca, Ep = 4.5 MeV, $\theta = 0°$; d = 2.991 meters [11].

including the n_{10} to n_{14} neutron groups from calcium-48, see Figure 3) is used as a measure of the calcium-43 concentration. The net integrated count from higher energy neutrons with energies between 2.416 and 4.151 MeV was used as a measure of calcium-48.

Results for the determination of calcium-43 are given in Table 3. The value in column 2 is the ratio of neutron counts representing calcium-43 to those representing calcium-48. A relative standard deviation of 4.34% was found for calcium-43 concentrations ranging from 0.145 (natural) to 2 atom of calcium-43 which represents total calcium, the internal ratio method is only applicable for comparatively low enrichments of calcium-48 up to about 0.4 atom ratio method. Although the time required to analyze a single sample by prompt neutron measurement is considerably shorter than by activation, the method cannot be applied to more than one sample at a time.

Table 3. Some determinations of calcium–43 by prompt neutron measurement.

I ^{43}Ca conc. known (atom %)	Neutron count ratio	Neutron count ratio per atom %	II ^{43}Ca conc. found (atom %)	Difference (II – I)	Relative error (%)
0.145	0.945	2.400	0.146	+ 0.001	+ 0.7
0.145	0.940	2.366	0.144	−0.001	−0.7
0.320	1.330	2.291	0.308	−0.012	−3.8
0.490	1.772	2.398	0.494	+ 0.004	+ 0.8
1.058	3.123	2.388	1.062	+ 0.004	+ 0.4
1.216	3.642	2.504	1.280	+ 0.064	+ 5.3
1.430	3.884	2.299	1.382	−0.048	−3.4
1.990	5.483	2.455	2.055	+ 0.065	+ 3.3

Number of samples in test series	= 15
Number of analyses in test series	= 24
Mean neutron count ratio per atom %	= 2.372
Mean error	= −0.0004 atom %
Relative standard error	= ± 4.34%
Slope of calibration line	= 2.378 per atom %
Intercept of calibration line; count ratio	= 0.597

IV. References

[1] Holmes, A., "Principles of Physical Geology", Thomas Nelson and Sons Ltd., London, 1964, p. 35.
[2] Health Physics, Official Journal of the Health Physics Society 3, 146 (1960).
[3] Junod, E., and Laverlochere, J., "Proceed. 3rd Intern. Coll. on Biology", Saclay 1963.
[4] Strelow, F. W. E., and Staerk, H., Anal. Chem. 35, 1154 (1963).
[5] Amiel, S., and Juliano, J. O., Israel Atomic Energy Commission, Rept. IA-933 (1964).
[6] Corless, J. T., Anal. Chem. 38, 810 (1966).
[7] Bethard, W. F., Schmitt, R. A., Olehy, D. A., Kaplan, S. A., Ling, S. M., Smith, R. H., and Dalle Molle, E., "Proceedings Symposium on Nuclear Activation Techniques in the Life Sciences", Amsterdam, 1967, p. 533.
[8] Peisach, M., and Pretorius, R., Anal. Chem. 39, 650 (1967).
[9] Brits, R. J. N., and Peisach, M., Unpublished data (1968).
[10] De Waal, T. J., Peisach, M., and Pretorius, R., Unpublished data (1968).
[11] McMurray, W. R., Peisach, M., Pretorius, R., van der Merwe, P., and van Heerden, I. J., Anal. Chem. 40, 226 (1968).

No. 29

SURFACE ANALYSIS OF MEDIUM WEIGHT ELEMENTS BY PROMPT CHARGED PARTICLE SPECTROMETRY

Colenso Olivier [1] and Max Peisach

Southern Universities Nuclear Institute
P.O. Box 17, Faure, C.P.
South Africa

MODERN TRENDS IN ACTIVATION ANALYSIS

Proceedings of the 1968 International Conference
held at the National Bureau of Standards
Gaithersburg, Maryland, October 7–11, 1968

James R. DeVoe, Editor
Philip D. LaFleur, Assistant Editor

Institute for Materials Research
Analytical Chemistry Division
National Bureau of Standards
Washington, D.C. 20234

Volume II of 2 Volumes

National Bureau of Standards Special Publication 312, Volume II

Nat. Bur. Stand. (U.S.) Spec. Publ. 312, Vol II, 676 pages (June 1969)

CODEN: XNBSA

Issued June 1969

SURFACE ANALYSIS OF MEDIUM WEIGHT ELEMENTS BY PROMPT CHARGED PARTICLE SPECTROMETRY

Colenso Olivier [1] and Max Peisach

Southern Universities Nuclear Institute
P.O. Box 17, Faure, C.P.
South Africa

I. Introduction

The limited penetration of charged particles with energies of a few MeV makes them suitable for the analysis of surface layers. Use has already been made of this property for the determination of surface concentrations of elements by the spectroscopy of elastically scattered charged particles [1-5]. Such methods have the advantage that small bombarding currents and short irradiations are sufficient for the analysis because charged particle scattering cross sections are usually large compared with reaction cross sections. However, the application is limited to the cases where the targets are light elements or the elements have widely differing mass numbers because the differential change of the energy of the scattered particle with the mass of the scatterer decreases with increasing target mass number [6]. In particular the method is of little use for the analysis of thick targets of the medium weight elements where both the surface element and the thick support have mass numbers between 50 and 70.

When charged particles induce nuclear reactions in surface layers the prompt charged particle products can best serve for an analytical method to determine surface concentrations because the energy of the product particle at the detector is determined not only by the energy of the bombarding particle and the nuclear reaction concerned, but also by the amount of energy lost by the bombarding particle in the target material before the nuclear reaction occurs and by the energy lost by the product particle between the points of its formation and detection. If prompt neutrons are measured, only energy lost in the first part of the path is likely to play a role in depth resolution. In this investigation the method using prompt protons from (d,p) reactions was evaluated for the determination of nickel films on copper and chromium films on nickel.

[1] Present address: Department of Chemistry, University of Stellenbosch, Stellenbosch, C.P., South Africa. This work forms part of the doctoral thesis to be submitted to the University of Stellenbosch by C. O. and is published with permission.

II. Experimental

A. Preparation of Standards

Standard thicknesses of nickel on copper and tantalum, of copper on tantalum and of chromium on nickel and tantalum were prepared by electroplating and weighing. Surface film thicknesses ranging from 10 to 5000 $\mu g/cm^2$ were used. These targets were irradiated in a 75-cm scattering chamber with a current of 0.5 to 1 μA of deuterons of 3.5 MeV obtained from the Van de Graaff accelerator of the Southern Universities Nuclear Institute.

B. Measurement

The energy of the protons formed by (d,p) reactions on the target and emitted at an angle, θ, to the bombarding beam was measured with a silicon semiconductor detector with a depletion layer of 700 μm and a resolution of less than 45 keV. This detector could measure protons up to 7 MeV. Since all the (d,p) reactions concerned were highly exoergic, in most cases the protons were produced with energies in excess of the range over which the available detector could be used. It was thus necessary to reduce the energy of the protons by covering the detector surface with a gold absorber of a suitable thickness. This absorber also served to eliminate relatively large fluxes of scattered deuterons. The appropriate thickness of absorber required for a detector was calculated from the known stopping power for protons [7]. A typical pair of curves showing the effect of gold thickness on the range of proton energies that could be measured with a detector capable of measuring up to 6 MeV protons, is shown as an example in Figure 1.

III. Results and Discussion

A. Energy Spectra of Prompt Protons

Typical spectra obtained from thin films of Cr, Ni and Cu on tantalum backings and of the protons from the backing itself are shown in Figure 2. The proton groups, p_i, refer to the ith excited state in which the product nuclide was formed, and the nuclide labelled in the figure refers to the target nuclide.

A common feature of the spectra in Figure 2 is the large extent to which the energy of each proton group had been broadened by the use of the absorber. However, the resolution was still sufficient to distinguish each target element.

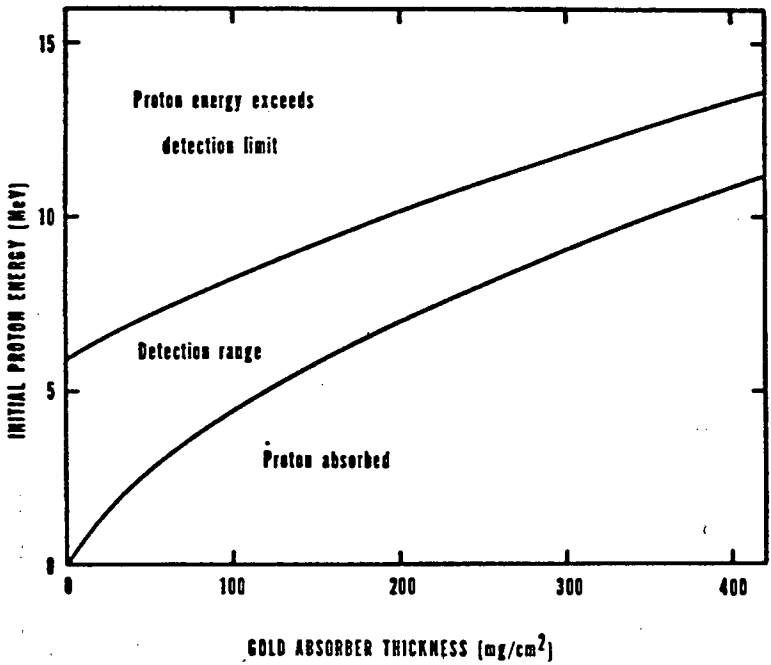

Figure 1. The effect of absorber thickness on the proton energy range that could be measured with a silicon semiconductor detector capable of measuring up to 6 MeV protons.

Tantalum backings were used because the Coulomb barrier for such a heavy element ($Z = 73$) was large. The cross section of the (d,p) reaction at 3.5 MeV was expected to be so small that prompt protons from it would be undetectable. This was not quite the case (see Figure 2).

The high energy peak from protons of the reaction $^{53}Cr(d,p_o)$ was observed, but was not included in Figure 2 for the sake of uniformity. The high abundance of chromium-52 and the comparatively large cross section of the reaction $^{52}Cr(d,p_o)$ gave rise to a prominent peak characteristic of this element and suitable for use for analytical purposes.

The energy spectrum obtained from nickel shows peaks which could be ascribed to protons from the two most abundant isotopes of reactions leading to the ground states and the first few excited levels. The peak marked Z is from reactions leading to higher levels which were not resolved.

No characteristic peak was found in the prompt proton spectrum of copper. The two unresolved peaks are due to protons from reactions leading to a large number of relatively closely spaced excitation states. The energy corresponding to the point X, refers to the maximum proton energy obtainable from ^{63}Cu under the conditions of the experiment, and Y to the corresponding energy for ^{65}Cu.

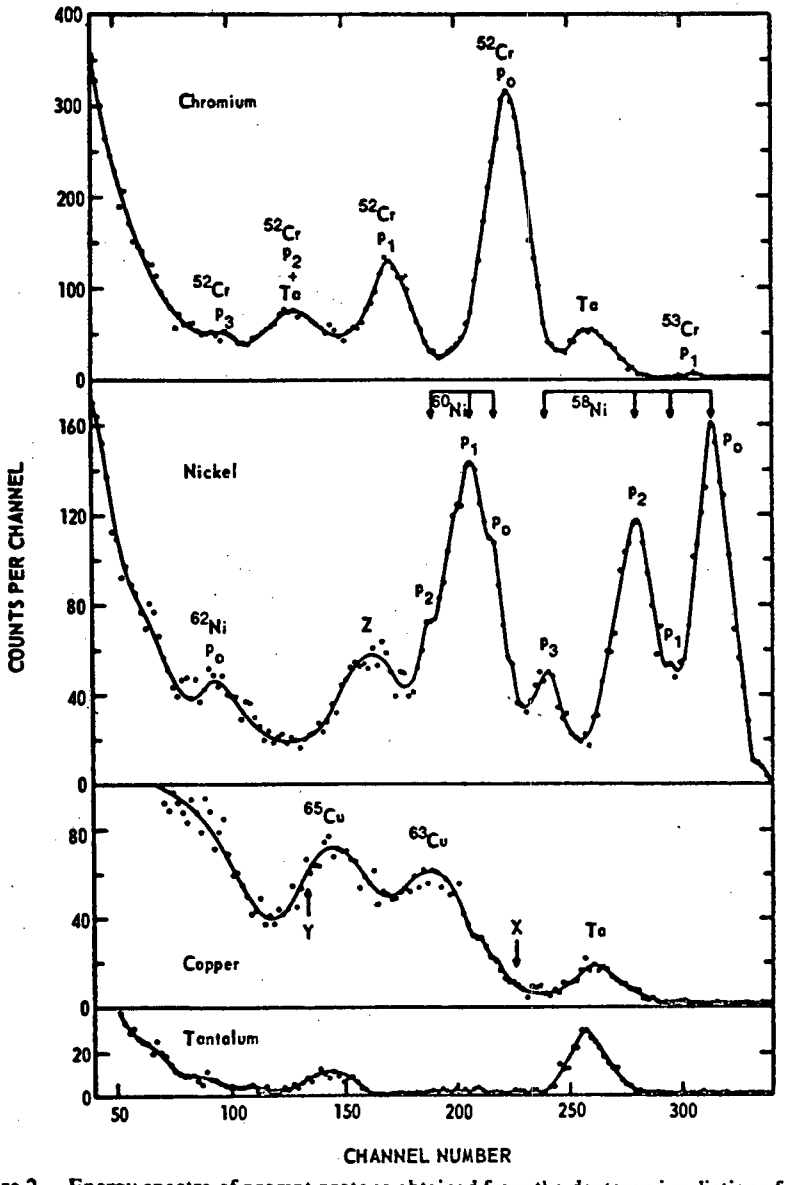

Figure 2. Energy spectra of prompt protons obtained from the deuteron irradiation of thin layers of chromium, nickel and copper on tantalum.

B. Analyses

The analysis of surface nickel on copper was of prime concern. A typical spectrum obtained from a film of nickel, about 300 $\mu g/cm^2$ thick on copper is shown in Figure 3. The peaks due to protons from nickel can readily be distinguished from those of copper. A measure of the nickel

thickness was obtained by integrating the counts over the "observed" proton energy range from 4.86 to 6.30 MeV, corresponding to "initial" proton energies between 9.36 and 10.32 MeV.

The calibration showing the variation of proton counts with nickel thickness is shown in Figure 4. The curve reflects the decreased yield

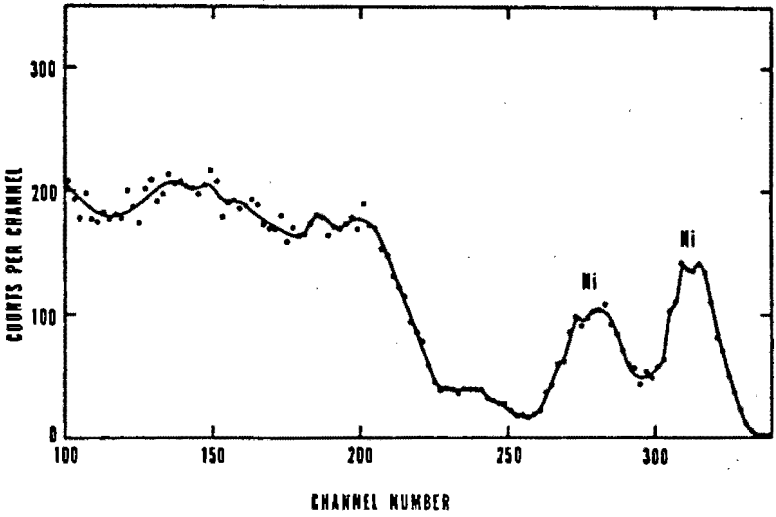

Figure 3. Energy spectrum of prompt protons obtained from a deposit of nickel on a copper backing irradiated with deuterons. $\theta=60°$, $E_d=3.5$ MeV, Au absorber = 196 mg/cm².

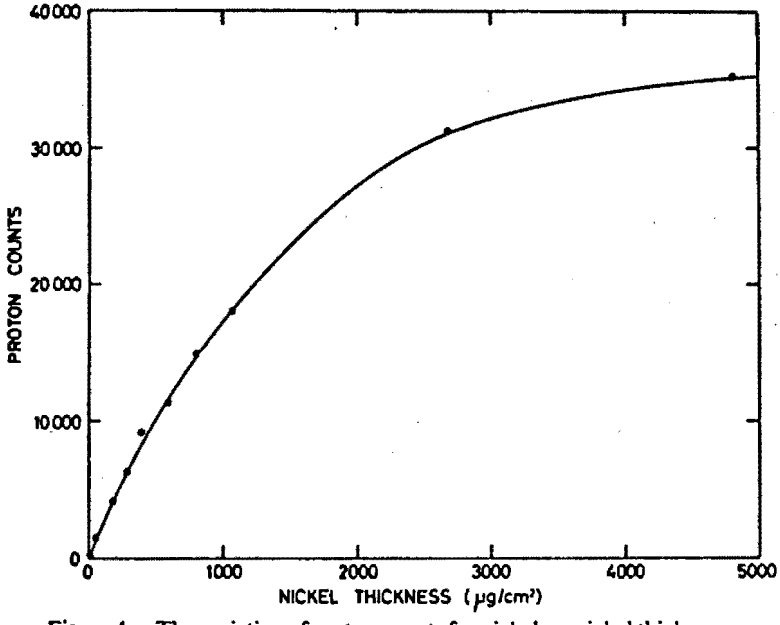

Figure 4. The variation of proton counts for nickel *vs.* nickel thickness.

obtained for thick films caused by the decrease in the cross section of the reaction with decreasing deuteron energy. However, it can be assumed that the calibration is linear up to 100 $\mu g/cm^2$. Results of a typical series carried out over this thickness region are listed in Table 1. The standard error was ± 2.2 $\mu g/cm^2$ over the whole region. This corresponds to a relative standard error of 2.2% for films of about 100 $\mu g/cm^2$, but the relative error increases for thinner films. With a bombarding deuteron beam of 3 mm^2 area used in this investigation and with a target inclined at 30° to the beam, the precision attained is equivalent to a relative standard error of $\pm 2.2\%$ on 24 μg of nickel.

Table 1. Some determinations of nickel films on copper by prompt proton counting.

Known nickel thickness ($\mu g/cm^2$)	Integrated proton counts per unit beam current	Measured nickel thickness ($\mu g/cm^2$)	Error[a] ($\mu g/cm^2$)
13.3	250	13.4	+ 0.1
17.8	418	20.6	+ 2.8
28.5	566	26.8	− 1.7
37.4	797	36.7	− 0.7
58.7	1233	55.2	− 3.5
76.5	1796	79.1	+ 2.6
97.8	2242	98.0	+ 0.2

[a] Standard error = $\pm$ 2.2 $\mu g/cm^2$

The determination of chromium on nickel is made possible by the fact that the peak due to p_o protons from chromium-52 is so prominent (see Figure 5). By curve stripping this peak can be resolved from the peaks representing nickel. The calibration giving the variation of proton counts with chromium thickness is similar to that obtained for nickel.

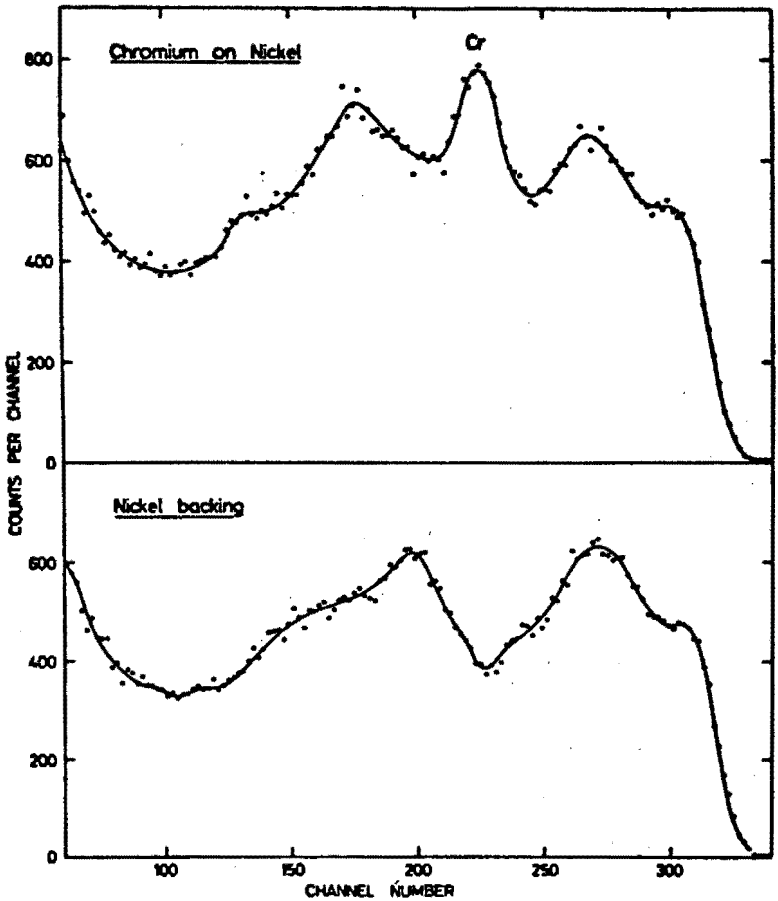

Figure 5. Energy spectrum of prompt protons from a thin chromium film on nickel compared with that obtained from the nickel backing. Chromium thickness = 160 θg/cm² (0.22 μm); $\theta = 60°$, $E_d = 3.5$ MeV, Au absorber = 196 mg/cm².

IV. References

[1] Rubin, S., Passel, T. O., and Bailey, L., Anal. Chem. 29, 736 (1957).
[2] Peisach, M., and Poole, D. O., J. S. Afr. Chem. Inst. 18, 61 (1965).
[3] Peisach, M., and Poole, D. O., Anal. Chem. 38, 1345 (1966).
[4] Patterson, J. H., Turkevich, A. L., and Franzgrote, E., J. Geophys. Res. 70, 1311 (1965).
[5] Anders, O. U., Anal. Chem. 38, 1442 (1966).
[6] Peisach, M., Poole, D. O. and Rohm, H. F., Talanta 14, 187 (1967).
[7] Williamson, C. F., Boujot, J.-P., and Picard, J., Report CEA-R3042 (1966).

Journal of Radioanalytical Chemistry Vol. 3 (1969) 345–351

ISOTOPIC DETERMINATION OF CALCIUM-43 BY PROTON ACTIVATION

R. J. N. BRITS, M. PEISACH

Southern Universities Nuclear Institute, P.O. Box 17, Faure, C.P. (South Africa)

(Received January 4, 1969)

An activation analysis method has been developed for the routine determination of ^{43}Ca. The calcium is chemically separated and converted to fluoride. When activated for 2 hours with 4.50 MeV protons, ^{43}Sc and ^{48}Sc are produced and the ratio of their activities is a measure of the isotopic concentrations of ^{43}Ca. ^{48}Ca serves as an internal standard to represent total natural calcium. The relative standard deviation is $\pm 1.5\%$ and the method can determine a change of $+0.004$ atom % ^{43}Ca in natural calcium. ^{42}Ca may interfere, if present in enriched concentrations.

The fact that ^{43}Ca has a low isotopic abundance in nature, 0.145%, indicates that it has potential use as an isotopic tracer of calcium, especially in those medical applications where radioactive tracers are undesirable. If a preparation enriched in ^{43}Ca is administered to a biological system, the extent of its dilution with natural calcium may be determined by isotopic analysis of a sample drawn from the system under investigation. Although such studies[1] have been carried out using ^{48}Ca, no such investigation with ^{43}Ca has yet been reported, despite the fact that the abundance of ^{43}Ca is almost 20% lower than that of ^{48}Ca. The lower natural abundance implies that an experiment involving dilution with natural calcium could be extended over a longer period of time.

Another field in which attention has in recent years been paid to the isotopic analysis of calcium is the extent to which possible isotopic fractionation occurs in natural processes.[2,3] Several workers have studied the isotopic composition of calcium by mass spectrometry.[4–9] Recently nuclear activation methods for such studies have been reported[10] in which the ratio of ^{48}Ca to natural calcium was obtained from the reactor activation of ^{48}Ca, and the determination of total calcium by titration. A similar study has been reported in which the isotopic ratio of ^{44}Ca to ^{48}Ca was determined by proton activation,[11] the concentration of ^{44}Ca serving as an internal standard for the determination of ^{48}Ca. If isotopic fractionation is determined solely by the mass difference between the isotopes concerned, a study based on the isotopic ratio $^{43}Ca/^{48}Ca$ would be more likely to reveal isotopic fractionation than one based on the isotopic ratio $^{44}Ca/^{48}Ca$. In addition, it should be noted that the natural isotopic concentration of ^{43}Ca

is of the same order as that of ^{48}Ca, so that the lighter isotope could possibly be a better internal standard than ^{44}Ca, which is at least eleven times more abundant than ^{48}Ca in nature.

It would thus be advantageous to develop a simple routine activation method for the isotopic determination of ^{43}Ca, because to date no such method has been reported. The only nuclear method that has been described used the spectroscopy of prompt neutrons from proton irradiation.[12]

By far the most common method of activation is to bombard a sample with thermal neutrons in a reactor, but ^{43}Ca cannot be activated in this way because neutron capture leads to a stable product. A possible method for determining ^{43}Ca by activation with fast neutrons is to follow the decay of 22-hour ^{43}K, formed by the reaction ^{44}Ca(n,p)^{43}K, and to use its activity as a measure of the ^{43}Ca content. The isotopic composition may then be obtained from a separate determination of total calcium.

An alternative method of activation is the use of accelerated charged particles. When protons of a few MeV are used to activate stable calcium isotopes, the main activities are formed by (p,n) reactions. The activity from the very abundant ^{40}Ca and from ^{42}Ca are short-lived and can be allowed to decay away within a few minutes, while the yield of ^{46}Sc is expected to be very small, because its half-life is very long and the target isotope from which it is produced has a low natural abundance. Thus the main activities expected from proton activation are ^{43}Sc, ^{44}Sc and ^{48}Sc produced from the corresponding calcium isobars.

The threshold for the reaction ^{44}Ca(p,n)^{44}Sc is 4.532 MeV. It thus follows that activation with protons of energies just below the threshold value, say 4.50 MeV, cannot result in the formation of ^{44}Sc, but both ^{43}Sc and ^{48}Sc can be produced in sufficiently high activities, because the cross sections for both reactions ^{43}Ca(p,n)^{43}Sc and ^{48}Ca(p,n)^{48}Sc are of the order of 100 mb, at this energy.[13] It would thus be possible to use the activity of the 44-hour ^{48}Sc as an internal standard to indicate the total content of natural calcium in the sample, while the 3.9-hour ^{43}Sc can give a measure of the content of ^{43}Ca.

Experimental

Sample preparation

As charged particle irradiation may cause high temperatures at the target, the material selected should be sufficiently refractory. Calcium fluoride has already proved suitable[14] and was thus used as target material. The calcium standards and samples for analysis were converted to calcium fluoride by evaporation with hydrofluoric acid in a platinum crucible. Targets were obtained by evaporating calcium fluoride in vacuum onto tantalum discs, when deposits 20 mm in diameter and ranging in thickness between 300 and 1000 μg/cm^2 were obtained. When equal weights of calcium fluoride were evaporated under similar conditions, it was found that the target thickness could be reproduced with a relative standard

error of $\pm 4\%$. For maximal precision, the analyses had to be carried out on samples and standards of equal thickness, but a thickness variation over the range 300 to 1000 $\mu g/cm^2$ could be used if slightly lower precision was acceptable. In this investigation the targets were approximately of equal thickness and about 800 $\mu g/cm^2$ thick.

The standards of the required isotopic concentrations were prepared by adding natural calcium to an enriched ^{43}Ca sample (81.12 atom %) obtained as calcium carbonate from the Oak Ridge National Laboratory, USA.

Irradiation and measurement

Twelve targets could simultaneously be irradiated on a rotating sample holder, cooled by circulating water or cooling gas, as previously described.[14] For activation, beams of 4.50 MeV protons in currents up to about 3 μA were used, as obtained from the 6 MV Van de Graaff accelerator at the Southern Universities Nuclear Institute. The beam diameter was between 8 and 10 mm; if larger diameter beams were available, higher beam currents could be used. Irradiations lasted for about 2 hours. The samples were measured either by γ-ray spectroscopy using Ge(Li) detectors, or by gross γ-ray counting with NaI(Tl) scintillators. In the latter case the individual activities were calculated from the decay data collected about 60 hours after irradiation using a computer programme based on the criterion of maximum likelihood.[15]

Results and discussion

γ-ray spectroscopy

A typical γ-ray spectrum obtained from a sample of natural calcium fluoride irradiated with 4.5 MeV protons is given in Fig. 1. It is obvious that very few radionuclides are generated in the activation, the only possible contaminating activities being positron and negatron emitters which do not decay with accompanying γ-emission.

The presence of ^{43}Sc was indicated by the gamma-ray of 374 keV. Furthermore, it was found that the rate of decay of the positron activity was consistent with the formation of 3.9-hour ^{43}Sc as the main product. In addition, small amounts of ^{13}N and ^{18}F were detected as components decaying with 10 min and 110 min half-lives. The origin of these two activities is not clear, but some ^{13}N could have been formed by the nuclear reaction ^{13}C(p,n)^{13}N from carbon deposited on the target by the decomposition of residual oil vapours at the point of incidence of the irradiation beam. ^{18}F could only have been produced from oxygen on the target primarily by the nuclear reaction ^{18}O(p,n)^{18}F, but also to a small extent by the nuclear reaction ^{17}O(p,γ)^{18}F. The Q-value for neutron emitting reactions such as (n,2n), (γ,n) and (p,pn) on ^{19}F is -10.442 MeV, which is too low for any ^{18}F to have been produced from natural fluorine.

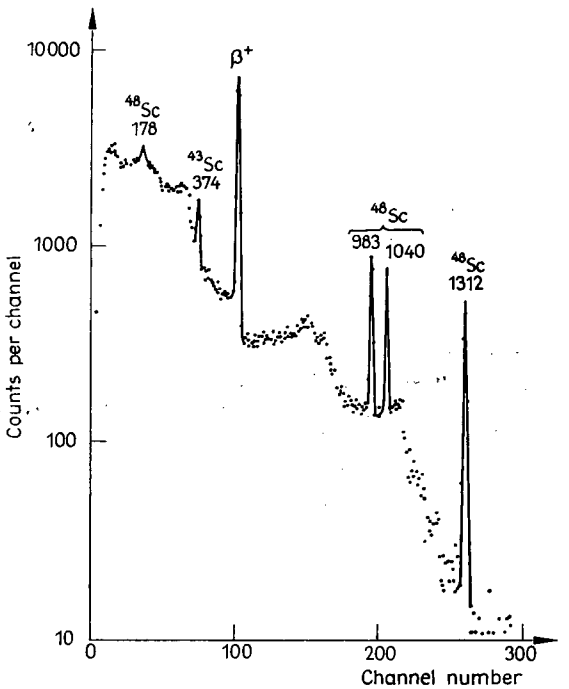

Fig. 1. Gamma-ray spectrum of natural calcium fluoride activated with 4.50 MeV protons, measured 2.300 hours after the end of irradiation

The presence of ^{48}Sc was indicated by gamma-rays with energies of 178, 983, 1040 and 1321 keV. Decay measurements confirmed the presence of this nuclide by its half-life of 44 hours. No other components could by detected even after the material has been decayed for several half-lives.

Because so few radionuclides are formed in the activation and as their half-lives are so widely different, the activity of each component can readily be obtained by measuring the decay of the gross activity. Such measurement could be delayed for a few hours to eliminate ^{13}N and to reduce the unwanted ^{18}F content.

Calibration

The activity ratio, *i.e.* the ratio of the measured activity of ^{43}Sc relative to that of ^{48}Sc, plotted against the known isotopic concentration of ^{43}Ca in standard samples, resulted in a linear calibration curve with a slope of 10.534 per atom %. This value is dependent on the experimental conditions of irradiation and measurement, and should be determined anew if there are any changes in the conditions.

The calibration line did not pass through the origin, but had an intercept which corresponded to an activity ratio of 0.4458 at zero concentration of ^{43}Ca.

It thus implied that ^{43}Sc was generated in the target material by another nuclear reaction, the most likely being

$$^{42}\text{Ca(p,}\gamma)^{43}\text{Sc.}$$

If the subscript m refers to the mass number, and A_m is the measured activity of the scandium isotope, it can readily be deduced that the activity ratio, R, is given by

$$R = \frac{A_{43}}{A_{44}} \propto \frac{(\sigma_{43}a_{43} + \sigma'_{42}a_{42})}{\sigma_{48}a_{48}} \cdot F(t) \qquad (1)$$

where $F(t)$ is the time-dependent factor whose value is determined by the duration of the irradiation, and

a_m is the isotopic concentration of the target calcium isotope,
σ_m the cross section for the reaction ^{m}Ca(p,n),
and σ'_m the cross section for the reaction ^{m}Ca(p,γ).

Hence, under fixed conditions of irradiation and measurements, and for samples in which the isotopic concentrations of ^{42}Ca and ^{48}Ca do not vary appreciably from their values in nature, it follows that the slope of the calibration line is proportional to the ratio $\frac{\sigma_{43}}{\sigma_{48}}$ and the intercept to the value $\frac{\sigma'_{42}}{\sigma_{48}} \cdot a_{42}$. The ratio of the cross sections for the two reactions leading to the formation of ^{43}Sc can thus be calculated to be

$$\frac{\sigma'_{42}}{\sigma_{43}} = \frac{0.4458}{10.534 \times 0.64} = 0.0661 .$$

This value is in excellent agreement with the value 0.0641 ± 0.0040 that may be obtained from the ratio of the measured cross section[13] of the reaction ^{43}Ca(p,n)^{43}Sc with 4.50 MeV protons and the extrapolated value of the cross section[16] for radiative proton capture of ^{42}Ca at the same energy.

Precision and accuracy

A test series of 36 analyses was carried out on 22 samples of known composition to determine the precision of the method. The results showed that the relative standard deviation was $\pm 1.54\%$.

Some typical results of analyses are given in Table 1. From the values in the table, the mean value of the net activity ratio was 10.550 per atom %. This value agreed with the slope of the calibration line, 10.534 per atom %, within the precision of the method. The results in Table 1 also include replicate analyses of natural calcium and of calcium enriched to 1.210 atom % ^{43}Ca. The results of the replicate analyses gave root mean square errors of $\pm 1.62\%$ and $\pm 1.94\%$, respectively, for 5 samples in each group. These results thus indicate that the method is capable of

Table 1

Some results of isotopic determinations of ^{43}Ca

Known ^{43}Ca concentration, atom % (*A*)	Activity ratio	Net activity ratio per atom %	Found ^{43}Ca concentrations, atom % (*B*)	Error (*B*) − (*A*)	Error %
(1) *Analytical results*					
0.379	4.419	10.483	0.3772	−0.0018	−0.47
1.004	11.05	10.562	1.007	+0.003	+0.30
1.450	15.55	10.417	1.434	−0.016	−1.10
1.769	19.20	10.602	1.780	+0.011	+0.62
2.010	21.64	10.544	2.012	+0.002	+0.10
(2) *Natural calcium*					
0.145	1.990	10.650	0.1466	+0.0016	+1.10
0.145	1.967	10.491	0.1444	−0.0006	−0.41
0.145	1.992	10.663	0.1468	+0.0018	+1.24
0.145	1.949	10.367	0.1427	−0.0023	−1.59
0.145	2.015	10.822	0.1490	+0.0040	+2.76
(3) *Enriched sample*					
1.210	13.37	10.681	1.227	+0.017	+1.40
1.210	13.33	10.648	1.223	+0.013	+1.07
1.210	13.29	10.615	1.219	+0.009	+0.74
1.210	12.70	10.127	1.163	−0.047	−3.88
1.210	13.25	10.582	1.215	+0.005	+0.41

Mean net activity ratio = 10.550 per atom %
Slope of calibration curve = 10.534 per atom %
Intercept of calibration curve: Ratio = 0.4458
Mean error = −0.00002 atom %
Relative standard deviation = ±1.54%

determining an enrichment of ±0.004 atom % at the level of the natural ^{43}Ca concentration.

The precision of the method is not appreciably different from the expected precision in determining the activity ratio when each activity is measured with a precision of ±1%. It thus follows that prolonged counting to decrease the statistical error on the measured activity, or an increase in the irradiation period to achieve the same result, may not be warranted.

The accuracy of the method may be deduced from the mean error, which is negligibly different from zero. The accuracy does, however, depend on the isotopic concentrations of ^{42}Ca and ^{48}Ca. It should be noted that the measurements determine the ratio of ^{43}Ca to ^{48}Ca. For most tracer uses such a ratio is sufficient. However, if the absolute isotopic concentration is required, this can readily be deduced if the concentration of ^{48}Ca is either assumed to be negligibly different from the value in nature, or is known. However, if the ^{42}Ca concentration varies

from sample to sample in a series of analyses, the *accuracy* of the determination of ^{43}Ca will be seriously affected even though the precision remains unchanged. In such cases the contribution to the ^{43}Sc activity from the lighter calcium isotope may be deduced if the samples, after decay, are reactivated with 3.0 MeV protons; all ^{43}Sc will then be formed by the reaction ^{42}Ca(p,γ)^{43}Sc, because the threshold for the nuclear reaction ^{43}Ca(p,n)^{43}Sc is 3.073 MeV.

Conclusions

A simple activation analysis method has been devised that is suitable for routine use for the determination of the isotopic concentration of ^{43}Ca. Apart from relatively short-lived positron emitters, only two radionuclides are generated, and their half-lives are sufficiently different to enable each to be separately determined from decay measurements.

Any method for measuring β, γ-emitting radionuclides may be followed, because γ-ray spectrometry is not really needed. In this investigation a scintillation detector was used because of its efficiency and convenience, but other γ-ray detectors, or even beta-counters, could, in principle, serve equally well.

This method thus provides an analytical tool which facilitates the use of ^{43}Ca as an isotopic tracer for calcium. This isotope has an advantage over ^{48}Ca because its concentration in nature is lower.

*

Financial assistance for this investigation was obtained from the South African Atomic Energy Board and from the South African Council for Scientific and Industrial Research.

References

1. G. D. McPherson, *Acta Orthop. Scand., Suppl.*, 78 (1965) 1.
2. E. Ingerson, *Bull. Geol. Soc. Am.*, 64 (1953) 301.
3. K. Rankama, Progress in Isotope Geology, Interscience, New York, 1963.
4. F. W. Aston, *Nature*, 57 (1934) 684.
5. M. M. Backus, W. H. Pinson, L. F. Herzog, P. M. Hurley, *Geochim. Cosmochim. Acta*, 28 (1964) 735.
6. J. T. Corless, K. A. Rahn, J. W. Winchester, *Trans. Am. Geophys. Union*, 44 (1963) 69.
7. A. J. Dempster, *Phys. Rev.*, 20 (1922) 631.
8. A. O. Nier, *Phys. Rev.*, 53 (1938) 282.
9. J. R. White, A. E. Cameron, *Phys. Rev.*, 74 (1946) 991.
10. J. T. Corless, *Anal. Chem.*, 38 (1966) 810.
11. J. A. Eisele, R. E. Larson, Intern. Conf. Modern Trends in Activation Analysis, Gaithersburg, October 1968.
12. W. R. McMurray, M. Peisach, R. Pretorius, P. van der Merwe, I. J. van Heerden, *Anal. Chem.*, 40 (1968) 266.
13. T. J. De Waal, Thesis, University of Stellenbosch, 1968.
14. M. Peisach, R. Pretorius, *Anal. Chem.*, 38 (1966) 956.
15. R. G. Monk, A. Mercer, T. Downham, *Anal. Chem.*, 35 (1963) 178.
16. M. Peisach, R. Pretorius, D. S. Rosettenstein, Convention Handbook, S. Afr. Chem. Inst. 20th Convention, Durban, 1967, p. 299.

No. 31

Microanalysis of Surface by Ion Beam Scattering

M. Peisach[1] and D. O. Poole[2]

[1]Southern Universities Nuclear Institute, Faure, C. P., South Africa

[2]South African Atomic Energy Board, Isotope Unit

INTRODUCTION

The limited penetration of charged particles with energies of a few MeV makes them suitable for the analysis of surface layers. By measuring the energy spectrum of the particles scattered from an incident beam of monoenergetic ions, the chemical composition of surfaces may be determined. Such measurements have been carried out with ions of hydrogen, helium and nitrogen using semi-conductor detectors to determine the energy of the scattered particle.

Earlier work had been carried out with ions of $^{1}H^{+}$ and $^{2}H^{+}$ using magnetic spectrometers to analyze the energy spectra of scattered beams [1-4]. Nevertheless, despite the lower resolution obtainable with semi-conductor detectors, they have already been used to measure thin layers of gold by scattering of accelerated hydrogen ions $^{1}H^{+}$ [5], thin surfaces by the scattering of accelerated helium ions, $^{4}He^{+}$ [6], and geological samples by the scattering of alpha particles, $^{4}He^{++}$, emitted by a radioactive source [7].

In this paper the use of ion beams for the microanalysis of surfaces is discussed.

THEORY

The Rutherford differential cross section P, per unit solid angle, at a mean scattering angle, θ, measured in centre-of-mass coordinates, for non-relativistic

eprinted from 'Electron and Ion Beam Science and Technology', . Bakish (Editor), Proc. 2nd Instern. conf. 1966, Amer. nst. Mining, Metall. Petr. Eng., Gordon and Breach, New York 1969), Vol II pp 1195-1213

bombarding ions is given by

$$P = \frac{(Z_1 Z_2 e^2)^2}{16\ E^2\ \mathrm{Sin}^4(\frac{\theta}{2})} \qquad (1)$$

where Z_1 and Z_2 are respectively the atomic number of bombarding ion and scattering atom, e is the electronic charge and E the energy of the bombarding ion.

The energy of the scattered ion, E' is given by

$$\frac{E'}{E} = 1-2(1-\mathrm{Cos}\theta)\ \frac{M_1 M_2}{(M_1+M_2)^2} \qquad (2)$$

where M_1 and M_2 are respectively the masses of the incident ion and the scattering atom. To convert the centre-of-mass angle θ to the laboratory angle θ_L, the value of θ may be expressed as

$$\theta = \theta_L + \mathrm{arc\ Sin}\ (\frac{M_1}{M_2}\ \mathrm{Sin}\theta_L) \qquad (3)$$

When a monoenergetic beam of ions is scattered by a target consisting of a monolayer of isotopic nuclei, the energy spectrum of the scattered particles measured at a selected angle is expected to consist of a single line. Due to the non-ideal behavior of the measuring apparatus, the line will appear as a narrow normal distribution, of which the width at half its maximum height, is a measure of the resolution of the system.

As the target thickness increases, more scattering nuclei are presented to the incident beam, so increasing the number of particles measured. However, the energies of the bombarding and scattered particles are degraded in traversing the target material, so that the energy spectrum will spread to lower energies. With thick targets where the energy lost along the path length of the particle may be sufficient to stop the particle, the energy spectrum will appear as a plateau ending with a maximum energy E'.

When attempting to differentiate between targets with different masses M_2 and M_2' it is desirable to have the energy difference between their corresponding values of

E' as large as possible, in order to overcome the inherent resolution limitations of the measuring system. It follows from equation (2) that the use of high energy ion beams is indicated. However, because the scattering cross section decreases with energy the increase in resolution has to be weighed against the decrease in count rate. Also, because the method is based entirely on elastic scattering, an upper limit is imposed on the energy of the bombarding ion; it should not reach that level where inelastic scattering becomes significant.

Selection of Experimental Conditions

Selection of Bombarding Particle

The nature of the ion beam used for surface analysis determines the depth to which the ion of a fixed energy will penetrate, as well as the extent to which peaks from M_2 and M_2^1 will be resolvable. It is clear that a fixed energy E, penetration will decrease with increasing mass of the particle. Accordingly if information of composition, or composition changes, is sought at depths below the surface, lighter elements would prove more useful. Conversely for the investigation of surfaces, heavy ions would a priori be expected to produce better results.

The bombarding particle most suitable to distinguish between M_2 and M_2^1 may be selected by comparing the variation of E' with the mass of the scatterer M_2 for different particles. If the "mass sensitivity", $S(M_1)$ for the particle M_1, is defined as the variation of E'/E with unit mass increase, at constant angle θ or θ_L we have

$$S(M_1)_\theta \equiv \frac{\partial}{\partial M_2}\left(\frac{E'}{E}\right)_\theta = \frac{2M_1(1-\cos\theta)(M_2-M_1)}{(M_1+M_2)^3} \qquad (4a)$$

$$S(M_1)_{\theta_L} \equiv \frac{\partial}{\partial M_2}\left(\frac{E'}{E}\right)_{\theta_L} = \frac{2M_1(1-\cos\theta)(M_2-M_1)}{(M_1+M_2)^3}$$

$$+ \frac{2M_1}{(M_1+M_2)^2}\sin\theta\,\tan(\theta-\theta_L) \qquad (4b)$$

from which the particle giving the greatest mass sensitivity for the mass number of the scatterer under investigation, may be selected. A comparison between the mass sensitivities of singly charged hydrogen, helium and nitrogen ions scattered at a laboratory angle of 135° is shown in Fig. 1 as a function of the mass number of scatter. At this angle, the use of hydrogen ions is inddicated for mass numbers less than 7, helium ions in the range 7 to 25 and nitrogen ions for mass numbers greater than 25 as determined by the points of intersection of the corresponding curves.

The mass number corresponding to the intersection points, vary with the angle of scatter; at 90° for example, the curves of $S(^4He^+)$ and $S(^{14}N^+)$ intersection at about 16, whilst for angles approaching 180° (laboratory angles) the intersection is at about 30. In general in c.m. coordinates the maximum mass sensitivity is obtained for

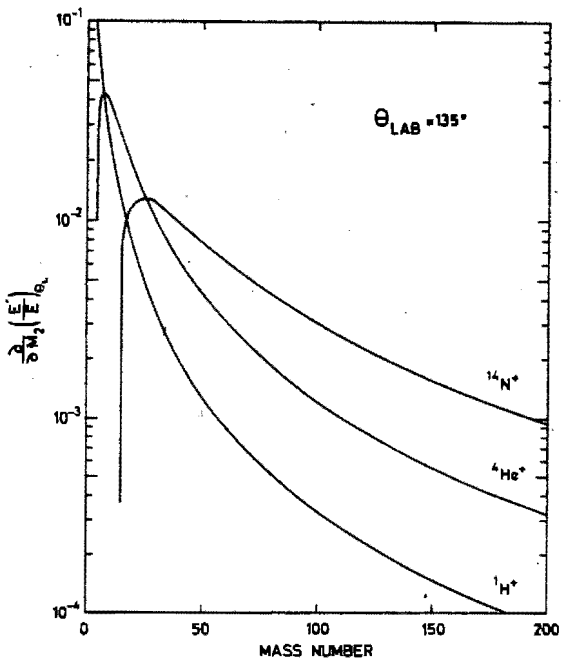

Figure 1. Mass sensitivity of different ion beams calculated at $\theta_L = 135^o$.

$M_2 = 2M_1$, but at a fixed laboratory angle θ_L the relationship is angle dependent.

Selection of Angle and Energy

Once the bombarding beam has been selected, the parameters that determine the experimental conditions are the scattering angle and the bombarding energy, which in turn have to be chosen so that the E' values obtained from M_2 and M_2' are separated by an amount compatible with the resolution of the detecting system. The selection of suitable experimental conditions would thus require repeatedly solving equation (2). For this purpose, the nomogram shown in Fig. 2 has been constructed.

The lines in the nomogram are labelled θ, E, B, $\Delta E/E$ and A. The angle θ is the scattering angle in centre-of-mass coordinates, but for most practical purposes and especially so for heavy elements with light-ion beams, the value is sufficiently close to the laboratory angle. Where light elements or heavy-ion beams are used, adjustments may be made by using equation (3). E refers to the energy of the incident ion and $\Delta E = E - E'$. B is the difference in energy between the scattered particles from two target nuclei M_2 and M_2' as obtained from equation (2) thus,

$$B = \left| (\Delta E)_{M_2} - (\Delta E)_{M_2'} \right| \qquad (5)$$

and represents the separation of two peaks in the energy spectrum. The mass factor, A, is defined by

$$A = \frac{M_1 M_2}{(M_1 + M_2)^2} \qquad (6)$$

For ease of operation extra scales have been included to convert M_2 to A for M_1 values of 1, 2, 3 or 4, but more scales may be added to suit.

The following two examples show how the nomogram may be used to select experimental conditions and to obtain qualitative data from experimental results, rapidly.

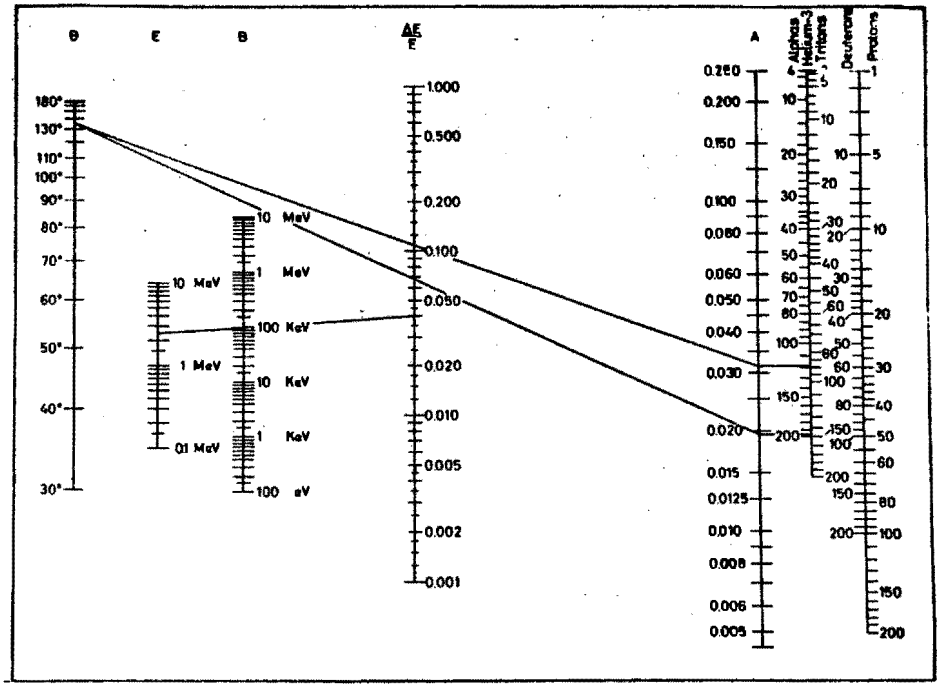

Figure 2. Nomogram for Selecting Experimental Conditions and for Rapid Evaluation of Experimental Data. The Lines Drawn Refer to Example 1 (see text).

Example 1

Thin sandwiches of tin on gold on aluminum were to be measured with a beam of helium ions. The resolution of the detecting system was about 50 keV so that it was desirable to have $B \geq 100$ keV, $M_1 = 4$, $M_2 = 197$ (for gold), $M_2' = 119$ (for tin). θ was arbitrarily chosen as 135°, being a convenient angle for measurement. To obtain the irradiation energy, the line joining $\theta = 135°$ to the A value for each metal was drawn to obtain $\Delta E/E$. The difference between them was plotted on the same scale and connected with the point B = 100 keV. This line cut the E scale at 2.5 MeV (see lines in Fig. 2).

Example 2

A geological sample was analyzed with 2.5 MeV helium ions scattered through 135°. The energy spectrum consisted of a series of plateaux with steps at ΔE values of 154, 497 and 920 keV. To identify the element associated with each step the energy of the scattered beam is compared with the incident beam energy, (or equivalent to an infinite mass for which $(\Delta E)_{M_2}$ in equation (5) is zero). Under these conditions $B = \Delta E$, so that by aligning the B value with E = 2.5 MeV a value of $\Delta E/E$ is obtained. A second line joining this value to $\theta = 135°$ gives the corresponding value of A and hence M_2. In this example it was found M_2 had values of 204, 64.5 and 32, being respectively Pb, Cu or Zn and S.

EXPERIMENTAL

Ion beams were obtained from the 5.5 MeV Van de Graaf accelerator at the Southern Universities Nuclear Institute, from which beams of $^1H^+$ ions up to 2.5 MeV, $^4He^+$ ions up to 3 MeV and $^{14}N^+$ ions up to 1.771 MeV were used for surface analysis. The upper energy for nitrogen ions was limited by the frequency measuring equipment which determined the magnetic field of the analyzing magnet of the accelerator.

A collimated beam with a cross sectional area of 5×10^{-3} cm^2 was used for surface analysis.

Scattering was measured in an evacuated scattering chamber in which the relative directions of incident and scattered beam could be externally adjusted, and in which the angle between the incident beam and the target surface could be pre-set. The scattered particles were measured with semi-conductor detectors which transmitted pulses to the counting apparatus.

2000 ohm-cm n-type silicon, as obtained from Messrs. Wacker-Chemie G.M.B.H., Munich, was used to construct surface barrier type semi-conductor detectors [8] with an active area of about 0.2 cm^2. With 5.48-MeV alpha particles from americium-241 these detectors gave resolutions of about 30 to 60 keV. The window thickness was about 0.05μ which gave rise to an energy loss not exceeding 50 keV for hydrogen and helium ions and about 160 keV for nitrogen ions, but this energy loss varied with the energy of the particle falling on the detector in such a way that no deviation from linearity could be observed in the calibration line relating pulse height to particle energy for the three types of ions studied. However, with increased detector bias, the pulse height increased as is shown for example in Fig. 3 for the 1166 keV nitrogen ion scattered from cadmium at 120° (lab) from a beam of 1700 keV incident nitrogen ions. For most measurements the detector bias was 50 volts.

MEASUREMENT OF METAL FILMS

From equation (2) the maximum energy, obtainable from scattering at a selected angle, per unit energy of incident particle, E'/E, is a function of the mass of the scattering nucleus. This function is shown in Fig. 4 calculated for helium ions for a laboratory angle of 135°, about the largest angle of scatter that could conveniently be measured in the experimental scattering chamber. The resolution attainable with a detector of 50 keV resolution and an incident beam of 2.5 MeV is shown for some elements.

Calibrated gold films ranging from about 0.2 to 40 μg/cm^2 in thickness, were deposited on various backing

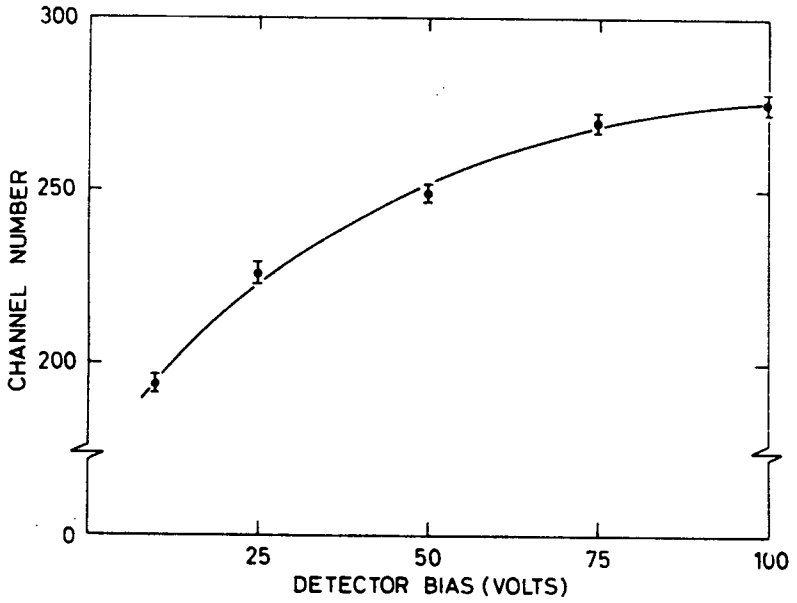

Figure 3. The variation of pulse height with detector bias. Measured with 1.70 MeV nitrogen-ions scattered through 120° (lab) off cadmium.

materials and measured with hydrogen [5] or helium ion [9] beams. The counts obtained from scattering off the gold, as obtained by integrating the counts under the peak due to gold in the energy spectrum, was used as a measure of the gold thickness. The results showed that the precision of the thickness measurement by scattering was better than ±3%, the precision with which the films could be calibrated by other means. The advantages of helium ion beams for such analyses have already been discussed [9].

Similar results were obtained with thin tin deposits, but for the analysis of tin plate, relatively thick tin deposits on an iron backing, the same procedure could not be used. Instead, inspection of the measured energy spectra showed that the broad peak due to tin was separated from a plateau due to the underlying iron (see Fig. 5),

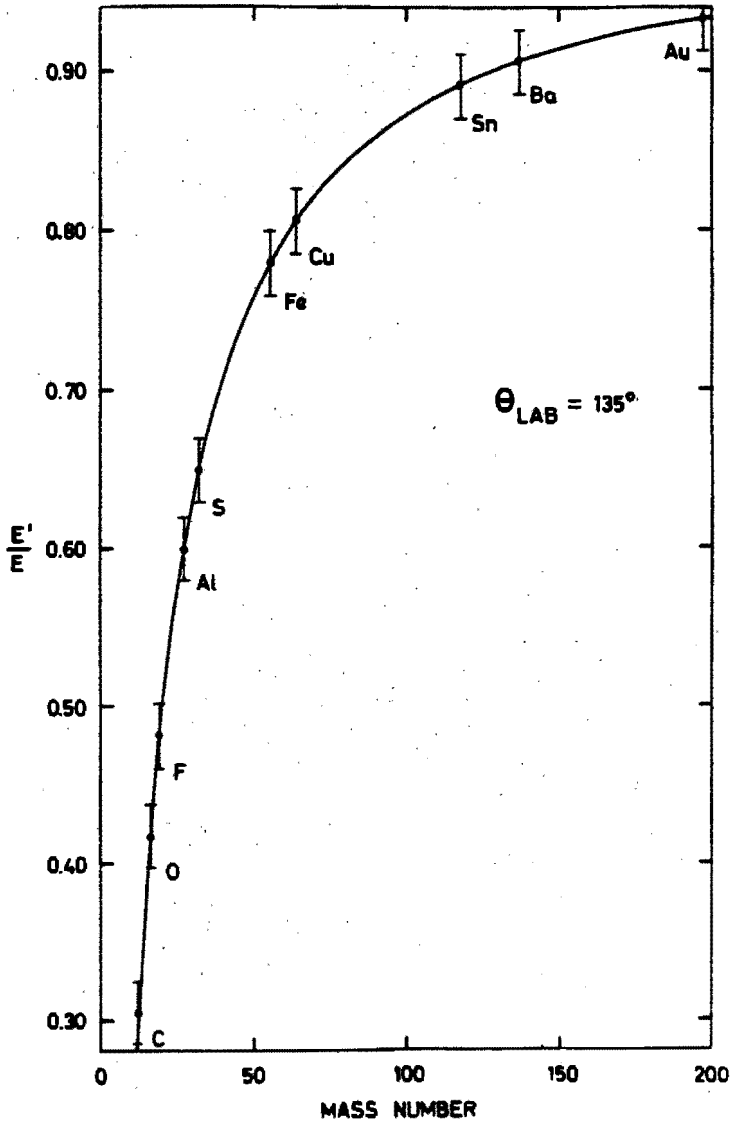

Figure 4. The variation of the energy of scattered helium ions with the mass number of the scattering nucleus; expressed as a ratio relative to the energy of the incident-ion and measured at 135° (lab). The error flags indicate resolution limits when a 2.5 MeV beam is used with a detector of 50 keV resolution.

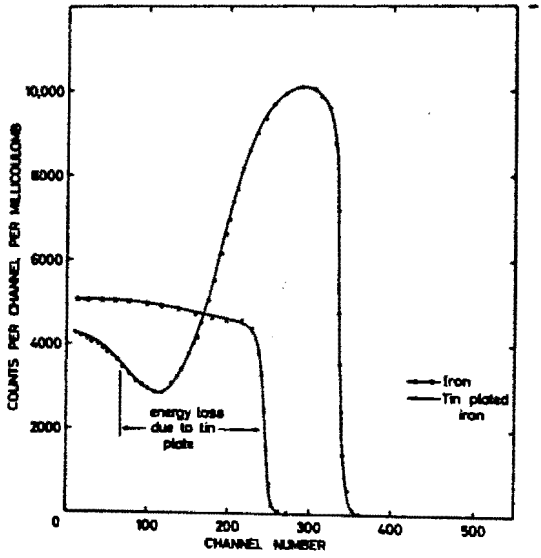

Figure 5. Energy spectrum of helium ions scattered from a thick tin coating on iron. The thickness of the tin may be obtained from the relative shift of the position for iron.

and that the maximum energy of the ion beam scattered from the iron had been degraded by energy loss of both the incident and scattered beams passing through the tin. This energy loss served as a means of measuring thick surface deposits. In the case of nitrogen ion beams, the beams were not sufficiently penetrating to show the underlying iron.

When a film of an element has to be measured on a backing consisting of an element with larger atomic number, the expected peak in the energy spectrum would appear superimposed on the continuum corresponding to the backing (see Fig. 8 of reference 9). In such cases the precision with which the film thickness can be measured is marred by the statistical errors inherent in the subtraction of large counts. Similarly the sensitivity of the analysis is expected to be somewhat less.

MEASUREMENT OF OXIDE FILMS ON ALUMINIUM [10]

The anodization of aluminium results in the formation of a uniform film of aluminium oxide over the metal, and the thickness of this film is a function of the anodizing conditions.

Standard thicknesses of aluminium oxide on aluminium were obtained by anodization of the metal, followed by a determination of the oxygen content by activation analysis using helium-3 beams. These standard films were analyzed by ion beam scattering. A typical spectrum obtained with helium-4 ions is shown in Fig. 6.

The spectrum clearly showed three plateaus, corresponding to relatively thick layers of three entities. The energies corresponding to the edges of two of these plateaus agreed with the energies calculated for surface atoms of oxygen and aluminium whilst the middle plateau, the energy corresponding to the edge of which varied with oxide film thickness, was identified as due to the ions scattered from the unanodized aluminium. As before, the energy difference between helium ions scattered from surface aluminium atoms in the aluminium oxide and aluminium atoms in the unanodized metal could be used as a measure of oxide film thickness.

Some results are shown in Fig. 6 where the maximum energy of helium ions scattered from the aluminium metal are shown plotted as a function of oxide film thickness. From this figure it is clear that the thickness of oxide films from 10 to 100 $\mu g/cm^2$ thick could readily be measured with a precision of about ±3%. This procedure could generally be applied to oxide films on metals, provided the film is thick enough to cause a moderate change in the energy spectrum of the ions scattered from the backing material.

When similar films were analyzed by nitrogen-ion scattering it was found that the low penetration of the beam made it impossible for ions scattered from the metal to be observed. It was also observed that the approximate experimental data as obtained from the nomogram (Fig. 2) was grossly in error for the case of oxygen, owing to the fact that the mass numbers of

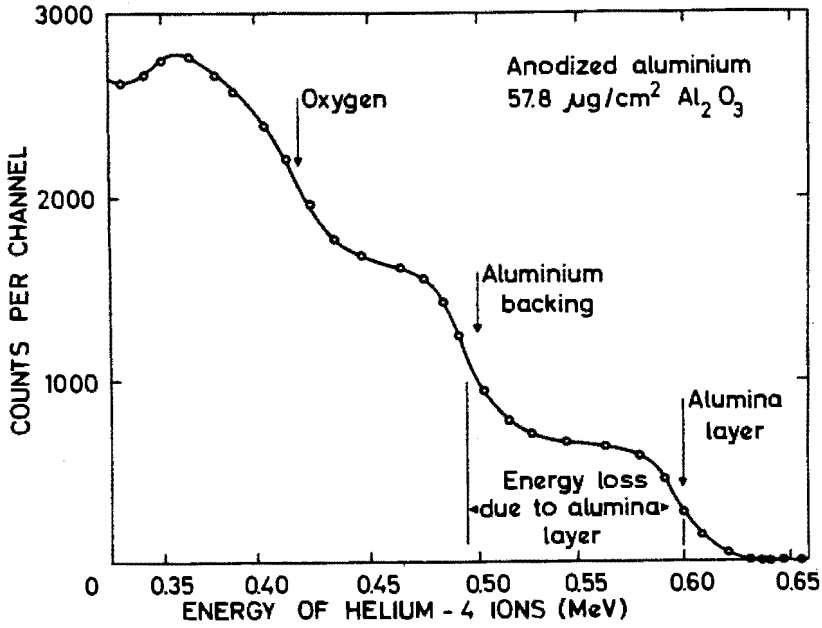

Figure 6. Energy spectrum obtained with 1000 keV helium ions scattered from anodized aluminium.

nitrogen and oxygen were so close that the assumption that the centre-of-mass angle was approximately the same as the laboratory angle, no longer applied.

Calculated values of E'/E for nitrogen-ion scatter from oxygen and aluminium are shown plotted in Fig. 8 as a function of laboratory angle. From these two curves the corresponding variation of B(Al-O) with scattering angle was obtained. This showed a maximum at about 75° after which the value decreased to 180°. However, even at 75°, the energy of nitrogen-ions scattered from surface oxygen would only be some 165 keV per MeV incident energy. To obtain somewhat higher energies, it was found

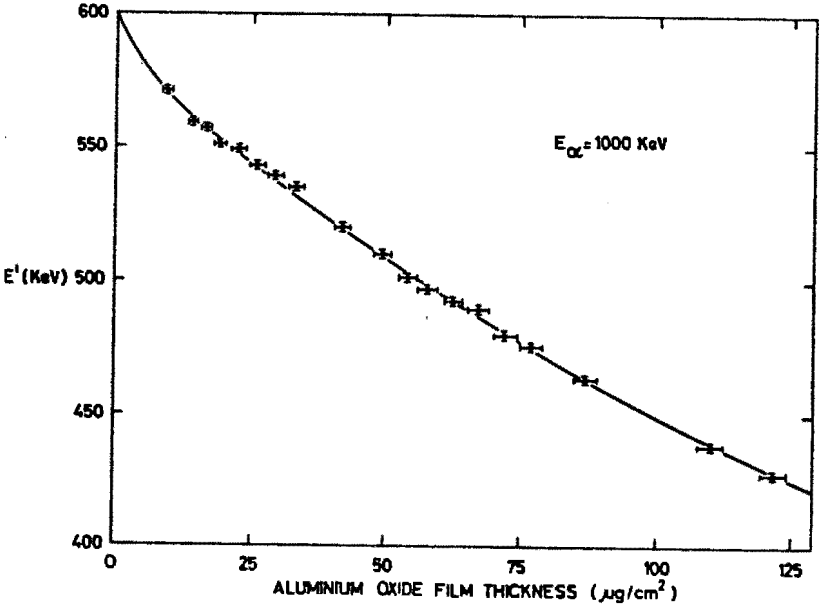

Figure 7. The variation of the energy of helium ions scattered from aluminium metal, as a function of the thickness of aluminium oxide on the surface.

to be more convenient to measure nitrogen ions scattered through 60° (lab). The separation B(Al-O) is still sufficiently large at 60° to enable the elements to be resolved.

Anodized aluminium with oxide films of about 30 $\mu g/cm^2$ when measured at a laboratory scattering angle of 60° with an incident beam of 1.70 MeV nitrogen-ions, appeared as an infinite layer of aluminium oxide.

ANALYSIS OF SELF-SUPPORTING ALUMINA FILMS [10]

Self-supporting alumina films ranging from 50 to 150 $\mu g/cm^2$ in thickness were analyzed by helium-ion scatter. A typical energy spectrum is shown in Fig. 9. As was

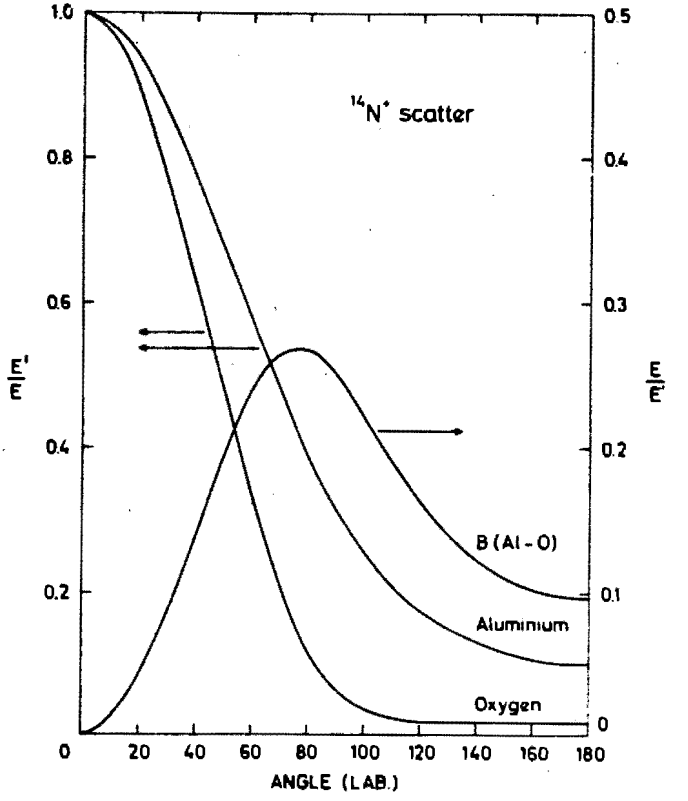

Figure 8. The variation of energy of nitrogen-ions scattered from aluminium and oxygen with angle of scatter (lab).

the case with metal films, the integrated count under the respective peaks could be used as a measure of the content of the respective element. Results showed that the precision of the analyses were about ±3%.

In Fig. 9 the shape of the peak for each element clearly shows it to be a double peak. As the number or particles scattered from a target of fixed mass at a fixed angle from a monoenergetic beam of fixed energy can only depend on the number of target nuclei per unit volume, the protruding peak indicates a region of higher density within the film. The profile of the peak could thus serve to obtain density variations within a thin target, which could not be similarly analyzed by other methods.

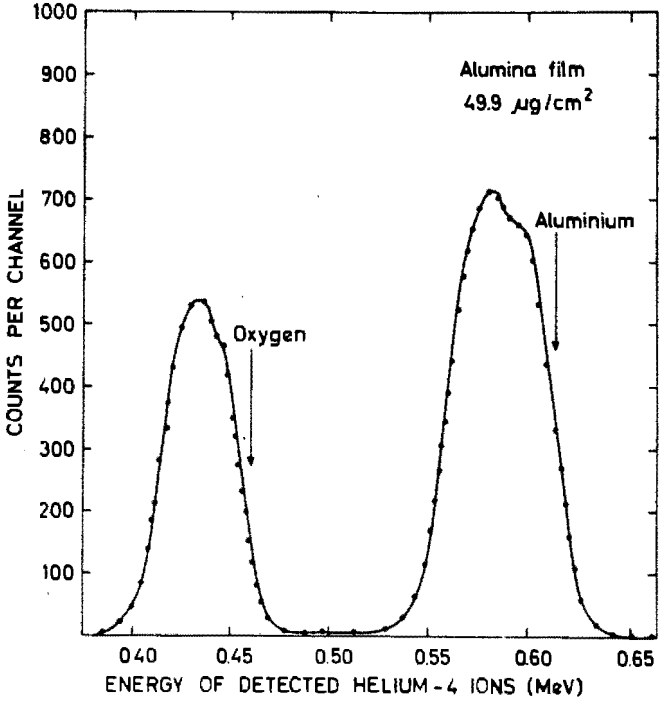

Figure 9. Energy spectrum obtained from helium ion scatter off a self-supporting film of aluminium oxide.

The same samples, analyzed by nitrogen-ion scatter appeared to be infinitely thick.

ANALYSIS OF FILMS OF COMPOUNDS

Where the thickness of a thin film of a compound has to be measured on a backing material with atomic number less than that of the constituent elements of the film, the spectra that are obtained resemble those obtained from self-supporting films. An example of one such spectrum is shown in Fig. 10; the spectrum was obtained from a thin layer of cadmium sulphide evaporated onto aluminium and measured with an incident nitrogen-ion beam of 1.70 MeV at a scattering angle of 75° (lab). The peak due to cadmium is higher than that due to sulphur because the scattering cross section increases with increasing atomic

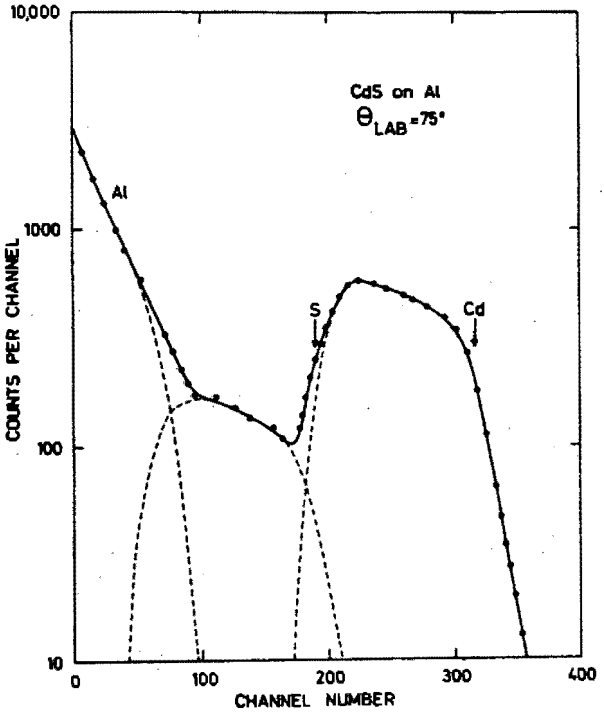

Figure 10. Energy spectrum obtained from nitrogen-ion scatter off a thin deposit of cadmium sulphide on aluminium.

number (see equation (1)). Although the elements are clearly resolved, the thickness of the deposit causes the "peak" to appear squat and to merge into that due to sulphur, which in turn merges with the continuum from the aluminium backing. It will be noted that the maximum energy of the nitrogen-ions scattered from aluminum is less than that calculated for surface aluminum. The difference between the measured and calculated energy can again serve as a measure of the film thickness of CdS, which can be obtained either from calibration or from a knowledge of the rate of energy loss of nitrogen-ions in CdS, $(dE/dx)_{N^+}$.

ANALYSIS OF GEOLOGICAL SAMPLES

Slices of geological samples when analyzed by ion-scattering appear as infinitely thick compounds and produce spectra consisting of a series of plateaus each ending at an energy characteristic of the element under the conditions of the measurement. Such spectra have been obtained for helium-ion scatter (see Fig. 11) and for alpha particle scatter [7]. With nitrogen-ions, the penetration is much less, so that local variations in the ore composition could have a marked effect on the analysis.

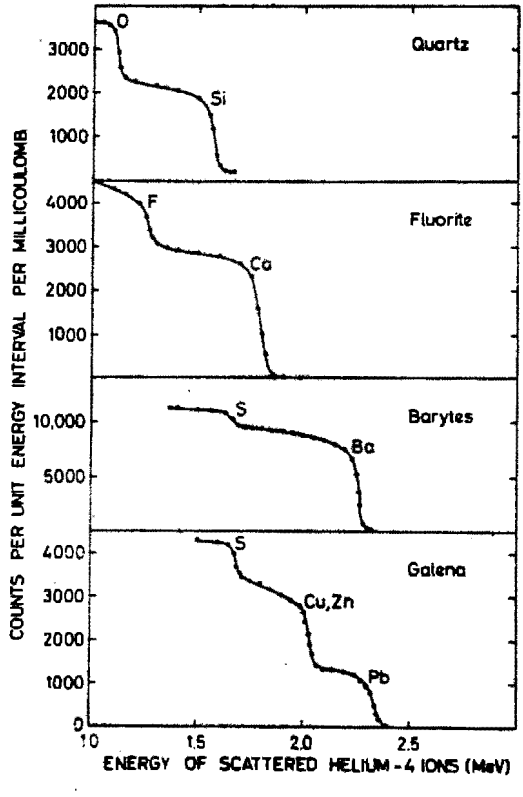

Figure 11. Spectra obtained from some geological samples analyzed by helium ion scatter.

ACKNOWLEDGMENTS

The authors acknowledge with thanks the willing assistance of Messrs. René Pretorius, Albert Bottega and Herman Rohm and the cooperation of the staff of the Southern Universities Nuclear Institute. Geological samples were kindly loaned by the Geology Department of the University of Stellenbosch.

One of us (D. O. P) thanks the South African A. E. B. for permission to include his work in this report.

REFERENCES

1. Rubin, S., Passell, T. O., Bailey, L. E., Anal. Chem. 29, 736 (1957)
2. Sippel, R. F., Phys. Rev. 115, 1441 (1959)
3. Buechner, W. W., Robertshaw, J. E. Trans. Amer. Nuc. Soc. 5, 197 (1962)
4. Green, F. L., Cooper, M. D., Robertshaw, J. E., Trans. Amer. Nuc. Soc. 5, 197 (1962)
5. Peisach, M., Poole, D. O., J. S. Afr. Chem. Inst. 18, 61 (1965)
6. Peisach, M., Poole, D. O. To be published.
7. Patterson, J. H., Turkevich, A. L., Franzgrote, E., J. Geophys. Res. 70, 1311 (1965)
8. Dearnaley, G., Whitehead, A. B., U. K. At. Energ. Res. Estab. rept R-3437 (1960)
9. Peisach, M., Poole, D. O., Proc. Intern. Conf. Modern Trends in Activation Analysis ICAA-II/37, (1965)
10. Peisach, M., Poole, D. O., Rohm, H. F., To be published.

THE DETERMINATION OF NICKEL ON METAL SURFACES BY PROMPT PROTON SPECTROMETRY

By C. OLIVIER* and M. PEISACH

OPSOMMING

Die konsentrasie van nikkel in oppervlaklae van metale is nie-destruktief bepaal deur gebruik te maak van die spektrometrie van onmiddellike protone wat onstaan tydens 'n bestraling met 3·5 MeV-deuterone. Die hoë-energie-protone van nikkel-58 is gebruik om die nikkelinhoud te meet. Die standaardfout van die bepaling vir oppervlakkonsentrasies tot 100 $\mu g/cm^2$ is $\pm 2{\cdot}2$ $\mu g/cm^2$.

SUMMARY

The concentration of nickel on surfaces of metals was determined non-destructively by the spectrometry of prompt protons which are generated during an irradiation with 3·5 MeV deuterons. The high energy protons from nickel-58 were used to measure the nickel content. For surface concentrations up to 100 $\mu g/cm^2$ the standard error in the determination was $\pm 2{\cdot}2$ $\mu g/cm^2$.

The limited penetration of charged particles with energies of a few MeV makes them suitable for the analysis of surface layers. Use has already been made of this property for the determination of surface concentrations of elements by the spectroscopy of elastically scattered charged particles.[1–5] Such methods are sensitive because charged particle scattering cross sections are usually large compared with reaction cross sections. However, the application is limited to cases where the targets are light elements, or the elements have widely differing mass numbers.[6] In particular, the method is of little use for the determination of nickel on thick targets of the medium-weight elements having mass numbers between 50 and 70.

To determine nickel on metal surfaces, it is a requirement that the prompt particles emitted from nickel should be distinguishable from those emitted by the elements in the substrate. However, unless some method is used to eliminate the effects of scattered particles, which usually exceed reaction products by at least one order of magnitude, it would be difficult to measure the prompt particles with sufficient precision. One method of doing this is to measure the prompt products, from exoergic reactions, which have energies greater than those attainable by elastically scattered particles.

If, however, the flux of scattered particles is very high, two (or more) scattered particles arriving coincidentally at the detector would be recorded as a single particle with a higher energy. In this way a low intensity continuum will build up in the spectrum over the energy region where only prompt reaction products were expected. To eliminate such summation, the detector may be covered with an absorber thick enough to stop scattered particles, but sufficiently thin to allow the desired products to reach the detector.

* Department of Chemistry, University of Stellenbosch, Stellenbosch, South Africa.

Since most (d, p) reactions are highly exoergic, the ground state protons would be produced at energies far in excess of those of the scattered deuterons. This would have the advantages that

(i) the absorber thickness would not be very critical, and
(ii) The energy spectrum of the transmitted particles would be relatively little distorted because of the low differential energy loss of energetic protons in matter.

Furthermore, these reactions have relatively high cross sections even at comparatively low bombarding energies of a few MeV, and hence offer a greater sensitivity when used for analysis. The Q-values of (d, p) reactions on the nickel isotopes and those of several other elements of the same transition series are listed in Table I together with the maximum energy of protons obtained from a bombardment with 3·5 MeV deuterons. The maximum energy of protons obtainable from the most abundant nickel isotope, (^{58}Ni), is appreciably higher than that obtained from the most abundant isotopes of the other elements listed in the table. Accordingly, an analytical method for

TABLE I

Energies of ground state protons from (d, p)-reactions induced by 3·5 MeV deuterons on some elements in the first transition series

Target Nuclide	% Natural Abundance	Q-value[7] (MeV)	Maximum Proton Energy MeV
Cr-50	4·31	7·0451	10·537
Cr-52	83·76	5·7169	9·217
Cr-53	9·55	7·4967	10·988
Cr-54	2·38	4·0294	7·529
Mn-55	100	5·0459	8·546
Fe-54	5·82	7·0742	10·567
Fe-56	91·66	5·4170	8·914
Fe-57	2·19	7·8179	11·308
Fe-58	0·33	4·3603	7·860
Co-59	100	5·2655	8·763
Ni-58	67·88	6·7788	10·272
Ni-60	26·23	5·5962	9·093
Ni-61	1·19	8·3749	11·864
Ni-62	3·66	4·6149	8·118
Ni-64	1·08	3·8779	3·441
Cu-63	69·09	5·6914	9·189
Cu-65	30·91	4·8359	8·334
Zn-64	48·89	5·7636	9·261
Zn-66	27·81	4·8289	8·327
Zn-67	4·11	7·9779	11·469
Zn-68	18·57	4·2779	7·777
Zn-70	0·62	3·8169	7·316

determining nickel based on prompt proton spectrometry, can be expected to be relatively free from interference from nuclides with mass numbers in the range 50 to 70. Any interference which might occur would be ascribable to low abundance nuclides, the most likely of which are chromium-50 and 53, iron-54 and 57 and zinc-67.

EXPERIMENTAL

Preparation of standards. Standard thicknesses of nickel on copper and tantalum, and of copper and chromium on tantalum were prepared by electroplating and weighing. The surface film thicknesses ranged from 10 to 5000 $\mu g/cm^2$, and the area of the circular deposit was about 2 cm^2 on discs of 19·5 mm diameter.

Irradiation. The standards, and sample discs of 20 or 25 mm diameter were irradiated in a 90-cm scattering chamber with a current of 0·5 to 4 μA of 3·5-MeV deuterons obtained from the Van de Graaff accelerator of the Southern Universities Nuclear Institute. The collimated irradiation beam had a circular cross section of 3 mm diameter. The current falling on the targets was measured with a current integrator. As it was not possible to cool the targets, low current densities were preferred even though the duration of an analysis was thereby increased.

Measurement. The energy of the protons formed from (d, p) reactions on the target and emitted at an angle, θ, to the bombarding beam was measured in a silicon semiconductor detector with a depletion layer of 700 μm and a resolution of less than 45 keV. This detector could measure protons up to 10 MeV. The scattered particles and

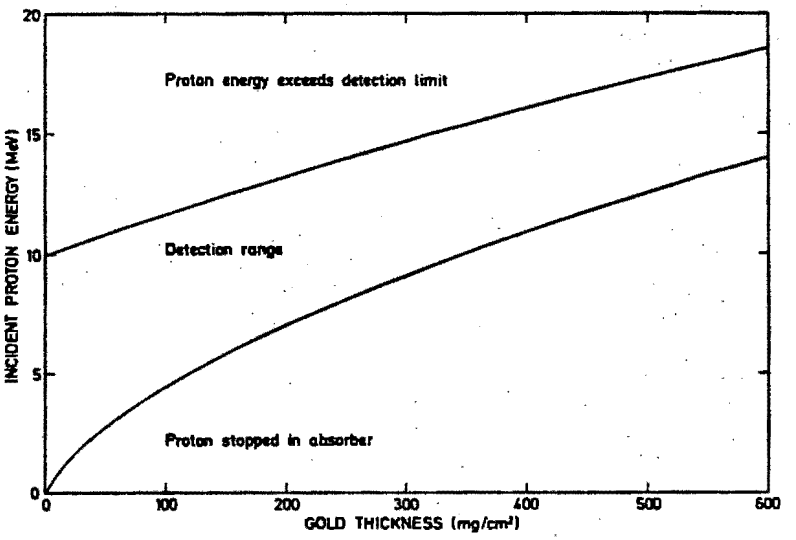

Fig. 1. The effect of absorber thickness on the proton energy range that could be measured with a silicon semi-conductor detector capable of measuring up to 10 MeV protons.

low energy protons were eliminated by placing a thin foil of gold as an absorber over the detector. The appropriate thickness of absorber required was calculated from the known stopping power for protons.[8] A typical pair of curves showing the effect of gold thickness on the range of proton energies which could be measured with a detector capable of measuring up to 10 MeV protons, is shown as an example in Figure 1.

RESULTS AND DISCUSSION

Energy spectra of prompt protons. Typical spectra obtained from thin films of Cr, Ni and Cu on tantalum backings, and of the protons from the backing itself, are shown in Figure 2. The proton groups p_i refer to the ith excited state in which the product nuclide was formed, and the nuclide labelled in the figure, refers to the target nuclide.

A common feature of the spectra in Figure 2 is the large extent to which the energy of each proton group had been broadened by the use of the absorber. However, the resolution was still sufficient to distinguish each target element.

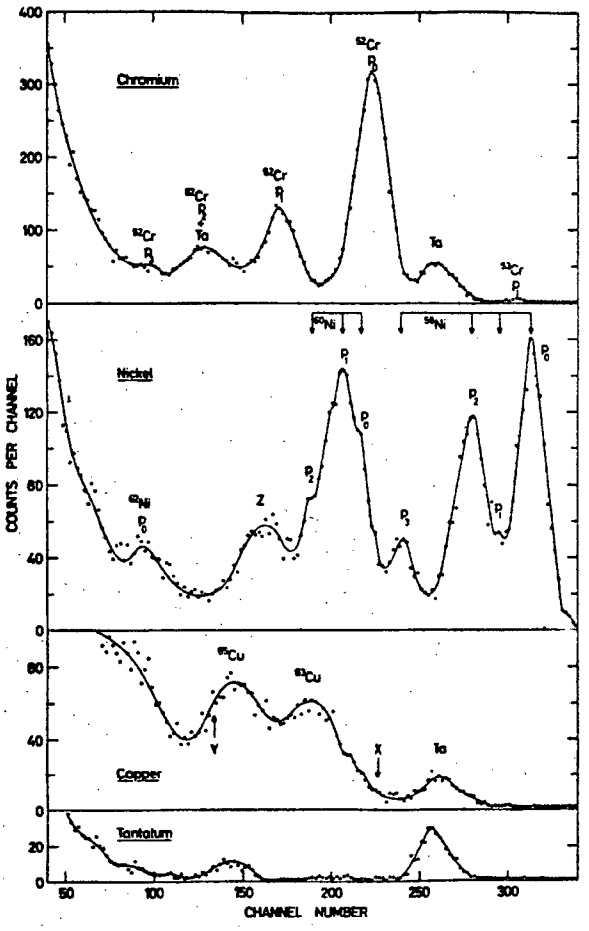

Fig. 2. Energy spectra of prompt protons obtained from the deuteron irradiation of thin layers of chromium, nickel and copper on tantalum.
$\theta = 60°$, $E_d = 3{\cdot}5$ MeV, Au absorber = 196 mg/cm².

Tantalum backings were used because the Coulomb barrier for such a heavy element, ($Z \equiv 73$), was large. The cross section of the (d, p) reaction at 3·5 MeV was expected to be so small that prompt protons from it would be undetectable. This was not quite the case (see Figure 2).

The high energy peak from protons of the reaction $^{53}Cr(d, p_0)$ was observed, but was not included in Figure 2 for the sake of uniformity. The high abundance of chromium-52 and the comparatively large cross section of the reaction $^{52}Cr(d, p_0)$ gave rise to a prominent peak, characteristic of this element and suitable for use for analytical purposes.

The proton energy spectrum obtained from nickel consisted of three prominent peaks which could be ascribed to the p_0 and p_2 groups from nickel-58 and a composite peak from nickel-60. These two nuclides are the most abundant nickel isotopes and would thus be the most likely ones to be measured for analytical purposes. The peak marked Z is from reactions leading to higher excitation states which were not resolved.

No characteristic peak was found in the prompt proton spectrum of copper. The two unresolved humps are due to protons from reactions leading to a large number of relatively closely spaced excitation states. The energy corresponding to the point X, refers to the maximum proton energy obtainable from ^{63}Cu under the conditions of the experiment, and Y to the corresponding energy for ^{65}Cu.

Analyses. Nickel is commonly electroplated on articles to improve resistance against corrosion, but objects made of iron or steel are seldom plated directly. Instead, the surface is first coated with a layer of copper from 6 to 70 mg/cm^2 in thickness before the nickel is deposited. It thus is most often necessary to determine nickel thicknesses on an underlying layer of copper. From Figure 2 no interference from copper may be expected when the counts under the high energy peaks in the nickel spectrum are integrated as a measure of the nickel content.

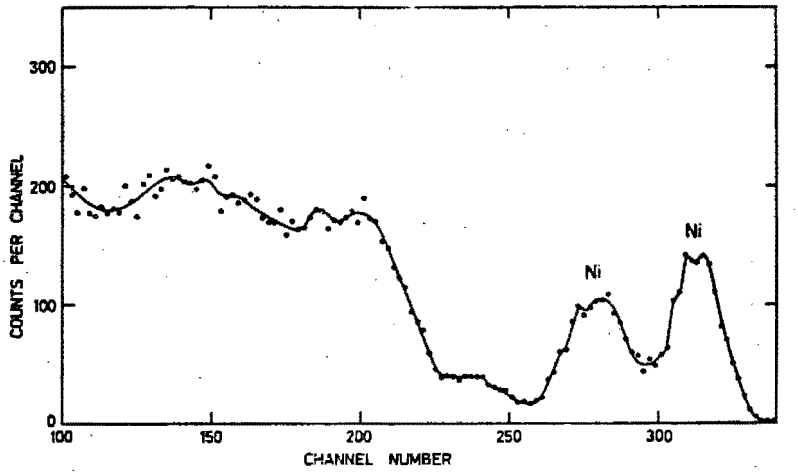

Fig. 3. Energy spectrum of prompt protons obtained from a deposit of nickel on a copper backing irradiated with deuterons.
$\theta = 60°$, $E_d = 3{\cdot}5$ MeV, Au absorber = 196 mg/cm^2.

Figure 3 shows the spectrum obtained from a typical case where a film of nickel approximately 300 $\mu g/cm^2$ in thickness had been plated on copper. The peaks due to protons from nickel, as marked in the figure, can readily be distinguished from those of copper. The energy region over which the counts from nickel were integrated was from 4·86 to 6·30 MeV which corresponded to energies between 9·36 and 10·32 MeV before the protons passed through the gold absorbers.

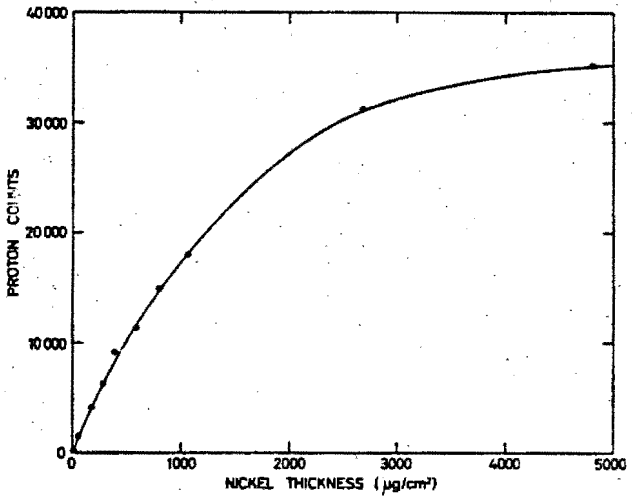

Fig. 4. The variation of proton counts from nickel, with nickel thickness.

TABLE II

Some determinations of nickel films on copper by prompt proton counting

Known nickel thickness ($\mu g/cm^2$)	Integrated proton counts per unit beam current	Measured nickel thickness ($\mu g/cm^2$)	Error ($\mu g/cm^2$)
13·3	250	13·4	+0·1
17·8	418	20·6	+2·8
28·5	566	26·8	−1·7
37·4	797	36·7	−0·7
58·7	1233	55·2	−3·5
76·5	1796	79·1	+2·6
97·8	2242	98·0	+0·2

Standard error = $\pm 2{\cdot}2$ $\mu g/cm^2$

The calibration, showing the variation of proton counts with nickel thickness is shown in Figure 4. The curve reflects the decreased yield obtained for thick films caused by the decrease in the cross section of the reaction with decreasing deuteron energy. However, it can certainly be assumed that the calibration is linear up to 100 $\mu g/cm^2$. Results of a typical series, carried out over this thickness region, are listed in Table II. The standard error was $\pm 2{\cdot}2$ $\mu g/cm^2$ over the whole region. This corresponds to a relative standard error of 2·2% for films of approximately 100 $\mu g/cm^2$, but the relative error increases for thinner films. With a bombarding deuteron beam of 3 mm^2 area used in this investigation, and with a target inclined at 30° to the beam, the precision attained is equivalent to a relative standard error of $\pm 2{\cdot}2\%$ on 24 μg nickel.

Possible Interferences. From the Q-values given in Table I, the only nuclides among the elements considered, which can yield protons with energies greater than those from nickel-58 are chromium-50 and 53, iron-54 and 57 and zinc-67. All the other nuclides have Q-values at least 1 MeV lower than that of nickel-58 and hence cannot produce protons which will interfere in the analysis. Although nickel-61 can also yield higher energy protons, it is obvious that this isotope cannot interfere with the determination of nickel. When the energy levels in the product nuclei are taken into account, it is found that the following proton groups have energies within the region of integration defined for the nickel analysis:

$$^{50}Cr(p_1),\ ^{53}Cr(p_1, p_2),\ ^{54}Fe(p_1, p_2),\ ^{57}Fe(p_2) \text{ and } ^{67}Zn(p_1, p_2, p_3).$$

Despite the fact that the possible sources of interference are nuclides with relatively low abundances in nature, their presence, unless corrected for, can introduce serious errors in the determination of nickel. Thus, test samples containing the interfering element on the surface in concentrations equal to that of nickel gave uncorrected results about 20% high with chromium, about 12% with iron and about 2% with zinc. However, the more abundant isotopes of the interfering element produced proton groups about 15 to 20 times as intense as the interfering ones, but in a different energy region of the spectrum. Their presence could thus be detected readily, and from their intensities, the extent of any interference in the nickel determination could be calculated and the required correction made.

The presence of interfering nuclides in the substrate poses a more involved problem, but it less likely because of the copper undercoat that is plated over the metal surface, as a result of which the energy of the deuteron beam on the surface of the substrate is at most, 2·9 MeV. From the variation of the cross section of (d, p) reactions with energy[9] the yield expected at this energy is at least 10 times less than at 3·5 MeV, and the energy of the proton groups produced would be lowered by an equivalent amount. Interferences from elements considered here would thus not be serious, but if other elements caused interference, the identity of the element would not be obvious and elimination of the interference would require separate investigation.

This work was financially supported by the South African Council for Scientific and Industrial Research and by the South African Atomic Energy Board to whom grateful acknowledgement is made.

This work forms part of a doctoral thesis to be submitted by C.O. to the University of Stellenbosch and is published with the permission of his Promotor.

Southern Universities Nuclear Institute,
P.O. Box 17,
Faure.

Received, November 28th, 1969.

REFERENCES

[1] S. Rubin, T. O. Passel and L. Bailey, *Anal. Chem.*, 1957, **29**, 736.
[2] M. Peisach and D. O. Poole, *J. S. Afr. Chem. Inst.*, 1965, **18**, 61.
[3] M. Peisach and D. O. Poole, *Anal. Chem.*, 1966, **38**, 1345.
[4] J. H. Patterson, A. L. Turkevich and E. Franzgrote, *J. Geophys. Res.*, 1965, **70**, 1311.
[5] O. U. Anders, *Anal. Chem.*, 1966, **38**, 1442.
[6] M. Peisach, D. O. Poole and H. F. Rohm, *Talanta*, 1967, **14**, 187.
[7] C. Maples, G. W. Goth and J. Cerny, *Nuclear Data*, 1966, **2A**, 429.
[8] C. F. Williamson, J.-P. Boujot and J. Picard, *Report CEA-R* 3042, 1966.
[9] C. Olivier and M. Peisach, *J. Radioanal. Chem.* (in press).

ELSEVIER Publishing Co.
Amsterdam

AKADÉMIAI KIADÓ
Budapest

Journal of Radioanalytical Chemistry Vol. 5 (1970) 391—402

DETERMINATION OF CHROMIUM ON METAL SURFACES BY PROMPT PROTON SPECTROMETRY

C. OLIVIER*, M. PEISACH

Southern Universities Nuclear Institute, P. O. Box 17, Faure (South Africa)

Surface concentrations of chromium were determined non-destructively on copper and nickel substrates by prompt proton spectrometry during irradiation with 3.5 MeV deuterons. Ground state protons from ^{52}Cr were used as a measure of the chromium content. The analysis required 5 to 30 min. The relative precision obtained was $\pm 1.8\%$ on copper and $\pm 2.4\%$ on nickel substrates, respectively.

Introduction

With the use of solid state detectors, procedures based on elastic scattering of charged particles have been developed to meet a variety of needs such as determining the thickness of oxide films on aluminium[1] or locating impurities in crystal channels.[2,3] Such methods depend on the difference in energy between particles scattered from the element being analyzed and that from the matrix material in which the required element is situated.

When thin layers of chromium have to be analyzed on substrates of metals having medium atomic weight, such as iron, nickel or copper, scattering methods become difficult to use because the number of particles scattered from the surface chromium is usually small compared to the number of scattered particles of equal energy obtained from the sub-surface layers of the substrate. Furthermore, the mass numbers of the chromium and that of the substrate element are so close together that the particles scattered from the surface layers have almost the same energy and severe demands are made on the resolution of the measuring system. For example, the energy difference between protons scattered from chromium and from iron through 165° is only 5 keV per MeV of the incident particle.

To overcome these difficulties, suitable nuclear reactions may be chosen such that the product particles obtained from the surface element and from the substrate may readily be resolved by the differences in their energies. The flux of particles falling on the detector will, however, not consist solely of particles produced in the nuclear reactions, but will also contain bombarding particles

* Permanent address: Department of Chemistry, University of Stellenbosch, Stellenbosch

that were scattered in the direction of the detector. Since the cross-sections for elastic scattering are usually much larger than the cross-sections of the nuclear reactions concerned, the reaction products will be difficult to measure if their energies lie in the energy continuum covered by the elastically scattered particles from the substrate. It is thus advantageous to use exoergic reactions from which product particles may be obtained with energies higher than attained by scattered particles.

The energy spectra as recorded by solid state detectors will show very high plateaux due to scattered particles, but in addition there may be a considerable continuum, caused by the summation of energies from two (or more) coincident particles, at higher energies in the region where nuclear products may be expected. To eliminate such summations, electronic pulse pile up rejection may be used, but it is simpler to cover the detector with an absorber just thick enough to prevent scattered particles from passing through and yet to allow the product particles to penetrate. Since (d, p) or (t, p) reactions are usually exoergic, these reactions would be suitable but most (d, α) reactions could not be used because of the limited penetration of alpha particles. In this investigation (d, p) reactions were used.

Table 1

Ground state Q-values and product particle energies from (d, p) and (d, α) reactions on stable isotopes of Cr, Fe, Ni and Cu

Target nuclide	Natural abundance, %	Q-value,[4] MeV		Maximum particle energy for $E_d = 3.5$ MeV and 0°, MeV	
		(d, p)	(d, α)	E_p	E_α
^{50}Cr	4.31	7.0451	4.9322	10.537	8.233
^{52}Cr	83.76	5.7169	4.5163	9.217	7.840
^{53}Cr	9.55	7.4967	7.6294	10.988	10.825
^{54}Cr	2.38	4.0294	5.2167	7.529	8.521
^{54}Fe	5.82	7.0742	5.1677	10.567	8.474
^{56}Fe	91.66	5.4170	5.6578	8.914	8.951
^{57}Fe	2.19	7.8179	8.2405	11.308	11.432
^{58}Fe	0.33	4.3603	5.4685	7.860	8.777
^{58}Ni	67.88	6.7788	6.5142	10.272	9.782
^{60}Ni	26.23	5.5962	6.0785	9.093	9.372
^{61}Ni	1.9	8.3749	8.7232	11.864	11.915
^{62}Ni	3.66	4.6149	5.6145	8.118	8.929
^{64}Ni	1.08	3.8779	5.1332	3.441	7.925
^{63}Cu	69.09	5.6914	9.3481	9.189	12.524
^{65}Cu	30.91	4.8359	8.9612	8.334	12.161

Nuclear reaction kinematics

When stable chromium, iron, nickel or copper nuclei are bombarded with deuterons of a few MeV, the most likely reactions yielding prompt charged particles are (d, p) and (d, α) reactions. The relative Q-values and the maximum energies attained by the prompt charged particles from reactions induced by 3.5 MeV deuterons are given in Table 1. Because the reactions are highly exoergic, many energy states can be excited in the product nuclei and the energy spectra of the prompt particles will thus extend from somewhat above 11 MeV to very low energies.

The bombarding beam loses very little energy in traversing the surface layers so that the energy spectra from the surface elements may be expected to consist of a series of narrow peaks whose widths are determined by the resolution of the measuring system. By contrast, the bombarding beam may be entirely stopped by the substrate, and hence the energy spectrum obtained from reactions in it may be expected to consist of undulating plateaux caused by the broadening and overlapping of individual peaks. In this broadened continuum low energy peaks from the surface elements may be difficult to discern. Accordingly, low energy reaction products will be of little interest for analytical purposes and may be eliminated together with the scattered particles.

Experimental

Preparation of standards and samples

Standard thicknesses of chromium were electroplated onto various metal discs usually over a circular area of 16 mm diameter. The thicknesses were obtained by weighing, but very thin deposits were also analyzed by neutron activation analysis. For comparison of spectra, thin films of nickel, iron and copper were electroplated onto tantalum. Metal discs thicker than the range of the bombarding deuterons were cut from sheets with over 99.9% purity.

Irradiation and measurement

Targets were irradiated inside a 90-cm scattering chamber with deuteron beams obtained from the 5.5 MV Van de Graaff accelerator of the Southern Universities Nuclear Institute. Beam currents ranged between 0.5 and 3.5 μA.

Using 3.5-MeV deuterons, the energy spectrum of prompt protons from (d, p) reactions were measured with a silicon semi-conductor detector mounted on a rotating arm which enabled the angle of measurement to be changed as required. The resolution of the detector and the measuring equipment was better than 45 keV.

The detector was covered with gold foils, each of about 15 mg/cm^2 thickness, to absorb the scattered deuterons and low energy protons. Four such foils were

sufficient to eliminate pulses from deuterons, but more foils were frequently used to enable the high energy protons, that would otherwise have passed through the detector volume, also to be stopped within the depletion layer of the detector. The effect of the absorber foils was to broaden the peaks obtained from each proton group and the broadening increased with absorber thickness.

Results and discussion

Energy spectra of prompt protons

Typical energy spectra of the prompt protons obtained from thin films of chromium, iron, nickel and copper on tantalum backings and of the protons from the backing itself are shown in Fig. 1. The positions of expected peaks, each marked in the figure by an arrow labelled with the target nuclide from which the particular proton group, p_i, originates, are calculated according to the known nuclear energy levels of the product nucleus and reaction kinematics. The energy scale in the figure refers to the energy of the particle before passing through the absorber. This scale is not linear because the rate of energy loss of the protons in the absorber decreases with increasing proton energy.

In the spectrum obtained from chromium the peaks due to proton groups from ^{52}Cr dominate because of the high abundance of this isotope. Of these peaks the two most prominent are those corresponding to the p_0 and p_4 proton groups but the latter lies in an energy region where there is a greater likelihood of obtaining protons from other elements. The p_0 group was accordingly preferred for analytical purposes and by integrating the number of counts under this peak, a value is obtained which is a quantitative measure of the concentration of chromium, while the energy of the protons indicates whether the chromium is in fact in the surface or below it. This integrated count is referred to as 'the chromium count'.

Just as in the case of chromium, the proton energy spectrum obtained from iron is virtually that of a single isotope, in this case ^{56}Fe. Each of the prominent peaks represents two or more proton groups that were not resolved under the conditions of measurement. The three proton groups with the highest energy, $^{56}Fe(p_0, p_1, p_2)$ sum to produce a spectrum peak which lies about 300 keV below that of $^{52}Cr(p_0)$. Although this separation exceeds the resolution of the measuring system, it can readily be seen that in samples containing a small surface concentration of chromium in the presence of a large surface concentration of iron, the chromium peak might be difficult to resolve as a result of overlapping by the tail of the composite peak from ^{56}Fe.

The proton energy spectrum from nickel consists of conveniently high energy peaks corresponding to $^{58}Ni(p_0)$ and $^{58}Ni(p_2)$ proton groups which enable nickel to be determined separately.[5] In addition the proton groups $^{60}Ni(p_0, p_1, p_2)$ generate

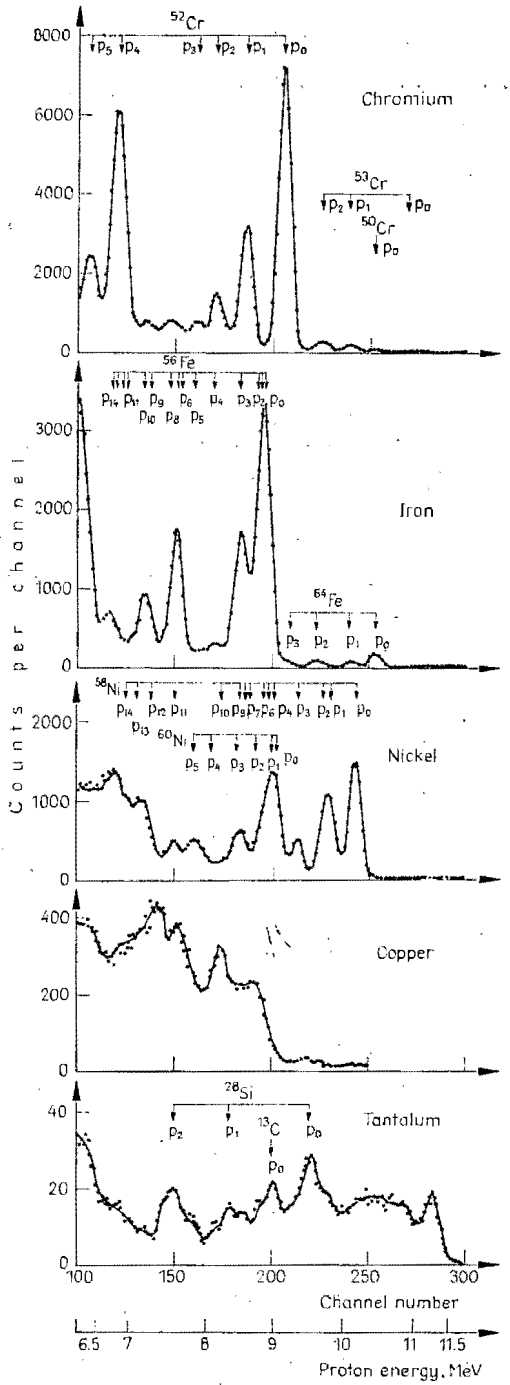

Fig. 1. Typical proton energy spectra obtained from thin films of chromium, iron, nickel and copper on tantalum irradiated with 3.5 MeV deuterons and measured at 60°

a composite peak lying within 200 keV from that of the ground state protons from ^{52}Cr. This composite peak probably also includes counts from the proton groups $^{58}Ni(p_4, p_5, p_0)$ which have similar energies. In the event of both chromium and nickel being present in surface layers the direct determination of chromium, as indicated above, would be impossible. It would then be necessary to use the number of counts obtained in the high energy nickel peaks as a means for calculating the extent of the interference in the energy region of interest for the chromium analysis.

The spectrum obtained from copper shows no major peaks. This is probably due to the fact that there are several proton groups which are produced with similar yields and with energies that cannot be resolved under the conditions of measurement used here. It is thus unlikely that copper could seriously hinder determinations of chromium except when present in relatively high surface concentrations.

The tantalum spectrum represents the background against which the measurements were made. Slight peaks appearing in the spectrum could be assigned to protons from silicon and carbon deposits of which formed from residual silicon vacuum oil vapours which decomposed at the heated point of incidence of the irradiation beam on the target.

The effect of backing material

1) *Iron.* Chromium is commonly electroplated on articles to improve their wear and appearance but objects made of iron or steel are seldom plated directly. Instead, the surface is first plated with a layer of copper from 6 to 70 mg/cm^2 in thickness, and sometimes further plated with nickel before the chromium is deposited. When 3.5 MeV deuterons are used to measure the thickness of chromium, the energy of the deuteron beam at the surface of the iron is at most 2.9 MeV, having lost the extra energy passing through at least 6 mg/cm^2 of copper.[6] It follows that the maximum energy of the $^{56}Fe(p_0)$ proton group would be at least 900 keV less than that of the $^{52}Cr(p_0)$ group from chromium on the surface. Under these conditions the $^{52}Cr(p_0)$ peak can readily be resolved from the spectrum of iron.

2) *Copper.* A typical spectrum obtained from a thick sample of copper is shown in Fig. 2. To facilitate comparison with the spectra in Fig. 1, the energy scales are the same in the two figures.

From Figs 1 and 2 it can be seen that the forward edge of the spectrum from thick copper just overlaps into the energy region covered by the peak from $^{52}Cr(p_0)$ protons. When the thickness of the chromium layer is less than about 100 μg/cm^2 it can be assumed that the deuteron beam undergoes a negligible energy loss when passing through it and that the energy spectrum of the protons from copper remains unchanged. The chromium count is then given by the difference between that of the pure and coated copper.

When the thickness of the chromium layer is between 100 and 300 $\mu g/cm^2$ this technique is no longer valid. The deuteron beam now loses at least 10 keV in the chromium surface layer with the result that the copper spectrum would undergo an apparent shift to the left equivalent to the energy lost in the chromium. Furthermore the yield of protons decreases with decreasing energy, so that the

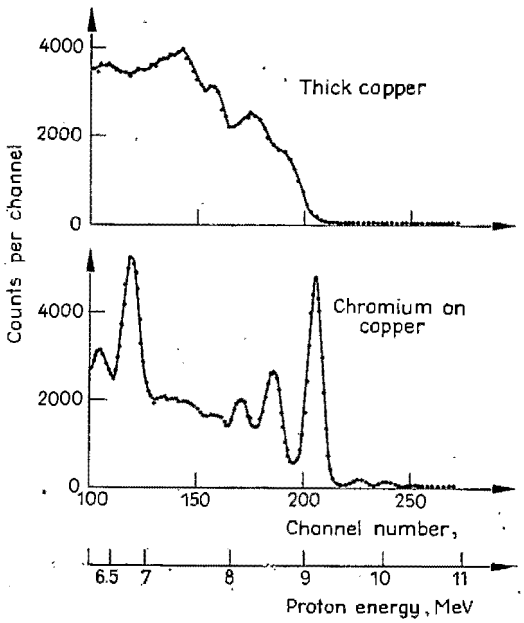

Fig. 2. Proton energy spectrum from a chromium film on copper compared with the spectrum from thick copper

number of counts that have to be subtracted to obtain the chromium count is now less than the value obtained from pure copper. Under these conditions the forward half of the peak representing the $^{52}Cr(p_0)$ proton group has the same shape as that obtained from a thin deposit of chromium and only the backward half is distorted by proton counts obtained from copper. By normalizing the known shape to the maximum and leading edge of the observed spectrum and integrating under the normalized curve a corrected value of the chromium count is obtained. Because of the added curve-fitting procedure larger relative errors are introduced but these are compensated for by the better statistical precision arising from the increased count from the thicker chromium layer.

When the thickness of chromium exceeds 300 $\mu g/cm^2$ the energy lost by the deuteron beam in it is at least 30 keV. This would cause such an apparent shift of the copper spectrum as to make the region of overlap relatively small, and hence would not cause any difficulty in determining the chromium count.

3) *Nickel.* A typical spectrum obtained from a sample of thick nickel is shown in Fig. 3. Whenever nickel is present as an undercoat for the chromium, the proton counts from the nickel will play the part of a large background count, the effect of which will be to reduce the precision of the chromium determination The analysis would be further complicated by the fact that just as was the case with copper, the nickel spectrum will undergo an apparent shift to lower energies

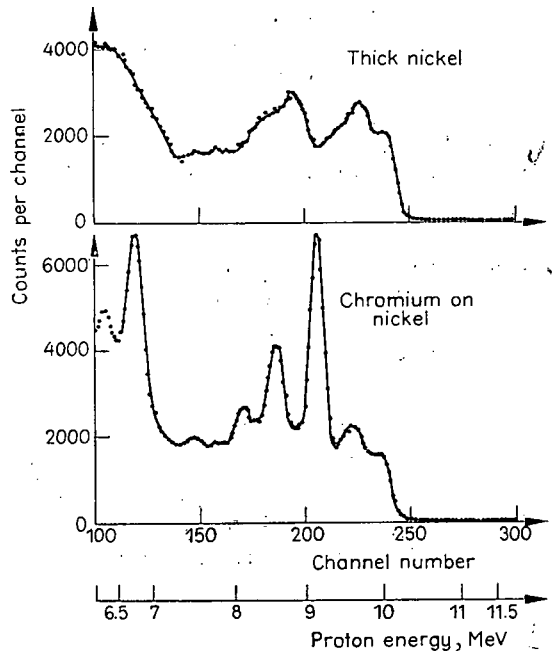

Fig. 3. Proton energy spectrum from a chromium film on nickel compared with the spectrum from thick nickel

according to the thickness of the chromium outer layer, but, unlike copper, the contribution from nickel does not become negligible.

The high energy hump in the spectrum of thick nickel (see Fig. 3) is almost entirely due to the ^{58}Ni isotope, and apart from a negligible contribution of counts from ^{50}Cr and ^{53}Cr, is not affected by the chromium content. A selected region near the top of this hump is integrated as a measure of the nickel contribution. This value is called 'the nickel count'.

To obtain the chromium count, the spectra of thick nickel and chromium-coated nickel are compared. The ratio of the two nickel counts is used to normalize the spectrum of thick nickel to that of the coated sample. Thereafter the normalized nickel spectrum is shifted an extend equivalent to the difference in the energies

between the tops of the nickel humps in the two spectra. The chromium count is then given by the difference between the integrated counts of the spectrum from the sample and the normalized spectrum over the energy region of the chromium peak. A secondary check is given by the resultant shape of the spectrum obtained if the normalized spectrum is subtracted from the observed spectrum of the sample.

This treatment of the analytical data is valid only if the nickel layer can be considered 'infinitely' thick. According to the extrapolation of the excitation curve for the (d, p) reaction on ^{58}Ni (see Section below), the yield of protons falls to about 1 % of its value at 3.5 MeV when the deuteron energy is 2.2 MeV. Accordingly, if the energy of the bombarding deuteron beam falls below 2.2 MeV within the nickel layer, the nickel may be considered 'infinitely' thick. This corresponds to a nickel deposit of 12.5 mg/cm^2. Such a restriction was, however, shown to be too stringent, because in the energy region of interest, the spectra obtained from varying thicknesses of nickel on tantalum were indistinguishable from those of thick nickel when the nickel exceeded 4.4 mg/cm^2. When this value is compared with the nickel thickness (6 to 40 mg/cm^2) normally applied as an undercoat for the electroplating of chromium, it follows that the undercoat can always be considered 'infinitely' thick.

The effect of deuteron energy

The variation of proton counts with deuteron energy between 2.45 and 3.90 MeV is shown in Fig 4, for thin targets of chromium, iron and nickel. In the case of chromium, only counts from the ^{52}Cr(p_0) group were considered but counts

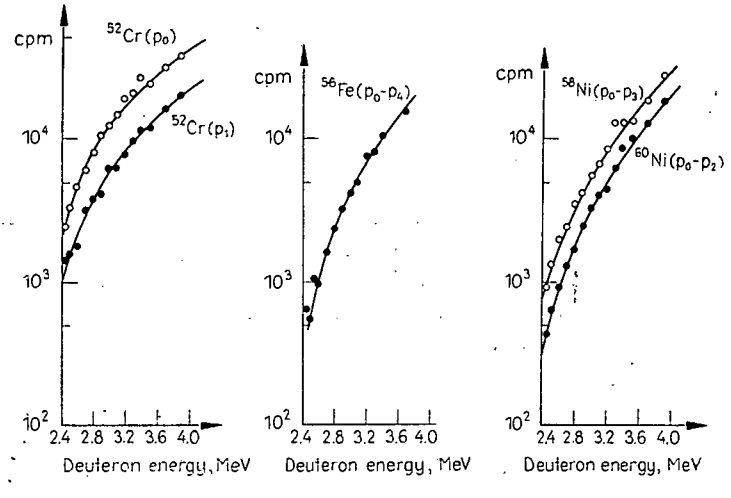

Fig. 4. The variation of proton count-rate from deuteron irradiated chromium, iron and nickel measured at 60° as a function of deuteron energy. Counts were summed for the proton groups indicated

were summed for the p_0 to p_4 proton groups from ^{56}Fe, the p_0 to p_3 groups from ^{58}Ni and the p_0 to p_2 groups from ^{60}Ni.

Since the proton yield increases with deuteron energy, it appears on the one hand that the higher the bombarding energy the more sensitive is the analysis likely to be. On the other hand the proton yield from heavier elements increases appreciably towards the end of the energy range studied, with the result that the higher background would lead to poorer precision. The energy of 3.5 MeV was selected as a reasonable compromise.

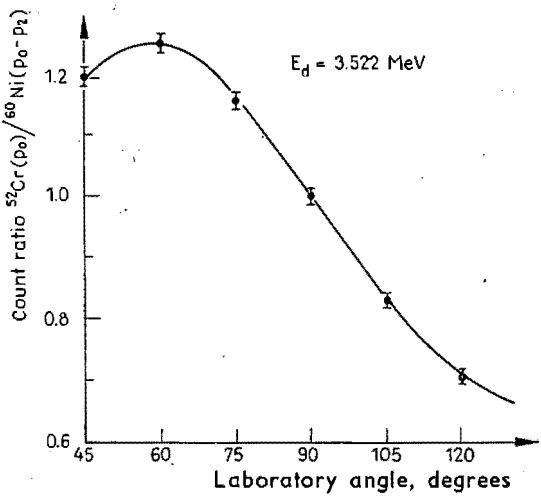

Fig. 5. The variation of the proton counts from chromium relative to that from nickel as a function of measuring angle. The data were arbitrarily normalized to unit value at 90°

The effect of the angle of measurement

By comparing the counts obtained with 3.5 MeV deuterons from different metals at the same measuring angle, it was found that the yield of proton counts from chromium changed more rapidly than that from nickel. The ratio of the chromium count to that from nickel is shown in Fig. 5 as a function of the measuring angle between 45° and 120°. These limits were imposed by the configuration of the measuring equipment.

Not only is the absolute yield from chromium higher at forward angles, but the yield relative to that of nickel is also much higher than at backward angles. Thus at forward angles better sensitivity and precision may be expected. Optimum conditions were shown to prevail at 60° and this angle was consequently chosen for the analytical determinations.

Calibration

Standard thicknesses of chromium on copper were used to calibrate the measuring system. The variation of proton counts obtained as a function of chromium thickness is shown in Fig. 6. The calibration curve deviates from linearity for film thicknesses exceeding 600 $\mu g/cm^2$, as a result of a decrease in the energy of the deuteron beam within the chromium layer and hence a decrease in the average reaction cross section. In the linear part of the calibration the number of counts recorded was 40.27 counts cm^2 per μg for an irradiation with 1 millicoulomb

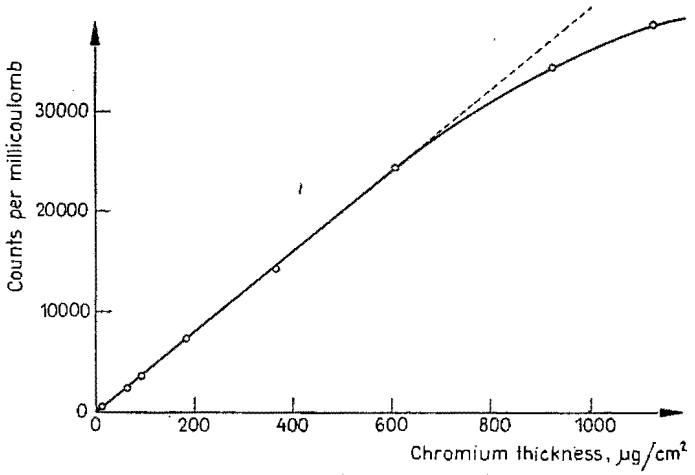

Fig. 6. The variation of proton counts with chromium thickness, which serves as a calibration curve

current. A different calibration curve is, however, needed when the experimental conditions, such as measuring angle or bombarding energy are changed.

If each calibration point is in turn taken to be an analyzed sample and the chromium thickness determined in terms of the others, the relative standard deviation was found to be $\pm 1.83\%$.

Precision and accuracy

From the above discussion the method seemed to be least precise when chromium films had to be measured over a substrate of nickel. This case was selected for determining the precision of the analysis with samples for which the chromium thickness was determined by weighing and checked by neutron activation analysis. Some results obtained under the same conditions as pertained to Fig. 6 are given in Table 2.

The standard error was ± 3.2 $\mu g/cm^2$ and the relative precision of the analyses, $\pm 2.40\%$, which was rather worse than the precision attained for the calibration of the method. This was expected as a result of the enhanced interference of proton

counts from nickel, compared to those from copper. Some of the samples had chromium films thicker than the 600 $\mu g/cm^2$ limit of the linear relationship between

Table 2

Some typical results of chromium determinations on nickel

Thickness, $\mu g/cm^2$		Counts per millicoulomb	Thickness determined, $\mu g/cm^2$	Counts per unit thickness[a]	Relative error, %
by weight	by neutron activation				
988.8	984.5	35,999	992.0	[b]	+0.32
490.9	498.5	19,711	489.5	40.15	—0.60
265.1	275.4	10,385	257.9	39.17	—2.72
166.6	157.4	6,716	166.8	40.31	+0.12
112.9	108.9	4,723	117.3	41.83	+3.90
—	73.5	3,003	74.6	40.86[c]	—

[a] For 1 mCb current.
[b] This value lies beyond the linear part of the calibration curve.
[c] Calculated from thickness as obtained by neutron activation.
No. of test samples: 16
No. of test analyses: 41
Relative standard deviation = $\pm 2.40\%$

counts and thickness. In those cases the thickness was read off the calibration curves. In other cases where the films were very thin, the test samples were not weighed and the proton counts were compared with the thickness as determined by activation analysis only.

The accuracy of the method could be judged from the mean error which was negligibly different from zero, and from the fact that the determinations showed no bias, whether compared with weighed standards or those analyzed by activation analysis.

*

The financial assistance obtained from the South African Atomic Energy Board and the South African Council for Scientific and Industrial Research is gratefully acknowledged. This work forms part of a doctoral thesis to be submitted by C.O. to the University of Stellenbosch and is published with the permission of his Promotor.

References

1. M. Peisach, D. O. Poole, H. F. Röhm, *Talanta*, 14 (1967) 187.
2. J. A. Davies, J. Denhartog, L. Eriksson, J. W. Mayer, *Can. J. Phys.*, 45 (1967) 4053.
3. E. Bogh, Proc. Intern. Conf. Solid State Physics Research with Accelerators. BNL-50083 (C-52), 1967, p. 76.
4. C. Maples, G. W. Goth, J. Cerny, *Nuclear Data*, 2A (1966) 429.
5. C. Olivier, M. Peisach, *J. S. Afr. Chem. Inst.* (in the press).
6. C. F. Williamson, J.-P. Boujot, J. Picard, CEA R-3042, 1966.

No. 34

Sonderdruck aus Radiochimica Acta 15, 123–127 (1971)

Activation Cross Sections for Deuteron-Induced Reactions on Calcium Isotopes up to 5.5 MeV

By TIELMAN J. DE WAAL*, MAX PEISACH and RENÉ PRETORIUS, Southern Universities Nuclear Institute, P. O. Box 17, Faure, C. P., South Africa

With 4 figures. (Received July 16, 1970)

Abstract

Calcium fluoride, of natural isotopic composition and isotopically enriched, was activated with deuteron beams up to 5.5 MeV using a Van de Graaff accelerator. Activation cross sections were determined by gamma-ray spectrometry for the following reactions:
$^{40}Ca(d, \alpha)^{38}K$; $^{42}Ca(d, n)^{43}Sc$; $^{43}Ca(d, n)^{44}Sc$; $^{43}Ca(d, n)^{44m}Sc$; $^{48}Ca(d, p)^{49}Ca$; $^{48}Ca(d, 2n)^{48}Sc$.
The relative accuracy of the excitation functions is $\pm$ 8% except for the reaction $^{43}Ca(d, n)^{44m}Sc$, where the accuracy is $\pm$ 15%.

Zusammenfassung

Kalziumfluorid von natürlicher Isotopenzusammensetzung und mit Isotopenanreicherung wurde mit Deuteronen bis zu 5,5 MeV mit Hilfe eines Van-de-Graaff-Beschleunigers aktiviert. Die Aktivierungsquerschnitte wurden durch Gammastrahlungsspektrometrie für folgende Reaktionen bestimmt:
$^{40}Ca(d, \alpha)^{38}K$; $^{42}Ca(d, n)^{43}Sc$; $^{43}Ca(d, n)^{44}Sc$; $^{43}Ca(d, n)^{44m}Sc$; $^{48}Ca(d, p)^{49}Ca$; $^{48}Ca(d, 2n)^{48}Sc$.
Die relative Genauigkeit der Anregungsfunktionen beträgt $\pm$8% mit Ausnahme der Reaktion $^{43}Ca(d, n)^{44m}Sc$, wo die Genauigkeit bei $\pm$15% liegt.

Résumé

A l'aide d'un faisceau de deutérons d'énergie atteignant 5,5 MeV, obtenu grâce à un accélérateur Van de Graaff, on a activé du fluorure de calcium naturel en vue de la production d'isotopes. Les sections efficaces d'activation ont été déterminées par spectrométrie γ pour les réactions suivantes:
$^{40}Ca(d, \alpha)^{38}K$; $^{42}Ca(d, n)^{43}Sc$; $^{43}Ca(d, n)^{44}Sc$; $^{43}Ca(d, n)^{44m}Sc$; $^{48}Ca(d, p)^{49}Ca$; $^{48}Ca(d, 2n)^{48}Sc$.
La précision relative des fonctions d'éxcitation est de $\pm$8%, sauf pour la réaction $^{43}Ca(d, n)^{44m}Sc$, où elle est de $\pm$15%.

Activation analysis is a useful, sensitive and often highly specific method for determining a wide variety of elements and their isotopes. This technique is most often used with neutrons from reactors or generators where the energy distribution in the irradiation flux can be altered by the analyst only to a limited extent. Under such conditions the variation of the activation cross section with the energy of the bombarding particle is of minor importance. This is no longer the case when activation is induced by charged particle beams, the energy of which can readily be altered to suit the needs of the analyst. A knowledge of the relevant excitation functions would then enable the proper choice of the bombarding energy to be made, in order to produce the highest yield of the required activity but at the same time to suppress interfering activities as much as possible. Such information is also of importance for radionuclide production and for studies of nuclear reaction mechanisms.

The increased interest shown by the medical profession in the use of stable calcium isotopic tracers has already resulted in the appearance of several nuclear methods for the determination of calcium isotopes [1–6]. One such method [6] uses deuteron activation and for it a knowledge of the excitation functions for the production of deuteron-induced radioactivities would be useful. In this investigation the activation cross sections were determined with a deuteron beam obtained from a Van de Graaff accelerator whose maximum energy was 5.5 MeV.

Experimental

Preparation of targets

Both calcium oxide and calcium fluoride have suitable thermal properties to withstand the high temperatures generated by charged particle beams. However, when targets of calcium oxide are exposed to the atmosphere they deteriorate as a result of chemical action. Furthermore, fluorine is to be preferred to oxygen in targets irradiated with deuterons because the most likely deuteron-induced reactions on fluorine lead either to stable nuclides or to fluorine-20 which has a half-life of only 11 sec. For these reasons calcium fluoride was used.

Enriched isotopes of calcium were obtained as carbonate from the Oak Ridge National Laboratory, U. S. A. These were converted to the fluoride by fuming with hydrofluoric acid in a platinum crucible. The targets of calcium fluoride, in which the calcium was either of natural isotopic composition or enriched in a particular isotope were prepared by distilling the heated material in vacuum onto tantalum discs, 0.25 mm thick. Deposits prepared in this way [5] had a thickness of about 200 $\mu g/cm^2$ which could be reproduced with a relative precision of about 4%. The thickness of each target was determined by weighing.

* Present address: S. A. Titan Products (Pty) Ltd., Umbogintwini, Natal, South Africa.

1. E. JUNOD and J. LAVERLOCHERE, 'Proc. 3rd Intern. Colloquium on Biology', Saclay, 1963.
2. S. AMIEL and J. O. JULIANO, Israel Atomic Energy Commission Rept. IA-933 (1964).
3. M. PEISACH and R. PRETORIUS, Anal. Chem. **38**, 965 (1966).
4. W. F. BETHARD, R. A. SCHMITT, D. A. OLEHY, S. A. KAPLAN, S. M. LING, R. H. SMITH and E. DALLE MOLLE, 'Nuclear Activation Techniques in the Life Sciences', I. A. E. A., Vienna, 1967, p. 533.
5. W. R. MCMURRAY, M. PEISACH, R. PRETORIUS, P. VAN DER MERWE and I. J. VAN HEERDEN, Anal. Chem. **40**, 266 (1968).
6. T. J. DE WAAL, M. PEISACH and R. PRETORIUS, Anal. Chem. **41**, 416 (1969).

Irradiation

Samples were irradiated with deuteron beams of between 1 and 10 μA obtained from the 5.5 MeV Van de Graaff accelerator of the Southern Universities Nuclear Institute. The energy spread in the beam was less than 0.1%. Up to 12 sample discs could be mounted on a rotating sample holder [3], which fitted into a vacuum chamber attached to the beam tube of the accelerator, and rotated at about 100 rpm.

Aluminium foils of different thicknesses were placed in front of each target thereby enabling data to be obtained simultaneously at 12 different deuteron energies. The energy of the beam in the middle of each target was determined from tabulated stopping powers [7]. The whole chamber was electrically insulated to obtain beam currents from readings with a current integrator [8], but these flux measurements were not sufficiently accurate for absolute determinations of cross sections. Activities formed in such multiple irradiations were however useful to obtain relative cross section values.

Accurate flux measurements were obtained when single targets were irradiated in a Faraday cup at different bombarding energies. The construction of the Faraday cup was such that secondary electron emission was negligible. The relative precision of the current measurements was 0.1% and its accuracy about 1%. In these irradiations no aluminium foil was used to degrade the energy of the bombarding beam.

Sets of relative cross sections obtained from the multiple irradiations were normalized to all the absolute values obtained from the single irradiations by the method of least squares.

Measurement of radioactivity

After irradiation, samples were analysed by gamma-ray spectrometry using a 3″ × 3″ NaI(Tl) scintillator or a 20 cc Ge(Li) detector, coupled to a multichannel analyser. Some of the radionuclides formed in the sample emitted beta-particles with appreciable energy. Because such negatrons tended to blanket lower energy photopeaks, it was found necessary to fit the detectors with a 'perspex' cap about 1.5 g/cm² in thickness to prevent the beta-particles from being recorded and to minimize bremsstrahlung formation.

The photopeak efficiency of the detectors was determined with substandards of sodium-22, manganese-54, cobalt-57 and 60, yttrium-88, caesium-137 and mercury-203, obtained from the National Physical Research Laboratory, Pretoria and the International Atomic Energy Agency, Vienna. The activities of the standards were known with an accuracy of about 1%.

Counting which started about 10 min after irradiation to allow time for very short-lived activities to decay, was continued periodically until sufficient data had been accumulated for the major components to be separately determined with the required precision by decay measurements.

Calculation of cross sections

The activity, A, produced in a sample containing N target nuclei by a bombardment with Φ particles/s · cm² for a time t_i is given by

$$A = \sigma \Phi N \left(1 - e^{-\lambda t_i}\right), \tag{1}$$

where σ is the activation cross section and λ the radioactive decay constant. The cross section can then be calculated from

$$\sigma = \frac{M \cdot C}{\mathcal{N} w a n \varepsilon \Phi \left(1 - e^{-\lambda t}\right)}, \tag{2}$$

where

$\mathcal{N}$ = Avogadro number = 6.0225×10^{23} molecules per g · mol
C = number of counts recorded per unit time with a detection efficiency ε, i. e. $\varepsilon A = C$,

and the target consists of w g of a compound with molecular weight M in which the number of atoms of target element is n and the fractional isotopic abundance of the isotope concerned is a i. e. $N = wan\mathcal{N}/M$. (In the case of both CaF_2 and CaO targets used here, $n = 1$.)

When using methods of gamma-ray spectrometry, the count rate, C, can more conveniently be replaced by C', the number of counts in the relevant photopeak of the gamma-ray spectrum recorded over a period t_c, the middle of which is a time t_d after the end of the irradiation. Correction can then be made for decay, and eq. 2 can be rewritten in terms of the measured parameters as

$$\sigma = \frac{M}{\varepsilon p a \mathcal{N}} \cdot \frac{C'}{t_c} \cdot \frac{\pi d^2}{4w} \cdot \frac{t_i \times 1.6 \times 10^{-19}}{Q} \times \frac{e^{\lambda t_d}}{\left(1 - e^{-\lambda t_i}\right)} \cdot 10^{24} \text{ barns}, \tag{3}$$

where

ε = the efficiency measured in photopeak counts per gamma-ray,
p = the gamma-ray intensity in gamma-rays per disintegration,
w = the total weight of target material
d = the diameter of the target area
Q = the integrated irradiation current in coulombs.

The third factor represents the surface concentration in g/cm².

Results and Discussion

Since the main stimulus for this investigation was to obtain data for isotopic dilution experiments and since in such investigations the isotopic composition of the samples is not much different from that of the natural element, only those reactions were considered from which measurable amounts of radionuclides were

7. C. F. WILLIAMSON, J.-P. BOUJOT and J. PICARD, Rept. CEA-R 3042 (1966).
8. E. BLIGNAUT and J. J. KRITZINGER, Nucl. Instr. Methods **36**, 176 (1965).

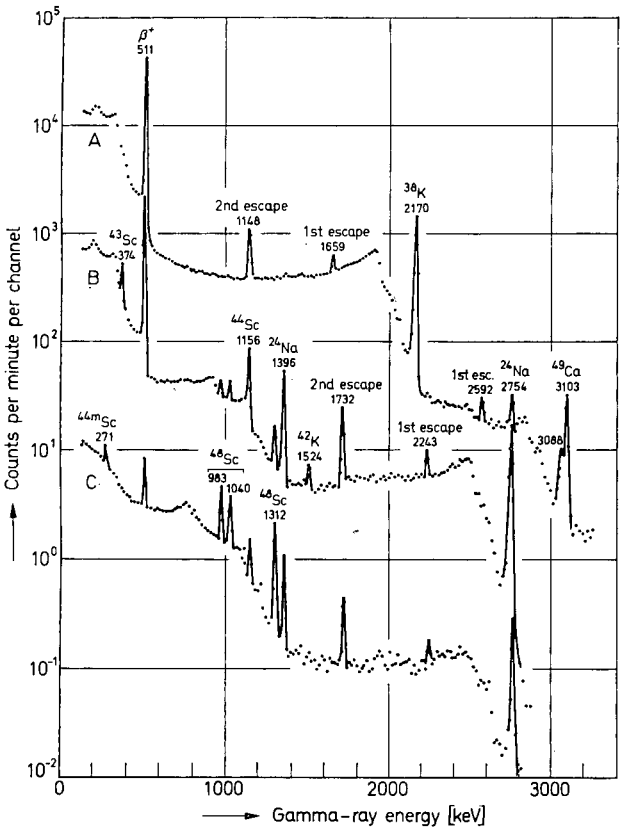

Fig. 1. Gamma-ray spectra obtained from the decay of a natural calcium fluoride target irradiated with 5.120 MeV deuterons. The 3088-keV peak is the second escape peak from the 4110-keV gamma-ray from ^{49}Ca (not shown in the figure). Curve A: after 0.168 h decay; Curve B: after 2.118 h decay; Curve C: after 90.633 h decay

generated in deuteron-irradiated calcium of natural isotopic composition. These radionuclides are listed in Table 1. Some typical spectra obtained from a single sample during its decay are shown in Fig. 1.

Some of the activities could have been formed from more than one calcium isotope. One of the ways in which scandium-44 and 44m could have formed is by a (d, γ) reaction on calcium-42, but (d, γ) reactions are very unlikely. This was confirmed experimentally by irradiating an enriched $^{42}CaF_2$ target at different deuteron energies up to 5.5 MeV. No scandium-44 or 44m was found. The same applied to the formation of scandium-48 from the reaction ^{46}Ca(d, γ)^{48}Sc. The yield of scandium-48 by this reaction was also expected to be minimal due to the low natural isotopic abundance of calcium-46. The formation of scandium-43 by the reaction ^{43}Ca(d, 2n)^{43}Sc was ignored because the highest energy used in this investigation (5.456 MeV) is below the calculated threshold of the reaction (5.472 MeV). It can thus be seen from Table 2 that each activity formed in a target of natural calcium, irradiated with deuterons having energies up to 5.5 MeV, could have been formed from only one reaction, except in the case of potassium-42 at bombarding energies somewhat above 5 MeV, when this nuclide could have been produced by the reactions ^{42}Ca(d, 2p)^{42}K and ^{44}Ca(d, α)^{42}K.

Table 1. *Nuclear data of radionuclides detected in natural calcium fluoride irradiated with 5.5 MeV deuterons* [9]

Radionuclide	Half-life	Main gamma-ray energies (keV)	Relative gamma-ray intensity (%)
^{38}K	7.71 m	2170	100
		(β^+)	200
^{42}K	12.36 h	1524	18
^{49}Ca	8.8 m	3103	89
		4110	10
^{43}Sc	3.92 h	374	22
		(β^+)	176
^{44}Sc	3.92 h	1156	100
		(β^+)	188
^{44m}Sc	2.44 d	271	86
^{48}Sc	1.83 d	983	100
		1040	100
		1312	100

(β^+) refers to positron decay and hence the appearance of 511 keV annihilation radiation.

Table 2. *Possible reactions leading to observed radionuclides in deuteron-irradiated natural calcium*

Radionuclide	Nuclear reaction	Q-value MeV [10]	Target abundance in nature %
^{38}K	^{40}Ca(d,α)^{38}K	4.6496	96.97
^{42}K	^{42}Ca(d,2p)^{42}K	−4.972 [11]	0.64
	^{44}Ca(d,α)^{42}K	4.2676	2.06
^{49}Ca	^{48}Ca(d,p)^{49}Ca	2.9189	0.18
^{43}Sc	^{42}Ca(d,n)^{43}Sc	2.6988	0.64
	^{43}Ca(d,2n)^{43}Sc	−5.229	0.145
$^{44,\ 44m}$Sc	^{42}Ca(d,γ)^{44}Sc	12.4092	0.64
	^{43}Ca(d,n)^{44}Sc	4.4816	0.145
^{48}Sc	^{46}Ca(d,γ)^{48}Sc	14.5029	0.0033
	^{48}Ca(d,2n)^{48}Sc	−2.718	0.18

There are two nuclides, potassium-42 and scandium-43, for which the most intense gamma-ray has a low relative intensity (see Table 1).

Analytical methods for the determination of isotopic concentrations based on counting potassium-42 would thus have poor precision except for very enriched specimens. Interest in the determination of cross sections for its production is thus lacking. Scandium-43, on the other hand, can be determined by counting positron annihilation gamma-rays instead of the weak 375-keV photons it emits. When this alternative method is resorted to, it should be borne in mind that scandium-44 also emits positrons and is indistinguishable from scandium-43 by its decay rate. When both of these scandium radioisotopes are present in an activated sample, as was the case in all samples measured in

9. C. M. LEDERER, J. M. HOLLANDER and I. PERLMAN, 'Table of Isotopes', 6th Ed. Wiley, New York (1968).
10. C. MAPLES, G. W. GOTH and J. CERNY, Nuclear Data **2**, 429 (1966).
11. F. EVERLING, L. A. KOENIG, J. H. E. MATTAUCH and A. H. WAPSTRA, 'Nuclear Data Tables', Part I, National Academy of Sciences, Washington (1961).

Table 3. *Cross sections of deuteron-induced reactions*

E_d (MeV)	Reaction cross sections (millibarns) $^{40}Ca(d, \alpha)^{38}K$	$^{42}Ca(d, n)^{43}Sc$	$^{43}Ca(d, n)^{44}Sc$	$^{43}Ca(d, n)^{44m}Sc$	$^{48}Ca(d, p)^{49}Ca$	$^{48}Ca(d, 2n)^{48}Sc$
5.456	4.77 ± 0.19	80.1 ± 7.5	76.6 ± 3.8	22.4 ± 4.5	134 ± 27	98.0 ± 3.9
5.120	3.57 ± 0.19	76.5 ± 7.6	74.8 ± 3.9		110 ± 17	73.2 ± 5.1
4.954	3.52 ± 0.25	57.8 ± 3.6	66.1 ± 2.7	8.7 ± 2.9	92.8 ± 8.9	46.5 ± 3.7
4.787	3.70 ± 0.19	67.1 ± 6.7	76.0 ± 7.6		94.1 ± 9.4	43.0 ± 4.3
4.450	2.76 ± 0.11	64.3 ± 6.0	78.5 ± 3.2	11.8 ± 3.9	88.2 ± 3.6	35.9 ± 2.8
4.404	2.81 ± 0.16	63.9 ± 6.5	81.1 ± 5.9		91.0 ± 9.1	32.2 ± 2.5
4.026	2.20 ± 0.15	50.0 ± 5.0	68.9 ± 6.9		72.0 ± 7.2	14.0 ± 2.7
3.950	2.05 ± 0.21	48.0 ± 3.2	73.4 ± 3.0	7.6 ± 2.4	63.1 ± 3.8	7.5 ± 1.0
3.612	1.86 ± 0.10	47.0 ± 4.7	58.8 ± 4.9		56.0 ± 5.5	
3.440	2.03 ± 0.12	40.9 ± 3.9	54.7 ± 2.6	9.8 ± 2.9	62.6 ± 2.5	
3.156	1.32 ± 0.10	24.8 ± 2.5	41.5 ± 8.2		35.0 ± 3.5	
2.937	1.03 ± 0.07	20.1 ± 2.0	28.8 ± 1.3	2.45 ± 0.70	33.6 ± 1.4	
2.675	0.478 ± 0.043	12.4 ± 1.2	21.2 ± 1.9		19.1 ± 1.9	
2.426	0.356 ± 0.023	6.37 ± 0.54	11.3 ± 0.6	1.34 ± 0.43	16.0 ± 2.5	
2.150	0.138 ± 0.011	2.66 ± 0.27	10.6 ± 2.0		7.15 ± 0.89	
1.910	0.044 ± 0.002	1.56 ± 0.13	2.53 ± 0.84	1.10 ± 0.31	4.98 ± 0.45	

this investigation, the contribution of scandium-44 to the yield of positron annihilation radiation can be determined from the intensity of the 1.159 MeV gamma-ray photopeak in the spectrum, thereby enabling scandium-43 to be determined by difference. The precision of this method of determining scandium-43 was checked using calcium which was isotopically enriched in calcium-42 (94.42 atom %, but still containing 0.06 atom % calcium-43) and calcium-43 (81.12 atom %, but with 0.65 atom % calcium-42). The activity of scandium-44m was obtained from the intensity of the 271-keV gamma-ray and of the 1.159 MeV gamma-ray of its daughter, scandium-44g. The activities of potassium-38 and calcium-49 were respectively determined from the intensities of the 2.170 and 3.10 MeV gamma-rays, while scandium-48 was determined from the intensities of all three gamma-rays listed in Table 1.

The cross sections at various deuteron energies below 5.5 MeV were determined for the nuclear reactions

$^{40}Ca(d, \alpha)^{38}K$
$^{42}Ca(d, n)^{43}Sc$
$^{43}Ca(d, n)^{44}Sc$
$^{43}Ca(d, n)^{44m}Sc$
$^{48}Ca(d, p)^{49}Ca$
$^{48}Ca(d, 2n)^{48}Sc$

and the results are listed in Table 3 and plotted in Figs. 2, 3 and 4. As was expected, the cross sections for (d, p) and (d, n) reactions were of comparable magnitudes, because both types proceed through a 'stripping'

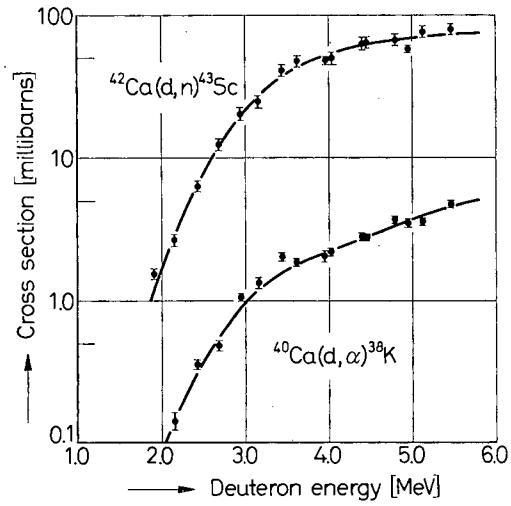

Fig. 2. Excitation functions for the reactions $^{40}Ca(d, \alpha)^{38}K$ and $^{42}Ca(d, n)^{43}Sc$

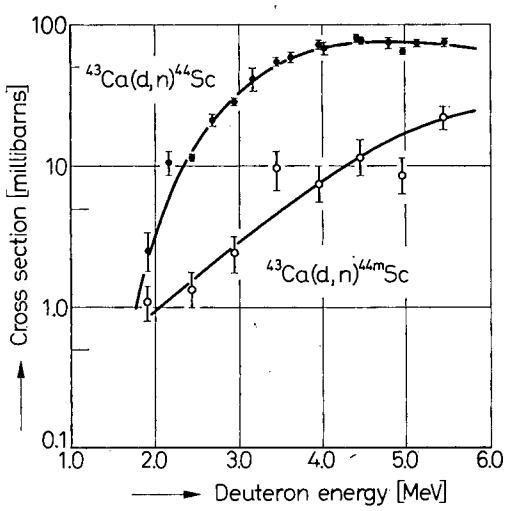

Fig. 3. Excitation functions for the reactions $^{43}Ca(d, n)^{44}Sc$ and $^{43}Ca(d, n)^{44m}Sc$

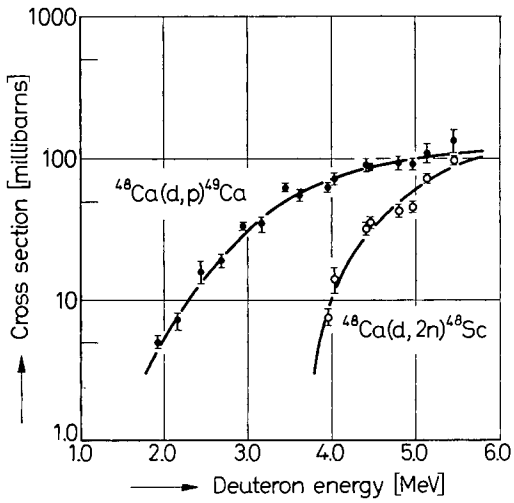

Fig. 4. Excitation functions for the reactions $^{48}Ca(d, p)^{49}Ca$ and $^{48}Ca(d, 2n)^{48}Sc$

mechanism. The slightly higher cross sections for the (d, p) reaction is explained by the Oppenheimer-Phillips process. The low cross section of the (d, n) reaction on calcium-43 leading to the metastable state of the scandium-44 nucleus can be ascribed to the high spin value (6^+) of this state, the 271 keV level, as compared to that of the ground state, (2^+).

Although the shape of the excitation function for the (d, α) reaction on calcium-40 is similar to that of (d, p) and (d, n) reactions on the other calcium isotopes, the absolute values of the cross sections at corresponding energies are very much lower because of the increased Coulomb effect experienced by the emitted alpha-particle.

The reaction ^{48}Ca(d, 2n)^{48}Sc is the only reaction studied which is endoergic. This is also the reason why the excitation function falls more rapidly than those of the other reactions, as the bombarding energy decreases.

Accuracy and precision

The energy of the beam from the Van de Graaff accelerator could be selected within $\pm$ 2 keV. However, the energy spread within the irradiated sample depended on the thickness of the target and the energy of the bombarding deuteron beam. For targets of 200 μg/cm^2 a beam of 2 MeV will lose about 35 keV while a beam of 5.5 MeV will lose 20 keV. If the bombarding energy is considered to be at the middle of the target, the energy spread would be between $\pm$ 17 keV and $\pm$ 10 keV, which is negligible.

The parameters that affect both the accuracy and the precision of the cross sections can be inferred from eq. (3). These are:

(i) errors in the bombarding flux.

The current integrator that was used to measure the bombarding current was calibrated immediately before and after use with a standard mercury cell and a standard resistance of about a megaohm. The integrated current falling on samples irradiated singly was measured with a relative accuracy of $\pm$ 1%. In addition to this source of error, variations in the beam current could introduce detectable errors in the activity generated in the target. These errors were less serious for multiple than single irradiations because changes in the bombarding beam current occurring over periods of about 1 sec and longer were spread over all the targets and affected all the activity yields similarly. The relative precision for multiple activations was thus very much better.

(ii) errors in determining the thickness of the target.

Since the area of the deposit could be well defined, the error in determining the average thickness was the error in weighing, which was not more than 1%. The uniformity of the target was determined by autoradiography and it was found that the thickness variation was within $\pm$ 3%.

(iii) errors in determining the activity.

The integrated counts in the photopeaks could readily be determined from the gamma-ray spectra, and the errors involved in measuring them were purely statistical as determined by the number of events counted and the relative importance of the subtracted background. In view of the fact that the cross sections decrease rapidly with decreasing energy, cross sections measured at lower energies involved larger precision errors that could exceed $\pm$ 15%. In the case of the reaction ^{43}Ca(d, n)^{44m}Sc, still larger precision errors of up to $\pm$ 33% were incurred due to the added uncertainties introduced in subtracting large backgrounds. The half-lives as given in Table 1 were accepted as correct.

(iv) errors involved in the absolute calibration of the spectrometer.

The activities of the sub-standards used to calibrate the spectrometer were known with a relative precision of $\pm$ 1%. Special care was taken to ensure that the sub-standards had the same geometrical form and a similar activity distribution as the irradiated samples. The automatic sample changer delivered samples to the counting position in a reproducible manner, thereby minimizing geometrical errors. The relative accuracy of the absolute calibration of the spectrometer was within 3%.

The above errors contributed to the uncertainties in the cross sections listed in Table 3. Every cross section was considered as a separate determination and each error value listed in the table is the root mean square error calculated from all the relevant experimental conditions pertaining to the measurement. Since the curves drawn in Figs. 2, 3 and 4 are obtained from several separate determinations and are influenced by values at adjacent energy points, values read off the curves can be accepted with an accuracy of $\pm$ 8%, except the excitation function of the reaction ^{43}Ca(d, n)^{44m}Sc, where an accuracy of $\pm$ 15% can be accepted.

Acknowledgements

Parts of this work were included in a doctorate thesis by R. P. and in a Master's thesis by T. J. DE W. presented to the Chemistry Department of the University of Stellenbosch and is published with the permission of their Promotors.

One of us (T. J. DE W.) thanks the South African Council for Scientific and Industrial Research for a bursary made available to him.

Additional financial assistance from the South African C. S. I. R. and the South African Atomic Energy Board is gratefully acknowledged.

PERGAMON PRESS
OXFORD NEW YORK LONDON PARIS

J. inorg. nucl. Chem., 1971, Vol. 33, pp. 2783 to 2789. Pergamon Press. Printed in Great Britain

ACTIVATION CROSS SECTIONS FOR PROTON-INDUCED REACTIONS ON CALCIUM ISOTOPES UP TO 5·6 MeV

TIELMAN J. de WAAL*, MAX PEISACH and RENÉ PRETORIUS
Southern Universities Nuclear Institute, P.O. Box 17, Faure, C.P., South Africa

(*Received* 23 *October* 1970)

Abstract—Calcium fluoride, of natural isotopic composition and isotopically enriched, was activated with proton beams up to 5·6 MeV using a Van de Graaff accelerator. Activation cross sections were determined by γ-ray spectrometry for the reactions:

$$^{43}Ca(p, n)^{43}Sc;\ ^{44}Ca(p, n)^{44}Sc \text{ and } ^{48}Ca(p, n)^{48}Sc.$$

The relative accuracy of the excitation functions is ±5 per cent except for the reaction $^{43}Ca(p, n)^{43}Sc$, where the accuracy is ±8 per cent.

INTRODUCTION

NUCLEAR methods have been used to determine ^{48}Ca by neutron activation [1, 2] and recently methods using charged particle activation have been developed [3–5] to determine the relative enrichment of ^{43}Ca and ^{48}Ca. To utilise this latter technique to its best advantage, a knowledge of activation cross sections would be essential. In addition, the variation of cross section with particle energy has to be known, because unlike neutrons, charged particles undergo a rapid change of energy within the sample. Although activation cross sections for deuteron-induced reactions have recently been reported[6], information on reactions induced by protons is not available. Such information is also of importance for radionuclide production and for studies of nuclear reaction mechanisms.

For target materials irradiated with a constant current of particles at a fixed energy, the specific activity produced would be directly proportional to the reaction cross section. At the end of the irradiation, the activity in the sample would be the sum of all the activities produced by various reactions on the components of the targets. By γ-ray spectrometry and decay measurements the various radioactivities may be resolved and hence individual cross sections may be determined relative to one another. Absolute values may be obtained if the activities are determined absolutely or by comparison with a reaction of known cross section.

*Present address: S.A. Titan Products (Pty) Ltd., UMBOGINTWINI, Natal, South Africa.

1. E. Junod and J. Laverlochere, *Proc. 3rd Intern. Colloquium on Biology*, Saclay (1963).
2. F. W. E. Strelow and H. Staerk, *Analyt. Chem.* **35**, 1154 (1963).
3. M. Peisach and R. Pretorius, *Analyt. Chem.* **38**, 956 (1966).
4. T. J. de Waal, M. Peisach and R. Pretorius, *Analyt. Chem.* **41**, 416 (1969).
5. R. J. N. Brits and M. Peisach, *J. Radioanal. Chem.* **3**, 345 (1969).
6. T. J. de Waal, M. Peisach and R. Pretorius, *Radiochim. Acta* In press.

In this investigation, the activation cross sections were determined with a proton beam obtained from a Van de Graaff accelerator with maximum energy of 5·6 MeV.

EXPERIMENTAL

Preparation of targets

Enriched isotopes of calcium were obtained as carbonate from the Oak Ridge National Laboratory, U.S.A. (see Table 1). These were converted to the fluoride by fuming with hydrofluric acid in a platinum crucible. The targets of calcium fluoride, in which the calcium was either of natural isotopic composition or enriched in a particular isotope were prepared by distilling the heated material in vacuum onto tantalum discs, 0·25 mm thick. The thickness of each target was determined by weighing.

Table 1. Isotopic composition of calcium targets

Isotope	Main enriched isotope (atom-%) ^{43}Ca	^{44}Ca	^{48}Ca	Natural Ca
^{40}Ca	12·78	1·35	15·67	96·97
^{42}Ca	0·65	0·04	0·31	0·64
^{43}Ca	81·12	0·05	0·07	0·145
^{44}Ca	5·40	98·56	2·02	2·06
^{46}Ca	0·05	0·01	0·05	0·0033
^{48}Ca	0·05	0·01	81·90	0·18

Irradiation

Samples were irradiated with proton beams of between 1 and 10 μA obtained from the 5·6 MeV Van de Graaff accelerator of the Southern Universities Nuclear Institute. Up to 12 sample discs could be mounted on a rotating sample holder [3], which fitted into a vacuum chamber attached to the beam tube of the accelerator, and rotated at about 100 rev/min. Aluminium foils of different thicknesses were placed in front of each target thereby enabling data to be obtained simultaneously at 12 different proton energies. The energy of the beam in the middle of each target was determined from tabulated stopping powers [7]. The whole chamber was electrically insulated to obtain beam currents from readings with a current integrator [8], but these flux measurements were not sufficiently accurate for absolute determinations of cross sections. Activities formed in such multiple irradiations were however useful to obtain relative cross section values.

Accurate flux measurements were obtained when single targets were irradiated in a Faraday cup at different bombarding energies. The construction of the Faraday cup was such that secondary electron loss was negligible. In these irradiations no aluminium foil was used to degrade the energy of the bombarding beam.

Sets of relative cross sections obtained from the multiple irradiations were normalised to all the absolute values obtained from the single irradiations by the method of least squares.

Measurement of radioactivity

After irradiation, samples were analysed by γ-ray spectrometry using a 3 in. × 3 in. NaI(Tl) scintillator or a 20 cm^3 Ge(Li) detector, coupled to a multichannel analyser. The detectors were fitted with a "Perspex" cap about 1·5 g/cm^2 in thickness to prevent beta-particles from being recorded and to minimise bremsstrahlung formation.

The photopeak efficiency of the detectors was determined with substandards of ^{22}Na, ^{54}Mg, ^{57}Co, ^{60}Co, ^{88}Y, ^{137}Cs and ^{203}Hg, obtained from the National Physical Research Laboratory, Pretoria

7. C. F. Williamson, J.-P. Boujot and J. Picard, *Rep.* CEA-R 3042 (1966).
8. E. Blignaut and J. J. Kritzinger, *Nucl. Instrum. Meth.* **36**, 176 (1965).

and the International Atomic Energy Agency, Vienna. The activities of the standards were known with an accuracy of about 1 per cent.

Treatment of data

When a target of w g, material with molecular weight M, deposited over a circular area of diameter d, is irradiated for a total integrated current of Q coulombs, the activity of a product radionuclide for which C counts are measured in the photopeak of the spectrum over a counting period t_c, is a measure of the activation cross section, σ which is obtained from

$$\sigma = \frac{M}{\epsilon p a . 6{\cdot}0225 \times 10^{23}} \cdot \frac{C}{t_c} \cdot \frac{\pi d^2}{4w} \cdot \frac{t_i \times 1{\cdot}6 \times 10^{-19}}{Q} \cdot \frac{e^{\lambda t_d}}{(1 - e^{-\lambda t_i})} \times 10^{24}$$

where t_i = duration of the irradiation
t_d = the time between the end of the irradiation and the middle of the counting period
ϵ = the counting efficiency in photopeak counts per γ-ray
p = the intensity of the γ-ray per disintegration
a = the fractional isotopic abundance of the target isotope
λ = decay constant of the radionuclide concerned.

The cross section measurements

When isotopic concentrations are determined in isotope dilution analysis, the values obtained do not usually differ much from those of the natural element. Accordingly, only those reactions were studied from which measurable amounts of radionuclides were generated in proton irradiated calcium of natural isotopic composition. The nuclear data of these radionuclides are given in Table 2. Some typical spectra obtained from the decay of a sample of natural composition irradiated with 5·1 MeV protons are given in Fig. 1.

The yields of scandium isotopes were obtained from integrating the counts under the appropriate photopeak and fitting the respective half-lives to the observed decay data. γ-Rays of 1156 keV from ^{44}Sc and each of the γ-rays of 983, 1040 and 1312 keV from ^{48}Sc were used to determine these radionuclides. The 374 keV γ-ray of ^{43}Sc was not used because of the unfavourable peak-to-background ratio for its photopeak (see Fig. 1). The yield of this isotope was obtained from the positron annihilation radiation. At proton energies below the threshold of the reaction ^{44}Ca$(p, n)^{44}$Sc, positron emission is due solely to ^{43}Sc (see Fig. 2), but above 4·530 MeV positron emission is due to both ^{43}Sc and ^{44}Sc and the two are not resolvable by decay measurements. Under these conditions the contribution of ^{44}Sc was determined from the intensity of the 1156-keV γ-ray photopeak in the spectrum, thereby enabling ^{43}Sc to be determined by difference.

Accuracy and precision

Bombarding energy. The uncertainty in the energy of the proton beam was ±2 keV. For targets of

Table 2. Nuclear data of radionuclides detected in natural calcium fluoride irradiated with protons up to 5·5 MeV

Radionuclide	^{43}Sc	^{44}Sc	^{48}Sc
Half-life	3·92 hr	3·92 hr	1·83 d
Main γ-ray energies (keV) and intensities (%)	374 (22)	1156 (100)	178 (6)
	(β^+) (176)		983 (100)
		1506 (0·8)	1040 (100)
		(β^+) (188)	1312 (100)
Method of production	^{43}Ca(p, n)	^{44}Ca(p, n)	^{48}Ca(p, n)
Q-value of reaction (keV)	−3004·3	−4429·0	−493·4
Reaction Threshold (keV)	3074	4530	504

(β^+) refers to decay by positron emission and hence, the observation of 511 keV annihilation radiation.

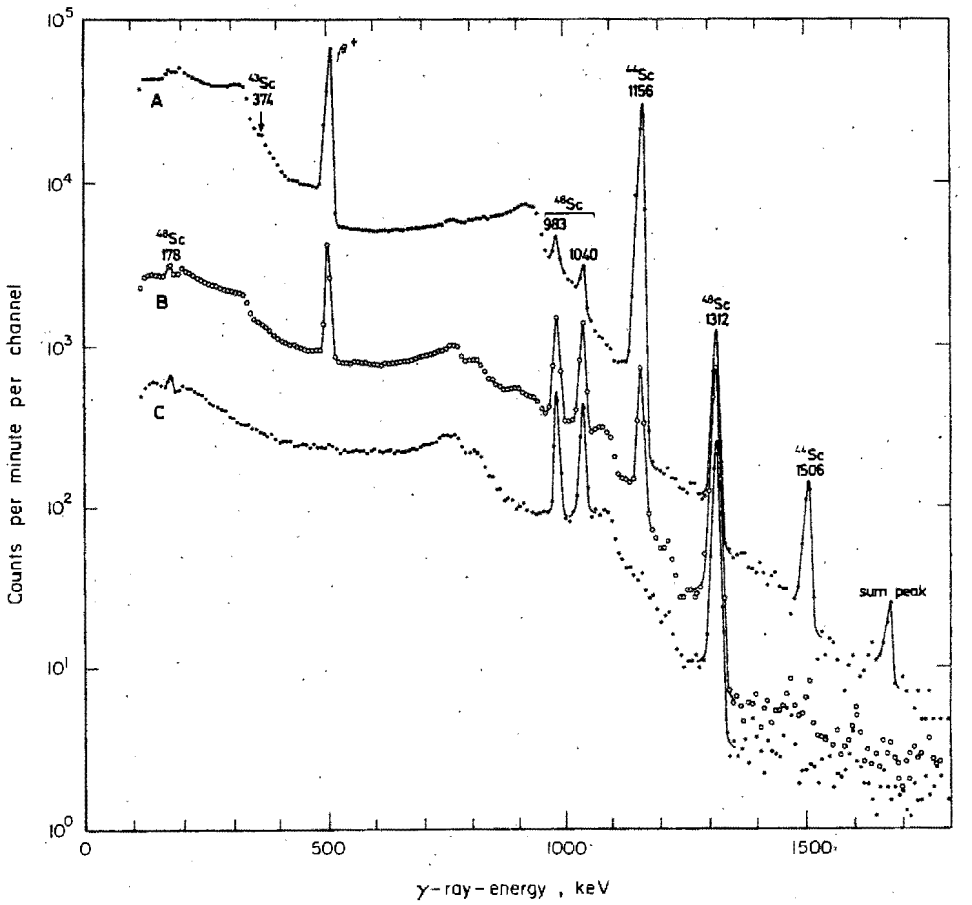

Fig. 1. γ-Ray spectra from natural calcium fluoride irradiated with 5·1 MeV protons. A—2·7 hr after the end of the irradiation; B—5·1 hr; C—23 hr.

200 μg/cm² the energy spread within the target would be ±11 keV at 2 MeV and ±5 keV at 5·5 MeV, which is negligible.

Bombarding flux. The current integrator was calibrated before and after use and the relative precision of current measurements in single irradiation was ±0·1 per cent with a relative accuracy of ±1 per cent. In addition to this source of error, variations in the beam current could introduce detectable errors in the activity generated in the target. These errors were less serious for multiple than single irradiations because changes in the bombarding beam current occurring over periods of about 1 sec and longer were spread over all the targets and affected all the activity yields similarly.

Target thickness. Since the area of the deposit could be well defined, the error in determining the average thickness was the error in weighing, which was not more than 1 per cent. The uniformity of the target was determined by autoradiography and it was found that the thickness variation was within ±3 per cent.

Activity determination. The errors involved in measuring the integrated counts were purely statistical as determined by the number of events counted and the relative importance of the subtracted background. Cross sections measured at lower energies involved larger precision errors that could exceed ±9 per cent. In the case of the reaction $^{43}Ca(p, n)^{43}Sc$, still larger precision errors of over ±15 per cent were incurred due to the added uncertainties introduced in subtracting the positron activity of ^{44}Se. The half-lives as given in Table 2 were accepted as correct.

Absolute calibration of the spectrometer. The activities of the sub-standards were known with

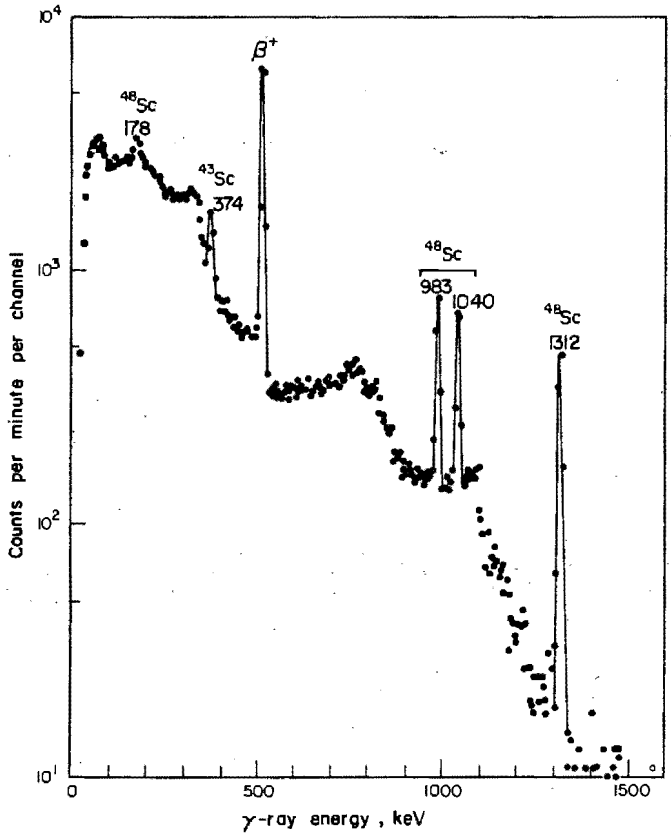

Fig. 2. γ-Ray spectrum from natural calcium fluoride, 2·3 hr after being irradiated with 4·5 MeV protons. The absence of ^{44}Sc is clearly evident.

a relative precision of ±1 per cent. Special care was taken to ensure that the substandards had the same geometrical form as the irradiated samples. The automatic sample changer delivered samples to the counting position in a reproducible manner, thereby minimising geometrical errors. The relative accuracy of the absolute calibration of the spectrometer was within 3 per cent.

The above errors contributed to the uncertainties in the cross sections listed in Table 3. Every cross section was considered as a separate determination and each error value listed in the table is the root mean square error calculated from all the relevant experimental conditions pertaining to the measurement. Since the curves drawn in Fig. 3 are obtained from several separate determinations and are influenced by values at adjacent energy points, values read off the curves can be accepted with an accuracy of ±5 per cent, except the excitation function of the reaction ^{43}Ca$(p, n)^{43}$Sc, where an accuracy of ±8 per cent can be accepted.

RESULTS AND DISCUSSION

The cross sections at various proton energies below 5·6 MeV were determined for the nuclear reactions

$$^{43}\text{Ca}(p, n)^{43}\text{Sc}$$
$$^{44}\text{Ca}(p, n)^{44}\text{Sc}$$
$$^{48}\text{Ca}(p, n)^{48}\text{Sc}.$$

The results are listed in Table 3 and the excitation curves are plotted in Fig. 3.

It is interesting to note that the 2·4d ^{44m}Sc was not detected from proton

Table 3. Cross sections of proton-induced reactions

$^{43}Ca(p, n)^{43}Sc$		$^{44}Ca(p, n)^{44}Sc$		$^{48}Ca(p, n)^{48}Sc$	
E_p (MeV)	Millibarns	E_p (MeV)	Millibarns	E_p (MeV)	Millibarns
5·574	243·6 ± 24·0	5·574	81·9 ± 7·1	5·474	254·1 ± 18·2
5·474	198·8 ± 19·9	5·474	75·6 ± 6·9	5·284	255·1 ± 18·1
5·183	227·3 ± 22·9	5·394	67·8 ± 6·0	5·083	214·5 ± 14·8
5·000	130·2 ± 13·1	5·183	45·7 ± 3·6	4·973	173·3 ± 20·1
4·792	131·3 ± 13·4	5·000	28·3 ± 2·1	4·883	196·1 ± 15·1
4·570	73·9 ± 10·1	4·993	34·7 ± 2·9	4·672	178·8 ± 12·6
4·340	52·6 ± 6·0	4·792	26·0 ± 2·1	4·470	159·9 ± 11·9
3·870	30·3 ± 4·0	4·570	6·1 ± 0·7	4·239	158·2 ± 11·8
3·610	26·0 ± 3·8			4·209	143·5 ± 10·5
3·350	14·3 ± 2·9			4·008	123·5 ± 9·8
				3·755	91·9 ± 7·6
				3·504	78·7 ± 6·0
				3·464	71·1 ± 4·9
				3·222	48·4 ± 3·5
				2·888	30·8 ± 2·2
				2·615	18·6 ± 1·7
				2·575	15·7 ± 1·2
				2·230	6·8 ± 0·5
				1·895	5·1 ± 0·6
				1·864	3·4 ± 0·4

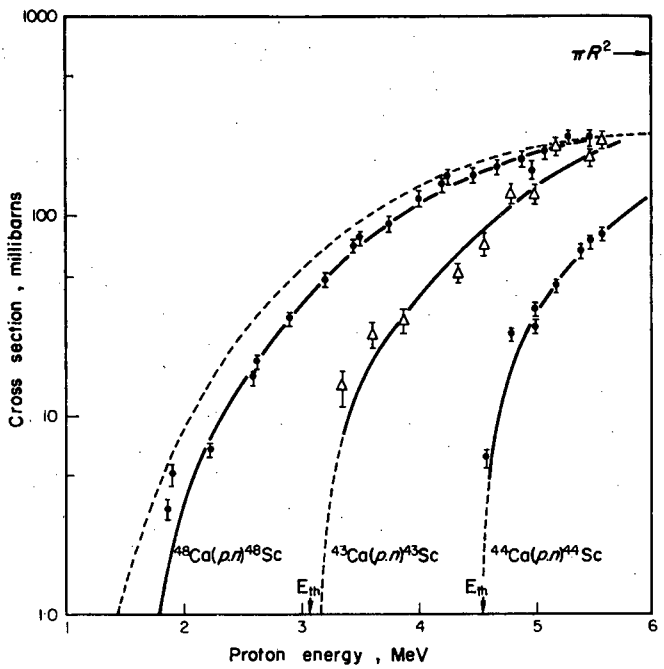

Fig. 3. The theoretically calculated excitation function (dashed) for the formation of a compound nucleus from a target with a nuclear radius $R = 1{\cdot}3.A^{1/3} \times 10^{-13}$ cm and $Z = 20$ is compared with the experimentally obtained excitation functions.

activation although it was produced by deuterons of equal energy[6]. This is probably due to the high spin, 6^+, of the metastable state, which can be populated from the very highly excited compound nucleus produced during deuteron irradiation, but which cannot be formed during proton irradiation because the compound nucleus is in a much lower state of excitation.

In addition to the listed reactions, some of the observed radionuclides may have been formed by the reactions $^{42}Ca(p,\gamma)^{43}Sc$ and $^{43}Ca(p,\gamma)^{44}Sc$. The latter reaction was not observed, since samples activated at energies below the threshold for the formation of ^{44}Sc by the (p,n) reaction, showed no indication of the presence of this radionuclide in the γ-ray spectrum (see Fig. 2). ^{43}Sc, however, was formed at proton energies below the threshold of the reaction $^{43}Ca(p,n)^{43}Sc$, and the cross section for its production by the $^{42}Ca(p,\gamma)^{43}Sc$ reaction has been measured[9]. From the known concentration of ^{42}Ca in the activated samples and from an extrapolation of the excitation curve of the (p,γ) reaction, corrections were made to the measured yield of ^{43}Sc to obtain the required cross section. Such corrections were usually small.

In the energy region under investigation, (p,n) reactions on calcium isotopes proceed through a compound nucleus mechanism[10]. The excitation functions could thus be compared with a theoretical curve calculated from the theory for compound nucleus formation[11]. Such a comparison is shown in Fig. 3 where the measured curves are shown in relation to the calculated one (shown dashed), which approaches the value πR^2 asymptotically as the bombarding energy increases. At bombarding energies above 2 MeV the cross section of the (p,n) reactions on ^{48}Ca approaches the theoretical value because, apart from proton decay, neutron emission represents the only major mode of de-excitation of the compound nucleus, and the degree of excitation of the compound nucleus is sufficiently high to meet the requirements of the theory[11] on which the calculations were based. This state of affairs is reached at a bombarding energy of about 5 MeV for the (p,n) reaction on ^{43}Ca and not at all for ^{44}Ca in the energy region studied, because the corresponding (p,n) reactions have relatively high thresholds.

Since proton emission from the compound nucleus is always a competing process, especially at lower energies, the cross sections of the (p,n) reaction will be less than the theoretical value, as is clearly illustrated by the curve for the reaction $^{48}Ca(p,n)^{48}Sc$ in Fig. 3. At high energies the cross sections may be expected to decrease because the compound nucleus may be de-excited by the emission of other particles when such emission becomes energetically possible.

Acknowledgements—Parts of this work were included in a doctorate thesis by R. P. and in a Master's thesis by T. J. de W. presented to the Chemistry Department of the University of Stellenbosch and is published with the permission of their Promotors.

This work was financially supported by the South African Council for Scientific and Industrial Research and by the South African Atomic Energy Board to whom grateful acknowledgement is made.

9. M. Peisach, R. Pretorius and D. S. Rosettenstein, *Convention Handbook*, p. 299. S. Afr. Chem. Inst. 20th Convention, Durban (1967).
10. W. R. McMurray, M. Peisach, R. Pretorius, P. Van der Merwe and I. J. Van Heerden, *Nucl. Phys.* **99A**, 17 (1967).
11. M. M. Shapiro, *Phys. Rev.* **90**, 171 (1953).

ELSEVIER SEQUOIA S. A.
Lausanne

AKADÉMIAI KIADÓ
Budapest

RADIOCHEM.RADIOANAL.LETTERS 8 /2/ 119-127 /1971/

DETERMINATION OF OXYGEN BY THE SPECTROMETRY OF PROMPT GAMMA-RAYS FROM TRITON-INDUCED REACTIONS

M.Peisach*

Chercheur Associé, C.N.R.S. - Laboratoire Pierre Süe
C.E.N.Saclay - B.P.No.2 - /91/Gif-sur-Yvette, France

Received 18 August 1971
Accepted 24 August 1971

The prompt gamma-rays from triton-induced reactions on oxygen were used for analysis. The method had a relative precision of 2 to 3.5% for surface oxygen concentrations from 50 to 3 μg/cm^2. The sensitivity with 1900 keV tritons was 0.13 μg/cm^2 on surfaces of steel or copper but 0.45 μg/cm^2 on aluminium where interfering gamma-rays were emitted.

INTRODUCTION

Triton-induced activation has been used for several years as a means of determining oxygen. In reactors the triton flux may be obtained by incorporating lithium-6 in the system, so that the primary reaction ^{6}Li/n,α/t produces an in situ flux of 2.7 MeV tritons. A detailed study of this method has recently been reported.[1] With triton beams from accelerators, metal surfaces can be irradiated directly and the induced activity of fluorine-18 can be used as a measure of the oxygen content. By this method a sensitivity of 5×10^{-3} μg.oxygen/cm^2 has been claimed.[2]

By measuring prompt γ-rays with a relatively large detector placed near to the target, sufficient data can be obtained over a period which is frequently short compared with the time

*Present address: Southern Universities Nuclear Institute, P.O.Box 17, Faure, C.P., South Africa.

needed for counting. Furthermore, if the triton beam has a relatively low energy, it may be possible to select conditions such that the count rate from oxygen is acceptable, while the yield from the matrix may be reduced by the Coulomb barrier effect.

The most likely reactions induced by tritons with energies up to 3 MeV, the highest energy available in this investigation, are /t,n/, /t,p/ and /t,α/ reactions. In the case of ^{16}O relatively few levels are available in the product nuclei[3] so that simple γ-ray spectrometry becomes feasible.

We can use a convention to label the γ-rays: S/a,b/, where s is the identity of the light nuclei product particle and a and b are the level numbers between which the transition occurs. The two γ-rays from the reaction $^{16}O/t,p/^{18}O$ are thus p/1.0/ and p/2.1/, and all /t,p/ reactions that do not produce ^{18}O in its ground state, have to be accompanied with the emission of p/1.0/ of 1982 keV. The more intense γ-rays from the reaction $^{16}O/t,n/^{18}F$ will be n/1.0/ of 940 keV, n/2.0/ of 1043 keV and n/3.0/ of 1085 keV. De-excitation of higher excited states frequently occurs in stages thus adding to the intensities of these three γ-rays. The more intense γ-rays from the reaction $^{16}O/t,\alpha/^{15}N$ are expected to be α/1.0/, 5271 keV, α/2.0/, 5299 keV and α/3.0/, 6324 keV. These γ-rays of high energy are thus expected to be found in an energy region where the intensities of γ-rays from other reactions are likely to be rather low, thereby making their use for analysis more attractive.

Only a single peak from the reaction $^{16}O/t,p/^{18}O$ was detected, corresponding to the γ-ray p/1.0/, thus indicating that the cross-section for the reaction leading to the second excited state of ^{18}O is probably low.

When the peaks from the reaction $^{16}O/t,\alpha/^{15}N$ are compared with the other peaks in the spectrum, the poorer resolution becomes obvious. No attempt was made here to isolate γ-rays corresponding to any particular direction of emission of the α particle. The integral curve shows the broadening expected from the Döppler effect. Because of the decreased resolution it became impossible to resolve the γ-rays α/1.0/ and α/2.0/. Qualitatively, γ-rays involving transitions from the 5th excited state of ^{15}N can still be identified, but for higher states the cross-sections are low because the energy available for the outgoing α particle becomes small relative to the Coulomb barrier. Each of the γ-rays n/1.0/, n/2.0/, n/3.0/, p/1.0/ and the pair α/1.0/ - α/2.0/ can be used independently for analysis.

One set of counts obtained from a gaseous sample of oxygen, bombarded with tritons having a mean energy of 1900 keV and normalised to 1 mC is respectively 1175.6; 1282.7; 303.3; 725.9; 401.8; for 1 μg oxygen per cm^2 or, 312.2; 340.7; 80.6; 192.8; 106.7 for 10^{16} oxygen atoms per cm^2. These values refer to measured counts and are not corrected either for absolute or for relative counting efficiencies.

Accuracy and precision

Examples of analyses using tritons of different energies are shown in Table 1. The results were based on the yield of

TABLE 1

Effect of bombarding energy

Triton energy /keV/	p/1.0/ counts measured		Ratio
	Aluminium 2	Aluminium 1	
2400	4752	4237	1.122
2300	4678	3803	1.230
2200	3970	3039	1.306
2100	3333	2811	1.186
2000	2433	2163	1.125
1900	1758	1440	1.221

Mean ratio by /t,pγ/ reaction: 1.198 ± 0.029
Mean ratio by /d,p/ reaction : 1.204 /ref. 4/
Relative standard deviation = 5.8%

p/1.0/ γ-rays, because it was expected that these values would be least precise as small gain changes in the measuring system could result in the inclusion of counts from 2032 keV ^{27}Al n/2.0/ γ-rays.

The accuracy of the method was tested by comparing the results with analyses using prompt-proton spectrometry from deuteron-induced reactions.[4] The ratio of the surface concentrations of oxygen on the two aluminium samples was in excellent agreement with the corresponding value from the /d,p/ method. It may thus be concluded that the two methods are comparably accurate.

The results given in Table 1 show a relative standard deviation of ±5.8%. This value is somewhat higher than expected from the statistical counting errors only, each count having

been measured within a statistical error of between 2 and 3.5%. The poorer precision may probably be accounted for by some interference from reactions induced in aluminium.

Results of analyses of two other metal surfaces containing more oxygen are given in Table 2. In the case of the steel sample, two additional peaks were observed corresponding to

TABLE 2

Analyses with 1900 keV tritons

γ-ray used	Copper		Steel	Surface concentration /atoms per cm^2/
	counts per 100 μC	Surface concentration /atoms per cm^2/	Counts per 100 μC	
n/1.0/	1020	32.67×10^{16}	486	15.57×10^{16}
n/2.0/	1148	33.70×10^{16}	542	15.91×10^{16}
p/1.0/	640	33.20×10^{16}	316	16.39×10^{16}
α/1+2.0/	342	32.05×10^{16}	158	14.81×10^{16}
	Mean:	32.91×10^{16}		15.67×10^{16}
By /d,p/ analyses		46.4×10^{16}		15.6×10^{16}

^{12}C n/2.1/, 1632 keV, and ^{12}C n/1.0/, 2313 keV γ-rays. The high intensity of these peaks points to the possibility of using them for determining surface concentrations of carbon.

The surface concentration of oxygen on the steel agreed well with the result obtained by prompt proton spectrometry. The large discrepancy between the results obtained by triton and by deuteron bombardment of the copper sample clearly indicates that the surface had undergone a change during the several weeks that elapsed between the analyses.

Sensitivity

Elements such as iron or copper contribute little to the radiation background when bombarded with tritons below 2 MeV, but aluminium, generates an appreciable amount of radiation. Using the criterion that the sensitivity of the method is the surface concentration of oxygen that would yield a count equivalent to three times the standard deviation of the background count, the sensitivity, for an irradiation current of 1 mC of 1900 keV tritons, is about 0.13 $\mu g/cm^2$ /5 x 10^{15} atoms/cm^2/ for iron and copper, but only 0.45 $\mu g/cm^2$ /or 1.7 x 10^{16} atoms/cm^2/ when aluminium is analysed. Clearly, the sensitivity can be improved if longer irradiations are acceptable, and if adequate screening against outside radiation is provided.

*

Thanks are due to Madame D.Magnac-Valette, of the Faculty of Sciences, Strasbourg for permission to use their facilities and to Madame I.Link and Mr.L.Kraus for their help with the electronic and measuring equipment. Mr.B.Vialatte assisted with some of the measurements and Dr.J.Siegka and Dr.G.Amsel of Ecole Normale Superieure, Paris kindly performed the /d,p/ analyses.

Financial support from the Pierre Süe Laboratory of the C.N.R.S. at Saclay made the investigation possible.

REFERENCES

1. J.J.M.de Goeij, J.P.W.Houtman, Proc. "Modern Trends in Activation Analysis", College Station, Texas /1965/ 372.

2. J.N.Barrandon, L.Quaglia, J.L.Debrun, M.Cuypers, G.Robaye, J.Radioanal.Chem., 4 /1970/ 115.

3. F.Ajzenberg-Selove, T.Lauritsen, Nucl.Phys., 11 /1959/ 235; F.Ajzenberg-Selove, Nucl.Phys., A152 /1970/ 108.

4. G.Amsel, D.Samuel, Anal.Chem., 39 /1967/ 1689; G.Amsel, B.Beranger, B.de Gelas, P.Lacombe, J.Appl.Phys., 39 /1968/ 2246; G.Amsel, J.P.Nadai, E.Dartemare, D.David, E.Girard, J.Moulin, Nucl.Instr.Methods, 92 /1971/ 481.

viously sticked to metal planchets. The average thickness of the paper was 7.2 ± 0.2 mg/cm^2 and the pipetted droplets were spread over a circular area about 8 to 15 mm in diameter. The resulting samples had an effective thickness between 18 and 32 mg/cm^2. Over this range of thicknesses, no change in count rate, due to self-absorption, could be observed, in agreement with previously reported results.[3] The aliquot samples were measured with a Ge/Li/ γ-ray spectrometer to determine the sodium-24 activity so as to be able to correct for pipetting errors, and the bromine concentrations were expressed relative to the activity of ^{24}Na.

Irradiation

Samples were irradiated for periods ranging from 10 sec to 5 min. Two reactor facilities were used, one in OSIRIS, where the thermal flux was 2.5×10^{18} m^{-2}s^{-1}, and the other in the EL3 reactor with a thermal neutron flux of 6.6×10^{16} m^{-2}s^{-1}.

Measurement

When bombardments were carried out in EL3, counting usually started at about 2 min after the end of the bombardment. In the case of samples irradiated in OSIRIS the recovery system involved a manual transfer stage which increased the dealy to about 6 min after the end of the bombardment.

The samples were mounted in a geometrically reproducible position below a thin NaI crystal 3 cm in diameter and 3 mm in thickness, covered with a 20 mg/cm^2 beryllium window. The crystal was optically connected to a photomultiplier and pulses were transmitted through a preamplifier to a multi-channel analyzer.

When relatively high bromine activities were measured, counting lasted for about 2 min. For routine analyses, samples were counted for a live time of 4 min, but because most samples were very active, the added decay of the bromine activity caused by the dead time of the counter could not be neglected, and for this reason clock time was also recorded. Most counts lasted about 5 to 6 min.

RESULTS AND DISCUSSION

X-Ray spectrometry

A typical spectrum obtained from a sample containing only aqueous ammonium bromide solution is shown in Fig.1. Shortly after the end of the bombardment, the spectrum consisted of a single peak corresponding to 11.9 keV and a slowly undu-

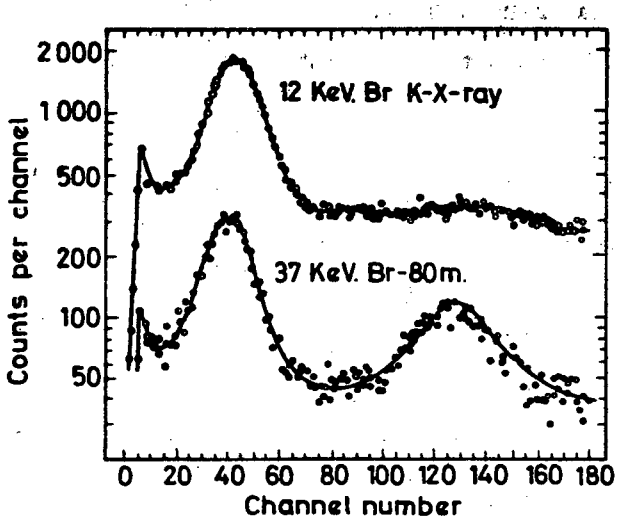

Fig.1. Energy spectrum of bromine activity from the neutron irradiation of ammonium bromide for 10 sec at a flux of about 2×10^{14} $m^{-2}s^{-1}$, taken 13 min and 33 s after bombardment /upper curve/ and 74 min and 37 s after the end of the bombardment

lating continuum. However, as the decay proceeded and the intensity of the continuum decreased another peak became more pronounced, corresponding to 37 keV γ-rays from about 50% of the decays of ^{80m}Br that were not internally converted. The initial

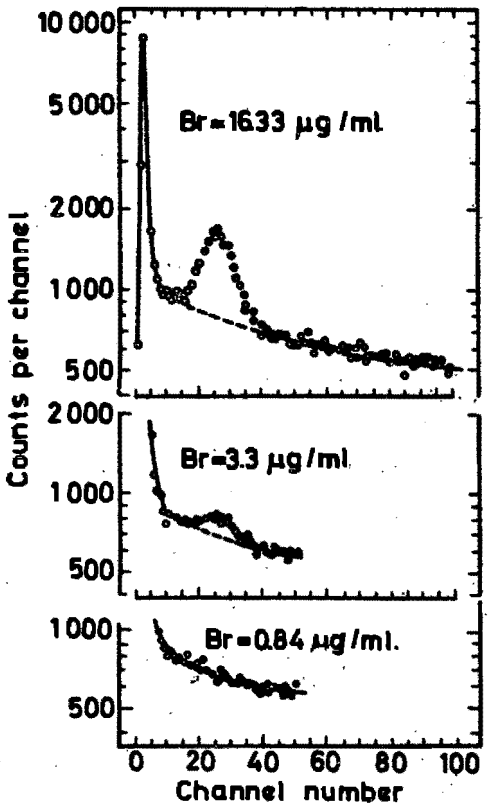

Fig.2. Energy spectra of natural blood plasma samples containing 16.33, 3.0 and 0.84 µg bromine per ml. Sample irradiated 1 min in a neutron flux of 6×10^{12} $m^{-2}s^{-1}$.

very sharp peak, which appears to be caused by 2 keV radiation, seems to be purely instrumental in origin, its intensity varying with the total activity of the sample.

The resolution of the bromine K X-ray peak, as given by the full width of the peak at one half of its maximum height

/FWHM/ was about 6.3 keV and hence was insufficient to resolve the 11.2 keV selenium K X-ray, obtained from the electron capture decay mode of ^{80}Br, from that of bromine. It may thus be expected that the rate of decay of the spectral peak would consist of terms referring to 6.1 min ^{82m}Br and 4.4 hr ^{80m}Br, both of which yield K X-rays of bromine and to 17.6 min ^{80}Br which yields selenium X-rays.

Examples of spectra from blood plasma samples with different bromine concentrations are shown in Fig.2.

Decay curve

Decay curves of ammonium bromide samples, synthetic blood plasma solutions containing various amounts of bromine, and of high-bromine natural blood plasmas were measured, after activation for different periods of time at different neutron fluxes. The decay rate was measured over long periods, depending on the activity of the samples, but all samples showed 4.4 hrs decay rate without indication of the presence of longer-lived radioactivity. ^{82}Br does not decay by X-ray emission, and was not observed.

The relative activities of the isotopes A, indicated by subscripts, were calculated using the nuclear data in Table 1. This ratio is time-independent for the conditions prevailing here. However, this relationship implies that the total decay proceeds through the emission of the K X-rays, since only K X-rays were measured to determine A. To correct for this simplification with the values in Table 1, the ratio becomes:

$$A_{80} : A_{80m} : A_{82m} = 7\ 79 : 443 : 10.000$$

TABLE 1

Bromine radioisotopes produced by thermal neutron capture[2]

Isotope	^{80m}Br	^{80}Br	^{82m}Br	^{82}Br
Half-life	4.4 h	17.6 min	6.1 min	35.5 h
Abundance of target nuclide /%/	50 . 52	50 . 52	49 . 48	49 . 48
σ /n,γ/ barns	2.9	8.5	3.0	0.26
Main γ-rays /keV/	37 49	/β⁺/[a] 618 666	46 777 1475	554 619 698 777 828 1044 1317 1475
Electron capture /ε/ relative intensity /%/	-	5	-	-
Internal conversion of γ-rays	/1/ 49 keV α = 400 $\frac{K}{L}$ = 3 /2/ 37 keV α_K = 1	-	46 keV α = 382 α_K = 268	negligible

/a/ /β⁺/ refers to the emission of positrons and hence the presence of 511 keV annihilation radiation

Experimental values obtained for a variety of conditions, and expressed relative to 10.000 counts of ^{82m}Br were in good agreement for ^{80m}Br, but somewhat high for ^{80}Br.

Precision

Samples of "synthetic" blood plasma solutions containing known amounts of bromine were used to determine the precision

TABLE 2

Precision of analyses

Sample	Known Br conc. µg/ml	Activity ratio measured	Found Br conc. µg/ml	Error µg/ml	Relative error /%/
A	3.024	0.5170	3.012	- 0.012	- 0.40
E	2.875	0.4965	2.903	+ 0.028	+ 0.97
B	2.419	0.3991	2.383	- 0.036	- 1.49
C	2.268	0.3799	2.280	+ 0.012	+ 0.53
G	2.195	0.3632	2.191	- 0.004	- 0.18
D	2.016	0.2656			
F	1.512	0.2406	1.536	+ 0.024	+ 1.59
H	0.826	0.1055	0.815	- 0.011	- 1.33
			r.m.s.error =	±0.0226 µg/ml	
			relative std deviation =	±1.15%	

of the method. The results are expressed as a ratio of bromine X-ray counts to counts from the 1369 keV γ-ray of ^{24}Na.

Some of the analytical results are listed in Table 2. The root mean square error of the method involves a concentration error of 0.023 µg/ml and a relative precision of ±1.2%. As only 10 µl were used for analysis, the data show a root mean square error of ±0.23 ng for bromine contents between 10 and 30 ng.

Sensitivity

In samples where the total radioactivity is small, the sensitivity of the method is high. Fig.3 shows a spectrum obtained from such a low-activity sample containing 11.59 ng

bromine, irradiated in OSIRIS for 10 sec and counted for 5 min.

The integrated net count for this sample was 5417 counts over a background of 2985 counts. If we accept that the sensiti-

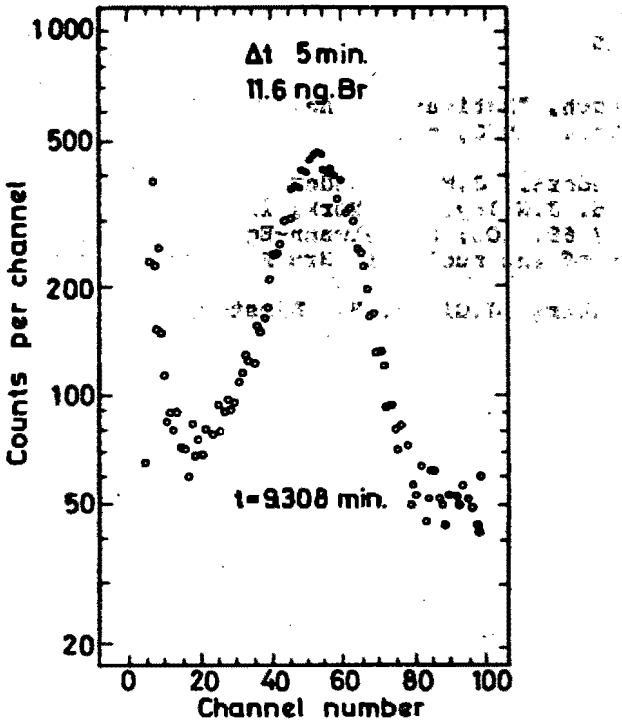

Fig.3. Spectrum of sample with low total activity, containing 11.6 ng bromine, 9.31 min after the end of the bombardment. Δt = 5 min. Sample irradiated for 10 sec at a neutron flux of 2×10^{14} $m^{-2}s^{-1}$

vity of the method is the weight of bromine required to produce a count equal to three times the standard deviation of the background count, the sensitivity of this method can be shown to be 0.35 ng.

When the sensitivity was determined in synthetic blood plasma solutions, the very high activity of the sample generated

a high background which made it difficult to discern peaks in samples containing less than 0.8 μg/ml bromine /see Fig.2/. In the presence of high radioactivities, the experimentally determined sensitivity was thus taken as 7 ng bromine.

REFERENCES

1. R.C.Koch, "Activation Analysis Handbook", Academic Press, New York, 1960, p.82.

2. C.M.Lederer, J.M.Hollander, I.Perlman, Table of Isotopes, 6th Ed. J.Wiley, New York, 1968; A.Artna, Nucl.Data B 1, /1966/ 69, 103; W.Seelmann-Eggebert, G.Pfenning, H.Munzel, Chart of the nuclides, 3rd Ed., Karlsruhe, 1968.

3. C.Shenberg, J.Gilat, H.L.Finston, Anal.Chem., 39 /1967/ 750.

No. 38

Sonderdruck aus Radiochimica Acta 17, 1–6 (1972)

Activation Cross Sections for Deuteron-Induced Reactions on some Elements of the First Transition Series, up to 5.5 MeV

By PAUL P. COETZEE* and MAX PEISACH, Southern Universities Nuclear Institute, P. O. Box 17, Faure, C. P., South Africa

With 12 figures. (Received December 21, 1970)

Summary

Deuteron activation was carried out with deuteron beams up to 5.5 MeV with a Van de Graaff accelerator. Absolute cross sections were determined by gamma-ray spectroscopy using a Ge(Li)- and/or NaI(Tl)-detector. Excitation functions were obtained for the nuclear reactions:

$^{50}Cr(d,p)^{51}Cr$; $^{55}Mn(d,p)^{56}Mn$; $^{58}Ni(d,n)^{59}Cu$; $^{64}Zn(d,n)^{65}Ga$; $^{50}Cr(d,\alpha)^{48}V$; $^{54}Fe(d,n)^{55}Co$; $^{60}Ni(d,n)^{61}Cu$.

Zusammenfassung

Mittels eines Van-de-Graaff-Generators wurde mit Deuteronen von maximal 5,5 MeV eine Deuteronenaktivierung durchgeführt. Die absoluten Wirkungsquerschnitte wurden mit Hilfe von Gammaspektroskopie an einem Ge(Li)- bzw. NaI(Tl)-Detektor bestimmt. Für folgende Kernreaktionen wurden Anregungsfunktionen ermittelt:

$^{50}Cr(d, p)^{51}Cr$; $^{55}Mn(d, p)^{56}Mn$; $^{58}Ni(d, n)^{59}Cu$; $^{64}Zn(d, n)^{65}Ga$; $^{50}Cr(d, \alpha)^{48}V$; $^{54}Fe(d, n)^{55}Co$; $^{60}Ni(d, n)^{61}Cu$.

Résumé

L'activation de deutérons a été effectuée à l'aide de faisceaux de deutérons d'énergie atteignant jusqu'à 5,5 MeV et produits dans un accélérateur Van de Graaff. Les sections efficaces absolues ont été déterminées par spectroscopie gamma avec un détecteur Ge(Li) et/ou NaI(Tl). Les fonctions d'excitation ont été obtenues pour les réactions nucléaires suivantes:

$^{50}Cr(d, p)^{51}Cr$; $^{55}Mn(d, p)^{56}Mn$; $^{58}Ni(d, n)^{59}Cu$; $^{64}Zn(d, n)^{65}Ga$; $^{50}Cr(d, \alpha)^{48}V$; $^{54}Fe(d, n)^{55}Co$; $^{60}Ni(d, n)^{61}Cu$.

Introduction

As a result of the rapid advances being made by charged particle activation analysis, the need is being felt for data potentially of use to the analyst. Much of the existing data was obtained using cyclotrons, with the result that information in the low energy region is often lacking. For this reason the systematic study of activation reactions on the isotopes of calcium [1, 2] was continued with the heavier elements. In this investigation the deuteron activation of some elements of the first transition series, up to zinc ($Z = 30$) was measured.

Experimental

Target preparation

Targets suitable for charged particle cross section measurements should be as thin as possible in order to reduce uncertainty in the effective bombarding energy. However, as the yield is a function of target weight it is necessary to compromise between the uncertainty in the bombarding energy and the amount of activity obtained. In this investigation the target thickness ranged from 400–1000 $\mu g/cm^2$ which corresponded to a energy loss of between 50 and 125 keV for 2 MeV deuterons and between 30 and 70 keV for 5.5 MeV deuterons.

Targets of natural isotopic composition were electroplated on tantalum backings.

When targets of enriched isotopes were required and only milligram quantities of material were available, other techniques were used such as molecular plating [3, 4], electrospraying [5, 6] vacuum deposition from a tungsten microcrucible [7] and the evaporation of small droplets [8]. Since the irradiation beam bombarded a portion of the total target area only targets of uniform thickness were accepted. The uniformity of the targets was checked by autoradiography after the samples had been activated.

Irradiation

Deuteron beams of between 0.5 μA and 12 μA were obtained from the 5.5 MeV Van de Graaff accelerator of the Southern Universities Nuclear Institute.

Several targets could be irradiated simultaneously on a rotating sample holder [9] which was cooled by circulating compressed air. Up to 12 samples could be accommodated and irradiations at different energies were carried out simultaneously by inter-

* Present address: Department of Chemistry, University of Stellenbosch, Stellenbosch, C. P., South Africa.

1. T. J. DE WAAL, M. PEISACH and R. PRETORIUS, Radiochim. Acta **15**, 123 (1971).
2. T. J. DE WAAL, M. PEISACH and R. PRETORIUS, J. Inorg. Nucl. Chem. (submitted).
3. W. PARKER and R. FALK, Nucl. Instr. Methods **16**, 355 (1962).
4. W. PARKER and M. COLONOMOS, Nucl. Instr. Methods **66**, 137 (1968).
5. D. CARSWEL and MILSTED, J. Nuclear Energy **4**, 51 (1957).
6. K. F. LAUER and V. VERDINGH, Nucl. Instr. Methods **21**, 161 (1963).
7. W. MENTI and M. MARTIN, Nucl. Instr. Methods **31**, 25 (1964).
8. W. PARKER, M. DE CROËS and K. SERVIER, Nucl. Instr. Methods **17**, 31 (1960).
9. M. PEISACH and R. PRETORIUS, Analytic. Chem. **38**, 956 (1966).

posing aluminium foils in front of each target to reduce the beam energy. The beam energy at the midpoint of the target was calculated from tables [10]. Under these conditions targets were activated with the same total current at different energies, thereby enabling relative cross sections and the shape of the excitation curve to be obtained experimentally.
Single samples were irradiated inside a Faraday cup which permitted the accurate measurements of the total current falling on the target. In this way absolute determination of cross sections could be made at selected bombarding energies, and all the single irradiations obtained in this way were used to normalize the relative values by the method of least squares.

Activity measurement

The irradiated samples were counted and analysed by gamma-ray spectrometry using a $3'' \cdot 3''$ NaI(Tl) scintillation detector or a 30 cc Ge(Li) detector.
The efficiency of the detectors was determined with standard activities of sodium-22, cobalt-60, yttrium-88, caesium-137 and americium-245, obtained from the National Research Laboratory, Pretoria and the International Atomic Energy Agency, Vienna.
The spectra were recorded for a preset time. However, a preset count single channel analyser connected in parallel was used to limit the counting period of very active samples. Spectra were automatically stored on magnetic tape.

Calculation of cross sections

The cross sections were calculated [1] from the equation

$$\sigma = \frac{M}{n\varepsilon p a N} \cdot \frac{C}{t_c} \cdot \frac{\pi d^2}{4w} \cdot \frac{t_i \cdot 1.6 \cdot 10^{-19}}{Q} \cdot \frac{e^{\lambda t_d}}{(1 - e^{-\lambda t_i})} \cdot 10^{24} \text{ barns.}$$

M = molecular weight,
a = fractional isotopic abundance,
ε = detection efficiency,
p = gamma-ray intensity in gamma-rays per disintegration,
n = number of atoms of target element per molecule,
N = Avogadro's number,
C = number of counts in the relevant photopeak,
t_c = counting time (live time),
d = diameter of target area,
w = total weight of target material,
t_i = irradiation time,
Q = integrated irradiation current in coulombs,
t_d = decay time

Results and Discussion

The reactions ^{50}Cr(d,p)^{51}Cr and ^{50}Cr(d,α)^{48}V

Enriched chromium-50 as Cr_2O_3, was used for the study of these two reactions. One-hour irradiations of the samples produced sufficient activity but the measurements were started approximately 5 days after the end of the irradiation to reduce interference from short-lived products.
In the case of the ^{50}Cr(d,p)^{51}Cr reaction, the 319 keV photopeak (Fig. 1) was integrated. Only the spectra were used in which the intensity of the 511 keV photopeak was comparatively low to avoid contributions from the Compton edge of the 511 keV photopeak being included in the count representing the activity of chromium-51.

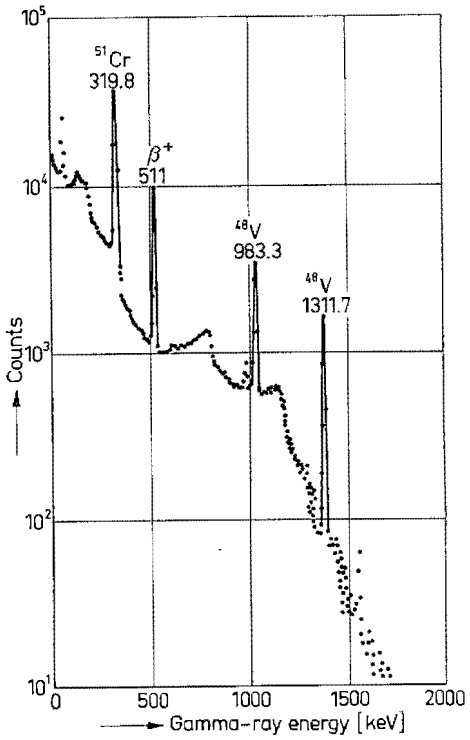

Fig. 1. Gamma-ray spectrum obtained from deuteron irradiated $^{50}Cr_2O_3$. $E_d = 5.5$ MeV

The activity of vanadium-48 was given by the integration of the counts forming the 1311-7 keV photopeak, as this peak was sufficiently resolved from all other activities.
The calculated values of the cross sections for these reactions are given in Table 1 and their corresponding excitation functions in Figs. 2 and 3.

Table 1. *Cross sections for the deuteron-induced reactions on* ^{50}Cr

E_d (MeV)	Reaction cross sections (Millibarns) ^{50}Cr(d,p)^{51}Cr	^{50}Cr(d,α)^{48}V
5.468	247 ± 11	7.1 ± 0.4
4.847	180 ± 9	4.1 ± 0.2
4.471	175 ± 8	3.4 ± 0.4
3.959	139 ± 6	2.8 ± 0.2
3.631	96 ± 5	1.34 ± 0.13
3.091	30.9 ± 2.5	0.42 ± 0.03
2.939	24.7 ± 2.0	0.37 ± 0.07
2.674	13.6 ± 1.0	0.12 ± 0.04
2.349	7.1 ± 0.4	0.06 ± 0.02

The reaction ^{55}Mn(d,p)^{56}Mn

The deuteron irradiation of manganese produced only one radioactive product, 2.58 h ^{56}Mn, whose activity could conveniently be measured. The simple gamma-ray spectrum obtained from it (Fig. 4) showed the intense

10. C. F. Williamson, J.-P. Boujot and J. Picard, CEA R-3042 (1966).

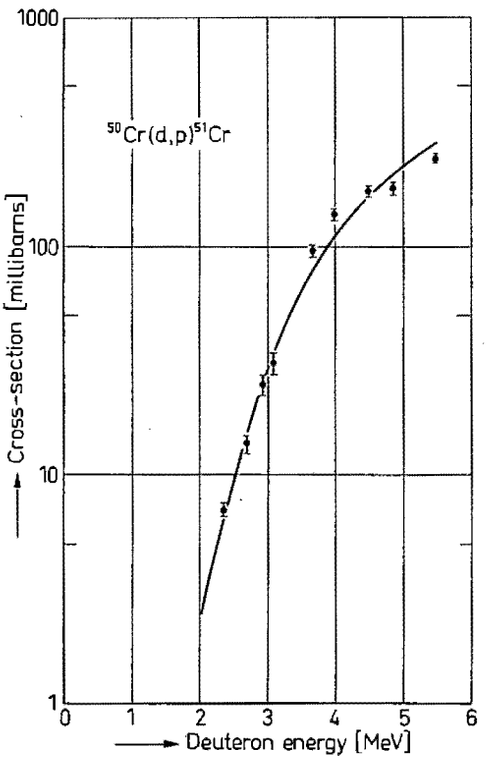

Fig. 2. The excitation function for the reaction $^{50}Cr(d,p)^{51}Cr$

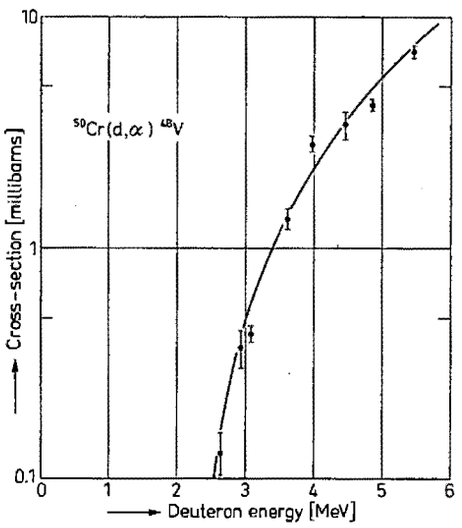

Fig. 3. The excitation function for the reaction $^{50}Cr(d,\alpha)^{48}V$

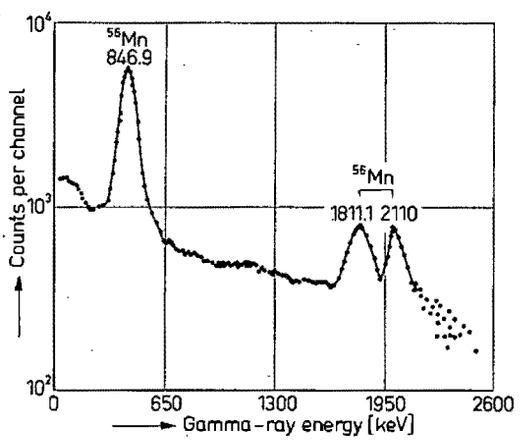

Fig. 4. The gamma-ray spectrum of manganese-56 obtained with a NaI(Tl) detector. $E_d = 5.5$ MeV

846.9 keV photopeak which was integrated to obtain a measure of the activity. The excitation function is given in Fig. 5 while the corresponding values of the cross sections are given in Table 2.

Table 2. *Cross sections for the reaction* $^{55}Mn(d,p)^{56}Mn$

E_d (MeV)	Reaction cross sections (Millibarns) $^{55}Mn(d,p)^{56}Mn$
5.471	208 ± 10
5.469	209 ± 10
5.191	174 ± 9
4.897	142 ± 7
4.868	153 ± 10
4.589	125 ± 6
4.462	140 ± 7
4.267	91 ± 4
3.925	83 ± 4
3.863	86 ± 5
3.575	40 ± 2
3.449	52 ± 3
3.184	28 ± 1
2.762	12.8 ± 0.6
2.451	6.4 ± 0.6
2.284	3.6 ± 0.2

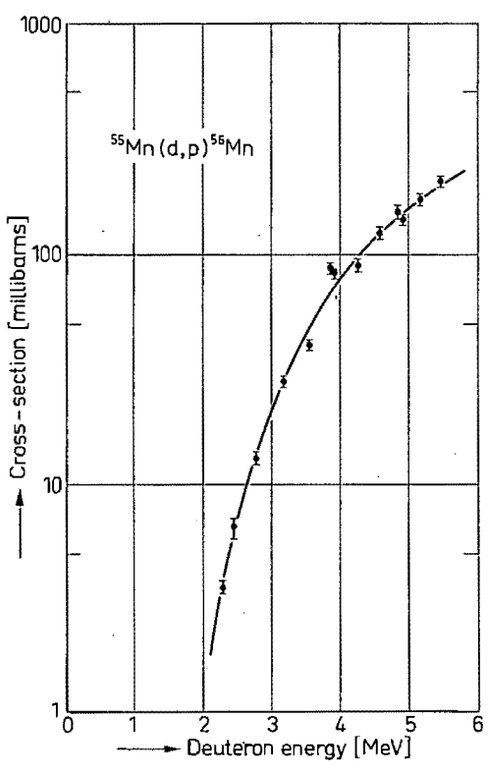

Fig. 5. The excitation function for the reaction $^{55}Mn(d,p)^{56}Mn$

The reaction $^{54}Fe(d,n)^{55}Co$

Most radioactive products which are produced in the deuteron activation of natural iron, have long half lives, and long irradiations would have been necessary to produce sufficient activity. Since such irradiations are impractical, short irradiations were carried out and 18.2 h cobalt-55 was the only product determined.

Table 5. *Cross sections for the reaction* $^{64}Zn(d,n)^{65}Ga$

E_d (MeV)	Reaction cross sections (Millibarns) $^{64}Zn(d,n)^{65}Ga$
4.894	64 ± 3
4.483	37 ± 2
3.955	20.1 ± 1.1
2.949	3.1 ± 0.2
2.345	0.39 ± 0.03

Accuracy and precision

The largest error affecting the precision of the cross section values arises from the determination of radioactivity. The errors involved in measuring them are statistical as determined by the number of events counted and the relative importance of the subtracted background. The relative precision was less than 0.5% when high activities were measured but reached up to 20% in the case of low activities.

A second important error lies in the absolute calibration of the spectrometer. The activities of the substandards used to calibrate the spectrometer were known with a relative precision of ±1% while the relative accuracy of the absolute calibration was less than 3%.

Since the area of the target could be well defined the error in determining its average thickness was the error in weighing which was within 2.5%.

The integrated current falling on samples irradiated singly was measured with a relative accuracy of ±1.5%. The energy of the beam from the Van de Graaff accelerator could be selected within ±2 keV.

The above errors contributed to the uncertainties in the cross sections listed here. Every cross section was considered as a separate determination and each error value is the root mean square error calculated from all the relevant experimental conditions pertaining to the measurement.

Acknowledgements

One of us (P.P.C.) thanks the South African Council for Scientific and Industrial Research for a bursary made available to him.

Additional financial assistance from the South African C.S.I.R. and the South African Atomic Energy Board is gratefully acknowledged.

Results reported here form part of a Master's thesis by P.P.C., presented to the University of Stellenbosch and is published with permission.

No. 40

Reprinted from the Proceedings of the National Conference on the Technological Applications of Nuclear Techniques. Atomic Energy Board, Pelindaba, South Africa, 1972.

THE USE OF CHARGED NUCLEAR PARTICLES FOR ANALYSIS

by

M. PEISACH and R. PRETORIUS

Southern Universities Nuclear Institute

SAMEVATTING

In aktiveringstudies kan die ligte elemente en elemente soos yster, waarvoor neutronaktiveringsanalise nie gevoelig genoeg is nie, bepaal word deur aktiveringsanalise met gelaaide deeltjies te gebruik. Pront deeltjiespektrometrie brei die aktiveringstegniek uit en stel 'n mens in staat om isotoopkonsentrasies vir die meeste ligte elemente te meet.

Gelaaide deeltjies se tempo van energieverlies na gelang van afstand is baie groter as dié van neutrone. Hulle kan dus gebruik word om die elementinhoud van oppervlakke te bepaal asook die wisseling in die konsentrasie van 'n komponent as 'n funksie van diepte onder die oppervlak deur die energiespektrum van elasties verstrooide gelaaide deeltjies en van die pront gelaaidedeeltjie-produkte van kernreaksies te gebruik.

Elementkonsentrasies van oppervlaklae kan met die opwekking van kenmerkende X-strale vanaf oppervlakatome met gelaaide deeltjiestrale bepaal word. In geskikte toestande kan oppervlakkonsentrasies van 10^{15} atome per cm^2 opgespoor en ontleed word. Deur goedgekollimeerde strale van gelaaide deeltjies te gebruik en dit al langs die kanale van 'n kristal te rig, kan die aard en ligging van onsuiwerhede vanaf die verstrooide deeltjies verkry word wat die kristal langs ander kanaalrigtings verlaat.

ABSTRACT

In activation studies the light elements and elements such as iron, for which neutron activation analysis is not sufficiently sensitive, may be determined using charged particle activation analysis. Prompt-particle spectrometry extends the activation technique and enables isotopic concentrations to be measured for most light elements.

The rate of energy loss with distance in matter is much greater for charged particles than for neutrons. They can thus be used to determine elemental compositions of surfaces and the variation of the concentration of a component as a function of depth below the surface, using the energy spectrum of elastically scattered charged particles and of the prompt charged particle products from nuclear reactions.

Elemental concentrations of surface layers may be determined by the excitation of characteristic X-rays from surface atoms with charged particle beams. Under suitable conditions, surface concentrations of 10^{15} atoms per cm^2 can be detected and analysed. Using well-collimated beams of charged particles directed along the channels of a crystal, the nature and position of impurities may be obtained from the scattered particles leaving the crystal along other channel directions.

1. INTRODUCTION

At the present state of accelerator technology, charged particle beams are obtainable which rarely penetrate more than a few millimetres in solids. Analyses carried out using charged particle beams are thus limited to thin samples, or other materials where the interest is in obtaining information about regions near to the surface of the sample. Bulk analyses can only be performed when the composition of the surface and near-surface region is assumed to represent the bulk composition. At first sight this restriction seems to be a disadvantage, but when charged particle beams are used correctly, they can provide information not obtainable with other analytical techniques. Indeed, the nature of information obtainable is truly unique and many institutions have obtained accelerators specifically for analytical use. The more recent such facilities include:

Type	Energy (MeV)	Location
Van der Graaff	2	École Normale Supérieure, Paris, France
"	3	LARN, Namur, Belgium
"	3	University of Sussex, England
"	5,5	Aarhus University, Denmark
"	5,5	Bell Telephones, USA
Cyclotron	30	AERE Harwell, England
"	40(under construction)	CNRS, Orleans, France

All these facilities are used in close cooperation with industries and research groups connected with such fields as metallurgy, electrochemistry, semiconductor materials, solid-state physics and chemistry.

In a short review paper such as this it is clearly impossible to deal adequately with each important application. Instead, the different aspects of charged particle usage will be discussed, starting with radioactivation analysis and thereafter dealing with (a) prompt techniques used during the bombardment, viz. scattering methods when no nuclear reactions are involved, and (b) prompt-product spectrometry from nuclear reactions. Thereafter mention will be made of two special techniques, viz. X-ray spectrometry from charged particle bombardment and the use of channeling of charged particles in single crystals.

2. RADIOACTIVATION ANALYSIS

The analysis of lighter elements such as oxygen, carbon, nitrogen, boron and beryllium, has a long history of high cost and technical difficulty. These elements have consequently been largely disregarded in reports on analytical data of so-called "pure" materials, even though modern technology has found that their presence, even in trace amounts, can have a most deleterious effect on the properties of materials. Neutron activation analysis has proved to be an unsuitable method for determining the light elements[1] as no readily measurable activities are formed during irradiation, while the sensitivities attained by most other analytical techniques have also proved to be inadequate[2]. Charged particle activation analysis has, however, been found to be a promising technique for determining most of the lighter elements in the ppm and ppb concentration ranges[3].

An important feature of charged particle activation analysis is the fact that the technique lends itself to automation. Large numbers of samples can be irradiated simultaneously by using a rotary-type target holder[4]. After irradiation the samples are removed from the irradiation chamber and packed into an automatic sample changer for measurement, by gamma-ray spectroscopy, of the induced radioactivity. The digital pulse height spectral data obtained from gamma-ray detectors and pulse height analysers, are stored on magnetic tape and processed by computer. Large numbers of samples may thus be analysed with a minimum amount of sample processing. In some cases, however, the presence of interfering activities in the sample necessitates the use of chemical separation after activation. Contamination caused during chemical processing, frequently a problem in other analytical methods, is negligible as such contamination is non-radioactive. Care must, however, be taken to prevent contamination before activation. In many cases the surface contaminants may be removed by etching the sample before activation.

Of all the light elements, the analysis of oxygen has probably attracted most attention. Schweikert and Rook[3] in the USA have determined oxygen in very pure silicon samples by charged particle activation analysis, for concentrations ranging from 10 ppb to 20 ppm. Their work is mirrored on the other side of the Atlantic by several groups carrying out oxygen analysis on so-called "pure" materials[5]. These studies in Europe are closely connected with recent developments in metallurgy and the drive to manufacture more highly purified metals, and the high scientific activity in this field is shown by the fact that regular six-monthly conferences are held to evaluate progress.

In analysing geological specimens, the urgency of the problem was less acute. Applications of radioactivation analysis by charged particle beams in this field thus started rather late. However, relatively short irradiations and the use of short-lived radionuclides makes this technique attractive for routine analysis of light elements. Figure 1 shows a series of spectra obtained[6] from a deuteron-bombarded sample of tourmaline measured at different stages of its decay. The prominence of gamma-ray peaks from ^{7}Be, ^{11}C, ^{28}Al, ^{24}Na and ^{56}Mn points to the ready use of this method for determining Li, B, Al, Na and Mn respectively as well as others such as Mg and Fe which were not present in the example.

3 PROMPT MEASUREMENT

Prompt particle spectrometry from charged particle bombardment is being used increasingly because of the development of technology requiring an accurate knowledge of surfaces and of variation of composition near the surface. The techniques being adopted can be divided into two classes, those in which a nuclear reaction does not occur, and those in which it does. The former group makes use of nuclear or Rutherford scattering of the bombarded particle, a process which occurs with relatively large

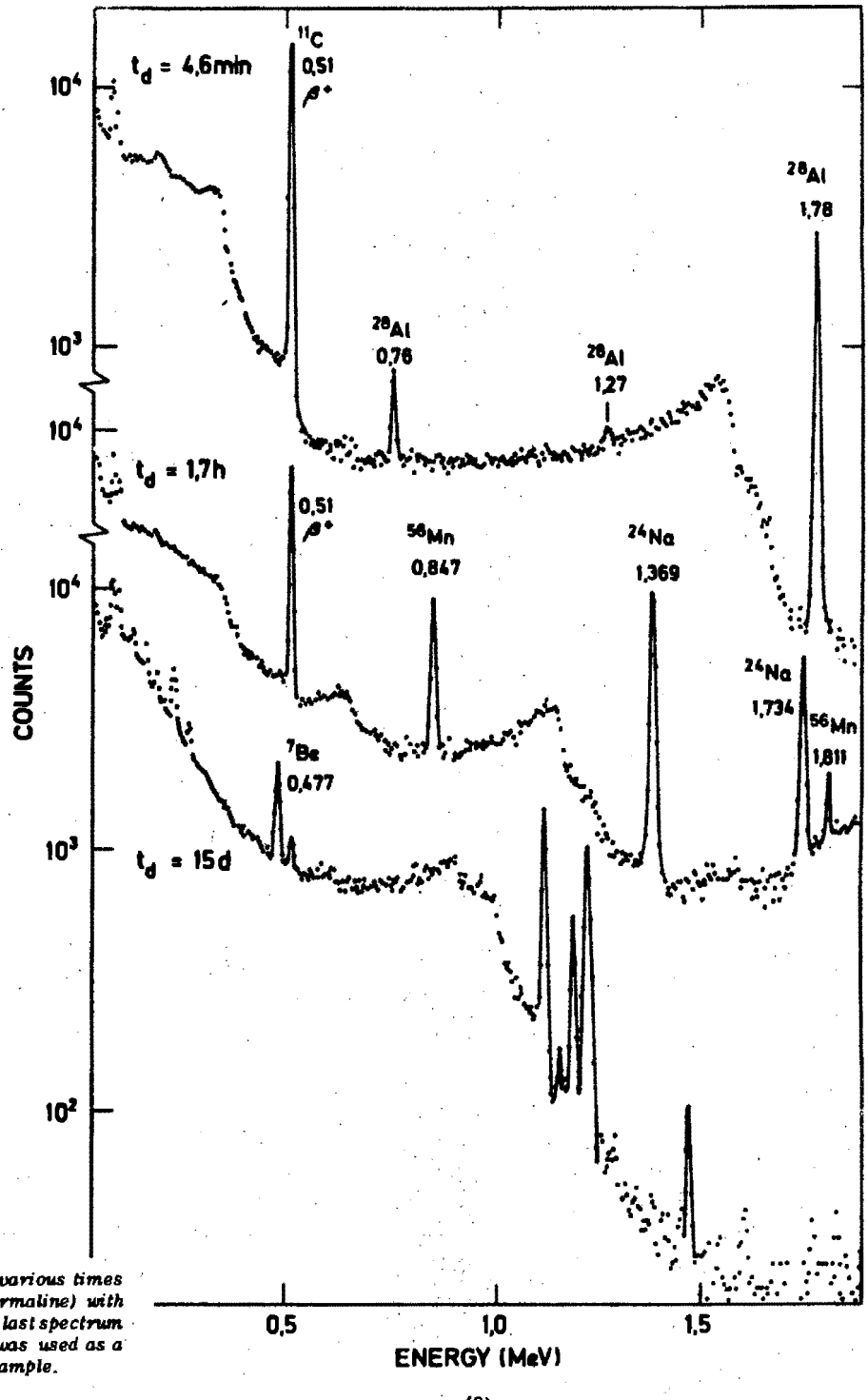

Figure 1. Gamma-ray spectra measured at various times after activation of a geological sample (tourmaline) with 5,5 MeV deuterons. The unmarked peaks in the last spectrum are due to activities from tantalum which was used as a backing material for mounting the powdered sample.

cross section. With particles of fixed bombarding energy, the energy of the scattered particle, measured in a pre-selected direction, is determined solely by the mass of the particle causing scatter while the intensity of the scattered beam is determined by the surface concentration of the scatterer.

The technique using scattered particles for surface analysis was first described by Rubin[7] but the form in which it is at present applied, using solid-state detectors to detect and measure the scattered particle, was described by Peisach and Poole[8]. Since then this technique has been used for a wide range of analyses, especially in connection with the construction of semiconductor devices. More recently, it was reported that glass samples are being analysed on a routine basis to determine elemental concentrations of various metals that had been implanted into the glass to change its optical properties. A similar application to determine elemental compositions of thin glass films is being studied by Peisach and Pretorius[9]. In this study the energy spectrum of scattered alpha

particles is used to determine most of the elements and the thickness of the sample, while a simultaneous measurement of prompt protons from (α,p) reactions gives a proton energy spectrum from which the concentrations of boron, sodium and aluminium can be obtained. Typical scattering spectra are shown in Figure 2, and prompt proton spectra in Figure 3. It is of course well known that the most spectacular use of scattering was the very first analysis of the moon's surface, when the work of Turkevich and his team[10] resulted in the placing on the moon of a radioactive alpha-particle emitter, curium-242, together with the necessary detectors, by Surveyor-V. A schematic representation of the apparatus is given in Figure 4. The entire apparatus weighed only 13 kg and measured about 15 cm x 15 cm x 13 cm. The absence of atmosphere on the moon was a marked advantage since vacuum equipment usually constitutes an essential part of the apparatus.

A recent report[11] described the use of scattering in connection with the printing industry. The major problem was to get information on the distribution in depth of various components, but elemental quantitative analyses were also of importance. Commercial paper is usually coated with a pigment, which also serves as the filler, and a binder. The interaction between the coating and the paper substrate gives rise to technological problems and it is important to obtain information on the distribution of the various components in the coating. Using 1,5 MeV alpha-particle beams, information was obtained as to the different behaviour of Zr and Pb siccatives used as additives to paper coatings, as well as differences between coated papers and polyesters. In addition, cases were found where Pb siccatives act differently depending on the presence or absence of Cu pigments.

There is much more scope for analytical applications if nuclear reaction products are measured, due to the wide range of nuclear reaction types and the range of bombarding energies and particles available. Since in any particular nuclear reaction the energies of the product particles are determined by kinematic relationships, spectrometry can frequently provide highly specific analyses. As before, the energy lost by a particle in escaping from the bombarded material may also be used to obtain information avout the depth distribution of the target nuclide. Obviously, no such information can be obtained where the measured product is a gamma ray (which loses intensity but not energy) but such analyses have advantages of specificity due to the high precision with which gamma-ray energies can be measured. Thus a very easy and rapid nondestructive procedure was developed[12] to determine the carbon content of steels over the carbon concentration range 0 04 to 0,69%. By bombarding the steel samples with deuterons carbon-12 produces carbon-13 in an excited state, which promptly decays with the emission of a gamma ray of 3 082 keV. This gamma ray is sufficiently intense to allow analyses to be carried out in a few minutes.

Attention may be drawn to another type of analysis where gamma-ray spectrometry is used to obtain information on concentration profiles. This is the case where the cross section for producing a particular excited state, followed by decay and with the emission of a characteristic gamma ray, shows a strong resonance and has negligible value on either side of the narrow resonance energy. The bombarding energy of the charged particle inducing the reaction may be selected above the resonance energy, so that when the energy of the particle falls to the resonance value as a result of energy loss within the material, the characteristic gamma ray is emitted. The yield of this radiation is thus a measure of the target-nuclide concentration at the depth where the bombarding particle attains the resonance energy. Such a case is the measurement of fluorine-concentration profiles through the use of the nuclear reaction $^{19}F(p,\alpha\gamma)^{16}O$ which has a sharp resonance at a proton energy of 872 keV.

Use of the above technique was made for the study of oxygen selfdiffusion in various oxides as a means of investigating point defects. Improvements in oxidation resistance of high-temperature alloys can be effected through the study of oxygen diffusion in the growing oxide scales. These investigations[13] used the resonance occurring at proton energies of 1 765 keV for the reaction $^{18}O(p,\alpha)^{15}N$, but the particle measured here was the emitted alpha particle. A double check on the depth profile measurements is available through a comparison between the energy loss in the proton beam and the loss of the alpha-particle energy emerging from the sample. Depth profiles up to 4 μm can be measured with a resolution of 0,1 μm.

A similar application, but one not making use of a resonance, has been reported[14] for the determination of chromium and nickel on metal surfaces. In this case prompt protons from (d,p) reactions are used. A typical spectrum

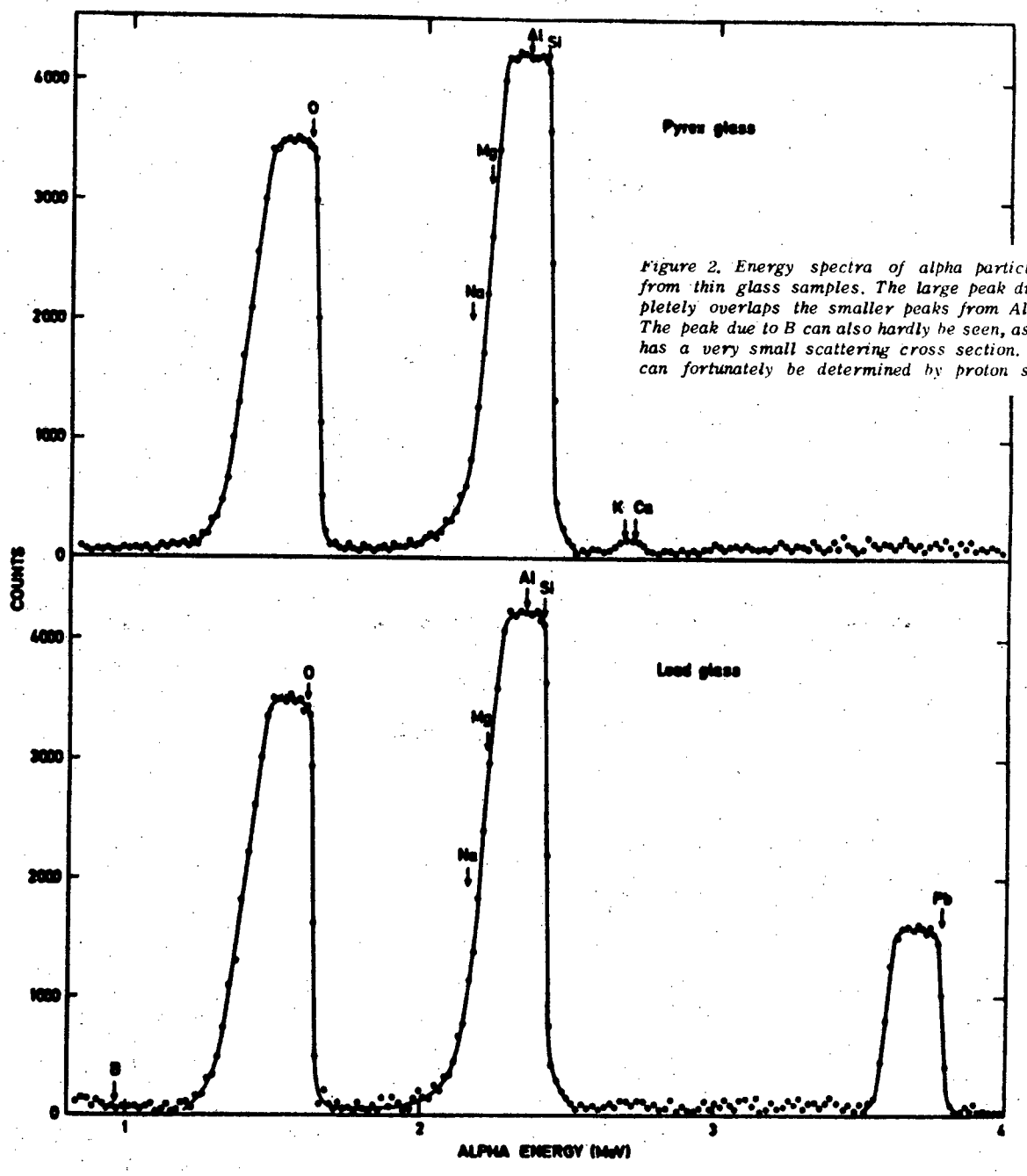

Figure 2. Energy spectra of alpha particles scattered from thin glass samples. The large peak due to Si completely overlaps the smaller peaks from Al, Mg and Na. The peak due to B can also hardly be seen, as this element has a very small scattering cross section. B, Na and Al can fortunately be determined by proton spectrometry.

(Figure 5) shows how readily the presence of chromium on a copper surface can be observed and measured.

4. X-RAY MEASUREMENT

Although the phenomenon of X-ray production by charged particle bombardment has been known for several years, interest in its possible use for analytical purposes has only recently been aroused by a paper published in 1970 by T.B. Johannesson, R. Akselsson and S.A.E. Johannesson[15]. The main advantage of X-ray production with heavy charged particles, as opposed to electrons, is due to the fact that the measured spectra are almost completely free of interfering brehmstrahlung. Also, the cross section for X-ray production by this method is extremely large, typically 100 to 10 000 barns, which are orders of magnitude greater than that of charged particle induced nuclear reactions which rarely exceed a barn. Such cross sections are directly proportional to the square of the charge of the bombarding projectile, and reach a maximum at energies where the velocity of the incident charged particle is comparable to that of the electron which is to be excited. The technique is extremely sensitive, and sensitivities of 10^{-12} g and better are readily achieved.

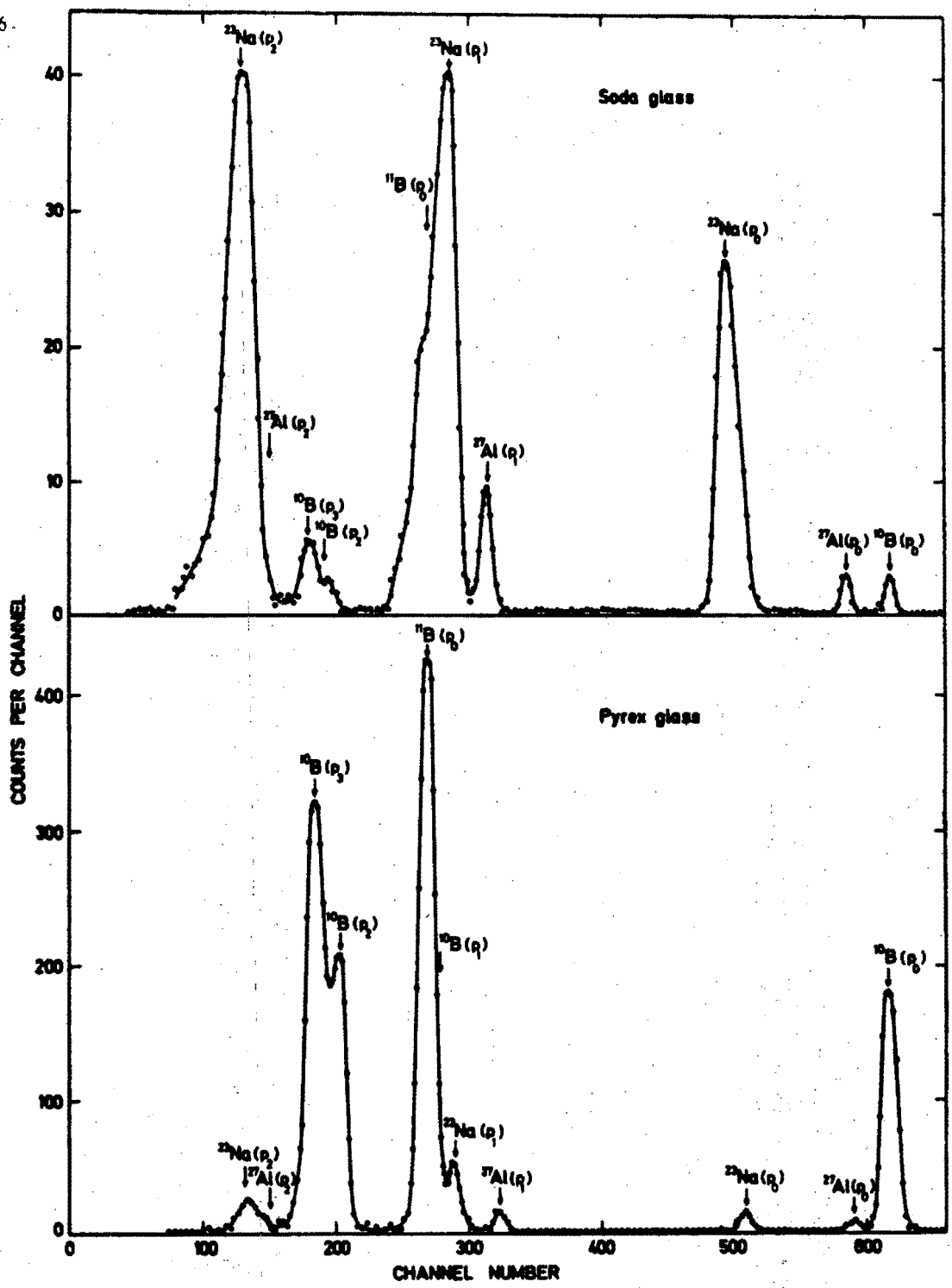

Figure 3. Spectra of prompt protons emitted during bombardment of soda and pyrex glass. The large difference in the boron and sodium content of the glasses is obvious.

The very high cross section from X-rays produced by charged particles, makes it possible to use extremely small beams of less than 1 nano-ampere. The serious heating problem that is associated with charged particle bombardment is thus obviated, thereby enabling biological materials to be analysed without decomposition of the sample. The X-ray yield from beams of extremely small dimensions is also usually sufficient for analysis and has led to the development of a proton microprobe with a beam diameter of about 3 microns[16], with which samples can be scanned over a limited area of 100 100 microns.

At Brookhaven National Laboratory, measurement of X-rays produced by charged particles is being used in pollution studies[17]. The potential of this method for the determination of pollutants is so promising that the IAEA has organised a study group, of which SUNI is a member, to investigate the use of this technique in pollution control.

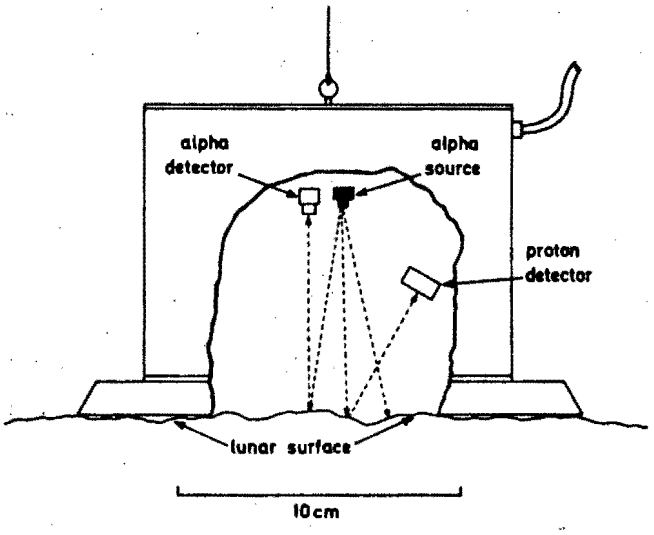

Figure 4. Schematic diagram of the apparatus used for the first chemical analysis of the moon's surface, during the landing of Surveyor-V. Analysis was carried out by measuring the energy of alpha particles scattered from the lunar surface. Protons from (α,p) reactions were also detected as a measure of Na, Al and B.

5. CHANNELING

When one looks at a ball-and-stick model of a single crystal, its transparency in certain directions becomes obvious. In these directions the regular arrangement of atoms seems to form open "channels" which, upon rotation of the model, alternate with planes or straight columns of atoms. A beam of charged nuclear particles aimed at a real crystal in the direction of such a channel will penetrate the crystal without colliding with the atoms forming the walls of the channel, as the positively charged nuclear particles are repulsed by the positive potential of the nuclei of these atoms and become steered down the channel by successive gentle collisions. The channeling effect thus prevents violent collisions with individual lattice atoms, and the yield of nuclear reaction products in a channeling direction will be drastically reduced from that observed when bombarding the crystal in a random direction.

The first experiment illustrating the channeling phenomenon was carried out approximately ten years ago and, since then, the effect has proved to be a useful tool to nuclear analytical chemists for determining the location of impurities within crystal lattices[18]. Figure 6 shows the principles involved for a simplified two-dimensional lattice, with the cross representing an impurity atom in a substitutional position, while the square and triangle represent impurities in two different interstitial positions. If analysis by charged particle scattering is carried out with a well-aligned (divergence $< 0{,}1^{o}$) beam, the direction in which the scattered particles from the impurities are measured can also be accurately defined by suitable collimation of the detector, thereby achieving a double alignment. It is clear from the figure that scattered particles from two of the impurities, designated by a cross and a square will be "blocked" by the row of atoms between it and the detector, resulting in a decrease in the yield of measured scattered particles, while the scattered yield from the third type of impurity is unaffected. The yield of scattered charged particles is thus first measured with the incident beam aligned with a channeling direction, and thereafter with alignment of the detector thereby enabling the lattice position of each type of impurity to be determined (see Figure 6).

Channeling has opened the way for many technical innovations. For example, electrical engineers can implant a desired impurity in a semiconducting crystal by ion bombardment along a channeling direction, thereby causing a minimum of radiation damage. Ion implantation of impurities into crystals in this way also permits penetration to greater depths, and can be used to control the distribution of such impurities in ways not possible with conventional diffusion techniques. After implantation the amount of implanted ions and their lattice positions may be determined as described above. A further advantage of ion implantation is that atoms of any element may be introduced into the substrate, whereas diffusion techniques are limited to those elements only which are soluble in the host material.

REFERENCES

1. ALBERT Ph.: L'analyses par Radioactivation, Youthier-Villans, Paris (1963).

2. MORRISON, G.H.: Trace Analysis; Physical Methods, p. 10, J. Wiley & Sons, New York (1966).

3. SCHWEIKERT, E.A. and H.L. Rook: Anal. Chem. 42, 1525 (1970).

   MARKOWITZ S.S. and J.D. Mahony: Anal. Chem. 34, 329 (1962).

   RICCI, E. and R.L. Hahn: Anal. Chem. 40, 54 (1968).

4. PEISACH, M. and R. Pretorius: Anal. Chem. 38, 956 (1966).

5. BARRANDON, J.N., L. Quaglia, J.L. Debrun, M. Cuypers and G. Robaye: J. Radioanal. Che. 4, 115 (1970).

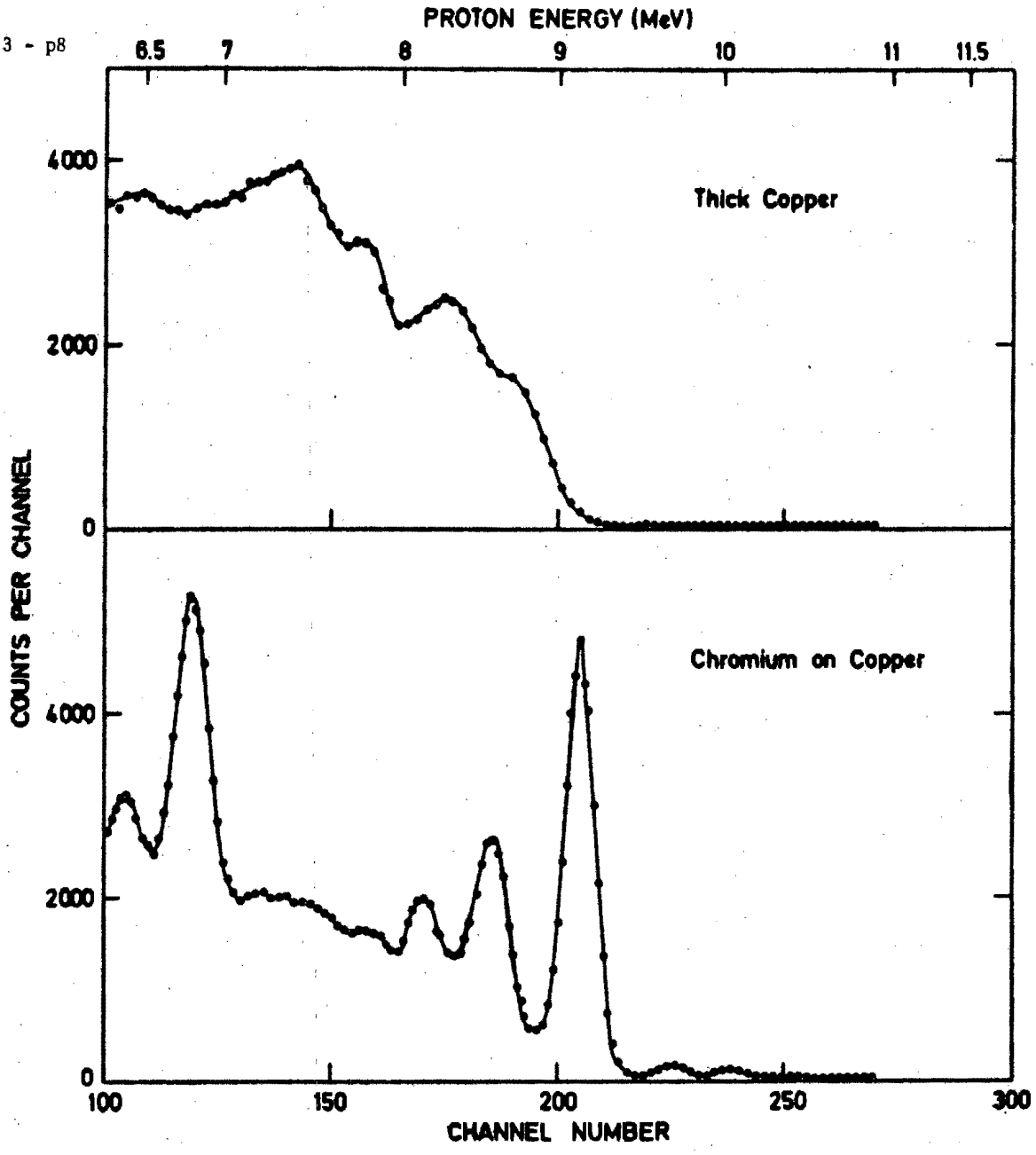

Figure 5. Proton-energy spectrum of a chromium film on copper compared with the spectrum from thick copper alone. Protons from (d,p) nuclear reactions were measured at an angle of 60° during bombardment with 3,5MeV deuterons.

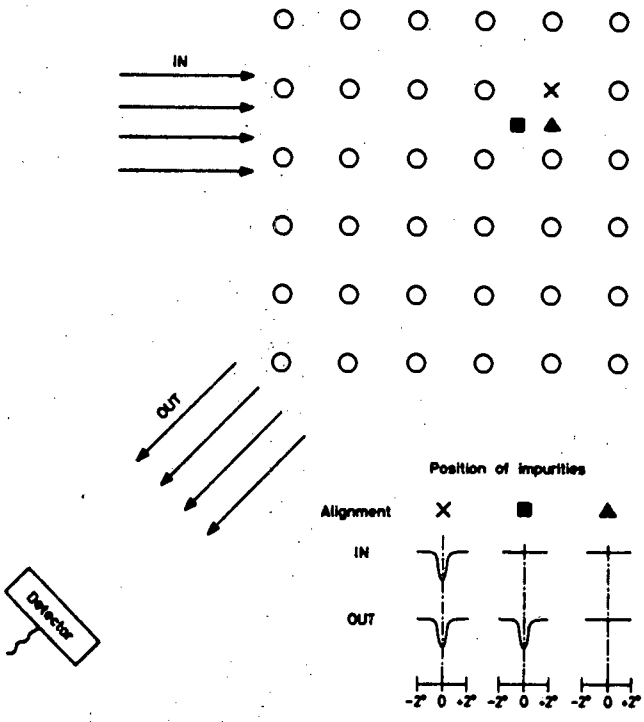

Figure 6. Illustration of how channeling of charged nuclear particles may be used for determining the lattice position of impurities in crystals. The simplified two-dimensional crystal lattice shows impurities in substitutional (X) and interstitial (■,▲) positions. By measuring the yield of scattered particles as a function of the alignment of the incoming beam and measuring direction, the position of the impurities may be determined.

AMSEL, G. and D. Samuel: Anal. Chem. 39, 1689 (1967).

AMSEL, G., B. Beranger, B. de Gelas and P. Lacombe: J. Appl. Phys. 39. 2246 (1968).

AMSEL, G., J.P. Nadai, E. D'Artemare, D. David, E. Girard and J. Moulin: Nucl. Instr. Methods, 92, 481 (1971).

6. PRETORIUS, R., F. Odendaal and M. Peisach: Proc. Intern. Conf. Chemical Analysis by Charged Particle Bombardment, Namur, Belgium, paper 4 (1971).
7. RUBIN, S. T.O. Passell and L.E. Bailey: Anal. Chem. 29, 736 (1957).
8. PEISACH M. and D.O. Poole: Proc. Intern. Conf.; Modern Trends in Activation Analysis, College Station, Texas, p. 206 (1965). Anal. Chem. 38, 1345 (1966).
9. PEISACH, M. and R. Pretorius: Preprints Modern Trends in Activation Analysis, Paris, paper M 92 (1972).
10. PATTERSON, J.H. A.L. Turkevich and E. Franzgrote: J. Geophys. Res. 70, 1311 (1965).
11. ERIKSSON, L. and G. Fladda: Proc. Intern. Conf. Chemical Analysis by Charged Particle Bombardment, Namur, Belgium, paper 16 (1971).
12. PIERCE, T.B., P.F. Peck and W.M. Henry: Analyst 90, 339 (1965).
13. AMSEL, G., J.P. Nadai, E. D'Artemare, D. David, E. Girard and J. Moulin: Nucl. Instr & Meth. 92, 481 (1971).

CALVERT, J.M., D.G. Lees, D.J. Derry and D. Barnes: Proc. Intern. Conf. Chemical Analysis by Charged Particle Bombardment, Namur, Belgium paper 3 (1971).

14. OLIVIER, C. and M. Peisach: J. of Radioanal. Chem. 5, 39 (1970).
15. JOHANSSON, T.B., R. Akselsson and S.A.E. Johansson: Nucl. Instr. Meth. 84, 141 (1970).
16. COOKSON, J.A. and F.D. Pilling: A.E.R.E. Harwell rept., AERE-R, 6300 (1970).
17. GORDON, B.M. and H.W. Kraner: Proc. Intern. Conf. Chemical Analysis by Charged Particle Bombardment, Namur, Belgium, paper 17 (1971).
18. MACKINTOSH, W.D. and J.A. Davies: Anal. Chem. 41, 26A (1969).

No 35

ELSEVIER SEQUOIA S. A.
Lausanne

AKADÉMIAI KIADÓ
Budapest

Journal of Radioanalytical Chemistry, Vol. 11 (1972) 105—122

PROMPT PROTON SPECTROMETRY FROM HIGH *Q*-VALUE (d, p) REACTIONS AND ITS USE FOR DETERMINING ^{10}B

C. OLIVIER,* M. PEISACH**

* *Department of Chemistry, University of Stellenbosch (South Africa)*
** *Southern Universities Nuclear Institute, Faure (South Africa)*

(Received September 8, 1971)

The analysis of boron in ore and glass samples was attempted by prompt proton spectrometry. A deuteron bombarding energy of 2.7 MeV was chosen to coincide with a region where the excitation function of the $^{10}B(d, p)^{11}B$ reaction did not vary appreciably with the energy. The intensity of the ground-state protons, emerging at an angle of 30°, was used as a measure of the boron content. Targets were prepared by a technique whereby approximately 300 $\mu g/cm^2$ deposits of powdered samples were centrifuged from a methanol suspension onto tantalum discs. Concentrations down to 0.2 % were determined. Possible interference by other elements, particularly nitrogen, magnesium and titanium, was investigated but found to be of little consequence mainly because of the high *Q*-value of the $^{10}B(d, p)^{11}B$ reaction.

Introduction

To date, the use for analysis of prompt charged particles from nuclear reactions induced by charged particles has been limited to the determination of ^{14}N, ^{16}O and ^{18}O, ^{32}P, ^{58}Ni and ^{60}Ni and ^{52}Cr.[1-5] It is thus evident that the full potential of this field has not yet been realized and that there exists scope for detailed study to extend the use of these methods to other elements and their isotopes.

The most likely reactions yielding prompt charged particles when stable nuclei are bombarded with deuterons of a few MeV are (d, p) and (d, α) reactions. The maximum energies attained by prompt protons from reactions induced by 2.7 MeV deuterons on isotopes with high *Q*-values for such reactions are given in Table 1. The energies of prompt α-particles are also included in the table. Since the isotopes of the rare gases are not expected to be components of other than gaseous samples, they are excluded from the table.

Because the reactions are highly exoergic, many energy states can be excited in the product nuclei and the energy spectra of the prompt protons will thus extend from somewhat above 12 MeV to very low energies. Since it could be expected that the bombarding beam will lose little energy in traversing very thin targets of the elements concerned, the energy spectra of prompt protons from such targets

Table 1

Ground state Q-values and product particle energies from (d, p) or (d, α) reactions on stable isotopes having Q-values for (d, p) reactions in excess of 8.0 MeV

Target nuclide	Natural abundance, %	Q-value, MeV [6]		Maximum particle energy for E_d = 2.7 MeV and 0°	
		(d, p)	(d, α)	E_p, MeV	E_α, MeV
^{47}Ti	7.28	9.403	6.845	12.074	9.232
^{10}B	19.78	9.231	17.819	11.811	16.362
^{33}S	0.76	9.198	8.566	11.858	10.692
^{43}Ca	0.145	8.911	7.868	11.584	10.167
^{87}Sr	7.02	8.876	8.002	11.562	10.498
^{25}Mg	10.13	8.870	7.049	11.524	9.145
^{50}V*	0.24	8.830	9.979	11.507	12.224
^{49}Ti	5.51	8.720	6.480	11.397	8.897
^{14}N	99.63	8.610	13.575	11.233	14.046
^{29}Si	4.70	8.393	6.014	11.059	8.254
^{61}Ni	1.19	8.375	8.724	11.048	11.093
^{77}Se	7.58	8.266	9.141	10.953	11.569

* Radioactive.

may be expected to consist of a series of narrow peaks whose widths are determined by the resolution of the measuring system. Alpha-particles, which may be considered as a possible source of interference in the analysis of boron by prompt proton spectrometry, can be eliminated together with the scattered deuterons by an absorber placed in front of the detector.

The variation in energy of ground-state protons as a function of the angle of measurement is presented in Fig. 1 for some of the above-mentioned isotopes. ^{47}Ti and ^{33}S have very low cross-sections for ground-state proton emission [7,8] and for this reason they are excluded from the figure. Because of their low abundance in the natural elements, ^{43}Ca (0.145%) and ^{50}V (0.24%) are also excluded, since the yields of protons emitted from targets containing even relatively high concentrations of calcium and vanadium are expected to be very low. Accordingly, attention was paid to the study of the possible analytical use of prompt ground-state protons for the determination of ^{10}B. The energy of the ^{10}B(p_0) proton group decreases rapidly with angle, and will, at wide measuring angles, overlap those of many proton groups of other elements. It is thus advantageous to measure at small angles, where least interference from other proton groups will then be experienced.

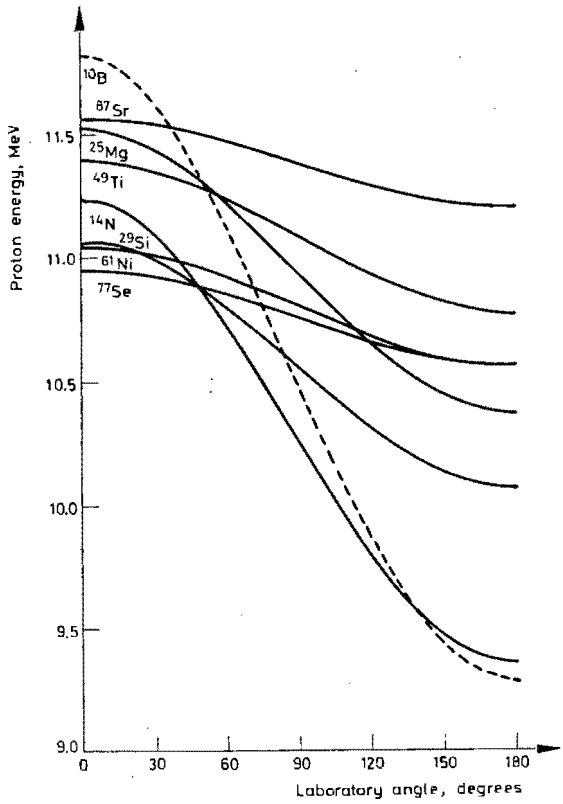

Fig. 1. The variation in energy of prompt ground-state protons, from (d, p) reactions induced by 2.7 MeV deuterons on some isotopes having high Q-values for this reaction, as a function of the angle of measurement

Experimental

Preparation of standards and samples

A technique similar to that used for preparing deposits of barium carbonate[9] for the routine counting of ^{14}C was used for preparing powdered deposits of elemental boron, boron nitride, glass, tourmaline and other inorganic compounds on tantalum discs.

Reference materials used were NBS standard glass samples Nos 92 and 93 and a tourmaline sample of which a complete analysis (NIM Report No. 939) was obtained from the National Institute for Metallurgy, Johannesburg, South Africa.

The apparatus used was a specially prepared centrifuge bucket, the design of which is shown in Fig. 2. It consisted of an aluminium centrifuge tube, the lower

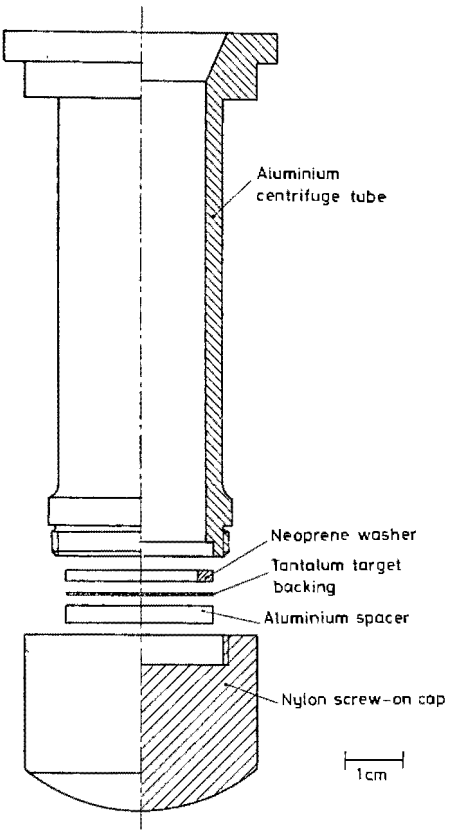

Fig. 2. Centrifuge bucket for preparation of the target deposits

end of which was a flat circular aluminium disc on which the tantalum disc rested. These discs were held in position by a base of nylon making a tight seal on a neoprene washer. The outer diameter of the centrifuge tube was made to fit the head of a 'Christ' centrifuge. The tantalum discs were 25 mm in diameter and 0.1 mm thick, while the inside diameter of the 2 mm thick neoprene washer was 20 mm, which was smaller than the inside diameter of the centrifuge tube. The area of deposition was 3.14 cm^2, and the average thickness of the deposits approximately 300 $\mu g/cm^2$.

Samples of the materials to be irradiated were ground to fine powders using a Siebtechnik mill with a Widia barrel and grinding stone. The particle size of the powders was about 0.5 μm and smaller, as measured by the average settling velocities of the suspended powders in distilled water.

Approximately 1 mg quantities of the powders were weighed out into 20 ml portions of methanol. High-frequency sound waves from an ultrasonic generator were used to bring the powders into uniform suspension. The suspension was

then poured into the aluminium bucket with a weighed tantalum disc in position, and centrifuged for 5 – 10 min at 3000 r.p.m.

After centrifugation the supernatant liquid was sucked off through a pipette, the tip of which rested on the edge of the neoprene washer to prevent the deposit being disturbed and to prevent the removal of part of the deposit from the tantalum disc during suction. The remaining methanol in the volume between the edges of the washer was evaporated with an infra-red lamp. Thereafter the tantalum disc was removed, dried in an oven at 120 °C and weighed.

The deposits thus prepared adhered sufficiently strongly to the tantalum for no loss in weight to be observed after irradiation. The preparation of evenly deposited targets was found to be successful in approximately 50% of cases.

Irradiation

The targets were irradiated inside a 90-cm scattering chamber with deuteron beams obtained from the 5.5 MV Van de Graaff accelerator of the Southern Universities Nuclear Institute. Rotation of the sliding rod sample mount around its own axis made possible variations of the target angle relative to the direction of incidence of the beam. A target angle of 20° was chosen. By moving the target holder in a small changing chamber, it was possible to change samples without breaking the vacuum in the large volume.

The collimated irradiation beam had a circular cross-section of 3 mm diameter. Although the small target angle of 20° resulted in an irradiated area of elliptical shape having a major axis of about 8.8 mm, this broadening was still sufficiently narrow for the beam to fall entirely within the boundaries of the target deposit of 20 mm diameter.

The beam current was measured with a current integrator which was connected to the target holder and a cylindrical tube which enclosed the target holder. The tube acted as a Faraday cup and thus corrected for secondary electron loss experienced with an open target. The beam entered through an aperture in the cup, while another hole of the same size in the same plane, but at an angle of 30° to the direction of incidence of the beam, allowed the prompt products to be measured.

Measurement

The energy spectra of the protons formed from (d, p) reactions on the target were obtained by means of a semiconductor detector and amplifier coupled to a pulse-height analyser. The detector could measure protons of up to 10 MeV and had a resolution of less than 45 keV. It was mounted on one of the two rotating arms of the scattering chamber and was covered with nine gold foils, each of about 15 mg/cm^2 in thickness, to absorb the scattered deuterons, low energy protons and α-particles. Since the (d, p) reactions of interest are highly exoergic, the absorber thickness is not very critical, because the ground-state protons will be

produced at energies far in excess of that of the scattered deuterons. The only restriction is that the protons must be stopped in the sensitive region of the detector. The appropriate thickness of the absorber required was calculated from the stopping power for protons.[10]

Effect of the angle of measurement

It has been pointed out that it is advantageous to measure the $^{10}B(p_0)$ protons at small angles. It was also established experimentally[11] that, for an incident deuteron beam of an energy in the region 1.45–3.15 MeV, the yield of $^{10}B(p_0)$ protons reaches a maximum in the vicinity of 30°. To obtain higher sensitivity, this direction was consequently chosen for analysis.

The effect of deuteron energy

The variation of proton counts with deuteron energies between 1.7 and 3.0 MeV is shown in Fig. 3 as obtained with a thin (114 $\mu g/cm^2$) target of boron nitride. Counts from the $^{10}B(p_0)$ and $^{14}N(p_0)$ groups are given separately. In both cases little variation in the proton yield occurs in the energy region 2.0–3.0 MeV. Thus, when targets of an appropriate thickness are bombarded with deuterons

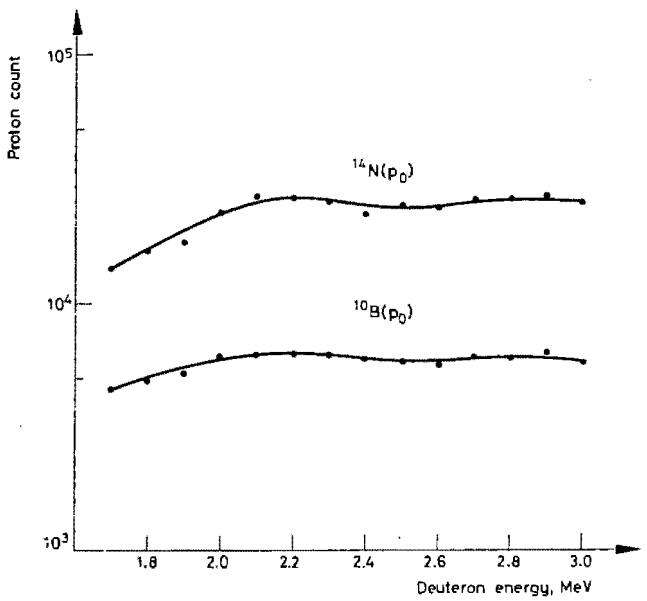

Fig. 3. The variation of proton counts measured at 30°, with deuteron energies between 1.7 and 3.0 MeV, as obtained with a thin target of boron nitride. Counts from the $^{10}B(p_0)$ and $^{14}N(p_0)$ groups are given separately

of 3 MeV or less in energy, very little variation in the count rate, if any, will be encountered while the deuterons traverse the target deposit, providing the energy does not fall below 2.0 MeV. Subject to this restriction, the count rate will be a function of the target thickness, which simplifies the analysis considerably. A bombarding energy of 2.7 MeV was selected in an attempt to decrease interference from heavy elements which already yield an appreciable count rate of protons above about 3 MeV. As far as the $^{14}N(p_0)$ group was concerned, no decrease in the relative yield could be achieved by changing the energy.

Effect of the target angle and the thickness of the deposit

The length of the path which the deuterons have to follow in traversing the target deposit depends on the angle which the target forms with the direction of incidence of the beam. It follows that the peak width increases with a decreasing angle, since the deuterons lose more energy through the longer path length and suffer more straggling. The energy loss of the prompt protons, however, is negligible. Most of the broadening of the peaks is caused by the absorber foils, so much so that by increasing the thickness of a boron target from 100 to 350 $\mu g/cm^2$ the peaks were only broadened from approximately 240 to 310 keV (full width at half height).

The deposit was usually about 300 $\mu g/cm^2$ thick, and the beam had to penetrate an effective thickness of about 880 $\mu g/cm^2$. For an elemental boron target the bombarding energy would be reduced to about 2.5 MeV,[10] which is still sufficiently high to ensure a constant rate of prompt proton production (see Fig. 3). Because of their lower stopping powers the same will apply to targets of other elemental compositions.

Effect of the distance between target and detector

The best distance for measurement was obtained by measuring prompt protons from an irradiated boron nitride target. Using the relative depth of the valley between the $^{14}N(p_0)$ and $^{10}B(p_0)$ peaks (see Fig. 4) in the spectra as a criterion, it was found that 55 mm between the detector and the centre of the target gave optimum results.

Effect of beam current

Boron counts, observed from the same target but irradiated with different beam intensities, showed a standard deviation of $\pm 3.23\%$ for a beam current between 0.3 and 1.0 μA. Higher beam currents resulted in a decrease in the boron count, caused by the loss of the deposited material accompanying the higher temperature involved.

Results and discussion

Energy spectra of prompt protons

Typical energy spectra of the prompt protons obtained from thin deposits of *boron*, boron *nitride*, *titanium* dioxide, cadmium *sulfide*, *calcium* fluoride, *strontium* chromate, *magnesium* oxide and *vanadium* pentoxide on *tantalum* backings, and of the protons from the backing itself are shown in Figs 4 – 7. The positions of expected peaks, each marked in the figures by an arrow labelled with the target nuclide from which the particular proton group, p_i, originates, are calculated from the known nuclear energy levels of the product nucleus and reaction kinematics. The energy scale in the figures refers to the energy of the particle before passing through the absorber. One effect of the absorber foils was to broaden the peaks obtained from each proton group; the broadening increases as the energy of the proton groups decreases.

The spectrum obtained from *boron* is characterized by the prominence of two peaks and the virtual absence of background counts in the energy region of interest. The peaks correspond to the p_0 and p_1 proton groups from ^{10}B. The high-yield p_0 group which lies in the high-energy region, where there is the least chance of obtaining protons from other elements, was accordingly chosen for analytical purposes. By integrating the number of counts under this peak, a value is obtained which is a quantitative measure of the concentration of boron. This integrated count is referred to as the boron count. The highly energetic α-particles also produced (see Table 1) are not detected, since their maximum range in gold[10] is less than 90 mg/cm^2, and they are therefore completely stopped in the absorber (135 mg/cm^2) placed over the detector.

In the spectrum obtained from boron *nitride*, the peak due to the p_0 proton group from ^{14}N dominates because of the high abundance (99.63 %) of this isotope and the large cross-section of the reaction concerned. In spite of the large yield of this proton group and the fact that the leading edge of this peak overlaps to some extent with the trailing edge of the peak from the $^{10}B(p_0)$ proton group, the latter peak is still clearly resolved from that of the $^{14}N(p_0)$ peak.

In the energy region of the $^{10}B(p_0)$ proton group, practically no counts were obtained in the spectrum from *titanium* dioxide. However, a prominent peak corresponding in energy to the $^{47}Ti(p_1)$ group is clearly distinguished and a small contribution by the $^{49}Ti(p_0)$ group is also observed. The $^{14}N(p_0)$ and $^{47}Ti(p_1)$ groups, which differ in energy by only about 50 keV, cannot be resolved from each other under the present experimental conditions. The presence of nitrogen was verified by changing the detecting angle from 30° to 90°, thereby increasing the energy difference between the two proton groups to approximately 500 keV. The integrated count under the $^{47}Ti(p_1)$ peak proved to be less than 10 % of that under the $^{14}N(p_0)$ peak.

In the spectrum obtained from cadmium *sulfide*, the $^{33}S(p_0)$ proton group was not observed. The prominent peak near the energy region of the $^{10}B(p_0)$ group is once again ascribed to the presence of nitrogen, which arises from the low con-

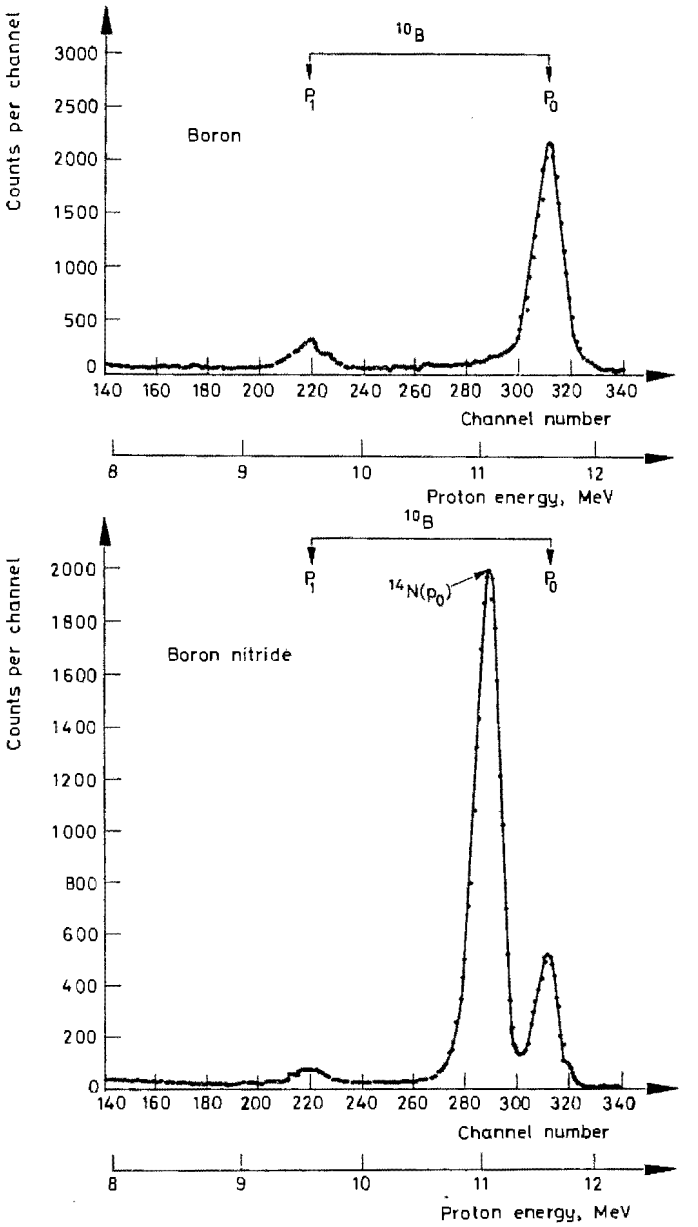

Fig. 4. Energy spectra of prompt protons obtained from the deuteron irradiation of thin deposits of boron and boron nitride on tantalum. $\Theta = 30°$, $E_d = 2.7$ MeV, Au absorber = 135 mg/cm²

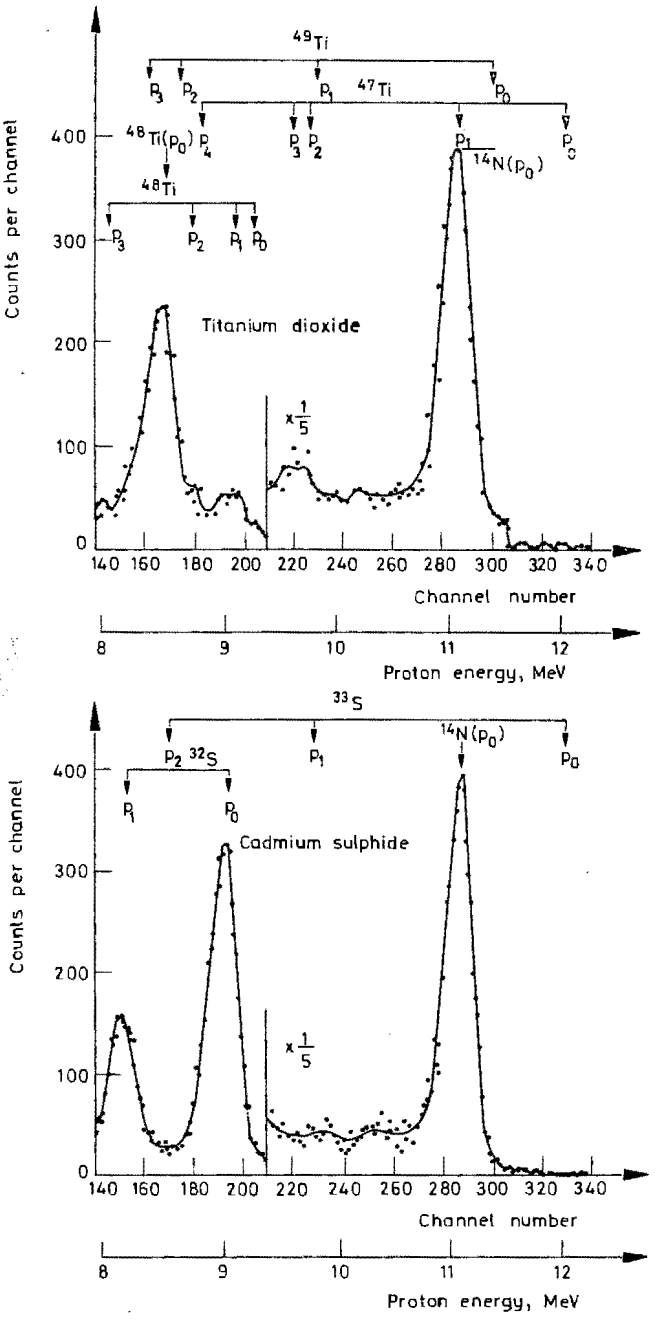

Fig. 5. Energy spectra of prompt protons obtained from the deuteron irradiation of thin deposits of titanium dioxide and cadmium sulfide on tantalum. $\Theta = 30°$, $E_d = 2.7$ MeV, Au absorber = 135 mg/cm^2

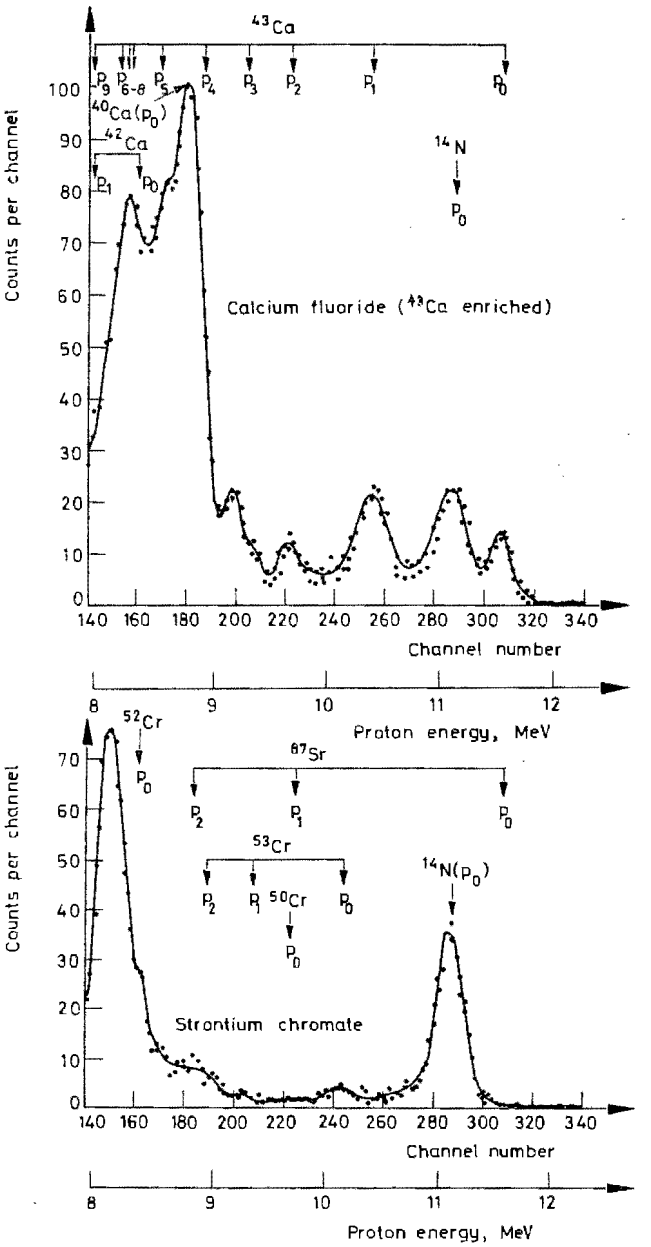

Fig. 6. Energy spectra of prompt protons obtained from the deuteron irradiation of thin deposits of calcium fluoride (^{43}Ca-enriched) and strontium chromate on tantalum. $\Theta = 30°$, $E_d = 2.7$ MeV, Au absorber = 135 mg/cm^2

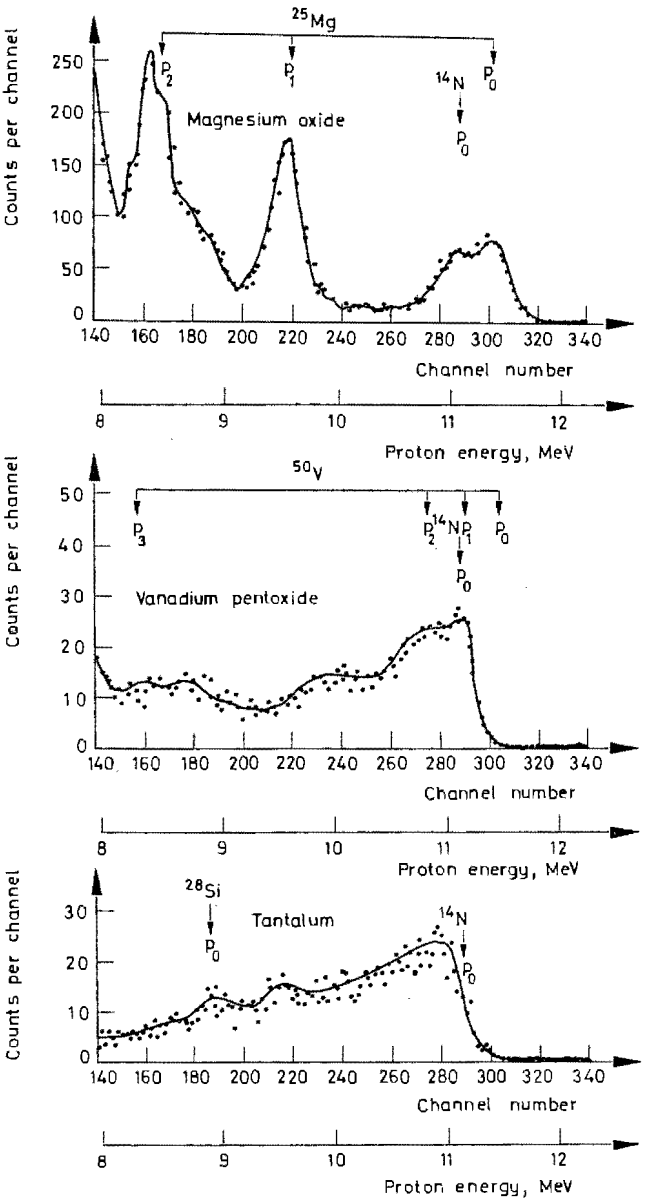

Fig. 7. Energy spectra of prompt protons obtained from the deuteron irradiation of thin deposits of magnesium oxide, vanadium pentoxide on tantalum. $\Theta = 30°$, $E_d = 2.7$ MeV. Au absorber = 135 mg/cm^2

centrations of ammonium sulfide still present in the precipitate, even though it had been repeatedly washed with distilled water. In the lower-energy region the other two prominent peaks observed correspond to the $^{32}S(p_0, p_1)$ proton groups.

For the spectrum obtained from *calcium* fluoride a target was prepared which was 81.12% enriched in ^{43}Ca. The peaks corresponding to the ground and first few excited states of the product ^{44}Ca, produced by the irradiation of ^{43}Ca, are clearly perceptible. The presence of nitrogen is again indicated.

In the spectrum obtained from *strontium* chromate the $^{87}Sr(p_0)$ proton group was not observed. Since the Coulomb barrier is relatively large for strontium ($Z = 38$), the cross-section of the (d, p) reaction at 2.7 MeV is apparently so small that prompt protons from it were not detected. On the other hand, a peak corresponding to the $^{14}N(p_0)$ proton group was again prominent.

In the spectrum obtained from *magnesium* oxide, peaks corresponding to the $^{25}Mg(p_0, p_1, p_2)$ proton groups are evident. A peak corresponding to the $^{14}N(p_0)$ group overlaps that of the $^{25}Mg(p_0)$ group. Depending on the method of preparation[12] this impurity might have been introduced in the magnesium oxide as either the nitrate or nitride.

In the spectrum obtained from *vanadium* pentoxide what may be $^{50}V(p_1, p_2)$ groups are just recognizable. Since the count rate was in any case very low, the presence of vanadium would not have a marked effect on the determination of boron.

Tantalum was used as backing material since the Coulomb barrier for such a heavy element ($Z = 73$) was large, and therefore the cross-section of the (d, p) reaction at 2.7 MeV was expected to be so small that prompt protons from it would be undetectable. This was not quite the case. The undulating plateau in this spectrum, whose leading edge corresponds to the peak of the $^{14}N(p_0)$ proton group, might have been caused largely by prompt protons from atmospheric nitrogen still present in the evacuated scattering chamber.

Analysis

Tourmaline and glass samples of known boron contents were used to determine the accuracy of the method. The reference material used was boron nitride. Typical energy spectra obtained from tourmaline, borosilicate glass and low-boron glass are shown in Figs 8 and 9. The $^{10}B(p_0)$ peak is clearly perceptible in each spectrum, although it is dwarfed by the $^{14}N(p_0)$ peak in the spectrum obtained from the low-boron glass. Nitrogen seems to be a low-concentration component of each sample even though no analytical results were available for this element. As was expected, the high content of silicon in every sample caused the very prominent peak corresponding to the proton group $^{28}Si(p_0)$. In the tourmaline samples, which contain aluminium, the spectra show a composite peak representing the $^{27}Al(p_0, p_1)$ proton groups.

To obtain the boron count in the boron nitride spectrum, a curve-fitting procedure had to be followed. By normalizing the shape of the leading edge of the

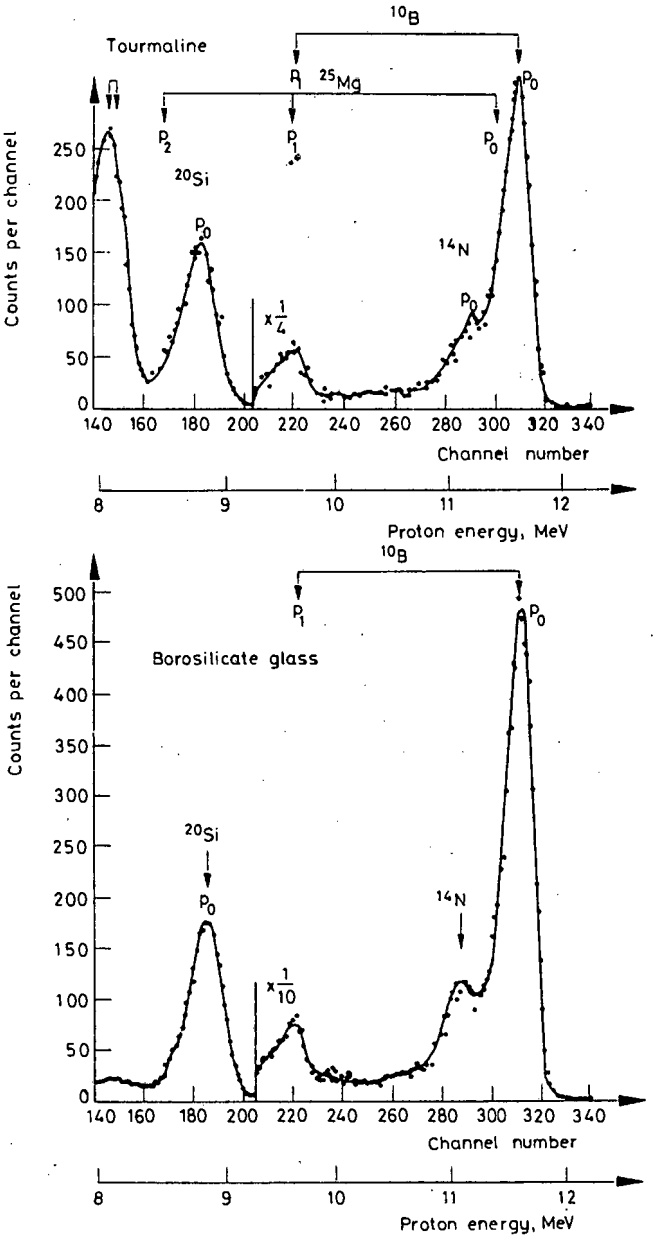

Fig. 8. Energy spectra of prompt protons obtained from the deuteron irradiation of thin deposits of tourmaline and borosilicate glass on tantalum. $\Theta = 30°$, $E_d = 2.7$ MeV, Au absorber = 135 mg/cm^2

$^{14}N(p_0)$ peak, a value is obtained which, after subtraction from the total integrated count of both peaks, gives the boron count. The forward edge was used for normalizing, since its shape is determined by protons detected from the surface of the target where little energy loss is experienced by the bombarding deuterons.

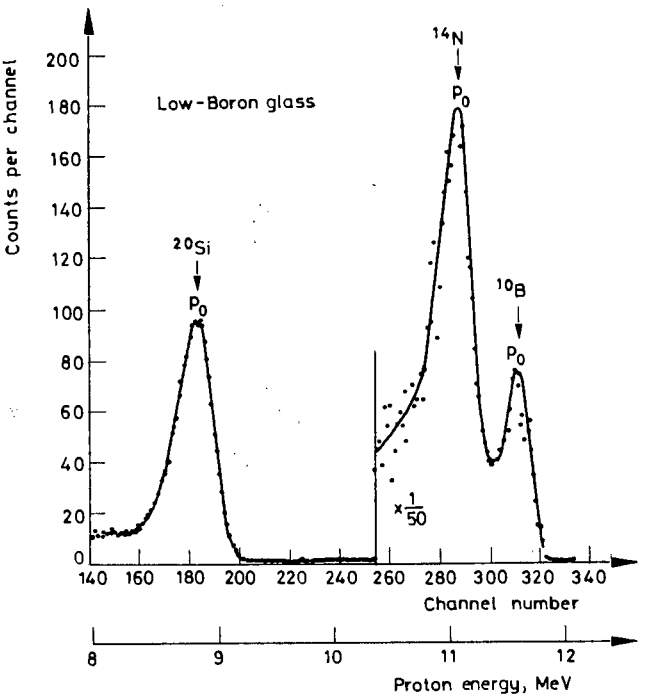

Fig. 9. Energy spectrum of prompt protons obtained from the deuteron irradiation of a thin deposit of low-boron glass on tantalum. $\Theta = 30°$, $E_d = 2.7$ MeV, Au absorber = 135 mg/cm

In contrast, the shape of the trailing edge may vary, because it is determined by protons from the back of the target deposit, and their energy is dependent on the amount of energy lost by the deuterons in penetrating the target material, and therefore on the sample thickness. A secondary check is given by the resultant shape of the boron peak obtained if the normalized $^{14}N(p_0)$ peak is subtracted from the observed spectrum. The same procedure is applicable for cases where the interfering peak has a higher count rate than that of the boron peak, as is the case with low-boron glass (see Fig. 9). In cases where the boron count was higher, for example with tourmaline and borosilicate glass (see Fig. 8), no great error is introduced when the shape of the trailing edge of the boron peak is normalized to that of other peaks in the same spectrum.

Calibration, precision and accuracy

Since little variation in the proton yield exists in the energy region concerned (see Fig. 3), a linear relationship was expected between 'the boron count' and 'concentration'. This assumption was tested by comparing the boron counts obtained from all samples after normalization to boron counts per unit percentage of boron. These results are given in Table 2.

Table 2

Some typical analytical results

Target	Thickness, μg/cm²	Counts[a] per 300 μg/cm²		Boron, %			Relative error, %
		Measured	Mean	Known	Determined[b] in target	Determined[b] mean value for sample	
Boron nitride	210.4	480.2	455.2±20.9	43.56	45.95	43.56[b]	+5.49
	214.9	450.3			43.09		−1.08
	220.9	473.9			45.35		+4.11
	305.6	435.2			41.65		−4.38
	329.1	436.4			41.76		−4.13
Tourmaline	222.5	422.6	450.1±19.6	3.25[e]	3.02	3.22	−7.08
	273.7	468.7			3.35		+3.08
	283.3	457.3			3.26		+0.31
	291.6	451.9			3.23		−0.62
Borosilicate glass	267.4	474.2	464.2±21.0	3.96[f]	4.13	4.04	+4.29
	269.9	440.2			3.83		−3.28
	299.2	478.5			4.16		+5.05
Low-boron glass	197.3	388.9	396.8±20.3	0.22[f]	0.19	0.19	−13.64[c]
	244.1	381.6			0.18		−18.18
	262.6	419.9			0.20		− 9.09
Boron powder	224.7	330.3	363.6±37.5	100	72.56	79.88	−27.44[d]
	232.0	424.8			93.32		− 6.68
	241.0	320.7			70.45		−29.55
	246.0	355.4			78.07		−21.93
	332.0	372.5			81.83		−18.17
	349.8	377.8			83.00		−17.00

[a] Expressed as counts per 300 μg/cm² target per unit percentage boron (by weight) as obtained from an irradiation with 0.1 mC current.

[b] Mean count from boron nitride used as calibration value for all these analyses.

[c] These values seem to indicate that the reported boron content of 0.22% is too high (see text).

[d] These values indicate large deviations for this sample (see text).

[e] Analysis supplied by National Institute for Metallurgy, Johannesburg, South Africa (NIM Report No. 939).

[f] Analyzed samples Nos 92 and 93 from U. S. Bureau of Standards.

The normalized count, expressed as the count that would have been obtained from a sample of standard thickness of 300 $\mu g/cm^2$ if irradiated with 0.1 mC current and normalized to unit percentage of boron by weight, is given in Column 3 of Table 2. These values, for the first three types of sample, have a mean value of 455.8 ± 19.4, i.e. a relative precision of 4.3%, and are in good agreement with the value 455.2 obtained from boron nitride for the slope of the linear calibration line correlating the boron content (in percentage by weight) to the observed normalized count. The mean value for each sample type, (Column 7) agrees very well with the known values. Relative errors are given in Column 8.

The marked increase in the relative error of the determination for the low-boron glass sample, and the appreciable discrepancy between the mean value determined by this method and the known boron content, seems to imply that the reported value of 0.22% is somewhat high. The value of 0.19% would have to be used to bring these results into line with those of other samples. The poorer precision for this sample can be ascribed largely to the relatively small numbers of counts that were obtained at the low level of boron. In the absence of interfering elements, when resolution becomes of minor importance, an improved precision may be obtained by placing the detector as near the target as is geometrically possible.

Clearly, the sample that had been accepted to be pure boron could not have been correctly described, because it would require an impurity amounting to more than 20% by weight to obtain agreement between these results and those from other samples.

Possible interferences

When the energy levels in the product nuclei are taken into account, it is found that the following proton groups have energies within the region of integration defined for the boron analysis (see Figs 4 – 7)

$$^{47}Ti(p_0, p_1), \quad ^{33}S(p_0), \quad ^{43}Ca(p_0), \quad ^{87}Sr(p_0),$$
$$^{25}Mg(p_0), \quad ^{50}V(p_0), \quad ^{49}Ti(p_0), \quad ^{14}N(p_0).$$

Of these the $^{25}Mg(p_0)$ group has the highest possibility of interfering, mainly because of its relatively high cross-section and the difficulty of resolving it from that of the required boron group. A test sample of magnesium oxide, containing magnesium and boron in equal concentrations, gave an uncorrected result about 0.6% high, which is well within the accuracy of the method. The proton groups $^{47}Ti(p_0)$, $^{33}S(p_0)$, $^{87}Sr(p_0)$ and $^{50}V(p_0)$ were not observed under the experimental conditions described, and the presence of natural elements containing these isotopes will therefore not affect the analysis. Although the $^{43}Ca(p_0)$ group was observed from a test sample containing about 40% ^{43}Ca, the presence of natural calcium will little affect the boron determination, because the count rate observed was low and because the natural abundance of ^{43}Ca is small (0.145%). As far as the presence of titanium is concerned, the small contributions from the $^{47}Ti(p_1)$

and $^{49}Ti(p_0)$ groups, which could not be determined accurately because of the presence of nitrogen in the test sample, may be ignored with confidence because of the very low count rates involved. The presence of nitrogen in the sample to be analyzed is easily coped with by the curve-fitting procedure described. As far as the backing is concerned, practically no counts were observed in the region of integration.

*

The financial assistance obtained from the South African Atomic Energy Board and the South African Council for Scientific and Industrial Research is gratefully acknowledged. Mr. H. S. PIENAAR, of the Department of Geology, University of Stellenbosch, is thanked for supplying the tourmaline sample. This work forms part of a doctoral thesis submitted by C. O. to the University of Stellenbosch and is published with the permission of his Promoter.

References

1. G. AMSEL, D. DANIEL, *Rev. Phys. App.*, 4 (1969) 383.
2. G. AMSEL, D. SAMUEL, *Anal. Chem.*, 39 (1967) 1689.
3. E. A. WOLICKI, A. R. KNUDSON, *Intern. J. Appl. Radiation Isotopes*, 18 (1967) 429.
4. C. OLIVIER, M. PEISACH, *J. S. Afr. Chem. Inst.*, 23 (1970) 77.
5. C. OLIVIER, M. PEISACH, *J. Radioanal. Chem.*, 5 (1970) 391.
6. C. MAPLES, G. W. GOTH, J. CERNY, *Nuclear Data*, 2A (1966) 429.
7. P. D. BARNES, C. K. BOCKELMAN, *Phys. Rev.*, 138 (1965) B597.
8. M. W. BRENNER, *Phys. Rev.*, 129 (1963) 765.
9. M. PEISACH, *J. S. Afr. Chem. Inst.*, 12 (1959) 57.
10. C. F. WILLIAMSON, J. P. BOUJOT, J. PICKARD, Report CEA-3042, 1966.
11. G. BREUER, *Z. Phys.*, 178 (1964) 268.
12. P. J. DURRANT, B. DURRANT, Introduction to Advanced Inorganic Chemistry, Longmans, Green and Co., London—New York, 1962, p. 442.

No 41

ELSEVIER SEQUOIA S.A.
Lausanne

AKADÉMIAI KIADÓ
Budapest

Journal of Radioanalytical Chemistry, Vol. 12 (1972) 139–149

DEUTERON ACTIVATION ANALYSIS OF GEOLOGICAL SAMPLES

R. PRETORIUS, F. ODENDAAL, M. PEISACH

Southern Universities Nuclear Institute, Faure, C. P. (South Africa)

Deuteron activation was found to be suitable for analysing geological samples, as no interfering activities are formed from oxygen, silicon and aluminium, which together make up more than 80% by weight of the earth's crust. To test the applicability of this method to geological samples, the mineral tourmaline was activated with 5.5 MeV deuterons obtained from the 6 MV van de Graaff accelerator at the Southern Universities Nuclear Institute. The induced activities were measured and analysed by gamma-ray spectrometry and the elements Al, Mg, B, Mn, Na, Fe and Li could readily be determined.

Introduction

Neutron activation has proved to be an excellent method for multi-elemental analysis of geological samples.[1–5] By combining chemical separation techniques[6] with sophisticated γ-ray spectrometry using high resolution lithium drifted germanium detectors[2,3,5] more than 60 elements may readily be determined.[4,5,7] For the analysis of rock samples retrieved from the moon, extensive use was made of neutron activation analysis.[7] The most attractive feature of this technique is its excellent sensitivity and specificity for determining most of the elements.[8,9] Sample preparation is usually minimal and in most cases the analysis can be carried out non-destructively. Certain elements, especially the lighter ones[8,9] can, however, not readily be determined by neutron activation analysis. It was consequently decided to investigate the possible use of charged particle activation as a complementary technique to neutron activation for the analysis of geological samples.

Deuteron activation should be particularly suitable for the analysis of geological samples as no large amounts of long-lived interfering activities are expected to be formed from oxygen, silicon and aluminium, which together make up more than 80% by weight of the earth's crust. The activities which could be formed from these elements during deuteron irradiation at an energy of 5.5 MeV are shown in Table 1. The short-lived activities ^{17}F, ^{28}Al and ^{30}P will decay almost completely within twenty minutes after the irradiation. The longer-lived activities ^{18}F (110 min) and ^{31}Si (2.6 hrs) could possibly cause problems. ^{18}F, however, is only a positron emitter and is formed from ^{17}O and ^{18}O, both of which have very low isotopic abundances in nature, while the longer-lived ^{31}Si only emits a 1.27 MeV γ-ray for 0.07% of its disintegrations and is also formed from a nuclide with a relatively low isotopic abundance (see Table 1).

Table 1

Activities expected to form from the main elements* in the earth's crust

Target nuclide	Isotopic abundance, atom %	Nuclear reaction	Half-life of product	Main γ-rays, MeV
^{16}O	99.759	$^{16}O(d, n)^{17}F$	66 s	β^+ (200)
^{17}O	0.037	$^{17}O(d, n)^{18}F$	110 m	β^+ (194)
^{18}O	0.204	$^{18}O(d, 2n)^{18}F$	110 m	β^+ (194)
^{29}Si	4.70	$^{29}Si(d, n)^{30}P$	2.6 m	β^+ (200); 2.24 (0.5)
^{30}Si	3.09	$^{30}Si(d, p)^{31}Si$	2.6 h	1.27 (0.07)
^{30}Si	3.09	$^{30}Si(d, \alpha)^{28}Al$	2.3 m	1.78 (100)
^{27}Al	100	$^{27}Al(d, p)^{28}Al$	2.3 m	1.78 (100)

*Oxygen = 46.7%, silicon = 27.7%, aluminium = 8.1%.

The applicability of deuteron activation analysis to geological investigations was examined by activating tourmaline samples. Tourmaline is a very interesting mineral occurring in granitic pegmatites and metamorphic rocks and its chemical composition is typical of most geological samples. The main compositional varieties of this mineral are the magnesium tourmalines or dravites, the iron tourmalines known as schorl and the alkaline tourmalines or elbaites which are usually rich in lithium. The chemical formulas of these three groups are:

Dravite $Na\ [Mg]_3\ \ Al_6\ B_3\ Si_6\ O_{27}\ (OH, F)_4$

Schorl $Na\ [Fe, Mn]_3\ \ Al_6\ B_3\ Si_6\ O_{27}\ (OH, F)_4$

Elbaite $Na\ [Li, Al]_3\ \ Al_6\ B_3\ Si_6\ O_{27}\ (OH, F)_4$.

There is a continuous series between dravite and schorl and between schorl and elbaite, but there appears to be an immiscibility gap between elbaite and dravite. It can be seen that the tourmalines are characterised by their Mg, Fe, Mn, Li and Al contents.

Irradiations were carried out with deuteron beams obtained from the 6 MV Van de Graaff accelerator at the Southern Universities Nuclear Institute.

Experimental

Preparation of samples and standards

Geological samples were prepared in a suitable form for irradiation by grinding to a fine powder and centrifuging a suspension of the powder in methanol onto tantalum or aluminium discs. This technique is described more fully elsewhere.[19] Standards were prepared from suitable compounds of the elements determined. A list of the standards used are given in Table 2. Targets from the standards were made either by the centrifuging technique mentioned above or by

Table 2

Compounds used as standards

Element determined	Standard	Method of target preparation
Lithium	LiF	Evaporation
Boron	BN	Centrifuging
Sodium	NaF	Evaporation
Magnesium	MgF_2	Evaporation
Aluminium	Al_2O_3	Centrifuging
Manganese	Std. Mn ore	Centrifuging
Iron	Fe_2O_3	Centrifuging

evaporation in vacuum onto tantalum or aluminium discs for those compounds having suitable melting points. The thickness of all targets were determined by weighing and varied between 200 and 300 $\mu g/cm^2$.

Irradiation and measurement

Targets were mounted on a rotating holder (see Fig. 1) which could be cooled by circulating water. The target holder fitted onto a vacuum chamber was connected to the beam tube of the accelerator. Irradiations were carried out with deuterons of 5.5 MeV and beam currents up to about 10 μA were used.

After irradiation, samples were placed in an automatic sample changer and analysed by γ-ray spectrometry using a Ge(Li) detector. Spectra were recorded on a 4 000 channel analyzer and transferred onto magnetic tape which could be read into an IBM 360–50 computer. Counting was repeated periodically until sufficient data had been accumulated to allow the major components to be separately determined.

Results and discussion

Gamma-ray spectrometry

γ-Ray spectra recorded during the decay of an irradiated schorl sample are shown in Fig. 2. Shortly after irradiation, the presence of ^{28}Al was proved by the photopeak at 1.78 MeV. The peak at 0.51 MeV was found by half-life measurements to be due mainly to ^{11}C (T = 20.5 min) which is a strong positron emitter formed from boron by the $^{10}B(d, n)^{11}C$ and $^{11}B(d, 2n)^{11}C$ reactions. After 1.7 hrs photopeaks from ^{24}Na (1.369 and 1.734 MeV) and ^{56}Mn (0.847 and 1.811 MeV) became prominent. The 1.734 MeV peak is the second escape peak from the 2.756 MeV γ-ray emitted during the decay of ^{24}Na. The last spectrum recorded 15 days after the end of the irradiation shows a peak at 0.477 MeV due to the decay of ^{7}Be (T = 53.4 days). All the other photopeaks in this spectrum were

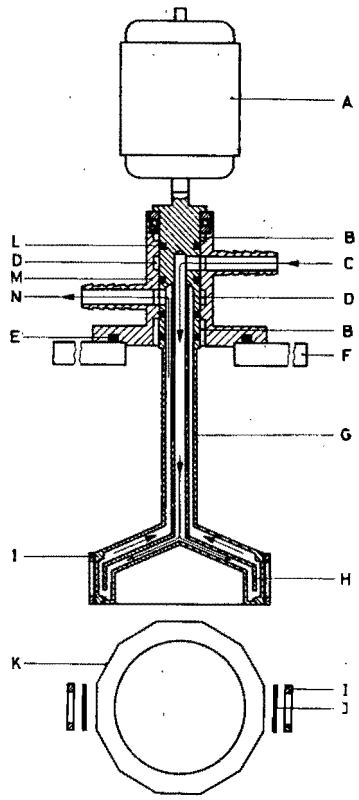

Fig. 1. Rotating sample holder cooled by circulating water.
A — motor and gear box, B — nylon bearings, C — water inlet, D — water chambers, E — vacuum seal, F — base plate, G — rotating cooled target holder, H — cooling water stream guide, I — target clamps, J — target, K — 12 flats for mounting target, L — water and vacuum seals, M — target holder support, N — water outlet

attributed to the tantalum backing and are formed from ^{182}Ta (T = 115 days) by the ^{181}Ta(d, p)^{182}Ta reaction.

Spectra recorded from an activated dravite sample are shown in Fig. 3. The first spectrum is for a sample on a tantalum backing while aluminium backings were used for the last two spectra recorded 44 hrs and 17 days after irradiation. Apart from radioisotopes already identified in the schorl sample, activities due to ^{27}Mg (9.46 min), ^{55}Co (18.2 hrs) and ^{22}Na (2.60 years) were also formed. The activities measured in tourmaline samples and the elements from which they are formed are listed in Table 3.

From Figs 2 and 3 it is clear that aluminium is more suitable than tantalum as a backing material for determining the longer-lived activities which are formed. Targets of each sample were thus prepared on aluminium as well as tantalum backings and irradiated for 30 min and 4 hrs, respectively.

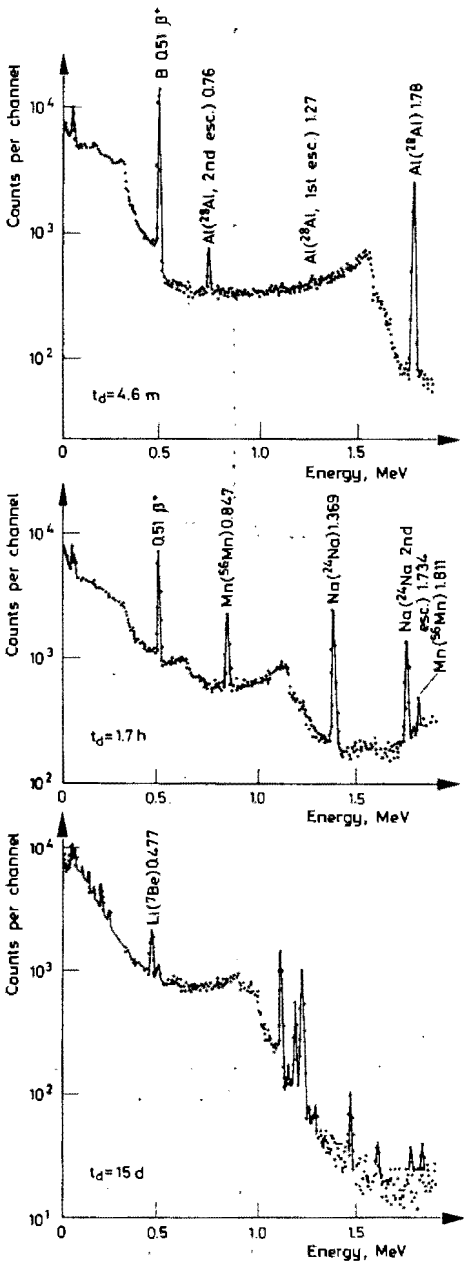

Fig. 2. γ-Ray spectra recorded during the decay of a schorl sample mounted on a tantalum backing and activated with a deuteron beam of 5.5 MeV

Table 3

Activities found and elements determined in tourmaline

Radio nuclide	Half-life	Nuclear reaction	Q value	Main γ-rays*	Element determined	Percentage interference
^{28}Al	2.3 m	^{27}Al(d, p)	5.499	1.78 (100)	Aluminium	
		^{30}Si(d, α)	3.121		(Silicon)	0.8
^{27}Mg	9.46 m	^{26}Mg(d, p)	4.212	0.84(70)	Magnesium	
				1.01(30)		
^{11}C	20.5 m	^{10}B(d, n)	6.466	β^+ (200)	Boron	
		^{11}B(d, 2n)	−4.990			
^{56}Mn	2.58 m	^{55}Mn(d, p)	5.046	0.84(99)	Manganese	
		^{58}Fe(d, α)	5.455	1.81(29)	(Iron)	6.19
				2.11(15)		
^{24}Na	15.0 h	^{23}Na(d, p)	4.734	1.37(100)	Sodium	
		^{27}Al(n, α)	−3.139	2.75(100)	(Aluminium)	6.00
		^{26}Mg(d, α)	2.909		(Magnesium)	0.3—9
^{55}Co	18.2 h	^{54}Fe(d, n)	2.832	β^+ (160)	Iron	
				0.48(12)		
				0.93 (80)		
^{7}Be	53.4 d	^{6}Li(d, n)	3.385	0.48(10)	Lithium	
		^{7}Li(d, 2n)	−3.868			
		^{10}B(d, αn)	−1.077		(Boron)	30—90
^{22}Na	2.60 y	^{24}Mg(d, α)	1.964	β^+ (180)	Magnesium	
				1.28(100)		

* Percentage of disintegrations leading to a specific γ-ray is given in parentheses.

Interferences

Some of the activities listed in Table 3 can be formed from more than one element in the tourmaline sample. The contribution of such interfering activities to the measured activity in the sample can, however, be determined by irradiating a known standard of the interfering element. Because both the sample and interference standard are irradiated simultaneously on the rotating target holder (see Fig. 1) the amount of interfering activity is given by the simple relationship:

$$\text{Interfering activity} = \text{activity (standard)} \cdot \frac{\text{thickness (sample)}}{\text{thickness (standard)}} \cdot \frac{\text{Wt.\% element (sample)}}{\text{Wt.\% element (standard)}}$$

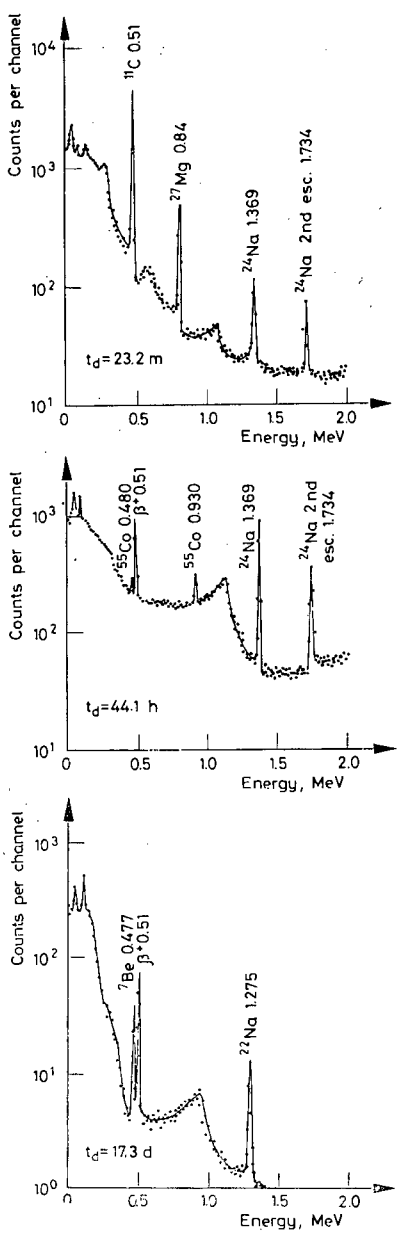

Fig. 3. γ-Ray spectra recorded during the decay of a dravite sample activated at a deuteron energy of 5.5 MeV. For the first spectrum (t_d = 22.3 min) the sample was mounted on tantalum, while aluminium was used as backing material for the last two spectra

The magnesium, boron and iron content of the samples can be uniquely determined (see Table 3) and the interfering activities formed from these elements for the determination of sodium, lithium and manganese, respectively, can be calculated by using the above-mentioned relationship. No activity is formed from silicon only, but fortunately the weight% of silicon in tourmaline[11] is practically constant, namely 17% and this value was used to calculate and subtract the silicon contribution to the measured ^{28}Al activity which was used as a measure of aluminium. ^{24}Na was detected in the aluminium backing material and is thought to have formed by the $^{27}Al(n, \alpha)^{24}Na$ reaction caused by neutrons originating in the aluminium backing itself during irradiation. An aluminium blank was irradiated to correct for such interference.

In the last two columns of Table 3 the interfering activities (in parentheses) as well as their percentage contribution to the measured activity are listed. The most serious interference is caused by boron when lithium is determined. For samples which have a relatively low lithium content as much as 90% of the measured ^{7}Be activity can be due to boron. Although the boron interference may be subtracted the statistical error which this entails can become prohibitively large. The interference of iron for the determination of manganese may also be quite serious depending on their relative abundances in the sample. Interference due to magnesium and the aluminium backing for sodium and of silicon, when determining aluminium, is small.

Quantization of measurements

The amount of radioactivity measured in the sample, A_{sample} is directly proportional to the weight, W_{sample}, of the particular element. By irradiating a standard simultaneously with the sample in the rotating target holder, a comparator technique is used, whereby both are subjected to the same irradiation flux. The weight of the unknown element in the sample can thus be given by

$$W_{sample} = W_{standard} \cdot \frac{A_{sample}}{A_{standard}} \quad (1)$$

where $W_{standard}$ – weight of the standard,
$A_{standard}$ – activity in standard.
The concentration of a certain element in the sample is then given by

$$\text{Wt.\% of element in sample} = N \cdot \frac{AW_{element}}{MW_{standard}} \cdot \frac{d_{standard}}{d_{sample}} \cdot \frac{A_{sample}}{A_{standard}} \cdot 100\% \quad (2)$$

where N – number of atoms of the element per molecule of standard,
AW – atomic weight,
MW – molecular weight,
d – thickness, g/cm^2.

Table 4

Some determinations of elements in tourmaline

Element determined	Measured activity	Sample	Wt.% known	Wt.% found
Aluminium (short irr.)	^{28}Al (2.3 m)	St. Tourm.	17.9	17.6 ±0.4
		Dravite	17.4 ±1.1	17.1 ±0.5
		Schorl	17.5 ±1.0	17.9 ±0.4
		Elbaite	21.7 ±1.1	20.6 ±0.4
Magnesium (short irr.)	^{27}Mg (9.46 m)	St. Tourm.	6.42	6.49±0.18
		Dravite	5.51±1.84	4.71±0.20
		Schorl	1.37±1.02	1.94±0.18
		Elbaite	0.20±0.18	0.30
Magnesium (long irr.)	^{22}Na (2.6 y)	St. Tourm.	6.42	7.20±0.31
		Dravite	5.51±1.84	7.10±0.40
		Schorl	1.37±1.02	2.45±0.21
		Elbaite	0.20±0.18	0.37
Boron (short irr.)	^{11}C (20.5 m)	St. Tourm.	3.24	3.28±0.16
		Dravite	3.11±0.15	3.00±0.14
		Schorl	2.95±0.23	3.10±0.12
		Elbaite	3.28±0.07	3.40±0.17
Manganese (long irr.)	^{56}Mn (2.58 h)	St. Tourm.	0.1	0.19
		Dravite	0.15±0.15	0.20±0.02
		Schorl	0.65±1.12	1.42±0.12
		Elbaite	0.59±0.42	0.98±0.07
Sodium (long irr.)	^{24}Na (15 h)	St. Tourm.	1.08	1.76±0.11
		Dravite	1.48±0.33	1.68±0.08
		Schorl	1.71±0.21	1.76±0.11
		Elbaite	1.82±0.19	1.51±0.12
Iron (long irr.)	^{55}Co (18.2 h)	St. Tourm.	2.19	2.10±0.16
		Dravite	2.6 ±2.5	2.85±0.21
		Schorl	9.9 ±2.5	9.50±0.48
		Elbaite	1.5 ±1.3	2.79±0.25
Lithium (long irr.)	^{7}Be (53.4 d)	St. Tourm.	0.01	0.09
		Dravite	0.07	0.09
		Schorl	0.16±0.16	0.12
		Elbaite	0.68±0.07	0.50±0.08

The γ-ray energies underlined in Table 3 were used as a measure of the various activities formed in the samples. Some determinations of elements in tourmaline are given in Table 4. The standard tourmaline sample was analysed at the National Institute of Metallurgy using various analytical methods, but unfortunately the accuracy of their determinations were not known. The dravite, schorl and elbaite samples were not analysed by other methods and the known weight percentage

for the various elements in them are average values for typical samples of each tourmaline group.[11] The given errors for these samples thus indicate the typical concentration range for a specific element in each group. Except for sodium, the found concentrations for the standard tourmaline sample agree within the errors of our method. Good agreement is also found between the typical values for the dravite, schorl and elbaite samples. It is, however, interesting to note that the found value for magnesium by measuring ^{22}Na is too high. The reason for this discrepancy has not yet been determined.

Advantages and limitations

The elements Mg, Al, Mn, Li, Na, Fe and B can readily be determined in typical geological samples by deuteron activation analysis. The method could play an important role as a complementary technique to neutron activation analysis since the latter method is not particularly suited for the determination of lithium, iron and boron.[8,9] The procedure can readily be automated so that large numbers of samples can be analysed on a routine basis. The rotating sample holder used in this experiment could only hold 12 samples but larger holders can be designed enabling many more samples to be irradiated simultaneously. Because the samples and standards are irradiated together irradiation time and flux need not be measured. Flux variations also have no effect on the analysis. This analytical method is, however, not generally suited for the determination of trace elements in geological samples but can be used for determining the major elements which have concentrations greater than approximately 0.1 weight%.

*

One of us (F.O.) thanks Dr. C. OLIVIER, his promotor, for permission to publish results which will form part of a M.Sc. thesis which is to be submitted to the University of Stellenbosch. Mr. T. W. STEELE and J. COOKE of the National Institute of Metallurgy, Johannesburg, are thanked for their analysis of the standard tourmaline sample. Special thanks are accorded to Mr. H. PIENAAR of the Geology Department at Stellenbosch University for supplying us with the tourmaline samples.

References

1. G. E. GORDON, K. RANDLE, G. G. GOLES, J. B. CORLIS, M. H. BEESON, S. S. OXLEY, *Geochim. Cosmochim. Acta*, 32 (1968) 369.
2. H. HIGUCHI, K. TAMURA, H. TAKAHASHI, N. ONUMA, H. HAMAGUCHI, Proc. Modern Trends in Activation Analysis, N.B.S., Gaithersburg, 1969, p. 334.
3. K. RANDLE, G. GOLES, Proc. Modern Trends in Activation Analysis, N.B.S., Gaithersburg, 1969, p. 347.
4. J. W. WINCHESTER, Proc. Symp. Nuclear Techniques for Mineral Exploration and Exploitation, Cracow, 1969, I.A.E.A., Vienna, 1969, p. 1.

5. G. E. GORDON, J. C. DRAN, P. A. BAEDECKER, C. F. L. ANDERSON, Proc. Modern Trends in Activation Analysis, N.B.S., Gaithersburg, 1969, p. 399.
6. F. GIRARDI, Proc. Modern Trends in Activation Analysis, N.B.S., Gaithersburg, 1969, p. 577.
7. G. H. MORRISON, *Anal. Chem.*, 43 (1971) 23A.
8. PH. ALBERT, L'analysis par Radioactivation, Gauthier-Villards, Paris, 1963.
9. G. H. MORRISON, Trace Analysis: Pysical Methods, J. Wiley, New York, 1963, p. 10.
10. C. OLIVIER, M. PEISACH, *J. Radioanal. Chem.*, 11 (1972) 105.
11. W. A. DEER, R. A. HOWIE, J. ZUSSMAN, An Introduction to the Rock-forming Minerals, Longmans, 1966, p. 92.

ELSEVIER SEQUOIA S.A.
Lausanne

AKADÉMIAI KIADÓ
Budapest

Journal of Radioanalytical Chemistry, Vol. 12 (1972) 251–259

PROMPT GAMMA RAYS FROM TRITON-INDUCED REACTIONS ON OXYGEN AND THEIR USE FOR ANALYSIS

M. PEISACH*

C.N.R.S., Laboratory Pierre Sue, C.E.N., Saclay, Gif-sur-Yvette (France)

Triton-induced reactions on oxygen were studied with a view to using the prompt γ-rays for analytical purposes. Five γ-rays were found to be potentially useful, of which three had a high intensity, the n(1, 0), n(2, 0) and p(1, 0) γ-rays, the other two being the n(3, 0) and the unresolved pair $\alpha(1, 0) - \alpha(2, 0)$. The γ-rays are labelled according to the convention $s(a, b)$, where s is the light prompt product and the γ-photon is emitted by de-excitation from level a to b in the heavy product nucleus. The method had a relative precision of 2 to 3.5% for surface oxygen concentrations from 50 to 3 μg/cm^2. The sensitivity with 1 900 keV tritons was 0.13 μg/cm^2 on surfaces of steel or copper which did not yield interfering γ-rays, but 0.45 μg/cm^2 on aluminium where interfering γ-rays were emitted.

Introduction

The determination of oxygen on metal surfaces has been studied by a large variety of nuclear methods, most of which use charged particles to induce the nuclear reaction. When activation methods are used, the activity most often determined is ^{18}F, but when the prompt nuclear products are measured, the spectroscopy of prompt protons[1] from the reaction ^{16}O(d, p)^{17}O, and of prompt neutrons[2] from the reaction ^{16}O(d, n)^{17}F offer sensitivities not easily attained by other methods.

Recent studies of the effect of the bombarding beam on the concentration of oxygen on metal surfaces have shown[3] that the oxygen concentration decreases during the bombardment and the extent of decrease is a function of the total amount of charge used in the irradiation. It thus follows that, to prevent oxygen loss, irradiations have to be carried out over a short period with low-intensity beams, a condition which presupposes that reactions with sufficiently high cross-sections are used to obtain the required precision.

Triton-induced activation has been used for several years as a means of determining oxygen. In reactors the triton flux may be obtained by incorporating ^{6}Li in the system under investigation, so that the primary reaction ^{6}Li(n, α)t produces an *in situ* flux of 2.7 MeV tritons for the secondary activation reaction ^{16}O(t, n)^{18}F. A detailed study of these consecutive reactions and the conditions under which

* On leave from Southern Universities Nuclear Institute, Faure C.P., South Africa.

they can be used have recently been reported.[4] With triton beams from accelerators metal surfaces can be irradiated directly, and the induced activity of ^{18}F can be used as a measure of the oxygen content. By this method a sensitivity of $5 \cdot 10^{-3}$ μg oxygen/cm^2 has been claimed.[5] Both these approaches thus indicate to what extent triton-induced reactions on oxygen can meet the above requirements.

By measuring prompt reaction products instead of radiation from radioactive decay, sufficient data can be obtained over a period which is frequently relatively short compared with the time needed for counting, but this advantage is often lost as a result of the small measuring solid angle that is needed to attain sufficient resolution. When, however, prompt γ-rays are measured with a relatively large detector placed near to the target, a high count rate may be obtained without appreciable loss of resolution. Furthermore, if the triton beam has a relatively low energy, it may be possible to select conditions such that the count rate from oxygen is acceptable, while the yield of γ-rays from the matrix elements may be comparatively low as a result of the Coulomb barrier effect.

For this reason the present study was undertaken using accelerator-produced triton beams below 3 MeV for measuring the oxygen concentration on surfaces of aluminium, iron and copper.

Principle of the method

The most likely reactions induced by tritons with energies below 3 MeV are (t, n), (t, p) and (t, α) reactions, but for most target nuclides these reactions are so exoergic that they could take place even at low bombarding energies, provided the triton can penetrate the Coulomb barrier. The product nucleus could then be produced in an excited state with many energy levels available for its decay, and the γ-rays emitted would then be expected to have a complex energy spectrum. However, a closer study of the case of ^{16}O shows that relatively few levels are available in the product nuclei so that simple γ-ray spectrometry becomes feasible.

Some nuclear data of the three reactions under discussion are given in Table 1, in which the Q-value refers to the ground state mass difference between ^{16}O and the heavy reaction product,[6] E_x is the energy difference between the excited nuclear level and the ground state taken as zero, E_γ is the energy of the emitted γ-ray, and the branching ratio[7] refers to the probability of de-excitation by means of the stated transition, expressed as a percentage. Where the different branching ratios for the various modes of decay of a particular level do not sum to 100%, minor transitions, resulting in low-intensity γ-rays, have been omitted. Since, for analytical purposes, especially at low oxygen concentrations, only the more intense γ-rays would be of interest, these are the only ones that have been listed. For the same reason the reactions of the two heavier isotopes of oxygen, which are present in relatively very low concentrations, have been ignored.

From Table 1 it is strikingly obvious that very few γ-ray energies are expected from (t, p) reactions with tritons in this energy range. We can use a convention

Table 1

γ-Rays from (t, n), (t, p) and (t, α) reactions on ^{16}O

Level, No.	E_x, keV	Transition	Branching ratio, %	E_γ, keV
Reaction $^{16}O(t, n)^{18}F$		$Q = 1.2696$ MeV		
1	940	(1, 0)	100	940
2	1 043	(2, 0)	100	1 043
3	1 085	(3, 0)	100	1 085
5	1 700	(5, 0)	30	1 700
		(5, 2)	70	657
6	2 104	(6, 0)	30	2 104
		(6, 1)	35	1 164
		(6, 2)	35	1 061
7	2 525	(7, 0)	80	2 525
		(7, 1)	20	1 585
8	3 063	(8, 0)	25	3 063
		(8, 1)	75	2 123
Reaction $^{16}O(t, p)^{18}O$		$Q = 3.7068$ MeV		
1	1 982	(1, 0)	100	1 982
2	3 550	(2, 1)	100	1 568
Reaction $^{16}O(t, \alpha)^{15}N$		$Q = 7.6882$ MeV		
1	5 270.6	(1, 0)	100	5 271
2	5 299.2	(2, 0)	100	5 299
3	6 323.5	(3, 0)	100	6 324
4	7 155	(4, 1)	100	1 885
5	7 301	(5, 0)	100	7 301
6	7 566	(6, 1)	100	2 295
7	8 312.6	(7, 0)	80	8 313
		(7, 2)	10	3 013
		(7, 3)	8	1 989
8	8 576	(8, 0)	33	8 576
		(8, 1)	63	3 305
9	9 053	(9, 0)	92	9 053
10	9 151.8	(10, 0)	100	9 152
11	9 154.9	(11, 0)	9	9 155
		(11, 1)	8	3 884
		(11, 2)	10	3 856
		(11, 3)	20	2 831
		(11, 4)	45	2 000
		(11, 5)	8	1 854

to label the γ-rays: $S(a, b)$, where S is the identity of the light nuclear product particle and a and b are the level numbers between which the transition occurs. The two γ-rays from the reaction $^{16}O(t, p)^{18}O$ are thus labelled p(1, 0) and p(2, 1), and it is clear that all (t, p) reactions that do not produce ^{18}O in its ground state

have to be accompanied by the emission of the γ-ray p(1, 0) of 1 982 keV, and the photopeak of this γ-ray is expected to be readily observable in the spectrum.

As the likelihood of producing an excited product nucleus generally decreases with the extent of excitation, it may be expected that the more intense γ-rays from the reaction $^{16}O(t, n)^{18}F$ will be n(1, 0), n(2, 0) and n(3, 0). It should be noted too that de-excitation of higher excited states frequently occurs in stages thus adding to the intensities of these three γ-rays. Following the same reasoning, the more intense γ-rays from the reaction $^{16}O(t, \alpha)^{15}N$ are expected to be $\alpha(1, 0)$, $\alpha(2, 0)$ and $\alpha(3, 0)$, but for this reaction it should be noted that the first excited level of ^{15}N is exceptionally high. These relatively intense γ-rays of high energy are thus expected to be found in an energy region where the intensities of γ-rays from other reactions are likely to be rather low, thereby making their use for analysis more attractive.

Experimental

Rectangular samples to be analysed, measuring about 10×17 mm and a few millimetres thick, were mounted on the sliding arm of a target holder placed at the end of one of the beam tubes of the 3 MeV Van de Graaff accelerator of the Centre Recherches Nucléaires at Cronenbourg, Strasbourg. These could be pushed into the path of a beam of tritons usually between 30 and 50 nA, but sometimes reaching 100 nA, as supplied by the accelerator. Gamma-rays from the nuclear reactions were measured with an 80 cm^2 Ge(Li) detector, the face of which was about 30 to 40 mm from the target, at 90° to the direction of the beam.

Physical and calibration data were obtained from oxygen gas in a gas cell, the centre of which was placed at the irradiation position for metal samples. A nickel window 2.54 mg/cm^2 in thickness allowed the beam to enter the cell with a loss of 310 keV for an incident beam of 3.3 MeV tritons, 355 keV for a beam of 2.6 MeV and 391 keV for a beam of 2.1 MeV. By varying the pressure in the cell, the amount of oxygen in the path of the beam could be varied.

Pulses from the detector were amplified and stored in a multichannel analyser during the analysis. After the spectrum had been obtained, the data were transferred to an off-line computer for processing.

Each irradiation was continued until data had been collected to obtain peaks in the spectrum with acceptably small statistical errors of counting, or until a total current of 100 μC had been used. In most cases 50 μC or less were sufficient.

Results and discussion

Gamma-ray spectroscopy

A typical γ-ray spectrum obtained for a sample of gaseous oxygen at 280 mm pressure, equivalent to a surface concentration of 526 $\mu g/cm^2$, is shown in Fig. 1. The total beam current used was 20 μC and the average bombarding energy as calculated from range-energy tables[8] was 2.069 MeV. As expected, the number of peaks is relatively small and most of the peaks can readily be identified.

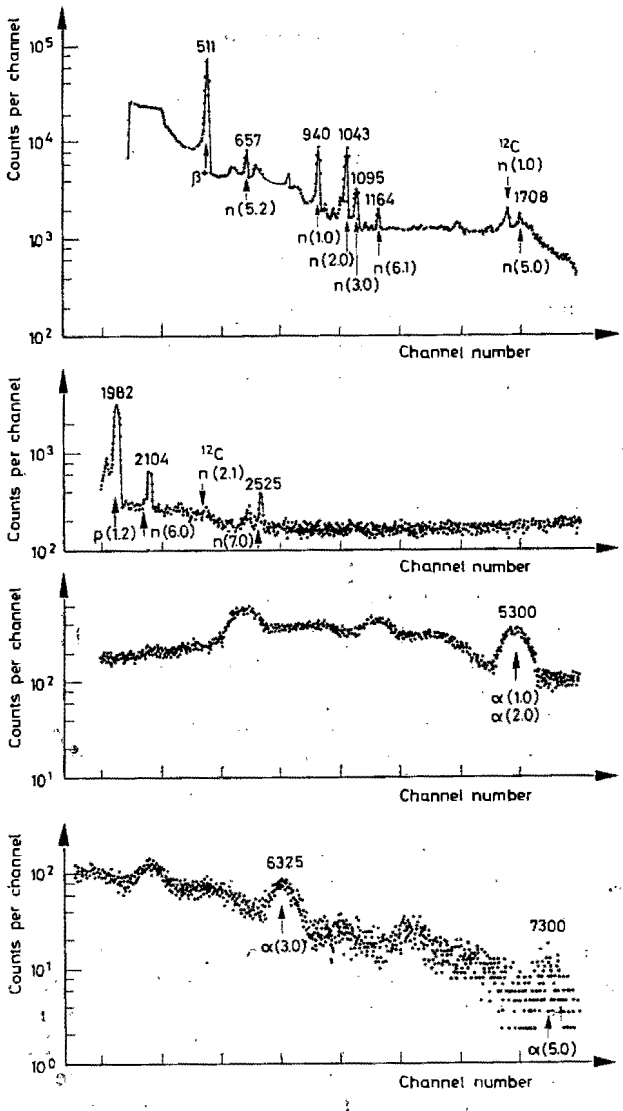

Fig. 1. Spectrum of prompt γ-rays, measured at 90° to the beam direction, during irradiation of an oxygen gas sample with tritons having a mean energy of 2 069 keV. Peaks are labelled with the energy in keV and according to the convention $s(a, b)$, where s is the prompt light particle product of the reaction, and the γ-ray quantum is emitted by de-excitation of the heavy product nucleus from level a to b. When the target nucleus is ^{16}O it is omitted in the figure

The very high yields obtained for the γ-rays n(1, 0), n(2, 0) and, to a lesser extent, n(3, 0), emphasize the well-known fact that the cross-section for the formation of ^{18}F by the reaction $^{16}O(t, n)^{18}F$ is high, but also show that these peaks can

be used for analytical purposes. Most of the γ-rays from this reaction listed in Table 1 are readily detectable in the spectrum, and are marked in Fig. 1 with an arrow indicating the calculated position of the peak. The γ-ray n(6, 2), which is a relatively weak γ-ray falling between the intense γ-rays n(2, 0) and n(3, 0), would be difficult to detect under the present experimental conditions. The value of the branching ratio for the γ-ray n(7, 1) is small and it would thus be difficult to observe in the relatively high continuum; it is expected to be only some 25% as intense as the γ-ray n(7, 0) whose low photopeak is shown in Fig. 1.

The only other listed transitions which have not been observed but which are energetically possible, are those involving the 8th excited state of ^{18}F. At the bombarding energy used here, the energy available for this reaction to produce the required excited state is not much above the threshold and hence the cross-section is expected to be low.

Only a single peak from the reaction ^{16}O(t, p)^{18}O was detected, corresponding to the γ-ray p(1, 0). Although the photopeak from this γ-ray is low compared to that of n(1, 0), it can still be used for analytical purposes because it falls in a region of the spectrum where the continuum is much lower. The photopeak from the γ-ray p(2, 1) was not observed, thus indicating that the cross-section for the reaction leading to the second excited state of ^{18}O is probably low.

When the peaks from the reaction ^{16}O(t, α)^{15}N are compared with the other peaks in the spectrum, the poorer resolution, as shown by the comparative widths of the peaks, becomes strikingly obvious. Under the conditions of analysis, no attempt was made to use α-particle spectroscopy to isolate γ-rays corresponding to any particular direction of emission of the α-particle. The integral curve, which was the one measured here, shows the broadening expected from the Doppler effect.

Very few of the γ-rays listed in Table 1 were detectable. Furthermore, because of the decreased resolution it became impossible to resolve the γ-rays α(1, 0) and α(2, 0) even though the levels involved in the transitions have a relative energy difference of almost 30 keV. However, the two γ-rays now produce a more intense peak which adds to the sensitivity of analysis. Qualitatively, γ-rays involving transitions from the 5th excited state of ^{15}N can still be identified, but when the higher states are involved, the energy available for the outgoing α-particle becomes small relative to the Coulomb barrier. Even from the 4th state the γ-ray yield is too small for analytical use as a result of the marked depression of the cross-section by Coulomb effects.

Attention should be drawn to two small photopeaks of γ-rays of 1 632 and 2 313 keV. These are due to the reaction ^{12}C(t, n)^{14}N induced on carbon deposited from traces of vacuum oil that decomposed on the nickel window at the point of incidence of the triton beam, and correspond to n(1, 0) and n(2, 1) γ-rays from ^{12}C.

The possibility thus exists for using γ-ray spectrometry to measure the radiation from the three expected reactions of ^{16}O for analytical purposes. If each of the γ-rays n(1, 0), n(2, 0), n(3, 0), p(1, 0) and the pair $\alpha(1, 0) - \alpha(2, 0)$ is used independently, it becomes possible to obtain 5 inter-related numerical values, each

of which is a measure of the oxygen content of the sample, but the relative values of which are fixed under constant conditions of measurement and at constant triton bombarding energy.

One such set of respective values obtained from a gaseous sample of oxygen, bombarded with tritons having a mean energy of 1 900 keV and normalised to 1 mC of total bombarding current, is: 1 175.6; 1 282.7; 303.3; 725.9; 401.8 for 1 μg oxygen per cm^2, or 312.2; 340.7; 80.6; 192.8; 106.7 for 10^{16} oxygen atoms per cm^2. These values refer to measured counts and are not corrected either for absolute or for relative counting efficiencies.

Accuracy and precision

Excitation functions were measured for each of the 5 γ-rays of interest for bombarding energies between 1 100 and 2 800 keV in steps of about 100 keV. In all cases the yield increased steadily with bombarding energy.

For analytical purposes, beams of any energy could be used, provided there was no interfering radiation from the matrix. Examples of analyses using tritons of different energies are shown in Table 2. The results were based on the yield of p(1, 0) γ-rays, because it was expected that these values would be least precise due to the fact that small gain changes in the measuring system could result in the inclusion of counts from the 2 032 keV n(2, 0) γ-rays from the (t, n) reaction induced on ^{27}Al.

Table 2

Results using tritons of different energies

Triton energy, keV	p(1,0) counts measured		Ratio
	Aluminium 2	Aluminium 1	
2 400	4 752	4 237	1.122
2 300	4 678	3 803	1.230
2 200	3 970	3 039	1.306
2 100	3 333	2 811	1.186
2 000	2 433	2 163	1.125
1 900	1 758	1 440	1.221

Mean ratio by (t, pγ) reaction: 1.198$\pm$0.070 ($\pm$5.8%).
Mean ratio by (d, p) reaction: 1.204 (Ref.[1]).

Pure aluminium foil with its oxide layer intact was analysed as Aluminium 1, and the thickness of the oxygen layer was compared with that of Aluminium 2, a sample which had been cleaned and re-oxidised by heating in air between 460° and 500 °C for 24 hrs. The thickness of the oxide film of Aluminium 2 was found to be 145 Å, in agreement with the expected value, as determined by the conditions of oxidation.[9]

The accuracy of the method was tested by comparing the results with analyses using prompt proton spectrometry from deuteron-induced reactions.[1] The ratio of the surface concentrations of oxygen on the two aluminium samples was found to be 1.198 ± 0.070, in excellent agreement with the corresponding value of 1.204 using the (d, p) reaction. Furthermore, a statistical analysis of the results indicated no bias. It may thus be concluded that the two methods are comparably accurate.

The results given in Table 2 show a relative standard deviation of $\pm 5.8\%$. This value is somewhat higher than expected from the statistical counting errors only. Each count had been measured within a statistical error of between 2 and 3.5%, so that the relative standard error of the ratio was expected to be somewhat below 5%. The poorer precision may probably be accounted for by some interference from reactions induced in aluminium.

Results of analyses of two other metal surfaces containing more oxygen are given in Table 3. In the case of the steel sample, two peaks featured strongly in the spectra, namely those corresponding to ^{12}C n(2, 1) and ^{12}C n(1, 0) γ-rays, from triton-induced reactions on ^{12}C. The high intensity of these peaks points to the possibility of using these γ-rays for determining surface concentrations of carbon.

Table 3

Analyses with 1 900 keV tritons

γ-Ray used	Copper		Steel	
	Counts per 100 μC	Surface concentration, atoms/cm^2	Counts per 100 μC	Surface concentration, atoms/cm^2
n(1, 0)	1 020	$32.67 \cdot 10^{16}$	486	$15.57 \cdot 10^{16}$
n(2 ,0)	1 148	$33.70 \cdot 10^{16}$	542	$15.91 \cdot 10^{16}$
p(1 ,0)	640	$33\,20 \cdot 10^{16}$	316	$16.39 \cdot 10^{16}$
α(1+2, 0)	342	$32.05 \cdot 10^{16}$	158	$14.81 \cdot 10^{16}$
Mean:		$32.91 \cdot 10^{16}$		$15.67 \cdot 10^{16}$
By (d, p) analyses:		$46.4 \cdot 10^{16}$		$15.6 \cdot 10^{16}$

The surface concentration of oxygen on the steel agreed well with the result obtained by prompt proton spectrometry. The large discrepancy between the results obtained by triton and by deuteron bombardment of the copper sample clearly indicates that the surface had undergone a change during the several weeks that elapsed between the analyses.

Sensitivity

The sensitivity of the method depends on the extent to which the matrix interacts with the bombarding beam. Elements such as iron or copper contribute little to the radiation background when bombarded with tritons below 2 MeV, but

aluminium generates an appreciable amount of radiation. Using the criterion that the sensitivity of the method is the surface concentration of oxygen that would yield a count equivalent to three times the standard deviation of the background count, the sensitivity for an irradiation current of 1 mC of 1 900 keV tritons is about 0.13 $\mu g/cm^2$ ($5 \cdot 10^{15}$ atoms/cm^2) for iron and copper, but only 0.45 $\mu g/cm^2$ (or $1.7 \cdot 10^{16}$ atoms/cm^2) when aluminium is analysed. Clearly, the sensitivity can be improved if longer irradiations are acceptable.

*

Thanks are due to Madame D. MAGNAC-VALETTE, Head of the Low Energy Division of the Faculty of Sciences, Strasbourg, for permission to use their facilities and to Madame I. LINK and Mr. L. KRAUS for their help with the electronic and measuring equipment. Mr. B. VIALATTE assisted with some of the measurements and Dr. J. SIEGKA and Dr. G. AMSEL of Ecole Normale Supérieure, Paris, kindly performed the (d, p) analyses.

Financial support from the Pierre Süe Laboratory of the C.N.R.S. at Saclay made the investigation possible.

References

1. G. AMSEL, B. BERANGER, B. DE GELAS, P. LACOMBE, *J. Appl. Phys.*, 39 (1968) 2246.
2. W. J. NAUDE, M. PEISACH, R. PRETORIUS, P. J. STREBEL, *J. Radioanal. Chem.*, 1 (1968) 231.
3. L. QUAGLIA, G. WEBER, *Radiochem. Radioanal. Letters*, 4 (1970) 89.
4. J. J. M. DE GOEIJ, J. P. W. HOUTMAN, Proc. Intern. Conf. Modern Trends in Activation Analysis, Texas A & M University, College Station, Texas 1965, p. 372.
5. J. N. BARRANDON, L. QUAGLIA, J. L. DEBRUN, M. CUYPERS, J. ROBAYE, *J. Radioanal. Chem.*, 4 (1970) 115.
6. C. MAPLES, G. W. GOTH, J. CERNY, *Nuclear Data*, 2A (1966) 429.
7. F. AJZENBERG-SELOVE, T. LAURITSEN, *Nucl. Phys.*, 11 (1959) 235; F. AJZENBERG-SELOVE, *Nucl. Phys.*, A152 (1970) 108.
8. C. F. WILLIAMSON, J. P. BOUJOT, J. PICARD, CEA R-3042, 1966.
9. R. K. HART, *Proc. Roy. Soc.*, 236A (1956) 68.

ELSEVIER SCIENCE B.V.
Amsterdam

AKADÉMIAI KIADÓ
Budapest

Journal of Radioanalytical Chemistry, Vol. 12 (1972) 313—322

THE DETERMINATION OF ^{10}B BY PROMPT PROTON SPECTROMETRY

C. OLIVIER,* M. PEISACH**

**Department of Chemistry, University of Stellenbosch, Stellenbosch (South Africa)*
***Southern Universities Nuclear Institute, Faure, C.P. (South Africa)*

Boron was analysed in ore and glass samples by prompt proton spectrometry, using deuterons of 2.7 MeV to coincide with a region where the excitation function of the $^{10}B(d, p)^{11}B$ reaction did not vary appreciably with energy.

Targets of approximately 300 $\mu g/cm^2$ thick of powdered samples were prepared by centrifugation. Concentrations down to 0.2% were determined. Possible interference by other elements, particularly nitrogen, magnesium and titanium, was investigated.

Introduction

To date the use for analysis of prompt charged particles from nuclear reactions induced by charged particles[1-5] has been limited to determination of ^{14}N, ^{16}O, ^{18}O, ^{32}S, ^{58}Ni, ^{60}Ni and ^{52}Cr. It is thus evident that the full potential of this field has not yet been realised.

Table 1[a]

Ground state Q-value and product particle energies from (d, p) or (d, α) reactions on stable isotopes having Q-values for (d, p) reactions in excess of 8.0 MeV

Target nuclide	Natural abundance, %	Q-value,[c] MeV		Maximum particle energy for E_d = 2.7 MeV and 0°	
		(d, p)	(d, α)	E_p, MeV	E_α, MeV
^{47}Ti	7.28	9.403	6.845	12.074	9.232
^{10}B	19.78	9.231	17.819	11.811	16.362
^{33}S	0.76	9.198	8.566	11.858	10.692
^{43}Ca	0.145	8.911	7.868	11.584	10.167
^{87}Sr	7.02	8.876	8.002	11.562	10.498
^{25}Mg	10.13	8.870	7.049	11.524	9.145
^{50}V[b]	0.24	8.830	9.979	11.507	12.224
^{49}Ti	5.51	8.720	6.480	11.397	8.897
^{14}N	99.63	8.610	13.575	11.233	14.046
^{29}Si	4.70	8.393	6.014	11.059	8.254
^{61}Ni	1.19	8.375	8.724	11.048	11.093
^{77}Se	7.58	8.266	9.141	10.953	11.569

[a] Isotopes of rare gases are excluded.
[b] Radioactive.

The most likely reactions yielding prompt charged particles when stable nuclei are bombarded with deuterons of a few MeV are (d, p) and (d, α) reactions. The maximum energies attained by prompt protons from reactions induced by 2.7 MeV deuterons on isotopes with high Q-values for such reactions are given in Table 1.

Because the reactions are highly exoergic, many energy states can be excited in the product nuclei and the energy spectra of the prompt protons will thus extend from somewhat above 12 MeV to very low energies. Since it could be expected that the bombarding beam will lose little energy in traversing very thin targets of the elements concerned, the energy spectra of prompt protons from such targets may be expected to consist of a series of narrow peaks whose widths are determined by the resolution of the measuring system. Alpha-particles, which may be considered as a possible source of interference in the analysis of boron by prompt proton spectrometry, can be eliminated together with the scattered deuterons by an absorber placed in front of the detector.

Experimental

Preparation of standards and samples

A technique similar to that used for preparing deposits of barium carbonate for the routine counting[7] of ^{14}C was used for preparing powdered deposits of elemental boron, boron nitride, glass, tourmaline and other inorganic compounds on tantalum discs.

Reference materials used were NBS standard glass samples Nos 92 and 93 and a tourmaline sample of which a complete analysis (NIM Report No. 939) was obtained from the National Institute for Metallurgy, Johannesburg, South Africa.

Samples of the materials to be irradiated were ground to fine powders with a particle size of about 0.5 μm as measured by the average settling velocities in water. Approximately one-milligram quantities of the powders were centrifuged onto tantalum discs producing a layer of about 300 $\mu g/cm^2$.

Irradiation

The targets were irradiated inside a 90 cm scattering chamber with deuteron beams obtained from the 5.5 MV Van de Graaff accelerator of the Southern Universities Nuclear Institute.

The collimated irradiation beam had a circular cross-section of 3 mm diameter. The target angle of 20° resulted in an irradiated area of elliptical shape having a major axis of about 8.8 mm, but this broadening was still sufficiently narrow for the beam to fall entirely within the boundaries of the target deposit of 20 mm diameter.

The beam current was measured with a current integrator which was connected to the target holder and a cylindrical tube which acted as a Faraday cup and thus corrected for secondary electron losses that were experienced with an open target.

Measurement

The semiconductor detector could measure protons of up to 10 MeV and had a resolution of less than 45 keV. It was covered with gold foils to absorb the scattered deuterons, low energy protons and α-particles. Since the (d, p) reactions of

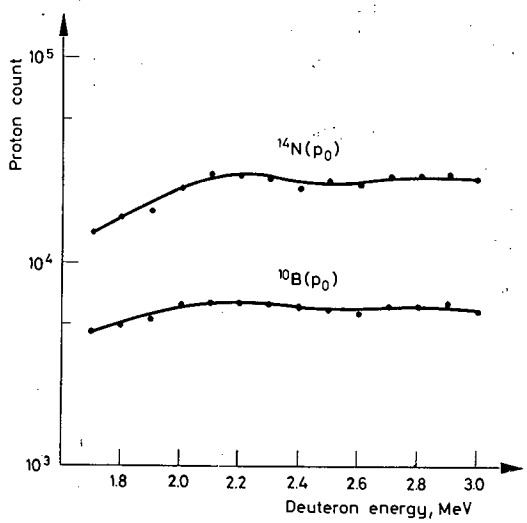

Fig. 1. The variation of proton counts measured at 30°, with deuteron energies between 1.7 and 3.0 MeV as obtained with a thin target of boron nitride. Counts from the $^{10}B(p_0)$ and $^{14}N(p_0)$ groups are given separately

interest are highly exoergic, the absorber thickness is not very critical. The only restriction is that the protons must be stopped in the sensitive region of the detector. The appropriate thickness of absorber required was calculated from the known stopping power for protons.[8]

The effect of the angle of measurement

It was advantageous to measure the $^{10}B(p_0)$ protons at small angles. It was also established experimentally[9] that, for an incident deuteron beam of energy in the region 1.45–3.15 MeV, the yield of $^{10}B(p_0)$ protons reaches a maximum in the vicinity of 30°. To obtain higher sensitivity, this direction was consequently chosen for analysis.

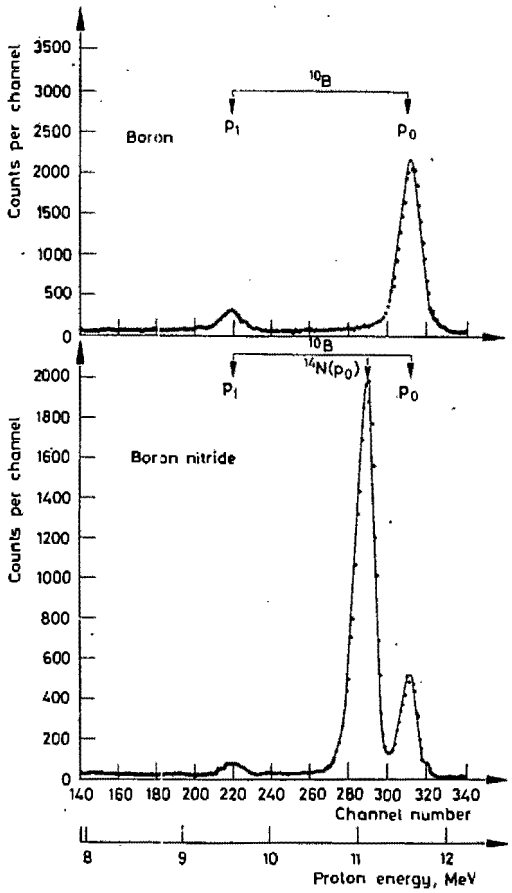

Fig. 2. Energy spectra of prompt protons obtained from the deuteron irradiation of thin deposits of boron and boron nitride on tantalum. $\Theta = 30°$, $E_d = 2.7$ MeV, Au absorber = = 135 mg/cm^2

The effect of deuteron energy

The variation of proton counts with deuteron energy between 1.7 and 3.0 MeV is shown in Fig. 1 as obtained with a thin (114 μg/cm^2) target of boron nitride. Counts from the $^{10}B(p_0)$ and $^{14}N(p_0)$ groups are given separately. In both cases little variation in the proton yield occurs in the energy region 2.0–3.0 MeV.

Providing the energy does not decrease below 2.0 MeV, the count rate will be a function of the boron content which simplifies the analysis considerably. A bombarding energy of 2.7 MeV was selected in an attempt to decrease interference from heavy elements which already yield an appreciable count rate of protons above about 3 MeV. No decrease in the relative yield of the $^{14}N(p_0)$ group could be achieved by changing the energy.

Effect of distance between target and detector

The best distance for measurement was obtained by measuring prompt protons from an irradiated boron nitride target. Using the relative depth of the valley between the $^{14}N(p_0)$ and $^{10}B(p_0)$ peaks (see Fig. 2) in the spectra as a criterion, it was found that 55 mm between detector and the centre of the target gave optimum results.

Effect of beam current

Boron counts, observed from the same target but irradiated with different beam intensities, showed a standard deviation of $\pm 3.23\%$ for a beam current between 0.3 and 1.0 μA. Higher beam currents resulted in a decrease in the boron count, caused by the loss of the deposited material accompanying the higher temperature involved.

Results and discussion

Energy spectra of prompt protons

The spectrum obtained from *boron* is characterized by the prominence of two peaks and the virtual absence of background counts in the energy region of interest. The peaks correspond to the p_0 and p_1 proton groups from ^{10}B. The high yield p_0 group which lies in the high energy region, where there is least chance of obtaining protons from other elements, was accordingly chosen for analytical purposes.

In the spectrum obtained from *boron nitride* the peak due to the p_0 proton group from ^{14}N dominates because of the high abundance (99.63 %) of this isotope and the large cross section of the reaction concerned. In spite of the large yield of this proton group and the fact that the leading edge of this peak overlaps to some extent the backward edge of the peak from the $^{10}B(p_0)$ proton group, the latter peak is still clearly resolved from the $^{14}N(p_0)$ peak.

Tantalum was used as backing material since the Coulomb barrier for such a heavy element ($Z = 73$) was large, and therefore the cross section of the (d, p) reaction at 2.7 MeV was expected to be so small that prompt protons from it would be undetectable. This was not quite the case (see Fig. 4). The undulated plateau in this spectrum whose leading edge corresponds to the peak of the $^{14}N(p_0)$ proton group, might have been caused largely by prompt protons from atmospheric nitrogen still present in the evacuated scattering chamber.

Analysis

Tourmaline and glass samples of known boron content were used to determine the accuracy of the method. The reference material used was boron nitride. Typical energy spectra obtained from tourmaline, borosilicate glass and low boron glass

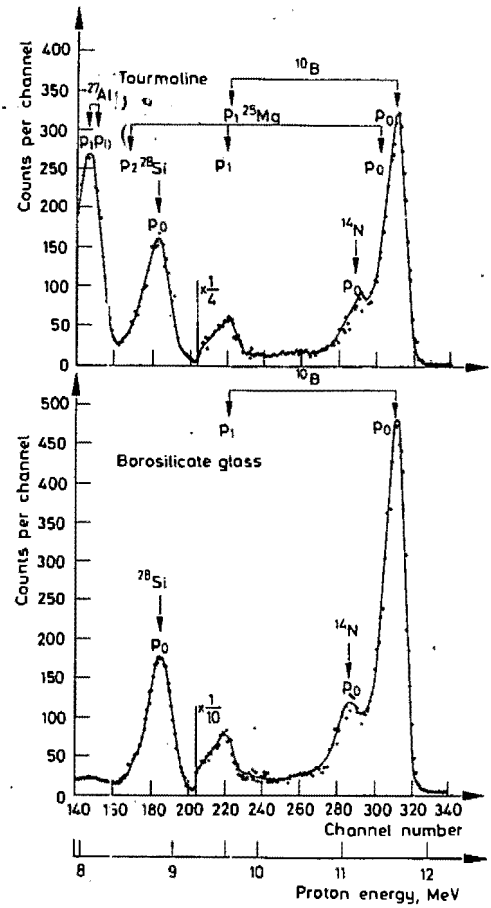

Fig. 3. Energy spectra of prompt protons obtained from the deuteron irradiation of thin deposits of tourmaline and borosilicate glass on tantalum. $\Theta = 30°$, $E_d = 2.7$ MeV, Au absorber = 135 mg/cm^2

are shown in Figs 3 and 4. The $^{10}B(p_0)$ peak is clearly perceptible in each spectrum, although it is dwarfed by the $^{14}N(p_0)$ peak in the spectrum obtained from the low boron glass. As was expected, the high content of silicon in every sample caused the very prominent peak corresponding to the proton group, $^{28}Si(p_1)$. In the tourmaline samples, which contain aluminium, the spectrum shows a composite peak representing $^{27}Al(p_0, p_1)$ proton groups.

To obtain the boron count in the boron nitride spectrum a curve fitting procedure had to be followed. By normalising the shape of the leading edge of the $^{14}N(p_0)$ peak a value is obtained, which after subtraction from the total integrated count of both peaks gives the boron count. The forward edge was used for normalising, since its shape is determined by protons detected from the surface of the target

where little energy loss is experienced by the bombarding deuterons. A secondary check is given by the resultant shape of the boron peak obtained if the normalised $^{14}N(p_0)$ peak is subtracted from the observed spectrum. The same procedure is applicable for cases where the interfering peak has a higher count rate than that of the boron peak, as is the case with low-boron glass (see Fig. 4).

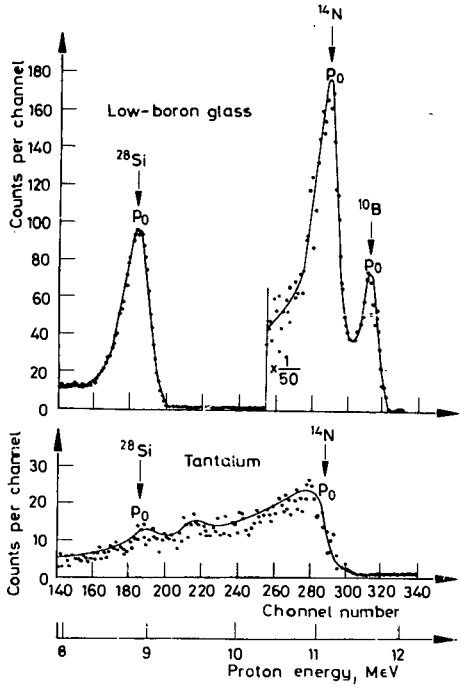

Fig. 4. Energy spectra of prompt protons obtained from the deuteron irradiation of a thin deposit of low-boron glass and from the tantalum backing. $\Theta = 30°$, $E_d = 2.7$ MeV, Au absorber = 135 mg/cm^2

Calibration, precision and accuracy

The normalised count, expressed as the count that would have been obtained from a sample of standard thickness 300 μg/cm^2 if irradiated with 0.1 mC current, and normalised to unit percentage of boron by weight, is given in column 3 of Table 2. These values, for the first three types of samples, have a mean value of 455.8 ± 19.4, i.e. a relative precision of 4.3%, and are in good agreement with the value 455.2, obtained from boron nitride for the slope of the linear calibration line correlating the boron content (in percentage by weight) to the observed normalised count.

The marked increase in the relative error of the determination for the low-boron glass sample, and the appreciable discrepancy between the mean value

Table 2

Some typical analytical results

Target	Thickness, $\mu g/cm^2$	Counts[a] per 300 $\mu g/cm^2$		Boron, %			Relative error, %
		Measured	Mean	Known	Determined[b] In target	Determined[b] Mean value for sample	
Boron nitride	210.4	480.2			45.95		+ 5.49
	214.9	450.3			43.09		− 1.08
	220.9	473.9	455.2	43.56	45.35	43.56[b]	+ 4.11
	305.6	435.2	±20.9		41.65		− 4.38
	329.1	436.4			41.76		− 4.13
Tourmaline	222.5	422.6			3.02		− 7.08
	273.7	468.7	450.1		3.35		+ 3.08
	283.3	457.3	±19.6	3.25[e]	3.26	3.22	+ 0.31
	291.6	451.9			3.23		− 0.62
Borosilicate glass	267.4	474.2			4.13		+ 4.29
	269.9	440.2	464.2	3.96[f]	3.83	4.04	− 3.28
	299.2	478.5	±21.0		4.16		+ 5.05
Low-boron glass	197.3	388.9			0.19		−13.64[c]
	244.1	381.6	396.8	0.22[f]	0.18	0.19	−18.18
	262.6	419.9	±20.3		0.20		− 9.09
Boron powder	224.7	330.3			72.56		−27.44[d]
	232.0	424.8			93.32		− 6.68
	241.0	320.7	363.6	100	70.45	79.88	−29.55
	246.0	355.4	±37.5		78.07		−21.93
	332.0	372.5			81.83		−18.17
	349.8	377.8			83.00		−17.00

[a] Expressed as counts per 300 $\mu g/cm^2$ target per unit percentage boron (by weight) as obtained from an irradiation with 0.1 mC current.

[b] Mean count from boron nitride used as calibration value for all these analyses.

[c] These values seem to indicate that the reported boron content of 0.22% is too high. See text.

[d] These values indicate large deviations from this sample. See text.

[e] Analysis supplied by National Institute for Metallurgy, Johannesburg, South Africa (NIM Report No. 939).

[f] Analysed samples Nos 92 and 93 from U.S. Bureau of Standards.

determined by this method and the known boron content, seem to imply that the reported value of 0.22% is somewhat high. The value of 0.19% would have to be used to bring these results into line with those of other samples. The poorer

precision for this sample can be ascribed largely to the relatively small number of counts that were obtained at the low level of boron. In the absence of interfering elements, when resolution becomes of minor importance, an improved precision may be obtained by placing the detector as near the target as is geometrically possible.

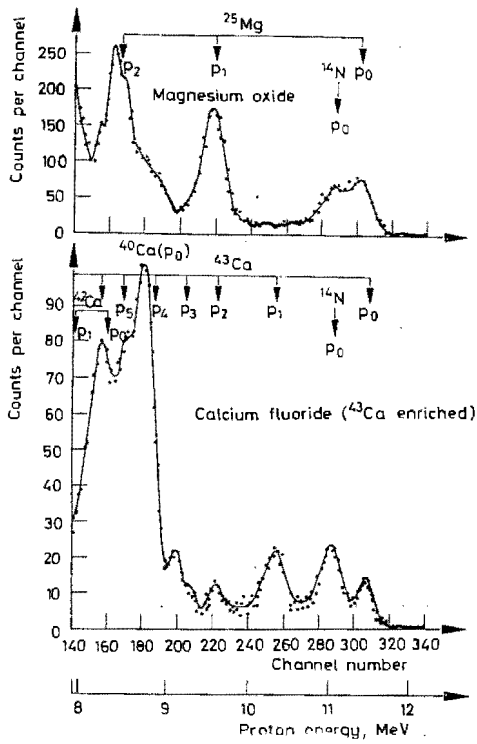

Fig. 5. Energy spectra of prompt protons obtained from the deuteron irradiation of a thin deposit of magnesium oxide and calcium fluoride (^{43}Ca enriched) on tantalum. $\Theta = 30°$, $E_d = 2.7$ MeV, Au absorber = 135 mg/cm^2

Clearly the sample that had been accepted to be pure boron could not have been correctly described, because it would require an impurity amounting to over 20% by weight to obtain agreement between these results and those from other samples.

Possible interferences

When the energy levels in the product nuclei are taken into account, it is found that the following proton groups have energies within the region of integration defined for the boron analysis: $^{47}Ti(p_0, p_1)$, $^{33}S(p_0)$, $^{43}Ca(p_0)$, $^{87}Sr(p_0)$, $^{25}Mg(p_0)$, $^{50}V(p_0)$, $^{49}Ti(p_0)$, $^{14}N(p_0)$.

Of these the $^{25}Mg(p_0)$ group has the highest possibility for interfering mainly because of its relatively high cross section and the difficulty of resolving it from that of the required boron group (see Fig. 5). A test sample of magnesium oxide containing magnesium and boron in equal concentrations, gave an uncorrected result of about 0.6% which is well within the accuracy of the method. The proton groups $^{47}Ti(p_0)$, $^{33}S(p_0)$, $^{87}Sr(p_0)$ and $^{50}V(p_0)$ were not observed under the experimental conditions described.

Although the $^{43}Ca(p_0)$ group was observed from a test sample containing about 40% ^{43}Ca (see Fig. 5) the presence of natural abundance of ^{43}Ca is small (0.145%). The presence of nitrogen in the sample to be analysed is easily coped with by the curve fitting procedure described. As far as the backing is concerned, practically no counts were observed in the region of integration.

*

The financial assistance obtained from the South African Atomic Energy Board and the South African Council for Scientific and Industrial Research is gratefully acknowledged. Mr. H. S. PIENAAR, of the Department of Geology, University of Stellenbosch, is thanked for supplying the tourmaline sample. This work forms part of a doctoral thesis submitted by C.O. to the University of Stellenbosch and is published with the permission of his Promoter.

References

1. G. AMSEL, D. DANIEL, *Rev. Phys. Appl.*, 4 (1969) 383.
2. G. AMSEL, D. SAMUEL, *Anal. Chem.*, 39 (1967) 1689.
3. E. A. WOLICKI, A. R. KNUDSON, *Intern. J. Appl. Radiation Isotopes*, 18 (1967) 429.
4. C. OLIVIER, M. PEISACH, *J. S. Afr. Chem. Inst.*, 23 (1970) 77.
5. C. OLIVIER, M. PEISACH, *J. Radioanal. Chem.*, 5 (1970) 391.
6. C. MAPLES, G. W. GOTH, J. CERNY, *Nuclear Data*, 2A (1966) 429.
7. M. PEISACH, *J. S. Afr. Chem. Inst.*, 12 (1959) 57.
8. C. F. WILLIAMSON, J. P. BOUJOT, J. PICKARD, Report CEA-R3042, 1966.
9. G. BREUER, *Z. Phys.* 178 (1964) 268.

No. 44

REPRINT

Journal of Radioanalytical Chemistry, Vol. 13 (1973) 193—200

ISOTOPIC DETERMINATION OF ^{46}Ca BY PHOTON ACTIVATION

M. PEISACH*

C.N.R.S. Laboratoire 'Pierre Süe', C.E.N. Saclay, Gif-sur-Yvette (France)

(Received February 17, 1972)

ELSEVIER SEQUOIA S.A.
Lausanne

AKADÉMIAI KIADÓ
Budapest

Journal of Radioanalytical Chemistry, Vol. 13 (1973) 193—200

ISOTOPIC DETERMINATION OF ^{48}Ca BY PHOTON ACTIVATION

M. PEISACH*

C.N.R.S. Laboratoire 'Pierre Süe', C.E.N. Saclay, Gif-sur-Yvette (France)

(Received February 17, 1972)

An activation analysis method has been developed for the routine determination of ^{48}Ca. The calcium is chemically separated, converted to the hydroxide, carbonate or chloride and activated for 30 min in the γ-ray flux generated by a primary electron beam between 40 and 57 MeV and a current of about 50 μA. A large number of samples can be activated simultaneously and the ratio of activities of ^{47}Ca and ^{43}K gives a measure of the isotopic concentration of ^{48}Ca. Naturally-occurring ^{44}Ca is used as an internal standard. The relative standard deviation is $\pm 3.3\%$.

Introduction

Isotopic dilution analysis has been used for some time to study the biological role of calcium. Preparations enriched in ^{48}Ca are administered to the biological system and information is obtained by measuring the isotopic dilution that results from the admixture of natural calcium.[1] To meet the need for a useful technique to determine isotopic concentrations of calcium isotopes, numerous nuclear methods have been developed, most of which make use of charged-particle beams to induce the required reaction. The methods that are based on the measurement of the prompt particles emitted from the nuclear reaction, such as neutron time-of-flight spectrometry from (p, n) reactions,[2] have the disadvantage that the full beam can be directed at only one sample at a time. To some extent this disadvantage is alleviated when activation methods are used,[3] by mounting the samples on a rotating sample holder so that many samples can be activated during a single irradiation, but then the beam is spread over all the samples and each receives the benefit of only a small proportion of the beam. It is only when penetrating radiation is used, as for example when thermal neutrons are used to activate ^{48}Ca by neutron capture,[4] that large number of samples can be activated together without appreciably decreasing the flux available to other samples in the same batch. However, the convenient use of another calcium isotope in the same sample as an internal standard, which is a marked advantage of charged particles, cannot readily be adapted to thermal neutron activation.

* On sabbatical leave from the Southern Universities Nuclear Institute, P.O. Box 17, Faure, C.P., South Africa.

Activation analysis using energetic photons combines both advantages. The radiation is highly penetrating, thereby allowing many samples to be placed in the same flux, and suitable radioactive products are generated from several calcium isotopes simultaneously, making a choice of an internal standard possible.

The nuclear reactions most likely to occur with photons of up to 50 MeV are (γ, n) and (γ, p) reactions and some properties of the radioactive products that may be expected from the photoactivation of calcium isotopes are listed in Table 1.

Table 1

Products from (γ, n) and (γ, p) reactions on calcium isotopes

Target nuclide	Natural abundance, %	(γ, n) Reaction			(γ, p) Reaction		
		Product	Half-life	Main γ-ray energies, keV	Product	Half-life	Main γ-ray energies, keV
^{40}Ca	96.97	^{39}Ca	880 ms	(β^+)	^{39}K	stable	
^{42}Ca	0.64	^{41}Ca	$8 \cdot 10^4$ y	no γ	^{41}K	stable	
^{43}Ca	0.145	^{42}Ca	stable		^{42}K	12.36 h	1 524
^{44}Ca	2.06	^{43}Ca	stable		^{43}K	22 h	372
							617
^{46}Ca	0.0033	^{45}Ca	165 d	12.5	^{45}K	16.3 m	175
							1 710
^{48}Ca	0.185	^{47}Ca	4.54 d	1 296	^{47}K	17.5 s	2 000
				810			2 600
				490			

(β^+) indicates decay by positron emission, and hence the presence of 511 keV annihilation radiation.

Nuclear reactions that occur with smaller probability need not be considered, because isotopic analyses are usually performed on separated samples of pure materials. Reference to Table 1 shows that the major isotope, ^{40}Ca, does not produce any activity except the very short-lived ^{39}Ca that decays before the sample can reach the counting apparatus. In addition, activities from ^{42}Ca and ^{46}Ca can be ignored, the former because its (γ, p) product is very long-lived and hence would be produced in small amounts, and the latter because of its low natural abundance. Thus, essentially only three radioactive products are present in photon-activated samples of calcium a few minutes after the end of the irradiation; ^{42}K and ^{43}K from (γ, p) reactions on ^{43}Ca and ^{44}Ca, respectively, and ^{47}Ca from the (γ, n) reaction on ^{48}Ca, and their activities can be used to determine the corresponding calcium isotopes.

In this work the activity of ^{47}Ca was measured to determine the isotopic concentration of ^{48}Ca. The results were expressed relative to the activity of ^{43}K used as a measure of the isotopic concentration of ^{44}Ca, which was selected as the internal standard.

Sample preparation

Samples for analysis were dissolved and the calcium was separated by precipitation. The precipitate was washed by centrifugation and transferred as a suspension in acetone to weighed foils of aluminium, which were then heated to evaporate the volatile liquid. Afterwards the foils were weighed and wrapped round the calcium deposit to form the target for irradiation. In the early experiments the calcium was precipitated as hydroxide because 2-min ^{15}O was the only other expected activity, but when it was established that irradiated samples could be stored for several hours before counting, the carbonate was used as the longer-lived activity from carbon could also be tolerated. Later it was found that the post-irradiation treatment was simplified if the calcium was in a water-soluble form. Consequently, after precipitation the calcium was converted to chloride by dissolution in hydrochloric acid, the excess acid evaporated and the residue dissolved in a drop of water that was then deposited onto the aluminium foil, evaporated to dryness and wrapped for irradiation.

Standards of the required isotopic concentrations were prepared by adding natural calcium to two enriched ^{48}Ca samples, obtained as calcium carbonate from the Oak Ridge National Laboratory, USA. The enriched samples consisted of ^{48}Ca (95.64 and 97.16 atom%, respectively) and ^{40}Ca, with negligible concentrations of the other stable calcium isotopes.

Irradiation and measurement

The samples were placed in the standard irradiation caps used at the Linear Accelerator facility at Saclay. These caps allow somewhat more than 1 cm^3 of space for the samples at the front of the pneumatic container which is used to deliver the samples to the irradiation position. The photon flux is generated by accelerated electrons impinging on a metal target and is anisotropic. The comparatively small volume of the irradiation caps ensures that all samples in it are irradiated with virtually the same flux. Up to 30 samples could readily be irradiated simultaneously.

Samples containing a few milligrams of the calcium compound were irradiated for about 30 min in the photon flux obtained from a 50 μA beam of electrons with energies between 40 and 50 MeV, but small samples and samples with low isotopic concentrations of ^{48}Ca were irradiated up to a maximum of 2 hrs.

After irradiation, samples in which the calcium was in a water-soluble form were unwrapped, sprayed with water and the solution acidified with hydrochloric acid to give a 10*N* solution. Other samples were completely digested in hydrochloric acid, but had to be evaporated just to dryness and redissolved in acid to obtain a solution with the correct acid concentration. The 10*N* acid solution was then passed through a 1-cm column of hydrated antimony pentoxide to remove ^{24}Na activity formed from sodium contamination and from (n, α) reaction on

aluminium with the fast photoneutrons generated by the photon flux. The eluate was made up to 5 ml, allowed to stand for sufficient time to eliminate positron activity by decay, and counted with a Ge(Li) γ-ray spectrometer some 12 to 24 hrs after irradiation, and thereafter at daily intervals if required.

Results and discussion

Gamma-ray spectroscopy

A typical γ-ray spectrum obtained from a sample of natural calcium carbonate irradiated in the photon flux produced by a primary electron beam of 45 MeV and measured about 5 days after irradiation is shown in Fig. 1. The shape of the spectrum changed little with decay. Spectra taken much earlier showed all the peaks found in Fig. 1, with the exception that the relative intensity of the peak from 160-keV γ-rays of ^{47}Sc gradually increased as the decay of ^{47}Ca generated

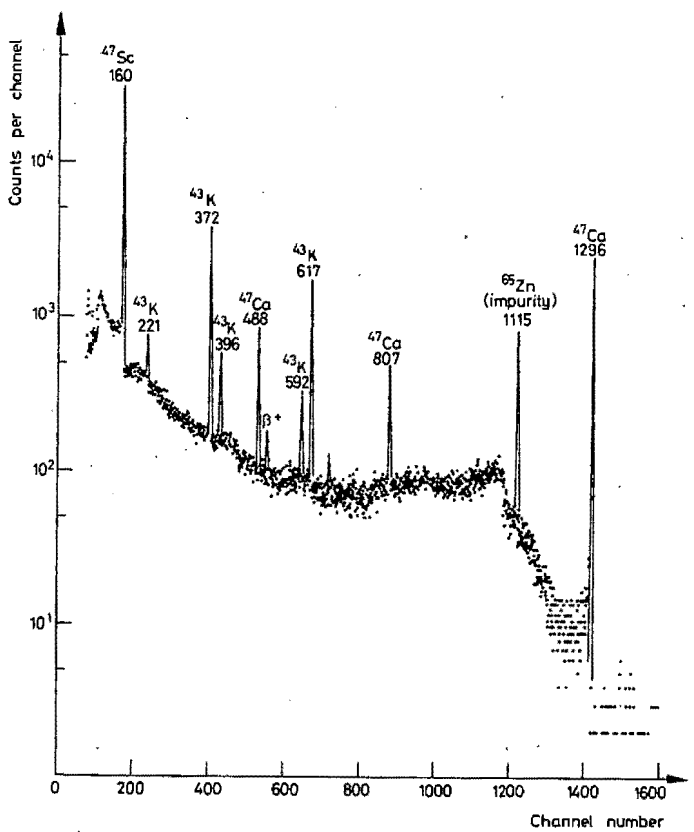

Fig. 1. γ-Ray spectrum from natural calcium carbonate measured for 60 min, 122.89 hrs after irradiation in a photon flux produced by a primary electron beam of 45 MeV. Peaks are identified by the radionuclide and the energy in keV

more daughter activity, and the peak from 1 524-keV γ-rays of ^{47}K, which had already decayed in the spectrum of Fig. 1, could be identified around channel 1 665 in spectra taken within the first few days after irradiation.

Despite there being several peaks, the spectrum was essentially a simple one showing the presence of only two major components, ^{43}K and ^{47}Ca, the γ-rays of which were identified by the peak positions in the spectrum and by their rates of decay. The intense peak corresponding to 1 115-keV γ-rays was due to ^{65}Zn formed from zinc impurities in the container which were not removed by the chemical treatment after irradiation. This impurity was relatively so long-lived that it could be treated as part of the background. Because few radionuclides were formed in the activation and as their half-lives were widely different, 22 hrs and 4.54 d, the activity of each component could readily be obtained by measuring the decay of the gross activity, and spectroscopy need not have been used.

In addition to the above radioactivities, the samples contained relatively high concentrations of ^{15}O, ^{11}C and other short-lived positron emitters, which were not removed but allowed to decay. As a result, the 16-min ^{45}K, most of which decayed away during the delay period, was seldom detected. However, separate irradiations performed specially to observe the formation of this product showed that readily measurable yields of ^{45}K were obtained despite the low abundance of the ^{46}Ca target isotope. It thus appears to be possible, in principle, to determine isotopic concentrations of ^{46}Ca if preparations enriched in this isotope are used as tracers in patients or other biological systems, provided the dead-time corrections caused by the high activities from the light elements do not introduce unacceptably high errors.

Calibration

It can readily be shown that under constant conditions of irradiation and measurement the ratio, R, of the activity of ^{47}Ca to that of ^{43}K is proportional to the relative concentrations of ^{48}Ca and ^{44}Ca, i.e.

$$R = \frac{A_{47}}{A_{43}} = k\frac{P_{48}}{P_{44}}, \qquad (1)$$

where A_{43} and A_{47} are the activities of ^{43}K and ^{47}Ca, respectively, at the end of the irradiation, and P_{44} and P_{48} are the isotopic concentrations of ^{44}Ca and ^{48}Ca, respectively, in the analysed sample, expressed in atom%. The proportionality constant k, which is obtained from the slope of the calibration line, includes values of the relevant cross-sections, half-lives, the time-dependent build-up factor for the activity growth during irradiation and the relative efficiencies of detection of the radiations measured.

If the isotopic concentrations of ^{44}Ca and ^{48}Ca are not much different from their values in nature, the activity ratio R can be used directly as a measure of the isotopic concentration in the sample. This simplification is valid for samples con-

taining up to 2 atom% of ^{48}Ca, for which the error introduced by the linearity assumption is about half the experimental error of the method. Generally, however, if an enriched tracer with isotopic concentrations of ^{44}Ca and ^{48}Ca, S_{44} and S_{48}, respectively, is diluted in the course of an investigation with natural calcium, the isotopic concentration of ^{48}Ca in the analysed sample is given by

$$P_{48} = \frac{S_{48}\left(0.185 - 2.06 \cdot \frac{R}{k}\right) - 0.185\left(S_{48} - S_{44} \cdot \frac{R}{k}\right)}{\left(0.185 - 2.06 \cdot \frac{R}{k}\right) - \left(S_{48} - S_{44} \cdot \frac{R}{k}\right)}. \quad (2)$$

Selection of the primary beam energy

The effect of varying the energy of the primary electron beam was found to be relatively small. Many replicate samples of natural calcium were activated in the photon fluxes from electron beams of energy ranging from 35 to 57 MeV. The variation of the mean activity ratio with the primary beam energy is shown in Fig. 2.

Although the physical threshold for the reaction ^{44}Ca(γ, p)^{43}K is about 12.2 MeV, electron beams of about 35 MeV produced relatively low yields of ^{43}K and the yield varied rapidly with comparatively small changes in energy. In this energy region the determination of the activity ratio was difficult, due to the low activity of ^{43}K, and the results were erratic. However, when the primary beam energy exceeded 40 MeV the relative yields of ^{43}K and ^{47}Ca changed slowly, while the absolute yields of these activities increased with increasing energy. It thus follows

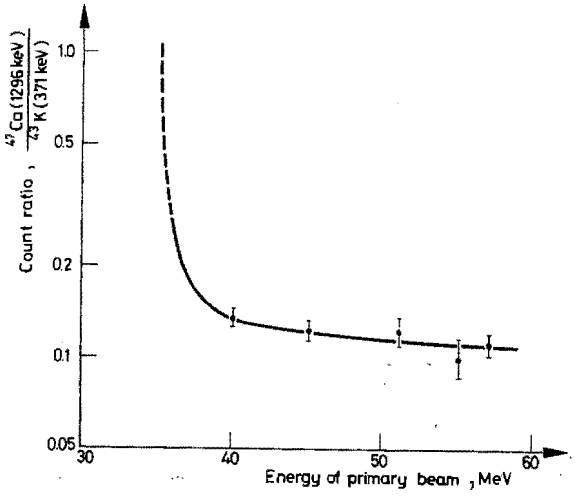

Fig. 2. The variation of the mean activity ratio with the primary beam energy

that for primary beams between 40 and 57 MeV, small changes in beam energy during an irradiation will have little effect on the activity ratio, and hence introduce negligible errors in the results.

Analyses of samples

The γ-ray spectrum (see Fig. 1) shows that the most intense spectral peak from ^{47}Ca is due to the γ-ray of 1 296 keV. The counts under this peak were integrated and used as a measure of the ^{47}Ca activity.

The two more prominent peaks from ^{43}K were those due to γ-rays of 372 and 617 keV. Both of these were used to determine the ^{43}K activity, but results from the former were more precise.

A test series of 24 analyses was carried out on 14 samples of different isotopic concentrations of ^{48}Ca. Some of the results in which the ^{44}Ca content was calculated from the counts of the 372-keV γ-ray are given in Table 2. The relative standard deviation was about $\pm 3.3\%$ for ^{48}Ca concentrations between 0.185 (natural) and 4.371 atom%. A similar series of results, but using the counts from the 617-keV γ-ray had a relative standard deviation of about $\pm 6\%$.

Table 2

Some isotopic analyses of ^{48}Ca

Samples	Atom% ^{48}Ca (known)	Atomic ratio $^{48}Ca/^{44}Ca$ (calculated)	Activity ratio $^{47}Ca : {}^{43}K$ (measured)	Atomic ratio (found)	Atom% ^{48}Ca (found)	Relative error, %
Enriched	4.371	2.213	0.6088	2.277	4.502	+3.0
	4.047	2.042	0.5434	2.032	4.038	−0.2
	3.172	1.587	0.4298	1.608	3.221	+1.5
	2.208	1.094	0.2858	1.070	2.166	−1.9
	1.993	0.985	0.2614	0.978	1.985	−0.4
	1.710	0.843	0.2265	0.848	1.725	+0.9
	1.417	0.697	0.1969	0.738	1.503	+6.1
	1.118	0.548	0.1399	0.525	1.074	−3.9
	0.847	0.414	0.1134	0.426	0.873	+3.1
	0.412	0.201	0.0548	0.206	0.425	+3.2
	0.388	0.189	0.0508	0.192	0.395	+2.1
Natural	0.185	0.0898	0.0242	0.0921	0.190	+2.7
			0.0243	0.0923	0.191	+3.2
			0.0227	0.0866	0.179	−3.3
			0.0236	0.0898	0.185	—
			0.0231	0.0881	0.182	−1.7

Number of analyses 24.
Number of samples analysed 14.
Relative standard deviation $\pm 3.3\%$.

Conclusion

A simple activation analysis method has been devised that is suitable for the routine determination of the concentration of ^{48}Ca relative to that of ^{44}Ca. The activities produced can be measured easily, even without γ-ray spectrometry. Large numbers of samples can readily be activated simultaneously and the activities are sufficiently long-lived to allow time for measurement, even from milligram samples. A relative precision of $\pm 3.3\%$ is attainable using an irradiation of only 30 min.

The irradiations were carried out at the Linear Accelerator facility of the Physics Division at Saclay, France. Financial assistance from the C.N.R.S. through Laboratoire 'Pierre Süe' is gratefully acknowledged. Special appreciation is expressed to the South African C.S.I.R. for a senior bursary held during the period of these investigations.

References

1. G. D. McPherson, *Acta Orthop. Scand. Suppl.*, 78 (1965) 1.
2. W. R. McMurray, M. Peisach, R. Pretorius, P. van der Merwe, I. J. van Heerden, *Anal. Chem.*, 40 (1968) 266.
3. M. Peisach, R. Pretorius, *Anal. Chem.*, 38 (1966) 856.
   T. J. de Waal, M. Peisach, R. Pretorius, *Anal. Chem.*, 41 (1969) 416.
4. E. Junod, J. Laverlochere, Proc. 3rd Intern. Colloquium on Biology, Saclay, 1963, p. 337 (1964).

No. 45

Thin Solid Films, *19* (1973) 297–312

ELEMENTAL ANALYSIS BY DIFFERENTIATED BACK-SCATTERING SPECTROMETRY*

M. PEISACH
Southern Universities Nuclear Institute, P.O. Box 17, Faure, C.P. (South Africa)
(Received August 16, 1973)

With thick targets, improved definition of spectral energies and improved precision in determining elemental surface concentrations have resulted from the use of arithmetic differentiation of the spectra.

A large number of pure compounds in pellet form were bombarded with beams of protons and $^4He^+$ ions up to about 4 MeV, and singly charged $^{14}N^+$ beams up to 1.6 MeV. Spectra were measured with surface barrier detectors and analysed by a programme which first smoothed the data before differentiation.

The method was tested on thin films, glass films of intermediate thickness, layers of powdered ore deposited on carbon foils and thick geological samples.

INTRODUCTION

It has been the experience in other fields of spectrometry, such as in the early days of γ-ray spectrometry or, more recently, Auger spectrometry, that the use of some form of differentiation increased the scope of that spectroscopic method. Usually differentiation was achieved by a development of the measuring technique but, in principle, differentiation achieved by other methods could serve equally well. It was difficult at this stage to predict the type of development that would occur in charged particle measuring devices which would enable us to differentiate back-scattering spectra as they were measured. However, the advent of computers as an accepted tool in the laboratory has now made it practical to effect mathematical differentiation of spectral data, either on-line or in a batch-wise process, while the data are being recorded. Over the past few years, arithmetic differentiation of back-scattering spectra has been used in our laboratory. In this paper, we describe some of the results we have obtained and discuss the implications of the method.

Back-scattering has been used for many years for analysing surface layers of materials[1]. When the bombarding beam does not lose an appreciable amount of energy in the target material, such as is the case for thin targets or surface layers, the back-scattered energy E is given by

* Paper presented at the International Conference on Ion Beam Surface Layer Analysis, Yorktown Heights, New York, U.S.A., June 18–20, 1973.

$$\frac{E}{E_0}=\left(\frac{M_1}{M_1+M_2}\right)^2\left[\cos\theta+\left\{\left(\frac{M_2}{M_1}\right)^2-\sin^2\theta\right\}^{1/2}\right]^2 \tag{1}$$

where E_0 is the energy (in laboratory coordinates) of the incident particle of mass M_1 and charge Z_1 being scattered off a target atom of mass M_2 and atomic number Z_2, and θ is the scattering angle.

The Rutherford cross section σ for elastic scattering is given by

$$\sigma=\frac{Z_1^2\,Z_2^2\,e^4}{4E}\left(\frac{M_1+M_2}{M_2}\right)^2\frac{\{(M_1/M_2)\cos\theta+k\}^2}{k(2-k^2-k\cos\theta)^2} \tag{2}$$

where

$$k=\left\{1-\left(\frac{M_1}{M_2}\sin\theta\right)^2\right\}^{1/2} \tag{3}$$

In the case of a thin target the energy spectrum of the back-scattered particles consists of peaks, each of which corresponds to an element in the target, the area under the peak being a measure of the elemental concentration. When targets of intermediate thickness are used, *i.e.* targets in which the bombarding beam undergoes appreciable energy loss but from which the minimum energy of the detected particles is still quite large, the spectra consist of elongated flat-topped peaks which may frequently overlap.

When thick targets are bombarded, the incident beam loses energy along its path through the material to the scatter site, after which the scattered particle again loses energy until it escapes from the target. The energy of the detected particle can thus range from E to almost zero, depending on the depth of the scatter site below the surface of the target. The spectra appear as a series of plateaux separated from each other by steps, the heights of which are used to determine the surface concentrations of the elements while the inflection point for each step is used to determine the energy at which the step occurs and hence to identify the element.

A method frequently used for analysing experimental results is shown in Fig. 1. Two straight lines are fitted to the plateau slopes on either side of the spectral step. The intersections between these lines and a third one, fitted to the step itself, are calculated. These intersections are denoted by (x_1, y_1) and (x_2, y_2) in Fig. 1. The spectral step height is given by y_1-y_2 and the channel number at which the step occurs by $\frac{1}{2}(x_1+x_2)$. This latter position is near, but usually does not coincide with, the inflection point.

THICK TARGETS

When a stepwise spectrum obtained from a thick target is arithmetically differentiated, ideally the result will consist of a line of zero slope, separated by a series of approximately gaussian peaks, in this case in the negative direction. The area between the zero line and each peak is a direct measure of the height of the corresponding step in the observed spectrum. However, by differentiation,

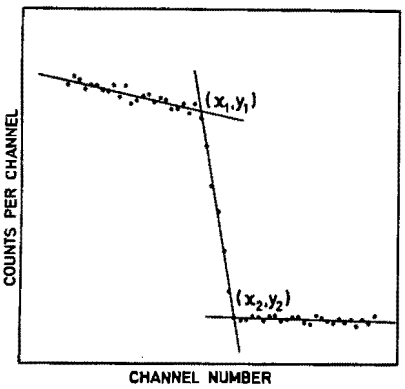

Fig. 1. The method often used for determining step height and step position. The step height is given by $y_1 - y_2$ and the position by $\frac{1}{2}(x_1 + x_2)$.

we have converted the stepwise spectrum to one whose shape is far more familiar to the analyst, and the analyses of such curves can be carried out using well-known and well-tried computer programmes. An additional advantage lies in the fact that most steps obtained on thick target spectra are sharp and their derivative therefore results in a well-defined turning point, the energy corresponding to which can much more readily be determined than that of an inflection point.

In the case of material in which the mass numbers of the elements concerned are widely separated, very little is gained by using the differential method since both the heights of the steps and the energies at which they occur can readily be deduced from the experimentally measured spectrum. An example of this is shown in Fig. 2, which is for a thick sample of manganous sulphate bombarded with 4 MeV α-particles; the differential below it clearly shows the three peaks corresponding, respectively, to the elements manganese, sulphur and oxygen in decreasing order of energy.

Figure 2 also clearly shows the Z_2^2 dependence of the scattering cross section. The yield obtained from sulphur is markedly lower than that obtained from manganese, even though the two elements are in equal atomic concentrations in the compound. Furthermore, oxygen and sulphur have approximately the same yield, although the atomic concentration of oxygen is four times that of sulphur.

To obtain these data, the original observed spectrum was smoothed and differentiated by a simplified least-squares procedure[2]. The smoothed count Y_j^* in channel j may be obtained in a region defined by m consecutive channels on either side of j from a polynomial f_x of degree $n < 2m+1$, where

$$f_x = \sum_{k=0}^{n} a_k x^k \tag{4}$$

and the coefficients a_k are obtained by the method of least squares. The final expression can then used to get the "best" value at the central point and a new set of a_k has to be calculated for the next channel, $j+1$. This method is tedious,

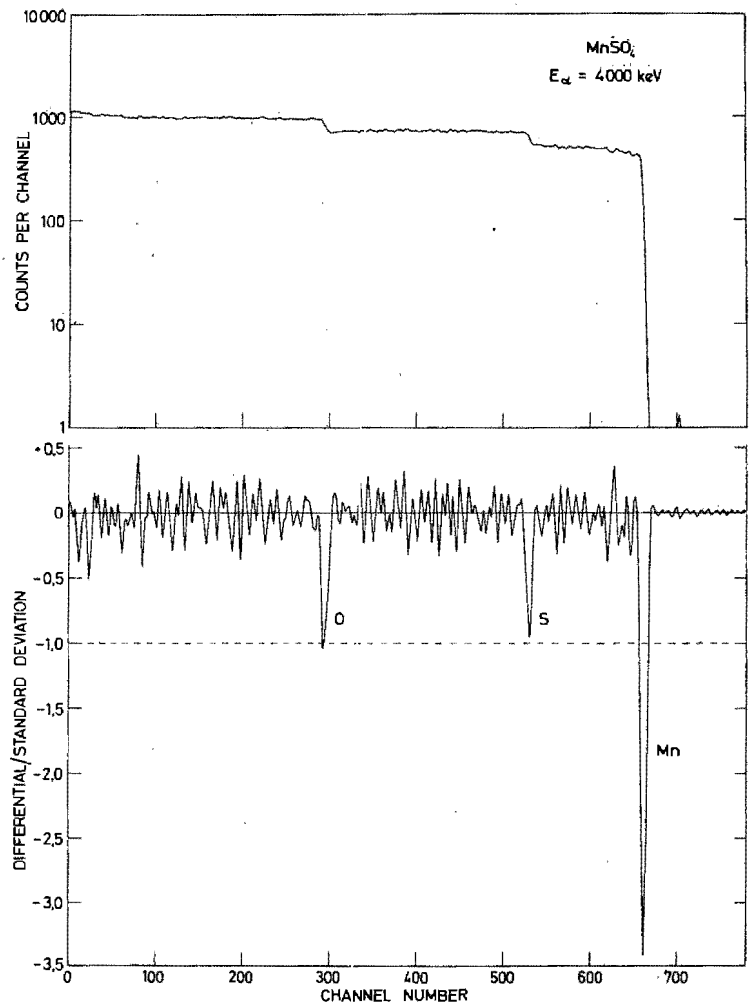

Fig. 2. Energy spectrum of elastically scattered α-particles from a thick target of manganous sulphate. $E_\alpha = 4000$ keV, θ(scatter) = 140° (lab).

but from the method of least squares a set of convoluting integers C_i and a normalizing factor N can be calculated which can be used to determine the Y_j^* from the observed values Y_j by

$$Y_j^* = \frac{1}{N} \sum_{i=-m}^{+m} C_i \, Y_{j+i} \tag{5}$$

in a manner exactly equivalent to the polynomial approach. The full procedure for obtaining the values C_i for different polynomials, and tabulated values of C_i for smoothing and differentiating are given in ref. 2. The value of m in the convolution stage should be small so that not more than one inflection in the observed

data occurs in the interval. In this work a cubic function was used for smoothing, a quadratic for differentiation and the number of channels chosen was the largest odd number less than the number of channels covered by the energy interval equivalent to the resolution of the detector. For quantitative results the values of the differential were used, but for visual interpretation the abscissae are given in units of "differential per unit standard deviation" in order to emphasize any meaningful peaks that may sometimes become evident in regions of low count rates. It should be noted that the logarithmic scale, needed to show different count rate regions with equal prominence, tends to emphasize curve slopes in the low count region. The above approach helps to eliminate such cases.

The back-scattered spectrum obtained from homogeneous material containing cobalt and iron is shown in the upper portion of Fig. 3. Because the mass numbers

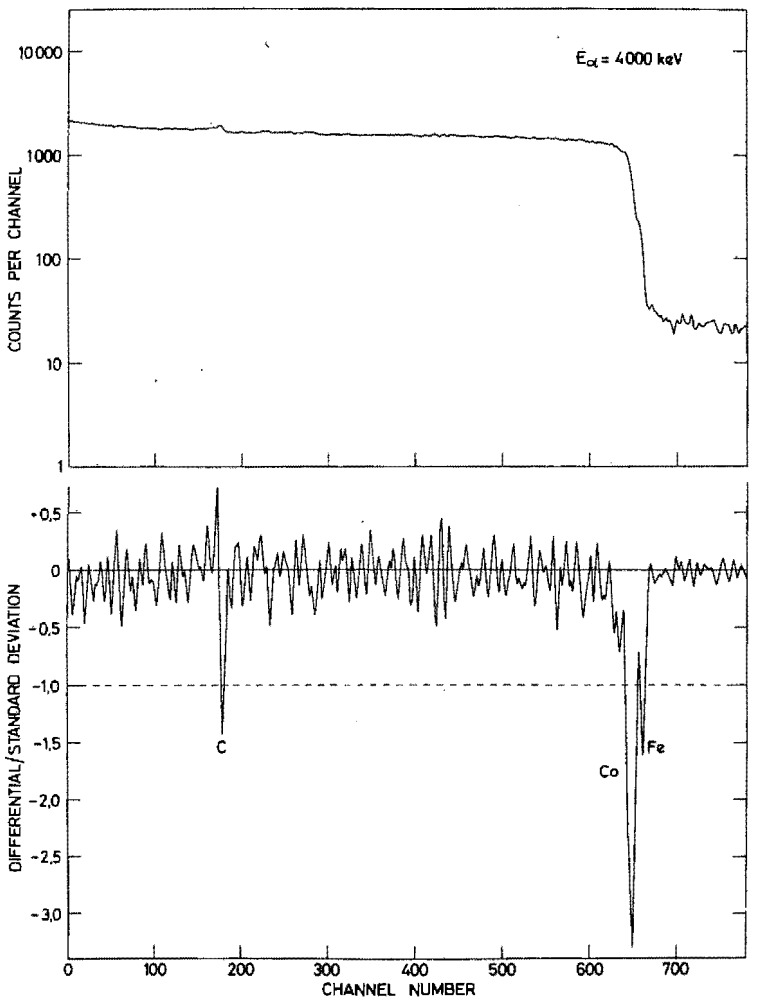

Fig. 3. Back-scattering (above) and differentiated spectra obtained from α-particle scattering from a thick target containing cobalt and iron. E_α = 4000 keV, θ(scatter) = 140° (lab).

of the most abundant isotopes of these two elements do not differ appreciably from each other, the two steps in the observed spectrum follow closely upon one another, and there is much to be said about the precision with which the surface concentration of each of these two elements can be obtained from the original spectrum. When the original spectrum is smoothed and differentiated, the peaks corresponding to the two elements can readily be resolved and stripped arithmetically or by computer programme, despite the fact that the peaks overlap at their bases. Should it be necessary, it would be a simple matter to obtain the shape of the differential peak for each element separately from thick targets of the pure metals.

The effect of detector resolution is shown in Fig. 4. The differentiated spectral peaks refer to manganese as obtained from bombarding a thick target of manganous sulphate with protons, α-particles and nitrogen ions. For these bombarding particles the detector resolution (full width at half height) as measured with a very thin layer of gold on a thin carbon foil was 18 keV for 3000 keV protons, 26 keV for 4000 keV α-particles and 53 keV for 1500 keV nitrogen ions. Despite this wide range, the precision with which the apex of each peak in the differentiated spectra can be determined varies little, even though corresponding peaks show increased widths and decreased heights with increasing mass of the bombarding particle.

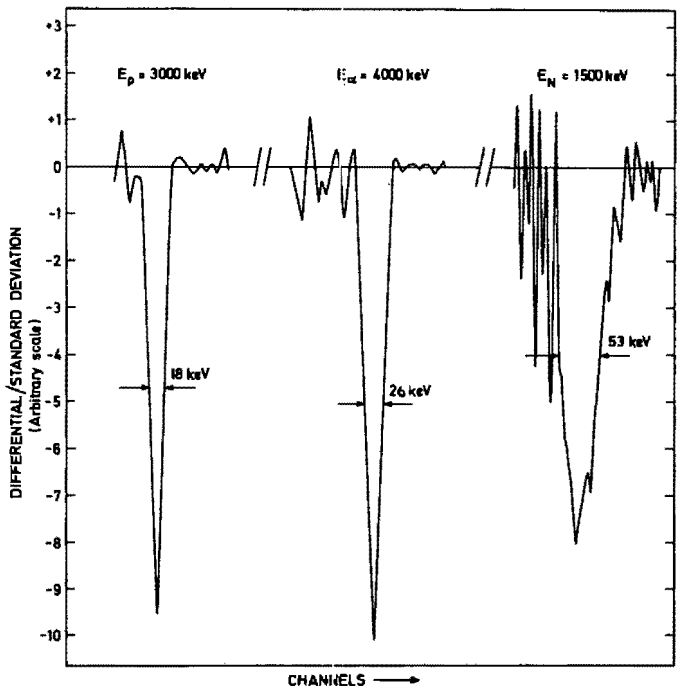

Fig. 4. The effect of detector resolution: Differentiated spectral peaks of manganese from thick targets of manganous sulphate bombarded with 3000 keV protons, 4000 keV α-particles and 1500 keV nitrogen ions. The widths at half height refer to the detector resolution.

Thick geological samples were analysed by differentiated back-scattering spectrometry. Figure 5 shows two spectra obtained from an ore sample from Spekboom near the contact zone between granite and amphibolite, where it is known that the potassium concentration in the amphibolite is a function of the distance from the contact zone. Scanning the ore across the contact zone (from -20 to $+70$ mm) resulted in a series of spectra of back-scattered α-particles and α-particle-induced X-rays, from which the required data were obtained.

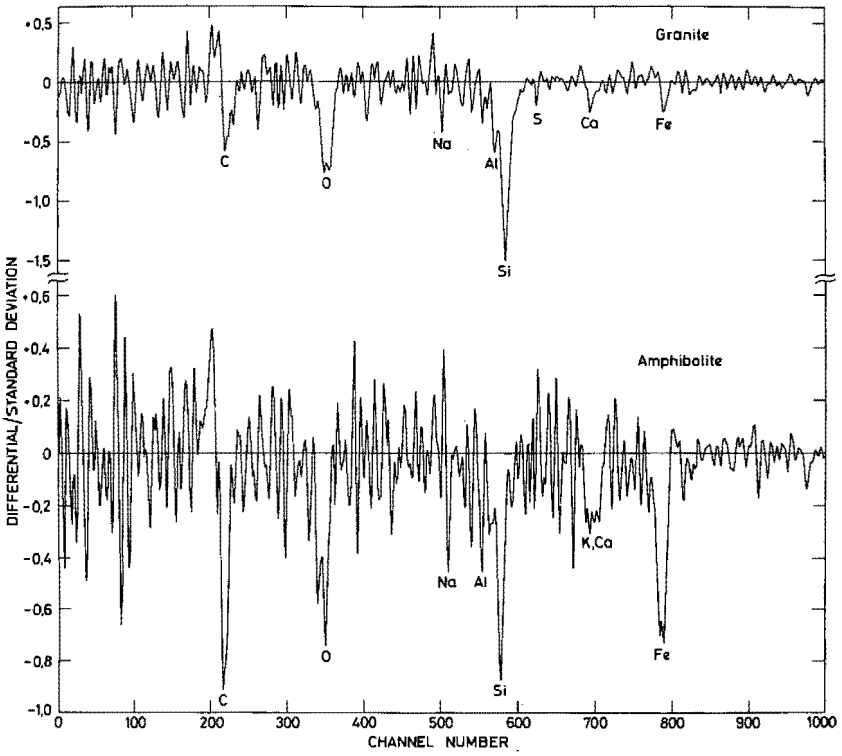

Fig. 5. Differentiated back-scattering spectra from the contact zone of granite (above) and amphibolite measured on a sample of Spekboom ore. $E_\alpha = 4000$ keV, θ(scatter) = 140° (lab).

Precision of energy and concentration determinations

The precision with which the energy and peak heights could be determined by the differentiation method was compared with that obtainable by the plateau step height method for a test series of 15 iron ore samples consisting of 5 of each of the ore types haematite, magnetite and pyrites. These ores were used because there were only two steps in each spectrum and the steps were sufficiently separated from each other to avoid prejudicing the step height method.

The results in Table I refer to energy precision. All values are expressed in "channel numbers" to avoid introducing errors of energy calibration. Attention is drawn to the fact that channel numbers corresponding to the various elements differ for the two methods. This is because the mean step height and the inflection

TABLE I

PRECISION OF ENERGY MEASUREMENTS*

Element	*Haematites*	*Magnetites*	*Pyrites*	*Mean (all data)*
Plateau step method				
O	311.82±2.28	309.60±2.31	–	310.71±2.46
S	–	–	499.90±0.82	499.90±0.82
Fe	611.40±0.53	610.93±0.18	609.80±0.59	610.71±0.82
Differentiation method				
O	317.17±2.23	316.01±1.41	–	316.59±1.86
S	–	–	503.61±0.28	503.61±0.28
Fe	612.77±0.48	612.80±0.28	612.07±0.76	612.45±0.76

* All values refer to "channel number" and errors are standard deviations.

point do not coincide. Because calibrations are usually obtained from thin samples using peak maxima, systematic errors could be introduced when dealing with thick targets. Table I shows that only in the ideal case of the heaviest element present, where the count rate drops to almost zero at the plateau step, do the two methods give comparable precision, but for lighter elements the differentiation method is the more precise.

Table II shows a comparison of the precision attainable by the two methods for concentration measurements. In this table the count ratio is given for the light element (O or S) relative to Fe in order to include errors involved in determining both elements but to avoid errors due to current integration. Both methods show improved precision when the relative heights of the steps become more nearly equal, but the relative precision is improved by differentiation. The absolute values of the ratios are in agreement within the precision of the methods, hence showing that the methods are equally accurate.

INTERMEDIATE THICKNESSES

The analysis of material of intermediate thicknesses presents a new set of patterns for the differentiated spectra. If the sample consists of several elements, each element will appear in the observed spectrum as an elongated approximately

TABLE II

PRECISION OF CONCENTRATION DETERMINATIONS*

	Plateau step method	*Differentiation method*
Haematites	0.1515±4.42%	0.1536±4.18%
Magnetites	0.1237±4.62%	0.1274±3.01%
Pyrites	0.7410±2.60%	0.7452±1.33%

* Values are expressed as the ratio of counts of the light element (O or S) relative to the counts from Fe, and the percentage errors are relative standard deviations.

flat-topped peak, the high energy edge of which corresponds to the shape of the spectrum obtained from an infinitely thick target, whilst the low energy edge is due to scattered particles obtained from the last layers of the target. In this way, the width of the scattered peak represents the total amount of energy lost by the bombarding material in the target. Such spectra when differentiated will result in a pair of peaks, one positive and one negative, the negative one having exactly the same characteristics as would have been the case with an infinitely thick target.

It is frequently not possible to estimate the thickness of an intermediate target from other measurements. The parameter that is usually obtained is the average thickness of the target, but if the target is in any way non-homogeneous an error is introduced in the one parameter from which all absolute values are calculated.

Using differentiated spectra it becomes possible to define the energy of the back-scattered particles from the rear of the target with as much definition as that obtained from the surface. The difference between these two energies is then directly a measure of the thickness of the target, at the point at which the beam strikes the target, and it is precisely at this point that the exact thickness of the target is required for absolute measurement. If the target consists of a series of elements, each element will exhibit a similar double peak, and each element will thus serve as a means of obtaining a duplicate value for the thickness. It is then possible to obtain, not only the energy lost by the bombarding beam within the target, but also, by using a series of energy–range tables and integrating the area between the differential peak and the zero line, the atomic composition of the material, and hence the thickness of the material in absolute measure can be obtained. It may be pointed out that the spacing of the positive peaks in the differentiated spectrum should closely resemble the spacing of the negative ones, thus making it possible to pair up positive and negative peaks even though the observed spectrum may show an overlapping of the various elemental plateaux.

There is a difference between the shape of the positive differentiated peak and that of the negative one. The positive peak is due to scattered particles arriving at the detector from the rear end of the target material, and hence the particles had to penetrate the entire thickness of the target, both on bombardment and after scattering, before arriving at the detector. On both portions of the path straggling occurred, with the result that the peak is much more diffuse than is the case from surface scattered particles. Since, however, the energy corresponding to the apex of a differential peak is very little affected by the resolution of the detector, we can consider the positive peak as one being measured with a detector of poorer resolution, which would account for the width of the differentiated peak. The energy of the peak still remains well defined, and hence average energy loss within the target can readily be determined.

It should be pointed out that, by using the shape of the peak itself, data on straggling can be obtained under varying conditions of bombardment.

An example of the use of differentiated spectrometry for targets of intermediate thickness is shown in Fig. 6. These data were obtained from the analysis of thin slivers of glass bombarded with α-particles. The slivers of glass were

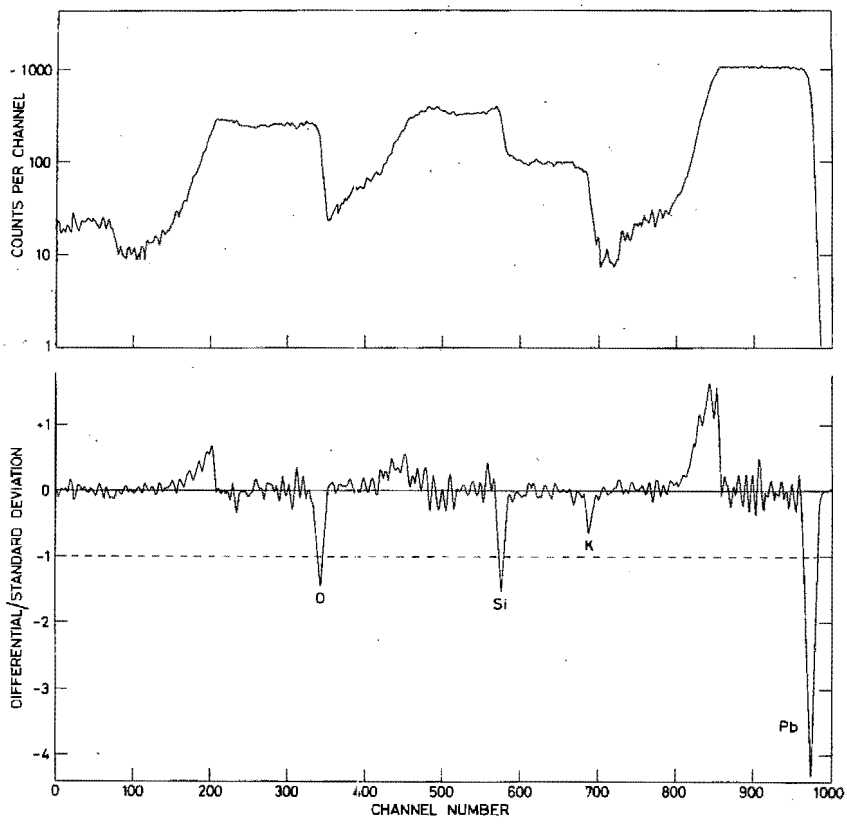

Fig. 6. Back-scattering of 4 MeV α-particles from a glass specimen. Note the plateaux formed for each component element in the upper spectrum and, in the differentiated spectrum, the elongated low energy tail of the positive peaks due to straggling.

obtained by rapidly blowing a bubble from the molten glass and mounting the thin fragments obtained from the glass over holes in a metal support. The spectra show most of the features discussed above. In this case, however, exact analysis of the major components of the glass was not possible, due to the fact that the scattering cross section for light elements is so much smaller than that for heavier ones. Relatively small concentrations of elements such as boron, which would seriously affect the energy loss of the bombarding beam within the target, would not readily be observed on the scattering spectrum. It follows, therefore, that the average thickness of the target would be incorrectly computed and this error would be carried over to the absolute determination of the major components. To correct for this, light elements were simultaneously determined by prompt proton spectrometry[3].

With proton energies as high as 3 MeV, charged particles are frequently observed from sources other than Rutherford scattering. Figure 7 shows spectra obtained from a deposit of calcium fluoride on carbon, where only the three labelled peaks are due to elastic scattering.

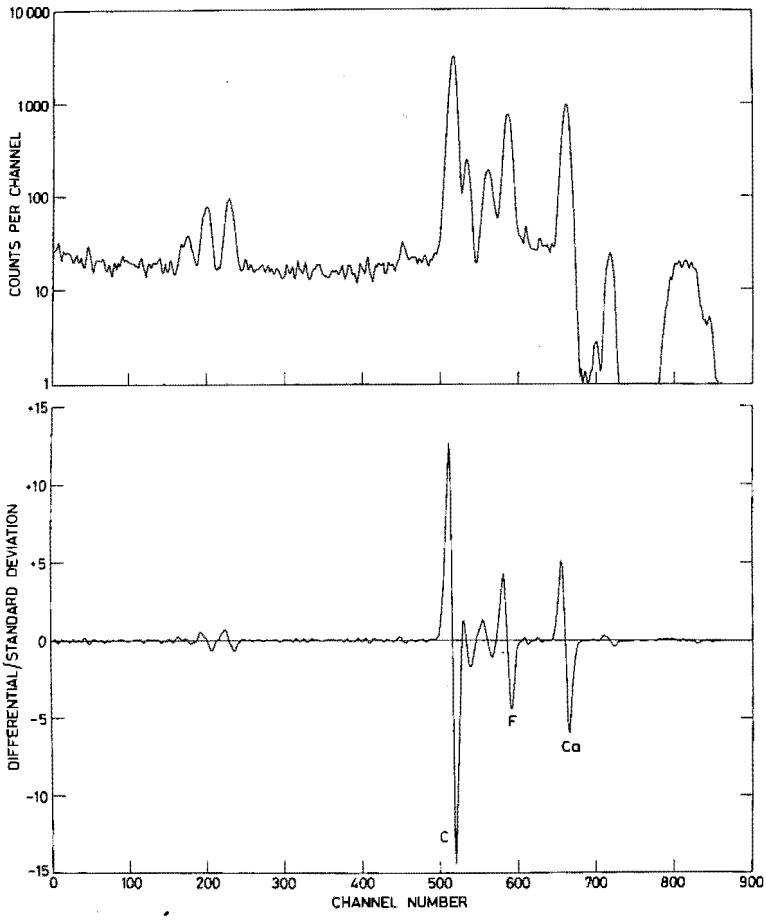

Fig. 7. Back-scattering at 140° (lab) of 3 MeV protons from calcium fluoride on carbon. Note the number of spectral peaks, of which only the three labelled ones are due to elastic scattering.

THIN TARGETS

Since the spectrum obtained from a thin target already consists of a series of peaks, the use of differentiation cannot introduce appreciable improvement in the determination of the energies concerned. When such spectra are differentiated the differential will consist of a pair of peaks, one positive and one negative, following immediately upon one another, the zero cross-over corresponding to the peak of the original spectrum. However, when observed spectra contain peaks that are poorly resolved, the differential will clearly show the existence of double peaks as a result of a widening of either the positive or the negative peak. In those cases standard stripping methods can then be used to analyse the spectra.

When finely powdered geological samples suspended in water or alcohol are sprayed onto thin carbon foils, ideally a thin sample should be produced which

will yield a back-scattering spectrum consisting of well-defined single peaks corresponding to each major and minor (but not trace) component. In practice, the particles that are sprayed onto the carbon foil, although small, are not uniform. As a result, the back-scattering spectrum (see Fig. 8) shows characteristics of both "intermediate" and "thin" samples and usually appears as a series of peaks with pronounced tailing towards the low energy side. Quantitative analyses from such data are frequently unsatisfactory, but the differentiated spectrum, consisting as it does of well-defined peaks, can be quantized easily and more precisely.

It is still a moot point whether the peak of an isolated thin target element corresponds exactly to the inflection point that would have been obtained for the same element in infinitely thick targets. It also remains to be established

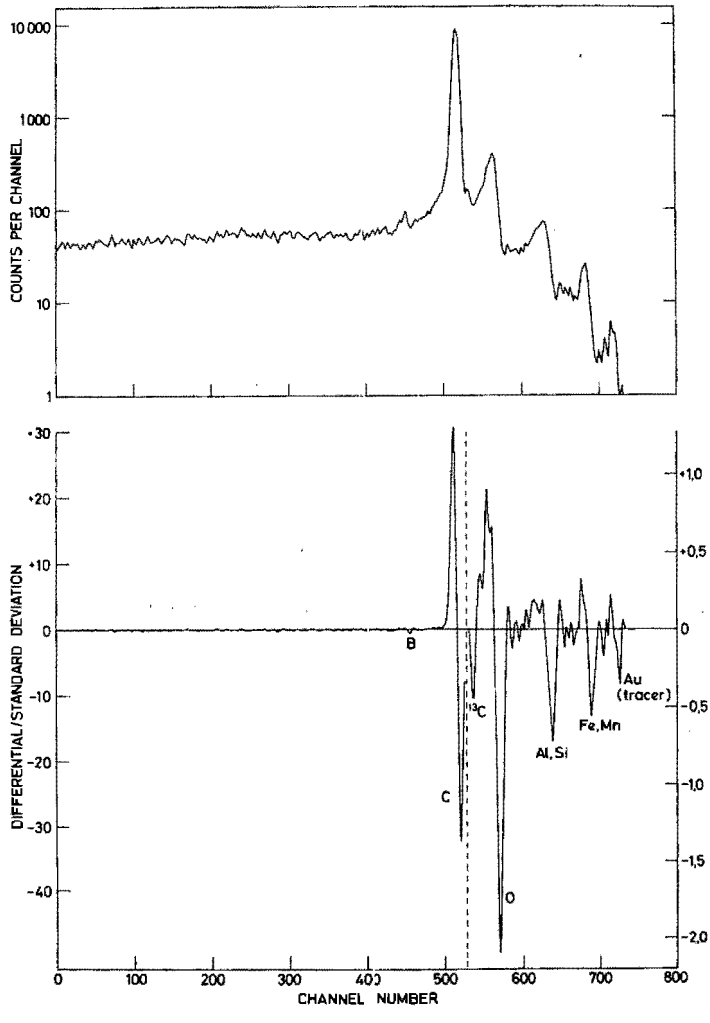

Fig. 8. Back-scattering from a powdered tourmaline sample deposited on a carbon foil. $E_p = 3000$ keV, θ(scatter) = 140° (lab).

whether the inflection point for intermediate target thicknesses is always found at the same energy, or whether there is a movement of the inflection point with sample thickness. Such studies are still proceeding.

CHANNELLING

In channelling experiments, back-scattering has become one of the standard procedures. Along random directions the spectra appear similar to those obtained from thick targets, with plateau edges clearly defined. As the bombarding direction approaches a channel direction, the intensity of back-scattering from surface atoms decreases and the plateau edge becomes rounded. On differentiation, the random direction spectrum would yield a symmetrical negative peak, while that obtained from a channelled direction would be tailed on the low energy side and the amplitude would be much lower. Since the amplitude of the differential peak is a measure of the slope of the observed spectrum at its inflection point, this amplitude is a good measure of the alignment of the crystal along a channel direction. The differentiation method, however, does not offer any advantage over the currently used one.

Evidence for crystal damage may be recognized by the appearance at the plateau edge in back-scattering spectra of a sharp peak, which becomes more pronounced along channel directions. This effect shows up on differentiation as a superimposed "thin sample" differential. When crystal damage is relatively slight, the differential peak already shows irregularities, from which the extent of damage may be inferred. Such a case is shown in Fig. 9.

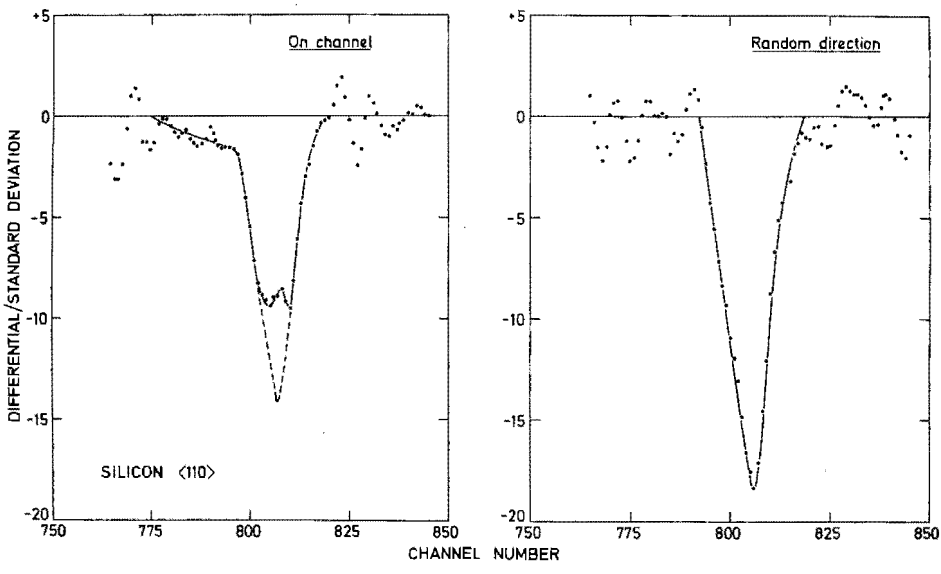

Fig. 9. Back-scattering of 1500 keV protons from a single crystal of silicon showing the effect of slight crystal damage, caused by prior bombardment of the crystal for a short time. Note the tailing on the low energy side in the left-hand spectrum.

Current studies of the shapes of the differential peaks along, near or off channel directions are aimed at obtaining a parameter which is independent of the integrated bombarding beam current, because of the difficulty in measuring low integrated currents with precision. One such method is to measure the energies E_l and E_h corresponding to an amplitude of 1/10 of the differential peak height on either side of the inflection point energy E and to use the parameter r, where

$$r = \frac{E - E_l}{E_h - E}$$

STATISTICAL CONSIDERATIONS

The mathematical derivation of the standard deviation of a point obtained for the differential or for the smooth curve has at this stage not yet been carried out. Instead, we have obtained the necessary values through the use of simulated

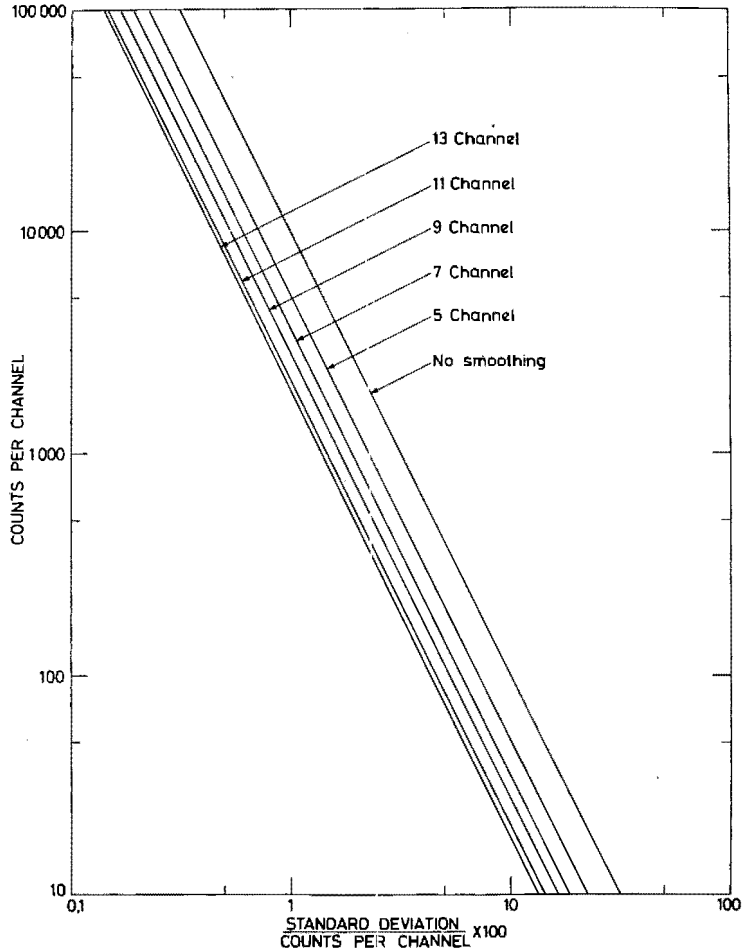

Fig. 10. The variation of the relative standard deviation with count rate, after smoothing over 5, 7, 9, 11 or 13 channels. The abscissa is expressed in 100 × (standard deviation)/(count rate).

data from which standard deviations were calculated. Plateaux such as would be obtained from infinitely thick targets have been simulated for up to 5000 channels and for counting rates ranging between 100 and 10 000 counts per channel. These plateau counts, for which the standard deviations were given by the square root of the count, were then smoothed by the least-squares method[2], involving between 5 and 13 channels per point, and the resulting smoothed plateau counts were used to calculate the standard deviation of the new points obtained. These results are given graphically in Fig. 10. Subsequently the data thus obtained were differentiated by the same procedure as used previously. From these data the average value of the differential was calculated and invariably found to be negligibly different from zero, while the standard deviation of the differential varied with the count rate. These results are shown graphically in Fig. 11.

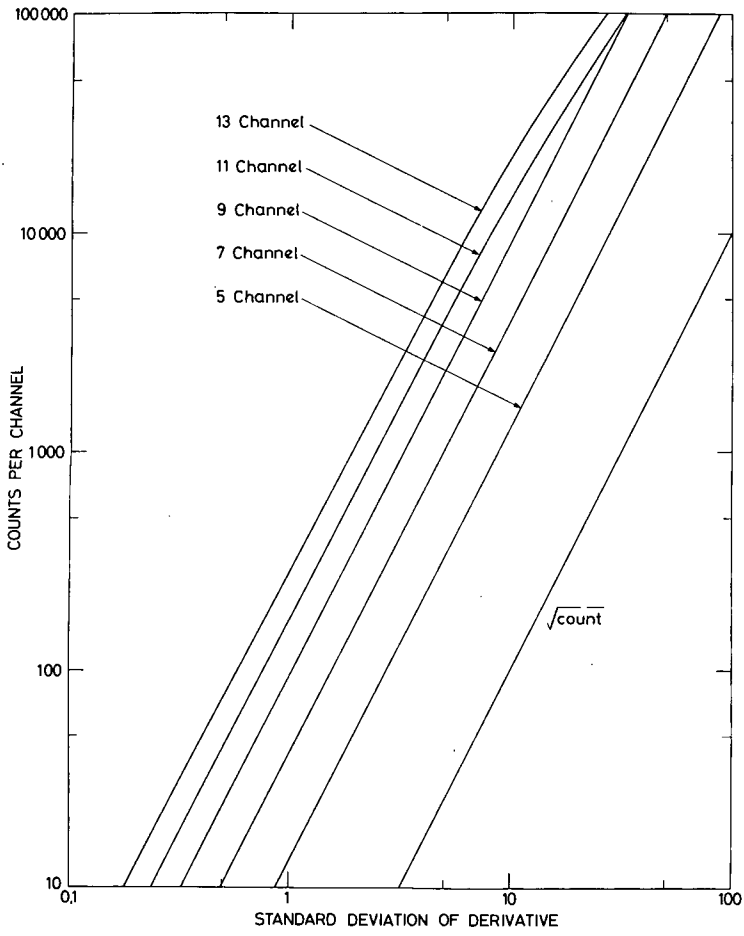

Fig. 11. The variation of the standard deviation of the derivative with count rate when differentiation involves 5, 7, 9, 11 or 13 channels.

The standard deviations obtained in this way were the values that were used in expressing the abscissae of the spectra shown previously.

At this stage, we do not yet recommend relying solely on the differentiated spectra for the analysis of a material. However, it is the differentiated spectrum that indicates the energy regions of interest where the observed spectrum has to be studied further. By using the ratio of the differential to the standard deviation, freak large value differential peaks arising purely from random fluctuations can be eliminated by inspection. However, the old adage that only good data lend themselves to mathematical manipulation still applies.

CONCLUSIONS

The advantages offered by arithmetic differentiation of back-scattering spectra can be summarized as follows.

(1) The energy corresponding to peaks or inflection points can be determined with precision.

(2) The determination of inflection points is little affected by the resolution of the detector.

(3) Surface concentrations of adjacent or nearly adjacent elements in the Periodic Table can be more readily measured.

(4) Thicknesses of intermediate samples, at the point where analysis is carried out, can be measured with fair precision.

(5) Differential peak shapes and low energy edge tailing can be useful for studies of straggling and channelling.

(6) A small extent of crystal damage can be detected.

ACKNOWLEDGEMENTS

The author is indebted to the staff of the Southern Universities Nuclear Institute for assistance with the preparation of samples and the measurements, to the South African Council for Scientific and Industrial Research and the South African Atomic Energy Board for financial support, and to the Board of Governors of S.U.N.I. and the organizers of the International Conference on Ion Beam Surface Layer Analysis for travel funds to present this paper at the conference. The Spekboom sample was supplied by the University of Natal, and other geological samples by the University of Stellenbosch.

REFERENCES

1 S. Rubin, T. O. Passell and L. E. Bailey, *Anal. Chem.*, *29* (1957) 736;
M. Peisach and D. O. Poole, *J. S. Afr. Chem. Inst.*, *18* (1965) 61;
M. Peisach and D. O. Poole, in J. P. Guinn (ed.), *Proc. 1965 Intern. Conf. on Modern Trends in Activation Analysis*, Texas A & M. University, 1965, p. 206;
J. H. Patterson, A. L. Turkevich and E. Franzgrote, *J. Geophys. Res.*, *70* (1965) 1311;
M. Peisach and D. O. Poole, *Anal. Chem.*, *38* (1966) 1345;
O. U. Anders, *Anal. Chem.*, *38* (1966) 1442.

2 A. Savitsky and M. J. E. Golay, *Anal. Chem.*, *36* (1964) 1627.

3 M. Peisach and R. Pretorius, *Proc. Intern. Conf. on Modern Trends in Activation Analysis, Saclay, France, 1972*, Paper M 92, in *J. Radioanal. Chem.*, in the press.

No. 46

SEPARATIONS IN RADIOCHEMISTRY WITH SPECIAL REFERENCE TO THE ISOLATION OF CARRIER-FREE ISOTOPES

BY M. PEISACH

Reprinted from *S. A. Industrial Chemist*

Volume 11, No. 1, January 1957

NATIONAL CHEMICAL RESEARCH LABORATORY
NASIONALE CHEMIESE NAVORSINGSLABORATORIUM

SOUTH AFRICAN COUNCIL FOR SCIENTIFIC AND INDUSTRIAL RESEARCH

SUID-AFRIKAANSE WETENSKAPLIKE EN NYWERHEIDNAVORSINGSRAAD

PRETORIA

LSG—36987

SEPARATIONS IN RADIOCHEMISTRY WITH SPECIAL REFERENCE TO THE ISOLATION OF CARRIER-FREE ISOTOPES

M. Peisach
National Chemical Research Laboratory, South African Council for Scientific and Industrial Research, Pretoria
Paper delivered at the Tenth Annual Convention of the South African Chemical Institute, Johannesburg, September 1956.

In all branches of chemistry separations play a very important role, but in radiochemistry the small amount of material generally involved renders normal analytical procedures difficult, if not impossible. When a target element has been bombarded in a cyclotron it is usually necessary to remove the product element in a "carrier-free" form, namely a form in which there are no other isotopes of the element present. In such separations one of the major analytical methods, precipitation, cannot be directly applied, as only rarely is there a sufficiently high concentration for precipitation to be effective. Consequently, the methods used in radiochemical separations differ from those of analytical chemistry owing to the ultra-micro scale of operation.

A numerical example might convey more clearly the amounts of material involved. When a tin target is bombarded with 8 M.e.v. deuterons, antimony-117 with a half-life of 2·8 hours is one of the main products. Under optimum conditions about 1 mc. Sb^{117} would be obtained. The weight of antimony produced is about $1{\cdot}05 \times 10^{-10}$ gm. and this has to be separated from about a gram of tin.

Another factor which plays a very important part is the duration of a radiochemical separation. It is obviously useless to be able to isolate a particular isotope in a few hours if its half-life is of the order of a few minutes. As a result, methods are frequently chosen for their speed, even though only a portion of the desired isotope may be recovered.

For convenience, the various techniques may be divided and discussed under the following headings.

Precipitation

For the isolation of carrier-free radioisotopes, precipitation procedures can take one of two forms; either the substance can be co-precipitated with a similar element, or it may be adsorbed on to another compound being precipitated as "scavenger".

In the case of true co-precipitation, the radioactive atom is incorporated into the crystal structure of the precipitate by isomorphous replacement, analogous to the formation of mixed crystals in macro amounts as, for example, the well-known case of radium and barium chlorides. Subsequent separation of the radioelement from its carrier may involve a good deal of difficulty, due to the two elements usually having similar chemical properties. The introduction of ion-exchange techniques has, to some extent, overcome this difficulty.

In addition to true co-precipitation, there are some cases where a mixed crystal may form which would have occurred had the radioisotope been present in macro amounts, e.g., lead-212 with silver chromate.[1] Anomalous mixed crystal formation can thus also lead to a homogeneous precipitate. A third type of co-precipitation resulting in an unhomogeneous precipitate, is the adsorption of a radioisotope onto a growing crystal, thus becoming trapped within the crystal structure, e.g., polonium-210 in potassium sulphate.[2]

Unlike co-precipitation which finds only limited application, adsorption of an isotope on to a precipitate is widely used, and depending on the conditions of precipitation, can be fairly specific. The selection of the precipitate is a matter of importance as it must be readily removable afterwards. Ferric hydroxide is such a precipitate, as after precipitation it can be extracted with ether from hydrochloric acid solution. Many carrier-free isotopes have been isolated using ferric hydroxide as "carrier", among them such widely differing elements as beryllium,[3] phosphorus,[4] manganese,[5] strontium,[6] zirconium,[6] lanthanum[6] and indium.[7] Other scavenger precipitates frequently used are manganese dioxide precipitated from nitric acid—used, for example, in separating tantalum from hafnium[8]—and sulphides such as bismuth sulphide (separating copper from zinc[9]), platinum sulphide (technetium from fission products[10]), cadmium sulphide (antimony from tin[7]) and copper sulphide (rhenium from tantalum[11]). An interesting example in which two different scavengers are used successively is the separation of tellurium from fission products.[6] Copper is added to the acid solution and precipitated as the sulphide. Tellurium, adsorbed on copper sulphide is separated and the scavenger removed by a second scavenger, this time by precipitation of ruthenium sulphide. Carrier-free tellurium is recovered after ruthenium is volatilised off from perchloric acid medium.

It frequently happens that in addition to the isotope required, a small amount of another radioactive element is co-precipitated. Since it is usually essential that the carrier-free isotope should be *radiochemically pure*, as opposed to *analytically pure*, milligram quantities of the interfering element are added as "hold-back carriers" to decrease the specific activity of the contaminant. Subsequent precipitation will yield a product containing the radioactive impurity in amount smaller by many orders of magnitude.

When milligram quantities of an isotopic substance are added, carrier-free separations are no longer chemically possible, and the separation techniques then become those of analytical chemistry. In recent years, however, newer techniques have been developed which are finding more and more application in radiochemistry.

1. *Precipitation from homogeneous solution*

When a precipitate is formed by adding one solution to another, it is inevitable that local supersaturation should arise even when the solutions are mixed with vigorous stirring under dilute conditions. As a result of such supersaturation excess reagents and other impurities may become occluded and be difficult to remove. If however, the precipitating agent is formed as a result of another reaction within the solution, precipitation will depend on the rate of this secondary reaction. By suitably controlling the secondary reaction, a pure precipitate may be obtained.

It is appreciated that the precipitation of the hydroxides of trivalent ions, especially iron and aluminium, results in a precipitate which is impure, as a result of adsorption of impurities, and difficult to filter, as a result of its gelatinous nature. However, when for example the pH of solutions of such ions is gradually lowered by hydrolysis of urea, the hydroxides precipitate slowly to yield a very much purer compound in a dense, more filterable form.[12] A pure precipitate of ferric hydroxide was obtained[13] when a soluble versene complex of iron was oxidised in homogeneous solution with hydrogen peroxide.

The hydrolysis of dimethyl sulphate in a solution containing lead, gave controlled precipitation of lead sulphate.[14] Similarly, controlled hydrolysis of dimethyl oxalate has been used[20] to separate americium from lanthanum by controlled precipitation of lanthanum oxalate. Homogeneous precipitation of thorium iodate was effected[15] by reducing periodate with ethylene glycol, which in turn, was produced by the hydrolysis of β-hydroxy ethyl acetate.

2. *The use of complexing agents*

Chelating agents, such as 8-hydroxy quinoline, cupferron and α-nitroso-β-naphthol, have been used for some time to form insoluble complexes, but in recent years, various reagents, such as EDTA (ethylenediamine tetraacetic acid) have been developed for the formation of soluble complexes. In radiochemical separations use is often made of this "masking action" to prevent the precipitation of an undesired compound. Thus tin in ammonical tartrate solution is not homogeneously precipitated by thioacetamide, but after the masking action is no longer required, the addition of calcium, which is preferentially chelated, allows stannous sulphide to precipitate.[23]

The masking action is not, however, specific but depends on the conditions of precipitation. Thus, in a mixture of iron (Fe^{3+}) and uranium (U^{6+}) EDTA forms chelates with each element, but at pH 5 in a buffer solution of ammonium acetate-acetic acid, iron is solubilised and only uranium precipitates with oxine for example, whereas at pH 9 in a buffer solution of ammonium hydroxide-sodium acetate, the reverse is the case.[19]

3. *Chromatographic precipitation*

This type of precipitation is conducted with a chromatographic column which acts as the source of the precipitating agent. Thus, a column of alumina treated with iodide has been used to separate silver, mercury and lead from each other by precipitation of their iodides.[16] The zones of precipitate do not migrate[17] and appear in order of solubility of the precipitates, with the least soluble appearing first. Usually the zones are not separated from each other by a clear band, but sometimes, slight changes of zone size during washing might result in clear bands.[18] It has been claimed[18] that chromatographic precipitation is more likely "to effect true and clean separation" than other, more common chromatography methods.

A modification of this method, in which only one of the components is precipitated, has been used for the separation of strontium and yttrium. The mixture is applied to a basic column and eluted with water. Strontium, not affected by its passage through the column, is eluted leaving yttrium hydroxide precipitated on the column.[21]

Another modification of chromatographic precipitation has been reported in which the precipitate may be displaced down the column. A nitric acid solution of bismuth, placed on a column of the chloride form of an anion resin, gave a precipitate of bismuth oxychloride which, on washing, moved down the column presumably by a process of dissolution and reprecipitation.[22]

Distillation

The separation of radioactive mixtures by volatilisation of one of the components is very frequently used for separating carrier-free isotopes. When a volatile substance has to be removed from a solution or melt, it is advisable to use an inert gas to sweep the substance from the still; separation of a gas from a solid is generally possible only after fusion.

As examples of distillatory separation mention may firstly be made of cases where the product itself is a gas, or readily convertable to a gas, and secondly, where it may be converted to a volatile compound, usually a halide. Of the first type there are the separations of the rare gases, argon, krypton and xenon produced by the irradiation of the corresponding halogens as their potassium salts,[8] and separated by fusing the salt or by boiling its aqueous solution *in vacuo*. The halogens may be removed in a similar way from their target metals selenium (which yields bromine by a (d,2n) reaction),[8] tellurium (iodine)[24] and bismuth (astatine).[8] Carbon-14 may be separated from nitrogen[25] by heating the aqueous solution of the target, ammonium nitrate, to remove the carbon dioxide and carbon monoxide formed during irradi-

ation, whilst tritium can be recovered[26] as $H_2{}^3O$ by heating the beryllium target in a current of oxygen.

Certain metals, osmium for example, can readily be volatilised as oxides, but this procedure is convenient only if the metal is present in large quantities. When carrier-free quantities of such elements are to be separated it is generally easier to use other methods. However, direct distillations of carrier-free metals are possible in those cases where the required product can be volatilised at a lower temperature than the target element. Thus when a cadmium target is heated *in vacuo*, carrier-free indium, produced by a (d,n) reaction, can be distilled and collected on a cold surface immediately above the heated vessel. This method, when applicable, offers a quick and clean-cut method of separation.

The second type of distillatory separation, conversion to a volatile salt, can be used to separate even very similar elements. For example, germanium bromide can be distilled from a gallium solution,[8] germanium chloride can be separated from arsenic, provided the latter is in its pentavalent form,[8] technetium bromide can be removed from a solution of molybdenum using carbon dioxide as "carrier" gas. An example of a two-stage distillation is the separation of antimony and indium from tin.[5] After preliminary separation by precipitation with carrier, the solution is acidified with perchloric acid. Addition of hydrochloric acid to the solution at 200°C removes all the tin, after which addition of hydrobromic acid removes antimony, leaving indium separated, in solution.

Distillation processes are also frequently used to remove the carrier which had been added for preliminary separation by precipitation. Thus in the separation of palladium from rhodium,[8] the palladium is first coprecipitated with selenium which is then distilled from perchloric acid solution. Similarly tellurium, separated from fission products by coprecipitation on ruthenium sulphide, is obtained carrier-free by volatilization of ruthenium.[8]

Electrodeposition

When electrolytic separation is applied to the carrier-free scale of operation, many unsuspected sources of error occur. Firstly, there is the danger of contamination. Scrupulous cleanliness is essential and frequently a preliminary electrolysis of reagent solutions is advisable. A second serious problem is sorption. It is well-known that a glass surface can act as a good absorber and it may happen that carrier-free quantities are quantitatively adsorbed on to the walls of the container. This difficulty may be overcome by coating the glass walls with wax, or, if it is not necessary to work with carrier-free material, by adding a small amount of isotopic carrier.

Redissolution is another problem. It has, for example, been found impossible to plate out certain oxides since they redissolved as fast as they were formed. The same difficulty arises even after the substance has been successfully plated out, as removal of adhering electrolyte by washing may also effectively remove the small amount of carrier-free element that has been deposited. Naturally the degree of redissolution will be less if washing is effected without switching off the potential across the electrodes, but even then losses of 20 per cent or more are not uncommon.[27]

Often it is sufficient to obtain the desired carrier-free isotope in the form of a deposit on an electrode, but when this is not the case a further difficulty may arise when the plate has to be stripped off the electrode. The best-known example is polonium which can only be redissolved by dissolving the entire platinum electrode. It is not unusual to find an element such as silver remaining strongly adherent to the electrode.

It is perhaps because of these difficulties that electrodeposition is seldom used for isolating carrier-free isotopes. In their review of the subject Garrison and Hamilton[8] cite only two cases of simple electrolytic separation, viz. the separation of copper from zinc and of silver from palladium.

With the observation by Lingane[28] and Griess[29] that polarographic data obtained from the dropping mercury electrode or solid electrodes could be applied to determine the potential at which electroseparation could be carried out, controlled potential electrolysis methods have been developed for a variety of cases such as the separation of silver and copper,[30] rhodium from indium[31] and copper, tin and lead from each other.[32] Such methods have not as yet been applied to carrier-free amounts. By using controlled potential methods in very small volumes of solution, however, it has been possible to separate and determine as little as 5×10^{-9} g. silver.[27]

Ion-exchange

With the production of better ion-exchange resins, both for anion and cation exchange, the principle of separation by ion-exchange has become well known in analytical chemistry. Since the method is equally suited for large and small amounts of material, this separation method finds ready application in separating carrier-free radioisotopes from each other as well as from relatively large amounts of non-isotopic carriers.

Exchange reactions may be carried out either in a batch process or by column operation. In the former, a fixed weight of resin is suspended in the solution under investigation and the system is allowed to attain equilibrium. Such operations are generally favoured for the determination of physical constants such as distribution coefficients, stability constants of complexes, and to establish conditions for separating similar ions. Columns are generally used when the objective is the separation of two ions; the techniques are then the well-known ones of chromatography. Although the interdependence of various factors has not yet been clarified, certain general principles for column separation have been established.[33]

1. The degree of separation increases with column length.
2. A low flow rate favours separation, probably allowing more time for diffusion in the resin.

3. Separation is improved with increased temperature.
4. Resin size is important, as decreased size reduces the distance for diffusion.
5. Increasing the amount of material decreases separation.
6. Increasing the exchange capacity of the resin favours separation.

Once the column operation details have been decided, i.e., length, flow rate, particle size, numerous effects will determine the extent of separation.[34]

1. Natural adsorption differences, e.g., valence, charge, radius, hydration.
2. Natural specificity of the exchanger.
3. pH.
4. Complex formation.
5. State of oxidation or reduction, i.e., absorption affinity.
6. Solvent—changes in dielectric constant.
7. Changes in ionic strength.
8. Selective precipitation.
9. Colloid formation.

The separation of the lanthanides and actinides is a good example of the application of column methods. By 1947 the first successful separation by ion-exchange chromatography was carried out, by elution with tartrate and citrate buffers.[44] The method was soon applied to large scale separation of rare earth elements[45] and has resulted in a marked reduction in price of the purified compounds of these elements. The method has proved useful even on very small scale separations. Using cation exchange Freiling and Bunney[35] were able to separate ten lanthanides produced by uranium fission. The eluent used was lactic acid of constant pH but of varying concentrations. A more rapid method, enabling the six more important fission-produced lanthanides to be separated within twelve hours, used a cation exchange column heated to 87°C. and eluted with lactic acid.[36] As the elements are eluted one at a time in decreasing order of atomic number, it is possible to predict the position of each element. In this way element 61, promethium, was identified[37] and later isolated in milligram quantities.

The identification of the actinides followed similar lines.[33] After americium and curium had been isolated by column techniques a search was made for elements 97 and 98. Using an ammoniumcitrate-citric acid eluent at pH 3·5, americium and curium were eluted and berkelium (element 97) was identified by counting its electron capture in a nucleometer.[38] With californium, element 98, the fractions had to be analysed with a pulse analyser in order to detect small amounts of one α-emitter in the presence of a large amount of curium, which is also an α-emitter. Working on the basis of lanthanide elutions, the exact position of the new element on the column was predicted, and so well was the experiment planned and executed, that the element was discovered in the first attempt even though it was calculated that there were only some 5,000 atoms of californium on the column.[39] This feat was surpassed in the identification of mendelevium, element 101.[40] The element was concentrated, identified by counting its spontaneous fission and an approximation of its half-life was made with only 17 atoms.

As an example of the application of a combined batch and column separation, mention may be made of the separation of carrier-free niobium from zirconium targets.[41] In concentrated hydrochloric acid containing a small amount of fluoride both niobium and zirconium form complexed anions which can be absorded on an Amberlite IRA400 anion resin in the chloride state. Niobium is very strongly retained by the resin, whereas zirconium can readily be eluted with 10N hydrochloric acid. A normal column operation gave the elution curve shown in Fig. 1. When, however, a solution containing carrier-free niobium in a mixture with macro quantities of zirconium, labelled with zirconium-95, was allowed to equilibrate with the resin in concentrated hydrochloric

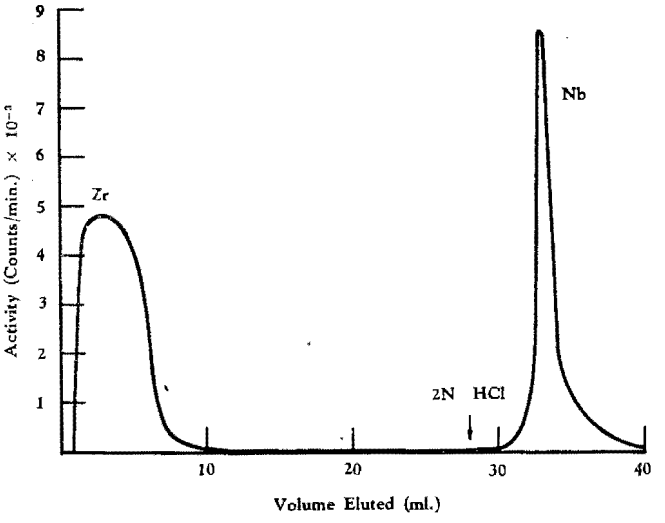

Fig. 1
Ion-exchange chromatographic separation of zirconium and niobium, by normal column procedure
Eluent: 10 N Hydrochloric acid for zirconium
2 N Hydrochloric acid for niobium

acid, niobium was absorbed by the resin, while zirconium remained largely in solution. Thereafter, the niobium-containing resin, separated by centrifugation and washed with concentrated hydrochloric acid, was packed in a column on top of a short length of fresh resin. The elution curve obtained is shown in Fig. 2. Separation of niobium was thus effected in a fraction of the time needed in normal column operations. The method of anion exchange with chloride-complexed metal ions has been applied to a large variety of metals.[42] The absorbed complex may be dissociated by eluting with a solvent in which the complex is no longer stable, thus reverting the metal to a cation which is no longer absorbed.

Solvent extraction

Solvent extraction methods are very suited for separating carrier-free isotopes, as the desired element may be transferred to an organic liquid phase, freed from impurities and re-extracted into an aqueous phase without the dangers of loss or contamination

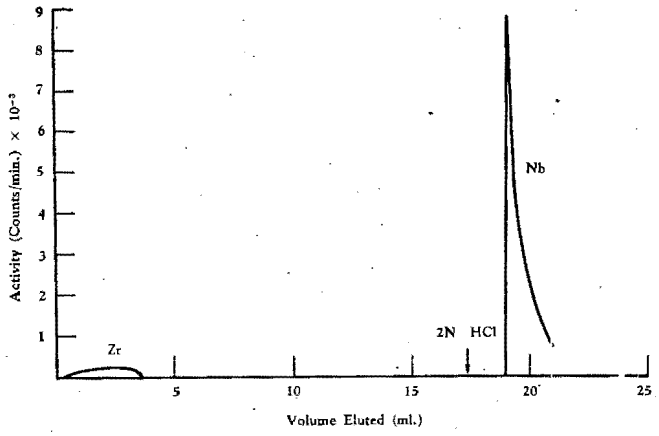

Fig. 2
Ion-exchange chromatographic separation of zirconium and niobium. Preliminary batchwise absorption in concentrated hydrochloric acid followed by column operation
Eluent: 10 N Hydrochloric acid for zirconium
2 N Hydrochloric acid for niobium

that accompany other methods. It is fortunate that, like ion-exchange methods, solvent extraction techniques apply equally to macro and ultra-micro quantities. As a result, values of partition coefficients obtained for larger quantities can be utilized when dealing with carrier-free isotopes. Gallium chloride, for example, extracted as $HGaCl_4$ from 7N HCl with ether or iso-propyl ether, was found to have a constant partition coefficient between 10^{-3} and 10^{-12}M.[43] However it should be remembered that at low concentrations the molecular state of the substance under investigation may frequently differ, e.g. by dissociation

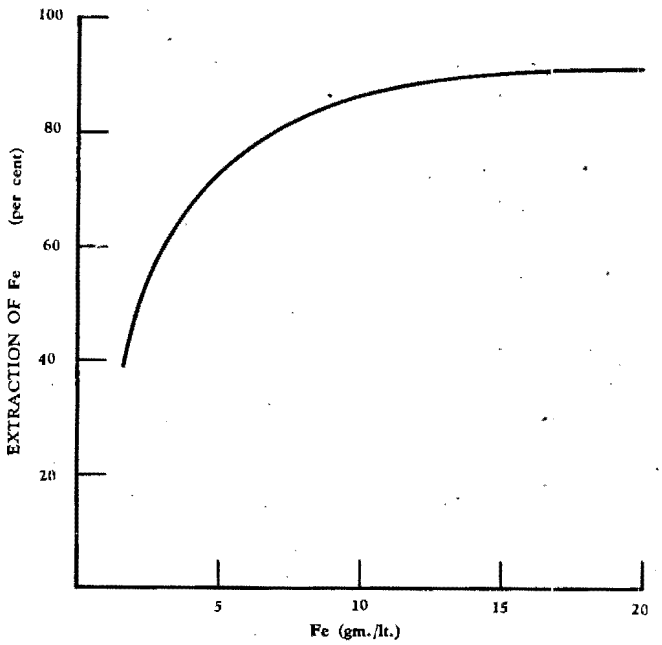

Fig. 3
Extraction of ferric chloride with iso-propyl ether from 5 N hydrochloric acid with different iron concentrations and initially equal volumes of each phase. After Dodson, Forney and Swift[46]

from that in higher concentrations and hence some difference in partition coefficient can be expected.

One of the more important examples of solvent extraction of simple salts is the case of ferric chloride, since it is frequently added during the separation of carrier-free isotopes. It may be removed by extraction from hydrochloric acid solution with many solvents such as diethyl ether, iso-propyl ether, amyl acetate and methyl butyl ketone, but unlike most compounds, the partition coefficient depends on its concentration. The percentage iron extracted by iso-propyl ether from an equal volume 6N hydrochloric acid is shown in Fig. 3.[46] It is obvious that while the method can be used to separate large amounts of ferric chloride, it cannot be applied to the separation of carrier-free radio iron.

The concentration of the acid can have a marked effect on the degree of extraction. Fig. 4 shows this effect for some elements extracted with ether from hydrochloric acid solution.[47]

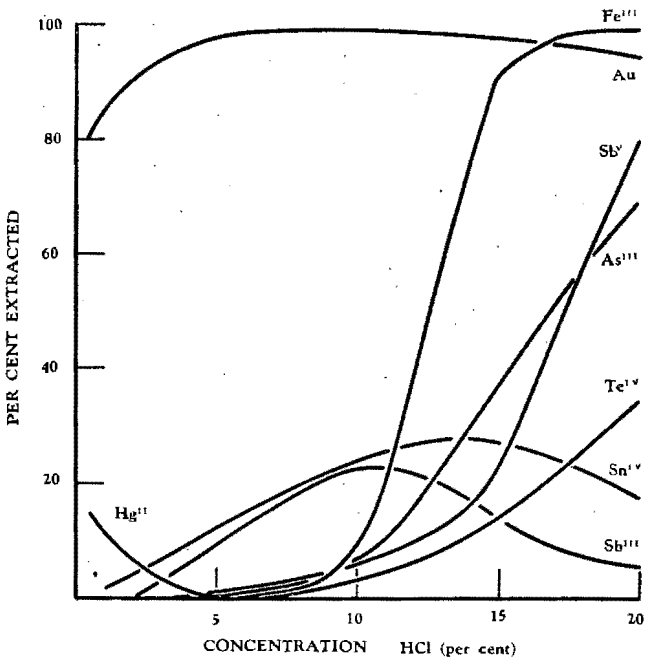

Fig. 4
The influence of hydrochloric acid on the extractability of chlorides, after Irving[47]

With a few exceptions, the behaviour of other halides is very similar to that of the chlorides. At corresponding acid concentrations tellurium is not extracted more than 3 per cent in hydrochloric acid while the value is over 30 per cent in hydrochloric acid. The reverse effect is seen in the case of indium which is completely (99 per cent) extracted from 6N hydrochloric acid, but only a trace (< 1 per cent from hydrochloric acid.[47] The extractability of nitrates is limited to uranium, thorium and cerium. Thiocyanates require a high concentration of ammonium thiocyanate in the aqueous phase and under these conditions scandium (94 per cent), indium (5 per cent) and beryllium (75 per cent) can conveniently be extracted.[47]

The extraction of complexes of metallic ions with organic compounds such as 8-hydroxyquinoline, dithizone and cupferron for the isolation and estimation of small amounts of metals, is a well-known technique in analytical chemistry. The specificness of these reagents depends largely on the conditions used, the most important being pH. For example, it may be possible to separate one element and, continuing with the same sample, to separate another by suitably adjusting the pH.

An example of the use of an extractable chelate is the case of the separation of iron from cobalt using acetylacetone.[48] In the pile irradiation of cobalt iron-59 is formed by $Co^{59}(n,p)Fe^{59}$ accompanied by $Co^{59}(n,\gamma)Co^{60}$. The activity of cobalt-60 far exceeds that of iron-59, but by use of the acetylacetone complex iron can be extracted with xylene at pH 4-7 to give carrier-free iron-59 without contaminating cobalt-60.

Radiocolloid Formation

In concentrations insufficient to exceed the solubility product, carrier-free isotopes may be converted to the colloidal state under those conditions which would have resulted in a precipitate had sufficient material been present. The explanation is not known, but it has been suggested that the carrier-free element conglomerates into colloidal aggregates through adsorption onto colloidal impurities already present in the solution.

This phenomenon has been successfully used in the isolation of carrier-free quantities of several elements, especially those forming insoluble hydroxides. The experimental procedure is then simplicity itself. The solution is merely made alkaline and drawn through a filter paper or sintered glass filter plate which retains almost all the radioelement. Washing with water does not dislodge the deposit, which however readily redissolves in acid.

The method has found application in the separation of beryllium-7 from lithium.[8] The lithium, dissolved in water, produced an alkaline solution which caused the formation of the beryllium radiocolloid. Other isotopes which have been separated by this method are magnesium-27 (from aluminium), scandium-46 (from titanium), yttrium-88 (from strontium) and bismuth-204,206 (from lead).[8]

In addition to the above methods of separation, general chemical separations can be applied, especially to the separation of radioisotopes in compounds prepared by the Szilard-Chalmers reaction. Other methods applicable to the separation of particular isotopes are also being developed. One such example is the separation of silver-111 by isotopic exchange.[49]

Acknowledgement

This paper is published by permission of the South African Council for Scientific and Industrial Research, Pretoria.

REFERENCES

1. Hahn, O., *Z. Elektrochem.*, 1932, **38,** 511.
2. Hahn, O., "Applied Radiochemistry", *Ithaca*, N.Y., Cornell University Press, 1936.
3. Crowley, J., Hamilton, J. G., and Scott, K., *J. Biol. Chem.*, 1949, **177,** 975.
4. *Science*, 1946, **103,** 703.
5. Maxwell, R. D., Gile, J. D., Garrison, W. M. and Hamilton, J. G., *J. Chem. Phys.*, 1949, **17,** 1340.
6. Overstreet, R., Jacobson, L., and Hamilton, J. G., *M.D.D.C.*, 1946, page 1275.
7. Maxwell, R. D., Haymond, H. R., Garrison, W. M., and Hamilton, J. G., *J. chem. Phys.*, 1949, **17,** 1005.
8. Cited by Garrison, W. M. and Hamilton, J. G., *Chem. Rev.*, 1951, **49,** 266.
9. Born, H. J., and Drehman, U., *Naturwissenschaften*, 1945, **32,** 159.
10. Parker, G. W., Reed, J., and Ruch, J. W., *A.E.C.D.*, 1948, page 2043.
11. Gile, J. D., Garrison, W. M., and Hamilton, J. G., *J. chem. Phys.*, 1950, **18,** 995.
12. Willard, H. H., *Anal. Chem.*, 1950, **22,** 1374.
13. MacNevin, W. M., and Dunton, M. L., *Anal. Chem.*, 1954, **26,** 1247.
14. Elving, P. J., and Zook, W. C., *Anal. Chem.*, 1953, **25,** 502.
15. Stine, C. R., and Gordon, L., *Anal. Chem.*, 1953, **25,** 1519.
16. Gapon, E. N., and Belen'kaya, I. M., *Kolloid. Zhur.*, 1952, **14,** 323.
17. Schäfer, H., and Neugebauer, W., *Z. anorg. allgem. Chem.*, 1953, **274,** 114.
18. Gapon, E. N., and Belen'kaya, I. M., C.A., 1954, **48,** 2443c. Issledovaniya v Oblasti Khromatog. Trudy Vsesoyuz Soveschchaniya Khromatog., *Akad. Nauk* S.S.S.R. *Otdel. Khim. Nauk*, 1950, pages 35-40, (published 1952).
19. Prible, R., and Malat, M., *J. Coll. Czech. Chem. Comm.*, 1950, **15,** 121.
20. Herman, J. A., *A.E.C.D.*, page 3637; Los Alamos Sci. Lab. Rept. L.A.M.S. 1625, 1953.
21. Finston, H. L., and Miskel, J., *Ann. Rev. Nuc. Sci.*, 1955, **5,** 269.
22. Samos, G., and Finston, H. L., Cited as private communication in Ref. 21.
23. Flaschka, H., *Z. Anal. Chem.*, 1952, **137,** 107.
24. Perlman, L., Morton, M. E., and Chaikoff, I. L., *Endocrinology*, 1942, **30,** 487.
25. Norris, L. D., and Snell, A. H., *Science*, 1947, **105,** 265.
26. O'Neal, R. D., and Goldhaber, M., *Phys. Rev.*, 1940, **57,** 1086.
27. Rogers, L. B., *Anal. Chem.*, 1950, **22,** 1386.
28. Lingane, J. J., *Ind. Eng. Chem., Anal. Ed.*, 1944, **16,** 147.
29. Griess, J. C. Jr., and Rogers, L. B., *J. Electrochem. Soc.*, 1949, **93,** 129.
30. Diehl, H., and Butler, J. P., *Analyst*, 1952, **77,** 268.
31. MacNevin, W. M., and Tuthill, S. M., *Anal. Chem.*, 1949, **21,** 1052.
32. Lingane, J. J., and Jones, S. L., *Anal. Chem.*, 1951, **23,** 1798.
33. Tompkins, E. R., *Anal. Chem.*, 1950, **22,** 1352.
34. Schubert, J., *Ibid.* 1950, **22,** 1359.
35. Freiling, E. C., and Bunney, L. R., *J. Amer. Chem. Soc.*, 1954, **76,** 1021.
36. Cuninghame, J. C., Sizeland, M. L., Willis, H. H., Eakin, J., and Mercer, E. R., *J. Inorg. Nuc. Chem.*, 1955, **1,** 163.
37. Marinski, J. A., Glendenin, L. E., and Coryell, C. D., *J. Amer. Chem. Soc.*, 1947, **69,** 2781.
38. Thompson, S. G., Cunningham, B. B., and Seaborg, G. T., *ibid.*, 1950, **72,** 2798.
39. Thompson, S. G., Street, K. Jr., Ghiorso, A., and Seaborg, G. T., *Phys. Rev.*, 1950, **78,** 298.
40. Ghiorso, A., Harvey, B. G., Choppin, G. R., Thompson, S. G., and Seaborg, G. T., *Phys. Rev.*, 1955, **98,** 1518.
41. Peisach, M., and van der Walt, S. J., (unpublished data).
42. Kraus, K. A., and Nelson, F., International Conference on Peaceful Uses of Atomic Energy, Session S2, 1955, paper 957.
43. Grahame, D. C., and Seaborg, G. T., *J. Amer. Chem. Soc.*, 1938, **60,** 2524.
44. Tompkins, E. R., Khym, J. X., and Cohn, W. E., *ibid.*, 1947, **69,** 2769.
45. Spedding *et al.*, see Disc. Faraday Soc., 1949, [7], 214; also *J. Amer. Chem. Soc.*, 1947, **69,** 2777, 2786, 2812; *ibid.*, 1948, **70,** 1671; *ibid.*, 1950, **72,** 2349, 2354, 5350; *ibid.*, 1951, **73,** 4840; *ibid.*, 1952, **74,** 856-7.
46. Dodson, R. W., Forney, G. J., and Swift, E. H., *J. Amer. Chem. Soc.*, 1936, **58,** 2573.
47. Irving, H. M., *Quat. Rev.*, 1951, **5,** 200.
48. Kenny, A. W., Maton, W. R. E., and Spragg, W. T., *Nature*, 1950, **165,** 483.
49. Meinke, W. W., and Sunderman, D. N., *Nucleonics*, 1955, **13,** [12], 58.

No. 47

S. Afr. J. med. Sci. (1958), **23**, 34

THE ASSOCIATION OF VITAMIN A ALCOHOL WITH RAT SERUM PROTEINS, *by C. F. Garbers, J. Gillman and M. Peisach (Joint Nutrition Research Unit of the University of the Witwatersrand and the Council for Scientific and Industrial Research, Medical School, Johannesburg, and National Chemical Research Laboratory, Pretoria).*

The evidence in the literature suggests that vitamin A alcohol is solubilised in the blood by combination with the more soluble fraction, most likely with the albumin [Dzialoszynski *et al.*, 1945; Ganguly *et al.*, 1952]. With the improved techniques available it became necessary to ascertain whether vitamin A is bound to a protein and if so to characterise the nature of this protein complex.

In the Nutrition Research Unit the association of vitamin A alcohol with rat serum proteins has been studied with the aid of labelled vitamin A [Garbers, 1956]. By using the appropriate experimental conditions all the vitamin A in the rats blood was present in the form of vitamin A alcohol - 2-C^{14}. This vitamin was found not to be associated either with the low or the high density lipoproteins, but was bound to the proteins which sediment out during the flotation of the liporoteins in the ultra-centrifuge, an observation also made by Krinsky *et al.* [1956] during the progress of our work.

Rat serum proteins were then fractionated by preparative electrophoresis on cellulose columns [Flodin, 1956] using a borate-phosphate buffer pH=8·6, μ=0·05. The protein concentration in these fractions was estimated by optical density measurements at 280 mμ and the location of vitamin A determined by radio activity measurements.

The radio activity was found to be associated with the α_1 - globulin. An excellent correlation was found between the vitamin A alcohol level as determined by colour reaction and as calculated from radio activity measurements on serum. Contrary to the generally accepted view the present investigation discloses that vitamin A alcohol is associated with the α_1-globulin and not with the albumin.

Since it is known that the α_1-globulin consists of various protein components, it was desirable to separate still further the constituents of this complex. This was indeed accomplished through the use of the borate-phosphate buffer. In the electrophoretic separation of the serum proteins, using this buffer, a protein component was found which migrated faster than the albumin. This component possessed the sedimentation rate of a globulin and is a glycoprotein. In the rat most of the mucopolysaccharides are associated with the α_1-globulin (or the albumin). Through the use of the complexing borate ion in the buffer system this glycoprotein component migrates faster than the albumin in the electric field. It might be thought that the migration of the vitamin A complex might also have been altered by the borate-phosphate buffer. However, the position of the vitamin A-protein complex was was unchanged when the non-complexing veronal buffer was used in the electrophoretic separation. Hence it can be concluded that vitamin A alcohol is associated with the α_1-globulin, but not with the α_1-lipoprotein and probably also not with the α_1-glycoprotein.

The authors express their thanks to Dr. D. A. Sutton for the interest he has shown in this work and for very many valuable discussions. We are further indebted to Dr. F. J. Joubert and Mr. P. van Berge for the ultra-centrifugal analysis, and to Mr. N. B. Wasserthal for technical assistance. This communication is published with the permission of the S.A.C.S.I.R.

REFERENCES

DZIALOSZYNSKI, L. M., MYSTKOWSKI, E. M. and STEWART, C. P. (1945). *Biochem. J.*, **39**, 63.
FLODIN, P. (1956). *Biochem. Biophys. Acta*, **22**, 151.
GANGULY, J., KRINSKY, N. I., MEHL, J. W. and DEUEL, H. J. (1952). *Arch. Biochem. Biophys.* **38**, 275.
GARBERS, C. F. (1956). *J. Chem. Soc.*, 3234.
KRINSKY, N. I., CORNWELL, D. G. and ONCLEY, J. L. (1956). *Fred. Proc.*, **15**, 113.

No. 48

THE CARRIER-FREE SEPARATION OF UZ FROM 100 kg URANYL NITRATE

J. VAN R. SMIT, M. PERISACH AND F. W. E. STRELOW

National Chemical Research Laboratory, South African Council for Scientific and Industrial Research, Pretoria, Union of South Africa

Reprinted from

UNITED NATIONS
PEACEFUL USES OF ATOMIC ENERGY

PROCEEDINGS OF THE SECOND INTERNATIONAL CONFERENCE, GENEVA, SEPTEMBER 1958

PERGAMON PRESS
LONDON . NEW YORK . PARIS
LOS ANGELES
1959

Reprint from 2nd UN Geneva Conference.
Printed by Pergamon Press, London.

The Carrier-free Separation of UZ from 100 kg Uranyl Nitrate

By J. van R. Smit, M. Peisach and F. W. E. Strelow*

The first member of the uranium-238 decay series, thorium-234, generally known as UX_1, decays by β emission to the unstable protoactinium-234, which exists in two isomeric states. Of these two nuclear isomers, UX_2 ($t_{1/2}$, 1.14 min) and UZ ($t_{1/2}$, 6.7 hr), the latter has until recently been generally believed to be the ground state (see, for example, Heerschap *et al.*[1]). In a re-investigation of the decay scheme of this so-called UX complex by means of a scintillation coincidence spectrometer, however, Johansson[2] found the reverse to be true.

Ong Ping Hok *et al.*[3] subsequently claimed to have proved UZ to be the ground state of protoactinium-234, but admitted that their suggested decay scheme still had many inconsistencies.

Since the branching factor for the transition to UZ is less than one per cent,[4] a large quantity of uranium is required for the preparation of sufficiently strong UZ sources for refined measurement. Quantities of up to 10 kg of uranyl nitrate (i.e., about 4.7 kg of uranium) have previously been used for this purpose.[3] This paper describes the methods used in this laboratory for the separation of UX_1 from 100 kg of uranyl nitrate and the subsequent milking off from the UX_1 of the UZ activity in a re-investigation of the decay scheme of the UX complex.

SEPARATION OF UX_1 FROM URANIUM†

Previous Work

Previous methods for separating UX_1 from uranyl nitrate solutions utilized a variety of techniques, such as coprecipitation on carbonate, hydroxide and sulphate precipitates, adsorption on animal charcoal, and recrystallization of uranyl nitrate from aqueous solution, resulting in enrichment of UX_1 in the aqueous phase. Radiochemical yields were usually low and separation incomplete. These older methods have been reviewed by Dyrssen.[5]

When crystalline uranyl nitrate is dissolved in ethyl ether the water of crystallization forms a small aqueous layer which contains most of the UX_1. This method has been extensively used in the separation of UX_1 from uranyl nitrate, often only as a first step to separate the bulk of the uranyl nitrate.

During the past few years a number of methods for the uranium–UX_1 separation have been described[5–8] in which cation exchange resins have been utilized, usually after first removing the bulk of the uranium by ether extraction. Owing to its high valency, Th^{4+} is very strongly adsorbed, while UO_2^{2+} is only moderately strongly held. If a solution of uranyl nitrate is percolated through a column of cation exchanger, therefore, the UX_1 is mainly adsorbed near the top of the column.

Uranium may then be selectively eluted from the column by dilute acid, and the UX_1 finally removed by eluting with a solution of a complexing agent for thorium, such as oxalic acid.

Choice of Separation Method

For processing a large bulk of uranium, ether extraction is attractive, since it enormously reduces the scale of the final uranium–UX_1 separation, and this has been applied in previous separations of up to 10 kg uranyl nitrate.

It was felt, however, that the hazard in using the quantities of ether necessary for 100 kg was too great. It was decided therefore to try to separate UX_1 directly from the whole mass of uranyl nitrate by means of an ion exchange column.

Dyrssen[5] systematically investigated the ion exchange method for the uranium–UX_1 separation and showed that UX_1 is much more strongly held by the sulphonated polystyrene resin, Dowex 50, than by sulphonated phenol-formaldehyde condensation resins such as Amberlite IR-100 and Wofatit KS. The latter require less 0.5*M* oxalic acid to elute UX_1, and so are much more suitable for handling gram quantities such as are obtained when the bulk of uranium is first removed by ether extraction. The retention by Dowex 50, however, offers promise of removing UX_1 without preliminary extraction.

* National Physical Research Laboratory, and National Chemical Research Laboratory, South African Council for Scientific and Industrial Research, Pretoria, Union of South Africa.

† Full details of the work on separation of UX_1 are presented in a M.Sc. thesis for the University of Pretoria. "Skeiding van mikrohoeveelhede torium en groot hoeveelhede uraan en die bereiding van 'n draervry monster Th^{234}" by F. W. E. Strelow.

Development of UX_1 Separation

A saturated solution of 100 kg of uranyl nitrate has a volume of about 65 litres, so that a high specificity and retention for UX_1 is essential to reduce handling to a minimum. The feasibility of applying Dowex 50 was therefore further investigated.

Preliminary experiments showed that sharp separation of UX_1 from its equilibrium mixture in 5 g of uranyl nitrate could be attained on a Dowex 50 column, 30 cm long and 1.2 cm in diameter, by eluting the uranium with $2N$ hydrochloric acid and recovering the UX_1 by elution with $0.5M$ oxalic acid, as recommended by Dyrssen.[5] The UX_1 on the column was located by scanning the column with an end-window G-M counter, which readily detects the hard β radiation of its 1.14-min UX_2 daughter.

The scale of operations was then increased to 2 kg of uranyl nitrate. When a saturated solution was passed through a similar column, it was found that only a small fraction of the UX_1 was retained and that the activity was spread evenly throughout the entire resin bed. It is not unusual for the selectivity of an ion exchange column to diminish for a pair of ions if the concentration level is too high, and it seemed possible that this applied in the present case.

In the next experiment, therefore, quantities of uranyl nitrate solutions of different concentrations, but each containing 50 g of the salt, were passed through columns of 200–400 mesh Dowex 50, each 25 cm long and 1.2 cm in diameter. The uranium was then eluted with dilute acid and the distribution of the activity remaining on the columns was measured as before. The results, plotted in Fig. 1, showed that the breakthrough capacity of the resin columns for UX_1 was highly dependent upon uranyl nitrate concentration. Adsorption of UX_1 is more efficient for lower concentrations, but little is to be gained by diluting the solution below a concentration of, say, 150 g/l. The final choice of dilution, however, is also determined by the desire to limit, to a minimum, the final volume of liquid to be processed. As a compromise, therefore, a concentration of about 250 g/l, corresponding to a six-fold dilution of saturated uranyl nitrate and a total volume of 400 litres, was selected. This was passed through ten columns in parallel, each containing about 100 ml of resin, at a flow rate of about 1 cm/min. The UX_1 was then confined to the upper two-thirds of each column. Details are elaborated later.

Elution of UX_1 from Resin Columns

Dyrssen[5] reported that removal of UX_1 from Dowex 50 by $0.5M$ oxalic acid was incomplete, so that other complexing agents such as citric acid, tartaric acid, ethylenediaminetetraacetic acid were investigated. They proved poorer elutriating agents than oxalic acid. An advantage of oxalic acid is that it is readily driven off on heating, permitting easy recovery of the UX_1.

To improve the efficiency of oxalic acid elution, a saturated solution, approximately $1M$ at our room temperature, was used. Since the UX_1 activity is

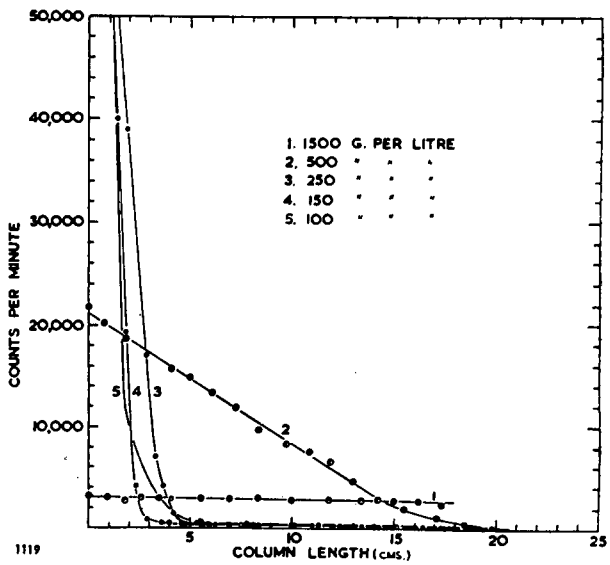

Figure 1. Distribution of UX_1 in Dowex 50 columns after 50 g of uranyl nitrate solutions of different concentrations were passed through each column

eluted from the resin mainly as the uncharged complex $Th(Ox)_2$ or as one or more negatively charged oxalate complexes, mass action indicates that desorption of UX_1 will increase with the square of the oxalic acid concentration or even a higher power. Increasing the oxalic acid concentration should thus enhance the efficiency of UX_1 desorption for a fixed amount of oxalic acid. This was confirmed by experiment, and, by use of saturated solutions, 95% recovery of UX_1 activity was achieved with eight to ten column volumes.

Since the solubility of oxalic acid rises steeply to $9.5M$ at 90°C,[9] the efficiency should increase further by eluting at elevated temperatures; but this was not considered necessary in the present work.

Purification of UX_1

The next step was to evaporate the UX_1 solution to dryness, followed by the removal of oxalic acid by sublimation. In our experiments, the solid residue usually amounted to several grams. This residue, consisting mainly of oxides of uranium which had been incompletely removed in the earlier elution step with dilute acid, was then taken up in hot aqua regia. After suitable dilution the solution, containing some finely dispersed insoluble particles, was now passed through a Dowex 50 column with a bed volume of about 3 ml, followed by washing with dilute acid to displace uranium. However, subsequent elution with more than fifteen column volumes of oxalic acid solution failed to remove more than about half the UX_1 activity. This was ascribed to the occlusion of some UX_1 by the insoluble particles, which had been retained in the column by the filtering action of the resin bed. The activity was therefore recovered instead by ashing the resin, followed by fusion with anhydrous sodium carbonate. After cooling, the melt was dissolved in dilute acid and any insoluble residue solubilized by fusion with potassium bisulphate.

To obviate possible interference in the UX_1–UZ separation by the large amount of salts introduced as a result of the fusions, the UX_1 was isolated by extraction into 60% tributyl phosphate in carbon tetrachloride. The activity was back-extracted with oxalic acid solution and, after sublimation of the oxalic acid, finally recovered almost free from salts or other impurities.

Separation of UZ from UX_1

In the past this has usually been achieved by coprecipitating the UZ activity on hydrated tantalic oxide.[10] However, yields obtained were poor and separation usually rather incomplete.

Dutch workers[4, 8] have recently developed an ion exchange method in which the UX complex is adsorbed on a column of low capacity cation exchanger. After allowing sufficient time for secular equilibrium to be established, UZ, with associated short-lived UX_2, was selectively eluted with a citrate solution. The initial fractions of UZ activity so obtained were contaminated by only about 0.2% UX_1. As the UX_1 contamination increases with continued elution, UZ yields of between 20 and 45% were considered sufficient. At this level the contamination amounted to about 1% of the initial UZ activity.

Kraus and Nelson,[11] in a systematic study of the anion exchange of metals in hydrochloric acid solution, have shown that the adsorbability of protoactinium, while negligible at concentrations below $3M$, rises sharply with increasing hydrochloric acid concentration. Thorium, on the other hand, shows negligible adsorption over the entire range of hydrochloric acid concentration.

This permits a simple column separation of UZ from UX_1. Thus, if a solution of the UX complex in concentrated hydrochloric acid ($\sim 12M$) is passed through a column of anion exchange resin, UZ is selectively adsorbed as the chloro complex, while UX_1 passes through. The column may now be washed free of UX_1 with concentrated hydrochloric acid and the UZ finally eluted with dilute hydrochloric acid. In view of the hydrolytic behaviour of protoactinium in very dilute acid medium, the relatively high acidity of $3M$ hydrochloric acid was employed, which still permits rapid elution.

It should be possible, in principle, to remove all traces of UX_1 from the column by washing sufficiently long with concentrated hydrochloric acid. On account of the low branching factor for UZ the ratio UZ:UX_1 activity in the UX complex (when in secular equilibrium) is of the order 1:200. Hence, preparation of a UZ source containing 0.1% UX_1 contamination would require separation with a decontamination factor of 200,000.

In this work it was found expedient to employ two anion exchange columns. The hydrochloric acid solution containing the UX complex was percolated through the first column and UX_1 washed out with $10M$ hydrochloric acid until the activity of single drops of effluent, as measured with a laboratory monitor, was not more than double the background level. UZ was next eluted with $3M$ hydrochloric acid and the eluate evaporated to dryness. The residue was redissolved in concentrated hydrochloric acid and passed through the second column. Only a few column volumes were now required to completely wash out UX_1 activity. UZ was then recovered by elution with $3M$ hydrochloric acid. Evaporation of this solution yielded a thin UZ source suitable for β spectroscopy. β and γ spectra of sources of UZ, prepared in this way, were re-examined after four days' decay. Over the entire energy range the observed counts lay within the statistical variation of background, proving the absence of UX_1.

Although the radiochemical yield at each step was not measured, careful monitoring throughout ensured no serious losses. Furthermore, the activity of the sources indicated a good overall yield.

METHOD

Materials

Uranyl nitrate solution. About 60 kg of 92%U_3O_8, obtained from Messrs. Calcined Products, Johannesburg, were dissolved in hot nitric acid. After insoluble material, mostly oxides of iron, was removed by filtration and centrifugation, the solution was evaporated and uranyl nitrate allowed to crystallize. A saturated solution of these crystals at room temperature was diluted six-fold to give a concentration of about 250 g/l. As carrier-free UX_1 was required, it was necessary to remove traces of long-lived natural thorium. The entire solution was passed through the cation exchange columns (see below) and the resin discarded. No further efforts were made to free the solution of other soluble impurities. This solution was then left for about three months to allow UX_1 to grow (to about 90% of saturation activity).

Ion exchange resins. For the separation of UX_1, 200–400 mesh, Dowex 50, cation exchange resin was used in the hydrogen form as received. The anion exchange resin was 100–200 mesh Amberlite IRA-400, hydroxide cycle, converted to the chloride form by batch treatment with hydrochloric acid.

Tributyl phosphate (TBP). A 60% (v/v) solution of TBP in AnalaR carbon tetrachloride was prepared and purified by repeated extraction with $0.5M$ oxalic acid solution, followed by washing with distilled water.

Concentrated hydrochloric acid. The concentrated hydrochloric acid used for the UZ separation was passed through a column of anion exchange resin to remove any traces of ferric iron, whose anion exchange properties resemble those of protoactinium.

Other reagents. In the procedure up to and including the sodium carbonate fusion stage, laboratory grade reagents were used; thereafter all reagents, except for TBP, were of analytical grade purity.

Apparatus

The apparatus is diagrammatically represented in Fig. 2. It consisted of ten glass columns in parallel,

each about 3.5 cm in diameter and 50 cm high. Beds of Dowex 50, supported by a sealed-in sintered glass disc, were packed into each column to a depth of about 10 cm. Conditions were arranged so as to allow the uranyl nitrate solution to pass through continuously. With a column head of 30 to 50 cm, a flow rate of about 1 cm/min was obtained. Under these conditions all the solution, about 400 litres, was processed in three to four days.

Procedure

The solution of uranyl nitrate was passed through the columns, checking the position of the UX_1 front with a monitor from time to time to ensure that breakthrough did not occur. When all the solution had been processed, the resin was transferred to one large glass column of about 12 cm in diameter. Uranium was eluted with $2M$ nitric acid until the yellow colour of the uranyl ions could no longer be distinguished in the effluent. The effluent was then evaporated to a small volume to drive off most of the acid and, after suitable dilution, was returned to the original uranyl nitrate solution.

About four more column volumes of $3M$ nitric acid were passed through the resin column to reduce the last traces of uranium held to a minimum. The nitric acid was washed out with two column volumes of distilled water and discarded. UX_1 was now recovered by elution with eight to ten column volumes of saturated oxalic acid, or until the activity of the lower portion of the column, as measured by a scanning monitor, was sufficiently reduced.

The effluent was evaporated to dryness and further heated to sublime off oxalic acid. The residue was taken up in the minimum amount of hot aqua regia and diluted six-fold with water. After filtering, the undissolved residue was washed with $2M$ nitric acid. The combined filtrate and washings were passed through a small Dowex 50 column, 5 mm in diameter and about 1.5 cm high, while continually monitoring to ensure that all the UX_1 was retained.

Uranium was then eluted from the column with about 20 ml of $3M$ nitric acid. Thereafter the resin was quantitatively transferred to the same filter used above. The filter and its contents were carefully ashed in a 25-ml platinum crucible and the ash fused with about 2 g of anhydrous sodium carbonate. After cooling, the melt was dissolved in a small volume of dilute nitric acid. Insoluble material was solubilized by a further fusion with potassium bisulphate.

The final solution was evaporated down to a volume of about 15 ml, and 30 ml of concentrated nitric acid were added. Sufficient solid ammonium nitrate was added to produce an almost saturated solution. The UX_1 was extracted with four or five 10-ml portions of 60% TBP in carbon tetrachloride. The UX_1 was back-extracted from the organic phase with five 10-ml portions of $0.5M$ re-sublimed oxalic acid. The oxalic acid solution was washed with three 5-ml portions of CCl_4 to remove last traces of TBP. The solution was then evaporated to dryness, the oxalic acid removed by sublimation, and the residue taken up in 2 ml of concentrated hydrochloric acid.

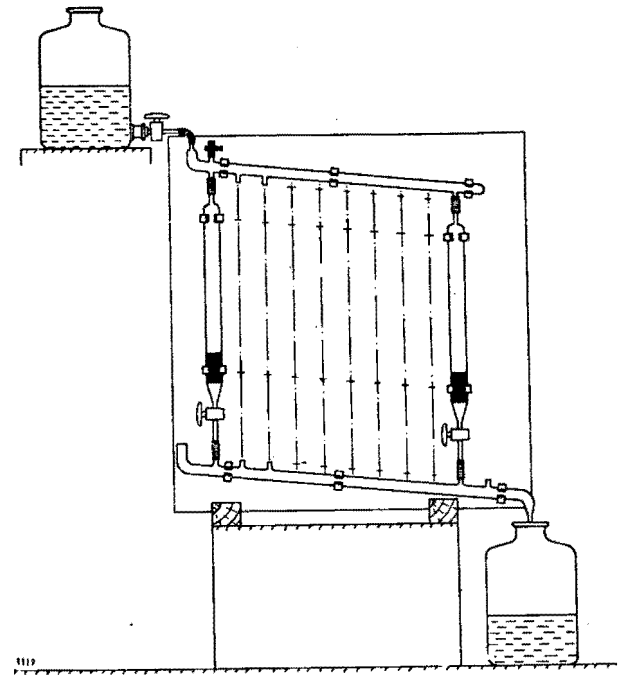

Figure 2. Diagram of apparatus for the separation of UX_1 from large quantities of uranyl nitrate solution

Two short columns of diameters 3 mm and 2 mm were packed with the anion exchange resin to a depth of 13 and 8 mm, respectively, and conditioned by passing 5 ml of concentrated hydrochloric acid through them prior to use. The UX_1 solution was percolated through the larger column and the column was washed with 2 ml of $10M$ hydrochloric acid. This procedure removed the bulk of UX_1, leaving UZ adsorbed on the column. The eluate was evaporated to dryness, taken up in 2 ml of concentrated hydrochloric acid, and was then ready for another milking, after allowing sufficient time for the 6.7-hr UZ to grow.

The column was then washed with small quantities of $10M$ hydrochloric acid until the activity of single drops of effluent was not more than double background level.

The UZ activity was recovered by eluting with 2 ml of $3M$ hydrochloric acid, evaporated to dryness and taken up in 1.0 ml of concentrated hydrochloric acid. This solution was passed through the smaller column and washed with $10M$ hydrochloric acid to remove last traces of UX_1. The UZ was then again eluted with $3M$ hydrochloric acid and the eluate collected in a small, shallow, conical glass container, the walls of which had been treated with silicones to render them water-repellent. The solution was evaporated by infrared heating to a volume of about 0.05 ml, after which it was transferred to the source-holder and evaporated to dryness.

Milking of UZ was completed in four to five hours. In this way, UZ sources were prepared on alternate days as long as the 24-day UX_1 activity was sufficiently strong.

REFERENCES

1. M. Heerschap, Ong Ping Hok and G. J. Sizoo, *The Beta-Radiations of UX_1 and UX_2*, Physica, *16*, 767–780 (1950).
2. S. A. E. Johansson, *Decay of UX_1, UX_2 and UZ*, Phys. Rev., *96*, 1075–1080 (1954).
3. Ong Ping Hok, J. T. Verschoor and P. Born, *The Decay of the UX-complex*, Physica, *22*, 465–480 (1956); Ong Ping Hok, *The Beta-Decay of Protoactinium Isotopes*, Thesis Vrije Universiteit, Amsterdam (1955).
4. W. L. Zijp, S. Tom and G. J. Sizoo, *The γ-β-Branching Ratio of UX_2. The Half-life of UZ*, Physica, *20*, 727–735 (1954).
5. D. Dyrssen, *The Preparation of Carrier-free Thorium-234 (UX_1) by Ion Exchange*, Svensk Kem. Tidskr., *62*, 153–164 (1950).
6. T. Vestermark, quoted by Dyrssen Ref. 5.
7. G. K. Schweitzer and I. B. Whitney, *Radioactive Tracer Techniques*, New York (1949).
8. F. Barendregt and S. Tom. *A Carrier-free Separation of UZ from UX*, Physica, *17*, 817–820 (1951).
9. C. D. Hodgman (Editor in Chief), *Handbook of Chemistry and Physics*, Chemical Rubber Pub. Co., Cleveland (1957).
10. E. Jacobi, *Trennung des UZ von UX*, Helv. Chim. Acta, *28*, 757–758 (1945).
11. K. A. Kraus and F. Nelson, *Anion Exchange Studies of the Fission Products*, Proceedings of the International Conference on the Peaceful Uses of Atomic Energy, Geneva 1955, P/837, Vol. 7, p. 113, United Nations, New York (1956).

No. 49

Communication to the Editor

SKIN DECONTAMINATION OF PHOSPHORUS - 32

W. R. McMURRAY, M.Sc. (Natal), D.Phil. (Oxon.).

M. PEISACH, M.Sc., Ph.D. (Cape Town), A.R.I.C.

Radioactivity Division:
Council for Scientific and Industrial Research,
Pretoria.

In radiochemical practice, the most stringent precautions against spillage of radioactivity and contamination of personnel cannot entirely eliminate the occasional accident. It is therefore necessary to be cognisant of the recognized methods of decontamination so that quick action can be taken after an accidental spill. The hands (in the event of ruptured gloves), arms and head are the most vulnerable parts of the body — the rest will usually be protected by clothing.

An example of the type of accident which can give rise to skin contamination occurred recently in this laboratory. The routine operation of removing radioactive liquid from a glass bottle (as received from Amersham Radiochemical Laboratory, England), is accomplished by piercing the rubber cap with a syringe needle and withdrawing solution into the syringe. In this instance, the cap gave way and up to 100 millicuries of carrier-free Phosphorus-32 (in the form of orthophosphate in hydrochloric acid) were splashed on to the surrounds. A radiation survey of the operator showed contamination on the lip as well as on the arms and an intense spot of activity above the rim of the short protective rubber gloves which were themselves very badly contaminated. The wrist activity gave a count-rate of 40,000 c.p.m. in a thin end window geiger counter.

This level of contamination is to be compared with a recommended upper limit of skin contamination of about $10^{-4}\mu c/cm^2$ for β-emitting isotopes and a corresponding geiger counting rate of about 150 c.p.m. Whereas the accepted maximum permissible level of radiation dose to the basal layer of the skin is 0·6 rad/week, the contamination level giving 40,000 c.p.m. corresponds to a dose to the epidermus exceeding 1·0 rad/hour. Admittedly, the normal wear of the surface layers of the skin will usually considerably reduce skin contamination in a matter of days and it is also true that P-32 absorption into the body is a relatively small hazard (a continuous burden of $10\mu c$ P-32 distributed through the body bone constitutes an acceptable risk), it is nevertheless certain that unnecessary radiation dose to any part of the body must be regarded as definitely undesirable.

An accepted procedure for the decontamination of the skin is as follows:

(i) Brush lightly with soap and water. If this fails:

(ii) Apply Titanium Dioxide paste and wash off with soap and water. As a further attempt:

(iii) Wash with EDTA-soap mixture. As a last resort:

(iv) Wash with a saturated potassium permanganate solution and after rinsing in water, remove the stain with a 5 per cent solution of sodium bisulphite.

Skin decontamination procedures should not be allowed to roughen or crack the skin as this will increase absorption of the radioactivity into the body.

In this particular case the more diffused contamination on face and arms was removed by step (i) but the intense activity on the wrist resisted all the above treatments. However, the desired result was achieved unexpectedly by shaving off the arm hairs. Evidently most of the activity was firmly absorbed on the hairs. We are thus led to add another step to the decontamination procedure:

(v) Hair removal.

Profiting further from this experience, operations of the type which led to the accident, will in future be conducted from behind a half-inch perspex screen with source manipulation through arm length neoprene rubber gloves attached to ports in the screen.

This note is published with the permission of the Council for Scientific and Industrial Research.

Reprinted from THE SOUTH AFRICAN INDUSTRIAL CHEMIST, December, 1958 LSG—40003

No 50

S. Afr. J. Med. Sci. (1958), **23**, 278—279.

A PRELIMINARY REPORT ON THE METABOLISM OF 2-C^{14}-PYRUVATE IN DIABETIC BABOONS,

by N. Savage, J. Gillman and C. Gilbert (C.S.I.R./University Joint Nutrition Research Unit and Department of Physiology, University of the Witwatersrand, Johannesburg) and M. Peisach (National Chemical Research Laboratory, Pretoria).

The elevation of the blood ketones and of the various serum lipids and the increase in the fat content of the liver in depancreatized baboons are controlled by a specific participation in metabolism of the endocrine glands [Gillman, Gilbert and Allan, 1958].

From a study of the altered metabolism supervening in the depancreatized baboon it was anticipated that some information might be forthcoming about the biochemical site of action of the various endocrine glands. As part of this study it became necessary to ascertain whether or not 2-C^{14}-pyruvate would be incorporated into the various lipid fractions of the serum and of muscle, liver and omental fat in a depancreatized insulin deprived baboon.

A pancreatectomized male baboon received intravenously a total of 500 μc. of 2-C^{14}-pyruvate over a period of three days. 103 μc. were injected 24 hours after the baboon last received insulin; a further 177 μc. were injected at the 48th hour, the remaining 220 μc. at the 81st hour; 20 hours thereafter the animal was placed under pentothal anaesthesia and pieces of liver, muscle and omental fat removed for isolation of lipids. Prior to the operation blood was removed for the isolation of serum lipids and blood ketones. Urine was collected over a 48 hour period prior to the operation for the isolation of urinary ketones.

Serum and tissue lipids were extracted by slight modification of standard procedures. The extracted lipids were then fractionated by standard methods and the cholesterol and free fatty acids of triglycerides and phospholipids isolated. Ketone bodies were isolated by a method to be described.

For the determination of the C^{14} activity all samples were combusted to CO_2 by the method of Van Slyke, Plazin and Weisiger [1951], and finally plated as $BaCO_3$. In most cases all samples were combusted in duplicate. In the various fractions the following results were obtained:

(1) *Triglycerides.* Despite a considerable rise in the triglyceride fractions of both liver and serum very low levels of radioactivity were detected in the fatty acids derived from the triglycerides of the serum, liver, muscle and omental fat.

(2) *Phospholipids.* The fatty acids of the phospholipids found in the liver and serum show C^{14} incorporation, at levels higher than those of the fatty acids of the triglycerides. The fatty acids of the phospholipids in muscle and omental fat show very low levels of radioactivity.

(3) *Cholesterol.* C^{14} is definitely incorporated into the cholesterol of the liver, serum and omental fat. Significant, but considerably less radioactivity, occurs in the cholesterol of muscle.

(4) *Ketones.* Blood ketones show comparatively little activity. The acetoacetate fraction of urine shows high levels of radioactivity. Lower, but none the less significant, levels of radioactivity are observed in the p-hydroxybutyric acid fraction.

The above results indicate that (1) in the insulin deprived baboon very little synthesis of the fatty acids of triglycerides occurs by way of pyruvate. In this connection it should be mentioned that in the livers of alloxanised diabetic rats, lipogenesis is suppressed [Stetten and Boxer, 1944], fatty acid is synthesised neither from acetate [Brady and Gurin, 1950] nor from pyruvate [Osborne, Chaikoff and Felts, 1951]; (2) the fatty acids of phospholipids found in the liver and serum can be synthesised in part from pyruvate; (3) Cholesterol found in the liver, serum and omental fat can be synthesised in part at least from pyruvate in the diabetic baboon in contrast to Bloch's and Rittenberg's [1945] failure to find such synthesis in normal animals; and (4) finally in diabetic baboons, ketone bodies of the urine can be derived in part from pyruvate in contrast again to Bloch's assertion [1947] that acetoacetate does not arise from a pyruvate precursor in normal animals.

We are indebted to Mr. J. Allan, Department of Surgery, for performing the pancreatectomy. The technical assistance of Mrs. R. Agulhas and Mr. D. Stirling is also gratefully acknowledged.

REFERENCES

BLOCH, K. (1947). *Physiological Reviews*, **27**, 574.
BLOCH, K. and RITTENBURG, D. (1945). *J. biol. Chem.*, **159**, 45.
BRADY, R. O. and GURIN, S. (1950). *J. biol. Chem.*, **186**, 461; **187**, 589.
GILLMAN, J., GILBERT, C. and ALLAN, J. C. (1958). *Brit. med. J.*, Nov. 22nd, 1260.
OSBORNE, M. J., CHAIKOFF, I. L. and FELTS, J. M. (1951). *J. biol. Chem.*, **193**, 549.
STETTEN, D. and BOXER, G. E. (1944). *J. biol. Chem.*, **156**, 271.
VAN SLYKE, D. D., PLAZIN, J. and WESIGER, J. R. (1951). *J. biol. Chem.*, **199**, 299.

No. 51

Reprinted from
THE JOURNAL OF THE SOUTH AFRICAN CHEMICAL INSTITUTE,
October, 1959, Vol. XII, pp. 116-118.

Oorgedruk uit
DIE JOERNAAL VAN DIE SUID-AFRIKAANSE CHEMIESE INSTITUUT,
Oktober 1959, Deel XII, bl. 116-118.

C.P.W.-P.M.B.

NOTES

THE ISOLATION OF RADIOSILVER BY ISOTOPIC EXCHANGE

by **M. PEISACH and S. J. VAN DER WALT**

NOTES

THE ISOLATION OF RADIOSILVER BY ISOTOPIC EXCHANGE

by

M. PEISACH and S. J. VAN DER WALT

Meinke and Sunderman[1] showed that sources of silver-111 could be prepared by isotopic exchange between dissolved and solid silver salts, and that about 98% recovery could be obtained with 5 mg silver carrier in the form of silver iodide on an inert grid. Since for nuclear spectroscopy it is essential that the amount of carrier should be as low as possible, this investigation was undertaken to determine how far the weight of silver iodide could be reduced without seriously affecting the recovery of radiosilver.

EXPERIMENTAL

Platinum grids were coated with varying weights of silver iodide by electroplating silver at 3 volts from a solution of 3M sodium cyanide, 0·5M sodium hydroxide and 0·01M silver nitrate, and converting it to iodide by electrolysis at 1·5 volts in a solution of 0·05M hydrogen iodide and 0·05M sodium bisulphite. The grids were washed and stored in 1:1 nitric acid.

For the exchange reaction the coated grids were rotated in a solution of radiosilver and the course of the reaction was followed by periodically measuring the activity of the solution. A plot of the percentage activity removed from solution against the duration of exchange is shown in Fig. 1 for grids with 1·45, 0·89, 0·23 and 0·14 mg silver iodide respectively. For small weights of silver iodide recovery is poor, and begins to fall sharply within a reasonably short time due to the photolytic decomposition of silver iodide. For recoveries of about 70% about 1 mg silver iodide is required.

To recover the isolated radiosilver, the silver iodide was dissolved in a solution of 3M sodium cyanide and 0·05M sodium hydroxide, and the silver was electroplated on to a platinum needle at 3 volts. The potential was then raised to 3·5 volts while the electrode was removed from solution and washed with a 1% solution of sodium nitrate. Fig. 2 shows the dependence of the rate of deposition of silver on the initial concentration of silver. For low concentrations of silver initial electrolysis removes the silver ions from solution in the immediate vicinity of the electrode and subsequent deposition will depend on the diffusion of ions towards the electrode. Accordingly, with decreasing concentration of silver there will be a large increase in the time required to recover the bulk of the silver. It can be shown from calculations of deposition rates that this method is impractical for the recovery of short-lived silver isotopes such as silver-112 and silver-113 and can be applied to longer-lived isotopes only when the weight of silver iodide carrier exceeds about 1 mg.

From the study of the exchange reaction as well as the subsequent recovery of exchanged silver by electrodeposition it is concluded that about 1 mg silver iodide is required. Since this amount of carrier produces a relatively thick source, the method of isotopic exchange cannot be used to prepare sources of radiosilver for nuclear spectroscopy.

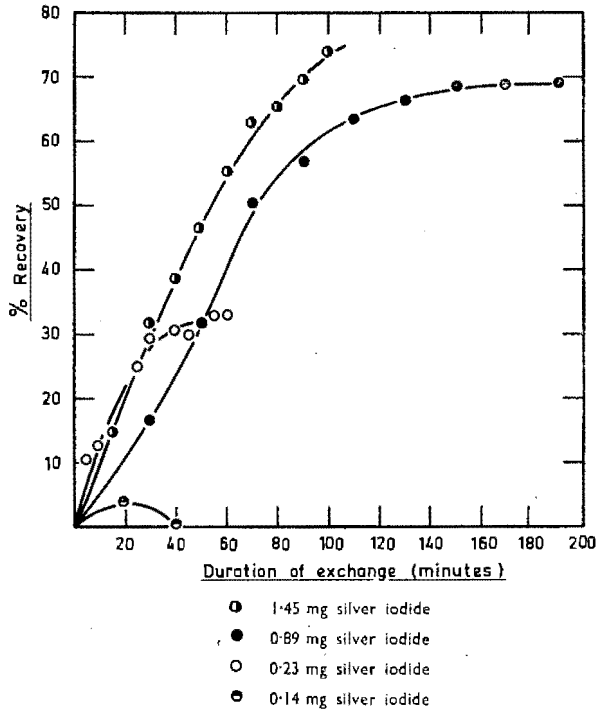

FIG. 1—The effect of the weight of silver iodide on the exchange reaction

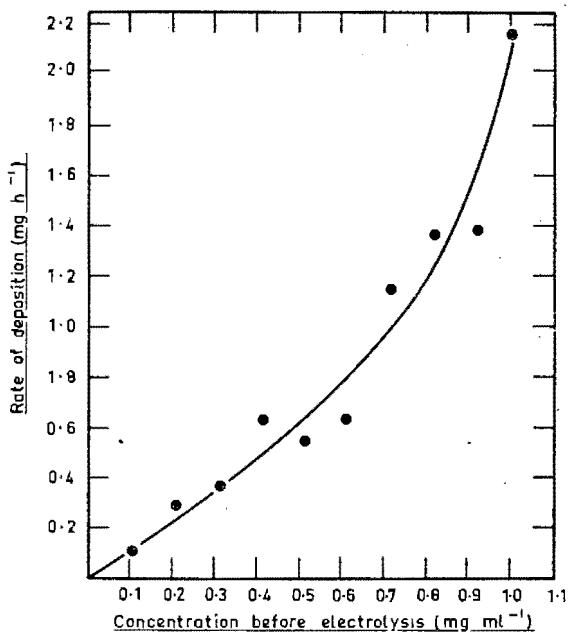

FIG. 2—The effect of concentration on the electrolysis of silver

This note is published with the permission of the South African Council of Scientific and Industrial Research.

National Chemical Research Laboratory,
South African Council for Scientific and Industrial Research,
Pretoria. *Received February* 2, 1959.

REFERENCES

[1] Meinke and Sunderman, *Nucleonics*, 1955, **13**, No. 12, 58.

No. 52

When high energy radiations such as alpha and beta particles, gamma and X-rays and accelerated ions pass through matter, their energy is transferred to the electrons in the system resulting in ionization and excitation of the molecules present. The study of chemical reactions produced by these ionized and excited molecules is called radiation chemistry. It differs from photochemistry in three important respects. Firstly, there is no selectivity since any component of the system can absorb energy by a primary act. Secondly, whereas one photon in photochemistry can generally excite only one molecule, in radiation chemistry the number of molecules affected is generally large and depends on the energy and nature of the incident photon or particle, and thirdly, these affected molecules are not homogeneously produced in the system, but are concentrated along the track of the photon or particle.

Closely allied to this field is the study of chemical effects of nuclear transformation. When a nucleus captures or emits a high energy photon or particle it may recoil with so much energy that in the process of thermalization it can break many chemical bonds in its immediate vicinity. These reactions, normally called "hot atom chemistry", are however not considered in this paper.

THE CHEMICAL EFFECTS OF RADIATION

M. PEISACH

Senior Research Officer
Radiochemistry Section, National Chemical Research Laboratory
Paper read at the XII Convention of the South African Chemical Institute, Port Elizabeth, July 1958

Early investigations had shown that, when dilute aqueous solutions were irradiated, hydrogen and hydrogen peroxide were the main products and that ferrous solutions were oxidized whereas ceric solutions were reduced, but the first real step in understanding the mechanism of this change was made by Weiss[1] when he postulated the formation of free atoms of hydrogen and hydroxyl radicals. At present it is generally accepted that the primary ionization is the removal of an electron from a water molecule. The ionized water is converted to hydroxyl radicals whilst the emitted electron usually has sufficient energy to cause further ionizations, each ionization resulting in a decrease in energy until the electron is finally captured. Thus, the reactions that occur are:

$$H_2O \longrightarrow H_2O^+ + e^-$$
$$H_2O + H_2O^+ \longrightarrow H_3O^+ + OH$$
$$H_2O + e^- \longrightarrow (H_2O^-) \longrightarrow H + OH^-$$

In addition to ionization, water molecules can become excited and undergo dissociation to hydrogen atoms and hydroxyl radicals directly. In gases the number of molecules dissociating through ionization is roughly equal to that dissociating by excitation.[2] It is likely that dissociation processes are of equal importance in liquids.[3]

Samuel and Magee[4] have calculated that along the track of, say, Co^{60} gamma-radiation several radical pairs (H and OH) can be produced in separate "hot spots" which may have an initial radius of about 3·7 Å and which are removed from the adjacent "hot pot" by about 5000 Å. Accordingly by the time diffusion has enlarged the radius of such a spot to a value large enough to overlap the next spot, recombination processes are virtually completed. Most of the molecular products of radiation are considered to be formed by recombination of the radicals by

$$H + OH \longrightarrow H_2O$$
$$H + H \longrightarrow H_2$$
$$OH + OH \longrightarrow H_2O_2$$

and that only those radicals which escape are available for reaction with other entities. It therefore follows that the molecular yield of hydrogen and hydrogen peroxide will be higher for radiations such as alpha-particles which produce denser ionization in their tracks than for gamma or X-rays.

These deductions are confirmed by experimental results. Hart[5] has summarized the yields of the radiation products of various systems irradiated by gamma and X-rays as well as tritium beta-particles and polonium

alpha-particles. Some of his values are selected in Table I.

Let the nett free radicals escaping recombination in stoichiometrically equal quantities be represented by reaction **1** and the nett radical recombination by reaction **2**. Reaction **3** gives the excess of hydrogen atoms and hydrogen peroxide surviving reaction **2** in accordance with the work of Dainton and Sutton[6] who showed that the molecular yield of H_2O_2 exceeds that of H_2.

$$H_2O \longrightarrow H + OH \quad \text{.....1}$$
$$H_2O \longrightarrow \tfrac{1}{2}H_2 + \tfrac{1}{2}H_2O_2 \quad \text{.....2}$$
$$H_2O \longrightarrow H + \tfrac{1}{2}H_2O_2 \quad \text{.....3}$$

If G_1, G_2 and G_3 refer to the number of water molecules decomposed per 1^{00} eV in reactions **1**, **2** and **3** respectively, it can be readily seen from Table I that with increasing density of ionization G_1 decreases and G_2 increases, and furthermore that the ratios $G_2/G_1 + G_2$ are in very good agreement with the values of 0·23 for CO^{60} gamma-rays, 0·315 for H^3 beta-rays and 0·887 for Po^{210} alpha-rays as calculated by Samuel and Magee.[4] Another interesting point is that the total number of water molecules decomposed per 1^{00} eV, $G_{tot.}'$ is about 4, substantially independent of the type of radiation used.

The initial effects of radiation on aqueous systems can thus be summarized as:—

1. the formation of free radicals and molecular products generally written as
   $H_2O \rightsquigarrow H, OH, H_2O_2, H_2$ **4**
2. the molecular yield of hydrogen and hydrogen peroxide is increased for densely ionizing radiation whilst radicals are the main products from gamma and X-radiation;
3. the number of water molecules decomposed per 1^{00} eV is about 4, independent of the type of radiation.

The Oxidation of Ferrous Solutions

The oxidation of ferrous solutions in the presence of oxygen and in oxygen-free solutions has been studied extensively since this reaction forms the basis of the Fricke dosimeter. The proposed mechanism of the oxidation[14] has been the subject of much discussion but it must now be considered as firmly established.

After the primary products of irradiation had been formed according to reaction **4** the following reactions take place:—

$$H_2O_2 + 2\,Fe^{++} \longrightarrow 2\,Fe^{+++} + 2\,OH^- \quad \text{.....5}$$
$$OH + Fe^{++} \longrightarrow Fe^{+++} + OH^- \quad \text{.....6}$$

and in the presence of oxygen

$$H + O_2 \longrightarrow HO_2 \quad \text{.....7}$$
$$H^+ + HO_2 + Fe^{++} \longrightarrow Fe^{+++} + H_2O_2 \quad \text{.....8}$$

or in the absence of oxygen

$$H^+ + H + Fe^{++} \longrightarrow Fe^{+++} + H_2 \quad \text{.....9}$$

In the presence of oxygen it is obvious that every OH radical oxidizes one ferrous ion, every molecule of hydrogen peroxide two and each H atom three ferrous ions. If $G(Fe^{III})$ air represents the number of ferric ions, formed per 1^{00} eV by G_H, G_{OH}, $G_{H_2O_2}$ and G_{H_2} the primary yield of the respective primary products then

$$G(Fe^{III})_{air} = G_{OH} + 2\,G_{H_2O_2} + 3\,G_H \quad \text{.....(a)}$$

is the observed standard yield in aerated solutions. Because of the material balance for water decomposition

$$2\,G_{H_2O_2} + G_{OH} = 2\,G_{H_2} + G_H \quad \text{.....(b)}$$

Combining these two equations

$$G(Fe^{III})_{air} = 2\,G_{H_2} + 4\,G_H \quad \text{.....(c)}$$

TABLE I

Comparison of yields for different systems with various irradiation, after Hart[5]

Radiation	*System*	G_1	G_2	G_3	$\frac{G_2}{G_1 + G_2}$	G_{tot}	*Ref.*
Co^{60} gamma-rays	Fe^{++}	2·86	0·69	0·78	0·19	4·33	7
Co^{60} gamma-rays	Br^-, O_2	2·74	0·92	—	0·20	3·66	9
Co^{60} gamma-rays	HCOOH	3·00	0·88	—	0·23	3·88	8
Co^{60} gamma-rays	HCOOH	2·35	0·46	1·42	0·16	4·23	10
2 MeV X-rays	Lactic Acid	3·08	1·04	—	0·25	4·12	11
H^3 beta-rays	HCOOH	2·35	1·02	—	0·30	3·37	8
Po^{210} alpha-rays	HCOOH	0·43	3·14	—	0·88	3·57	8
$B^{10}(n, a)\,Li^7$	HCOOH	0·26	2·94	—	0·92	3·20	8

and the corresponding equation for the oxygen-free case

$$G(Fe^{III})_{air\text{-}free} = G_{OH} + 2G_{H_2O_2} + G_H = 2G_{H_2} + 2G_H \quad \text{.....(d)}$$

The ratio of these two values is

$$1 + \frac{G_H}{G_{H_2} + G_H}$$

Using published values[15] of 0·4 for G_{H_2} and 3·68 for G_H, adjusted to a $G(Fe^{III})_{air}$ value of 15·5, the theory predicts a ratio of 1·90. A thorough study of the radiolysis of ferrous sulphate solutions was recently made by Allen and Rothschild[13] who found a value of $1{\cdot}90 \pm 0{\cdot}03$ in excellent agreement with theory. In earlier researches values between 2·0 and 4·0 were obtained but these high results were attributed to organic impurities in the solutions, the effect of which is to increase $G(Fe^{III})_{air}$ and to decrease $G(Fe^{III})_{air\text{-}free}$.

In the absence of oxygen it was observed[13] that the oxidation rate decreased as oxidation proceeded. This decrease was ascribed to reduction of ferric ions according to

$$Fe^{+++} + H \longrightarrow Fe^{++} + H^+ \quad \text{.....10}$$

and it was shown that the decrease in rate depended only on the ratio of ferric to ferrous ions present.

Taking into account the back-effect of reaction **10** Allen and Rothschild[13] deduced that equation (**d**) now becomes

$$G(Fe^{III})_{air\text{-}free} = 2G_{H_2} + 2G_H \left(\frac{1}{1 + \frac{k_{10}\,(Fe^{III})}{k_9\,(Fe^{II})}} \right)$$

where (Fe^{III}) and (Fe^{II}) represent the molar concentrations of ferric and ferrous ions respectively and k_9 and k_{10} the rate constants for reactions **9** and **10** respectively. By plotting the reciprocal of the observed yield against the ferric to ferrous ratio they obtained a straight line, the slope of which gave the value $0{\cdot}081 \pm 0{\cdot}010$ for the ratio k_{10}/k_9. By assuming 10^{00} eV/l as unit dosage, the rate of change of ferric iron concentration with dosage can be obtained from equation (**e**):

$$\frac{d\,(Fe^{III})}{d\,(dose)} = \frac{7{\cdot}35}{1 + \frac{0{\cdot}081\,(Fe^{III})}{c - (Fe^{III})}} + 0{\cdot}8 \quad \text{.....(e)}$$

where c is the total iron concentration and 7·35 the value of $2G_H$.

On integration this becomes

$$8{\cdot}085\,\frac{dose}{c} = 0{\cdot}919\,\frac{(Fe^{III})}{c} - 0{\cdot}0736\,\ln\left(1 - 0{\cdot}992\,\frac{(Fe^{III})}{c}\right) \quad \text{.....(f)}$$

When their experimental values of $\frac{dose}{c}$ are plotted against $\frac{(Fe^{III})}{c}$ the points fall in excellent agreement with the curve calculated from equation (**f**) as depicted in Fig. 1.

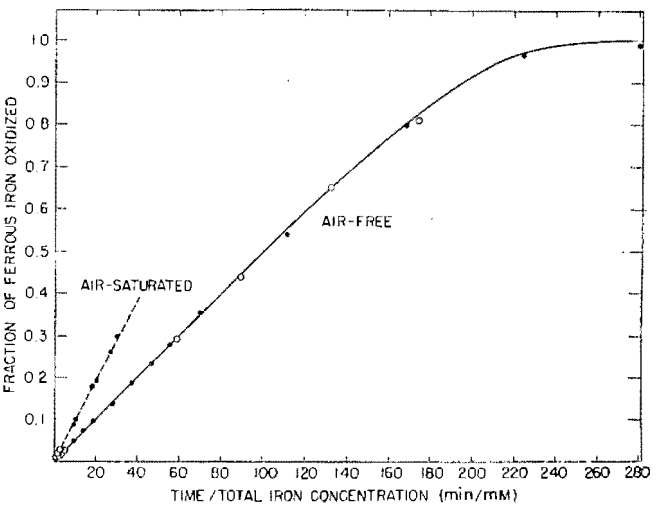

Fig. 1

Gamma-ray oxidation of air-free ferrous solution in 0·8N H_2SO_4
After Allen and Rothschild[13]
● *1·09 mM Fe.* O *10·1 mM Fe.*
Dose rate 3·80 × 10^{19} eV/l.–min.
The curve is calculated according to equation **f** *(see text)*

These authors also applied a similar treatment to the study of the effect of oxygen concentration. In a closed system, as the oxygen concentration drops the value of the ferric yield of aerated solutions drops and approaches that of de-aerated solutions. In this case the yield was dependent upon the ratio of ferrous iron to molecular oxygen, the two substances competing for reaction with H atoms according to reactions **9** and **7** respectively.

The effect of *p*H on the initial oxidation yield at constant oxygen concentration is small.[16] After prolonged irradiation the oxidation rate falls due to reactions **10** and **11** playing an increased role as a result of the high ferric ion concentration.

$$HO_2 + Fe^{+++} \longrightarrow Fe^{++} + O_2 + H^+ \quad \text{.....11}$$

In air-free solutions the effect of *p*H is involved.[17] In this case there is a decrease in the oxidation rate as irradiation proceeds until a steady state is reached. The build-up of ferric-ion concentration cannot by itself account for the entire effect. Since solutions of ferric sulphate were not reduced by gamma-radiation but reduction did take place when saturated with hydrogen, it was likely that reaction with hydrogen could lead to the observed decrease in oxidation rate. This could be ascribed to

$$OH + H_2 \longrightarrow H + H_2O \quad \text{.....12}$$

which leads to an increase of hydrogen atoms capable of

reducing ferric to ferrous ions by reaction **10**. There is thus competition between Fe^{++} and H_2 for reaction with OH and at the same time added competition from Fe^{+++} for reaction with H. By a careful determination of reaction rates at various *p*H values it was shown[17] that only those reactions involving ferric ions are *p*H-dependent. Since, however, reaction **9** is almost unaffected by a large change of hydrogen-ion concentration it is likely that the reaction is not a three-body process but should be written as

$$H_2^+ + Fe^{++} \longrightarrow Fe^{+++} + H_2 \quad \textbf{9a}$$

as was first postulated by Weiss.[14]

The effect of organic impurities has already been mentioned. From the investigations of the effect of hydrocarbons,[18] alcohols[19] and organic acids[20] the overall effect in the presence of oxygen can be explained by the following mechanism:—

$$OH + RH \longrightarrow R\cdot + H_2O \quad \textbf{13}$$
$$R\cdot + O_2 \longrightarrow RO_2\cdot \quad \textbf{14}$$
$$RO_2\cdot + Fe^{++} \longrightarrow Fe^{+++} + RO_2^- \quad \textbf{15}$$
$$RO_2^- + H^+ \longrightarrow ROOH \quad \textbf{16}$$
$$ROOH + Fe^{++} \longrightarrow RO^- + Fe^{+++} + OH \quad \textbf{17}$$

which results in the oxidation of many ferrous ions. The addition of small amounts of chloride ion prevents this series of reactions by preferential reaction with the OH radical:—

$$OH + Cl^- \longrightarrow Cl + OH^- \quad \textbf{18}$$
$$Cl + Fe^{++} \longrightarrow Fe^{+++} + Cl^- \quad \textbf{19}$$

and this is the purpose of the addition of sodium chloride to the ferrous sulphate dosimeter.

The effect of cupric ions on the ferrous oxidation in aerated solutions is very marked, the G value dropping from 15·5 to about 0·6.[21] This is due both to the preferential reaction of cupric ions with HO_2 radicals, preventing reaction **8** and to the reduction of ferric by cuprous:—

$$Cu^{++} + HO_2 \longrightarrow Cu^+ + H^+ + O_2 \quad \textbf{20}$$
$$Cu^{++} + H \longrightarrow Cu^+ + H^+ \quad \textbf{21}$$
$$Cu^+ + Fe^{+++} \longrightarrow Cu^{++} + Fe^{++} \quad \textbf{22}$$

The Reduction of Ceric Solutions

The currently accepted mechanism for the reduction of ceric ions by radiation is that given by Allen.[22] Following the formation of the primary products according to reaction **4** the reduction proceeds as follows:—

$$H + Ce^{+4} \longrightarrow Ce^{+3} + H^+ \quad \textbf{23}$$
$$H_2O_2 + Ce^{+4} \longrightarrow Ce^{+3} + HO_2 + H^+ \quad \textbf{24}$$
$$HO_2 + Ce^{+4} \longrightarrow Ce^{+3} + H^+ + O_2 \quad \textbf{25}$$
$$OH + Ce^{+3} \longrightarrow Ce^{+4} + OH^- \quad \textbf{26}$$

As in the case of ferrous solutions it follows that

$$G(Ce^{III}) = G_H + 2\,G_{H_2O_2} - G_{OH} \quad (\textbf{g})$$

which, with equation (**b**) reduces to

$$G(Ce^{III}) = 4\,G_{H_2O_2} - 2\,G_{H_2} \quad (\textbf{h})$$

Since the hydrogen yield can be measured directly, the primary yields of G_H, G_{OH} and $G_{H_2O_2}$ can now be obtained from measurements based on the ferrous and the ceric systems.

When thallous ions are added to ceric solutions the value of G (Ce^{III}) increases from 2·4 to 7·9.[23] Thallous ions now compete with cerous ions for the hydroxyl radicals and instead of producing a nett back-oxidation *via* reaction **26**, the cerous yield is increased:—

$$Tl^+ + OH \longrightarrow Tl^{++} + OH^- \quad \textbf{27}$$
$$Tl^{++} + Ce^{+4} \longrightarrow Tl^{+++} + Ce^{+3} \quad \textbf{28}$$

By studying the effect of the thallous to cerous ratio the rate of constants for reactions **26** and **27** may be compared in a manner similar to the ferrous-ferric case treated above. The ration for k_{27}/k_{26} was found to be 38[3] showing that thallous ions remove hydroxyl radicals 38 times as efficiently as cerous ions.

Aqueous Solutions of Organic Compounds

The reactions of organic compounds in dilute aqueous solutions can also be explained by secondary reactions following the initial decomposition of water by reaction **4**. The radiolysis of aqueous formic acid yields carbon dioxide and hydrogen as the main products[24] and the process may be explained by some of the following reactions:—

$$H + HCOOH \longrightarrow H_2 + HCOO\cdot \quad \textbf{29}$$
$$OH + HCOO\cdot \longrightarrow CO_2 + H_2O \quad \textbf{30}$$
$$OH + HCOOH \longrightarrow H_2O + HCOO\cdot \quad \textbf{31}$$
$$H + HCOO\cdot \longrightarrow H_2 + CO_2 \quad \textbf{32}$$
$$2\,HCOO\cdot \longrightarrow HCOOH + CO_2 \quad \textbf{33}$$

At present there is insufficient information available to decide which of the three processes, reactions **29** and **30**, reactions **31** and **32** or reactions **29**, **31** and **33**, is the correct one but as a result of investigations with deuteroformic acid, DCOOH, there is evidence that it is the HCOO· radical and not ·COOH which takes part in the reaction.

The decomposition is enhanced over 50 times when small amounts of hydrogen peroxide are added, whilst oxygen inhibits decomposition. The large change in decomposition rate with hydrogen peroxide must be attributed to a chain mechanism which is considered to proceed *via*

$$HCCO\cdot + H_2O_2 \longrightarrow H_2O + CO_2 + OH \quad \textbf{34}$$

The oxygen inhibition probably acts as

$$HCOO\cdot + O_2 \longrightarrow HO_2 + CO_2 \quad \textbf{35}$$

followed by

$$HCOO\cdot + HO_2 \longrightarrow H_2O_2 + CO_2 \quad \textbf{36}$$

The nature of the products from the radiolysis of aqueous solutions of benzene depends on the conditions of radiation. In the absence of oxygen, lightly ionizing radiation such as *X*- or gamma-rays produce phenol, diphenyl and small amounts of terphenyl in

addition to hydrogen peroxide and hydrogen from the water,[25, 26] but with densely ionizing radiation such as neutrons or alpha-particles, hydroquinone and pyrocatechol are also observed.[27] Although the yields reported by various authors differ markedly from each other, the mechanism which best fits the results for gamma-radiation[26] is as follows for the production of phenol and diphenyl:—

$$C_6H_6 + OH \longrightarrow C_6H_5OH \longrightarrow C_6H_5\cdot + H_2O \quad \text{.....37}$$

$$C_6H_5\cdot + OH \longrightarrow C_6H_5\cdot OH \quad \text{.....38}$$

$$C_6H_5\cdot + H \longrightarrow C_6H_6 \quad \text{.....39}$$

$$2C_6H_5\cdot \longrightarrow C_6H_5\cdot C_6H_5 \quad \text{.....40}$$

and for the small amounts of terphenyl by:—

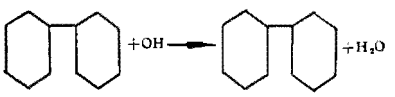

.....41

followed by

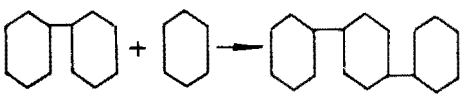
.....42

In aerated solutions the production of diphenyl, reaction **40**, is completely suppressed whilst the yield of phenol is increased. This clearly indicates the removal of phenyl radicals by the reaction

$$C_6H_5\cdot + O_2 \longrightarrow C_6H_5O_2\cdot \quad \text{.....43}$$

which is confirmed by the linear increase of the phenol yield with dosage until all the oxygen is exhausted after which the yield drops rapidly to that of air-free solutions. In addition to the major product, phenol, ring opening occurs leading to a dialdehyde which has been formulated[28] as mucondialdehyde (CHO—CH=CH—CH=CH—CHO). Since no such product could be detected in oxygen-free irradiations, it is suggested that, after the formation of the organic peroxyl radical, the hydroperoxide is formed which loses water to form the dialdehyde.

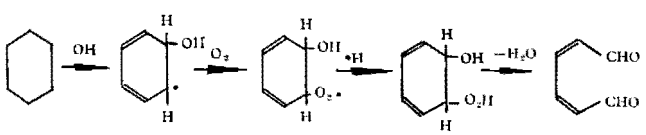

Other Organic Systems

A detailed review of the many organic systems that have been studied has recently been published.[27] Since, on irradiation, energy can be absorbed by any component and by any atom in the molecule, it would at first sight seem unlikely to have any specificity of reaction. Nevertheless, some reactions that occur are markedly specific, presumably due to transfer of ionization or excitation energy from the site of primary attack to the reaction site.[29]

Specificity of attack may be observed when alcohols are irradiated.[30] The main product from primary alcohols are dimers produced by combination of two hydroxyalkyl radicals. The bond of the alcohol molecule which is preferentially broken is on the first carbon atom other than the carbon-hydroxyl bond; ethanol, for example, undergoes the following overall reaction:—

$$2\,CH_3CH_2OH \longrightarrow \begin{matrix} CH_3—CH—OH \\ | \\ CH_3—CH—OH \end{matrix} + H_2 \quad \text{.....44}$$

via radical production

$$CH_3CH_2OH \longrightarrow CH_3—CH—OH + H \quad \text{.....45}$$

These radicals can also be further oxidized to aldehydes, or, in the case of secondary alcohols, to ketones, but tertiary alcohols yield only ketones.

Of industrial importance is the polymerization of ethylene to produce polyethylene at relatively low temperatures and pressures. At room temperatures and pressures from 20 atmospheres the products from gamma-irradiations have similar properties to the normal thermal product. The mechanism of this polymerization is as yet not firmly established, but it is obvious that some chain mechanism is involved as the yields are very high, G (C_2H_4) varying up to ~12,000 depending on the conditions used.

The presence of a carbonyl group may also lead to specificity of attack. Thus gamma-irradiation of carboxylic acids causes both decarboxylation and dehydrogenation.[29] Thus

$$R — CH_2COOH \longrightarrow R — CH_3 + CO_2 \quad \text{.....46}$$

or

$$R — CH_2 — CH_2 — (CH_2)_n — COOH \longrightarrow R — CH = CH — (CH_2)_n — COOH + H_2 \quad \text{.....47}$$

Although it was shown that the proportion of the two yields varies greatly, no satisfactory explanation is yet available. Another example of degradation is the removal of ammonia from amino-acids in aqueous solutions, but in these systems reaction probably occurs through the agency of the radicals from the primary decomposition of water.

Both oxidation and reduction were shown to take place when Seitz[30] proved the *X*-irradiation of aqueous solutions of dyes produced irreversible oxidation and reversible reduction. Weiss and his co-workers studied the effect of radiation on steroids.[32, 33, 34] They found that in air-saturated solutions in organic solvents oxidation occurred at positions 3, 5, 6 and 7, but in air-free aqueous solutions dehydroxylation and dehydrogenation took place.

Chemical Dosimetry

For any radiation-induced reaction to be suitable for an accurate quantitative measurment of absorbed radiation, it should be one whose products can be measured easily, the yield should be proportional to the dosage and be independent over a wide range of intensities and types of radiation. At present there is no chemical system which satisfies all these demands, but the Fricke dosimeter,[35] which measures the oxidation of 10^{-3}M ferrous solution in air-saturated 0·8N sulphuric

acid containing about 10^{-3}M chloride, seems to satisfy the requirements of most workers and is very widely used.

The Fricke dosimeter has the advantage that the oxidative mechanism is very well understood and that the yield has been measured accurately by a variety of ways. The best value to date gives G (Fe^{III}) with Co^{60} gamma-rays $15{\cdot}45 \pm 0{\cdot}11$.[36] The dosimeter is capable of measuring dose rates up to 1,000 r/min without much lowering of the yield[37] and dosages of up to 200,000 r can be measured. For other types of radiation the value of G (Fe^{III}) drops with ionization intensity to 4·2 for Li^7 and He^4 recoil products from the neutron irradiation of boron[38] (B^{10} (n, a) Li^7).

Alkyl iodide dosimeters have proved useful for measuring small dosages. Chloroform-water mixtures, when irradiated, produce hydrochloric acid by a chain mechanism so that by using indicators in the proper *p*H range, dosages as small as 10—100 r can be measured.[39,40] Suttle[41] showed that bromoform used with crystal violet gave a detectable colour with a dose as small as 5 r.

For gaseous systems Harteck and Dondes[42] have developed the nitrous oxide system for high-level dosimetry. Upon irradiation nitrous oxide yields nitrogen, oxygen and nitric oxide, the latter being converted to nitrogen dioxide by reaction with oxygen. By measuring the total pressure due to the nitrogen and oxygen, dosages from 5×10^4 to 3×10^9 r may be measured. The amount of nitrogen dioxide formed in the lower part of this range is too small for easy measurement, but from about 5×10^6 r the pressure of NO_2 may be used as an additional check. If the nitrogen dioxide yield is sufficiently high, the dosage can be measured colorimetrically from the unopened vessel.

Possible Industrial Uses of Radiation

As large radiation sources become commercially available it is possible that industrial applications will become feasible. Already use can be made of radiation for sterilizing pharmaceutical products and intensive research is in progress on the preservation of foods. In the chemical field it seems that the use will be restricted to the production of expensive chemicals or to those reactions which proceed through a chain mechanism to give large yields. Examples of such chain mechanisms are chlorinations and polymerizations, the latter having strong possibilities in the field of plastics.

Recently Harteck and Dondes[43] discussed the possibility of using a nuclear reactor for the manufacture of nitric acid. They deduced that a 550 mW reactor using enriched uranium and costing 20 million dollars could with a burn-up of about 6 million dollars worth of fuel per year produce annually electricity valued at 4 to 6 million dollars and 70,000 tons nitrogen fixed as nitrogen dioxide. At current market values this fixed nitrogen is worth about 60 million dollars as nitric acid. In addition large amounts of nitrous oxide would be formed, for which there is at present no large scale use.

Other uses are no doubt being investigated and it is estimated[44] that the next 10 to 15 years will see big developments in this field.

REFERENCES

1. Weiss, J., *Nature*, **153**, 748 (1944).
2. Hirschfelder, J. O., *J. Phys. Chem.*, **52**, 447 (1948).
3. Hart, E. J., *J. Chem. Educ.*, **34**, 586 (1957).
4. Samuel, A. H. and Magee, J. L., *J. Chem. Phys.*, **21**, 1080 (1953).
5. Hart, E. J., *Ann. Rev. Phys. Chem.*, **5**, 146 (1954).
6. Dainton, F. S. and Sutton, H. C., *Trans. Faraday Soc.*, 49, 1011 (1953).
7. Allen, A. O., *Radiation Research*, **1**, 85 (1954).
8. Hart, E. J., *Radiation Research*, **1**, 53 (1954).
9. Hochanadel, C. J., *J. Phys. Chem.*, **56**, 587 (1952).
10. Hart, E. J., *J. Amer. Chem. Soc.*, **76**, 4312 (1954).
11. Johnson, G. R. A., Scholes, G. and Weiss, J., *J. Chem. Soc.*, 3091 (1953).
12. Weiss, J., *Ann. Rev. Phys. Chem.*, **4**, 143 (1953).
13. Allen, A. O. and Rothschild, W. G., *Radiation Research*, **7**, 591 (1957).
14. Rigg, T., Stein, G. and Weiss, J., *Proc. Roy. Soc.*, **A211**, 375 (1952).
15. Hochanadel, C. J. and Lind, S. C., *Ann, Rev. Phys. Chem.*, **7**, 83 (1956).
16. Allen, A. O., Hogan, V. D. and Rothschild, W. G., *Radiation Research*, **7**, 603 (1957).
17. Rothschild, W. G. and Allen, A. O., *Radiation Research*, **8**, 101 (1958).
18. Vermeil, C., Cottin, M. and Haissinsky, M., *J. Chim. Phys.*, **49**, 437 (1952).
19. Dewhurst, H. A., *Trans. Faraday Soc.*, **48**, 905 (1952).
20. Hart, E. J., *J. Amer. Soc.*, **74**, 4174 (1952).
21. Hart, E. J., *Radiation Research*, **2**, 33 (1955).
22. Allen, A. O., *Radiation Research*, **1**, 85 (1954).
23. Sworski, T. J., *Radiation Research*, **4**, 483 (1956).
24. Hart, E. J., *J. Amer. Chem. Soc.*, **73**, 68 (1951); *J. Phys. Chem.*, **56**, 594 (1952).
25. Sworski, T. J., *Radiation Research*, **1**, 231 (1954).
26. Stein, G. and Weiss, J., *J. Chem. Soc.*, 3245 (1949).
27. Collinson, E. and Swallow, A. J., *Chem. Rev.*, **56**, 471 (1956).
28. Daniels, M., Scholes, G. and Weiss, J., *J. Chem. Soc.*, 832 (1956).
29. Collinson, E. and Swallow, A. J., *Quart. Rev.*, **9**, 311 (1955).
30. Seitz, W., *Strahlentherapie*, **61**, 140 (1938).
31. McDonell, W. R. and Newton, A. S., *J. Amer. Chem. Soc.*, **76**, 4651 (1954).
32. Keller, M. and Weiss, J., *J. Chem. Soc.*, 2709 (1950).
33. Coleby, B., Keller, M. and Weiss, J., *J. Chem. Soc.*, 66 (1954).
34. Allison, R., Coleby, B. and Weiss, J., *Nature*, **175**, 720 (1955).
35. Fricke, H. and Morse, S., *Am. J. Roentgenol.*, Radium Therapy, **18**, 430 (1927).
36. Schuler, R. H. and Allen, A. O., *J. Chem. Phys.*, **24**, 56 (1956).
37. Hine, G. J. and Brownell, G. L. (Editors), "Radiation Dosimetry" (New York), Academic Press (1956), p. 384.
38. McDonell, W. R. and Hart, E. J., *J. Amer. Chem. Soc.*, **76**, 2121 (1954).
39. Taplin, G. V. and Douglas, C. H., *Radiology*, **56**, 577 (1951).
40. Taplin, G. V., Douglas, C. H. and Sanchez, B., *Nucleonics*, **9**, (2), 73 (1951).
41. Suttle, J. F., USAEC Report LA-1615 (1954).
42. Harteck, P. and Dondes, S., *Nucleonics*, **14** (3), 66 (1956).
43. Harteck, P. and Dondes, S., *Nucleonics*, **14** (7), 22 (1956).
44. Spence, R., *Chem. and Ind.*, 1532 (1954).

No. 53

The Transport of Vitamin A in Rat Serum with Special Reference to the Occurrence of Unidentified Metabolites of Vitamin A in the Rat

By C. F. GARBERS, J. GILLMAN and M. PEISACH

Biochem. J. (1960) **75**, 124
Printed in Great Britain

The Transport of Vitamin A in Rat Serum with Special Reference to the Occurrence of Unidentified Metabolites of Vitamin A in the Rat

By C. F. GARBERS,* J. GILLMAN
Joint Nutrition Unit of the South African Council for Scientific and Industrial Research and the University of the Witwatersrand, Johannesburg

AND M. PEISACH
National Chemical Research Laboratory, South African Council for Scientific and Industrial Research, Pretoria, South Africa

(*Received* 13 *July* 1959)

Despite the suspected association of vitamin A alcohol with serum proteins, the mechanism of vitamin A transport in serum is still not fully known. Bennhold (1938) was led to believe that both vitamin A and the carotenoids were associated with the globulins, a view which was later supported by Pett & le Page (1940) after alcoholic fractionation of serum. According to Dzialoszynski, Mystkowski & Stewart (1945), however, vitamin A was said to accompany those proteins of the blood which were precipitated by full or three-quarter saturation with ammonium sulphate. Accordingly it was inferred that vitamin A was most likely attached to albumin.

* Present address: Department of Chemistry, University of Stellenbosch, Stellenbosch, South Africa.

The interpretation of results obtained from ammonium sulphate fractionation of chicken, cow and pig plasma is complicated by large losses, particularly of vitamin A ester (Ganguly, Krinsky, Mehl & Deuel, 1952). Nevertheless, it appeared from the observations of Ganguly *et al.* (1952) that 40–60% of the vitamin A alcohol in chicken, cow and pig plasma could be recovered from the proteins precipitating at half-saturation, whereas the vitamin A esters seemed to be associated with the proteins precipitated at lower salt concentrations. After fractionation of chicken and rat plasma by dialysis against distilled water, vitamin A ester was found with a protein fraction which precipitated more readily on dialysis than did the protein carrying vitamin A alcohol.

While our work was in progress, Krinsky, Cornwell & Oncley (1956) reported that during flotation of the lipoproteins of human plasma in the ultracentrifuge the vitamin A alcohol–protein complex sedimented together with the other proteins. From their studies on the transport of vitamin A and of the carotenoids in human plasma Krinsky, Cornwell & Oncley (1958) arrived at the view that since albumin, isolated by two different experimental procedures, did not contain significant amounts of vitamin A alcohol, some protein other than albumin was the carrier of the vitamin A in the blood.

The available evidence would suggest therefore that vitamin A is made soluble in the blood by association with a protein.

With the aid of improved techniques now available for the fractionation of serum proteins by preparative electrophoresis and with the aid of [2-^{14}C]vitamin A, it is hoped in this investigation to identify the vitamin A-carrying serum protein (Garbers, Gillman & Peisach, 1958). Thereafter we shall draw attention to the presence of uncharacterized products of vitamin A in the rat's serum and their possible importance in metabolism.

MATERIALS AND METHODS

[2-^{14}C]*Vitamin A*. This was prepared from [2-^{14}C]vitamin A acid by reduction with lithium aluminium hydride after esterification with diazomethane (Garbers, 1956). The [2-^{14}C]vitamin A alcohol (radioactivity: 1·07 mc/m-mole) was dissolved in purified hexane, stabilized with DL-α-tocopherol (5%) and stored at −20° under N_2 until used for the preparation of doses.

Preparation of doses. Peanut oil was extracted with ethanol, residual ethanol in the oil was removed *in vacuo* and the oil then distilled in a 5 in. rotating disk molecular still (Distillation Products Inc., Rochester, N.Y., U.S.A.). The first third of the distillate was discarded and the residue distilled at 200–220° at 0·03 mm. Hg. α-Tocopherol was added to the oil to the extent of 0·1 mg./100 g. [2-^{14}C]-Vitamin A was dissolved in this oil so that each dose (0·2 ml. of oil) contained 100 i.u. of labelled vitamin A.

Treatment of experimental animals. Male albino rats of the Wistar strain were used in all experiments. Vitamin A-deficient animals were produced by feeding the following diet to weanling animals: casein, 15%; dextrinized corn starch (corn starch cooked in boiling water, dried at a low temperature and ground to a fine powder), 71%; brewer's yeast, 10%; Steenbock's salt mixture no. 40 (NaCl, 9·49%; $MgSO_4$,$7H_2O$, 10%; Na_2HPO_4,$12H_2O$, 14·59%; K_2HPO_4, 28·28%; $CaHPO_4$, 28·29%; calcium lactate pentahydrate, 6·26%; iron citrate hexahydrate, 2·44%; KI, 0·65%), 4%.

(i) Expts. 1–3 and 5. After 5–6 weeks on the vitamin A-free diet the rats started to lose weight, and fat (5–10%) containing vitamin A (Gillman, Norton, Rivett & Sutton, 1956) was included in the diet. The amount of fat consumed by the rats per day contained the equivalent of 2 i.u. of vitamin A/day. With this amount the rats failed to grow (or grew only slowly), but continued to live. When the amount of vitamin A supplemented was decreased, the rats gradually lost weight and died. Before use the animals were fed with the vitamin A-free diet until signs of deficiency developed, whereupon they received five successive daily doses of 100 i.u. of [2-^{14}C]vitamin A in 0·2 ml. of refined peanut oil by stomach tube. Groups of 5, 15, 6 and 18 rats were used for Expts. 1–3 and 5 respectively.

(ii) Expt. 4. A group of 10 male albino rats (average wt. 34 g.) was weaned on a vitamin A-free diet as above. When these rats started to lose weight (average wt. 157 g.), the diet was supplemented twice weekly with 175 i.u. of [2-^{14}C]vitamin A in peanut oil for 6 weeks (average weight at the end of this period 221 g.). The vitamin A administered allowed marginal storage in the liver and a normal blood-vitamin A concentration (Lewis, Bodansky, Falk & McGuire, 1942).

Collection of blood. The rats were anaesthetized with ether 2–43 days after administration of the last dose and blood was collected from the dorsal aorta. The blood was allowed to clot for 2 hr. and the serum was collected and pooled. Under these experimental conditions the serum contained only vitamin A alcohol with little or no vitamin A esters. The serum for electrophoresis fractionation was dialysed at 2° for 12 hr. against the buffer used for the electrophoresis separation. The vitamin A concentrations of the serum did not decrease during the dialysis.

Vitamin A analyses. Serum proteins were denatured by addition of an equal volume of absolute ethanol. The serum–ethanol mixture was extracted once with an equal volume of light petroleum (b.p. below 40°) followed by two further extractions with half the volume of light petroleum (b.p. below 40°). The extracts were combined and evaporated under N_2 in an Evelyn tube, and the vitamin A in the residue was estimated by the Carr–Price colour reaction with the Evelyn spectrophotometer.

Liver samples were ground with Na_2SO_4 and extracted with ether according to the method of Ames, Risley & Harris (1954). The turbidity which sometimes developed after the addition of the Carr–Price reagent was eliminated by filtering a measured portion of the ether extract through alumina and eluting the vitamin A with hexane–ethanol (92:8, v/v) (Thompson, Ganguly & Kon, 1949).

If the vitamin A concentration in serum or tissue was to be calculated from radioactive assay, the vitamin was

extracted similarly, the solvent evaporated and the residue was subjected to combustion. The $^{14}CO_2$ formed was isolated as $Ba^{14}CO_3$. If required, samples of serum or tissue were also made directly to produce $^{14}CO_2$ by combustion, and $Ba^{14}CO_3$ was isolated.

Vitamin A-breakdown products in the urine. Repeated samples of urine were obtained from vitamin A-deficient rats by making a fistula in the bladder. The neck of the bladder immediately below the entrance of the ureters was isolated by blunt dissection and a small incision made in the ventral wall. A polyethylene tube (no. 1) was passed through the incision into the bladder and tied in position with non-absorbable thread. The cannula was exteriorized and led into a glass saddle affixed to the back of the rat (van Zyl, 1957). After 1–2 days the urine was clear and its flow regular. Four days after the operation the rats were fed by stomach tube 500 i.u. of [2-^{14}C]vitamin A in 0·2 ml. of peanut oil. Through the use of a special metabolism cage (C. F. Garbers & C. Gilbert, unpublished work) urine samples were collected from the saddle and blood samples from the tail at fixed intervals. The blood and urine samples were subjected to combustion separately and the $Ba^{14}CO_3$ was isolated and analysed.

Water and the vitamin A-free diet were supplied without restriction to the experimental animals throughout the experiment.

Combustion of samples and assay of radioactivity. Combustion of samples was according to the method of Evans & Huston (1952), the oxidizing mixture of van Slyke, Plazin & Weisiger (1951) being used. The CO_2 formed during the combustion was isolated as $BaCO_3$ and weighed. The CO_2 was generated from the $BaCO_3$ and absorbed in N-NaOH. From this solution the carbonate was precipitated as $BaCO_3$ on 20 cm.^{2} planchets (approx. 3 mg. of $BaCO_3$/cm.^{2}; Peisach, 1959) and counted with 34% efficiency in a proportional-counter converter (Nuclear Measurements Corp., type P.C.C.-10) screened in 3 in. of steel; gas: Tracerlab proportional gas. The results are expressed as counts/min. and are corrected for self-absorption.

Concentration of lipoproteins from rat serum. This was effected by preparative ultracentrifuging of rat serum at solution densities of 1·063 and 1·20 g./ml. in the Spinco model E analytical ultracentrifuge according to the method of de Lalla & Gofman (1954). The lipoprotein fractions were changed by combustion directly to CO_2 for radioactive assay. The sedimented proteins were dialysed against borate buffer, pH 8·6, to remove most of the KBr before combustion.

Fractionation of rat-serum proteins. The method as described by Porath (1956), in which electrophoresis is carried out on columns from which the proteins are subsequently eluted with buffer, was used. The supporting medium was partially acetylated cellulose powder (Campbell & Stone, 1956, 1957). Two columns were used: column *a* (2 cm. × 32 cm.), washed with borate–phosphate buffer (0·0115 M-$Na_2B_4O_7$–0·0155 M-NaH_2PO_4, pH 8·6, *I* 0·05), was developed for 18 hr. at 18 mA and column *b* (2·2 cm. × 39 cm.), washed with veronal buffer (0·1 M-sodium diethylbarbiturate–0·02 M-diethylbarbituric acid, pH 8·6, *I* 0·05), was developed for 40 hr. at 15 mA. The proteins were eluted at a rate of 10–15 ml./hr. Volume of fractions collected: 2·0–2·1 ml. All these manipulations were carried out at 2°. The buffer used was first kept *in vacuo* to remove dissolved gases and then saturated with N_2.

The protein content of the fractions was determined by measurements of *E* at 280 mμ in a Beckman DU or Unicam SP. 600 spectrophotometer. The homogeneity of the fractions was tested by paper electrophoresis or sedimentation experiments or both.

Concentration of protein solutions for sedimentation experiments. If the protein solutions in the borate–phosphate buffer were too dilute for sedimentation experiments, the fractions were concentrated by evaporation in a vacuum desiccator. The proteins dissolved in the veronal buffer were precipitated with ethanol in the presence of Zn^{2+} ions (Cohn *et al.* 1950) as follows: the protein solution eluted from the column with veronal buffer was mixed with an equal volume of precipitating solution (11·502 g. of $ZnSO_4,7H_2O$, 3 g. of acetic acid and 400 ml. of 95% ethanol, diluted to 1000 ml. with water) at −5°. In trial experiments it was found that the pH, measured with the aid of a glass electrode (instrument standardized against phosphate buffer), of the resulting protein suspension diluted with 4 ml. of NaCl solution (0·02 M) was approx. 6·0 (Cohn *et al.* 1950). After precipitation the supernatant was kept, the precipitate was freeze-dried and dissolved in disodium ethylenediaminetetra-acetate solution [3·308 g. of disodium ethylenediaminetetra-acetate and 77·6 ml. of 0·1 N-NaOH made to 1000 ml.; pH 7·0 (measured with the aid of a glass electrode), *I* 0·05].

Sedimentation. Sedimentation runs were made in the Spinco model E analytical ultracentrifuge at room temperature and at top speed (59 780 rev./min.). After the sedimentation runs, all the mother liquors and protein solutions of the fraction analysed were subjected to combustion and assayed for radioactivity.

Paper electrophoresis. Whatman no. 3 MM paper was suspended horizontally over a Perspex rack in a labyrinth-type of apparatus (van Kampen & Zondag, 1955). Proteins were stained with bromophenol blue (Hardwicke, 1954) and the glycoproteins with the periodic acid–Schiff stain (Björnesjö, 1955).

RESULTS

Zone electrophoresis of rat-serum proteins

Expt. 1. *Electrophoresis fractionation of rat-serum proteins with borate–phosphate buffer (Campbell & Stone*, 1956, 1957; *Porath*, 1956): *mobilities of the* α_1*-glycoprotein and the macroglobulin.* Fig. 1 shows the distribution obtained when rat-serum proteins, which were collected from rats 3 days after administration of the last dose, were fractionated by electrophoresis on a partially acetylated cellulose-powder column. A component migrating faster than the albumin in the electric field can be readily observed. Two consecutive fractions, nos. 7 and 8, were pooled and their homogeneity and nature investigated by paper electrophoresis and by sedimentation runs in the ultracentrifuge. Fig. 2 indicates the sedimentation-boundary diagrams of fractions 7 and 8. Fractions 7–18 were investigated similarly and the results of the analysis (Fig. 1) showed that the albumin peak consisted of at least three components, namely the albumin, the macroglobulin and the third com-

ponent which migrated faster than the albumin under the experimental conditions. This last-named component stained positive for a glycoprotein by the method of Björnesjö (1955) and possessed the sedimentation properties of a globulin. When this component was re-examined by paper electrophoresis in the veronal buffer (pH 8·6, I 0·05), it possessed a mobility slightly less than that

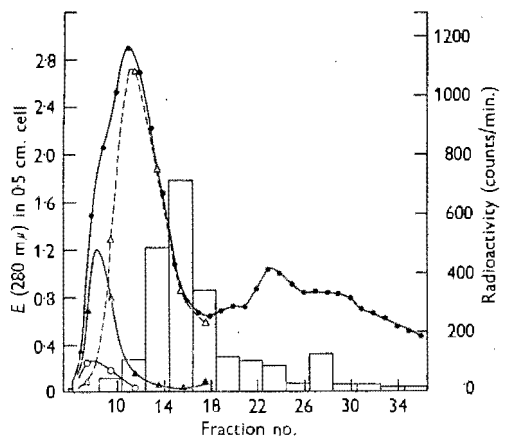

Fig. 1. Zone-electrophoresis fractionation on a cellulose-powder column (2 cm. × 32 cm.) of rat-serum proteins (3 ml.) with the borate–phosphate buffer (pH 8·6, I 0·05). A current of 18 mA was applied for 17 hr. ●, Total protein; △, albumin; ▲, α_1-glycoprotein; ○, macroglobulin. Histograms indicate radioactivity. The curve for the α_1-glycoprotein was obtained from the experimentally determined points together with the assumption that at any point (from fractions 6 to 16) the sum of the concentrations of the albumin, α_1-glycoprotein and macroglobulin (determined with the aid of sedimentation experiments) equalled the concentration of the total protein (determined spectroscopically).

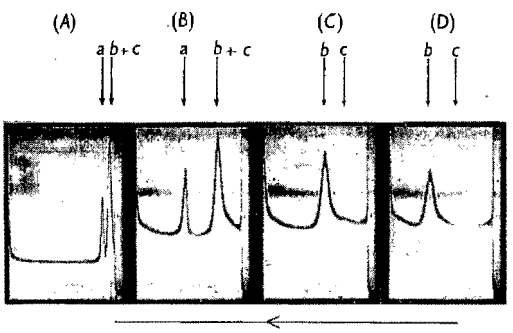

Fig. 2. Sedimentation-boundary diagrams of the combined fractions 7 and 8 in borate–phosphate buffer. Speed 59 780 rev./min. Exposures A, B, C and D were taken 8, 32, 56 and 80 min. respectively after reaching top speed. a, Macroglobulin; b, glycoprotein; c, albumin.

Table 1. *Correlation between the vitamin A concentrations of rat-serum as calculated from Carr–Price measurements and radioactive assay*

Values for the vitamin contents of serum are the averages of duplicate analyses unless indicated otherwise.

Expt.	No. of rats	No. of days between feeding of last dose and collection of serum	Vitamin A (i.u./100 ml. of serum) calc. from: Carr–Price measurements	Radioactive assay on fat-soluble components (*a*)	Radioactive assay on serum (*b*)	Percentage of activity not extractable	*b*/*a*	Counts/min. on α_1-globulin (*c*)	Counts/min. on globulins (*d*)	*d*/*c*
1 (Fig. 1)	5	3	111	112	121	7·5	1·08	2247	2247	1
2 (Fig. 3)	15	2	101	—	131	23*	1·30*	1446	1977	1·37
3 (Fig. 4)	6	4	53†	45·6†	75	39·2	1·64	970	1530	1·58
4 (Fig. 6)	7	7	Lost	135	189·8	29	1·41	2440	3640	1·49
4	3	43	74†	66·7	86·2	22·6	—	—	—	—
5	13	2	101	—	134	24·6*	—	—	—	—
5	5	10	73	—	100·1	27·1*	—	—	—	—

* Calculated from radioactive assay and Carr–Price measurements on serum.
† Results from single analysis on serum.

of the albumin and is therefore most likely an α_1-glycoprotein (Garbers & Joubert, 1958). Analyses of the fractions revealed the radioactivity to be associated with the α_1-globulin. The radioactivity is not associated with the albumin, since one would then expect the radioactivity to be proportionally distributed over the albumin peak (Fig. 1).

The vitamin A content of the serum in Expt. 1 calculated from Carr–Price measurements and radioactive assay on whole serum and the fat-soluble components from serum agree well (Table 1).

Expt. 2. Electrophoresis fractionation of rat-serum proteins with borate–phosphate buffer: isolation of the lipoproteins. Fig. 3 shows the result when the serum-protein fractions eluted from the column after electrophoresis were analysed for radioactivity. The radioactivity was identified not only on the α_1-globulin but also on other globulins. From the latter approx. 27 % of the total radioactivity was eluted (Table 1). It is possible that some of the radioactivity was carried on the β-globulin (Fig. 3).

The lipoproteins from the same serum were also isolated by flotation in the ultracentrifuge according to the method of de Lalla & Gofman (1954). The radioactivity was associated neither with the low- nor with the high-density lipoproteins, but with the proteins which sediment during flotation of the lipoproteins in the ultracentrifuge. The results are summarized in Table 2.

The vitamin A content of the serum obtained by radioactive assay exceeded the vitamin A level as determined by Carr–Price colour reaction by 29·7 % (Table 1).

Expt. 3. Electrophoresis fractionation of rat-serum proteins with veronal buffer: mobility of the macroglobulin in this buffer. Fig. 4 shows the distribution obtained when rat serum, obtained from the rats 4 days after administration of the last dose, was fractionated by zone electrophoresis in veronal buffer.

In Expt. 1 it was established that when the borate–phosphate buffer is used for the electrophoretic fractionation of rat-serum proteins, two components (macroglobulin and α_1-glycoprotein) migrated faster than the albumin. The ultracentrifugal analysis of the pooled fractions 15 and 16 of this experiment reveals that when the non-complexing veronal buffer is employed for the

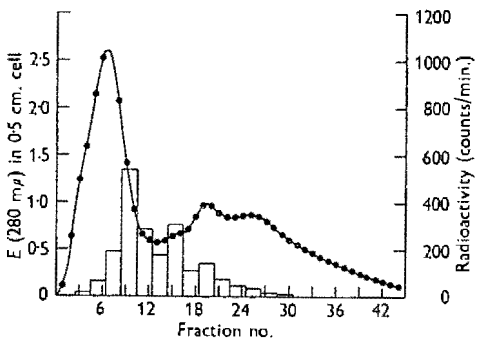

Fig. 3. Zone-electrophoresis fractionation of rat-serum proteins (3 ml.). Conditions were identical with those of Fig. 1. A current of 18 mA was applied for 18 hr. ●, Total protein. Histograms indicate radioactivity.

Table 2. *Isolation of lipoprotein fractions*

Description of fractionation	Radioactivity (%) in: Lipoprotein fraction	Radioactivity (%) in: Sedimented proteins
Ultracentrifugal flotation fractionation at solution density 1·063	1·1	98·1
Ultracentrifugal flotation fractionation at solution density 1·20	3·9	94·2

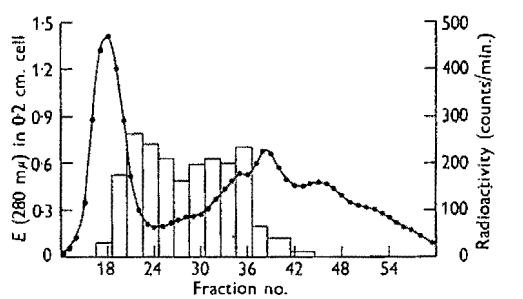

Fig. 4. Zone-electrophoresis fractionation of rat-serum proteins (3·5 ml.) on a cellulose-powder column (2·2 cm. × 36 cm.) with veronal buffer (pH 8·6, I 0·05). A current of 15 mA was applied for 36 hr. ●, Total protein. Histograms indicate radioactivity.

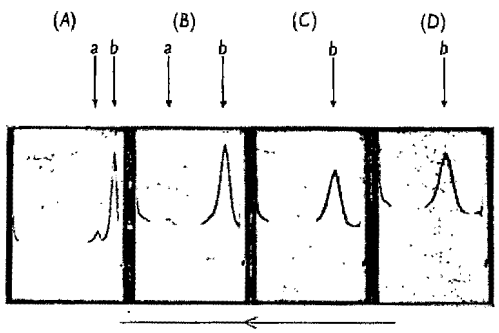

Fig. 5. Sedimentation-boundary diagrams of the combined fractions 15 and 16 in ethylenediaminetetraacetic acid solution. Speed 59 780 rev./min. Exposures *A*, *B*, *C* and *D* were taken 8, 32, 56 and 80 min. respectively after reaching top speed. *a*, Macroglobulin; *b*, albumin.

electrophoresis of rat serum, only the macroglobulin is found to migrate faster than the albumin (Fig. 5).

Analysis of the protein fractions revealed that approx. 63·4 % of the radioactivity recovered in these fractions was associated with the α_1-globulin and the remainder with other globulins.

Here again the vitamin A concentrations differed when determined by Carr–Price colour reaction and by radioactive assay on the whole serum. It was found that 39·2 % of the radioactivity was not extractable from serum by the conventional methods employed during the Carr–Price estimation (Table 1).

Expt. 4. Electrophoresis fractionation of rat-serum proteins with veronal buffer: mobility of the α_1-glycoprotein in this buffer. The vitamin A administered to the rats in Expts. 1–3 and 5 was not sufficient to allow storage. The association of vitamin A with the serum proteins in rats having reserves of vitamin A in the liver was investigated. Under the experimental conditions described, the rat livers contained an average of 31·2 i.u. of vitamin A/g. of liver (range 21–44 i.u./g.) 1 week after administration of the last dose. The analysis of the serum is reported in Table 1.

A procedure similar to that described in Expt. 3 was followed for the fractionation of a sample of pooled serum obtained from a group of seven rats 1 week after administration of the last dose. When the protein fractions eluted from the column after electrophoresis were analysed, 67 % of the radioactivity recovered was associated with the α_1-globulin and the remaining 33 % with the other globulins (Fig. 6).

The position of the α_1-glycoprotein was determined by spotting on paper portions of the fractions, obtained after electrophoresis and staining for glycoproteins, followed by elution and subsequent quantitative estimation of the dye as recommended by Björnesjö (1955). As is expected from an α_1-globulin component, the mobility of the glycoprotein is smaller than that of the albumin (Fig. 6). The presence of globulin components could also be demonstrated by paper-electrophoresis techniques in fractions 14–20 of the albumin peak. In the veronal buffer the macroglobulin still migrates faster than the albumin (Expt. 3), whereas in the borate–phosphate buffer both the α_1-glycoprotein and the macroglobulin migrate faster than the albumin during electrophoresis (Expt. 1).

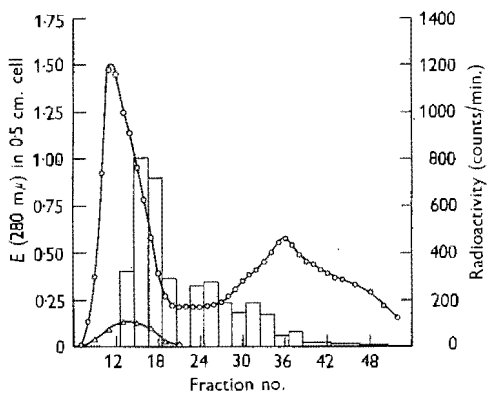

Fig. 6. Zone-electrophoresis fractionation of rat-serum proteins (4 ml.) on a cellulose-powder column (2·2 cm. × 36 cm.) with the veronal buffer (pH 8·6, *I* 0·05). A current of 15 mA was applied for 40 hr. ○, Total protein; △, glycoprotein. Histograms indicate radioactivity.

It has been observed before that the mobilities of certain components in sera change in buffers containing borate (Consden & Powell, 1955; Goldwasser & Mathews, 1955; Aronsson & Grönwall, 1957; Cooper, 1958). This increased mobility of the α_1-glycoprotein is most likely due to the action of the borate ion with the glycol groupings, leading to increased charges on the glycoproteins. As the position of the peak of radioactivity on the α_1-globulin is unaltered when either the borate–phosphate buffer or the veronal buffer is employed, the radioactivity is probably also not associated with the α_1-glycoprotein.

Influence of time on the amount of radioactivity not extractable from serum

The results obtained in Expts. 1–3, where serum samples were collected 3, 2 and 4 days respectively after administration of the last dose of labelled vitamin A, indicated that the radioactivity could not always be completely extracted by the conventional methods used for the extraction of vitamin A from serum. A similar investigation (Expt. 5) verified these results, and a difference of 24·6 and 27·1 % still existed between the vitamin A concentration of the serum determined by Carr–Price colour reaction and that calculated from radioactive assay 2 and 10 days after administration of the last dose (Table 1).

Similarly, in Expt. 4, where the experimental animals had reserves of labelled vitamin A in the liver, a discrepancy was found between the radioactivity in whole serum and the radioactivity in the fat-soluble components extracted from serum 1 week after administration of the last dose. To assess whether this discrepancy is persistent in serum, three rats from this group were maintained on a vitamin A-free diet for a period of 43 days after administration of the last dose. During this period the rats continued to grow (average increase in weight: 22 g.), and at the end of this period 29·2 % more radioactivity was found in whole serum than in the fat-soluble components extracted from the serum (Table 1).

Comparison of the concentrations of vitamin A in rat serum as calculated from radioactive assay and from Carr–Price measurements on serum

In the paragraph 'Treatment of experimental animals' conditions are described that enabled us to create a physiological condition which allowed the animal to survive without having any vitamin A in the blood or tissues as judged by the Carr–Price colour reaction. Administration of 500 i.u. of labelled vitamin A to these animals resulted in the appearance of vitamin A in the blood. This vitamin A was all labelled, since the vitamin A content of the fat-soluble components extracted from the serum was of the same order whether determined by radioactive assay or Carr–Price colour reaction. However, on occasions not all the radioactivity was confined to the fat-soluble extracts. In other words, part of the radioactivity derived from the labelled vitamin A was present as a component (or components) not extractable from serum by conventional methods. Furthermore, this second labelled component(s) could not be separated from the serum by dialysis.

The normal occurrence of this second labelled component(s) in the serum was suspected from the results of Expts. 4 and 5. Despite the varying conditions under which these experiments were conducted, this second labelled component(s) was still present in quantities varying from 23 to 29% of the total radioactivity in serum (Table 1).

The large amount of radioactivity (39·2%) which could not be extracted from the serum in Expt. 3 was found in rats greatly depleted of vitamin A before the labelled vitamin A was fed. In this connexion it should be mentioned that during the period of depletion and before radioactive vitamin A was fed one rat developed panophthalmia.

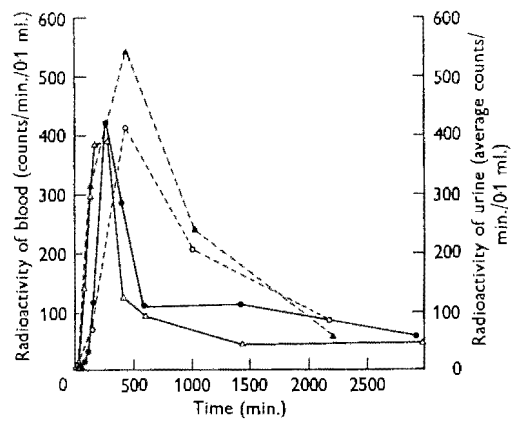

Fig. 7. Appearance of radioactivity in the blood and urine of vitamin A-deficient rats after administration of 500 i.u. of [2-^{14}C]vitamin A. Rat 1: ●, radioactivity in whole-blood samples; ○, radioactivity in urine samples. Rat 2: △, radioactivity in whole-blood samples; ▲, radioactivity in urine samples.

If the results presented in Table 1 are considered with the data obtained from the electrophoresis fractionation of the serum proteins, it is evident that: (i) one peak of radioactivity on the α_1-globulin is to be found when the vitamin A concentrations of the serum calculated from the radioactive assay and from the Carr–Price estimation correlate well (Fig. 1); (ii) a discrepancy between the vitamin A concentration calculated from total radioactivity and from the Carr–Price measurements on whole serum was found with two peaks of radioactivity, namely one on the α_1-globulin and the second on other globulins.

No proof can be offered that part or all of the radioactivity eluted from the column was indeed present as vitamin A. However, the correlations presented in Table 1 more than suggest that the fat-soluble components extracted from the ethanol-denatured serum contain vitamin A alcohol as the only radioactive component on the α_1-globulin. The radioactivity not extractable from the ethanol-denatured serum is associated mostly with the α_2-globulin.

Breakdown products of vitamin A in the urine

Labelled water-soluble products (11·7% of the dose) derived from [2-^{14}C]vitamin A are excreted in the urine of rats within 24 hr. after the intraperitoneal injection of 9200 i.u. of [2-^{14}C]vitamin A to depleted rats (Wolf, Kahn & Johnson, 1957).

Under our experimental conditions the excretion of radioactivity in the urine reached a maximum during the period 4–10 hr. after the oral administration of 500 i.u. of [2-^{14}C]vitamin A (Fig. 7). In the two experiments conducted, the radioactivity excreted in the urine during the 48 hr. after oral administration was 6·8 and 11·5% of the administered dose. The bulk of this radioactivity, 69·4 and 82·4% respectively, was excreted during the first 24 hr. period.

The radioactivity in the blood reached a maximum after approx. 4 hr., and at the end of 48 hr. the livers of the animals contained radioactivity corresponding to 20·6 and 19·8% respectively of the administered dose.

DISCUSSION

Our investigations in the rat disclose that vitamin A alcohol is transported by a globulin component of the serum protein. In this respect the transportation of vitamin A in the rat is similar to that described for man by Krinsky *et al.* (1958). In the rat the globulin component could be still further characterized. The vitamin A alcohol appears to

accompany the α_1-globulin but probably not the α_1-glycoprotein.

The finding that vitamin A alcohol is not associated with the lipoproteins clearly dissociates the transporting mechanism of vitamin A alcohol from that of the vitamin A esters, which are transported in rat serum, as in man, by the low-density lipoproteins (Garbers, 1958).

The amount of vitamin A in rat serum, as determined by Carr–Price colour reaction, cannot always account for all the radioactivity in the serum after the oral administration of labelled vitamin A to depleted rats. Another component(s) derived from vitamin A therefore is present in the blood. Unfortunately, in this investigation no evidence can be presented as yet whether there is one or more such component. The results to date indicate that in the serum of rats with little or no reserves of vitamin A the concentration of this second component(s) is equivalent (in terms of radioactivity) to approx. 20–30 i.u. of vitamin A/100 ml. of serum. The transport of the second component(s) derived from vitamin A seems to be different from that of vitamin A alcohol.

The evidence for and against the presence in serum of an intermediary product of vitamin A not detectable by the methods usually employed for the chemical estimation of vitamin A has been reviewed (Moore, 1957). Experiments suggest that on feeding vitamin A to depleted rats the vitamin A absorbed is first transformed into an intermediary product which in turn is utilized for promoting growth and for preventing xerophthalmia (Moore, 1957). Once this intermediary product reaches a particular concentration, vitamin A alcohol may be expected in the blood and ultimately in the liver and kidneys.

A situation can be visualized where rats are depleted of their stores of vitamin A and eventually also of the vitamin A in the blood. In such circumstances the intermediary product nevertheless may still be present in the blood, thus accounting for survival of vitamin A-deficient rats despite the failure to demonstrate vitamin A in the blood by conventional methods. On feeding labelled vitamin A to these rats, the labelled vitamin A again appears in the blood and depots. However, in short-term experiments the intermediary product may still not be labelled. In such circumstances there may be adequate amounts of the intermediate, i.e. the more immediately utilizable form of vitamin A. Accordingly the vitamin A administered to the depleted rat is not required for metabolism and therefore the vitamin A concentration rises in the blood and also later in the depots. On the other hand, depending on the state of depletion of the animal and the amount of labelled vitamin A fed, a situation could arise where there is so little of the vitamin A intermediate present in the blood that the feeding of labelled vitamin A would lead rapidly to the formation and appearance in the blood of the labelled vitamin A intermediate at the same time as the labelled vitamin A alcohol accumulates in the blood. The finding that this second labelled component(s) occurs in varying quantity in rat serum does not necessarily exclude it (them) from being a normal product(s) of vitamin A metabolism.

le Gallic (1947) provided suggestive experimental evidence for the presence in the blood of albino rats of a component having vitamin A bioactivity, but which was not detectable by the Carr–Price colour reaction. Since le Gallic's experiments and the investigations of others of the 'lard factor', the so-called 'hidden forms' of vitamin A have received renewed attention. It has now been shown that herring eggs also possess more bioactivity than can be accounted for by the Carr–Price colour reaction (Fisher *et al.* 1956). Subsequently, Plack, Thompson & Kon (1958) and Plack, Kon & Thompson (1959) identified vitamin A aldehyde as a constituent of herring eggs. Evidence which might indicate the presence of retinene in the rat's liver was also presented (Scharpenseel & Wolf, 1958).

In our experiments, this second labelled component(s) in the rat serum may be merely a breakdown product(s) of vitamin A and not an active intermediate product(s) of vitamin A. It is known that compounds similar in structure to vitamin A are absorbed, transported in the blood and stored in the liver (Ames, Swanson & Harris, 1955).

The rat normally does not excrete any vitamin A in the urine. Furthermore, the labelled products in the urine after feeding [2-^{14}C]vitamin A are water-soluble (Wolf *et al.* 1957) and may be either the active intermediate(s) or merely a breakdown product(s) thereof or of vitamin A. If the labelled products in the urine are breakdown products of vitamin A, they are most likely derived from the circulating blood. However, there is a possibility that the labelled products are elaborated and excreted by the kidneys or, less likely, by the urinary passages. However, if the component(s) in the urine is the same as that in the serum, it follows from the results obtained that the kidneys have the ability to concentrate this component(s), especially as the average excretion of radioactivity/unit volume in the urine is greater than in the blood, where the radioactivity is due to [2-^{14}C]-vitamin A and the other component(s). As the synthetic vitamin A was labelled at $C_{(2)}$, the second labelled component(s) in the serum is to be expected to be relatively large or to be covalently linked to the proteins, otherwise it (they) should separate during dialysis.

Whether this second labelled component(s) in rat serum belongs to the hidden forms of vitamin A or whether it (they) is merely a decomposition product is now being investigated in this Laboratory.

SUMMARY

1. With the aid of [2-^{14}C]vitamin A it was established that vitamin A alcohol is transported in rat serum in association with the α_1-globulin. The vitamin A alcohol is not associated with the lipoproteins.

2. When a borate–phosphate buffer is employed for the electrophoretic fractionation of rat-serum proteins, the mobility of the α_1-glycoprotein is greater than that of the albumin.

3. By employing veronal buffer and borate–phosphate buffer for the electrophoretic fractionation of rat-serum proteins, it could be concluded that vitamin A alcohol is probably also not associated with the α_1-glycoprotein.

4. A labelled component(s) derived from [2-^{14}C]-vitamin A and associated with the α_2-globulin can occur in serum and most likely is a normal constituent of serum, occurring in a concentration equivalent to 20–30 i.u. of vitamin A. It has not been possible as yet to establish whether these derivatives of vitamin A are active intermediates or degradation products.

5. On giving [2-^{14}C]vitamin A orally to vitamin A-depleted rats, 7–12% of the radioactivity is excreted in the urine within 48 hr. after administration.

We are grateful to Dr D. A. Sutton and Dr J. R. Nunn for their encouragement and helpful suggestions and to Dr F. J. Joubert and Mr P. C. van Berge for assistance with the ultracentrifuging experiments. We are indebted to Dr C. Gilbert for carrying out the bladder cannulations, and to Mr N. B. Wasserthal, Mrs A. A. Slaa and Miss M. Tardrew for technical assistance. This paper is published by permission of the South African Council for Scientific and Industrial Research.

REFERENCES

Ames, S. R., Risley, H. A. & Harris, P. L. (1954). *Analyt. Chem.* **26**, 1378.

Ames, S. R., Swanson, W. J. & Harris, P. L. (1955). *J. Amer. chem. Soc.* **77**, 4136.

Aronsson, T. & Grönwall, A. (1957). *Scand. J. clin. Lab. Invest.* **9**, 338.

Bennhold, H. (1938). *Die Eiweisskörper des Blutplasmas.* Dresden and Leipzig: Theodor Stekinopf.

Björnesjö, K. B. (1955). *Scand. J. clin. Lab. Invest.* **7**, 153.

Campbell, P. N. & Stone, N. E. (1956). *Biochem. J.* **62**, 9P.

Campbell, P. N. & Stone, N. E. (1957). *Biochem. J.* **66**, 19.

Cohn, E. J., Gurd, F. R. N., Surgenor, D. M., Barnes, B. A., Brown, R. K., Derouaux, G., Gillespie, J. M., Kahnt, F. W., Lever, W. F., Liu, C. H., Mittelman, D., Mouton, R. F., Schmid, K. & Uroma, E. (1950). *J. Amer. chem. Soc.* **72**, 465.

Consden, R. & Powell, M. N. (1955). *J. clin. Path.* **8**, 150.

Cooper, D. R. (1958). *Nature, Lond.*, **181**, 713.

de Lalla, O. & Gofman, J. W. (1954). *Meth. biochem. Anal.* **1**, 459.

Dzialoszynski, L. M., Mystkowski, E. M. & Stewart, C. P. (1945). *Biochem. J.* **39**, 63.

Evans, E. A. & Huston, J. L. (1952). *Analyt. Chem.* **24**, 1482.

Fisher, L. R., Harrison, G. F., Kon, S. K., Plack, P. A., Thompson, S. Y. & Todd, P. E. E. (1956). *Proc. Nutr. Soc.* **15**, xi.

Ganguly, J., Krinsky, N. I., Mehl, J. W. & Deuel, H. J. (1952). *Arch. Biochem. Biophys.* **38**, 275.

Garbers, C. F. (1956). *J. chem. Soc.* p. 3234.

Garbers, C. F. (1958). *Nature, Lond.*, **182**, 1018.

Garbers, C. F., Gillman, J. & Peisach, M. (1958). *S. Afr. J. med. Sci.* **23**, 34.

Garbers, C. F. & Joubert, F. J. (1958). *Nature, Lond.*, **182**, 530.

Gillman, J., Norton, K. B., Rivett, D. E. A. & Sutton, D. A. (1956). *Biochem. J.* **63**, 458.

Goldwasser, E. & Mathews, M. B. (1955). *J. Amer. chem. Soc.* **77**, 3135.

Hardwicke, J. (1954). *Biochem. J.* **57**, 166.

Krinsky, N. I., Cornwell, D. G. & Oncley, J. L. (1956). *Fed. Proc.* **15**, 113.

Krinsky, N. I., Cornwell, D. G. & Oncley, J. L. (1958). *Arch. Biochem. Biophys.* **73**, 233.

le Gallic, P. (1947). *C.R. Soc. Biol., Paris*, **141**, 1214.

Lewis, J. M., Bodansky, O., Falk, K. G. & McGuire, G. (1942). *J. Nutr.* **23**, 351.

Moore, T. (1957). *Vitamin A*, p. 285. Amsterdam: Elsevier Publishing Co.

Peisach, M. (1959). *J. S. Afr. chem. Inst.* **12**, 57.

Pett, L. B. & le Page, G. A. (1940). *J. biol. Chem.* **132**, 585.

Plack, P. A., Kon, S. K. & Thompson, S. Y. (1959). *Biochem. J.* **71**, 467.

Plack, P. A., Thompson, S. Y. & Kon, S. K. (1958). *Biochem. J.* **68**, 2P.

Porath, J. (1956). *Biochim. biophys. Acta*, **22**, 151.

Scharpenseel, H. W. & Wolf, G. (1958). *Fed. Proc.* **17**, 491.

Thompson, S. Y., Ganguly, J. & Kon, S. K. (1949). *Brit. J. Nutr.* **3**, 50.

van Kampen, E. J. & Zondag, H. A. (1955). *Chem. Weekbl.* **51**, 535.

van Slyke, D. D., Plazin, J. & Weisiger, J. R. (1951). *J. biol. Chem.* **191**, 299.

van Zyl, A. (1957). *J. Endocrin.* **16**, 213.

Wolf, G., Kahn, S. G. & Johnson, B. C. (1957). *J. Amer. chem. Soc.* **79**, 1208.

No. 54

(*Reprinted from Nature, Vol.* 187, *No.* 4731, *pp.* 58-59, *July* 2, 1960)

Radiolytic Oxidation of Ferrous Solutions with Standardized Internal Sources of Phosphorus-32

THE 'Fricke' solution is the most common chemical dosimeter in use at present, but the G-value of the oxidation is still not universally accepted. We have redetermined this value by radiolysis with 100–250 mc. phosphorus-32 dissolved in air-saturated 0·8 N sulphuric acid containing 10^{-3} M ferrous ions (as ferrous ammonium sulphate) and 10^{-3} M chloride (as sodium chloride). The energy dissipated by the radioactive decay was determined from standardization of the radioactivity by 4π-proportional counting as well as 4π-liquid scintillation counting, and an acceptance of the calculated value[1] of 0·69 MeV. for the average energy per disintegration of phosphorus-32.

The standardization values as obtained by the 4π-liquid scintillation method are about 1·1 per cent higher than those from 4π-proportional counting. This discrepancy is consistent and quite reproducible[2]. For some years now it has been believed that the proportional counting method was very nearly 100 per cent efficient for high-energy beta emitters such as phosphorus-32 [3], but recent work[4] using sodium-24 and phosphorus-32 incorporated in the same compound, $^{24}NaH_2{}^{32}PO_4$, in which each radionuclide was separately standardized, the former by β–γ coincidence and the latter by 4π-proportional counting, showed that the self-absorption correction for phosphorus-32 amounted to about 1 per cent. It is thus possible that the newer 4π-liquid scintillation method may be more accurate than 4π-proportional counting.

Carrier-free phosphorus-32, produced by neutron irradiation of sulphur, contains some phosphorus-33. The relative amounts of the two isotopes were determined by measuring the radioactivities of the lines corresponding to mass-charge ratios between 47 and 51 as obtained by the isotope separator of the National Physical Research Laboratory, Pretoria. The phosphorus-33 content was $1{\cdot}6 \pm 0{\cdot}16$ per cent of the total activity.

Corrections for the loss of energy through the walls of the containers were made by measuring the apparent yield, G_r, for each of 22 spherical glass containers of radius r and extrapolating the plot of G_r against $1/r$ to zero. Fig. 1 shows the results obtained (standardization by proportional counting). The

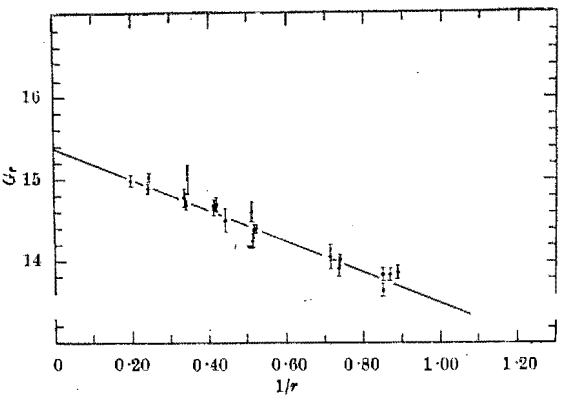

Fig. 1. Variation of apparent G-value with radius^{-1}

errors marked are standard errors for each flask, and the straight line is that calculated by the method of least squares, each point being given a statistical weight in accordance with the number of replicate determinations made with the corresponding flask. The same data were used to determine the '95 per cent error' of the G-value at infinite radius. The results obtained were :

for 4π-proportional counting	$15{\cdot}39 \pm 0{\cdot}04$ ions/100 eV.
for 4π-liquid scintillation counting	$15{\cdot}21 \pm 0{\cdot}04$ ions/100 eV.

The assumption of linearity of G_r with $1/r$ is justified by the fact that the discrepancies between values obtained from the straight line and those calculated from data published by Hine and Brownell[1] lie within the experimental errors.

M. Peisach

Radiochemistry Section,
National Chemical Research Laboratory,

J. Steyn

Radioactivity Division,
National Physical Research Laboratory,
South African Council for
Scientific and Industrial Research,
Pretoria.

[1] Hine, G. J., and Brownell, G. L., "Radiation Dosimetry" (Academic Press, New York, 1956).
[2] Steyn, J., Proc. Symp. Metrology Radionuclides, Vienna, 1959 (in the press).
[3] Pate, B. D., and Yaffe, L., *Canad. J. Chem.*, 33, 15, 925, 1656 (1955).
[4] Campion, P. J., Taylor, J. G. V., and Merritt, J. S., Proc. Symp. Metrology Radionuclides, Vienna, 1959 (in the press).

Printed in Great Britain by Fisher, Knight & Co., Ltd., St. Albans.

No. 55

Reprinted from
THE JOURNAL OF THE SOUTH AFRICAN CHEMICAL INSTITUTE,
April, 1960, Vol. XIII, pp. 34-44.

Oorgedruk uit
DIE JOERNAAL VAN DIE SUID-AFRIKAANSE CHEMIESE INSTITUUT,
April 1960, Deel XIII, bl. 34-44.

C.P.W.-P.M.B.

RADIOLYSIS OF FERROUS SULPHATE SOLUTIONS WITH STANDARDISED INTERNAL SOURCES OF PHOSPHORUS-32

by **M. PEISACH and J. STEYN**

RADIOLYSIS OF FERROUS SULPHATE SOLUTIONS WITH STANDARDISED INTERNAL SOURCES OF PHOSPHORUS-32*

by

M. PEISACH† and J. STEYN‡

OPSOMMING

Die radiolitiese opbrengs van ferri-ione in die "Fricke"-dosismeteroplossing (10^{-3}M ferro-ammoniumsulfaat en 10^{-3}M natriumkloried in lugversadigde 0·8N swawelsuur) is bepaal deur middel van interne bestraling met fosfor-32. Die radioaktiwiteit is gestandaardiseer met beide 4π-eweredigheidstelling en 4π-vloeistofsintillasietelling. Dit is bekend dat hierdie twee telmetodes vir fosfor-32 resultate lewer wat 1% van mekaar verskil en gevolglik is respektieflike G-waardes van 10·62 $\bar{E}^{-1}$ en 10.50 $\bar{E}^{-1}$ ione per 100 eV gevind, waar $\bar{E}$ die gemiddelde energie is wat per disintegrasie vrygestel word deur fosfor-32. Met $\bar{E}$ = 0·690 MeV is hierdie G-waardes ooreenstemmend 15·39 ± 0·04 en 15·21 ± 0·04.

SUMMARY

The radiolytic yield of ferric ions in the "Fricke" dosimeter solution (10^{-3}M ferrous ammonium sulphate and 10^{-3}M sodium chloride in air-saturated 0·8N sulphuric acid) was determined with internal sources of phosphorus-32. The radioactivity was standardised with 4π-proportional counting and 4π-liquid scintillation counting methods. These two procedures which are known to give results differing by about 1% for phosphorus-32 gave G-values of 10·62 $\bar{E}^{-1}$ and 10·50 $\bar{E}^{-1}$ ions per 100 eV respectively, where $\bar{E}$ is the average energy dissipated per disintegration of phosphorus-32. For $\bar{E}$ = 0·690 MeV the G-values are correspondingly 15·39 ± 0·04 and 15·21 ± 0·04.

INTRODUCTION

The simplest and most widespread chemical dosimeter for the measurement of radiation dosage is the "Fricke" dosimeter which consists of a 10^{-3}M solution of ferrous sulphate in air-saturated 0·8N sulphuric acid.[1] The initial effect of ionising radiation on an aqueous system is to produce hydrogen atoms, hydroxyl radicals, molecular hydrogen peroxide and molecular hydrogen and possibly other chemical species in much lower concentrations. These primary products may now oxidise the dissolved ferrous ions by the reactions:

$$Fe^{++} + OH \longrightarrow Fe^{+++} + OH^-$$
$$H + O_2 \longrightarrow HO_2$$
$$HO_2 + Fe^{++} \longrightarrow Fe^{+++} + HO_2^-$$
$$HO_2^- + H^+ \rightleftharpoons H_2O_2$$
$$H_2O_2 + Fe^{++} \longrightarrow Fe^{+++} + OH + OH^-$$

The effect of organic impurities (RH) in the system is to increase the ferric ion concentration by the chain involving the reactions:

$$OH + RH \longrightarrow R\cdot + H_2O$$
$$R\cdot + O_2 \longrightarrow RO_2\cdot$$
$$RO_2\cdot + Fe^{++} \longrightarrow RO_2^- + Fe^{+++}$$
$$RO_2^- + H^+ \longrightarrow ROOH$$
$$ROOH + Fe^{++} \longrightarrow RO^- + Fe^{+++} + OH$$

*A paper read in Cape Town at the Fourteenth Annual Convention of the S.A. Chemical Institute on February 12, 1960.

but this chain reaction can be prevented by the addition of chloride which causes the oxidation of only one ferrous ion per hydroxyl radical by the reations:

$$OH + Cl^- \longrightarrow OH^- + Cl$$
$$Fe^{++} + Cl \longrightarrow Fe^{+++} + Cl^-$$

Accordingly the "Fricke" dosimeter solution includes 10^{-3}M sodium chloride.

The determination of the G-value, *i.e.*, the yield in ions per 100 eV energy absorbed, of the dosimeter solution depends on the measurement of the increase in the ferric ion concentration and on a knowledge of the amount of energy absorbed by the system. To determine the ferric ion concentration spectrophotometric measurements are made of the optical density of the solution at 304-305 mμ, the absorption peak of ferric ions. To determine the energy, methods that have been used are ion current measurements, ionisation chamber methods, internal radiation methods [1] and colorimetry. In the early determinations there was a good deal of uncertainty about the G-value, results ranging from about 14 to 21 [2,3], but more recently, in the period 1955 to 1957 the accepted value fell to between 15 and 17 [4,5]. At present the most favoured value seems to be 15·5 but even this is not universally accepted. [6]

In the present publication the energy absorbed by the solution was determined from an accurate standardisation of the amount of radioactive material present in the solution, when carrier-free phosphorus-32 was dissolved in the dosimeter solution to act as radiation source.

EXPERIMENTAL

Principle of the method. To measure the radiation yield we define G as the number of ferric ions produced per 100 eV. Hence the number of ions produced by E MeV is

$$G E \times 10^4$$

and if E is the energy absorbed per c.c. of solution, then the concentration of ferric ions, c, in g ions per liter is

$$c = \frac{G E}{N} \times 10^7$$

where N is the Avogadro number.

For solutions which obey the Beer-Lambert law, we have

$$kc = \log \frac{I_0}{I_t} = D_t$$

where k is the molar extinction coefficient of the ferric solutions, D_t the optical density and I_t the intensity of transmitted light for the irradiated solution compared with I_0, that of the unirradiated one. Hence

$$D_t = \frac{k G E}{N} \times 10^7 \qquad \text{.. .. ..} \quad (1)$$

To determine E we have to consider the decay of the radionuclide.

If A_o is the measured disintegration rate in disintegrations per second per c.c. at time t = o then the number of atoms disintegrating from zero time to time t is

$$N_o - N = \frac{A_o}{\lambda} (1 - e^{-\lambda t}) \text{ per c.c. solution.}$$

If $\overline{E}$ is the average energy in MeV dissipated per disintegration then

$$E = \frac{A_o \overline{E}}{\lambda} (1 - e^{-\lambda t}) \text{ MeV/c.c.} \qquad \text{.. .. ..} \quad (2)$$

Now, substituting in equation (1)

$$D_t = \frac{k\,G\,A_0\,\bar{E}}{N\lambda}(1 - e^{-\lambda t}) \times 10^7 \quad .. \quad .. \quad .. \quad .. \quad .. \quad (3)$$

and a plot of D_t against $(1 - e^{-\lambda t})$ should be a straight line through the origin with slope proportional to G.

The above deduction did not take into account any energy lost from the system by radiation through the walls of the container. The proportion of energy lost in this way is a function of the dimensions of the container and in the case of spherical flasks the fraction of energy lost would decrease with increasing radius. Accordingly, the true G-value can only be obtained by extrapolating the plot of the apparent G-value against r, the radius of the flask, to infinite radius, or what is usually easier, to extrapolate the plot against $\frac{1}{r}$ to zero.

Reagents and apparatus. Since the effect of organic impurities could be marked even if present in relatively small concentrations, it was decided to take all the necessary precautions to ensure a high degree of purity for the water used to prepare the "Fricke" solution. Water from the laboratory supply was distilled in an all-silica still, after which it was refluxed successively with alkaline potassium permanganate and acid sodium chromate solutions. The distillate from the chromate treatment was finally redistilled and this water was used to prepare the dosimeter solution and to wash all the apparatus which came into contact with the irradiation solution.

The sulphuric acid, ferrous ammonium sulphate and sodium chloride used were all of Merck's *"pro analysi"* grade. The "Fricke" solution was made up in 2 l. batches, each batch containing 0·7845 g ferrous ammonium sulphate as hexahydrate, 0·1170 g sodium chloride and sufficient sulphuric acid to form a 0·8N solution. The solution was aerated with cleaned compressed air for about 24 hours before radioactive material was added.

Phosphorus-32 was obtained as carrier-free phosphate, in acid solution, from The Radiochemical Centre, Amersham, England. In the earlier irradiations specially prepared sulphuric acid solutions were ordered, but later batches were in hydrochloric acid and were converted to chloride-free sulphuric acid solutions by repeated evaporation with concentrated sulphuric acid in platinum-ware. The total amount of activity used for the irradiations varied between 125 and 250 mc.

The containers in which the irradiations were carried out (Fig. 1) were selected spherical glass flasks with a narrow constriction at the neck, so that the flask could be filled to the same volume every time. Samples of the irradiated solution were removed by a capillary-tipped pipette which passed through the constriction. The mean internal diameter of each of 22 flasks, ranging in capacity from about 6 to over 540 c.c., was determined by volume measurement and checked by direct measurements externally, corrected for wall thickness.

For the measurement of the ferric ion concentration the optical density of samples of the solution was determined in 1 cm silica cells at 304-305 mμ with a Unicam S.P. 500 spectrophotometer. As the temperature coefficient of the molar extinction coefficient is +0·7%, temperature control at 21·0 ± 0·2·C was sufficient.

The nuclear measurement equipment consisted of two type 532/A I.D.L. power supply units, two type 1009A and one 1009E Dynatron scalers, a Hewlett-Packard high speed decade scaler and one model 107P R.I.C. and one model N302 Hamner non-overloading linear amplifiers of the Chase-Higinbotham type. In addition, for scintillation counting the photomultiplier was an E.M.I. type 6097S tube and was used with a liquid scintillator solution consisting of a mixture of 82 parts toluene and

18 parts ethyl alcohol as solvent, and primary and secondary solutes respectively, 14 g/l. P.P.O. and 0·5 g/l. P.O.P.O.P. as supplied by Messrs. Nuclear Enterprises Ltd.

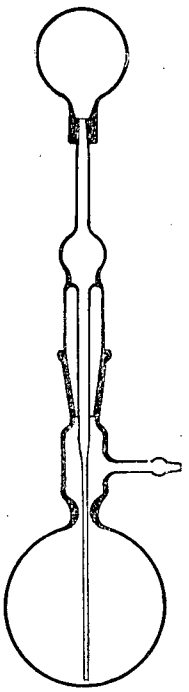

Fig. 1—Irradiation flask showing the capillary-tipped pipette with its rubber bulb attached, in position. For irradiation under aeration the rubber bulb is removed and the air supply is attached instead

SUPPLEMENTARY DETERMINATIONS

(1) *Calibration of absorption cells.* A total of 16 1 cm silica absorption cells were calibrated relative to one another by comparing the intensity of transmitted light of the same "Fricke" solution at 304-305 mμ. All later measurements made with these cells were corrected accordingly.

(2) *Determination of the molar extinction coefficient* (k). Several determinations of k were made with standardised ferric solutions in 0·8N sulphuric acid. The concentration of ferric iron ranged from zero to 0·45 mM in a solution with total iron concentration of 1·000 mM. The value obtained is in good agreement with previously reported values, as is shown in Table I.

(3) *Purity of the emitter.* Carrier-free radiophosphorus is produced by neutron irradiation of sulphur. Since natural sulphur consists mainly of the isotope S^{32} with about 0·75% S^{33} and 4·2% S^{34}, it may be expected that the (n, p) reaction which produces phosphorus-32 should be accompanied by a similar reaction producing phosphorus-33. The half-life of phosphorus-34 is so short (12·4 seconds) that it need not be taken into account. Both phosphorus-32 and 33 are β-emitters and their half-lives are 14·3 days and 25 days respectively, so that both these isotopes will be present for the duration of the irradiation experiment.

TABLE I

The molar extinction coefficient of ferric iron

Reference	k reported [mole^{-1} cm^{-1}]	Temp. [°C]	k calc. 21°C [mole^{-1} cm^{-1}]
11	2150	20	2165
12	2094	20	2109±20
1	2174	23·7	2133
6	2196	25	2135±6
			This work 2122±9

The purity of the radioactive emitter was confirmed and the relative amounts of the two isotopes present were determined by means of the isotope separator of the Nuclear Physics Division of the National Physical Research Laboratory. A sample of the radioactive solution, as received, was added to about 1 g of chemically pure phosphoric acid and heated *in vacuo* to about 300°C to remove most of the moisture. The residue was transferred to the sample holder of the isotope separator and analysed. Radioactivity was found corresponding to a large variety of mass-charge ratios, but the series of lines between mass-charge ratios of 47 and 51 proved most convenient for analysis. A typical analysis of the radioactivity of this group is shown diagrammatically in Fig. 2. The shaded portions represent the activities of strips cut out from the target receiver plate and measured. The activity of mass 48 was found to contain only phosphorus-32, presumably as $[P^{32}O^{16}]+$, whereas the activity at mass 49 contained comparable proportions of phosphorus-32 and 33. From these two lines the isotopic composition of the radioactivity was determined.

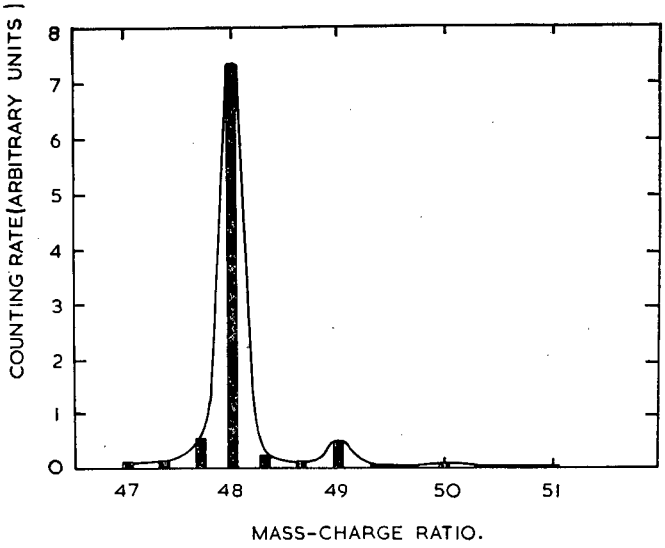

Fig. 2—Isotopic analysis of the radioactive emitter

The strips corresponding to masses 48 and 49 were counted under identical conditions and the absorption of the β^- radiations in aluminium was determined. Using the absorption data of mass 48, which contained only phosphorus-32, the absorption data of mass 49 was corrected to give the relative concentration of phosphorus-33. It was found that 1·6 $\pm$ 0·16 per cent (estimated total error) of the activity was due to the heavier isotope. If it is assumed that the relative average energies dissipated per disintegration of the two isotopes are in the ratios of their respective maximum energies, then the calculated energy dissipated by the mixture is about 98·6% of that dissipated by pure phosphorus-32 with the same total activity. Since the two isotopes would both contribute to the counting rate, A_0, the total energy, E, absorbed by the system as given by equation (2) has to be corrected for the phosphorus-33 content. In all results given subsequently this correction has been made.

(4) *The relationship between* D_t *and* $(1 - e^{-\lambda t})$. To establish that the ferric ion concentration, as measured by the optical density of the solution, D_t, increased linearly with $(1 - e^{-\lambda t})$ one irradiation experiment was carried out in which measurements were taken periodically for each of 22 flasks without interruption over some 190 hours. The results showed that for the larger flasks D_t increased linearly with the decay of phosphorus-32. However, for smaller flasks there was an apparent deviation from linearity, in the plot of D_t against $(1 - e^{-\lambda t})$. This effect was due to the fact that for the smaller flasks the volume of solution removed for measurement represented an appreciable proportion of the total volume. Consequently, when a large number of measurements was made there was an appreciable change in the geometrical shape of the liquid during its irradiation and hence the fraction of energy escaping from the solution, and therfore its radiation dose rate could no longer be assumed directly proportional to $(1 - e^{-\lambda t})$ over the entire irradiation period. In order to prevent this effect, reliable results could be obtained when the number of samples taken for measurement from the smaller flasks was kept as small as was consistent with the accuracy required.

(5) *The effect of oxygen concentration.* During irradiation a stage will eventually be reached where there is a marked decrease in the G-value due to oxygen deficiency. To show that, under the conditions described in this publication, this stage was never reached, an experiment was carried out where two parallel series of solutions were irradiated in which one was left undisturbed whilst the other was continuously aerated with a very slow stream of air. It was found that the G-values determined on the undisturbed solutions were not significally different from those of the aerated ones.

Procedure. Immediately prior to irradiation several samples of the "Fricke" solution were removed for use as reference solutions in the optical measurements. The addition of the carrier-free phosphorus-32 marked the beginning of the irradiation. The solution was then dispensed into the spherical irradiation flasks as quickly as possible and left in a thermostatically controlled bath at 21°C. Small samples of the solution were removed from the larger flasks at various times for absolute measurement of radioactivity.

The solutions as drawn from the flask had too high an activity to be counted directly, and were diluted with distilled water containing 200 mg/l. of phosphate carrier as NaH_2PO_4. From each of these diluted solutions a large number of sources were prepared for both the 4π-proportional and the 4π-scintillation counting methods.

For proportional counting, sources were prepared as almost weightless deposits on thin films of cellulose acetate made conducting by the vacuum evaporation of gold on to it. The sulphuric acid in the sample had to be neutralised with ammonia gas

to prevent the acid attacking the film. Counting was carried out in the same N.P.R.L. 4π-proportional counter normally used for international comparisons of radioactivity standards.[14] For liquid scintillation counting samples of the diluted solutions were weighed out and transferred to the counting cells by means of small weighing pipettes, mixed with 12 c.c. liquid scintillation solution and counted by the new 4π-scintillation counting method developed in this Laboratory[7].

The growth of ferric ion concentration during irradiation was followed spectrophotometrically. Measurements were made in the absorption peak of ferric ions at 304-305 mμ and it was found convenient to make the first set of measurements some 5 to 7 days after the start, depending on the level of activity used. Thereafter measurements were taken periodically over a period of about a month. Two aliquots were removed from each flask and their optical density measured in the calibrated silica cells against samples from two of the reference solutions. In this way errors due to differences in the cells, possible contamination of the reference solution, and other such sources were reduced. After measurement, the samples were returned to the flasks so that the spherical geometry of the irradiation mixture could be retained. The mean value of D_t from all these determinations and the corresponding value of $(1 - e^{-\lambda t})$ were used in equation (3) to calculate the apparent G-value.

RESULTS AND DISCUSSION

The linear relationship between D_t and $(1 - e^{-\lambda t})$ is shown in Fig. 3. It is now possible to calculate an apparent G-value for each flask, provided that the constants in equation (3) and the particular value of A_0 for the irradiation experiment are known. The constants used to calculate all the results in this investigation are:

$N = 6{\cdot}025 \times 10^{23}$ atoms per g mole (Avogadro number)

$\lambda = 5{\cdot}61 \times 10^{-7}$ sec^{-1} corresponding to a half-life of 14·3 days

$k = 2122 \pm 9$ mole^{-1} cm^{-1} at 21°C (*vide supra*)

$\overline{E} = 0{\cdot}690$ MeV (calculated — *vide infra*)

The value of $\overline{E}$ has been calculated[9] from the experimentally determined maximum value of β^- energy and an assumed allowed shape of the beta spectrum. Several experimental determinations have been made[9] and the results are in fair agreement with this value; accordingly the calculated value is used here. Any error inherent in this value will also be reflected in the G-value calculated from it. Should a better value be determined in the future, the results given below will have to be adjusted accordingly.

The results of the absolute standardisation of radioactivity, A_0, for the different experiments are given in Table II and the errors listed therein are the standard errors (given by $\frac{\sigma}{\sqrt{n}}$). The ratio of the activities as found by the two standardisation methods has a mean value of 1·0114, *i.e.*, the 4π-liquid scintillation counting method gives results about 1·14% higher than the 4π-proportional counting method. This discrepancy is consistent and quite reproducible[7]. To decide between the results of the two methods is not straightforward. For some years now it was believed that the proportional counting method had an efficiency of very nearly 100% for high energy beta emitters, such as phosphorus-32[10]. On the other hand, the liquid scintillation counting method is a new development still lacking the status of the older method. However, recent work[8] has produced evidence to show that the efficiency of proportional counting of phosphorus-32 may not be as high as was believed. By incorporating two different radionuclides in the same compound, one of which could be

standardised by the β–γ coincidence counting method, it was shown[8] that the self-absorption for phosphorus-32 amounted to about 1%. It is thus possible that of the two methods used here the 4π-liquid scintillation counting method may be the more accurate after all.

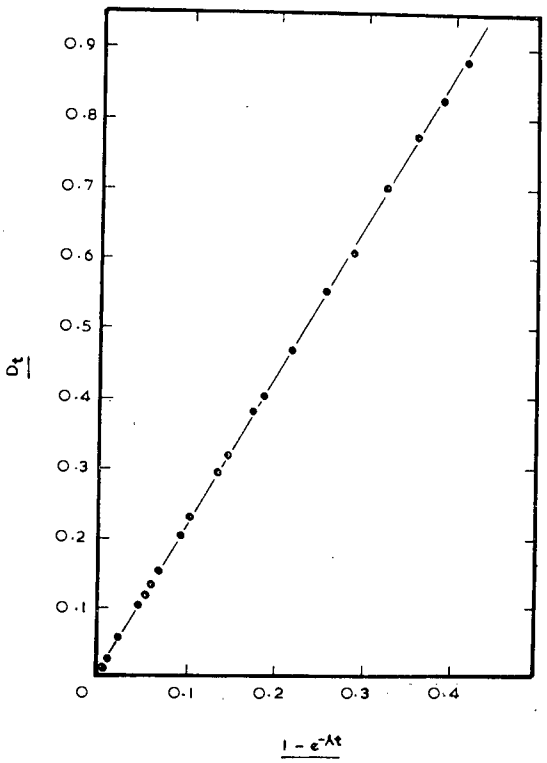

Fig. 3—The variation of the optical density with the decay of the P^{32}

TABLE II

Absolute standardisation of radioactivity

Experiment	Proportional counting (P) [sec^{-1} c.c.$^{-1}$]	Scintillation counting (S) [sec^{-1} c.c.$^{-1}$]	Ratio $\frac{S}{P}$
1	3·4826±0·0075 × 10^6	3·5299±0·0037 × 10^6	1·0136
2	3·4495±0·0034	3·4882±0·0009	1·0112
3	3·9522±0·0037	3·9787±0·0037	1·0067
4	1·9905±0·0018	2·0187±0·0020	1·0142
5	2·6698±0·0026	2·7000±0·0034	1·0113
		Mean ratio	1·0114

The apparent G-values, G_r, obtained for each flask, are plotted against $\frac{1}{r}$ in Fig. 4 and the errors shown are standard errors. The straight line in the figure is that calculated by the method of "least squares", each point being given a statistical weight in the calculation according to the number of determinations made with the corresponding flask. G_r, for the zero value of $\frac{1}{r}$, *i.e.*, an infinite flask, is obtained from the

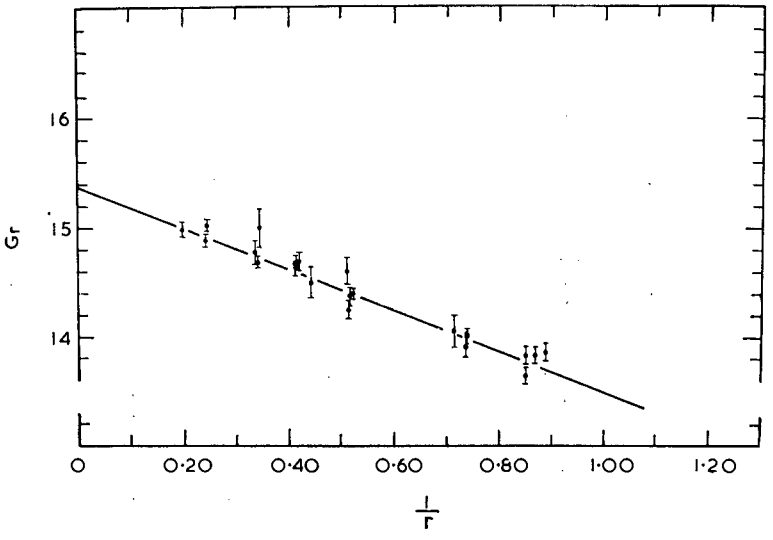

Fig. 4—Variation of apparent G-value with radius^{-1}

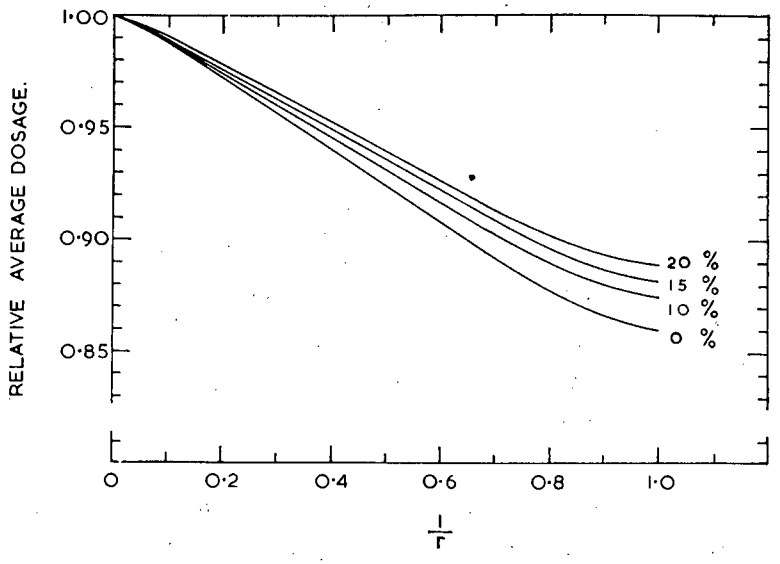

Fig. 5—The average dosage inside a spherical uniform beta source relative to that inside an infinite sphere, after Hine and Brownell.[9] The curves are drawn for 0, 10, 15 and 20% back-scatter

straight line and the corresponding error is the "95% error" calculated from the same data; this value of G_r is the G-value of the radiation reaction.

The assumption of a linear relationship between G_r and $\frac{1}{r}$ requires justification. The problem of determining the average radiation dosage inside a spherical uniform beta source has been treated by Hine and Brownell,[9] from whose data Fig. 5 has been prepared, showing the variation with radius of the ratio of the average radiation dosage inside a sphere of radius r to that inside an infinite sphere. The effect of back-scatter from the walls of the container is shown by the curves of Fig. 5 drawn for 0, 10, 15 and 20% back-scatter.

When these curves are made to coincide with the value of the calculated straight line of Fig. 4 at $\frac{1}{r} = 0{\cdot}2$, *i.e.*, near the value corresponding to the largest flask used in the experiment, it is found that the values obtained from the 15 and 20% back-scatter curves (Fig. 5) do not differ appreciably from the corresponding values from the straight line (Fig. 4) for $\frac{1}{r}$ from zero to unity. This relationship is shown diagrammatically in Fig. 6.

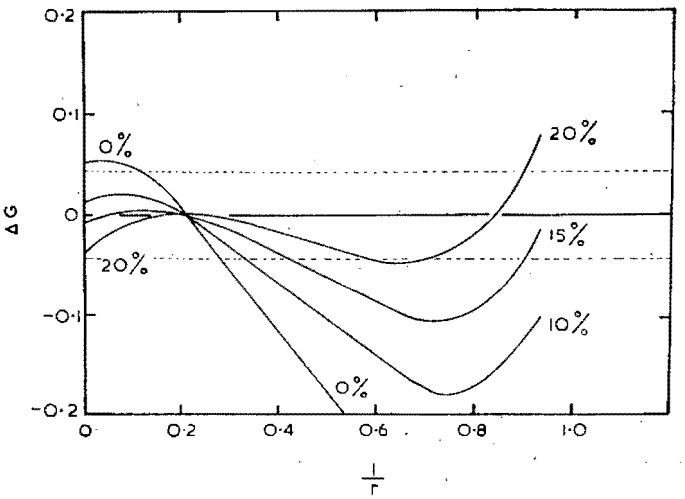

Fig. 6—The inherent error introduced in the G-value if G_r is assumed to vary linearly with $\frac{1}{r}$ (see text). For comparison the dotted lines show the 95% error of G at $\frac{1}{r}=0$

If G_l is the value of G_r obtained from the straight line at any value of $\frac{1}{r}$ and G_c is the corresponding value obtained on the basis of the curves in Fig. 5 then

$$\Delta G = G_c - G_l$$

represents the inherent error made by assuming a linear relationship between G_r and $\frac{1}{r}$. Fig. 6 shows the plot of ΔG against $\frac{1}{r}$. It is clear that ΔG is within the

experimental error for almost the entire range of $\frac{1}{r}$ less than unity, if the back-scatter contribution is between 15 and 20%. This value for the back-scatter contribution also agrees with the value of 15% found[13] from measurements with aluminium, and it is concluded that a linear relationship between G_r and $\frac{1}{r}$ is justified.

The radiolytic yield of ferric ions in the "Fricke" solution was thus found to be 15·39 ± 0·04 ions per 100 eV by proportional counting and 15·21 ± 0·04 by liquid scintillation counting. As these values depend on that of $\overline{E}$ they may be given as 10·62 $\overline{E}^{-1}$ and 10·50 $\overline{E}^{-1}$ respectively.

The authors acknowledge their appreciation to Dr. W. E. Frahn and his co-workers for their assistance with the isotopic analysis of the radioactive material and to D. van As, H. L. Lawrenz, P. J. Horn and Mrs. M. M. Pols for technical assistance.

†Radiochemistry Section,
National Chemical Research Laboratory,
S.A. Council for Scientific and Industrial Research,
Pretoria.

‡Radioactivity Division,
National Physical Research Laboratory,
S.A. Council for Scientific and Industrial Research,
Pretoria.

Received January 2, 1960.

REFERENCES

[1] Weiss, Allen and Schwarz, *International Conf. Peaceful Uses of Atomic Energy*, Geneva, 1955, P/155.
[2] Hardwick, *Discussions Faraday Soc.*, 1952, **12**, 205.
[3] Hart, *Annual Rev. Phys. Chem.*, 1954, **5**, 142 *et seq.*
[4] Dainton, *ibid.*, 1955, **5**, 215.
[5] Garrison, *ibid.*, 1957, **8**, 150.
[6] Brynjolfson and Holm, *Proc. Symposium Metrology Radionuclides*, Vienna, 1959. In the press.
[7] Steyn, *idem.*
[8] Campion, Taylor and Meritt, *idem.*
[9] Hine and Brownell, *Radiation Dosimetry*, Academic Press, New York, 1956, p. 694 *et seq.*
[10] Pate and Yaffe, *Can. J. Chem.*, 1955, **33**, 15, 925, 1656.
[11] Donaldson and Miller, *J. Chim. Phys.*, 1955, **52**, 578.
[12] Swallow, Discussion on reference 11, *ibid.*, 1955, **52**, 585.
[13] Failla, *Progress Nuclear Energy*, Series VII, 1956, **1**, 156.
[14] *Standards of physical measurement and means for their utilisation, as well as other testing facilities available in the South African National Physical Research Laboratory*, C.S.I.R. publication, in the press.

Sonderdruck aus Radiochimica Acta 2, 197–201 (1964)

No. 56

Reactor-Produced Carrier-Free Iridium-194

By M. PEISACH*, Israel Atomic Energy Commission, Soreq Research Establishment.

With 4 figures. (Received October 23, 1963)

Summary Reactor irradiation of natural osmium leads to osmium-194 by second order neutron capture. When converted to osmium tetroxide, millicurie amounts of carrier-free iridium-194 can be recovered repeatedly from the decay of a single sample of osmium-194 by vacuum distillation. The half-life of pure iridium-194 was found to be 17.4 ± 0.1 hours.

Zusammenfassung Bei Bestrahlung von natürlichem Os im Reaktor entsteht durch Neutroneneinfang zweiter Ordnung ^{194}Os. Nach Umwandlung in OsO_4 können aus einer zerfallenden ^{194}Os-Probe wiederholt Millicuriemengen von trägerfreiem ^{194}Ir durch Vakuumdestillation gewonnen werden. Die Halbwertszeit des reinen ^{194}Ir wurde zu 17.4 ± 0,1 h gefunden.

Résumé L'irradiation d'osmium naturel dans un réacteur nucléaire fournit de l'osmium-194 par capture de neutrons de second ordre. Après la conversion en tétraoxyde, on peut obtenir d'un même échantillon de ^{194}Os plusieurs fois quelques millicuries de ^{194}Ir, sans entraîneur, par distillation sous vide. La période trouvée pour ^{194}Ir pur est 17.4 ± 0,1 heures.

Introduction

Natural iridium consists of two isotopes, each of which has a large cross section for thermal neutron capture, so that, unlike many other elements, high specific activities are obtainable with even moderate reactor fluxes. Thus, in a thermal neutron flux of 10^{13} neu-

* Present address: Southern Universities Nuclear Institute, Faure, South Africa.

trons/cm.² sec., the short-lived iridium-194 can be obtained with a specific activity of over 60 curies per gm. when irradiated to saturation, and the long-lived iridium-192, for which irradiation to saturation would require a long time, can be obtained at over 100 curies per gm. after only about 6 weeks. As a result the need to find methods to increase the specific activity of irradiated iridium has not been very pressing. Nevertheless, the enrichment of radio-iridium by SZILARD-CHALMERS reactions has been studied in the phthalocyanine [1] and the hexachloro compounds [2, 3]. Except where isotopically pure iridium-193 is used as target material, these methods lead to mixtures of iridium-192 and 194. In cases where the presence of residual long-lived iridium-192 can have detrimental effects, the use of the conveniently short-lived iridium-194 is restricted and a need arises for a method of production giving a radiochemically pure product.

Carrier-free radionuclides are produced by neutron irradiation when the radioisotope of the target element formed by neutron capture, decays by beta emission to form a new element which can then be separated chemically.

$$M_Z^A\,(n,\gamma)\,M_Z^{A+1} \xrightarrow{\beta^-} M_{Z+1}^{A+1}.$$

Examples of such a process are the production of iodine-131 from the irradiation of tellurium and silver-110 from palladium. To prepare iridium-194 by this method would thus require the prior formation of osmium-194.

With its long half-life of about 700 days [4] osmium-194 could serve as a useful source of carrier-free iridium-194, samples of which could be milked from the parent nuclide at its saturation level of activity about once every five days, or, very conveniently for laboratory purposes, about once daily at half saturation, for several years. It can be produced in reactor irradiations from natural osmium by two consecutive neutron captures from the 41% abundant osmium-192 [4].

$$^{192}\mathrm{Os}\,(n,\gamma)\,^{193}\mathrm{Os}\,(n,\gamma)\,^{194}\mathrm{Os} \xrightarrow[\sim 700d,]{\beta^-} {}^{194}\mathrm{Ir}.$$

It could also be obtained from the reaction ^{192}Os (t, p) ^{194}Os but this reaction has not yet been carried out experimentally.

When osmium-192 is irradiated in a thermal neutron flux, the atoms of osmium-193 may, in addition to decay, be lost by several different nuclear reactions. If, however, it is assumed that the reaction cross section for all other nuclear reactions is small compared with that for neutron capture, it can be shown by the method used by RUBINSON [5] that the activity of osmium-194, and hence of a target containing N_A atoms of osmium-192 in a constant thermal neutron flux of Φ neutrons/cm.² sec. is given by

$$A_t = \lambda_c N_c = \frac{N_A \Phi^2 \sigma_1 \sigma_2}{\lambda_B(\lambda_B - \lambda_c)} F,$$

where N_C is the number of atoms of osmium-194 produced and the "growth factor", F is given by

$$F = \lambda_B\left(1 - e^{-\lambda_C t}\right) - \lambda_C\left(1 - e^{-\lambda_B t}\right).$$

The decay constants λ_B and λ_C refer respectively to osmium-193 and osmium-194, σ_1 to the first order neutron capture cross section of the reaction ^{192}Os (n, γ) ^{193}Os and σ_2 to the second order, ^{193}Os (n, γ) ^{194}Os. It is further implied that the neutron flux is not large enough to cause third order reactions with osmium-194 to any appreciable extent, an effect which may begin to show at fluxes exceeding about 10^{15} neutrons/cm.²sec. Provided that the irradiated osmium is stored long enough to allow short-lived osmium activities to decay, only three radioisotopes, osmium-185, 191, and 194, would remain. Of these the first decays to stable rhenium-185 and the second to stable iridium-191 through the very short-lived 4.9 sec. nuclear isomer, leaving osmium-194 as the only source of radio-iridium. Osmium metal can readily be converted to osmium tetroxide, a volatile solid at room temperature, whose vapour pressure is shown in Figure 1. When irradiated osmium as its tetroxide is kept condensed in a cooled vessel, the activity of the daughter, iridium-194, would built up and should remain behind on the walls of the vessel when the parent osmium tetroxide is distilled off. Thus by repeated distillation the osmium tetroxide remains pure and successive samples of carrier-free

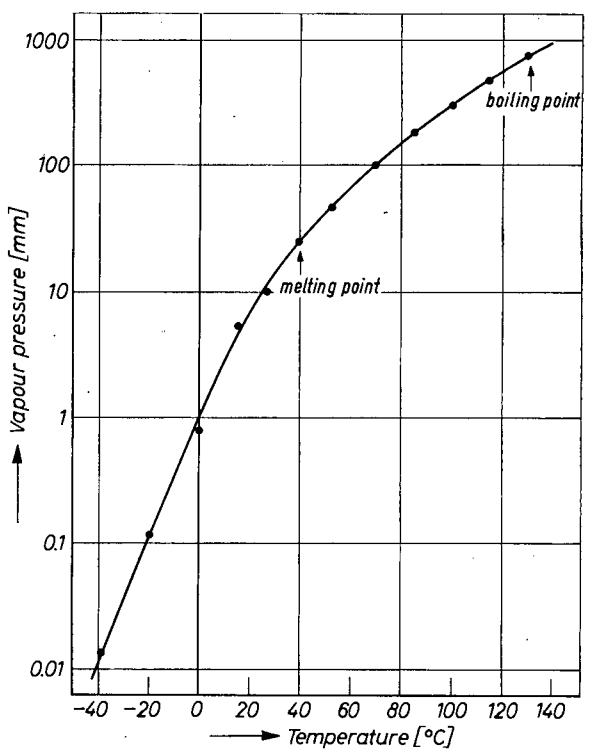

Fig. 1. Vapour pressure of osmium tetroxide [6]

1. W. HERR, Z. Naturforsch. 7b, 201 (1952).
2. U. CROATTO, G. GIACOMELLO and A. G. MADDOCK, Ricerca Sci. **21**, 1788 (1951); **22**, 265 (1952).
3. W. HERR and K. HEINE, Z. Naturforsch. **15**a, 323 (1960).
4. M. LINDNER, Physic. Rev. **84**, 240 (1951).
5. W. RUBINSON, J. Chem. Physics **17**, 542 (1949).
6. GMELINS Handbuch der Anorganischen Chemie. 8th edition. System No. 66 Osmium, Verlag Chemie GmbH, Berlin 1939, p. 38.

iridium-194 should be recoverable, without any possibility of contamination by iridium-192.

Experimental

Preparation and Irradiation of Target

Spectroscopically pure osmium metal powder, (supplied by Messrs. Johnson, Matthey and Co., Ltd.) was weighed and sealed, under vacuum, in a quartz vial, in which it was irradiated for about 24 hours at a thermal neutron flux of about 3×10^{13} neutrons/cm.^{2} sec. After irradiation the sample was left for about 4 months during which the osmium-193 decayed away completely and the activity of osmium-191 fell to about 5×10^9 dps per gm. and of osmium-185 to about 1×10^7 dps per gm. A longer decay period would have been advantageous as the radiation hazard would have decreased without appreciably affecting the activity of the 700-day osmium-194.

Preparation of Osmium Tetroxide

The experimental vacuum apparatus is shown diagrammatically in Figure 2. The entire system which would come into contact with osmium tetroxide vapour was scrupulously cleaned before assembly, in order to

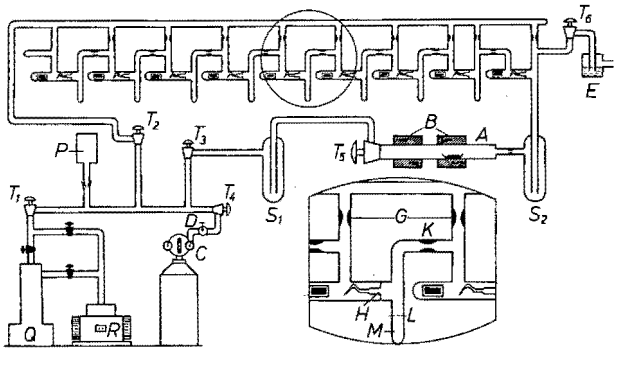

Fig. 2. Schematic representation of apparatus for the formation of osmium tetroxide and the recovery of iridium-194. *A* quartz combustion tube, *B* movable ring furnaces, *C* pure oxygen supply, *D* needle valve, *E* bubbler, *G* constrictions for sealing under vacuum, *H* break-seals, *K* constriction, *L* cutting mark, *M* sample tube T_1, T_2, T_3, T_4, T_5, T_6, stopcocks, S_1, S_2 gas traps, *P* Pirani gauge head, *Q* Oil diffusion pump, *R* Rotary backing pump

prevent decomposition of the very strongly oxidising OsO_4 by organic or other oxidisable impurities on the glass walls. There were no greased joints or vacuum stopcocks in this part of the system; instead, connection between one part of the line and the next was made through break-off seals opened with magnetic hammers sealed in glass and placed in the apparatus at the required points.

The vial containing the irradiated osmium powder was cracked open in a metal boat, which was then inserted into the combustion tube, *A* (Figure 2), through the socket of the large stopcock, T_5. The stopcock was then replaced and the system flushed with pure oxygen from *C*, at atmospheric pressure and room temperature. Thereafter, the osmium was converted to osmium tetroxide by heating the tube *A* with movable ring furnaces, *B*, to about 700 °C while maintaining the steady current of oxygen. The OsO_4 was condensed in a gas trap, S_2, cooled with a mixture of dry ice and alcohol to − 80 °C. It was not advisable to cool S_2 with liquid nitrogen as this would have condensed some oxygen as well. Excess oxygen escaped through the stopcock T_6 and a bubbler, *E*. The course of the combustion was followed by measuring the increase in activity (of Osmium-185 and 191) at S_2 and the decrease at *A*. When conversion was completed, the oxygen supply was closed off, stopcock T_6 was sealed off, T_3 and T_4 were closed, T_1 and T_2 were opened, and, with the gas trap S_2 still cooled, but this time with liquid nitrogen, the entire vacuum apparatus was evacuated to a pressure lower than 10^{-5} mm. Hg. The combustion tube was then sealed off and pumping was continued for more than 2 days. During this time the glass walls of the system were kept warm to facilitate outgassing.

The gas trap, S_2, was then sealed off, the OsO_4 distilled into the first of the tubes, *M*, and sealed in it, ready for use, after which the gas trap was removed and discarded. The sections were then sealed off at the constrictions, *G*, to produce a train of tubes each sealed in vacuum and connected to the next through a break-seal, *H*.

Recovery of Iridium-194

The osmium tetroxide was kept condensed at the base of the tube *M* for about a day, during which time iridium-194 activity built up to about half saturation. The next tube *M* was then cooled in liquid nitrogen and the osmium tetroxide allowed to heat up to room temperature. When the seal was broken, OsO_4 distilled into the cooled tube leaving the iridium-194 behind. After about an hour, when the distillation was virtually completed, the cooled tube was sealed at *K* and the original cut off the apparatus at *L*, producing a simple test tube from which the iridium activity could be removed by washing the walls with concentrated nitric acid.

Purification of Iridium-194

As the distillation of OsO_4 was a diffusion process it was expected that small amounts of osmium would be found together with the iridium. Gamma ray spectra of samples of the nitric acid solution confirmed the presence of osmium activity. It was further noted that samples that had been left to stand for a long time before distillation contained relatively more osmium activity, probably due to autoradiolytic decomposition from the intensely radioactive osmium-185.

To remove the last traces of osmium, from the iridium, a few milligrams of unirradiated osmium powder and some concentrated hydrochloric acid were added to the concentrated nitric acid solution. The mixture was heated to dissolve the carrier osmium and then eva-

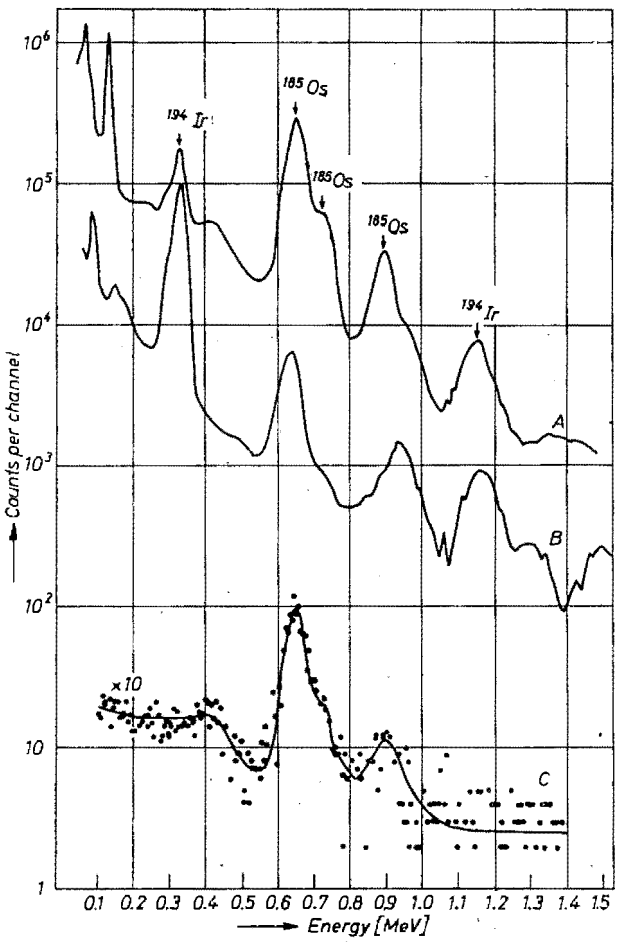

Fig. 3. Gamma ray spectra of iridium-194 samples. (A) Showing impurity of osmium-185 after distillation, (B) Impurity removed by chemical treatment, (C) Pure sample after decay of 10 days (enlarged ten times)

porated to dryness to remove osmium tetroxide. The process was repeated twice after which a solution made with concentrated nitric acid did not show the presence of any osmium.

Discussion

Purity of Iridium-194

Gamma-ray spectra of the recovered iridium-194 directly after the distillation of osmium tetroxide (Figure 3 A) show prominent peaks at 646, 718, and 880 KeV, due to osmium-185, completely obscuring the much lower intensity peaks of iridium-194 in the same region. From the activity of such samples, measured about 10 days afterwards when all iridium activity had decayed, the decontamination factor was found to range from 5×10^{-5} to 8×10^{-6}. After chemical purification, the gamma-ray spectrum (Figure 3 B) shows no obvious osmium peaks. When purified samples were allowed to decay for 10 days, the gamma-ray spectrum, enlarged ten times (Figure 3 C) revealed only the smallest trace of osmium. Decontamination factors calculated from these very low activities were in the range of 10^{-4} to 10^{-6} for the purification stage. The method of purification thus gave an enrichment of the relative activity of iridium-191 of not less than 10^{10} and usually about 10^{12}, resulting in a product in which the radiochemical impurities were difficult to detect. It is obvious that the radioactive osmium in the iridium-194 could be reduced still further if the irradiated sample was allowed to decay for a much longer period.

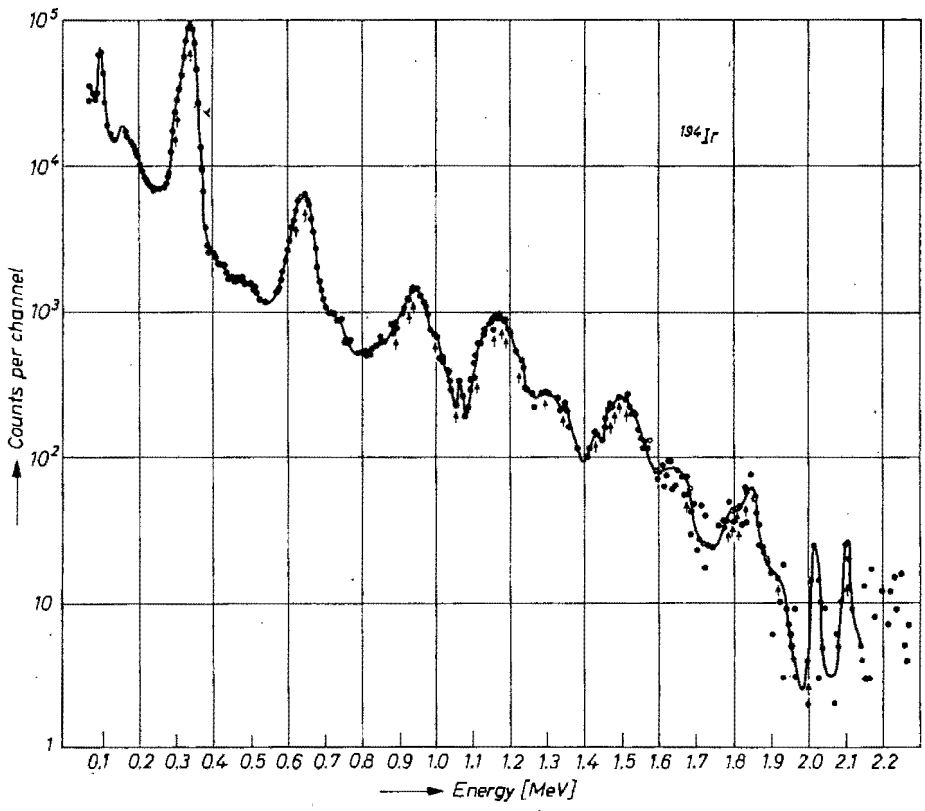

Fig. 4. Gamma ray spectrum of pure iridium-194. Arrow markings show the energies of known gamma rays

The complete gamma-ray spectrum for pure iridium-194 as obtained with a 3″ × 3″ NaI(Tl) scintillation detector is given in Figure 4. The arrow markings in the figure show the energies of known gamma rays obtained from external conversion spectra with high resolution spectrometers [7, 8].

Yield of Iridium-194

The activity of iridium-194 samples obtained over a period of about a month, corrected for the growing-in period, had a mean value of 1400 ± 200 dps per g. osmium, in good agreement with the calculated value. Hence, an irradiation lasting a little over 3 months (2500 hours) at a flux of 3×10^{13} neutrons/cm.^{2} sec. would yield about 16 μc per g. osmium, or, millicurie amounts could readily be obtained from a 10 g. sample irradiated for 3 months at a flux of 10^{14} neutrons/cm^2. sec. It should be noted that because the activity of osmium-194 (and hence of iridium-194) depends on Φ^2, the use of high reactor fluxes would result in a sharp rise in the yield.

The Half-Life of Iridium-194

Half-life measurements made on many samples showed that the accepted value of 19 hours was too high. The decay was followed either by beta ray counting, through absorbers to eliminate the softer beta rays but transmitting the 2.2 MeV. β^- ray, or by gamma ray counting of the intense 325 keV radiation or the lower intensity 622–645 keV gamma rays. No deviation from linearity within the statistical errors of counting, was observed over more than 5 half-lives. The mean half-life was found to be 17.4 ± 0.1 hours (Table 1). The half-life obtained from following the rate of growth of iridium-194 in a freshly separated osmium sample was less reliable as a result of the very high background activity from osmium-185 and 191.

Table 1. *Half-life of iridium-194*

Method	Result	Reference
	Hours	
Counting strong β^- rays	17.41 ± 0.09	This work
325 keV γ	17.4 ± 0.1	This work
622–645 keV γ	17.5 ± 0.25	This work
Growth of ^{194}Ir in ^{194}Os	18.0 ± 1.0	This work
^{194}Ir from ^{194}Os	18	[4]
Decay of γ-ray peaks	19	[7]
β^- rays from enriched ^{193}Ir	19	[10]
Absorption measurements	19.0 ± 0.2	[11]
Decay of 1.65 MeV γ	18.8	[11]
Decay of β-spectrum	19.5	[12]
	20.7 ± 5	[9]

Table 1 lists the reported half-lives of iridium-194. As most investigations on this nuclide dealt with its complex decay scheme, it is not surprising that very little attention was paid to its half-life. SEREN, FRIEDLANDER and TURKELL [9], stated that the "half-life in literature is 19 hours. We find 20.7 ± 5". Others [7, 10] refer to the decay being "consistent with a 19-hour half-life" or the radiation being "attributed to the 19-hour ^{194}Ir". It is of interest to note that the lowest value previously reported was 18 hours [4] obtained from the iridium-194 separated from osmium-194.

To account for the apparent half-life of 19 hours, the relative yields of iridium-192 and 194 obtained from the irradiation of natural iridium have to be taken into account. After a very short irradiation the iridium-192 contributes somewhat less than 5% to the total activity, and the proportion increases somewhat with longer irradiations. The presence of so little relatively long-lived activity can lead to appreciable errors. The decay of an irradiated iridium sample followed for 20 hours showed an apparent half-life of 18.6 hours, which increased to about 19.2 hours when followed for over 30 hours, the period over which counting was continued in previous investigations [7, 11]. In all these cases the points did not deviate from linearity, within the statistical error calculated from the count rate. It is unfortunate that the work on the irradiation of enriched iridium-193 [10], which would have given a product containing relatively much less iridium-192, did not deal more thoroughly with the half-life, as the apparent value would have been appreciably less than 19 hours.

Acknowledgements

The advice on the design and the assistance during operation of the vacuum apparatus given by NATHAN OCHERT, ALEXANDER ROTH, and ISAAC LEDERER and of the staff of the Vacuum Technology Department are gratefully acknowledged. AMOS NUTES and YORAM GURFINKEL are thanked for their help with electronic equipment. Thanks are due to the staff of IRR-1 for supplying the irradiations.

7. M. W. JOHNS and S. V. NABLO, Physic. Rev. **96**, 1599 (1954).
8. J. KERN and G. BÄCKSTRÖM, Nuclear Physics **19**, 461 (1960).
9. L. SEREN, H. N. FRIEDLANDER, and S. H. TURKELL, Physic. Rev. **72**, 888 (1947).
10. C. E. MANDEVILLE, J. VARMA, and B. SARAF, Physic. Rev. **98**, 94 (1955).
11. L. J. GOODMAN and M. L. POOL, Physic. Rev. **71**, 288 (1947).
12. C. M. WITCHER, Physic. Rev. **60**, 41 (1941).

No. 57

CURRENT INTEREST IN NUCLEAR CHEMISTRY

M. Peisach

Southern Universities Nuclear Institute, Faure, C.P.

Based on a paper read to the Western Province branch of The South African Chemical Institute, 12th March 1964.

Reprinted from The South African Industrial Chemist, September, 1964.

CURRENT INTEREST IN NUCLEAR CHEMISTRY

M. Peisach*

Based on a paper read to the Western Province branch of The South African Chemical Institute, 12th March, 1964.

Modern teaching tacitly assumes that the nucleus of an atom plays no part in Chemistry. From this point of view, the term "Nuclear Chemistry" is a paradox. It is, however, an apt description of the field of research that has arisen from the efforts of chemists in the study of sub-atomic particles, their properties and reactions, their effects on matter and their uses.

In a short paper such as this, little more can be done than to touch lightly on some of the main topics of current activity. The topics selected are

Radioisotope Production
and Analysis by Radioactivation.

Some mention of Chemical Effects of Nuclear Transformation will be made, but the very important and closely allied field of Radiation Chemistry is considered beyond the scope of the present paper.

RADIOISOTOPE PRODUCTION

We read in Genesis that "in the beginning" the world was in a state of randomness, disorder and implied instability. We can expect just that kind of system to have existed if we imagine the world to have been the cooling offshoot of a nuclear reaction mass of some parent star. Our relics of those days are natural long-lived radioactive species that have not yet reached the stable state. Most of them are the heavy elements, but some lighter ones such as some rare earth isotopes, and others like potassium–40 (1.3×10^9y.), vanadium–50 (6×10^{15}y.) and rubidium–87 (4.7×10^{10}y.) have survived to become of interest to nuclear geochemists.

It was in the early thirties of the present century that artificially produced radioactive material first became available. Irene Curie and Joliot prepared 2.6-min. phosphorus–30 by bombarding aluminium with energetic α–particles from polonium[1]. They proved the radioactive product to be phosphorus by dissolving the aluminium in hydrochloric acid and collecting phosphine from the evolved gases.

Isotope Production by neutron irradiation

With the advent of nuclear reactors, neutrons became available in enormous fluxes. As a result, the production of radioactive materials expanded rapidly to cover virtually every element.

When w g. of a target of formula weight, M, is irradiated for a time, t, in an irradiation flux, Φ per cm² per second, the activity, A, formed from a nuclear reaction whose reaction probability (cross section) is δ, is given by

$$\frac{A}{w} = \frac{N \sigma \Phi a}{M} (1 - e^{-\lambda t}) \quad \text{.....(I)}$$

where λ is the decay constant of the radioactive species formed and the target isotope in question comprises a fraction a of the whole target. N is the Avogadro number.

(1) *Neutron capture*

Most radionuclides are produced in reactors by neutron capture, which leads to the formation of an isotopic nuclide with mass one unit higher than the target atom. For many purposes the specific activity obtainable is sufficient, but it frequently happens that the obtainable specific activity is too low. As an example the production of radio-iodine can be considered.

For medical purposes radio-iodine is administered to patients and its rate of concentration by the thyroid is measured. If stable iodine–127 is irradiated to form iodine–128, the weight of iodine that would have to be administered to obtain the desired radioactivity, would be sufficient to upset the entire iodine metabolism of the patient. Instead, the specific activity has to be enriched by other means, or, so called, carrier-free preparations are carried out to obtain a product in which the only isotope of the element of interest is the radioactive species. Radio-iodine can thus be made by the following methods:

*Southern Universities Nuclear Institute, Faure, C.P.

(*a*) Iodine–125 (57.4 d) is obtained from the neutron irradiation of xenon and allowing radioxenon to decay. Separation of small amounts of radiocaesium formed from the decay of other xenon isotopes is usually necessary[2] [3].

$$Xe^{124}\ (n, \gamma)\ Xe^{125} \xrightarrow[\text{capture}]{\text{electron}} I^{125}\ \text{(carrier-free).}$$
18 hr.

(*b*) Iodine–128 (25.0 m) can be obtained enriched by Szilard-Chalmers reaction (*vide infra*) from the irradiation of iodoform[4] or other iodo-compounds[5] [6] where the bulk of the target iodine is retained in the organic form and iodine–128 is extracted.

I^{127} (n, γ) I^{128} extracted (high specific activity).

(*c*) Iodine–129 (1.6×10^7y) is too long-lived and is not usually used for medical purposes.

(*d*) Iodine–130 (12.5 hr) can be obtained in a mixture with other iodine isotopes from uranium fission.

(*e*) Iodine–131 (8.05 d), although available from fission products, is usually obtained as a decay product of radiotellurium[7] [8].

$$Te^{130}\ (n, \gamma)\ Te^{131} \xrightarrow{\beta^-} I^{131}\ \text{(carrier-free).}$$
25 m.

(*f*) Iodine–132 (2.3 hr) can be obtained from the decay of fission product tellurium–132 and is usually supplied in the form of adsorbed tellurium on a column from which iodine–132 solutions can be eluted[9] [10].

$$U\ (n, f)\ Te^{132} \xrightarrow{\beta^-} I^{132}\text{(carrier-free).}$$
78 hr.

Among radionuclides that can be obtained carrier-free from the decay of an (n, γ) product are niobium–95 (from zirconium), technetium–99 (from molybdenum), rhenium–105 (from ruthenium), silver–111 (from palladium), antimony–125 (from tin), gold–199 (from platinum) and others.

(2) *Consecutive neutron capture*

An interesting recent innovation was the use of two consecutive (n, γ) reactions to yield an isotope decaying by β^--emission as a precursor for a carrier-free radioisotope[11]. The activity of the second product is given by

$$\frac{A}{w} = \frac{Na.\,\Phi^2}{M}\ \frac{\sigma_1\,\sigma_2}{\lambda_1\,(\lambda_1 - \lambda_2)}\ .\ F \text{.....(II)}$$

where σ_1 and σ_2 refer respectively to the first and second neutron capture, and λ_1 and λ_2 respectively to the decay constants of the radioactive nuclide formed from the first and second (n, γ) reaction. The "growth factor", F, is given by

$$F = \lambda_1\,(1 - e^{-\lambda_2 t}) - \lambda_2(1 - e^{-\lambda_1 t}) \text{.....(III)}$$

Using natural iridium it is impossible to obtain a carrier-free preparation of iridium–194 uncontaminated with iridium–192. However, isotopically pure iridium–194 has been obtained[11] by the neutron irradiation of osmium in which consecutive neutron capture yields osmium–194.

$$Os^{192}\ (n, \gamma)\ Os^{193}(n, \gamma)\ Os^{194} \xrightarrow{\beta^-} Ir^{194}\ \text{(carrier-free).}$$
32 hr. 700 d.

After irradiation, the osmium can be converted to its tetroxide, which is sufficiently volatile to be distilled off to recover iridium–194. (See Figure 1).

From equation (II) it is evident that the yield is dependent on the product ($\sigma_1\sigma_2$) and on the flux as Φ^2. Accordingly, this procedure should be useful for those neutron capture reactions whose products have large capture cross sections and in reactors with large thermal neutron fluxes.

(3) (*n, p*) *reactions*

Among carrier-free radionuclides produced by (n, p) reactions, three of interest to organic chemists are carbon–14, from the neutron irradiation of nitrides, phosphorus–32, from irradiated sulphur, and sulphur–35 from irradiated potassium chloride. Recently, the use of fast neutrons has shown that small quantities of sodium–24 may be obtained from magnesium[12] by the reaction

Mg^{24} (n, p) Na^{24}.

With the current tendency to use shorter-lived radioisotopes where possible, the use of cobalt–58 instead of cobalt–60 as a cobalt tracer has increased. Even in hydrology where tracer experiments last some time, cobalt–58 (71d) is preferred above cobalt–60 (5.26 y) so that the use of tracer in one year should not interfere with its use the next. By neutron irradiation of nickel[13] [14] carrier-free solutions are obtained from the nuclear reaction Ni^{58} (n, p) Co^{58}.

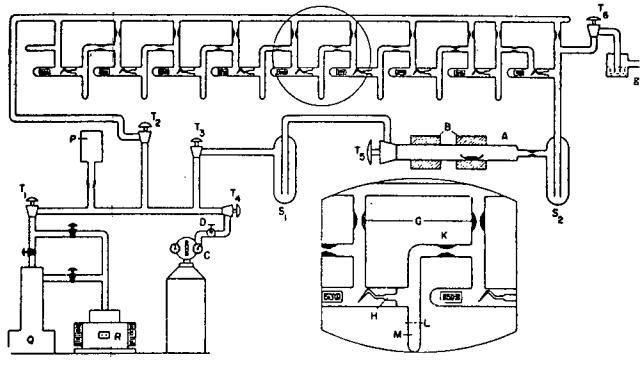

Fig. 1

Schematic representation of apparatus for the formation of osmium tetroxide and the recovery of iridium-194

A quartz combustion tube, B movable ring furnaces, C pure oxygen supply, D needle valve, E bubbler, G constrictions for sealing H break-seals, under vacuum, K constriction, L cutting mark, M sample tube, T_1, T_2, T_3, T_4, T_5, T_6, stopcocks, S_1, S_2 gas traps, P Pirani gauge head, Q Oil diffusion pump, R Rotary backing pump.

(4) (*n, α*) *reactions*

Because of the high Coulomb barrier for alpha-particle release, (n, α) reactions e.g. Al^{27} (n, α) Na^{24}, usually require fast neutrons. A notable exception is the formation of tritium by the reaction

Li^6 (n, α) H^3,

which is highly exoergic (Q = 4.79 MeV). As a result the triton is released with considerable energy and has been used for the formation of fluorine–18 from the oxygen in the anions of lithium salts, e.g. Li_2CO_3[15] [16] or $LiNO_3$[17] by the reaction

O^{16} (t, n) F^{18}.

Isotope production with charged particles

Whereas neutron irradiation can, with very few exceptions, lead to neutron-rich nuclides, other methods of production are required for neutron-deficient ones. Accelerators such as cyclotrons or Van de Graaff machines provide the answer. In this way carrier-free preparations of manganese–54, chromium–51, copper–64 and zinc–65 can be obtained.

With the use of larger accelerators the acceleration of nuclei such as Li^6, Li^7, C^{12}, N^{14}, O^{16} and Ar^{40} has become possible. By using accelerated ions such as these, nuclides in the neutron-deficient region far from the stability line can be obtained. Chackett and Chackett[18] were able to obtain gold–188 and other very light isotopes of mercury, gold and platinum from the irradiation of tantalum with 6+—charged ions of carbon–12, carbon–13 and nitrogen–14.

The spectacular work of Ghiorso *et al*[19] led to the formation of Lawrencium, element–103,

Cf^{252} (B^{11}, 6n) Lw^{257}

800 y. 8 sec.

Fission

As an isotope production process, fission yields about 200 different radionuclides. Their production modes, yields and properties have been studied for many years, but even to-day still holds the attention of many.

Uranium fission is the source of large amounts of carrier-free caesium–137, promethium–147, barium–140, and the long-lived strontium–90 which is one of the major health hazards in fall-out.

Current research is largely directed towards determination of primary fission yields and elucidation of the charged distribution of fission products. A large variety of fissionable nuclides, is under investigation and their fission characteristics are being investigated for a wide spectrum of bombarding charged particles, fast neutrons and photons.

ANALYSIS by RADIOACTIVATION

It is remarkable how closely allied the fields of radioactivation analysis and radioisotope production are. Just as the first artificial radioisotope was produced by charged particle bombardment, so also was the first activation analysis, when 6 p.p.m. gallium were detected in iron irradiated with deuterons[20]. In the same way also, activation analysis really became an important analytical tool with the growth and availability of neutron sources.

The most common nuclear reaction used for activation analysis is (n, γ) and the weight of the element present in the sample is determined by the intensity of the induced radioactivity. The same equation as for radioisotope production, equation (I), may be used to determine appropriate conditions for irradiation or the limits of sensitivity for available measuring conditions. It may readily be shown that, for an irradiation neutron flux of 3×10^{13} neutrons per cm^2 per sec. the sensitivity of detection for most heavy elements is 10^{-11} to 10^{-12}g. Very few analytical procedures have such a sensitivity and a comparable range of application.

Research trends in activation analysis

Coupled with recent methods of gamma-ray spectroscopy, radioactivation analysis can provide a rapid qualitative and quantitative analytical tool with wide applications. A large group at Houston, Texas, is developing automated analysis procedures coupled with computer analysis to determine many elements simultaneously and by remote control for the investigation of the surface of the moon. Similar work in Europe deals with the use of ion-exchange to effect rapid separation and analysis. This, then, is one of the current directions of development.

Another direction of development appears to be the trend to develop methods of analysis of very high specificity so that procedures for the estimation of one element, or a small group of elements, become possible. This trend together with the desire for non-destructive methods has produced some interesting results, and with more study of nuclear properties will doubtlessly lead to many others.

Delayed neutrons

When a radioactive nuclide decays to an excited state of the daughter nuclide, de-excitation is possible by various processes. If, however, the excited state lies above the binding energy of a neutron, neutron emission becomes possible. The neutron emitter would then be the excited daughter nucleus, but as the emission of a neutron is instantaneous, its rate will be determined by the decay of the precursor and would have the same half-life. A schematic representation is given in Figure 2.

Analytical aspects of delayed neutron emission have been described for fissionable elements and for nuclear reactions leading to nitrogen–17[21] [22]. Of the neutrons emitted during fission, about 1% appear as delayed

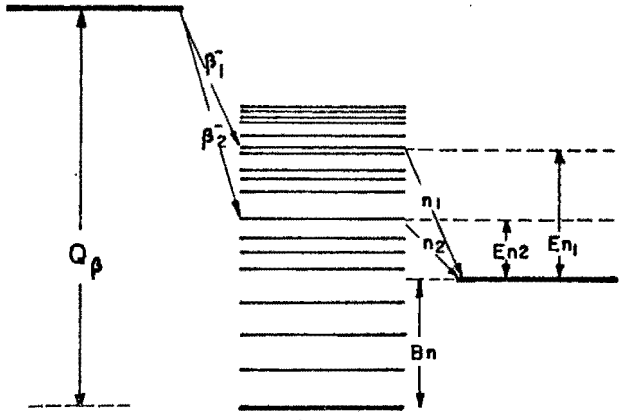

Fig. 2
Schematic Representation of Delayed Neutron Emission

neutrons. These arise from the decay of short-lived precursor fission products and are mostly heavy isotopes of halogens, e.g.

Bromine–87 (54 sec.); Bromine–88 (16 sec.); Bromine–89 (4.5 sec.); Bromine–90 (1.6 sec.); Iodine–137 (24 sec.); Iodine–138 (6.3 sec.); Iodine–139 (2.0 sec.); Antimony–135 (< 0.4 sec.); Arsenic–85 (0.43 sec.)

The high beta and gamma ray backgrounds from other fission products do not interfere with neutron counting so that by integrating the delayed neutron counts over a suitably fixed period, non-destructive analysis of fissionable elements is possible. By utilizing the differences in fission characteristics, it becomes possible to analyse mixtures or to determine isotopic concentrations. For example, while uranium–235 can undergo fission by thermal neutrons, uranium–238 requires fast neutrons so that irradiation first with

thermal neutrons only and then in a mixed neutron flux enables the isotopic composition to be determined. Similarly plutonium in breeder reactors can by thermal neutron fission be determined in the presence of uranium–238.

Nuclear reactions leading to the formation of nitrogen–17, a delayed neutron emitter (precursor) with a half-life of 4.14 seconds, can be utilized for analytical purposes. A lithium solution irradiated with thermal neutrons can lead to nitrogen–17 by the successive reactions

$$Li^6\ (n, \alpha)t;\ O^{18}\ (t, \alpha)N^{17}$$

thus, for known O^{18}-concentration (e.g. natural water) the lithium content may be measured, or for known lithium content, oxygen may be isotopically analysed for oxygen–18([23]).

"Knock on" particles

With fast neutron irradiations of hydrogenous media, "knocked-on" hydrogen nuclei may attain sufficient energy to induce nuclear reactions. An intimation that the nitrogen–13 detected in organic compounds irradiated with fast neutrons could be of value for analytical purposes was made by Gilmore and Hull([24]). While investigating the possible formation of nitrogen–13 by an (n, 2n) reaction for the determination of nitrogen, they found relatively large interference from reactions

$$C^{12}\ (p, \gamma)\ N^{13}$$

and $C^{13}\ (p, n)\ N^{13}$

as a result of reactions caused by knock-on protons in the organic media investigated.

By a similar argument, a non-destructive method was developed independently for the determination of deuterium concentration in water([25]). When a pure water sample containing deuterium is irradiated with neutrons, "knock-on" deuterons can be produced with sufficient

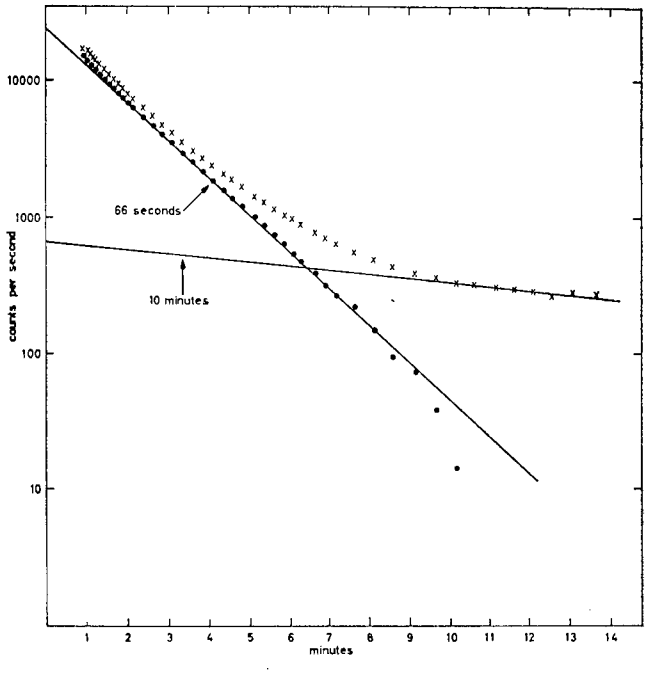

Fig. 3

Decay of the positron annihilation gamma radiation showing the 66s decay of F^{17} obtained from a 48% D_2O sample irradiated for 66 seconds at an epi-cadmium neutron flux of 6.7×10^{11} n/cm² sec. The 10 min. component is due to nitrogen-13.

energy to induce the formation of fluorine–17 by the nuclear reaction

$$O^{16}\ (d, n)\ F^{17}$$

the activity of which gives a direct measure of the deuterium concentration. In the same investigation, nitrogen–13 was detected from the reaction of knock-on particles with the polyethylene container. (See Figure 3).

Photoneutron emission

The photodisintegration of deuterium and the emission of photoneutrons require gamma ray energies greater than 2.23 MeV. A counting system based on the photodisintegration of deuterium is then naturally biased against all energy quanta below the photoneutron threshold of 2.23 MeV.

Few radionuclides produced by neutron irradiation of common elements emit gamma rays over 2.23 MeV in their decay. If, in addition, only those whose half-lives lie between 1 and 100 hours are considered, the number is small indeed. (See, for example, Table 1). It thus becomes possible to determine a small group of elements non-destructively and with high specificity.

Using a source of sodium–24 (15 hr., 2.75 MeV), the first application of photoneutron emission for analysis was to determine deuterium([26]) ([27]). A sample containing deuterium was placed near a large source of sodium–24 and its neutron emission was compared with a standard deuterium sample.

Essentially the same type of arrangement (see Figure 4) was used for the determination of sodium([28]). After neutron irradiation, the sample was immersed in a bottle of D_2O surrounded with a ring of six BF_3 neutron counters, and counted. Table 1 shows that a sample containing manganese, gallium or lanthanum would give high results due to the interference from manganese–54, gallium–72 or lanthanum–140, respectively. Of these only gallium constitutes a problem. The other two can readily be allowed for because their decays (2.58 hr. and 40 hr.) differ widely from sodium–24. It is fortunate that samples normally submitted for sodium analysis do not contain much gallium.

TABLE I

Photoneutron count rates for common elements likely to interfere in sodium analysis, compared with the count rate for sodium

Element	Isotope	Half-life (hrs.)	Activity (a) Calculated	Activity (a) Observed	Sodium equivalent (d) (μg).
Sodium.....	Na^{24}	15.0	14.84	14.90	1
Manganese....	Mn^{56}	2.58	12.65	11.99	1.24
Gallium.....	Ga^{72}	14.1	3.28	3.04	4.90
Lanthanum....	La^{140}	40.2	0.515	0.50	2.98×10^1
Magnesium....	Na^{24}	15.0	0.00247 b)	0.003 b)	4.97×10^3
Aluminium.....	Na^{24}	15.0	0.00142 b)	0.0017 b)	8.76×10^3
Potassium.....	K^{42}	12.4	0.00059	0.00058 c)	2.53×10^4

a) Normalised counts per minute for 1 μg metal irradiated for 1 hour at a thermal neutron flux of 10^{13} n/cm²-sec. and counted 1 hour after irradiation.

b) For a fission-spectrum neutron flux of 10^{12} n/cm²-sec, assuming a thermal to fission flux ratio of 10:1.

c) Measured for Analar grade $KHCO_3$ containing approx. 0.03% Na and corrected for the sodium-24 contribution.

d) Weight of element, in μg, yielding a neutron count rate equivalent to 1 μg Na 1 hour after the end of irradiation.

Clearly, each of the above elements, Mn, Ga, La or Na can be determined under suitable conditions. The determination of lanthanum could be of value where rare earths have to be analysed. By this method photoneutrons from deuterium can be used as a measure of lanthanum only withou any chemical separation; interference from sodium–24 could be reduced by allowing it to decay, before measuring the longer-lived lanthanum–140. Similarly, manganese can be measured in steel or blood samples([29]), provided the sodium to manganese ratio by weight is reduced to less than 30.

Further developments are possible by utilizing the photoneutron emission from beryllium for which the threshold is about 1.6 MeV., but because many nuclides emit radiation over 1.6 MeV, the method of photoneutron counting would require other discriminatory steps to make the analysis more specific.

CHEMICAL EFFECTS OF NUCLEAR TRANSFORMATIONS

The preceding sections discussed nuclear effects. In this section attention is also focused on the other parts of a molecule or solid when one of its constituent atoms is involved in a nuclear transformation.

When an atom of mass M undergoes a nuclear reaction, such as radiative neutron capture, and emits a gamma ray of energy $E\gamma$ (frequently between 5 and 8 MeV), the nucleus will acquire a recoil energy $E^2\gamma/2Mc^2$. Thus, a bromine atom releasing a 5 MeV gamma ray will have a recoil energy of some 167 eV, or about an order of ten times that of the chemical bond. It is clear that a polyatomic molecule should be expected to dissociate if one of its constituent atoms undergoes radiative neutron capture.

This effect was first demonstrated by Szilard and Chalmers([30]) who showed that radio-iodine could be extracted with a sodium sulphite solution from neutron irradiated ethyl iodide. Since then many similar reactions have been studied academically and as a production method for high specific activity radionuclides. For good enrichment it is generally best to select organic compounds, stable complexes or oxygenated anions with which the radionuclide, after recoil, does not exchange. In this way high specific activity radio-antimony, radioiron and radiochromium have been prepared from NH_4SbF_6([31]), $K_4Fe(CN)_6$([32]) and K_2CrO_4([33]) respectively. It should be noted that prolonged irradiation will decrease the specific activity of the product as a result of radiolysis of the target compound.

In condensed phases the yield from Szilard-Chalmers reactions is almost never complete, but the mechanism by which some radionuclides should be retained in the molecular form of the target is by no means clear. In the simple calculation it was assumed that the atom is released without sharing its energy with the rest of the molecule. If the energy is shared with the rest of the molecule as translation, then for diatomic molecules with atoms having masses M_1 and M_2 the translation energy is $E^2\gamma/2(M_1 + M_2)C^2$ thus reducing the recoil energy of M_1 by the factor $M_2/M_1 + M_2$. Now, if M_2 is small, the recoil energy may become comparable with the bond strength and the retention probability increases([34]) ([35]).

Part of the retention could probably be explained by repenetration. The highly energetic ("hot") atoms can be assumed to undergo reaction in two stages. Firstly at high energies, much of the energy degradation would take place by collision with isotopic nuclei and could lead to retention by displacement of isotopic atoms in the molecules by head-on collision. Examples of such reactions have been indicated([36]) ([37]) by the trapping of highly energetic fission product iodine. Secondly, diffusion controlled lower energy reactions could occur by radical formation and excitation when the hot atom had lost most of its initial energy. This modified "hot spike" theory([38]) has been able to account for some experimental results, but it is still not generally accepted and the subject still forms the basis of a good deal of current investigation.

An intriguing problem is to determine what the relative contributions of ionization and free radical processes are. In most cases elucidation is difficult, but in the case of isomeric transition the dominating reaction mechanism must be ionic. Because of the low energy radiation generally emitted in isomeric transition, hot atom reactions are considered unlikely. Nevertheless, when internal conversion occurs, i.e. when an electron from the K or L shell is ejected instead of a gamma ray, the atom can become highly excited as a result of the emission of Auger electrons (electrons which fall in to fill vacant inner sites do not emit their excess energy by photon emission, but by ejection of a further electron). The atom then attains a high positive charge and undergoes hot atom reactions by ionic processes. In this way lower isomers of tellurium–127 and –129 can be separated([39]) even though their decay energies are about 107 keV whereas no separation can be obtained with zinc–69 isomer whose decay proceeds by an unconverted 435 keV gamma ray.

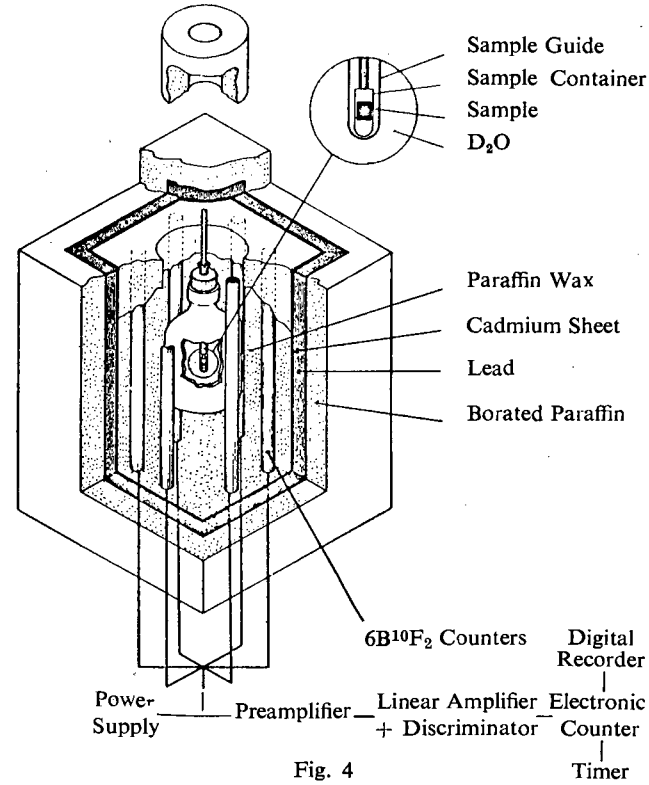

Fig. 4

Photoneutron measurement assembly and block diagram of electronic circuit.

SUMMARY

Three aspects of nuclear chemistry have been touched upon, and it has been shown that in isotope production the present interest appears to be towards better methods of producing carrier-free radionuclides, especially from reactor irradiated material; in activation analysis the interest is in rapid and non-destructive analysis on the one hand and high specificity on the other, while hot atom chemistry is still looking for a good theory to explain the different effects at different levels of "hotness".

REFERENCES

(1) CURIE, I. and JOLIOT, F., Nobel Prize Lecture, 1935,
(2) PEISACH, M. and PAISS, Y., Israel Atomic Energy Comm. rept. **IA-775**, 117 (1962).
(3) MYERS, W. G. and VANDERLEEDEN, J. C., J. Nucl. Med.. **1**, 149 (1960).
(4) PEISACH, M., Israel Atomic Energy Comm. rept. **IA-685**, 66 (1961).
(5) BRUSTAD, T. and BAARLI, J., J. Chem. Phys. **22**, 1311 (1954).
(6) SCHULER, R. H. and McCAULEY, C. E., J. Chem. Phys. **25**, 1080 (1956).
(7) TOTH, G., J. Inorg. Nucl. Chem. **19**, 186 (1961).
(8) DOIS, M. and ROSA, U., U.S. Patent 3, 114, 608 (1963).
(9) STIENNON-BOVY, R. and HAEGEMAN-GELADI, G., "Production and use of short-lived radioisotopes from reactors", I.A.E.A. Vienna, (1963) 141.
(10) ARNOTT, D. G. and PERUMA, C. P., Intern. J. Appl. Radiation and Isotopes **2**, 85 (1957).
(11) PEISACH, M., Radiochim. Acta (1964) (in press).
(12) SHIKATA, C., SHIKATA, E. and SHIBATA, N., Nippon Genshiryoku Gakkaishi (J. Atomic Energy Soc. Japan) **4**, 149 (1962) (in English).
(13) PEISACH, M., J.S. African Chem. Inst. (1964) (in press).
(14) MELLISH, C. E. and PAYNE, J. A., Nature **178**, 275 (1956).
(15) STANG, L. G. Jr., TUCKER, W. D., DOERING, R. F., WEISS, A. J., GREENE, M. W. and BANKS, H. O. Proc. 1st UNESCO Intern. Conf. Paris, 1957, "Radioisotopes in scientific research" Vol. **1**, Pergamon press (1958).
(16) PEISACH, M., Israel Atomic Energy Comm. rept. **IA-620**, 18 (1960).
(17) BRESESTI, M., DEL TURCO, A. M. and OSTIDICH, A., Radiochim. Acta **2**, 49 (1963).
(18) CHACKETT, K. F. and CHACKETT, G. A., J. Inorg. Nucl. Chem. **4**, 225 (1957).
(19) GHIORSO, A., SIKKELAND, T., LARSH, A. E. and LATIMER, R. M., Phys. Rev. Letters **6**, 473 (1961).
(20) SEABORG, G. T. and LIVINGOOD, J. J., J. Am. Chem. Soc. **60**, 1784 (1938)
(21) AMIEL, S and PEISACH, M., Israel Atomic Energy Comm. rept. **IA-784** (1962).
(22) AMIEL, S. and PEISACH, M., Atomnaya Energiya **14**, 535 (1963).
(23) AMIEL, S. and PEISACH, M., Anal. Chem. **35**, 323 (1963).
(24) GILMORE, J. T. and HULL, D. E., Anal. Chem. **34**, 187 (1962).
(25) AMIEL, S. and PEISACH, M., Anal. Chem. **34**, 1305 (1962).
(26) HAIGH, C. P., "Second Radioisotope Conference, Oxford, 1954", Vol. II, Butterworth, London (1954).
(27) ODEBLAD, E., Clin. Chim. Acta **1**, 67 (1956).
(28) AMIEL, S. and PEISACH, M., Anal. Chem. **35**, 1072 (1963.)
(29) STOLL, Z., PEISACH, M. and AMIEL, S., Israel Atomic Energy Comm. unpublished data (1963).
(30) SZILARD, L. and CHALMERS, T. A., Nature **134**, 462 (1934).
(31) WILLIAMS, R. R., J. Phys. Chem. **52**, 603 (1948).
(32) TOMPKINS, E. R., COHN, W. E., ADAMSON, A. W. and WILLIAMS, R. R. in "Radiochemical studies: The Fission Products", N.N.E.S. IV-9, McGraw-Hill, New York, (1951) Bk **1**, 199.
(33) HARBOTTLE, G. and MADDOCK, A. G., J. Chem. Phys. **21**, 1686 (1953).
(34) SUESS, H., Z. physik. Chem. **B 45**, 297, 312 (1940).
(35) STEINWEDEL, H. and JENSEN, J. H. D., Z. Naturforsch. **2a**, 125 (1947).
(36) DENSCHLAG, H.-O., HENZEL, N. and HERMANN, G., Radiochim. Acta **1**, 172 (1963).
(37) PAISS, Y. and AMIEL, S., Israel Atomic Energy Comm. rept. **IA-822**, 93 (1963).
(38) HARBOTTLE, G. and SUTIN, N. "Advances in Inorganic Chemistry and Radiochemistry" Editors EMELEUS, H. J. and SHARPE, A. G., Academic Press, New York, **1**, 267 (1959).
(39) SEABORG, G. T., FRIEDLANGER, G. and KENNEDY, J. W., J. Am. Chem. Soc. **62**, 1309 (1940).

No. 58

Reprinted from
THE JOURNAL OF THE SOUTH AFRICAN CHEMICAL INSTITUTE,
April, 1965, Vol. XVIII, pp. 1-5.

Oorgedruk uit
DIE JOERNAAL VAN DIE SUID-AFRIKAANSE CHEMIESE INSTITUUT,
April 1965, Deel XVIII, bl. 1-5.

C.P.W.-P.M.B.

THE PREPARATION OF POTASSIUM HEXACYANOCOBALTATE(III) LABELLED WITH COBALT-58 AND -60 FOR HYDROLOGICAL STUDIES

by **M. PEISACH**

THE PREPARATION OF POTASSIUM HEXACYANOCOBALTATE(III) LABELLED WITH COBALT-58 AND -60 FOR HYDROLOGICAL STUDIES

by

M. PEISACH*

OPSOMMING

Kobalt-58, in 'n reaktor vervaardig deur die kernreaksie $^{58}Ni(n,p)^{58}Co$, en kobalt-60 deur $^{59}Co(n,\gamma)^{60}Co$, word gebruik om spoorderoplossings van $K_3Co(CN)_6$ te berei vir hidrologiese ondersoeke. Kobalt-58 word geskei met 9N HCl op 'n anioon-uitruilhars en geëlueer met N HCl. Kobalt-60 word regstreeks verkry deur neutronbestraling van kobaltchloried. Tot 300 mC ^{60}Co word op een slag bewerk.

SUMMARY

Reactor-produced cobalt-58, by the reaction $^{58}Ni(n,p)^{58}Co$ and cobalt-60, by $^{59}Co(n,\gamma)^{60}Co$ were used to prepare tracer solutions of $K_3Co(CN)_6$ for hydrological studies. Cobalt-58 was separated by anion-exchange resin with 9N HCl and eluted with N HCl. Cobalt-60 was obtained by direct neutron irradiation of cobalt chloride. Batches containing up to 300 mC ^{60}Co were handled.

INTRODUCTION

Aqueous hexacyanocobaltate(III) has been demonstrated to be superior to other cobalt complexes for hydrological tests in limestone[1] and for use in measuring the period of retention in percolating filters.[2,3] Material labelled with cobalt-60 was used for hydrological tracing, but because its long half-life made subsequent tests on the same site open to doubt, the shorter lived 71-day cobalt-58 may sometimes be preferred. This paper describes the preparation of the tracer material labelled either with cobalt-58 or with cobalt-60.

When used for hydrological studies, the hexacyanocobaltate tracer solutions are mixed with relatively large amounts of carrier. Because problems from too low a specific activity are unlikely to arise, cobalt-60 could be prepared by the reaction $^{59}Co(n,\gamma)^{60}Co$ by the direct irradiation of a suitable cobalt salt in a reactor. Cobalt-58, as prepared by the reaction $^{58}Ni(n,p)^{58}Co$, however, yields a high specific activity (carrier-free) product. Thus, in this procedure it was necessary to dilute the cobalt-58 with stable cobalt to obtain the required specific activity.

EXPERIMENTAL

Preparation and irradiation of nickel.—Nickel carbonate, low in iron and cobalt, as supplied by The British Drug Houses, Ltd., was used to prepare the target material. The common impurities were iron (<40 p.p.m.), cobalt (<20 p.p.m.) and zinc (<25 p.p.m.). Of these, the most serious was cobalt, which, on activation would produce cobalt-60 contamination, and which therefore had to be removed before irradiation. Cobalt-60 tracer was used to check the efficiency of this process.

* Present address: Southern Universities Nuclear Institute, Faure, South Africa.

The nickel carbonate was dissolved in hydrochloric acid and the acid concentration adjusted to 9N. A small amount of cobalt-60 solution was added as tracer and the solution passed through a column of Amberlite IRA-400, 30 cm in length and 2·5 cm in diameter, when all the cobalt activity was retained in the top centimeter.[4,5] Nickel, free from cobalt, was precipitated from the eluate with cobalt-free sodium carbonate. Weighed amounts of the washed and dried precipitate were sealed in quartz vials for irradiation in aluminium cans placed in a dummy fuel element of the reactor core of IRR-1.

The separation of cobalt-58.—The nickel carbonate was irradiated, and left for about a week to allow short-lived products, such as 2·5-hour ^{65}Ni and 15-hour ^{24}Na produced in the aluminium can by the reaction ^{27}Al(n,α)^{24}Na, to decay. The ampoule was then smashed, and the powder dissolved in hydrochloric acid to give a solution 9N with respect to acid.

Radiocobalt was separated from the irradiated nickel in two stages. In this way the volumes eluted could be kept manageably small. Firstly, the solution was passed through the same column as used for purification, where most of the nickel was recovered. Secondly, the radiocobalt, with some nickel eluted from the first column, was passed through a smaller column of Amberlite IRA-400, 10 cm in length and 1 cm in diameter, to remove all remaining nickel salts. A typical elution curve for the first stage is shown in Fig. 1 where the 36-hour ^{57}Ni, produced by the reaction ^{58}Ni(n,2n)^{57}Ni, served as a tracer for nickel.

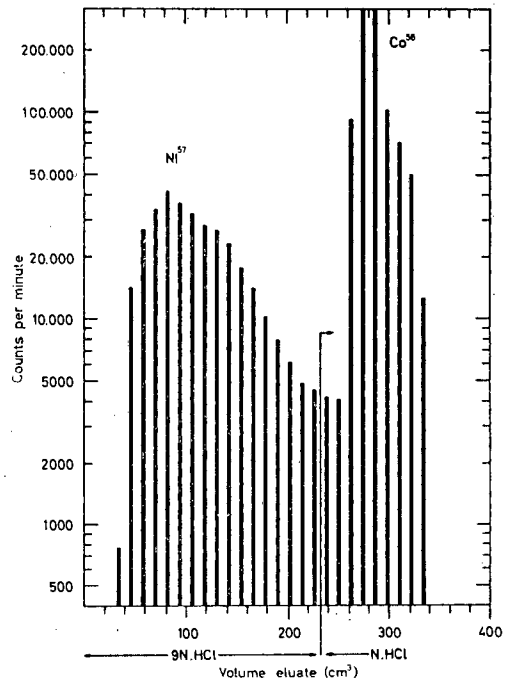

FIG. 1—Typical elution curve for the preliminary separation of cobalt-58 from nickel.

The cobalt-58 eluate was concentrated, its activity measured and cobalt chloride added to obtain the required specific activity. The solution was then evaporated just to dryness to remove the excess acid and the residue taken up in water slightly acidified with hydrochloric acid for conversion to potassium hexacyanocobaltate(III).

The yield of cobalt-58 obtained at IRR-1 corresponded to a saturation activity of 103 mC per g nickel at a flux of 10^{13} neutrons/cm^2 sec. This is compared with corresponding irradiations elsewhere in Table 1.

TABLE I

Yield of cobalt-58 normalised to saturation activity for 1 g nickel irradiated at a flux of 10^{13} neutrons/cm^{2}sec

Reference	Yield [mC]	Remarks
Mellish and Payne[6]	89.8	Harwell Hollow uranium bar
	85.2	Thermal flux $1{\cdot}4\times10^{12}$n/cm^{2}sec
	82.6	,, ,, $1{\cdot}2\times10^{12}$
	85·0	,, ,, $1{\cdot}0\times10^{12}$
Levin and Bochkarev[7]	37·5	
Shikata, Shikata and Shibata[8]	44·3	JRR–1 Hole 2
	73·3	JRR–1 Hole 1
This work	103	IRR–1 Position 46
Calculated	197·3	σ=105 mb[9] (fission spectrum neutrons)
	206·7	σ=111 mb[10]

Preparation and irradiation of cobalt.—Cobalt metal was not convenient as a target material because it required relatively harsh conditions for its dissolution. Similarly, cobalt oxide would have to be dissolved in acid, excess of which was detrimental at later stages of processing. Cobalt chloride, being readily soluble in water, is suitable as a target, but its water of crystallisation has to be removed to prevent pressure building up from radiolysis.

Cobalt chloride, containing small amounts of impurities such as iron (<30 p.p.m.), nickel (<12 p.p.m.) and zinc (<50 p.p.m.), was dried, weighed and sealed in quartz vials for irradiation. The vial was kept for the short-lived radionuclides, notably ^{38}Cl and ^{24}Na, to decay and then smashed, the cobalt chloride dissolved in water and the solution, acidified with a few drops of hydrochloric acid, was used for conversion to potassium hexacyanocobaltate(III).

Self-absorption in cobalt chloride.—Because both cobalt and chlorine have relatively high thermal neutron capture cross sections, it was expected that the activity obtained from irradiated cobalt chloride would be lower than calculated because of neutron self-absorption within the sample. Fig. 2 shows the activity of a 10 g sample contained in a cylindrical vial of diameter d plotted as a function of d and calculated relative to the hypothetical case where no self-absorption exists.

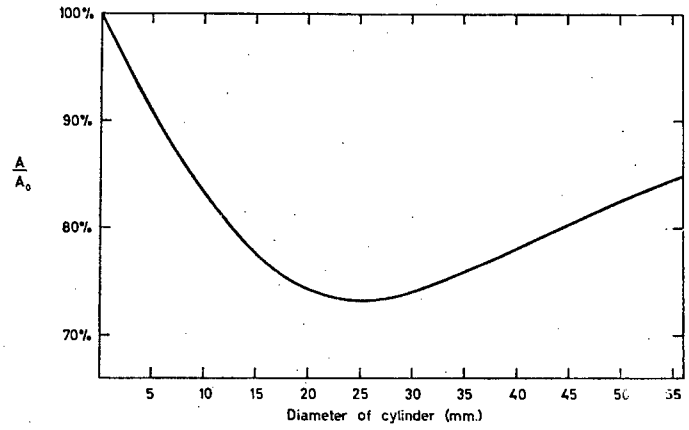

FIG. 2—Self-absorption in cobalt chloride. The dependence of the relative activity produced in a 10-g sample contained in a cylindrical vial, on the diameter of the vial.

At the reactor core position where the samples were irradiated there was an appreciable variation of flux with height, so that it was undesirable to irradiate a long sample. Rather than to minimise self-absorption, the self-absorption of the sample was calculated[11] and the irradiation duration increased accordingly.

Preparation of potassium hexacyanocobaltate(III).—The solution of radiocobalt, as ^{58}Co or ^{60}Co, was treated with a slight excess of potassium cyanide solution and the resulting buff precipitate of cobaltous cyanide, which gradually darkened to yellow-brown, filtered off and thoroughly washed with water. It was then stirred with a 10% excess of 37% w/v aqueous potassium cyanide. A greenish precipitate, probably $K_2Co[Co(CN)_6]$, formed but it was readily converted to a deep yellow solution of $K_3[Co(CN)_6]$ by the addition of hydrogen peroxide at room temperature in neutral solution, or without the hydrogen peroxide by heating to about 70°C.

Gamma ray measurements showed that the cobalt-58 contained less than 0·1% of cobalt-60, whilst no impurity could be detected in the cobalt-60. The activities of the preparations were calibrated by comparison with standards and by ionisation chamber measurements. Normally, batches containing about 100 mC cobalt-60 were processed, but when 300 mC were required, samples were irradiated to a somewhat higher specific activity and diluted with non-radioactive hexacyanocobaltate as required.

Two tests were carried out to determine cationic cobalt. In the one, cobalt was precipitated with carrier cobalt as sulphide and the activity measured; in the second, the solution was passed through a cation-exchange column and the activity retained on the column measured. All samples were assayed to be better than 99%.

DISCUSSION

The yield of cobalt-58.—Although the reaction $^{58}Ni(n,p)^{58}Co$ is exoergic (Q=+0·39MeV), the high coulomb barrier raises the effective threshold neutron

energy to about 1·5 MeV. The yield calculated from the effective cross section for fission spectrum neutrons,[9,10] (Table 1) is very much higher than that obtained, showing that the energy distribution in the irradiation neutron flux differed appreciably from that in fission. The extent of moderation of the neutron flux can be seen by comparing the measured and calculated yields, but the result is qualitative rather than quantitative without corresponding measurements with threshold detectors at higher neutron energies. The relatively high yield obtained at IRR-1 (see Table 1) showed that the extent of moderation was less than elsewhere and confirmed that the irradiation site was suited for radioisotope production with fast neutrons.

Radiochemical purity of the products.—In the case of cobalt-60, the nuclear reactions $^{59}Co(n,p)^{59}Fe$ and $^{59}Co(n,2n)^{58}Co$ will lead to contamination by iron-59 and cobalt-58. Using the accepted value for the reaction cross sections for fission spectrum neutrons[9] and allowing for the contribution of thermal neutrons, the iron-59 was calculated to contribute $1{\cdot}7\times10^{-2}$ % of the activity of the samples. Because the threshold for the formation of cobalt-58 is so high, about 10·2 MeV, the probable contribution of cobalt-58 was calculated to be less than 4×10^{-4} %. Radioactivation of impurities would contribute less than 10^{-4} % of the activity. Such low levels of impurity would be difficult to detect and the level would fall still further during the course of the investigation, because their half-lives are less than that of cobalt-60. Accordingly, the cobalt-60 was accepted as radiochemically pure.

In the case of cobalt-58, the more important impurities were removed during purification and could not lead to radioactive contaminants. The main nuclear reaction leading to radiocontamination is $^{60}Ni(n,p)^{60}Co$ which would produce cobalt-60 activity of about $2{\cdot}8\times10^{-2}$ % and this impurity would not be chemically separable. Moreover, because of its longer life, the relative contribution of cobalt-60 would increase with the age of the preparation and the duration of the experiment. Accordingly, this limits the purity of cobalt-58. Other nuclear reactions such as $^{58}Ni(n,\alpha)^{55}Fe$ and $^{62}Ni(n,\alpha)^{59}Fe$ produce radio-iron which would not follow cobalt through the chemical processing.

Israel Atomic Energy Commission,
P.O. Yavne, Israel.

Received July 14th, 1964.

REFERENCES

1 E. A. Halevy, A. Nir, Y. Harpaz and S. Mandel, *Proc. U.N. Intern. Conf. Peaceful Uses At. Energy, 2nd Geneva*, 1958 P/1613.
2 G. E. Eden and K. V. Melbourne, *Intern. J. Appl. Radiation Isotopes*, 1960, **8**, 172.
3 E. Halevy and A. Nir, *J. Geophys. Res.*, 1962, **67**, 2403.
4 N. V. Sidgwick, *The Chemical Elements and Their Compounds*, Vol. II, Clarendon Press, Oxford, 1950.
5 G. E. Moore and K. A. Kraus, *J. Am. Chem. Soc.*, 1952, **74**, 843.
6 C. E. Mellish and J. A. Payne, *Nature*, 1956, **178**, 275.
7 V. I. Levin and V. V. Bochkarev, *C.A.*, 1962, **56**, 11145.
8 C. Shikata, E. Shikata and N. Shibata, *J. At. Energy Soc. Japan*, 1962, **4**, 105.
9 J. C. Roy and J. J. Hawton, *At. Energy Can. Ld.*, 1960, AECL-1181.
10 J. F. Barry, *Reactor Science and Technology, J. Nucl. Energy: Pt A and B*, 1962, **16**, 467.
11 J. Gilat and Y. Gurfinkel, *Nucleonics*, 1963, **21**, No. 8, 143.

No. 59

GERMANIUM (GERMANYL) FERROCYANIDE

BY
M. PEISACH,
W. PUGH,
AND
F. SEBBA

This Communication was published in the
Journal of the Chemical Society, March, 1950, pages 949—950.

Preprinted from the Journal of the Chemical Society, 1950.

192. *Germanium (Germanyl) Ferrocyanide.*

By M. PEISACH, W. PUGH, and F. SEBBA.

Ionised ferrocyanides react with acid solutions of germanium dioxide to form an insoluble white precipitate. The reaction can be used as a qualitative test for germanium and, under proper conditions, leads to a product of definite composition, namely *germanyl ferrocyanide*, $[Ge(OH)_2]_2Fe(CN)_6$ or $(GeO)_2Fe(CN)_6,2H_2O$.

INSOLUBLE ferrocyanides of quadrivalent titanium, zirconium, thorium, and tin are well known (Gmelin, "Handbuch der Anorganischen Chemie," 8th Edn., System No. 59, Part B, 1930, p. 604), but no corresponding compound of germanium has been described hitherto. Many years ago, one of us (F. S.) observed that a white precipitate appeared when an acid solution of germanium chloride was treated with potassium ferrocyanide. The nature of this precipitate and the conditions necessary for the preparation of *germanyl ferrocyanide* are now described.

The formation of a white precipitate, or even a colloidal opalescence, on treatment with ferrocyanide may well serve as a useful qualitative test for germanium. This element is usually associated in minerals with arsenic and is separated from other metals by distillation of the volatile chloride from hydrochloric acid solutions. However, even with the utmost precautions to keep arsenic in the quinquevalent state the distillate contains some arsenic which then inteferes with the simple test for germanium by precipitation as the white sulphide. Neither tervalent nor quinquevalent arsenic gives a precipitate with ferrocyanides (Gmelin, *op. cit.*, p. 607). Hence, if the distillate is treated with potassium ferrocyanide solution the appearance of a precipitate is evidence of the presence of germanium. One part of germanium in 10,000 parts of solution gives an opalescence; larger amounts give a white gelatinous precipitate.

The nature and appearance of this precipitate vary with the conditions. In slightly acid solution there may be a time lag of an hour or more before precipitation, but it is shortened by increasing the acidity of the solution and by raising the temperature; the optimum conditions appear to be an acidity at least equivalent to 4N-hydrochloric acid and a temperature of 50—60°. The appearance of opalescence or a precipitate, depending on the concentration of germanium, is then a matter of seconds. Sulphuric, acetic, and chloroacetic acid are much less effective in coagulating the initial sol; and if the temperature exceeds 70° the inital white precipitate becomes blue rather quickly.

This colour change is undoubtedly due to the formation of Prussian-blue by decomposition of the excess of ferrocyanide in the strongly acid solution (Gmelin, *op. cit.*, p. 584). It takes place slowly in the cold, even in the dark and in the absence of air, but rapidly if a large excess of ferrocyanide is employed. Consequently, in the early part of the work it was impossible to get a product of uniform composition. Later, it was found that if the ratio of ferrocyanide to germanium does not exceed one g.-ion per g.-atom the precipitate darkens only slowly during several days. This is fortunate because the gelatinous precipitate cannot be filtered off and, as it is highly retentive of adsorbed electrolytes, its washing by decantation and centrifugation occupies several days. Under the most favourable conditions encountered the final product had acquired a pale mauve tinge. This product was found to contain two atomic proportions of germanium for each ferrocyanide radical and its analysis corresponds with the empirical formula $(GeO)_2Fe(CN)_6,2H_2O$ or $[Ge(OH)_2]_2Fe(CN)_6$. *X*-Ray structure analysis is the only means of establishing unequivocally which is the actual structure. No compound even approximating in composition to $GeFe(CN)_6$ has been detected in this work, and this is in accord with the general chemistry of germanium, for there is no recorded compound of this element in which the occurrence of a simple quadrivalent germanium ion has been estalished.

A similar zirconyl ferrocyanide, $(ZrO)_2Fe(CN)_6$, has been described by Weibull (*Lunds Univ.*

Arsskr., 1881—82, II, 18, No. 5, 40), though Venable and Mochlmann (*J. Amer. Chem. Soc.*, 1922, **44**, 1705) obtained products with ferrocyanide–zirconyl ratios as high as 3 : 4. Our experience with the germanium ferrocyanide leads us to suspect, however, that the American authors' products were highly contaminated with Prussian-blue.

Experimental.

Germanyl Ferrocyanide.—Pure germanium dioxide (4 g.) was dissolved in hot 5N-sodium hydroxide (100 ml.). The solution was diluted to 400 ml., filtered from a trace of undissolved oxide, neutralised with hydrochloric acid, and treated with concentrated hydrochloric acid to bring the acidity to 5N. The temperature was adjusted to 60°. Precipitation was made with 0·2M-potassium ferrocyanide (200 ml.).

The only practical way of washing the pure, white, bulky, and gelatinous precipitate was by settling and decantation. Because each settling period was of the order of a day the whole process of washing was extremely tedious and led to continuous darkening of the product. After the fourth wash the precipitate was dried *in vacuo* for several days, becoming then more granular. Further washing with water was then possible in a much shorter time and without appreciable decomposition. Finally, the moist precipitate was centrifuged 10 times with small amounts of ether to ensure complete removal of adsorbed hydrochloric acid. Alcohol could not be used for this purpose, for it tended to peptise the material. The product was then dried *in vacuo*.

It was a pale mauve powder which was quite stable in air and showed no tendency to become blue after many weeks' exposure to the laboratory atmosphere. Some samples that had been less thoroughly washed did become blue on storage. A thin film of Prussian-blue could often be seen over the surface of the precipitate in the centrifuge tube.

Analysis.—Germanium was determined as Mg_2GeO_4 by a modification of Muller's method (*J. Amer. Chem. Soc.*, 1922, **44**, 2493). Modification was necessary because *germanyl ferrocyanide* is insoluble in water and in acids. It does however dissolve in caustic alkalis and in aqueous ammonia. An ammoniacal solution of the sample was therefore treated with ammonium sulphate–magnesium sulphate solution, the proportions of the reagents being carefully controlled in accordance with Muller's directions. The precipitate of magnesium ammonium germanate, after being washed, was ignited to Mg_2GeO_4. The ferrocyanide in the filtrate from the germanium determination was determined, after acidification with sulphuric acid, by titration with standard permanganate by the method of de Haen (*Annalen*, 1854, **90**, 160) or with standard ceric sulphate using ferroin as internal indicator (Vogel, "Quantitative Inorganic Analysis," Longmans, 1947, p. 383). In a few cases too, the total iron was determined volumetrically after decomposition of a fresh sample with concentrated sulphuric acid (Kjeldahl). Excellent agreement was obtained by all methods.

In all, over 30 analyses were made of samples of 4 different preparations {Found: Ge, 34·2; $Fe(CN)_6$, 49·6; Fe, 13·0. $[Ge(OH)_3]_2Fe(CN)_6$ requires Ge, 34·2; $Fe(CN)_6$, 49·84; Fe, 13·1%}.

Confirmation that the compound contains either co-ordinated water or hydroxyl groups was obtained by pyrolysis. A weighed sample, mixed with copper oxide to decompose volatile cyanogen compounds, was heated in a combustion train in pure dry air and the water liberated was absorbed in "Anhydrone." The water absorbed amounted to 8·6% (Calc. for $2H_2O$, 8·5%).

Properties.—Pure germanyl ferrocyanide is a white solid which, like all other ferrocyanides, is slowly decomposed by strong acids with formation of Prussian-blue. It is insoluble in water and in moderately strong acids, but dissolves readily in alkalis, with decomposition, forming soluble germanates and alkali ferrocyanides. Heat decomposes it; at 130° it loses about one-third of its weight, and the vapours smell strongly of cyanogen compounds; at a red heat in air it loses half its weight and the vapours carry germanium as well, probably the result of reduction by carbon to the volatile germanous oxide. When desiccated *in vacuo* over sulphuric acid it becomes extremely hygroscopic; it will then absorb up to one-third of its own weight of water.

University of Cape Town.

[*Received, January 9th*, 1950.]

Printed in Great Britain by Richard Clay and Company, Ltd., Bungay, Suffolk.

No. 61

REPRINT

Journal of Radioanalytical Chemistry, Vol. 16 (1973) 445—452

SOME ANALYTICAL INVESTIGATIONS INTO THE USE OF X-RAYS EMITTED DURING CHARGED-PARTICLE IRRADIATION

M. PEISACH,* D. A. NEWTON, P. F. PECK, T. B. PIERCE

Analytical Sciences Division, A. E. R. E., Harwell, Nr. Didcot,

ELSEVIER SEQUOIA S.A.
Lausanne

AKADÉMIAI KIADÓ
Budapest

Journal of Radioanalytical Chemistry, Vol. 16 (1973) 445—452

SOME ANALYTICAL INVESTIGATIONS INTO THE USE OF X-RAYS EMITTED DURING CHARGED-PARTICLE IRRADIATION

M. PEISACH,* D. A. NEWTON, P. F. PECK, T. B. PIERCE

Analytical Sciences Division, A. E. R. E., Harwell, Nr. Didcot, Berkshire (England)

X-radiation emitted as a result of charged particle irradiation offers a means of extending the scope of analytical methods based on the measurement of prompt radiation. X-ray yields from a number of pure materials have been examined over a range of particle energies and X-ray measurement applied to the determination of a number of constituents in aluminium alloys. An examination of the distribution of silicon and germanium across an electronic component has been carried out using a small diameter incident ion beam.

Introduction

Analytical techniques based on the measurement of prompt radiations emitted as a result of charged-particle irradiation have primarily been concerned with the detection of radiations of nuclear origin or of particles resulting from elastic scattering processes. Thus gamma-radiation, charged-particles and neutrons from nuclear reaction and a number of elastically scattered ions have been counted to provide information to match the requirements of specific analytical problems.[1] Radiations from nuclear reactions have, in general, been applied to the determination of lighter elements, although techniques are being extended to provide measurement of elements of higher atomic number such as iron[2] zinc[3] chromium nickel and copper[4] and chromium, manganese and iron.[5] The majority of these applications have required sample irradiation with particles with energies of between 0. 5 and 5 MeV and at these energies, substantial outputs of X-radiation are generated from many elements which can also offer the basis of analytical determination. X-ray methods can therefore be applied with experimental techniques which are closely similar to those already in use and for many applications, X-rays can be measured at the same time as other prompt-radiations.

*On leave from Southern Universities Nuclear Institute, P.O. Box 17, Faure C. P., Republic of South Africa.

X-ray measurement to some extent complements other prompt-radiation techniques, since it offers a means of analytical determination of intermediate and heavy elements which are not, at present, comprehensively covered by existing methods. An additional attraction is the extension of X-ray measurement to multi-element analysis using established techniques of X-ray spectroscopy to provide information about several components present in the sample. Substantial interest has been shown in the use of charged-particles with energies of the order of tens or hundreds of keV for exciting characteristic X-radiation and a number of systematic studies have been made at these particle energies which have been directed at measuring X-ray production efficiencies and at assessing the analytical potential of particle excited X-rays.[6,7] However, the strong dependency of X-ray production upon incident particle energy has stimulated interest in the use of more energetic charged-particles for X-ray excitation and a limited number of papers have appeared which have examined the production and application of X-rays produced by particles with energies of the order of MeV.[8,9] Such studies have shown that the absolute excitation cross-sections may be very high, offering the basis for sensitive analytical determination, and the low bremsstrahlung background of ion-induced X-ray radiation offers a high signal to background ratio[10] so that parts per million sensitivies appear to be a very real possibility. The multielement capability of the technique has also been demonstrated by the accumulation of spectra from a variety of materials in which contributions from a number of elements have been identified. High-resolution semiconductor techniques offer a convenient means of measurement of X-rays for analytical purposes, although the use of X-ray crystal spectrography may well be necessary for certain applications where the resolution of the semiconductor detector is inadequate. The analytical potential of charged-particle excited X-rays both to complement the existing prompt-radiation techniques and to extend accelerator based analytical methods, suggests the technique warrants further investigation and this paper summarises some work carried out to measure X-ray yields from a number of elements over the energy range most frequently used in this laboratory for prompt-radiation measurements and to apply the technique to the solution of two specific problems, the determination of a number of elements in samples of aluminium alloys and, in conjunction with small-diameter incident ion beams, to examine the distribution of elements across an electronic component.

Experimental

Protons with energies of between 1.0 and 2.8 MeV were produced with the electrostatic generator IBIS at A.E.R.E. Harwell. The beam-line used was that designed for micro-beam work permitting small beams with diameters down to 3 μm diameter to be produced on the target with a special quadrupole assembly.[11] However, very small ion beams were used only for examining spatial distributions by beam scann-

ing or for irradiating very small samples and larger beams were used for bombarding larger homogeneous samples. The target chamber contained a moveable sample table with holders for two samples placed one on either side of a quartz disc. The table could be moved in three dimensions by stepping motors under command from a controller placed outside the chamber vacuum so that either the samples or the quartz disc could be moved into the particle beam as required. The movement of the table could be controlled over wide limits to permit a particular region of the sample to be lined up for irradiation. The size and position of the beam was viewed on the quartz disc through two microscopes, with one in front and the other behind the sample table. The ion beam was moved relative to the sample for scanning by electrostatic deflection and beam movement was discontinuous, X-rays being counted while the ion beam was stationary on the target and all counting circuits were inhibited while the beam movement was taking place. By this means, the recorded X-ray yield could be identified with the irradiation of a particular region of the sample surface. If the intensity of the incident ion beam was sufficient to damage the sample surface when stationary for the time required to accumulate sufficient counts, the ion beam could be rapidly scanned to a regular raster pattern so that heat could be dissipated over a larger area.

X-rays were measured by means of a silicon detector and output pulses from the detector were fed, after amplification, to a 4096 channel pulse-height analyser. Spectra were punched on paper tape for storage and subsequently processed in either a PDP-8 or an IBM 370/165 computer depending upon the mathematical manipulations required. The ion dose falling on the target was measured by beam-current integration and the integrator used to control the analyser so that the X-ray yield could be accumulated for a known, pre-set particle dose.

Samples were mounted in metallurgical mounting resin and were polished with a succession of finer grinding powders to give a good surface finish when viewed under a microscope. "Specpure" materials were irradiated for yield measurements and several were mounted in one sample holder to permit yields from a number of elements to be obtained without there being any need to let the target chamber up to air. No indication was found of cross-contamination when several materials were polished in the same mount.

A number of different computer programs were available for processing the X-ray data, varying from simple display and peak-area calculation techniques to more complex data interpretation methods and contouring programmes to simplify the presentation of surface scanning data.

X-ray yield measurements

The intensities of X-radiation emitted as a result of charged-particle irradiation has been measured by a number of workers for particles of different energies and in some cases excitation cross-sections have been calculated.[8, 12] A primary interest for analytical work is the X-ray count that can be detected by an appropriate count-

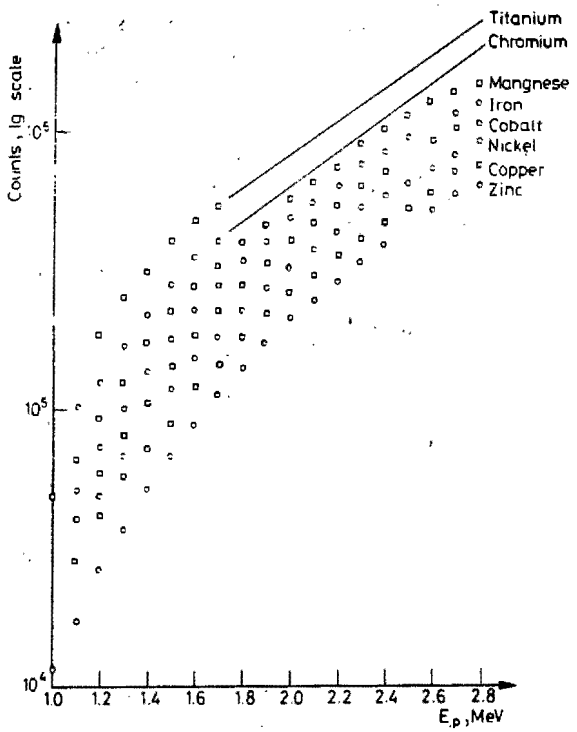

Fig. 1. Yields of K_α X-rays from first transition series elements

er in a practical system, since this defines the best interference-free sensitivity that can be obtained and gives an indication of the potential of the technique for analysis under the most favourable conditions. In the analysis of a real sample, this sensitivity will be modified by the effect of radiation from other components contributing to the accumulated spectrum. In addition, the detectable X-ray yield is important in the use of microbeams since at high-resolution, small beam-currents of the order of only a few nano-amperes may be attainable so that the time taken to accumulate a statistically acceptable number of counts will govern the scanning speed that can be used and hence the detail with which the sample can be examined. Consequently, a number of elements were irradiated with protons of energies of between 1.0 and 2.8 MeV and the X-ray yields measured with a silicon detector. The yields of K_α X-rays for elements of the first transition series are shown in Fig. 1 demonstrating the decrease in yield with increasing the atomic number as expected and also the high yield measured by the detector. While the conversion of the data given in Fig. 1 to useable analytical sensitivities can only be achieved from a knowledge of the composition of the sample to be examined and the nature of the expe-

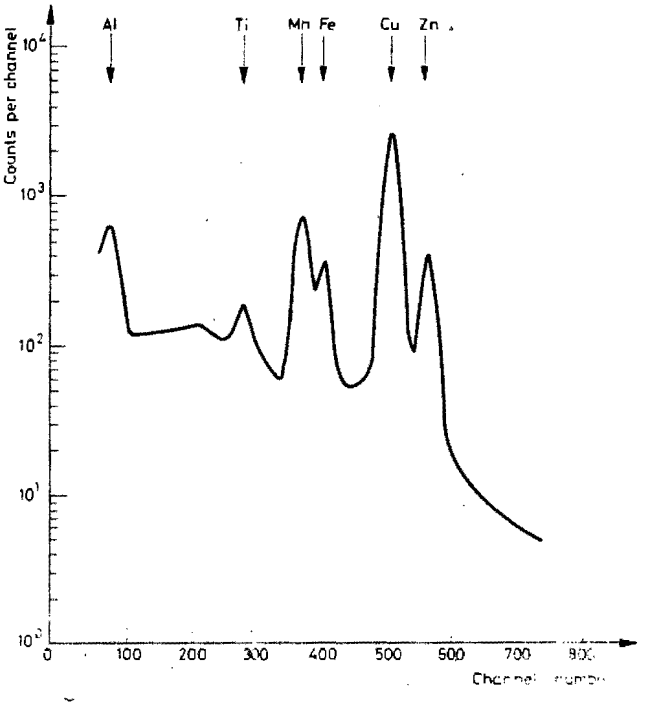

Fig. 2. X-ray spectrum of a standard alloy

rimental system to be used, clearly the high yields obtained do offer a sensitive method of analysis which can be applied to the examination of small samples and adequate counts can be obtained at beam currents expected for micro-beam work o make the use of X-ray measurement in conjunction with micro-beams a practical proposition.

The micro-analysis of aluminium alloys by measurement of charged-particle excited X-rays

The measurement of charged-particle excited X-rays has been applied to the determination of a number of elements in fragments of aluminium alloys. Small quantities of the alloys, typically weighing a few milligrams, were mounted in resin and polished until a flat area suitable for irradiation was produced. This area was then irradiated with 2.8 MeV proton beams approximately 10 μm in diameter and the emitted X-ray spectra were accumulated during irradiation. A typical spectrum from a standard aluminium alloy is shown in Fig. 2 with the characteristic X-rays from minor components in the samples identified. In addition to the lines shown

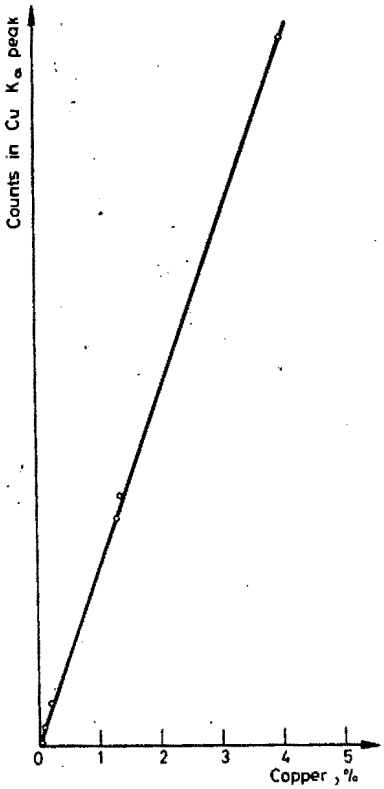

Fig. 3. Calibration curve for determination of copper in aluminium alloy

in Fig. 2 for the elements titanium, manganese, iron, copper and zinc, contributions to the spectra of the samples were found from chromium and nickel. In general the elements were present at levels of greater than 0.1% although in cases where the combination of X-ray lines were favourable, determinations were carried out at levels of the order of a few hundred ppm.

Interpretation of the X-ray spectra were carried out by simple graphical methods whenever this was possible but computer techniques were used to enable more complex spectra to be put on a quantitative basis. As an example of the analytical data obtained, a calibration curve for the line intensity of copper in standard alloys, plotted against concentrations found by chemical techniques is given in Fig. 3. A linear dependency of the count rate of the K_α line of copper against copper content is shown and provides a basis for analytical determination. An aluminium matrix clearly simplifies measurement and avoids the presence in the spectrum of intense lines from the matrix which could complicate analytical measurement by overlap with wanted lines. Absorbers were not used to improve the detection of any

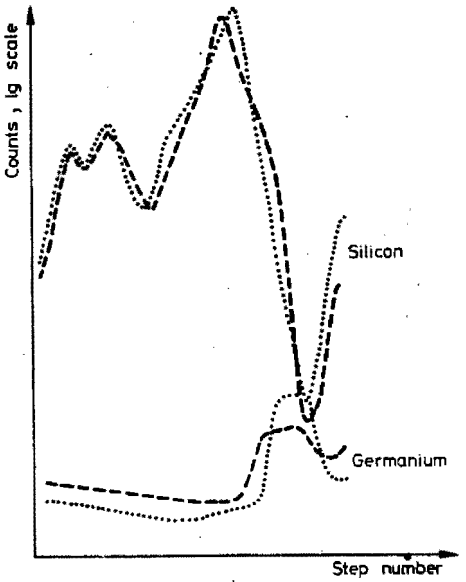

Fig. 4. Distribution of silicon and germanium across an electronic component found by micro-beam scanning. ····· Run 1, - - - - - run 2

particular element and to reduce the effect of possible interferences, since the purpose of using the non-dispersive detector system was to accumulate information from several elements during a single irradiation to reduce the demand on accelerator time required for analysis and to lower the unit cost of the measurements.

Examination of elemental distributions by measurement of X-rays produced by microbeams

Prompt gamma-radiation or particles from nuclear reaction processes or from elastic scattering have been produced by small-diameter ion beams to provide local analyses of larger samples and beam diameters down to about 3 μm have been produced and used for analytical purposes.[13] These small-diameter ion beams clearly offer a genuine microprobe capability for analytical techniques based upon nuclear reactions which can be extended to X-ray measurement by the use of a suitable detector system. Movement of the ion beam relative to the sample permits the different regions of the sample to be examined and systematic variations followed by scanning according to a pre-determined line or raster pattern. The use of microbeam techniques in conjunction with X-ray measurement is illustrated by results obtained for the examination of an electronic component which was placed after

polishing on the table in the target chamber. Irradiation was with 2.8 MeV proton beams, 5 μm in diameter and the beam was scanned relative to the sample to provide a step-wise examination of the composition of the sample surface. X-ray spectra from each irradiation were stored on paper tape and subsequent processing permitted both qualitative and quantitative information to be determined from each spectrum and hence each irradiation. Variations in composition with position could thus be followed. X-ray lines from silicon, germanium and gold were identified in the various spectra and the contours of line intensity of the several elements were produced. Fig. 4 shows line scans of the variation in intensity of the silicon K_α and the germanium K_α lines across the component. Step size was 2.5 μm and the change in concentration of the two elements with position can clearly be seen thus illustrating the sensitivity of the technique to spatial variations in concentration. Figure includes results for two separate scans carried out parallel but with the beam displaced laterally by about 10 μm indicating the good reproducability of line yield with position that can be obtained.

References

1. T. B. Pierce, Proc. of the International Meeting on Chemical Analysis by Charged Particle Bombardment, Namur, 1971, J. Radioanal. Chem., 12 (1972) 11.
2. T. B. Pierce, Proc. of the Second Conference on Practical Aspects of Activation Analysis with Charged Particles, Euratom report EUR 3896 d-f-e Brussels 1968, p. 119.
3. J. F. Chemin, J. Roturier, B. Saboya, G. Y. Petit, Proc. of the International Meeting on Chemical Analysis by Charged Particle Bombardment, Namur, 1971, J. Radioanal. Chem., 12 (1972) 221.
4. C. Olivier, M. Peisach, Modern Trends in Activation Analysis, National Bureau of Standards, Publication 312, p. 946.
5. G. Deconninck, G. Demortier, Colloqium on the Application of Nuclear Methods to the Basic Metal Industries, I.A.E.A. Vienna.
6. P. B. Needham, B. D. Sartwell, Advances in X-ray Analysis, Vol. 14 (1971) p. 184.
7. J. A. Cairns, R. S. Nelson, J. S. Briggs, Atomic Energy Research Establishment Report A.E.R.E. R-6887, 1971.
8. G. A. Bissinger, J. M. Joyce, E. J. Ludwig, W. P. McEver, S. M. Shafroth, Phys. Rev., A1 (1970) 841.
9. T. B. Johansson, R. Akselsson, S. A. E. Johansson, Nucl. Instr. Methods. 84 (1970) 141.
10. D. M. Poole, J. L. Shaw, Atomic Energy Research Establishment Report AERE-R 5918, 1968.
11. J. A. Cookson, F. D. Pilling, Atomic Energy Research Establishment Report AERE-R 6300, 1970.
12. H. W. Lewis, B. E. Simmons, E. Merzbacher, Phys. Rev., 91 (1953) 943.
13. T. B. Pierce, Proc. Soc. Chem., 7 (1970) 59.

No. 62

REPRINT

ELSEVIER SEQUOIA S.A.
Lausanne

AKADÉMIAI KIADÓ
Budapest

Journal of Radioanalytical Chemistry, Vol. 16 (1973) 551—558

THE ELEMENTAL AND ISOTOPIC DETERMINATION OF LITHIUM BY THE COINCIDENCE MEASUREMENT OF COMPLEMENTARY PARTICLES

R. PRETORIUS,* P. P. COETZE,** M. PEISACH*

**Southern Universities Nuclear Institute, P. O. Box 17, Faure, Cape (South Africa)*
***Department of Chemistry, University of Stellenbosch, Stellenbosch (South Africa)*

The coincident measurement of both nuclear products at their complementary angles was used to determine ^{6}Li by the reactions $^{6}Li(d, \alpha)^{4}He$ and $^{6}Li(p, \alpha)^{3}He$, and ^{7}Li by the reaction $^{7}Li(p, \alpha)^{4}He$. Elemental lithium was determined in natural samples or samples of known isotopic composition. Isotopic analyses could be carried out over the entire range from 0 to 100 atom% with a relative standard deviation of about 4%. The CMCP technique is highly specific and effectively eliminates interference and background.

Introduction

Although the analytical use of prompt particle spectrometry has in recent years been increasing rapidly, the technique has generally been limited to the measurement of prompt photons, neutrons, hydrogen or helium ions. In principle, measurement of the heavier recoiling product nucleus could be used equally well for analytical purposes but in practice this can only be achieved if the recoiling particle has sufficient energy to reach the detector. Since the total amount of energy available in a nuclear reaction is determined by the energy of the bombarding particle and the Q-value of the reaction, sufficient energy can be transferred to the recoiling product nucleus either by using a high energy irradiation beam or by selecting a high Q-value reaction or a suitable combination of both.

It is obvious that the escape of the recoiling product nucleus can be facilitated through the use of thin targets. In addition thin targets are also indicated when energy measurements have to be made as the distortion of the energy spectrum is directly related to the energy lost by the particles. For equal energies lighter ions will undergo a smaller energy loss than heavier ones and therefore spectrometry of the recoiling nucleus would more likely be successful for reactions involving light elements. An added advantage results from the fact that light recoiling ions carry off a relatively larger proportion of the available energy than do heavier ones.

In a nuclear reaction resulting in the formation of only two product particles, measurement of one of these particles at a selected angle will determine the energy of its complementary particle and the direction in which it is emitted. The fixed relationships between the energies and directions of complementary particles can be calculated from well known nuclear reaction kinematics.[1] If both particles are measured in coincidence with one another a very high degree of specificity can be attained and a recent paper[2] in which the use of this technique is first described for analytical purposes, the advantages of the method are discussed. Coincident measurement of complementary particles (CMCP) is highly efficient because for every particle measured in one detector there is another particle emitted to the second detector placed at the appropriate complementary angle.

Deuteron bombardment of lithium

When lithium is bombarded with deuterons, among the reactions that occur are

$^{6}Li(d, \alpha)\,^{4}He$ Q = 22.375 MeV,
$^{7}Li(d, \alpha)\,^{5}He$ Q = 14.164 MeV.

These reactions meet the requirement of high Q-values so that deuteron beams of a few MeV can be used. The recoiling "heavy" product is a helium-ion which, in the case of ^{6}Li is indistinguishable from the light product. The two products from each of these reactions can, in principle, escape from the target and thicknesses of a few hundred micrograms per cm^2 would still enable energy spectra to be measured without appreciable distortion. However, the half-life of ^{5}He is $T = 2 \cdot 10^{-21}$ sec whilst the time of flight to the detector a few cm away will exceed 10^{-11} sec, a time long compared to its half-life. Recoiling ^{5}He ions will therefore decay to a neutron and a randomly-emitted alpha particle which no longer bears a kinematic relationship with the alpha-particle generated in the reaction. Hence, only ^{6}Li can be measured by the CMCP technique.

Proton bombardment of lithium

Reactions analogues to the above, but induced by protons are

$^{6}Li(p, \alpha)\,^{3}He$ Q = 4.021 MeV,
$^{7}Li(p, \alpha)\,^{4}He$ Q = 17.347 MeV.

In this case both the "light" and the "heavy" product nuclei are stable so that the CMCP technique is directly applicable to the measurement of both isotopes.

As an example of the energies and directions involved, Table 1 lists the complementary angles and energies for a proton bombarding energy of 1.9 MeV. At this energy the reaction with ^{6}Li, which is usually the less abundant isotope, has a maximum cross section.

Table 1
Complementary angles and energies
for (p, α) reactions on ^{6}Li and ^{7}Li at E_p = 1.9 MeV

^{6}Li (p, α) ^{5}He				^{7}Li (p, α) ^{7}He			
Angle φ, degrees	Alpha energy, MeV	Angle φ, degrees	Helium-3 energy, MeV	Angle, degrees	Alpha energy, MeV	Angle, degrees	Alpha energy, MeV
0.0	3.812	180.0	2.110	0.0	11.754	180.0	7.493
10.0	3.782	164.6	2.139	10.0	11.714	167.5	7.533
20.0	3.697	149.5	2.224	20.0	11.596	155.1	7.651
30.0	3.561	135.0	2.360	30.0	11.406	152.9	7.841
40.0	3.383	121.3	2.538	40.0	11.152	131.0	8.095
50.0	3.175	108.4	2.746	50.0	10.848	119.5	8.399
60.0	2.949	92.3	2.972	60.0	10.505	108.8	8.742
70.0	2.716	85.3	3.205	70.0	10.137	95.1	9.110
80.0	2.488	75.0	2.433	80.0	9.760	87.2	9.487
90.0	2.272	65.4	3.649	90.0	9.385	77.3	9.862
100.0	2.074	56.4	3.847	100.0	9.025	67.7	10.222
110.0	1.899	48.1	4.021	110.0	8.688	58.5	10.559
120.0	1.750	40.3	4.171	120.0	8.385	49.5	10.862
130.0	1.625	32.9	4.296	130.0	8.120	40.9	11.127
140.0	1.526	25.9	4.395	140.0	7.898	32.4	11.349
150.0	1.449	19.1	4.471	150.0	7.722	24.2	11.525
160.0	1.396	12.6	4.525	160.0	7.596	16.1	11.651
170.0	1.364	6.3	4.557	170.0	7.519	8.0	11.728
180.0	1.354	0.0	4.567	180.0	7.494	0.0	11.753

Experimental

Enriched ^{6}Li and ^{7}Li were obtained from the Oak Ridge National Laboratory, U.S.A. These were isotopically diluted with natural lithium to form preparations with the required isotopic concentrations. The salts were then converted to lithium fluoride by precipitation with hydrofluoric acid.

Samples of lithium as LiF were evaporated onto thin carbon foils of 20 – 30 $\mu g/cm^2$. The thickness of the target material was between 10 and 200 $\mu g/cm$. It is necessary to use thin backings because if one of the particles is emitted in the backward direction, its complementary particle is usually emitted in the opposite forward direction.

The samples were mounted in a vacuum chamber which fitted onto the beam tube of the 5.5 MV Van de Graaff accelerator at the Southern Universities Nuclear Institute. Beam currents between 0.2 and 1.0 μA were used and irradiations lasted between 3 to 10 min per sample. Charged particle spectra were measured with two surface barrier detectors placed at the appropriate complementary angles. Special precaution was taken to ensure that the irradiation beam and both detectors lay in the same plane, as the specific kinematic relationships only apply under such conditions. Pulses from charged particles detected by the backward detector coincident with those measured by the forward one were analysed by a multi-channel analyser.

Results and discussion

Observation of complementary particles

Using proton bombardment and having the backward detector placed at 110° to the direction of the beam, the coincidence counts in the backward detector were measured as a function of the direction of the forward one (see Fig. 1). The maximum coincidence count rate for each reaction falls as the complementary angle as calculated in Table 1.

Deuteron irradiation

Energy spectra recorded from the deuteron bombardment of lithium fluorine are shown in Fig. 2. The upper spectrum, taken without coincidence shows the high

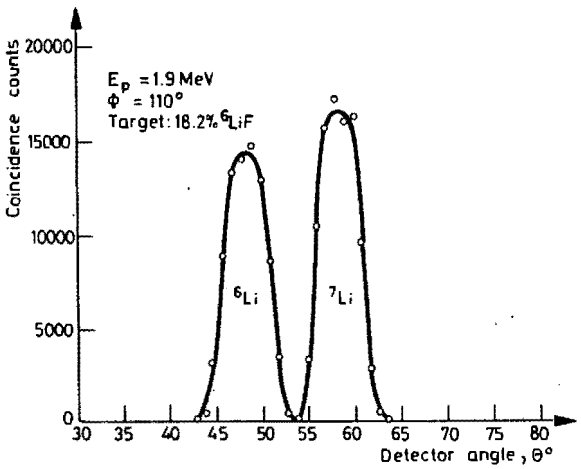

Fig. 1. Coincidence count rate, from proton-induced reactions on lithium isotopes measured by the backward detector at 110°, as a function of the direction of the forward detector

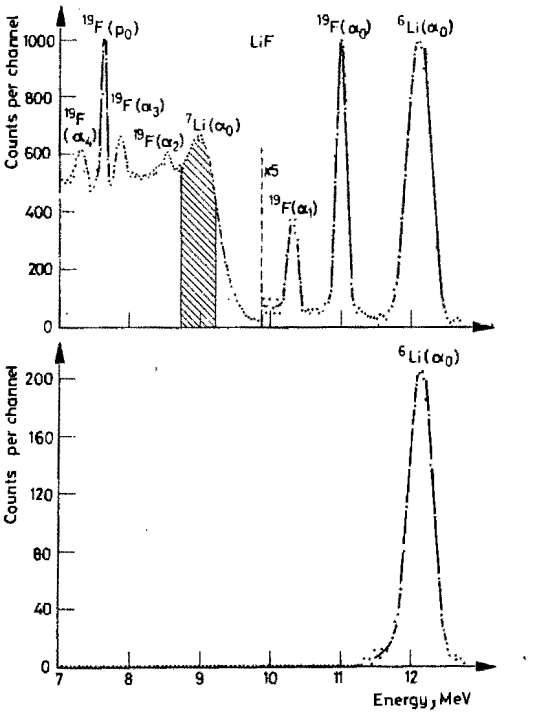

Fig. 2. Prompt particle energy spectra from deuteron bombarded lithium fluoride. Upper spectrum: without coincidence. The continuum at lower energies is due to alpha particles from the decay of ^{5}He. The shaded area is the region chosen for integration as a measure of ^{7}Li content. Lower spectrum: CMCP technique applied. Note that the peak height due to lithium-6 is as in the upper spectrum

energy peak due to ^{6}Li and other peaks due to reactions on fluorine. The continuum at lower energies is due to alpha-particles from the decay of ^{5}He from the reaction $^{7}Li(d, \alpha)\,^{5}He$. When only coincident particles are measured, the lower spectrum is obtained, showing only a peak due to ^{6}Li. It is clearly evident that the count rate measured for this peak was not affected by the coincidence requirement.

Since only one isotope is measured by the CMCP technique, isotopic analysis results were obtained by using ^{19}F as an internal standard or by reference to the intensity of the continuum, as shown by the shaded area in Fig. 2 that was taken as a measure of the ^{7}Li content.

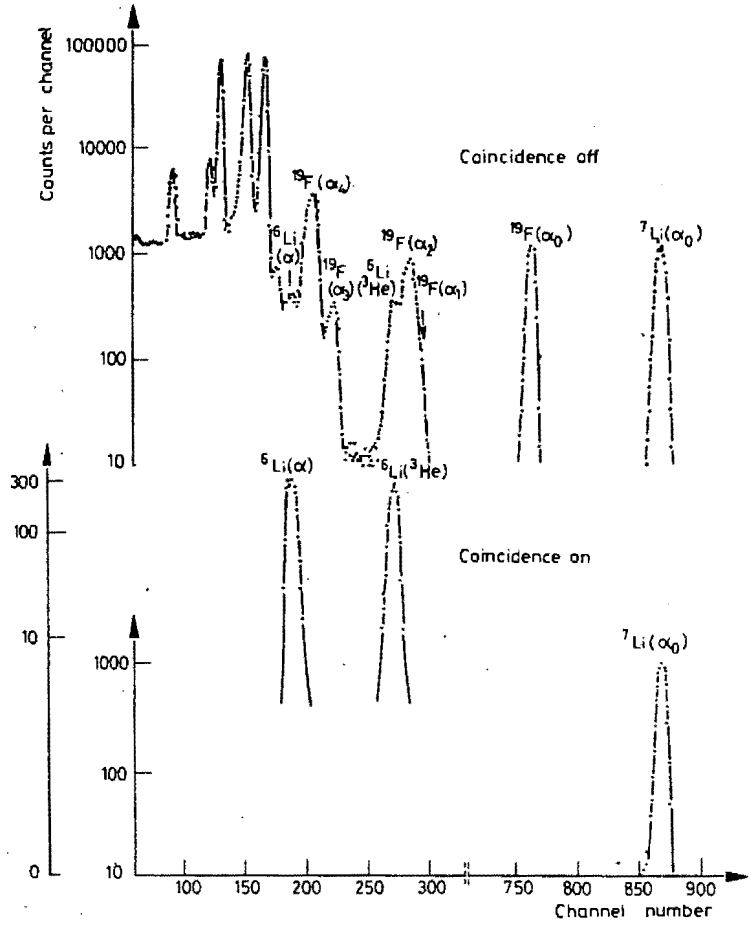

Fig. 3. Prompt particle spectra from proton bombarded lithium fluoride. E_p = = 1.9 MeV. Uppermost spectrum: without coincidence in which peaks from lithium-6 are obscured. Second spectrum: the two peaks from the reaction $^{6}Li(p, \alpha)\,^{3}He$ as measured by the CMCP technique with the backward detector at 110° and the forward one at 48.1°. Lowest spectrum: single peak obtained with CMCP technique for the reaction $^{7}Li(p, \alpha)\,^{4}He$. Forward detector at 58.5°. Both lower spectra show absence of interferences and background

Proton irradiation

Without coincidence, the spectrum shown in the top part of Fig. 3 is obtained. As before, many peaks are evident, mostly from reactions on ^{19}F. Although the high energy alpha particles can readily be used as a measure of ^{7}Li, determination

Table 2
Some isotopic determinations of lithium by proton irradiation

Known ^{6}Li, atom%	Count ratio, ^{6}Li/^{7}Li	Found ^{6}Li, atom%	Error, atom%	Relative error, atom%
3.02	0.1391	3.24	+0.22	7.3
5.01	0.2344	5.35	+0.34	6.8
6.26	0.2694	6.10	-0.16	2.6
6.73	0.3005	6.75	+0.02	0.3
7.02	0.3140	7.03	+0.01	0.1
7.32	0.3073	6.89	-0.43	5.9
7.53	0.3305	7.38	-0.15	2.0
7.85	0.3653	8.09	+0.24	3.1
8.24	0.3834	8.46	+0.22	2.7
8.64	0.3787	8.36	-0.28	3.2
10.23	0.4519	9.82	-0.41	4.0

Relative standard deviation of all determinations is ±4.3%.

of ^{6}Li is strongly hampered. This interference is totally eliminated by the CMCP technique as is shown in the lower two spectra in the figure. The peaks from ^{6}Li were obtained with the forward detector at an angle of 48.1°, and the single peak from ^{7}Li at 58.5°. Since no energy discrimination was imposed on the forward detector, two energy peaks are obtained corresponding to ^{3}He and ^{4}He ions detected in the backward detector from the reaction ^{6}Li(p, α)^{3}He. In the case of the reaction ^{7}Li(p, α)α, the two product particles are identical and hence only one peak can be recorded.

For elemental analysis of natural samples, or of samples of known isotopic composition, only ^{7}Li need be determined.

Analytical results

Some results of isotopic analyses are given in Table 2, as obtained from proton irradiation. The relative standard deviation of a series of such analyses was found to be ± 4.3%. Similar analyses performed under deuteron bombardment[2] gave a relative standard deviation of ± 3.5%. The apparently reduced precision using proton bombardment could be ascribed to the fact that separate determinations had to be made for ^{6}Li and ^{7}Li with the forward detector positioned at the appropriate complementary angle each time. If two detectors were used in the forward direction,

each permanently placed at the correct complementary angle, the two isotopes could simultaneously be determined by a single irradiation.

*

The financial assistance obtained from the South African Council for Scientific and Industrial Research and the Atomic Energy Board is gratefully acknowledged. One of us (P. P. C.) thanks his Promotor for permission to publish results which will form part of a doctoral thesis to be submitted to the University of Stellenbosch.

References

1. R. D. Evans, The Atomic Nucleus, McGraw-Hill, New York, 1955, p. 411.
2. R. Pretorius, Radiochem. Radioanal. Letters, 10 (1972) 297.

No 63

REPRINT

Journal of Radioanalytical Chemistry, Vol. 16 (1973) 559—566

ANALYSIS OF GLASS BY SIMULTANEOUS SPECTROMETRY OF SCATTERED ALPHA PARTICLES AND PROMPT PROTONS

M. PEISACH, R. PRETORIUS

Southern Universities Nuclear Institute, P. O. Box 17, Faure, Cape (South Africa)

ELSEVIER SEQUOIA S.A.
Lausanne

AKADÉMIAI KIADÓ
Budapest

Journal of Radioanalytical Chemistry, Vol. 16 (1973) 559—566

ANALYSIS OF GLASS BY SIMULTANEOUS SPECTROMETRY OF SCATTERED ALPHA PARTICLES AND PROMPT PROTONS

M. PEISACH, R. PRETORIUS

Southern Universities Nuclear Institute, P. O. Box 17, Faure, Cape (South Africa)

The energy spectrum of alpha particles scattered from a beam of 4 MeV was used to determine heavy elements and oxygen and silicon in glass. Simultaneously, but with a separate detector, the energy spectrum of prompt protons from (α, p) reactions were used to determine boron, sodium and aluminium. Both detectors were placed at 135° to the direction of the beam, but the proton detector was covered with an absorber to stop backscattered alpha particles. Glass samples analysed by other methods and standard glass powders from the U.S. Bureau of Standards were used as references.

Introduction

The energy spectrum of charged particles scattered from the surface of a sample can readily be used to determine the elemental composition of the major components of the material. Because the charged particles of a few MeV do not penetrate very deeply into solids such analyses are valid if the entire sample is thin, or if the elemental composition in the surface layers are representative of the composition of the bulk. This method of analysis should thus be applicable to determining major components of glass, since thin specimens can be obtained simply and quickly.

Composition of glasses varies over a wide range, but most ordinary glass types consist typically of 40 – 70% SiO_2, 5 – 15% Na_2O and 3 – 8% K_2O with other major components that may be B_2O_3, Al_2O_3, BaO and PbO, and minor elements such as Mg, Ca, Mn, Zn and As depending on the type of glass. The more abundant isotopes of most of these elements have mass numbers that are sufficiently far apart to enable the elements to be identified and determined by scattering techniques. However, the relatively high concentrations of silicon present in almost all common glasses may be expected to produce high intensity peaks in the energy spectrum that could overlap the relatively low peaks expected from sodium and aluminium, thereby making it impossible to observe these elements. The determination of boron may also be difficult because of the much smaller scattering cross section of this element. Accordingly other methods had to be found to determine these important components.

The (α, p) reactions on ^{10}B, ^{23}Na and ^{27}Al are exoergic, producing ground state protons with relatively high energies. For most other elements this reaction is endoergic and protons obtained from them will have much lower energies. In addition the Coulomb barrier for alpha particle reactions increases appreciably with increasing atomic number resulting in low reaction cross sections for bombarding energies of a few MeV. By using alpha beams, analyses may thus be carried out for the three elements not accessible by the scattering technique, without interference from other glass components. It may be noted that the use of alpha particles is also advantageous for the scattering analysis since the relative energy change per unit mass number of target is much higher for alpha particles than protons or deuterons.[1]

Experimental

Preparation of specimens

Very thin slivers of glass were made from glass tubing by melting the sample to form a clear molten mass from which a large bubble was rapidly blown. Thin specimens 6–10 mm. diameter were visually selected according to the extent to which the pieces exhibited the colourful diffraction of light. Each specimen was mounted on an aluminium annulus 4 – 5 mm wide and 16 mm outer diameter which was covered with an adhesive. Samples of powdered glass were carefully melted in a platinum crucible and a drop of molten material was attached to a platinum-tipped tube from which the bubble could be blown. Excessive air bubbles in the melt caused glass bubbles to rupture before they were sufficiently thin.

Glass powders with particle diameters less than 1 μm were centrifuged onto backings of tantalum[2] to produce specimens of up to 300 $\mu g/cm^2$ in thickness over a circular area of about 20 mm diameter. Such targets were, however, only used for measurements of prompt protons.

Irradiation and measurement

Before mounted specimens were irradiated, the average thickness of the sample was determined by measuring the decrease in energy suffered by alpha particles from ^{241}Am when passing through the glass. Only specimens less than about 400 $\mu g/cm^2$ in thickness were selected. Targets for bombardment were mounted in a 90 cm-scattering chamber with two surface-barrier semi-conductor detectors each at 135° to the direction of the bombarding beam on either side of it. The detector for measuring prompt protons was covered with an aluminium absorber foil 5. 74 mg/cm^2 thick and a single collimator with an aperture of 5. 5 mm was placed in front of the detector. The detector used to measure scattered alpha particles carried a collimator of 3. 5 mm and another of 4. 5 mm placed 30 mm away

to restrict the solid angle subtended at the target, because of the large cross section for scattering relative to that for the (α, p) reaction.

Beam currents of about 100 to 150 nA were used and the transmitted current was measured in a Faraday cup. In the case of centrifuged specimens where heavy backings were used, a Faraday cup was constructed around the target. Beam currents of up to 200 μC were sufficient for an analysis.

Results and discussion

Spectrometry of scattered alpha particles

A typical energy spectrum of scattered alpha particles is shown in the upper part of Fig. 1. For each major element the spectrum contains a distorted square-like peak, the high-energy edge of which is a sharp cut-off. This edge represents the

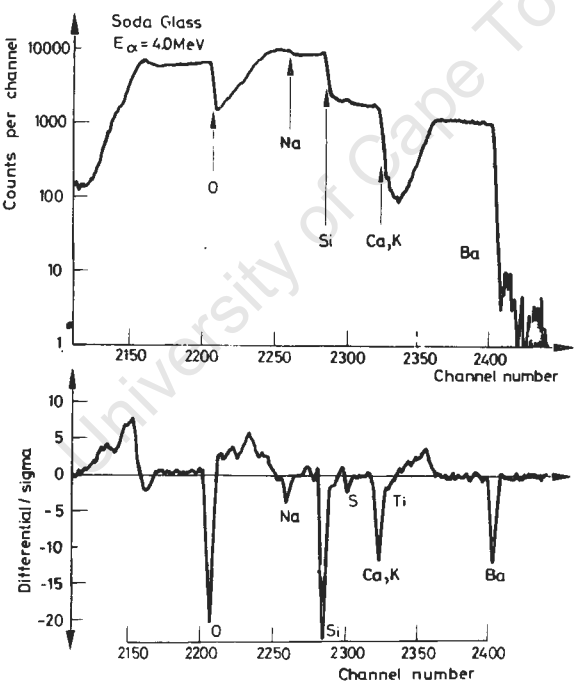

Fig. 1. Elastic scattering of 4 MeV alpha-particles from soda glass. Upper curve: Observed spectrum showing plateaux from which thicknesses can be determined. Lower curve: Differentiated spectrum with derivative values expressed relative to the standard deviation of the observed count. This curve was used for element identification of major components and for determining their concentration in the sample

maximum energy E' of an alpha-particle scattered from an atom of the element mass M_2 situated on the surface of the specimen, and is given by the relationship

$$\frac{E'}{E} = 1 - 2(1 - \cos\theta)\,\frac{M_1 M_2}{(M_1 + M_2)^2}$$

for a beam of initial energy E of particles mass M_1 scattered through a centre-of-mass angle θ. By contrast, the low-energy edge of the peak which represents the energy of an alpha particle scattered from the back of the specimen falls more gradually as a result of degradation of the beam by straggling. The apparent width of the peak is a measure of the average thickness of the specimen over the irradiated area. However, the width of the elemental peak increases with decreasing mass of the scatterer; the energy of the scattered particle decreases with decreasing mass of scatterer, but the rate of energy loss in matter increases with decreasing particle energy, so that particles scattered from light elements at the back of the specimen will be detected with a relatively greater energy loss than is the case for heavy elements. The average thickness of the specimen over the irradiated area can thus be calculated from each elemental peak using energy loss tables[3] for the appropriate element.

Since the Rutherford scattering cross section $d\sigma/d\Omega$ for a bombarding particle of charge Z_1e scattered from a target of charge Z_2e is

$$\frac{d\sigma}{d\Omega} = \frac{(Z_1 Z_2 e^2)^2}{16E^2 \sin^4(\theta/2)} \quad \text{cm}^2 \cdot \text{atom}^{-1} \cdot \text{steradian}^{-1},$$

it can readily be seen that in a single sample consisting of equal numbers of atoms of several elements, the ratio of the number of particles scattered from each element will be proportional to the ratio of the corresponding values of (Z_2).^{2} The number of atoms of an element in the vicinity of the surface will thus determine the height of each peak, which may therefore be used as a measure of the concentration of the element.

Inspection of the spectrum in the upper part of Fig. 1 will show that it is not easy to determine the height of the step corresponding to every observable element. However, if the differential of the curve is plotted as a function of energy (or channel number), as is shown in the lower part of Fig. 1., several advantages become obvious. The sharp high-energy edge of the elemental peaks now appear as well-defined negative peaks, the minimum of which corresponds to the inflexion point of the elemental peak and can be readily used as a means of identifying the element. The rather poorly defined but equally prominent positive peaks show the inflexion points of the low-energy peak edges and may be used to calculate the

true specimen thickness. Furthermore, the area between the differential peak and the base line is a direct measure of the height of the elemental peak and hence is a measure of the elemental concentration.

In Fig. 1 the ordinate are expressed relative to the standard deviation of the observed count in order to make significant peaks clearly apparent.

Spectrometry of prompt protons

Typical prompt proton energy spectra for two different glass types are shown in Fig. 2. Under the conditions of the experiment, protons with energy above about

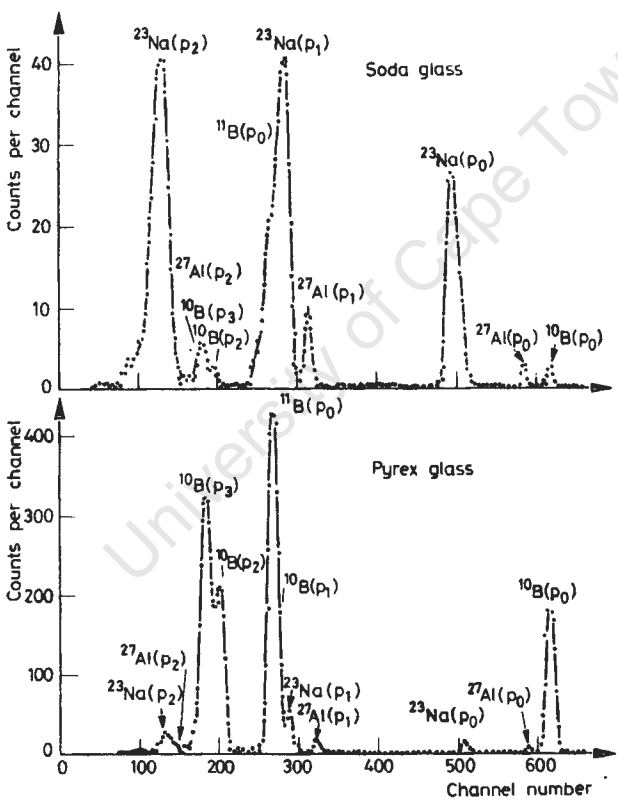

Fig. 2. Prompt proton spectra from different glass types, obtained under alpha-particle bombardment at 4.0 MeV. The peaks are labelled with the target nuclide present in the glass and the value (p_i) refers to the protons emitted from the corresponding (α, p) reaction if the product nucleus is formed in its ith excited state. The subscripts of (p_i) correspond to the ith level number in Table 1

1300 keV would penetrate the aluminium absorber. Table 1 lists the sources from which such protons would be formed, and by comparison between the data in the table and the identified peaks in Fig. 2 it is clear that all listed nuclides except ^{19}F were present in glass samples.

Table 1
Proton energies above 1300 keV from (α, p) reactions,*
E_α = 4000 MeV, θ = 135°

Target nuclide	Ground state Q-value,[4] keV	Level		Proton energy, keV
		No.	E_X, keV	
^{10}B	4064	0	0	5398
		1	3090	2795
		2	3680	2309
		3	3850	2170
^{11}B	784	0	0	2766
^{19}F	1675	0	0	4227
		1	1277	3080
^{23}Na	1822	0	0	4561
		1	1809	2910
		2	2938	1893
^{27}Al	2378	0	0	5235
		1	2230	3170
		2	3510	1999
		3	3770	1763
		4	3790	1745

*Only elements with $Z \leq 14$ were considered since the Coulomb barrier <7.5MeV.

The peaks in the spectrum show relatively little overlapping and there are sufficient free-standing peaks to obtain the characteristics of the peak shape for peak-stripping procedures if necessary. The integrated counts under the peak is a measure of the total content of the nuclide in the sample and the method is made absolute by standardisation against analysed glass samples. Such samples were obtained from the National Bureau of Standards, Washington, U.S.A. and from Consolidated Glass Works, Germiston, South Africa.

Results

Relative concentrations of major elemental components in the glass were obtained from scattering data where Rutherford scattering cross sections were assumed to be valid. From these data the approximate thickness of the sample was calcu-

Table 2
Preliminary analyses of some glass types*

Element		Soda glass	Pyrex glass	Red glass	Yellow Uranium glass	Lead glass
Scattering	SiO_2	71.1	81.4	60.9	62.4	55.6
	CaO, K_2O	8.69	–	8.62	7.40	7.46
	ZnO	–	–	16.0	–	–
	BaO	2.08	–	–	2.23	–
	PbO	–	–	–	–	22.8
Proton spectrometry	B_2O_3	<0.01	14.65	0.11	0.73	<0.02
	Na_2O	16.0	1.49	13.1	11.7	11.8
	Al_2O_3	2.08	2.24	0.33	3.00	2.43

*All values are percentage by weight.

lated using tabulated stopping powers of elements.[3] The approximate weight concentration of B as B_2O_3, Na as Na_2O and Al as Al_2O_3 were calculated from the proton spectrometry data, in which quantisation was achieved by intercomparison between the sample to be analysed and a suitable standard. It was essential that the standard specimen had a thickness comparable to that of the sample so that variations in the excitation function over the energy range of the bombarding alpha particle within the glass specimen, affected the standard and sample equally. A more accurate value for the thickness of the sample was then calculated using the approximate data for B, Na and Al in addition to the relative concentrations from scattering. Weight concentrations were then calculated from the amended sample thickness.

Preliminary results of analyses for a variety of glass types are listed in Table 2. Each analysis represents mean values from replicates. Values expressed for calcium

should be considered as the sum of the calcium and potassium contents, as these two elements could not be resolved. In Red glass and Yellow Uranium glass an unknown element of mass approximately 105 was detected which was assumed to be palladium (atomic weight 106.4) while a small concentration of a heavy element, presumably Uranium was also found in the latter.

*

The financial assistance obtained from the South African Council for Scientific and Industrial Research and the Atomic Energy Board is gratefully acknowledged. Special thanks are expressed to Mr. J. Conrady of Consolidated Glass Works Ltd., Germiston, South Africa for providing analyses of several glass samples. Mr. Alan Wolfromm assisted with the computer programme for thickness and composition calculations.

References

1. M. Peisach, D.O. Poole, H.F. Röhm, Talanta, 14 (1967) 187.
2. M. Peisach, J. S. Afr. Chem. Inst., 12 (1959) 57; C. Olivier, M. Peisach, J. Radioanal. Chem., 11 (1972) 105.
3. C.F. Williamson, J.P. Boujot, J. Picard, Rept. C.E.A. R-3042, 1966.
4. C. Maples, G.W. Goth, J. Cerny, Nucl. Data, A2 (1966) 429.

No. 64

REPRINT

Journal of Radioanalytical Chemistry, Vol. 19 (1974) 269–275

RAPID NEUTRON ACTIVATION OF BROMINE USING 6.1–MINUTE BROMINE–82M: APPLICATION TO THE DETERMINATION OF BROMINE IN BLOOD PLASMA

M. PEISACH,* B. MAZIERE,** C. LOC'H,** D. COMAR,** C. KELLERSHOHN**

**Southern Universities Nuclear Institute, Box 17, Faure, C.P. (South Africa)*
***Commissariat à l'Energie Atomique, Département de Biologie, Service Hospitalier*

ELSEVIER SEQUOIA S.A.
Lausanne

AKADÉMIAI KIADÓ
Budapest

Journal of Radioanalytical Chemistry, Vol. 19 (1974) 269–275

RAPID NEUTRON ACTIVATION OF BROMINE USING 6.1–MINUTE BROMINE–82M: APPLICATION TO THE DETERMINATION OF BROMINE IN BLOOD PLASMA

M. PEISACH,* B. MAZIERE,** C. LOC'H,** D. COMAR,** C. KELLERSHOHN**

**Southern Universities Nuclear Institute, Box 17, Faure, C.P. (South Africa)*
***Commissariat à l'Energie Atomique, Département de Biologie, Service Hospitalier Fréderic Joliot (Laboratoire Pierre Süe), 91-Orsay, (France)*

Une méthode rapide de dosage du brome dans le plasma sanguin par analyse par activation neutronique est décrite. En mesurant le brome 82m par spectrométrie X, l'analyse dans des échantillons plasmatiques de 10 µl peut être faite en 10 minutes. En présence de grandes concentrations de sodium et de chlore, telles que celles du plasma normal, la plus petite quantité de brome décelable est d'environ 5 ng. Les erreurs statistiques mises à part, l'erreur expérimentale introduit une marge d'incertitude d'environ ±2%. On compare les avantages de différents détecteurs utilisés.

INTRODUCTION

A rapid determination of bromine by neutron activation analysis is possible through the use of 6.1-minute bromine-82m. This nuclide is produced from the stable bromine–81 isotope, which has an abundance of 49,96 atom% in natural bromine. The cross section for the formation of the radioisotope by neutron capture with thermal neutrons is about 3 barns, so that reactors providing neutron fluxes between 10^{12} and 10^{15} $n \cdot cm^{-2} \cdot sec^{-1}$ can produce sufficient activities from relatively short irradiations 10^{15} $n \cdot cm^{-2} \cdot sec^{-1}$ to enable microgram and nanogram quantities of bromine to be determined.

The sensitivity of determining bromine-82m activities can be enhanced by the appropriate choice of detector. With the use of low energy gamma-ray or X-ray detectors, the energy spectrum covered during a measurement can be restricted to radiation not exceeding 100 keV in energy. Under such conditions, the radiation measured from neutron activation of natural bromine is restricted to 37 and 49 keV gamma-rays from 4.4 hour bromine-80m and 46 keV gamma-rays from 6.1-minute bromine-82m. These radiations are all internally converted to produce bromine X-rays.[1] The 37-keV gamma-ray has a conversion coefficient $\alpha_k = 1$ so that only about half these radiations will contribute to the measured K X-rays of 11,9 keV, in contrast with the other two aforementioned gamma-rays which are virtually entirely internally converted: the values of the respective conversion coefficients for X-ray production from the 49 keV gamma-ray of ^{80m}Br and the 46-keV gamma-ray of ^{82m}Br are about 400 and 382 and over 70% of

the decays result in K X-rays. In addition to these radiations, there is a small intensity of selenium K-rays of 11.2 keV produced from the electron capture mode of decay of 17.6 min bromine-80 having a relative probability of about 5%. It thus follows that X-rays gene ated from the radio-bromine isotopes will consist almost entirely of those originating from bromine-82m decaying with a half-life of 6.1 minutes together with a small contribution of a 4.4 hour component originating from bromine-80m and a 17.6 minute component from bromine-80.

To enable the analyses to be carried out as quickly as possible, but without loss of precision, the counting period should be extended until most of the bromine-82m had decayed. Correction factors from the above thre-component decay system were obtained from pre-computed tables using measured intensities of the components.

The sensitivity limit attainable with gamma-ray spectroscopy is determined by the re ative intensities of the gamma-rays of interest and interfering radiation which arise fror other causes viz., bremsstrahlung effects resulting from the production of a radiation continuum caused by energetic beta-particles from the sample, backscatter effects resulting from the detection of usually low energy gamma-rays scattered from the sample to the detector by extraneous matter and Compton effects caused from the detection of electrons from gamma-rays scattered in the detector. These effects cannot be eliminatec entirely, even from samples which contain only radio-bromine isotopes, but their effec can be decreased by using detectors with comparatively small sensitive volumes in which the probability of interaction is small for energetic gamma-rays, and by removing material of large atomic number from the vicinity of the detector, thereby decreasing the intensity of bremsstrahlung.

Blood plasma contains both sodium and chlorine at a concentration level of about 3 mg/ml, whereas the bromine concentration is about 3 ppm in normal plasma. Thermaneutron activation of plasma thus produces relatively large yields of chlorine-38 and sodium-24, the effect of which will be to reduce the sensitivity for determining bromine.

This work reports the results of studies carried out with two different detecting systems to develop a suitable technique for the rapid determination of bromine in blood plasma and for evaluating the precision, accuracy and sensitivity of the technique.

Experimental

Materials

Dilute aqueous solutions of ammonium bromide were used to establish the conditior for analysis and to collect physical data.

Synthetic plasma solutions were prepared containing 5.77 g NaCl and 2.74g Na_2CO_3 per liter.

This corresponded to concentrations of 3.30 g/l of sodium and 3.50 g/l of chlorine as found in average blood plasma. Varying quantities of ammonium bromide were added to these solutions as required.

Liquid blood plasmas were analysed as received.

Preparation of samples for counting

Pipetted volumes from 5 to 20 μl were deposited on discs of filter paper. The average thickness of paper was 7.2±0.2 mg/cm^2 and the pipetted droplets were spread over a circular area of about 8 to 15 mm diameter. The resulting samples had an effective thickness between 18 and 32 mg/cm^2. Over this range of thicknesses, no change in count rate, due to self-absorption, could be observed, in agreement with previously reported results.[2] In cases where relatively old samples of liquid plasma were irradiated, undispersed solid material sometimes obstructed the action of the automatic pipette. In such cases, and all samples where there was doubt about the correct volume pipetted, bromine activity was expressed relative to the activaty of sodium-24 in the sample, determined later with a Ge(Li) spectrometer.

Two different modifications of the procedure were used. In the first, liquid plasma measuring about 200 μl was sealed in a polyethylene vial for irradiation, and samples for counting were prepared from the activated liquid. The disadvantage of this procedure lay in the loss of time, and hence loss of activity of bromine-82m, during pipetting and preparation of the sample. The second modification involved the deposition of the required volume of plasma onto filter paper before activation and then counting the paper directly after its return from the reactor. Although counting could start much sooner the disadvantage of this technique lay in the possibility of contamination before activation and possible interference from fluctuations in the bromine content of the paper.

Irradiation

Samples were irradiated in aluminium or polyethylene containers for periods varying from to 10 sec to 5 min. Three reactor facilities were used viz:

OSIRIS, Saclay, France, thermal neutron flux $2.5 \cdot 10^{14}$ n · cm^{-2} · sec^{-1}
EL 3 Saclay, France, thermal neutron flux $6.6 \cdot 10^{12}$ n · cm^{-2} · sec^{-1}
SAFARI I Pelindaba, South Africa, thermal neutron flux $1.3 \cdot 10^{13}$ n · cm^{-2} · sec^{-1}.

Measurement

Bromine activities were recorded with two different spectrometers, using either a NaI(Tl) scintillator 3 cm diameter x 3 mm thick having a resolution of about 6,3 keV at

12 keV, or a Si(Li) detector of 30 mm^2 area and 3 mm thick having a resolution of 262 eV at 6.4 keV. Both detectors had thin beryllium windows, the latter being 0.025 mm thick.

Because the scintillator had a very much higher efficiency, count rates were appreciably higher than with the Si(Li) detector, due to the activities from chlorine and sodium. To avoid excessive errors due to dead-time correction, samples were mounted about 25 to 40 mm away from the crystal face. In contrast to this, paper discs counted with the Si(Li) detector were mounted as close to the detector window as possible, typically about 4 mm from the window. For routine analysis samples were counted for a fixed live time of the measuring system, but because of the high activities the added decay of bromine-82m caused by the dead-time of the measuring system could not be neglected, hence real time was recorded at the start and end of each count.

Under fixed conditions and using the pre-irradiation pipetting technique, it was found that the difference between live time and clock time was surprisingly constant. Accordingly extended counting periods of up to 500 sec could be used and tables calculated from accurately determined decay curves were used to correct the measured nett count to corrected undecayed activity at the end of the irradiation (see Table 1).

Results and discussion

Gamma-ray spectrometry

Typical spectra obtained with the NaI(Tℓ) scintillator and the Si(Li) detector may be compared in Fig. 1. The much improved resolution of the latter makes it possible to observe the presence of selenium X-rays and both the Kα and Kβ X-rays of bromine. Howeve the spectra from the NaI scintillator were recorded with a much greater count rate, so th despite the better resolution of the semi-conductor diode, the precision of the results are about equal.

As the decay proceeds, the intensity of the X-rays decreases and it becomes possible to observe[3] the peak from the unconverted 37 keV gamma-ray of bromine-80m.

Comparison of the two curves obtained from a sample with about 8 ng bromine clearly illustrates the gain in sensitivity effected by the Si(Li) detector. Using the criterion of sensitivity as being the weight of bromine which gives an integrated count equal to three times the standard deviation of the background, the sensitivity limit in a blood plasma sample is about 5 ng bromine.

Calculations

The blank sample gave the shape of the spectral continuum under the combined peak corresponding to Se K and Br Kα and Kβ X-rays. This shape was fitted to the low ene

Table 1
Extract from decay correction calculations

Time at start of count, min	Count duration, min				
	3	4	5	6	8
1	1.2903	1.3536	1.4183	1.4844	1.6207
2	1.4290	1.4984	1.5693	1.6417	1.7907
3	1.5810	1.6570	1.7345	1.8136	1.9762
4	1.7473	1.8302	1.9149	2.0011	2.1782
5	1.9288	2.0192	2.1113	2.2052	2.3975
6	2.1264	2.2247	2.3249	2.4267	2.6352
7	2.3412	2.4479	2.5564	2.6667	3.0465
8	2.5741	2.6895	2.8068	2.9258	3.0465
9	2.8258	2.9503	3.0768	3.2050	3.4659

These data are dependent on the relative yields of radiobromine isotopes as affected by the neutron energy distribution at the activation facility used.

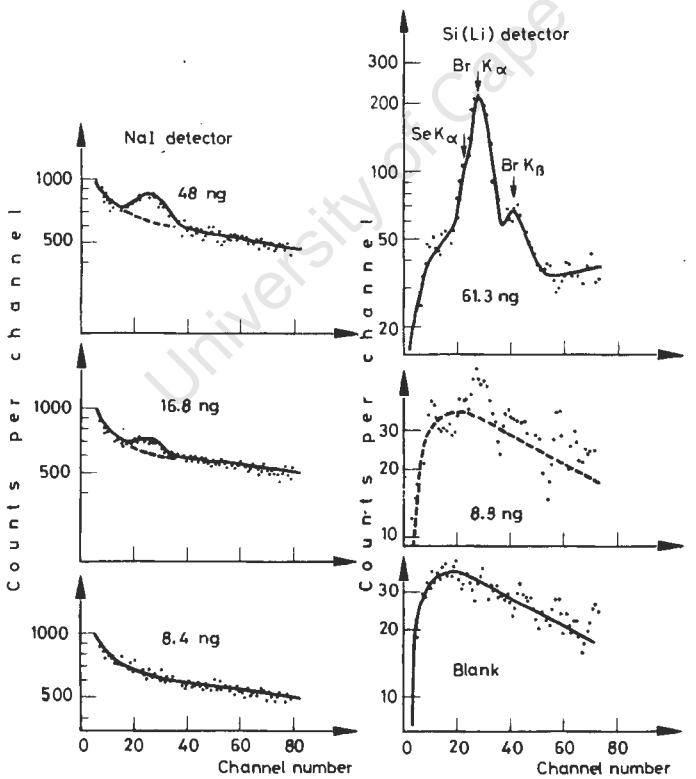

Fig. 1 Portions of gamma-ray spectra from different weights bromine in 10 μl aliquots of plasma

edge of the peaks and the corresponding background was subtracted. Using tables such as Table 1 computed from decay curves the activity at the end of the irradiation was calculated and converted to bromine content by comparison with synthetic standards.

Precision and accuracy

Precision was determined by repeated analysis of a single sample. Some replicate analyses of a series of 16 analyses are shown in the upper portion of Table 2, and analyses of known samples in the lower part. The relative precision is ±6%, the root mean square error is 2,8 ng bromine and the results do not show bias within the precision of the method.

Table 2
Some results of analyses

Known Br content, ng	Nett integrated count at t = 0 A_0	Found Br content, ng	Error, ng
(a) Replicate analyses. Precision test. Si(Li) detector			
35.0	265.1	31.1	-3.0
35.0	303.3	35.6	+0.6
35.0	295.4	34.6	-0.4
35.0	315.0	36.9	+1.9
35.0	297.1	34.8	-0.2
35.0	283.6	33.3	-1.7
No. of test analyses = 16			
Mean value of A_0 = 298.8±18.2			
Overall relative precision = 6.1% due to statistical errors (5.8%) and added experimental errors (2.0%).			
(b) Test analyses. Accuracy test. Both detectors.			
8.8	109.1	12.8	+4.0
8.9	46.2	5.4	-3.5
21.9	202.1	23.7	+1.8
30.7	274.5	32.2	+1.5
35.0	295.9	34.7	-0.3
43.5	350.4	41.1	-2.4
48.2	433.1	50.8	+2.6
61.3	491.9	57.7	-3.6
37 test analyses on 22 samples prepared			
Root mean square error (all analyses) = ±2.8 ng bromine.			

Conclusion

The method using Si(Li) detectors is suited for routine use. If the usual statistical errors of counting are acceptable, single irradiations followed by a single relatively long counting period enables results to be obtained with a relative precision of about ±6% within 10 minutes. Analyses are nondestructive and repeat irradiations can be carried out to improve precision.

*

Financial support from the Commissariat à l'Energie Atomique, France and the Southern Universities Nuclear Institute, South Africa is gratefully acknowledged. Thanks are due to the South African Atomic Energy Board and the French C. E. A. for the use of their facilities. Special appreciation is expressed to the South African C. S. I. R. for a travel and senior bursary held by one of us (M.P.) to enable the bulk of this work to be done in France.

References

1. C. M. LEDERER, J. M. HOLLANDER, I. PERLMAN, Tables of Isotopes, 6th ed., Wiley, New York, 1968; A. ARTNA, Nucl. Data, B1 (1966) 69, 103; W. SEELMANN–EGGEBERT, G. PFENNING, H. MUNZEL, Chart of the nuclides, 3rd Ed. Karlsruhe, 1968.
2. C. SHENBERG, J. GILAT, H. L. FINSTON, Anal. Chem, 39 (1967) 750.
3. M. PEISACH, D. COMAR, C. KELLERSHOHN, Radiochem. Radioanal. Letters, 8 (1971) 267.

No. 60

THE SYSTEM SODIUM CHLORIDE

THE SYSTEM SODIUM CHLORIDE—SODIUM SULPHATE—WATER, WITH REFERENCE TO THE RECOVERY OF SODIUM CHLORIDE AND SODIUM SULPHATE FROM NATURAL BRINES IN SOUTH AFRICA

By M. PEISACH

National Chemical Research Laboratory, Pretoria

A study of the system $NaCl—Na_2SO_4—H_2O$ has been made with a view to acquainting manufacturers of common salt in the Union, with the principles and possibilities of salt and sodium sulphate production from the brines available to them. Calculations based on values found in the literature, showed that pure sodium chloride and pure sodium sulphate could be obtained from a brine containing these two substances in suitable concentrations. To achieve separation of the constituents a three-stage process is required. In the first stage, brine is concentrated by evaporation; refrigeration as the second stage yields pure sulphate, while the third stage, solar evaporation followed by recycling the solution of the correct density, results in pure sodium chloride.

A DETAILED SURVEY of the supply of common salt in South Africa has recently been made by Shuttleworth.[1] Apart from a relatively inaccessible deposit of rock salt in South West Africa, the main salt resources of the Union consist of inland salt pans lying in a belt between Mafeking and De Aar. In addition there are coastal pans at Saldanha Bay and near Port Elizabeth, but due to transportation costs, these cannot supply salt to the interior. With few exceptions, the brines of the inland pans are characterized by a high sodium sulphate content and relatively low concentrations of calcium and magnesium salts. It is not uncommon to find brines in which the sodium sulphate exceeds 20 per cent of the total dissolved solids, while values over 30 per cent have been reported.[1] The preparation of pure sodium chloride from such brines presents difficulties not often met with in other countries.

Therefore, it has been considered of value to review and examine the system $NaCl–Na_2SO_4–H_2O$ with reference to the working up of such brines. The magnesium and calcium salts are usually present in the brines in such relatively low concentrations that, from a practical point of view, and for the sake of simplicity, their presence has been ignored.

A thorough study of the application of the phase rule to the recovery of sodium chloride from South African brines was made by Pelling.[2] The methods he suggested for the recovery of pure sodium chloride from brines containing sodium sulphate were:

(i) direct evaporation at the boiling point, followed by cooling the mixture to between 21·5 and 25°C.,
(ii) removal of sodium sulphate by refrigeration and
(iii) crystallization of impure sodium chloride with subsequent removal of sodium sulphate by washing with dilute brine.

While the "evaporation" and the "washing" methods were described in detail, the method involving the refrigeration of brines was only briefly outlined. This paper deals in greater detail with the possible application of the refrigeration process to the recovery of pure sodium chloride and pure sodium sulphate from South African brines.

The phase diagram

The system $NaCl–Na_2SO_4–H_2O$ has been investigated by several authors, notably by Chretien,[3] Schreinemakers and de Baat,[4] and Seidell,[5] but as a rule they concentrated on certain aspects of the system. The information found in the literature has been collected and is presented in a form in which it can be applied to the practical problems of salt recovery.

It is usual to represent ternary equilibria graphically by means of a three-dimensional plot on triangular composition axes and a vertical temperature axis. Figure 1 shows such a prismatic plot lying on one of the faces of the prism and depicts the surface of crystallization, i.e., any point on this surface represents an equilibrium between the solution and one or more solid phases. The portion cut away corresponds to the solution, while the surface is divided into a number of areas with intersecting lines as their boundaries. Within each of these areas, a single phase crystallizes in equilibrium with the solution. This is called a primary phase, and the areas are primary phase fields.

The three-dimensional surface of crystallization in Figure 1, however, is not very convenient for calculations. If a solution is cooled till crystallization takes place, without loss of water by evaporation, the course of crystallization can be conveniently followed on a two-dimensional projection of the surface of crystallization on the triangular base of the prism. This projection is shown in Figure 2. Projections of the primary phase fields are labelled with the corresponding primary phases. The inclinations of the intersecting lines between the primary phase fields with respect to temperature are shown by means of arrows. The line AB, which separates the primary phase fields of solid NaCl and solid anhydrous Na_2SO_4, ends at the boiling point (760 mm.) of a solution mutually saturated with both solids.

The significance and use of the various parts of this diagram are best illustrated by an example.

Consider a solution represented by the point X in Figure 2. As the composition of such a solution

Transvaal Chemical Manufacturers' Association

Annual dinner-dance—By a member

"THE plans of mice and men are apt to gang agley", but this cannot be said of the Association's Annual Dinner-Dance, held on September 23 last. From the commencement of the Cocktail Party till the last of the dancers wended their weary way home, it can be justifiably said, I think, that all of us had a most enjoyable evening.

Events commenced in a most convivial atmosphere when members had the pleasure of meeting the Minister of Economic Affairs, Dr. A. J. R. van Rhijn and Mrs. van Rhijn at the Cocktail Party before dinner. I would appeal to members, however, to mix to a greater extent at future functions of this nature thus taking the opportunity to meet one's fellow members in the Association and establishing an acquaintanceship which can foster a closer relationship between all of us.

One can agree that the success of an annual function of this nature is due to the fact that the speeches given are apt and very pertinent, which particularly applied to this year.

Dr. van Rhijn undoubtedly showed his friendliness towards the chemical industry and the profession, and when he concluded his speech one could be pardoned for being slightly swollen-headed. After his kindly remarks to the chemical manufacturers he made the important point "That it is only by our own efforts we shall progress" and we must agree with him when he said "to succeed we must endeavour to see that one and all of us do a proper day's work".

Our Chairman must certainly be congratulated on his fluent Afrikaans and his remarks were well received.

The Dinner and Dance were enjoyed by all and there was proof of this when in "the wee sma' hours" the ballroom was still well filled.

I would like to take the opportunity of thanking one and all—both visitors and members who came and joined us—for making this affair such a success, and one we'd hoped for. A special word of thanks must be paid to our very hardworking Chairman, Mr. S. Goodman, and the Executive Committee for the time they devoted to ensure that this function would be a happy and enjoyable one.

I hope to see all the same faces next year, as well as a number of new ones.

New soap germicide—hexachlorophene—now available in the Union

Hexachlorophene, a chlorinated bisphenol developed in the United States of America, is one of the newest aids to hygiene and sanitation introduced into this country by one of our members.

Hexachlorophene (which is also known as G-11) is a unique germicide in that it is non-irritating and also retains its bactericidal activity in the presence of soaps, thus overcoming the limitations of other "phenolics" whose potency is nullified under similar circumstances.

This fact has been confirmed by the Medical Profession so that today hexachlorophene liquid soap is recognized in the new revision of the United States Pharmacopoeia.

Our member reports that the liquid soap containing hexachlorophene has been extensively tested in the Union of South Africa by a large laboratory where the bactericidal effect was confirmed and the presence of a residual germicidal film on the skin was demonstrated.

The soap is now being used by a large number of surgeons as a simple and effective method of achieving asceptic technique without the use of prolonged and painful application of scrubbing brushes.

Industrially this type of soap has been found to reduce the incidence of dermatitis and to lessen the possibility of secondary infections resulting from cuts and abrasions.

In food industries and wherever there is a danger of bacterial contamination by contact, the use of such soaps can go a long way to prevent transmission of disease if used by all food handlers.

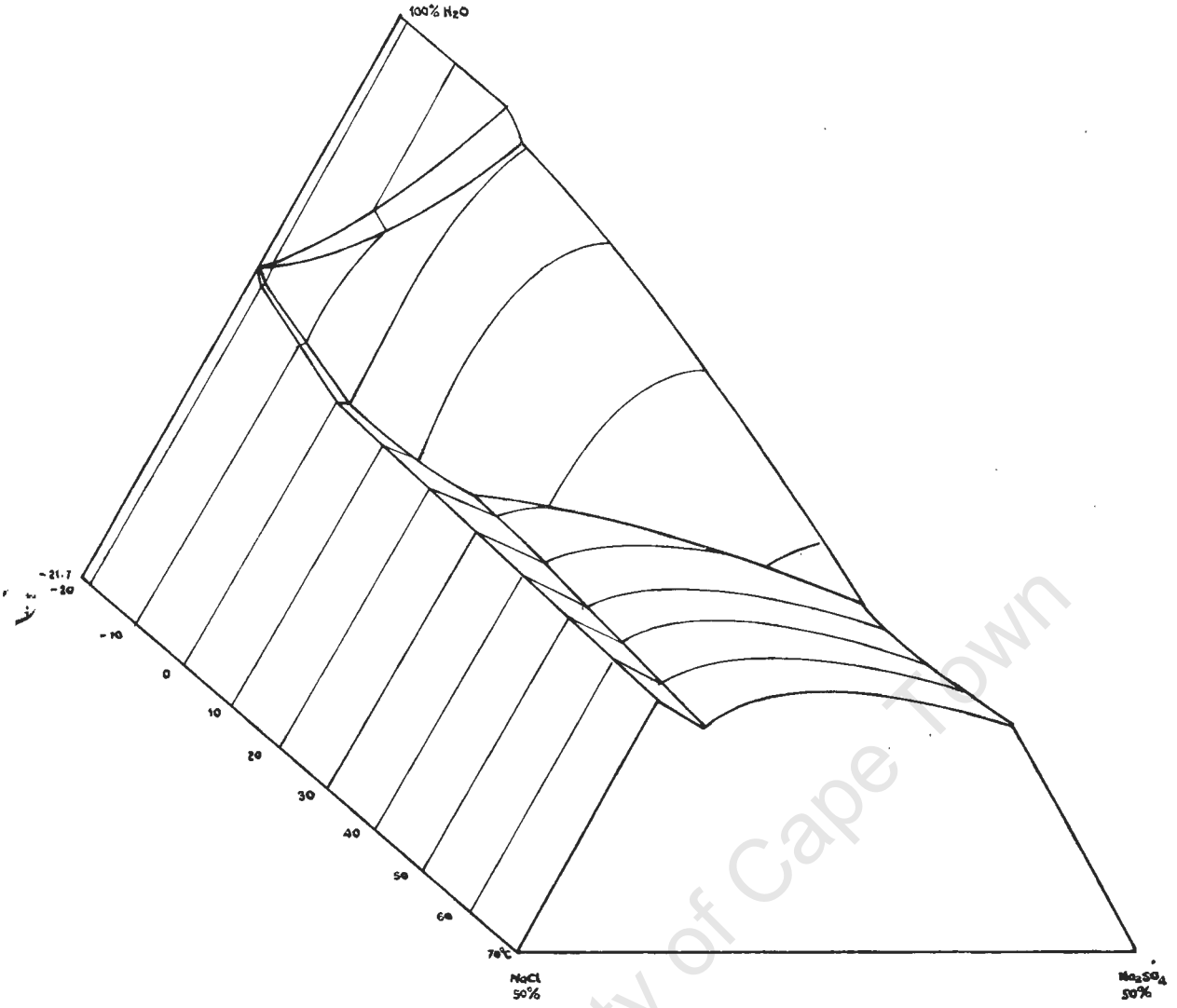

Fig. 1
Prismatic Plot of the System
$NaCl$—Na_2SO_4—H_2O

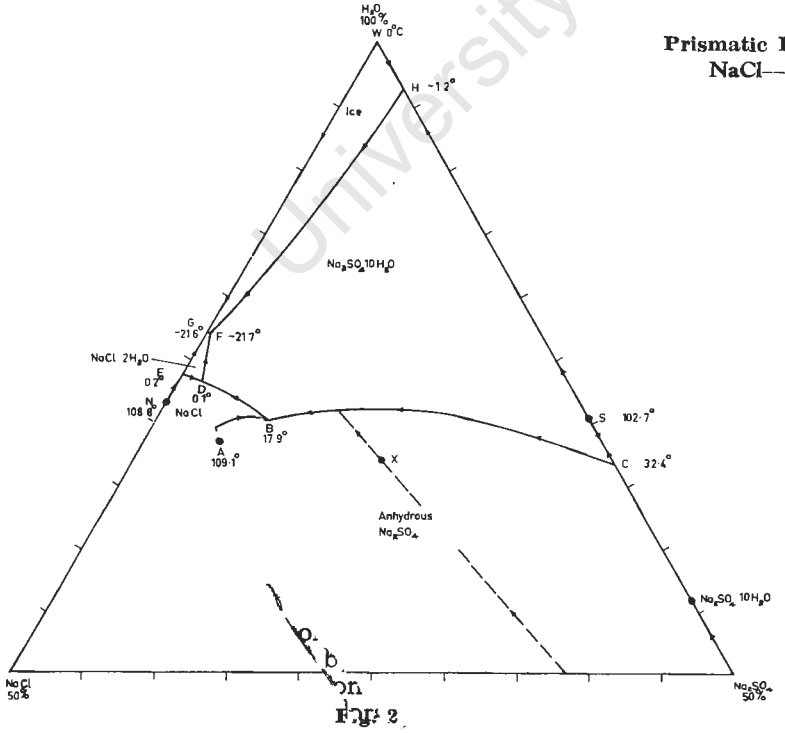

Fig. 2
Projection of Surface of Crystallization

temperatures. Therefore, conclusions drawn from the discussion of the system are also approximately true for temperatures not much different from 25°C. For other conditions of temperature and concentration, an argument similar to the one discussed in the above example can be used.

The effect of cooling concentrated brines

The nature of the solid phases which separate on cooling depends on the composition of the original brine, as will be seen from the two examples discussed below.

As before, consider the system represented by the point Y isothermally evaporated at 25°C. until the solution is nearly saturated. This point may be represented by Z (Figure 3). If the solution is now cooled to, say, −10·6°C., Z will not change its position on the diagram, but must now be considered in relation to the isothermal section at the new temperature (Figure 4). In the chosen example, Z lies in the area LTR and represents a system consisting of a solution of composition R in equilibrium with a mixture of solid sodium chloride and the decahydrate of the sulphate. The two solids crystallize together, so that in this particular case pure sodium chloride could not be obtained.

However, when the isothermal sections at 25°C. and at −10·6°C. are plotted on the same axes, Figure 5, the curve JKM crosses the line RT at V, which corresponds to a solution in which the sodium sulphate content is 34·4 per cent of the total dissolved solids. Thus, brines in which the proportion of sodium sulphate exceeds this value, will on evaporation to the saturation point at 25°C. produce a system represented by, say, Z′. As this point lies above RT, the only solid phase in equilibrium with the solution at −10·6°C. is $Na_2SO_4.10H_2O$, which, therefore, would crystallize from the solution on cooling to this temperature. Here, therefore, a pure component separates.

Thus, brines differing only in the sodium sulphate content will behave differently when cooled. In either of the above examples, the sulphate content in the residual solution is greatly reduced, so that this solution can be used to recover sodium chloride.

Practical applications

On the basis of the above discussion, the practical aspects of salt winning may now be discussed. As has already been pointed out, the usual method of evaporation results in a contaminated product. However, the separation of pure compounds is possible if evaporation and cooling processes are applied under controlled conditions. It is clear that the concentration of the salts and the temperature prevailing at the pans will greatly influence the conditions. For this discussion it is assumed that the temperature at which evaporation takes place is 25°C., but similar calculations can be made at other temperatures. The composition and density of the solution at the drying-up point at various temperatures are given in Table II.

TABLE II

Composition of solution at drying up point

Temperature °C.	Weight salt in 100g. solution		Per cent Na_2SO_4 in total dissolved solids	Density g./c.c.	Reference
	NaCl	Na_2SO_4			
10	24·4	3·43	12·3	1·223	5
10·2	24·3	3·39	12·2	1·224	3
*15	23·2	5·41	18·9	1·236	3
17·5	22·3	7·31	24·7	1·247	3
20	22·5	7·36	24·7	1·246	3
*21·5	22·0	7·50	25·4	1·244	5
*25	22·7	7·06	23·7	1·241	3
30	23·0	6·68	22·5	1·237	3

*The values corresponding to these temperatures differ somewhat from those cited by Pelling.[2] While his values are mainly based on the work of Seidell[5] and of Schreinemakers and de Baat,[4] these include the results of the very detailed investigations of Chretien.[3]

For the temperatures chosen above, brines can b classified according to whether the sodium sulphate content is below 23·7 per cent, the composition of the drying-up point at 25°C. (see Table II), between 23·7 and 34·4 per cent and above 34·4 per cent of the total dissolved solids. A somewhat modified classification will be necessary if different chilling or evaporation temperatures are used. Each of these types of brines has to be treated according to slightly differing procedures.

When the sodium sulphate is less than 23·7 per cent of the total dissolved solids, pure sodium chloride can be obtained without cooling. Controlled evaporation will result in a pure salt without contamination by the sulphate, which concentrates in the solution. The concentration of the dissolved salts changes until the solution attains the composition of the drying-up point (see Table II) and has a density of 1·241 g. per c.c. When the solution reaches this density, evaporation should be stopped, as sodium sulphate begins to crystallize. The amount of residual solution, which depends on the proportion of sulphate in the original brine, may be so small that further treatment may not be economically feasible. However, should it be necessary to process the solution further it may be diluted with water or fresh brine to a density of about 1·21 g. per c.c. and treated as brine containing sodium sulphate between 23·7 and 34·4 per cent of the total dissolved solids even though the actual proportion of sodium sulphate may be below this range.

In the case of brines containing a higher proportion of sodium sulphate—between 23·7 and 34·4 per cent of the total dissolved solids—pure sodium chloride cannot be obtained by evaporation alone. It has already been shown that cooling a saturated solution will also produce an impure product. It is thus advisable to concentrate the brine to a predetermined density, the exact value depends on the proportion of sodium sulphate, before cooling it to, say, −10°C. (+14°F.). During refrigeration, pure $Na_2SO_4.10H_2O$ settles out leaving a solution which now contains very little sulphate. Evaporation

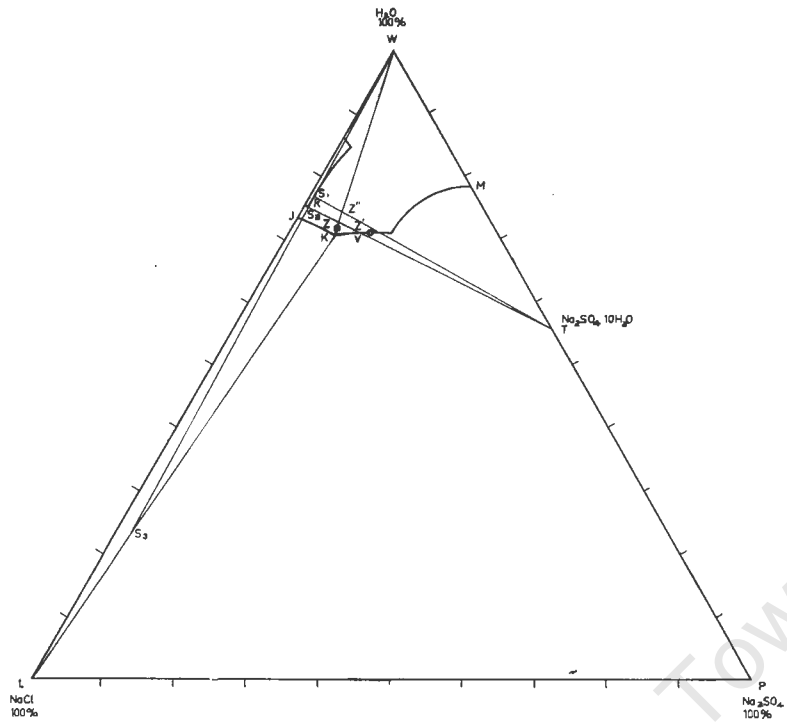

Fig. 5

Isothermal Sections at —10.6 deg. and 25 deg. C.

of this solution will yield pure NaCl and, as before, the concentration of the sulphate in the solution will increase until the drying-up point is reached. The solution can now be pumped back into the original or concentrated brine and the cycle of operations repeated. Thus pure $Na_2SO_4.10H_2O$ and pure NaCl may be recovered without loss of any raw material.

The treatment of brines, in which the sodium sulphate exceeds the above range, is very much the same as above, with the exception that the original brine may be concentrated to the saturation point. As before, chilling to —10°C. will produce pure $Na_2SO_4.10H_2O$ and evaporation at 25°C. pure NaCl. The solution remaining after the drying-up point has been reached can again be recycled. Alternatively, the brine may be evaporated to the drying-up point, during which process pure Na_2SO_4 crystallizes. The solution may now be diluted to a density of 1·21 g. per c.c. and treated as a brine in which the sodium sulphate is between 23·7 and 34·4 per cent of the total dissolved solids.

Numerical example

A numerical example may illustrate the process. Suppose after the initial evaporation the solution contains 6 g. Na_2SO_4 and 20 g. NaCl per 100 g. solution, i.e. the sodium sulphate is about 23 per cent of the total dissolved solids. The density of the concentrate at 25°C., was found experimentally to be 1·217 g. per c.c. in agreement with calculation.

When such a solution is cooled to —10·6°C., $Na_2SO_4.10H_2O$ crystallizes so that, from Figure 5

Weight solid $Na_2SO_4.10H_2O$: total weight system = S_1Z'' : S_1T, where Z'' represents the composition of the brine concentrate and S_1 the solution in equilibrium with the solid at —10·6°C. From the curve, this ratio was found to be 0·115. From 100 g. of brine concentrate, therefore, 11·5 g. pure $Na_2SO_4.10H_2O$ would be obtained and would leave 88·5 g. solution.

During subsequent evaporation at 25°C. the representative point moves along WS_1 to the curve JKM until at S_2, on the curve, pure sodium chloride begins to crystallize. As isothermal evaporation continues, the pure salt crystallizes out until at S_3 the solid sulphate just begins to form. If evaporation is stopped at this stage

Weight solid NaCl : total weight system = S_3K : LK. This value was found to be 0·57.

During evaporation, the weight of water removed from the 88·5 g. solution was calculated to be 58·5 g. The remaining system weighed 30·0 g. of which 17·1 g. were solid NaCl.

To summarize, 100 g. concentrated brine treated in the way outlined above yields 11·5 g. pure $Na_2SO_4.10H_2O$ (or 5·1 g. calculated as anhydrous Na_2SO_4) and 17·1 g. pure NaCl. The remaining solution, weighing 12·9 g. and having a density of 1·241 g.

per c.c. can be recycled with fresh brine. The recovery of the pure salts is 85·3 per cent for the chloride and 84·8 per cent for the sulphate. It may be pointed out that complete evaporation of the chilled brine (represented by S_1) will yield a product with an average sodium sulphate content of about 4·4 per cent, as compared with 23 per cent for the product from the complete evaporation of unchilled brine.

Similar calculations were made for chilling temperatures of 0°C. and about 5°C. The results of the calculations are summarized in Table III below.

TABLE III

Effect of cooling brines to different temperatures. (Calculated for 100g. brine containing 20 per cent w/w NaCl and 6 per cent w/w Na_2SO_4)

Cooling temperature °C.	−10·6	0	*About* 5	*No cooling*
Weight pure $Na_2SO_4.10H_2O$ g.	11·54	11·09	9·21	nil
Weight pure NaCl g.	17·06	16·36	13·89	0·75
Recovery Na_2SO_4 per cent	84·8	81·5	67·7	nil
Recovery NaCl per cent	85·3	81·8	69·5	3·8
Weight solution to be recycled g.	12·89	15·67	27·34	85·0
Average per cent Na_2SO_4 in NaCl from complete evap. of chilled brine	4·35	5·26	8·84	23·1

Technical considerations

The industrial methods of salt winning may now be reconsidered in the light of the results in Table III.

(a) Evaporation of the brine without cooling

If the brine is allowed to evaporate without preliminary cooling, only a small amount (3·8 per cent) of the available sodium chloride will crystallize as a pure product. Subsequent evaporation will result in a product contaminated with sulphate, and, if the brine is evaporated to dryness, the average sodium sulphate content of the product will be 23·1 per cent. The disadvantage of this method is the high sulphate content of the sodium chloride obtained; alternatively, if evaporation is stopped before the sulphate begins to crystallize, the percentage recovery of sodium chloride is very small.

(b) Complete evaporation after cooling

The introduction of refrigeration greatly improves the purity of the main product, and yields pure sodium sulphate, which constitutes a useful by-product of the process. When the remaining brine is completely evaporated the average sodium sulphate content of the salts is about 4–10 per cent, depending on the refrigeration temperature. From Table III it is clear that at the lower cooling temperatures smaller amounts of sodium sulphate are left in solution, and hence on evaporation, a purer product may be recovered. However, since the costs involved to cool a brine to −10°C. are very much greater than to cool it to 0°C., and since there is very little increase in the sodium sulphate content of the salt obtained from the brine cooled to 0°C., it would appear that this temperature could be used industrially.

(c) Partial evaporation after cooling

To obtain pure sodium chloride as well as pure sodium sulphate, partial evaporation of the chilled brine is advocated. The course of evaporation may be followed by measurements of the density of the brine, and, when the appropriate density has been attained (see Table II) the remaining solution can be recycled. This procedure, involving the three stages—cooling, evaporation and recycling—is the recommended procedure, since the extra operation is counterbalanced by the uniformity of the sodium chloride obtained in a high degree of purity.

Economic factors involved in the application of the above process to the production of common salt and sodium sulphate under South African conditions have not been considered. In the United States, however, the process has been used commercially for several years. At Monahans, Texas, a plant, using the same principle, produces sodium sulphate from a brine containing 7–8 per cent w/w Na_2SO_4.[6] As the sodium chloride concentration of the brine is not high enough, more of this salt is added to the raw brine before chilling, in order to decrease the solubility of sodium sulphate. Although the consumption of sodium chloride is over 40 tons per day, none is recovered, all being discarded in the tailing liquors.

A similar process has been worked out[7] for application to Swedish brines. Since these are rich in calcium and potassium, the process has been planned for the recovery of sodium chloride and of potassium by crystallization of both NaCl and $KCaCl_3$.

This paper is published by permission of the South African Council for Scientific and Industrial Research.

REFERENCES

1. Shuttleworth, R. G., "The supply of common salt and related chemicals in South Africa" (1952). Internal Report, obtainable, free of charge, from the Council for Scientific and Industrial Research, Pretoria.
2. Pelling, A. J., J. South African Chem. Inst., 1925, **8**, No. 1, 3–6. J. Chem. Met. Mining Soc. S.A., 1925, **25**, 242, 297.
3. Chretien, A., Ann. Chim., 1929, **12**, 9–145.
4. Schreinemakers, F. A. W., and de Baat, W. C., Z. phys. Chem., 1909, **65**, 589.
5. Seidell, A., Amer. Chem. J., 1902, **27**, 52–62.
6. Weismann, W. I., and Anderson, R. C., Mining Eng., 1953, **5**, 711–15.
7. Assarsson, G. O., Sveriges Geol. Undersökn., Ser. C. No. 501. Arsbok, 1948, **42**, 1.